WASHABLE BAGHOUSE OPERATION AND DESIGN AS APPLIED TO MILK POWDER PRODUCTION

A thesis submitted in partial fulfilment of the requirements

for the

Degree of

Doctor of Philosophy in Chemical and Process Engineering

in the University of Canterbury

by John R. Gabites

2007

Our deepest fear is not that we are inadequate.
Our deepest fear is that we are powerful beyond measure.
It is our light, not our darkness that frightens us most.
We ask ourselves, who am I to be brilliant?
Actually, who are you *not* to be?
You are a child of God and your playing small does not serve the world.
There is nothing enlightened about shrinking so that other people won't feel insecure around you.
We are all meant to shine, as children do.
We were born to make manifest the glory of God that is within us.
It is not just in some of us; it is in everyone.
And as we let our own light shine, we unconsciously give other people permission to do the same.
As we are liberated from our own fear, our presence automatically liberates others

Marianne Williamson

Abstract

The use of washable baghouses for fines collection in milk powder plants has been investigated. The main aim of this study was to increase the fundamental understanding of both operation and design of washable baghouses for application in milk powder plants. This work has focussed on the industrial scale. Industrial plant operating data has been collected, plant designs compared and analyses conducted on powder produced at the industrial scale.

The amount of powder that becomes fines, the small size fraction of powder entrained in spray dryer outlet air streams, has been shown to be significantly greater than the traditionally vague estimate of 10 % to 20 %. The ratio of fines flows to total powder flows ranged from 49 ± 8 % to 86 ± 2 % depending on the powder type and plant operating conditions. A simple yet reliable method was developed to quantify fines flows based on measured powder size distributions of samples taken from around the plant. These estimates were supported by readings from an online optical scintillation instrument, which was shown to be capable of measuring fines flows at concentrations approximately four times the supposed maximum stated by the instrument's manufacturer.

Observations in another part of this work supported previous Fonterra observations showing that the amount of bulk fat in skim milk powder (SMP) has a large influence on the baghouse differential pressure. Fines flows measured by the optical scintillation instrument and analysis of other plant operating data showed that a change in bulk fat in SMP does not appear to cause any change in fines concentration. Observations of the surface of SMP by scanning electron microscopy, and electron spectroscopy for chemical analysis, both showed that fat is over-represented on the surface of the particles, and that only small increases in the bulk fat content are required to cause large increases in the surface fat coverage. It is hypothesised that increased fat on the surface of particles increases the clumping of SMP before deposition on the bags. Consequently, the powder forms more porous cakes and is less likely to penetrate into the interior of the filter bags, which also makes it easier to pulse clean powder from the filter bags. Therefore, the baghouse differential pressure is reduced.

The design of pulse-jet baghouses from the literature was found to rely heavily on the authors past experience and approach, giving rise to large variation in recommended values of the key

design parameters. A procedure for determining the optimal combination of these parameters was developed. This procedure showed that the main Fonterra washable baghouses are far from optimal because of their high air-to-cloth ratios, long bags and high elutriation and annular velocities. This procedure also showed that the Fonterra vibrating fluid bed washable baghouses are much closer to the optimum, which is the probable reason these washable baghouses have had almost no operational issues.

Observations of the movement of the bags from below showed significant movement for bags near the inlet of the baghouse, indicating that this was the probable cause of the high bag damage in this zone. It is suggested that increasing the outer gap (distance between the baghouse wall and the bag on the edge of the bag bundle) be investigated further in an attempt to slow the annular velocity around the edge of the bag bundle and reduce bag movement. It is also recommended that stainless steel inspection hatches installed in the wall of a baghouse for this research, be included in all current and future washable baghouses because use of these hatches reduced the overall clean-in-place turn around time by 20 %.

Computational fluid dynamics simulations of the air flow patterns within the Clandeboye Dryer 2 chamber were carried out using a commercial code CFX10.0. These simulations are possibly the first to include the influence of a spray dryer's internal fluid bed airflow on the flow patterns within a spray dryer. As expected, the simulations showed the main air jet oscillated and precessed about the central axis with no apparent distinct frequency. In turn, the recirculation zones between the main jet and the chamber walls fluctuated in size. Different fluid bed flows within the industrial range had only a local influence on the air only flow field by reducing the length of the main jet. A different outlet boundary condition (including a flow resistance representing the baghouse) also appeared to have little influence on the overall flow field. Good agreement was found between the movements of the main jet via simulations and from telltale tufts installed in the plant dryer. This supported other indications that the simulations were an accurate representation of the actual flows.

It was concluded that this project achieved its main aim of improving the fundamental understanding of washable baghouse operation and design, especially for application in milk powder plants. Also this project, as well as a change in production schedules, has helped to reduce downtime associated with the washable baghouses in the Fonterra Clandeboye Dryer 2 plant by an estimated 50 hours per annum.

Acknowledgements

I would like to express my sincere thanks to my supervisor, Professor John Abrahamson whose warmth, enthusiasm and support made every aspect of this project achievable, exciting and fun. John, thank you so much for instilling in me the skills you have and the opportunities you provided made me humbled to be able to work with you. I also wish to thank my co-supervisor Dr James Winchester. James, thank you so much for the well thought out conversations, the deep interest you showed and the encouragement to keep going when times got tough.

I would like to acknowledge the CAPE technical staff of Bob Gordon, Frank Weerts, Tony Allen and Trevor Berry. I know I was not an easy customer but thank you for your advice and getting the job done, well almost. Thanks to Richard Snoek for his willingness to spend a summer being a CAPE technician. I also wish to thank Hilary Takurangi (my little sister), and Dr Stephanie Day from WASS for their articulate proof reading and improving my writing style.

The financial assistance from the Foundation for Research Science and Technology (FRST) and Fonterra Co-operative Group Ltd is gratefully acknowledged - I would not have been here without it. Thanks also for the interest, the assistance and the laughs provided by the Fonterra Clandeboye powder plant staff.

Thank you to Nathan Bushnell for his assistance with CFX and more importantly his friendship. Also, a big thanks for the laughs, the willingness to go for a pint and the support from Jock Brown, Jack Rutherford, Dave Walker, Bram Beuger and Rahul Shastry.

I am forever grateful for the kindness, support and welcoming homes of Bruce and Suzanne Gabites and Murray and Christine Facer. Thank you for making this process as easy as you could, being extremely understanding of my transient lifestyle and being there when I needed you. Finally, to my greatest teachers, Mum and Dad: I can never thank you enough for the gifts you have given me, the support, the encouragement and the unconditional love. I obviously picked the best parents because the person I am is a direct reflection of the parents you are.

Table of Contents

ABSTRACT ..... **I**

ACKNOWLEDGEMENTS ..... **III**

NOMENCLATURE ..... **XI**

1. INTRODUCTION **1-1**

1.1. Background **1-1**

1.1.1. History of Washable Baghouses in the New Zealand Dairy Industry 1-4

1.2. Scope of Thesis **1-7**

1.2.1. Significance of Thesis 1-8

2. BACKGROUND **2-1**

2.1. Baghouses **2-1**

2.1.1. Separation Principles 2-2

2.1.2. Filter Bags 2-3

2.1.3. Baghouse Types 2-5

2.2. Pulse-Jet Baghouses **2-8**

2.2.1. Pulse-Jet Baghouse Research 2-12

2.3. Theory **2-13**

2.3.1. Differential Pressure Models 2-13

2.3.2. Pneumatic Conveying Correlations 2-15

2.3.3. Power Spectrum 2-16

2.4. Milk Powder Plants **2-16**

2.4.1. Milk Powder 2-17

2.4.2. Fonterra Clandeboye 2-18

2.4.3. Washable Baghouse Research in the New Zealand Dairy Industry 2-19

2.5. Experimental Techniques **2-21**

2.5.1. Scanning Electron Microscopy 2-21

2.5.2. Particle Size Analysis 2-22

2.5.3. Electron Spectroscopy for Chemical Analysis 2-22

3. HISTORICAL DATA INVESTIGATION 3-1

3.1. Introduction 3-1

3.1.1. Aims 3-2

3.2. Theory 3-2

3.2.1. Fan Operating Conditions 3-2

3.2.2. Total Solids of Milk Concentrate 3-3

3.2.3. Milk Powder Sticky Point 3-4

3.2.4. Filter Cake Porosity and Thickness 3-4

3.3. Assumptions 3-5

3.4. Methods 3-6

3.4.1. Plant Log Book Data 3-6

3.4.2. Air Flow Instrumentation 3-7

3.4.3. Assumptions Tested 3-7

3.5. Results 3-7

3.5.1. Thought Flow Diagram 3-7

3.5.2. 2003/2004 Season Trends 3-11

3.5.3. Airflow Instrumentation 3-18

3.5.4. Individual Product Groups 3-22

3.5.5. Product Averages 3-35

3.5.6. Assumptions 3-39

3.6. Conclusions 3-41

3.7. Recommendations 3-42

4. FINES LOADINGS 4-1

4.1. Introduction 4-1

4.1.1. Aims 4-2

4.2. Theory 4-3

4.2.1. Particle Size Distribution Method 4-3

4.2.2. Particle Flow Measurement Techniques 4-7

4.2.3. Pneumatic Conveying Correlations 4-13

4.3. Methods 4-13

4.3.1. Particle Size Distribution Method 4-13

4.3.2. Online Instrument 4-14

4.3.3. Pneumatic Conveying Correlations 4-16
4.4. Instrument Location 4-17
4.4.1. Instrument Measurement Range 4-20
4.4.2. Installation 4-21
4.5. Results 4-23
4.5.1. Particle Size Distribution Method 4-23
4.5.2. Online Instrument 4-27
4.6. Fines Loadings Discussion 4-30
4.6.1. CPM 5003 Calibration Curve 4-34
4.6.2. Particle Size Distribution Method Assumptions 4-35
4.6.3. Accuracy of Particle Size Distribution Method Curve Fitting 4-36
4.7. Use of Optical Scintillation Instrument 4-38
4.7.1. Evaporator Swaps 4-38
4.7.2. Feed Line Swaps 4-41
4.7.3. Changes in Atomisation Equipment 4-43
4.7.4. Suitability of the Trialled Instrument 4-45
4.8. Pneumatic Conveying Correlations 4-47
4.8.1. Molerus and Wellman 4-47
4.8.2. Maynard 4-49
4.8.3. Williams 4-50
4.8.4. Future Development 4-51
4.9. Conclusions and Recommendations 4-51

5. FILTER BAG SCANNING ELECTRON MICROSCOPY 5-1
5.1. Introduction 5-1
5.1.1. Aims 5-2
5.2. Assumptions 5-2
5.3. Methods 5-2
5.4. Results 5-3
5.4.1. New Bags 5-3
5.4.2. Used Bags 5-6
5.4.3. CIPed Bags 5-9

5.5. Conclusions 5-15

6. SINGLE CELL BAGHOUSE 6-1

6.1. Introduction 6-1

6.2. Design Idea 6-2

6.3. Construction 6-4

6.3.1. Structure 6-4

6.3.2. Baghouse Shell 6-6

6.3.3. Instrumentation & Pipe work 6-12

6.4. Commissioning 6-20

6.5. Further Work 6-20

6.6. Future Use of Rig 6-22

6.7. Conclusions and Recommendations 6-24

7. FAT IN SKIM MILK POWDER 7-1

7.1. Introduction 7-1

7.1.1. Aim 7-4

7.2. Theory 7-5

7.3. Assumptions 7-7

7.4. Methods 7-8

7.5. Results 7-10

7.5.1. Differential Pressure 7-10

7.5.2. Filtration Velocity 7-13

7.5.3. Fines Concentration 7-14

7.5.4. Filter Cake Resistance 7-17

7.5.5. SEM Images 7-23

7.5.6. Proposed Mechanisms 7-26

7.6. Future Work 7-27

7.7. Conclusions and Recommendations 7-28

8. DESIGN OF PULSE-JET BAGHOUSES 8-1

8.1. Background 8-1

8.1.1. Aim 8-1

8.2. General Pulse-Jet Baghouse Design 8-2
8.2.1. Baghouse Design Parameters 8-2
8.2.2. Design Procedures 8-12
8.2.3. Milk Powder Collection 8-16
8.3. Fonterra Washable Baghouse Designs 8-17
8.3.1. Main Washable Baghouses 8-18
8.3.2. Vibrating Fluid Bed Washable Baghouses 8-25
8.3.3. Discussion 8-30
8.4. Recommended Design Changes 8-33
8.5. Future Research 8-35
8.6. Conclusions and Recommendations 8-35

9. BAG MOVEMENT 9-1
9.1. Introduction 9-1
9.1.1. Aims 9-3
9.2. Theory 9-3
9.3. Assumptions 9-4
9.4. Methods 9-5
9.5. Results 9-7
9.5.1. Observations From Below Bag Bundle 9-7
9.5.2. Inspection Hatches 9-9
9.5.3. Periods of Industrial Scale Bag Movement 9-9
9.5.4. Natural Period of Laboratory Scale Bag 9-13
9.5.5. Bag Movement Modelling 9-15
9.5.6. Observation of Cleaning Pulse 9-18
9.6. Future Research 9-21
9.7. Conclusions & Recommendations 9-22

10. SPRAY DRYER CFD MODELLING 10-1
10.1 Computational Fluid Dynamics 10-1
10.1.1 Governing Equations 10-3
10.1.2 Turbulence Modelling 10-4
10.1.3 Particle Tracking Theory 10-8

10.2 Introduction to Spray Dryer CFD Modelling 10-10
10.2.1 Aims 10-12
10.3 Model Description 10-12
10.3.1 Geometry 10-12
10.3.2 Mesh 10-13
10.3.3 Transient Air Flow Simulation 10-15
10.4 Transient Air Flow Results 10-18
10.4.1 Influence of SFB Flow 10-27
10.4.2 Influence of Outlet Boundary Condition 10-30
10.4.3 Air Flow Patterns Mesh Independence 10-36
10.4.4 Air Flow Patterns Validation 10-40
10.5 Steady State Particle Tracking Simulation Details 10-42
10.6 Steady State Particle Tracking Results 10-47
10.6.1 Particle Trajectories 10-47
10.6.2 Fines Fractions 10-50
10.6.3 Particle Tracking Mesh Independence 10-55
10.6.4 Particle Independence Study 10-56
10.7 Future Work 10-57
10.8 Conclusions and Recommendations 10-60

CONCLUSIONS AND RECOMMENDATIONS 11-1
11.1 Conclusions 11-1
11.1.1 Historical Data Investigation 11-1
11.1.2 Fines Loadings 11-1
11.1.3 Filter Bag Scanning Electron Microscopy 11-3
11.1.4 Single Cell Baghouse 11-4
11.1.5 Fat in Skim Milk Powder 11-4
11.1.6 Design of Pulse-Jet Baghouses 11-5
11.1.7 Bag Movement 11-6
11.1.8 Spray Dryer CFD Modelling 11-6
11.2 Recommendations 11-8

REFERENCES R1

APPENDICES A1

Appendix A - Background Information on Milk Powder Plants A1

A1 – Fonterra Clandeboye Dryer 2 Process Description A2

A2 – Fonterra Whareroa Powder 2 Process Description A15

A3 – Fonterra Clandeboye Dryer 2 Process Block Diagram A24

A4 – Fonterra Edendale Dryers 2 and 3 Visit Report A28

Appendix B - Supporting Information for Torbar 402 Averaging Pitot Tube B1

B1 – Torbar 402 Averaging Pitot Tube Differential Pressure to Volumetric Air Flow Conversion Calculation B2

B2 – Torbar 402 Averaging Pitot Tube Differential Pressure Transmitter CAPEX B3

Appendix C – Paper submitted to Food and Bioproducts Processing (2007) C1

Appendix D – Laboratory Scale Single Cell Baghouse funding proposal submitted to Fonterra D1

Appendix E – Publications from Baghouse Design work E1

E1 – Design of washable baghouses for fines collection in milk powder plants, presented in 5th World Congress on Particle Technology (2006) E2

E2 – Design of baghouses for fines collection in milk powder plants, submitted to Powder Technology (2006) E13

Appendix F – Clandeboye Dryer 2 Baghouse Inspection Hatches CAPEX F1

Appendix G – Paper presented in 5th International Conference on CFD in the Process Industries (2006) G1

Nomenclature

Roman Symbols

Symbol	Explanation	Units
a	Constant in optical scintillation instrument equation	–
A	Cross sectional area of a pipe	m^2
A_b	Filtration area of single filter bag	m^2
A_f	Total baghouse filtration area	m^2
A_n	Filter system factor	–
A_{Bags}	Cross sectional area of bags in baghouse	m^2
A_{BB}	Cross sectional area of bag bundle	m^2
A_{BH}	Baghouse footprint area	m^2
A_T	Material factor	–
b	Extinction coefficient	m^{-1}
b_{av}	Average value of extinction coefficient	m^{-1}
B	Application factor	–
c	Powder concentration in air stream	g / m^3
c_{in}	Baghouse inlet solids concentration	g / m^3
c_{out}	Baghouse outlet air solids concentration	g / m^3
c_{rms}	root mean square concentration	g / m^3
C	Logarithmic layer constant	–
d_e	Rossin Rammler distribution measure of fineness	µm
d_i	Standardised residual	–
d_p	Particle size	µm
$d_{p,norm}$	Normal fines return line powder particle size	µm
$d_{p,SFB}$	Static fluid bed particle size	µm
$d_{p,BH}$	Baghouse particle size	µm
D	Dust load factor(used in Chapter 8)	–
D	Diameter of spray dryer chamber (used in Chapter 10)	m
D_b	Diameter of filter bag	m
D_{BB}	Diameter of bag bundle	m
D_{BH}	Diameter of baghouse	m
D_T	Dust loadings	gr / ft^3
D_1	Lumped density for protein, lactose and minerals	kg / m^3
D_2	Water density	kg / m^3
D_3	Fat densities	kg / m^3

D_4	Concentrate solids density ratio	–
D_5	Non fat solids density ratio	–
e_i	Residual	%
E	Young's modulus (used in Chapter 9)	Pa
E	Expansion ratio (used in Chapter 10)	–
f	Combined filter bag and cake permeability (used in Chapter 2)	m / Pa s
f	Opening boundary loss coefficient (used in Chapter 10)	–
F	Bulk flow behaviour factor	–
F_g	Gravitational force	N
F_o	Other forces	N
F_D	Drag force	N
F_1	RNG k – ω turbulence model blending function	–
F_2	SST turbulence model second blending function	–
g	Constant in optical scintillation instrument equation	–
G	Gap from the edge of bag bundle to baghouse wall	m
h	Internal energy	J / kg
H	Fan operating head (used in Chapter 3)	mm H_2O
H	Tropical climate factor (used in Chapter 8)	–
H_c	Operating head of fan at equivalent point on the fan curve	mm H_2O
I	Intensity of received light (used in Chapter 4)	cd
I	Flue gas flow factor (used in Chapter 8)	–
I	Moment of inertia (used in Chapter 9)	m^4
I_0	Intensity of transmitted light	cd
I_{av}	Average light intensity	cd
I_{rms}	Root mean square received light intensity	cd
k	Turbulent kinetic energy	m^2 / s^2
k_b	Clean filter bag resistance	Pa s / m
k_b'	Clean filter bag resistance	m^{-1}
k_c	Filter cake resistance	s^{-1}
k_c'	Filter cake resistance	m / kg
K	Torbar 401 constant	0.7476 $K^{0.5}$ m / s
K_1	Plume Parameter	m^3 / m^2
l	Path length of light beam	m
L	Cake thickness (used in Chapter 3)	m
L	Length of beam (used in Chapter 9)	m
L_b	Length of filter bag	m

L_1	Baghouse #1 fines return line equivalent pipe length	m
L_2	Baghouse #2 fines return line equivalent pipe length	m
m	Mass flow of particles	g / s
$\overline{m}$	Mass of bag and cage per unit length	kg / m
m_c	Concentrate mass flow	tonne / hr
m_{col}	Mass flow of collected powder	g / s
m_{ds}	Total powder flow	kg / hr
m_{in}	Mass flow of powder fed to baghouse	g / s
m_{out}	Mass flow of powder in outlet air stream from baghouse	g / s
m_p	Particle mass	kg
m_{BH}	Total mass flow of powder from chamber to baghouses	kg / hr
$m_{BH,\#1}$	Mass flow of powder from Baghouse #1	kg / hr
$m_{BH,\#1,In}$	Mass flow of powder to Baghouse #1	kg / hr
$m_{BH,\#1,Out}$	Mass flow of powder emissions from Baghouse #1	kg / hr
$m_{BH,\#2}$	Mass flow of powder from Baghouse #2	kg / hr
$m_{BH,\#2,In}$	Mass flow of powder to Baghouse #2	kg / hr
$m_{BH,\#2,Out}$	Mass flow of powder emissions from Baghouse #2	kg / hr
m_{SFB}	Mass flow of powder through Static Fluid Bed	kg / hr
m_{Sift}	Mass flow of powder through Sifter	kg / hr
m_{VFBH}	Mass flow of powder from Vibrating Fluid Bed Baghouse	kg / hr
$m_{VFBH,In}$	Mass flow of powder to Vibrating Fluid Bed Baghouse	kg / hr
$m_{VFBH,Out}$	Mass flow of powder emissions from Vibrating Fluid Bed Baghouse	kg / hr
MS_E	Mean square or error	%
M_1	Protein, lactose and minerals lumped density constant	1.635 for skim & whole milk, 1.530 for MPC
$M_{1,3}$	Average particle diameter by volume	μm
n	Baghouse extractor fan speed (used in Chapter 3)	%
n	Number of data points in a data series (used in Chapter 4)	–
n	Number of filter bags in a baghouse (used in Chapter 8)	–
N	Number of data points in a series	–
N	Fan operating speed (used in Chapter 3)	rpm
N	Bag density in bag bundle (used in Chapters 8 & 10)	m^{-2}
N_c	Fan operating speed at equivalent point on the fan curve	rpm
Op	Opacity	%
p	Pressure	Pa
P	Static pressure (used in Chapter 3)	bar
P	Particle size factor (used in Chapter 8)	–
P_{fc}	Concentrate feed line pressure	bar

P_{fr}	Fines return line pressure	kPa
P_{yy}	Power spectrum of data set y	–
Q	Inverse of the normal cumulative probability (used in Chapter 4)	–
Q	Volumetric air flow	m^3 / s
Q_c	Volumetric air flow through a fan at equivalent point on the fan curve	m^3 / s
Q_{in}	Dryer inlet air volumetric flow	m^3 / s
$Q_{BH,in}$	Baghouse air volumetric flow	m^3 / s or m^3 / min
Q_{out}	Dryer outlet air volumetric flow	m^3 / s
Q_{SFB}	Static fluid bed air volumetric flow	m^3 / s
r	Radial distance	mm
R	Mass fraction of powder above a given particle diameter	–
RH	Relative humidity	%
RH_{out}	Relative humidity of dryer outlet air	%
S	Filter drag	Pa / m / s
S	Specific gravity of air (used in Chapter 3)	–
St	Strouhal number	–
S_E	Internal energy source term	W / m^3
S_M	Momentum source terms in the x, y, or z directions	N / m^3
t	Time	s
t	Filtration cycle time (used in Chapters 2 – 4, 7)	s
T	Temperature of air (used in Chapters 3 & 10)	^oC
T	Gas temperature factor (used in Chapter 8)	–
T_c	Temperature of concentrate	^oC
T_{in}	Dryer inlet air temperature	^oC
T_{out}	Dryer outlet air temperature	^oC
$T_{MPC\ 70}$	Temperature of milk protein concentrate 70 powder	^oC
T_{SFB}	Static fluid bed air temperature	^oC
T_{SMP}	Temperature of skim milk powder	^oC
T_{Sticky}	Sticky point temperature of milk powder	^oC
T_{WMP}	Temperature of whole milk powder	^oC
TS_c	Concentrate total solids	%
u	Velocity component in the x direction	m / s
u_τ	Friction velocity	m / s
u^+	Dimensionless near wall velocity	–
U	Velocity vector	m / s

U_g	Gas velocity vector	m / s
U_{in}	Main inlet air velocity	m / s
U_p	Particle velocity vector	m / s
U_t	Tangential velocity	m / s
U_T	Terminal velocity	m / s
U_{SFB}	Static fluid bed inlet air velocity	m / s
U_0	Spray dryer inlet velocity	m / s
V	Velocity component in the y direction	m / s
V_e	Elutriation velocity	m / s
V_f	Air to Cloth Ratio	$m^3 / m^2 / s$ or $m^3 / m^2 / min$
V_{fe}	Final filtration velocity	$m^3 / m^2 / min$ or ft / min
V_{fn}	Nominal filtration velocity	$m^3 / m^2 / min$
V_{Anl}	Annular velocity	m / s
w	Velocity component in the z direction	m / s
W	Mass per unit area of dust cake	kg / m^2
x_f	Fat content of powder on dry basis	%
x_{mc}	Moisture content of powder on dry basis	%
x_p	Particle location	m
X_b	Perimeter-to-perimeter bag distance	m
X_{BH}	Fines Fraction	–
X_{SFB}	Ratio of powder flow through the Static Fluid Bed to the total powder flow	–
y^+	Dimensionless distance from the wall	–
Y	Fast Fourier transform of data series y	–
$\overline{Y}^T$	Complex conjugate of Y	–
z	Distance from ejector (used in Chapter 6)	mm

Greek Symbols

Symbol	Explanation	Units
α	Cantilever beam model numerical constant	1.875
Δx	Bag displacement	m
Δy	Distance from the wall	m
ΔP	Baghouse differential pressure	mm H_2O
ΔP	Pressure drop across an averaging Pitot tube (used in Chapter 3)	bar
ΔP_b	Pressure drop across a filter bag	Pa
ΔP_c	Pressure drop across a filter cake	Pa
ΔP_{fr}	Pressure drop in a pneumatic conveying line	Pa
ΔP_g	Pressure drop in a pneumatic conveying line due to the carrier gas	Pa
ΔP_s	Pressure drop in a pneumatic conveying line due to solids	Pa
$\Delta P_{s,norm}$	Normal pressure drop in a pneumatic conveying line due to solids	Pa
$\Delta Q_{3,BH}$	Volume percent of Baghouse powder in a given particle size range	%
$\Delta Q_{3,SFB}$	Volume percent of Static Fluid Bed powder in a given particle size range	%
$\Delta Q_{3,Sift}$	Volume percent of Sifter powder in a given particle size range	%
$\Delta Q_{3,Sift,i}$	Actual volume percent of Sifter powder in particle size range i	%
$\Delta Q_{3,Sift,Pred,i}$	Predicted volume percent of Sifter powder in particle size range i	%
ε	Cake porosity (used in Chapter 3)	–
ε	Eddy dissipation rate (used in Chapter 10)	m^2 / s^3
ϕ	Baghouse collection efficiency	%
Φ	Viscous shear dissipation function	W / m^3
γ	Rossin Rammler distribution spread parameter	–
η	Pulse cleaning efficiency	%
κ	von Karman constant	0.4187
λ	Thermal conductivity	W m / K
μ	Viscosity of air	kg / m / s
ρ	Fluid density	kg / m^3
ρ_b	Powder bulk density	g / mL
ρ_c	Density of concentrate	kg / m^3
ρ_f	Density of fluid	kg / m^3
ρ_p	Density of particle	kg / m^3
$\rho_{p,norm}$	Normal density of fines return line powder	kg / m^3
τ_w	Wall shear stress	$kg / m / s^2$
ω	Frequency of turbulence (Used in Chapter 10)	Hz
ω	Circular frequency	Hz
ω_{fat}	Percentage fat in the dry solids	%

Abbreviations

Abbreviation	Explanation
BH	Baghouse
BH #1	Number One Main Baghouse
BH #2	Number Two Main Baghouse
BMP	Butter Milk Powder
CAPE	Department of Chemical and Process Engineering
CAPEX	Application for Capital Expenditure
CD1	Fonterra Clandeboye Dryer 1
CD2	Fonterra Clandeboye Dryer 2
CD3	Fonterra Clandeboye Dryer 3
CFD	Computational Fluid Dynamics
CIP	Clean In Place
CP	Cream Powder
DC	Direct Current
ESCA	Electron Spectroscopy for Chemical Analysis
ED2	Fonterra Edendale Dryer 2
ED3	Fonterra Edendale Dryer 3
ID	Internal Diameter
OD	Outer Diameter
MPC	Milk Protein Concentrate
MPC 70	Milk Protein Concentrate with 70% dry basis protein content
MPC 80	Milk Protein Concentrate with 80% dry basis protein content
NIR	Near Infrared Radiation
PLC	Process Logic Computer
PSD	Particle Size Distribution
RHS	Rolled Hollow Sections
RTV	Room Temperature Vulcanizing
SEM	Scanning Electron Microscopy
SFB	Static Fluid Bed
SMP	Skim Milk Powder
SST	Shear Stress Transport
PTFE	Polytetrafluroethylene
TA	Fonterra Te Awamutu site
UK	United Kingdom
USA	United States of America
WMP	Whole Milk Powder
WPC	Whey Protein Concentrate
WP2	Fonterra Whareroa Powder 2
VF	Vibrating Fluid Bed

1. Introduction

1.1. Background

A recent change in the design of milk powder plants has seen the traditional cyclone system (Figure 1-2) used for fines recovery replaced with washable baghouse systems (Figure 1-3). Fines are defined as the small size fraction of milk powder that becomes entrained in the spray dryer outlet air streams.

The first such new design installed in New Zealand by Fonterra Co-operative Group Ltd (Fonterra), the world's largest exporter of milk products, was a retrofit of the Whareroa Powder 2 plant; the cyclones were replaced with a Lubbers designed washable baghouse in the 2000/2001 season. Three GEA Niro A/S designed milk powder plants were built at Clandeboye (Dryer 2, 2000/2001 season) and Edendale (Dryer 2, 2001/2002 season; Dryer 3 2002/2003 season). The three identical plants have two main washable baghouses for the drying chamber air and a single washable baghouse for the vibrating fluid bed air. A single baghouse was installed at Lichfield with the new Whey Protein Concentrate dryer ready for the 2002/2003 season. The world's largest milk powder plant was built on the Clandeboye site in the 2004 off-season. This plant has five Intensiv designed washable baghouses; four off the chamber for the main drying and static fluid bed air streams, and a single washable baghouse for the vibrating fluid bed air. Two new plants were built on the Te Awamutu site for the 2005/2006 season (Dryer A and Dryer B). Dryer A has two baghouses and Dryer B one, all of which are Intensiv designed.

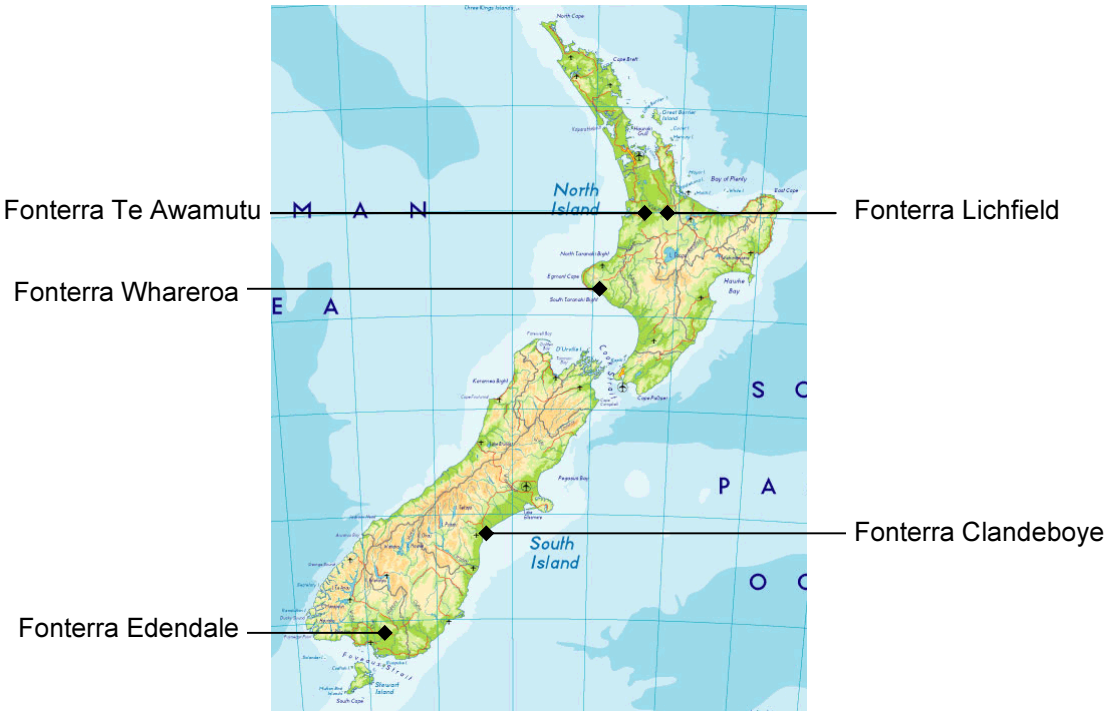

Figure 1-1: Location of Fonterra milk powder plants with washable baghouses in New Zealand

Baghouses were traditionally used to remove fines not recovered by cyclones attached to spray dryer systems (Figure 1-2). Fonterra currently operates 12 milk powder plants with this cyclone/baghouse set-up. These baghouses were always thought to be a source of microbial contamination because powder may have long residence times in the bags. Therefore approximately 10 % of these cyclone fines were downgraded to stock food. Another disadvantage of this traditional system was that cyclones often had issues with wall deposits that lead to blockages, thus interrupting dryer operation.

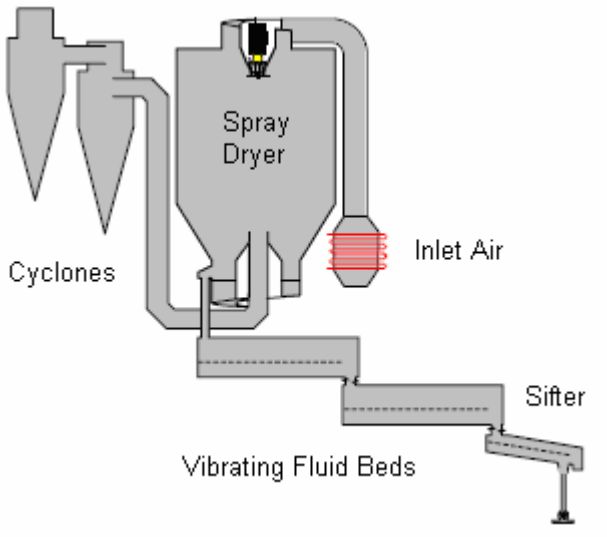

Figure 1-2: Schematic of traditional milk powder plant (source: Fonterra)

Washable baghouses (Figure 1-3), with their ability to be cleaned-in-place (CIPed), have changed the perception of baghouses as being a source of microbial contamination. A CIP involves the recovery of product residues, a pre-rinse with water to remove loose dirt, cleaning with a detergent (typically 1 % sodium hydroxide solution at approximately 70 ^{o}C), a second water rinse, disinfecting with acid and a final water rinse (Bylund, 2003).

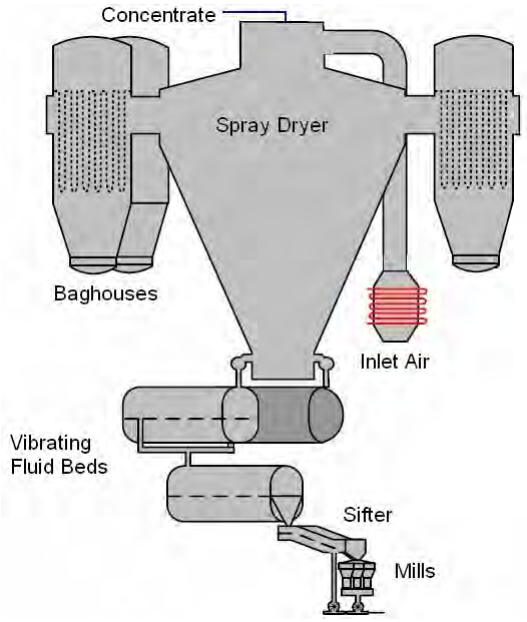

Figure 1-3: Schematic of modern milk powder plant (source: Fonterra)

Because washable baghouses can be CIPed, all fines collected by them retain the microbial product quality of the dryer chamber powder, thereby increasing profits. Because all fines are collected in a single stage, fewer unit operations are required. This leads to reduced building space requirements, lower capital costs and simplified plants (Westergaard, 2003). The final advantage of the new system is that baghouse collection is a gentler form of product collection when compared to cyclones. This is more suited to the high fat and high protein powders of the New Zealand dairy industry (Machen, 2001).

1.1.1. History of Washable Baghouses in the New Zealand Dairy Industry

Despite the numerous advantages of this new fines collection system, high differential pressures, some blinding and bag damage due to bag movement have caused frequent interruptions to the dryer operation. A history follows of the washable baghouse operational issues encountered within the Clandeboye Dryer 2 (CD2) plant, many of which are applicable to other Fonterra sites.

At the peak of the dairy season, the milk to be processed at Clandeboye is almost equal to the capacity of the site. Any reduction in site capacity due to production issues is very costly. For example, it was estimated that the 66 hours of downtime due to baghouse issues in the 2002/2003 season cost Fonterra Clandeboye $300,000.

One of the main causes of this downtime was because the baghouses were operating at high differential pressures. Consequently, the baghouse extractor fan speeds had to be increased to maintain the required chamber vacuum, thus creating an increase in electricity costs. If the baghouse differentials exceed a set point of 180 mm H_2O, the plant automatically switches to running on water rather than product. This can be costly downtime, especially at the peak of the season.

During these periods of running on water, the filter bags were able to be pulse cleaned without the presence of incoming powder, in an attempt to reduce the differential pressure. If the differential pressure did not decrease, the filter bags were deemed to be completed blinded; likely that small powder particles filled the voids in the bag fabric. Consequently, the plant was shut down and the filter bags replaced. If a total replacement took place in the

two main baghouses, six hours of downtime was required and the bag replacement cost was between $19,200 and $52,800 depending on the type of bags used.

A further problem was significant caking around the top of the bags, particularly when producing skim milk powder (SMP). This caked powder was often so bad, operators had to shake the filter bags or even poke the powder clumps with metal rods to remove it.

Excessive bag damage due to bag movement was also common. Again, these damaged bags had to be replaced, as powder lost through the bags to atmosphere with the dryer outlet air stream equated to lost profits and had the potential to violate resource consents. Bags were damaged when they rubbed against each other and against sharp sections of the internal cages that support them. The movement causing this rubbing arose not only from the nature of pulse cleaning but also the dirty airflows in the baghouse. The weak finger joint holding the two sections of the bag cages together was believed to allow greater bag movement in the bottom 3 m of the bags, and also create more sharp sections for bags to rub on.

In an attempt to improve bag life, a number of different suppliers of filter socks were used. Filtercorp, Madison and Intensiv bags were all trialled with limited success. These companies also offered a new type of filter sock, a pleated bag that has an increased filtration area in a shorter length because of the pleats. However, these bags often blew out of shape because they were not structurally sound at the pulse cleaning pressures used.

The performance of the baghouse CIP had been a major disappointment of the GEA Niro A/S baghouses. Firstly, large amounts of powder caked onto the bags, particularly when producing SMP. To remove this powder, long initial water flushes were needed at the beginning of the CIP. Also, contact of high protein powder with the caustic solution of a CIP creates a gel layer that appeared to remain on the filter bags after a CIP. Compounding this problem were issues with the CIP set that prolonged the CIP time further. For example, when pumps ran dry (because of insufficient water supply) and fluid beds filled with water (because of poor drainage), the CIP sequence had to be put on hold to resolve these dilemmas. Finally, at the completion of the CIP, all bags had to be dried out before the plant could return to production. Altogether, this process could easily take over 10 hours. Therefore, it was more effective, both in terms of cleanliness and down time, for all the bags to be replaced. This six to seven hour task was much quicker than the full baghouse wash and dry out.

Issues with the main air inlet to the spray dryer added to the baghouse problems. Firstly, condensate leaked from the main drying air radiator into the drying air stream. This led to high humidity levels in the dryer, and consequently sticky powder clogged the baghouses. These high humidity levels in the dryer were remedied when the leaks in the air radiator were fixed and then a new radiator installed in the 2004 off season. Plant operators learnt from this experience the need for strict control of dryer air humidity levels because of their impact on baghouse performance.

A second issue with the main drying air was because of the incorrect position of a weld in the air distributor. This caused the air flow pattern down the dryer to favour one side. Consequently, milk powder often fouled patches of the dryer wall. The incorrect weld upsetting the air flow was removed and hence, the chamber fouling problem eliminated. Coupled with this, the lance angles were adjusted to ensure the desired concentrate spray angle was achieved. It was believed that a non uniform air flow pattern within the dryer would have created an imbalance in fines loadings on the two main baghouses.

Operating data showed that the higher the fat content of SMP, the lower the baghouse differential pressure. A cream dosing system was implemented at Clandeboye in 2003 which enabled cream to be dosed to standardise fat levels in skim milk. This gave greater control over the skim milk powder composition so that SMP with higher fat contents could be produced, thus having a positive effect on baghouse differential pressures. However, the mechanism behind this phenomenon was unknown.

A second observation of importance was that evaporator swaps had an impact on baghouse differential pressures. Previously, as an evaporator neared the end of a run and the total solids of the concentrate decreased slightly, an increase in baghouse differential pressures resulted. When the total solids returned to the set point because of concentrate flow from the new evaporator, the differential pressure would decrease but not to the initial levels. To help overcome this variation in concentrate total solids, a low solids diversion loop was installed in the concentrate feed line. The collected low solids concentrate is now slowly blended back into the concentrate fed to the dryer.

1.2. Scope of Thesis

As it stands, little is known about the effective operation and design of washable baghouses for fines collection in milk powder plants. The main aim of this project is to increase the fundamental understanding of baghouse operation and design. This project will be judged a success if at its completion, the downtime at the CD2 plant can be reduced from 66 to 50 hours, the bag lifetime is increased by 50 % and the milk powder processing capacity of the plant is increased by 1 %.

A more detailed description of baghouses and milk powder plants is given in Chapter Two. A search of the open literature is also presented highlighting previous baghouse research. However, there are only a limited number of publications on the fabric filtration of milk powder or studies into milk powder collection by cyclones or baghouses.

Chapter Three covers the review of the 2003/2004 dairy season operating data from the Clandeboye Dryer 2 plant. The aims here were to deduce which operating parameters the baghouse differential pressure is most sensitive to and to compare the baghouse operating data for the three products produced in CD2 during this season.

Three methods were used to investigate the amount of fines produced for each powder. They were (a) a particle size distribution method, (b) an optical scintillation instrument which was checked by independent isokinetic sampling and (c) use of pneumatic conveying pressure drop correlations. These methods are outlined and the results are discussed in Chapter Four.

An in-depth plant study involved three areas of research. Firstly, SEM imaging of new, used and CIPed filter bags was carried out, the results of which are found in Chapter Five. Secondly, a single bag laboratory scale baghouse was designed and constructed. The details of this are explained in Chapter Six. Finally, investigation into the mechanism behind reduced baghouse differential pressures with increased fat in skim milk powder is located in Chapter Seven.

Chapter Eight details a baghouse design study. This baghouse design study had several aims. They were (a) determine the key baghouse design parameters and suggest suitable values for these, (b) develop a design procedure, (c) determine the most suitable of the available air-to-cloth ratio guidelines, and (d) review the current Fonterra washable baghouse designs.

The bag movement investigation found in Chapter Nine comprised three parts. Firstly, the cause of an identified high bag damage zone was to be deduced. Secondly, the natural and operational frequencies of industrial and laboratory scale bags were determined. Finally, a simple cantilever beam model was applied to these.

A computational fluid dynamics investigation of the CD2 dryer is found in Chapter Ten. This study investigates the transient flow patterns within the spray dryer and includes steady state particle tracking.

1.2.1. Significance of Thesis

Every new milk powder plant being built in New Zealand and around the world is using the washable baghouse system. Also, Fonterra are investigating retrofitting all their current milk powder plants that use the cyclone system with washable baghouses. Therefore, this thesis is very significant as a better understanding of washable baghouse operation and improved designs is required to prevent the operational issues outlined above occurring in these new installations. Because of the status of the New Zealand dairy industry as a world leader, it is likely that this work will also be of significant interest to companies, both processing and design, outside New Zealand.

2. Background

This chapter provides detailed information about baghouses and milk powder plants. An outline of the current state of knowledge on the subjects of pulse-jet baghouses and washable baghouse use in the diary industry is also presented. The chapter also includes information about the key experimental techniques used during this project.

2.1. Baghouses

Baghouses are a form of fabric filter, 'the oldest and most reliable of many methods for removing dusts from an air stream' (Ruthven, 1997). A baghouse consists of many individual filter elements contained in a single housing with a gas inlet and outlet, a dust storage hopper and a cleaning mechanism (Orr, 1977).

The filtration process found within a baghouse is basically as follows: the particle laden air stream, or dirty air stream, is forced to flow through a surface filter (Neiva and Goldstein, 2003); particles larger than the fabric interstices are deposited by a simple sieving action (Dickenson, 1992) and form a powder layer known as the cake (Silva et al., 1999) while the clean gas passes through the filter (Parker, 1997); initially the filtration efficiency is low until loose flocs build up on the fabric surface which then provide an effective filter for removal of fine particles (Richardson et al., 2002). The filter requires cleaning from time to time to avoid excessive build up of solids and therefore high pressure drops (Richardson et al., 2002): this is achieved using one of the methods described below.

Baghouses are used in a number of chemical and process industries. For example, baghouses for the control of industrial particulate pollution are used in the power generation, chemicals, foods, metals and minerals industries (Cora and Hung, 2002; Dickenson, 1992). The use of baghouses will continue to grow in the coming years as constraints on environmental emissions become more stringent (Ellenbecker and Leith, 1980).

The expectation for increased baghouse use is because of the advantages this form of dust collection equipment has over alternatives such as cyclones, electrostatic precipitators and wet scrubbers. Baghouses can have collection efficiencies that exceed 99 % (Croom, 1995;

Ruthven, 1997; Turner et al., 1998) with proper fabric selection, adequate sizing and good design (Dickenson, 1992) as particles as small as 0.3 μm can be collected (Croom, 1995).

Baghouses have moderate pressure drops and power consumption (Ruthven, 1997), and because of the smaller space requirements, baghouses require lower capital investments than other alternative dust collectors (Croom, 1995). Finally, the dust is recovered in a dry, reusable fashion and no water is required to saturate the exhaust gases, as in the case of the wet scrubber (Ruthven, 1997).

There are some limitations to the use of baghouses which are a result of gas and particle characteristics. Baghouse operation suits only low temperatures of up to 260 ^{o}C (Croom, 1995; Ruthven, 1997), although the use of metal and ceramic filters can extend operating temperatures to 540 ^{o}C (Croom, 1995). It is agreed that humid gas streams (Masters, 1972; Turner et al., 1998), situations where liquid condensation is a possibility (Ruthven, 1997) and corrosive gas streams (Turner et al., 1998) should be avoided. It is suggested (Masters, 1972) that baghouses cannot be used for products requiring high hygiene standards in handling. However, modern washable baghouses should eliminate these concerns because they can be CIPed. Masters (1972) also warns that baghouses cannot be used for collection of hygroscopic powders or particles/agglomerates that are in stringy form. Although not stated, it is likely that hygroscopic and stringy agglomerates will adhere strongly to the bag surface and interior such that they can not be removed by cleaning. Other disadvantages of baghouse use are that maintenance for bag replacement can be expensive and is also an unpleasant task (Ruthven, 1997). Also, because of the large hold up of powder on arrays of vertical surfaces in air, baghouses may be hazardous with combustible or explosive dusts (Ruthven, 1997).

2.1.1. Separation Principles

For particle separation to occur from a gas stream, the particles must be transported to the surface of the fibres of the filter medium and be retained there (Löffler et al., 1988). According to Löffler et al. (1988), particles are transported to the fibre surface by one of two mechanisms, stochastic or deterministic motion. Stochastic motion is caused by Brownian motion (Löffler et al., 1988). This motion increases the chances of particles coming into contact with the filter cake or filter elements (Croom, 1995) and is the most important

mechanism for sub-micron particles (Ruthven, 1997), that is, those below 0.2 μm (Croom, 1995). Deterministic motion of particles toward the fibre surfaces is a result of inertial, gravitational or electrostatic forces (Löffler et al., 1988). It is agreed (Cora and Hung, 2002; Croom, 1995; Ruthven, 1997) that the primary mechanism for attracting dust particles to the filter medium is direct impaction. In this situation a particle collides directly with a filter element (Croom, 1995). This mechanism accounts for almost 99 % of the baghouse collection of particles greater than 1 μm in aerodynamic diameter (Bethea, 1978).

Electrostatic forces may arise between the dust and filter element and therefore attract particles into the filter or dust cake (Croom, 1995). If these forces produce agglomerates, the cleanability of the filter increases and hence, these electrostatic forces may be set up intentionally (Croom, 1995). Gravity settling causes particles to settle onto the filter media or fall to the dust hopper below (Croom, 1995).

Other particle collection mechanisms that may apply are: sieving, when larger particles than the openings in the filter are caught (Croom, 1995); interception, that is interrupting the path of particles when they pass within half a diameter of the filter element (Croom, 1995); and precoat, when a layer of process dust or flow aid is intentionally built up on the filter surface to serve as a filter medium for smaller particles (Ruthven, 1997).

2.1.2. Filter Bags

The selection of the filter media is a key to baghouse performance (Croom, 1995). A choice is made between woven or non-woven, natural or synthetic fabrics, the temperature and chemical resistance of the fabric and bag weight, strength and permeability (Bergmann, 2001). This choice is made by considering the filtration velocity, dust properties and cleaning method (Croom, 1995).

The filter bags used in the New Zealand dairy industry are polyester needlefelts. Such filter bags are a three dimensional medium as filtration occurs at the surface as well as within the structure (Löffler et al., 1988). Fibres lie in a random arrangement and a support scrim may be included to reinforce the interior of the bags, allowing them to handle higher tensile stresses (Löffler et al., 1988).

Croom (1995) states that the development of these needlefelts has improved efficiency to 99.99 % and reduced filter drag because a smaller amount of fine material penetrates into the medium compared with woven fabrics. This in turn reduces the electricity costs for the fans associated with the baghouse. Also, development of these needlefelts has increased bag life because of less abrasion and wear (Croom, 1995).

There are several possible surface finishes that can be applied to fabric filters to ensure fabric quality, modify the surface characteristics of the bag and regulate the filter bag permeability (Lydon, 2004). They include singeing, calendaring, polytetrafluroethylene (PTFE) membranes and chemical finishes. Surface finishes also allow for higher filtration performance and increase bag life times (Lydon, 2004). These are explained in the following paragraphs.

Singeing involves contacting the surface of the bag with a hot metal strip or passing a hot flame over the surface to remove short protruding fibres (Lydon, 2004). These fibres would impede cake discharge because of mechanical adhesion (Lydon, 2004) and therefore encourage dust accumulation on the bag (Löffler et al., 1988).

Calendering is achieved by passing the filter fabric between hot pressurised rollers at a speed and temperature appropriate for the fabric (Lydon, 2004). This process softens the filtering surface fibres, welding some together and forms a skin (Humphries, 1981). Calendaring improves surface smoothness (Löffler et al., 1988) and changes the cake discharge behaviour such that the smooth surface gives particles less opportunity to adhere mechanically (Weigert and Ripperger, 1997). However, calendaring may reduce the filter surface area and decrease the bag permeability (Lydon, 2004). Also, calendaring creates smaller pores which retain smaller particles, thus increasing the resistance, and excessive calendaring may decrease the mechanical stability of the filter (Weigert and Ripperger, 1997).

PTFE membranes can be laminated to the fabric surface (Lydon, 2004). It has been shown that PTFE membranes are able to be cleaned much more efficiently than singed and untreated felts as dust deposits on the surface rather than inside the fabric and therefore, true dust cakes form (Ellenbecker and Leith, 1983). PTFE membranes also make the bags more durable (Lydon, 2004).

Chemical finishes, such as Ravlex^{TM} (Lydon, 2004), can be impregnated into the filter material to improve repellency and cleanability (Löffler et al., 1988) as well as provide resistance to heat, chemicals and abrasion (Lydon, 2004).

Penetration of powder into the bag fabric, which may decrease the bag life, increases with the filtration velocity (Agarwal, 2005; Leith and First, 1977a; Leith et al., 1978). 'Blinding' occurs when particles become trapped inside the bag fabric and adhere to its surface (Weigert and Ripperger, 1997). Typically, condensation, improper cleaning or excessive dust loads are the causes of blinding (Bergmann, 2001). Weigert and Ripperger (1997) report that the intensity of blinding depends on the filter medium, the intensity of the cleaning process and the particle size, shape and adhesiveness. Blinded bags result in high differential pressures which can cause dust to pass directly through the pores of the bag fabric (Zielinski, 2003). Because of the large driving force between the dirty and clean side of the bag, high emissions can result, therefore, permanently blinded bags need to be replaced (Zielinski, 2003).

2.1.3. Baghouse Types

Baghouses are classified by the type of cleaning method used to remove the particulate matter from the surface of the filter medium (Agarwal, 2005). The method used depends on the bag fabric used, the baghouse design and housing configuration (Dickenson, 1992). The choice of cleaning mechanism not only affects the size of the baghouse, but also its cost, maintenance requirements and dependability (Orr, 1977). The three most common types are the shaker, reverse flow and pulse-jet (Dickenson, 1992). In each case, sufficient energy must be imparted to the fabric to overcome the adhesive forces holding the dust to the bags (Turner et al., 1998).

2.1.3.1.Shaker

With a shaker type (Figure 2-1) dirty air enters the bags from the bottom and flows from the inside to the outside of the bags. The filter elements inflate during operation and do not require internal support (Dickenson, 1992). When the bags are cleaned, the dirty air flow is stopped and the tops of the elements (closed ends) shaken by a vibrating mechanism to shake off the collected dust (Dickenson, 1992). The shaking mechanism may be operated by mechanical, vibratory or air-pulsed methods (Richardson et al., 2002).

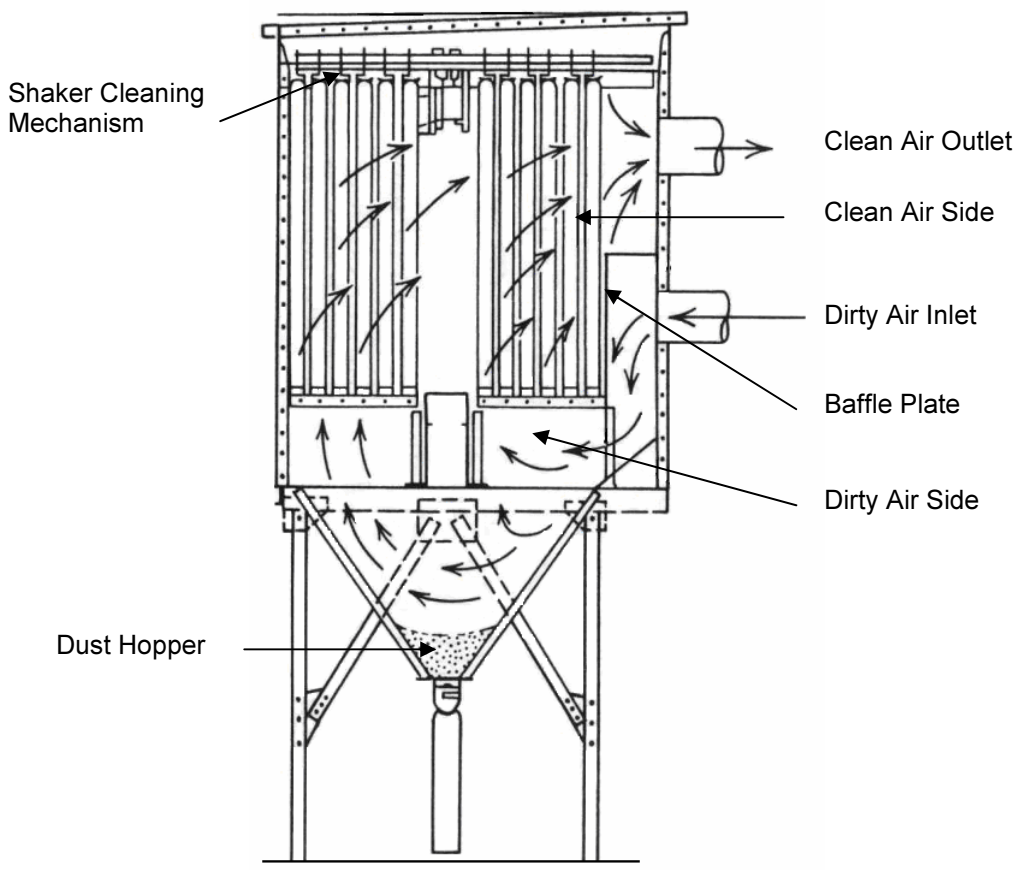

Figure 2-1: Shaker type of baghouse (source: Ruthven, 1997)

Cleaning by the shaker mechanism is usually achieved off-line as the incoming air must be stopped or diverted to another filter (Agarwal, 2005). Hence these filters operate batchwise in their filtering and cleaning modes (Agarwal, 2005). Cleaning can be done online but is less effective (Dickenson, 1992).

A shaker type baghouse is suitable for a wide range of conditions but is not suitable for some fabrics and high dust loadings (Billings and Wilder, 1970). Woven fabrics are adequately cleaned by shaking but non-woven fabrics are not (Richardson et al., 2002). Shaker baghouses are generally not as efficient as the pulse-jet type, hence the market has moved away from use of shaker baghouses (Agarwal, 2005). Bag failure in the top of the bag is common because of the extensive flexing the fastened end must undergo to effectively shake the free end of the bag (Billings and Wilder, 1970). Also, this type of baghouse tends to block more quickly as shaking does not release the dust cake completely (Agarwal, 2005).

2.1.3.2.Reverse Flow

In reverse-air cleaning (Figure 2-2) gas flow to the bags is stopped in the compartment being cleaned and reverse air flow is directed through the bags (Turner et al., 1998). With reverse air flow, because gas flow during filtering is from the inside to the outside of the bags (Agarwal, 2005), cleaning is used to deflate and collapse the elements causing the dust cake to collapse and break away (Dickenson, 1992). To prevent the complete collapse of the filter bags during cleaning, rings are sewn at intervals into the bags (Ruthven, 1997).

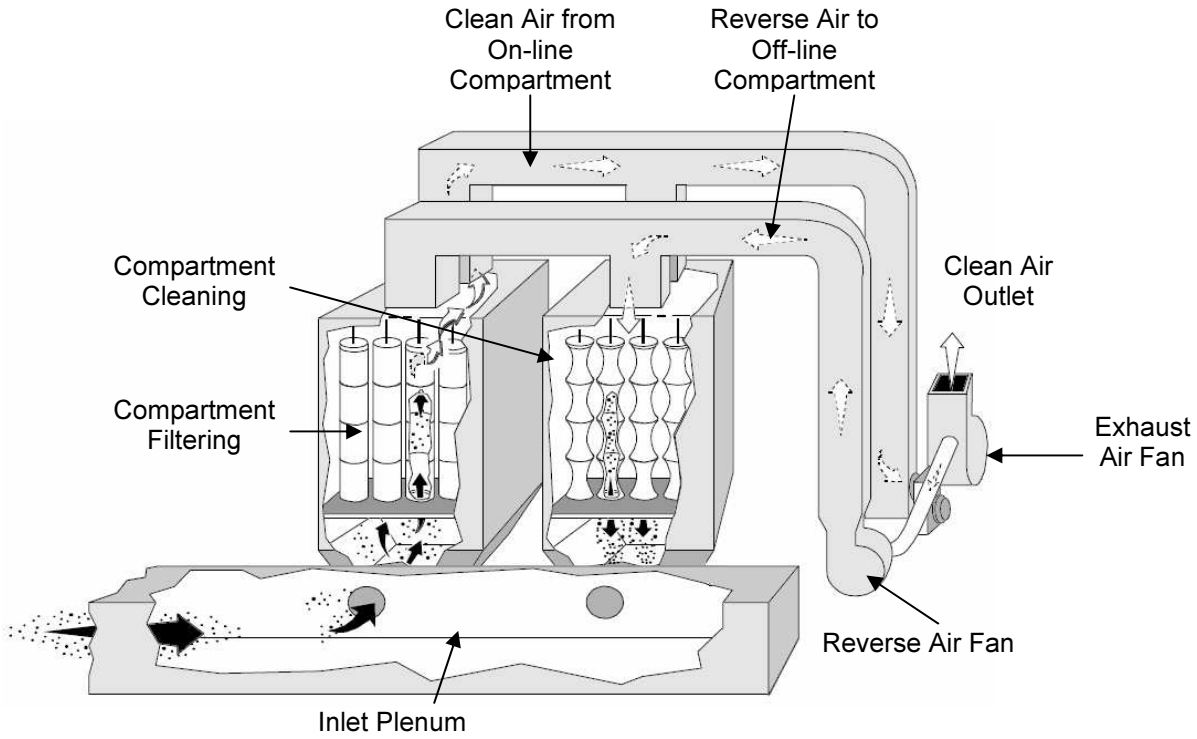

Figure 2-2: Reverse flow type of baghouse (source: Turner et al., 1998)

The source of reverse air is generally a separate fan system capable of supplying clean, dry air for one or two compartments (Turner et al., 1998). Reverse flow cleaning uses a relatively low pressure (≈ 14 – 28 kPa), high volume air supply (Croom, 1995).

The reverse flow baghouse has the same wide range of applications as the shaking type, as long as dust is released easily from the fabric (Billings and Wilder, 1970). Therefore bags made from felts are not easily cleaned by reverse flow (Billings and Wilder, 1970) and woven fabrics are generally used (Ruthven, 1997).

Reverse flow baghouses are perceived to be more expensive than the shaker and pulse-jet type because of the requirement of additional fans, ducts and dampers (Billings and Wilder, 1970). This type of baghouse is not as efficient as the pulse-jet type because it cannot generate sufficiently high gas velocities to fully dislodge the filter cake (Agarwal, 2005). Other disadvantages include some lack of control of the cleaning intensity and flexing of the filter bag for cleaning, leading to bag attrition (Billings and Wilder, 1970).

2.1.3.3.Sonic Cleaning

Sonic cleaning is the fourth type of cleaning, which is not as common as the shaker, reverse flow, or pulse-jet types. Sonic cleaning can be used to provide additional fabric vibrations (Orr, 1977) or occasionally as the only cleaning energy (Turner et al., 1998). Sound is usually generated by a plate vibrator, a siren or a resonance whistle using compressed air (Orr, 1977). The horns usual operate in the 125 to 160 Hz range and produce sound pressures of 120 to 145 db (Turner et al., 1998). When properly used, sonic cleaning can greatly reduce the mass of dust on bags considerably, but can also lead to increased penetration through the bag (Turner et al., 1998).

2.2. Pulse-Jet Baghouses

This study focuses on the pulse-jet type of baghouse used in the New Zealand dairy industry. In pulse-jet baghouses (Figure 2-3), the dirty air flows from the outside to the inside of the filter and collects the dust on the outside (Dickenson, 1992; Ruthven, 1997). Therefore, filter elements are supported by internal wire cages to maintain the filter shape (Orr, 1977). Unlike the shaker and reverse flow type baghouses, bags in a pulse-jet baghouse are not attached at both ends to the baghouse structure (Turner et al., 1998). Instead, the bag and cage are generally hung from the top plate (Ruthven, 1997) known as the tube sheet or cell plate.

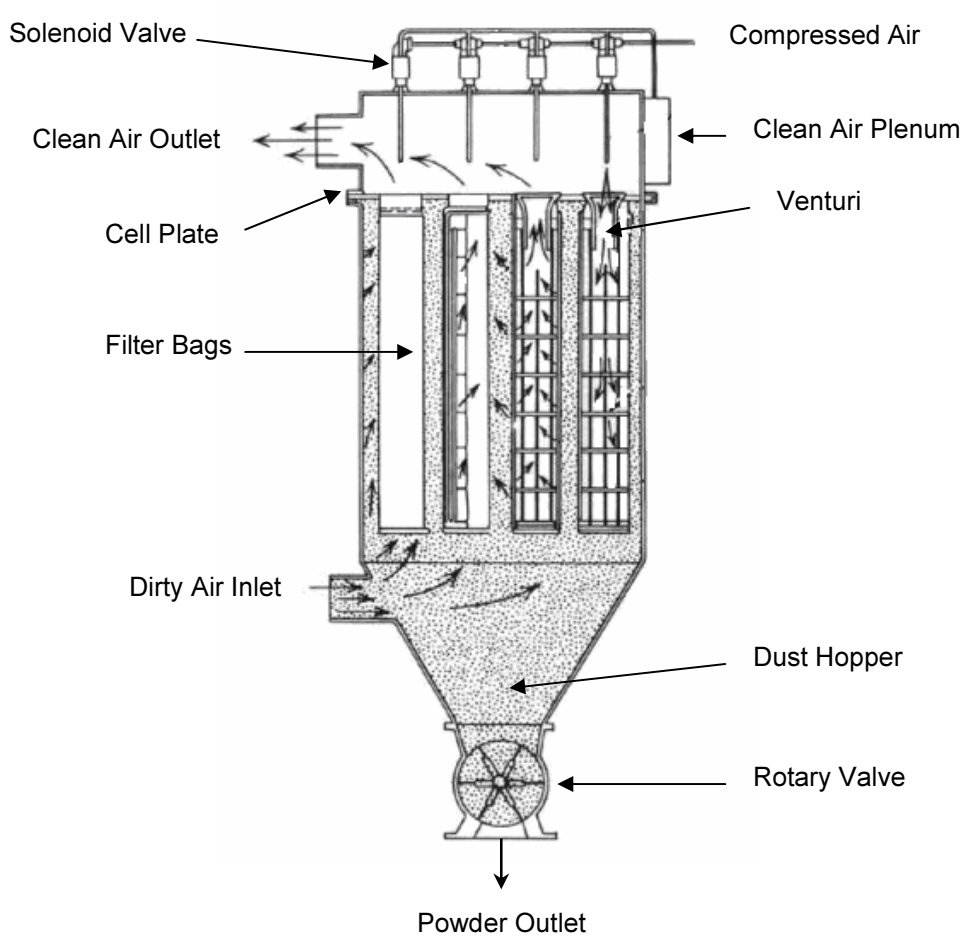

Figure 2-3: Pulse-Jet type of baghouse (source: Ruthven, 1997)

Pulse-jet cleaning uses a sharp pulse of compressed air released at the top of the bag (Billings and Wilder, 1970) to force a burst of air down through the bag and expand it violently (Turner et al., 1998). The pulse is introduced on the clean side of the filter (Dickenson, 1992) by directing it through a blowpipe or nozzle centred over each filter (Croom, 1995). Each element may also contain a venturi extending inside the bag (Ruthven, 1997). This jet of air induces flow in the form of cleaned air from other bags (Ruthven, 1997) and the combined air flow amounts to a temporary five to seven times increase in the volumetric flow rate of the original pulse (Orr, 1977).

As Figure 2-4 shows, the cleaning pulse produces a momentary expansion of the filter (Orr, 1977) and gives rise to some combination of shock, fabric deformation and flow reversal (Billings and Wilder, 1970). The fabric reaches its extension limit and the dust separates from the bag (Turner et al., 1998). Air escaping through the bag carries the separated dust

away from the fabric surface (Turner et al., 1998). At the same time, the severe flow prevents any inflow during the cleaning interval (Dickenson, 1992). Thus, dust is removed without more than a brief interruption to filtration (Billings and Wilder, 1970).

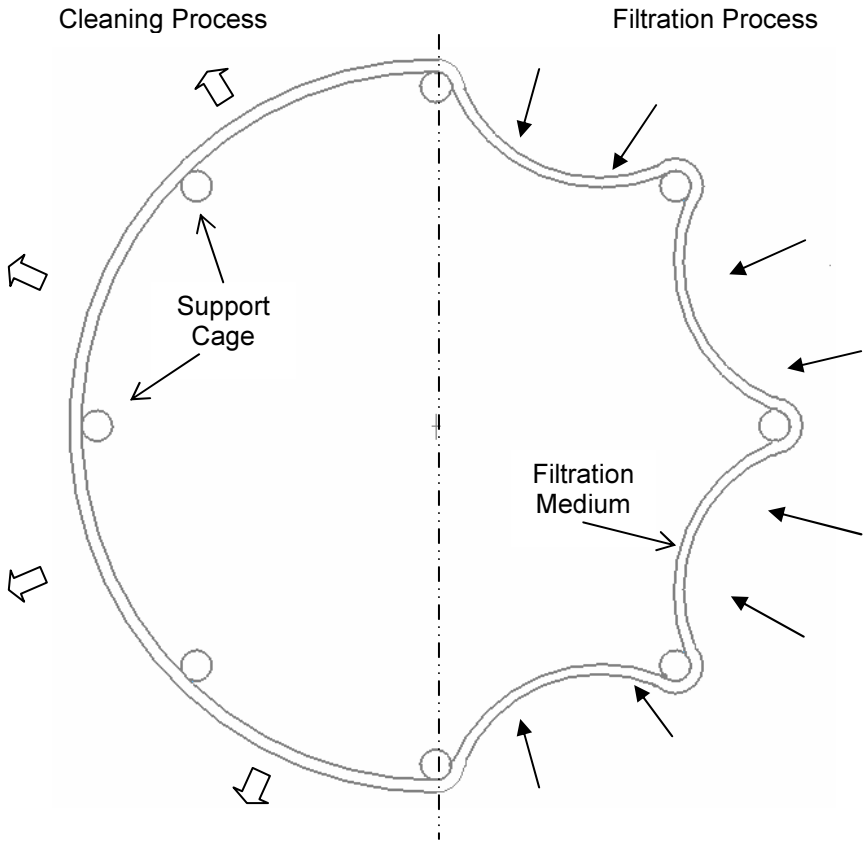

Figure 2-4: Diagram of bag and cage during cleaning and filtration in a pulse-jet baghouse

A solenoid valve on the compressed air line is energized by a timer for about 0.1 s (Billings and Wilder, 1970; Croom, 1995; Dickenson, 1992; Orr, 1977) and the compressed air pressure is usually between approximately 400 and 800 kPa (Billings and Wilder, 1970; Croom, 1995; Ruthven, 1997). Within the baghouse, a pulse usually occurs every 6 to 10 s (Orr, 1977), and the pulse frequency for each bag is adjusted as required between one to ten minute intervals (Dickenson, 1992). The effectiveness of cleaning can be adjusted by changing the compressed air pressure and the duration of the pulse (Ruthven, 1997). The frequency of cleaning can also be adjusted (Billings and Wilder, 1970). For a long bag life, a minimum number of cleaning cycles is preferred (Ruthven, 1997).

The major advantage of the pulse-jet baghouse over the shaker and reverse flow types is that it cleans better than any other method (Croom, 1995). As only a small percentage of the total

filtration area is cleaned at once, higher average filtration velocities are possible (Dickenson, 1992), typically three to four times higher than those of the shaker or reverse flow baghouses (Billings and Wilder, 1970). Therefore, the pulse-jet baghouse is smaller and has a lower capital cost because it uses less fabric and, in some cases, extra compartments for off-line cleaning are not required (Turner et al., 1998).

Because of such a short cleaning duration, pulse-jet baghouses are useful at high dust loadings (Billings and Wilder, 1970). Pressure fluctuations are almost negligible because of the rapid cleaning (Orr, 1977). As there are no moving parts, the pulse-jet type also has an advantage in terms of maintenance (Billings and Wilder, 1970), when compared to the shaker and reverse flow types.

Felted fabrics are more suited to pulse-jet baghouses (Billings and Wilder, 1970). The three major reasons for this are that: woven fabrics would be over cleaned and therefore lead to excessive leakage of dust following cleaning; because inlet velocities are high, felts with softer surfaces may withstand more abrasion; and felts form more porous dust cakes so less cleaning is required to maintain the same differential pressure (Billings and Wilder, 1970).

Although pulse-jet baghouses use higher filtration velocities, these velocities also need to be limited to prevent re-entrainment of dust from clean to dirty bags (Dickenson, 1992). It is agreed by Dickenson (1992), Ruthven (1997) and Turner et al. (1998) that re-entrainment of dust is followed by re-deposition onto bags, which can be a problem even at low filtration velocities.

High filtration velocities also cause higher pressure drops, which in turn, increase operating costs (Turner et al., 1998) and can damage fragile filters and thus reduce filter life (Croom, 1995). Bag damage can also occur because of pulse cleaning pressures that are too high (Billings and Wilder, 1970). Because the bottom ends of bags in pulse-jet baghouses tend to move in the turbulent gas flows during filtration, there is the potential that bags may rub against each other and accelerate wear (Turner et al., 1998). Long filter bags are also difficult to clean effectively using the pulse-jet method (Billings and Wilder, 1970; Orr, 1977).

2.2.1. Pulse-Jet Baghouse Research

Löffler and fellow researchers have published extensively on their research into cleaning pulse-jet baghouses. Klingel and Löffler (1984) investigated how changes in pulse cleaning pressure and filtration velocity influenced the residual dust (the dust remaining after cleaning) on a 2.44 m long pilot scale filter bag. These authors concluded that a decrease in differential pressure is not a sufficient measure of cleaning efficiency, and that it may not be economically justified to clean more intensively.

The cleaning mechanisms in the same pilot scale pulse-jet baghouse used by Klingel and Löffler (1984) were investigated by Löffler and Sievert (1987). Their results showed that large inertia forces act upon the dust cake in the upper bag regions because of the rapid pressure increase and consequent bag acceleration. In the lower region of the bag, it was postulated that, because of smaller inertia forces, the dust cake was mainly removed by reverse air flow.

Further work carried out by Löffler and co-workers include modelling the effects of structural inhomogeneities in fibrous filters on pressure drop and particle collection (Schweers and Löffler, 1994); investigating the influence of high temperatures on particle adhesion (Berbner and Löffler, 1994); and developing a method to prepare dust cakes for microscopic examination (Schmidt and Löffler , 1990).

Research carried out on pulse cleaning has been extensive. For example, the effect of modified cleaning pulses to limit dust seepage through a filter bag was studied by Leith et al. (1978) and the performance of different venturis in pulse-jet filters by Morris et al. (1991). Tsai et al. (2000) and Morris and Allen (1996) investigated how operating parameters such as the filtration velocity, filtration pressure drop, dust type and gas humidity influenced adhesion forces and therefore, cleaning efficiency. Dust cake removal characteristics have been studied by several authors including Ellenbecker and Leith (1983), Humphries (1981) and Koch et al. (1996). These three authors agree that the degree of dust cake removal during cleaning is influenced by the filter type.

2.3. Theory

The background theory applied in a number of chapters in this thesis follows. Theory applied specifically in an individual chapter is located near the beginning of that chapter.

2.3.1. Differential Pressure Models

There have been two approaches to baghouse differential pressure approximations. The first approach fits experimental pressure drop data to a curve by regression analysis (Löffler et al., 1988). Billings (1974), Rothwell (1987) and Leith and First (1977b) have also used this approach.

The work in this thesis uses a second approach where pressure drop through the filter bags (ΔP) is assumed to be the sum of the bag pressure drop (ΔP_b) after cleaning (Löffler and Sievert, 1987) and the cake pressure drop (ΔP_c), as shown by

$$\Delta P = \Delta P_b + \Delta P_c \tag{2-1}$$

Because the flow is at low Reynolds numbers (Re < 1), Darcy's Law can be applied (Löffler et al., 1988). The simplest model of this form is that of Billings and Wilder (1970) given by Equation 2-2.

$$\Delta P = k_b V_f + k_c c V_f^2 t \tag{2-2}$$

The parameters in Equation 2-2 are:

- k_b [Pa s / m] – cleaned filter bag resistance
- V_f [m / s] – filtration velocity
- k_c [s^{-1}] – resistance due to the deposited cake
- c [kg / m^3] – dust concentration in the air stream
- t [s] – filtration time

Ellenbecker and Leith (1983) define the efficiency of a cleaning pulse η, as being the fraction of powder on the filter bag prior to cleaning that is transferred to the hopper. This parameter is included in their model. Thus, Equation 2-2 is modified to include the efficiency of the cleaning pulse as Equation 2-3 shows:

$$\Delta P = k_b V_f + \frac{k_c c V_f^2 t}{\eta} \tag{2-3}$$

Now the cake resistance k_c reflects the material actually retained in the cake.

Equation 2-3 assumes that the filter collects all incoming dust (there is no lost powder through the baghouse and no powder entering the baghouse falls to the dust hopper before reaching the filter bags), and that at steady state the mass of dust per unit area collected during a filtration cycle is equal to the mass per unit area of dust falling to the hopper as a result of the cleaning pulse.

Löffler et al. (1988) do not lump the fluid viscosity μ [Pa s] into their resistance terms as has been done in Equation 2-3. Equation 2-4 shows the corresponding equation from Löffler et al. (1988) where the filter bag resistance k_b' [m^{-1}] and cake resistance k_c' [m / kg] have different units from those presented above, and W [kg / m^2] is the mass per unit area of dust cake given by Equation 2-5.

$$\Delta P = k_b' \mu V_f + k_c' \mu W V_f \phi \qquad (2\text{-}4)$$

$$W = c V_f t \qquad (2\text{-}5)$$

The reaming term in Equation 2-4 is an overall collection efficiency ϕ, representing the fact that not all powder entering the baghouse is collected. This collection efficiency assumes that all powder entering the baghouse reaches the filter bags.

The bag resistance in the models presented above is shown as a constant. However, the bag resistance is likely to increase over several cleaning cycles as small particles fill the voids and are not removed by pulse cleaning. Also, despite the cake differential pressure being proportional to the filtration velocity squared (Equations 2-2 and 2-3), the flow is laminar, not turbulent (Ruthven, 1997) and hence Equation 2-4 is proportional to velocity.

The models above give the differential pressure at any time since the last pulse clean. In this thesis, unless stated, the operating or average differential pressure over a cleaning cycle is implied when referring to the baghouse differential pressure.

More advanced differential pressure models are available. Neiva and Goldstein (2003) developed a model for calculating the pressure drop build up that takes account of the changes in cake properties caused by compressive stresses. Kavouras and Krammer (2003) proposed a model that takes account of different generations of cake which result from patchy cleaning.

These models require detailed knowledge of the dust cake growth, which is currently not known for the case of milk powder cakes in the New Zealand dairy industry. Therefore, these models were not used here.

This work uses the model of Billings and Wilder (1970) for the baghouse differential pressure. This model is the simplest of the three presented above and was chosen because the pulse cleaning efficiency and the collection efficiency of a filter bag is unknown in the washable baghouses used in the New Zealand dairy industry, and these efficiencies can be absorbed into the cake resistance k_c if they are approximately constant.

2.3.1.1. Filter Drag

The filter drag S [Pa s / m] is the resistance that occurs through the fabric and dust layer as given by Equation 2-6 (Cora & Hung, 2002):

$$\Delta P = SV_f \tag{2-6}$$

This parameter was used in Chapter Three to compare baghouse operation for different milk powders. Such a comparison is much easier using the filter drag than the filter cake resistances, which would need to be determined from Equation 2-2. The filter drag was also used in Chapter Five to show the influence of a CIP on the average baghouse pressure drop.

The inverse of the filter drag gives an estimate of the combined bag and cake permeability f [m / Pa s] determined from

$$f = \frac{1}{S} \tag{2-7}$$

This permeability estimate was used in Chapter Five to compare the permeability data obtained from bag suppliers for new filter bags, with new bag permeability values calculated from plant operating data.

2.3.2. Pneumatic Conveying Correlations

The pressure drop in a pneumatic conveying line (ΔP_{fr} [Pa]) is the sum of the pressure drop caused by the carrier gas (ΔP_g [Pa]) and the pressure drop due to the presence of solids (ΔP_s [Pa]), that is

$$\Delta P_{fr} = \Delta P_g + \Delta P_s \quad (2\text{-}8)$$

Several authors (Klinzing, 1997; Maynard, 2006; Mills, 2004; Molerus and Wellman, 1981) outline procedures for calculating the pressure drop caused by solids and gas, which are functions of the following properties: the length and cross sectional area of the pipe; the gas density and velocity; the density, velocity and mass flow of solids; and friction factors for both the gas and solids. The use of a pneumatic conveying line pressure drop being a function of the amount of solids present was used in Chapters Three, Four and Seven.

2.3.3. Power Spectrum

The power spectrum is a measure of the power at various frequencies from a noisy signal (MathWorks, 2004). The power spectrum can be easily determined using Matlab 7.0 (MathWorks Inc, Natick, USA). Given a data series y containing N data points, the power spectrum Pyy is given by Equation 2-9 where Y is the discrete Fourier transform of y, found by taking the fast Fourier transform, and $\overline{Y}^T$ is the complex conjugate of Y.

$$Pyy = \frac{Y\ \overline{Y}^T}{N} \quad (2\text{-}9)$$

A greater coverage of the Fast Fourier Transform and power spectra is given by Press et al. (1989). Time series analysis in the form of the power spectrum was applied in Chapters Nine and Ten.

2.4. Milk Powder Plants

The milk powder process consists of unit operations of milk selection and pre-treatment, concentrate manufacture, homogenization, drying and packing (Spreer, 1998). Raw milk is heat treated by an officially approved pasteurisation process to limit any pathogenic contamination (Spreer, 1998). Solid impurities are then removed by clarification and the milk separated into cream and skim milk by centrifugal separators (Bylund, 2003). To gain good control of the final product composition, milk is standardised by adding cream and lactose solutions to the skim milk to obtain the desired protein, lactose and fat levels.

Falling-film evaporators are generally used for concentration of milk from a solids content of between 9 – 13 % to 40 – 50 % (Bylund, 2003). These evaporators are multi staged (Bylund, 2003) and use a combination of mechanical vapour recompression and thermal vapour recompression. Final drying of the product occurs in a spray dryer (Bylund, 2003). This process involves dispersion of the concentrate into very fine droplets, evaporation of the water as the dispersed droplets mix into a stream of hot air, and separation of the milk powder particles from the drying air (Bylund, 2003).

A detailed process description and block flow diagram, which outline the milk powder process in more detail, have been written for the Fonterra Clandeboye Dryer 2 and the Fonterra Whareroa Powder 2 plants, and are located in Appendices A1 and A2. A process block diagram for the Fonterra Clandeboye Dryer 2 plant can be found in Appendix A3. Finally, a comparison of the GEA Niro A/S designed CD2, ED2 and ED3 MSD 2000 plants is located in Appendix A4.

2.4.1. Milk Powder

Milk powders are usually free flowing agglomerates of complex particle sizes and shapes that have been formed by the process of spray drying (Ozkan et al., 2003). The differing particle sizes and shapes are a result of variations in milk concentrate properties such as density, viscosity and surface tensions and variations in dryer operating parameters such as concentrate flow, atomisation energy and dryer inlet and outlet air temperatures (Bloore, 2002).

Lactose, protein, fat, and ash, as well as a small amount of water, constitute the components of milk powder. Powders are classified on different combinations of these components, as shown in Table 2-1.

The majority of milk powders are used in food processing: cream powder is a raw material in ice cream; whey powders are used in powdered soups, cake mixes and baby foods; and skim milk powder is used in the food processing industries such as bakeries, ice-cream factories, the manufacturing of chocolate or for reconstituting (Masters, 1972).

Table 2-1: Approximate percentage composition of different milk powders

Powder	Lactose	Protein	Fat	Moisture	Ash
Skim Milk	51.0	36.0	1.0	3.5	8.5
Butter Milk	47.8	31.5	5.8	3.5	8.6
Whole Milk	36.6	27.9	26.6	3.0	5.9
Cream	12.3	11.5	71.5	2.7	2.0
Whey Protein Concentrate	7.4	80.4	5.6	3.8	2.8
Milk Protein Concentrate	17.0	72.0	1.5	4.5	5.0

Compositions sourced as follows: SMP, WMP, CP and WPC from Kim et al (2002); BMP from Masters (1972); MPC from Fonterra.

2.4.2. Fonterra Clandeboye

Fonterra Clandeboye is located at Clandeboye, 7.8 km north east of Temuka, South Canterbury, South Island, New Zealand. This site is the second largest of the Fonterra manufacturing sites, with the Whareora site located 2.5 km south of Hawera, Taranaki, North Island, New Zealand being the largest. Clandeboye has the capacity to process up to 11.2 million litres of raw milk per day into milk powders, cheeses, butter, whey protein powders and lactose.

Three milk powder plants (Figure 2-5) are situated on this site. Both dryers one and two are GEA Niro A/S designs that have evaporation capacities of approximately 24 tonne / hr of water. CD1 is a compact design using rotary disc atomisation, whereas CD2 is a MSD 2000 design with pressure nozzle atomisation. CD1 processes predominantly SMP, but also some WMP. CD2 mainly produces milk protein powders and some WMP, but has also produced SMP. CD3 is the world's largest milk powder plant as it can produce up to 25 tonne / hr of milk powder. This equates to an evaporation capacity of approximately 45 tonne / hr. CD3 is a Stork wide-body design and processes only WMP. The CD2 milk powder plant was the main focus of this study.

Figure 2-5: Fonterra Clandeboye milk powder plants

2.4.3. Washable Baghouse Research in the New Zealand Dairy Industry

Research into the use of a pulse-jet bag filter instead of cyclones to collect SMP, WMP and sodium caseinate powder from a pilot scale spray dryer was carried out by Stapper et al. (1976) at the New Zealand Dairy Research Institute. This research investigated the difference in baghouse performance using different inlet air configurations; compared the performance of different filter fabrics; and established the influence of the air to cloth ratio, powder loadings and pulse cleaning pressure on the baghouse differential pressure. Stapper et al. (1976) found that the baghouse differential pressure increases with a) powder loadings for a constant filtration velocity and filtration cycle time, b) the air to cloth ratio for a constant powder loading and filtration cycle time and c) a decrease in the pulse cleaning pressure for a constant velocity, powder loading and filtration cycle time. These authors also found that a bottom entry dirty air inlet had a higher differential pressure than a top entry, and that cross contamination of products caused by powder hold up in the filter bags was negligible.

Machen (2001) investigated methods for determining when a baghouse needs to be CIPed. This work was carried out on the Fonterra (then Kiwi Co-operative Dairies Ltd) Whareroa Powder 2 washable baghouse. Plant historical data from a number of product groups was used to determine the plant parameters that influenced the baghouse differential pressure. It was found that time of operation with the same bags had the greatest impact. Parameters shown to have no apparent influence were the concentrate density and feed flow rate.

Models were developed by Machen (2001) to determine the time before a maximum allowable differential pressure for a product group was reached, and thus, a CIP was required. However, use of these models led to unrealistically long times between CIPs possibly because Machen (2001) did not take into account background colour of the powder or its microbiological quality.

Scanning electron microscope images of filter bags in Machen's (2001) study identified the presence of resin-like clumps between the bag fibres. It was postulated that these clumps added strength to the bag. The SEM images also showed that the surface of the filter bag was covered with some type of coating that was not present on the clean side of the filter bags.

Machen (2001) also found some issues arising in the Whareroa Powder 2 baghouse CIP. A major problem was redeposition of soil (solid milk powder removed by the CIP from internal surfaces of the plant) onto filter bags during the caustic recirculation step. Also, the formation of a gel from the powder residue on the filter bags at low rinse temperatures was observed. Determining when the filter bags were dry after a CIP was also an issue.

Wiryawan and Trinh (2003a, 2003b, 2003c, 2003d) wrote a series of internal reports for Fonterra on their work characterising a washable baghouse. This work compared particle size distributions from three locations within the Whareroa Powder 2 washable baghouse, investigated the mechanical and tensile strength as well as the abrasion resistance of filter bag fabrics, and carried out trials on a pilot scale baghouse studying the influence of different filter bags, filter bag ages and powder loadings on the average differential pressure with time.

Mechanical strength tests (Wiryawan & Trinh, 2003a) indicated that the new filter bags coated with a surface layer (Intensiv and Filtercopr bags) were stiffer and more resistant to puncture than the same aged filter bags. This difference was attributed to degradation in the surface layer of the old bag. The tensile tests conducted (Wiryawan and Trinh, 2003b) showed that a used filter bag was stiffer, and therefore less deformable, as well having a lower tensile strength than new filter bags. These findings suggest that pulse cleaning performance will decrease as the filter bags age: the bags will become less flexible, and will not be able to impart as great an acceleration on to the filter cake. As a result, old bags may overcome smaller cake adhesion forces compared with new bags.

The abrasion experiment results of these authors (Wiryawan & Trinh, 2003c) were carried out by water blasting samples of bag fabric in front of a stainless steel support. The results suggested that filter bags made from single layer woven materials shrank when damaged by abrasion. The implications of this finding are that filter bags may shrink because of a CIP and thus be less permeable after a CIP. The results also showed that the surface coating of Leubbers' filter bags had a tendency to peel off when exposed to abrasive forces.

Finally, the filtration experiment work of Wiryawan and Trinh (2003d) showed three key points. First, the average differential pressure over time for a new bag from two different suppliers filtering SMP showed no difference. The authors suggested this indicated that it is the formation of a filter cake rather than the type of filter bag that determines the steady state differential pressure. Secondly, the powder loading was shown to influence the rate of formation and thickness of the filter cake and thirdly, used filter bags were seen to have a higher permeability and therefore lower differential pressure than new bags. It was proposed that wear on used filter bags causes a change in their structure, making them more permeable.

2.5. Experimental Techniques

2.5.1. Scanning Electron Microscopy

SEM is a very common technique for viewing objects at high magnification. There are several advantages of this technique over other methods such as optical microscopy and transmission electron microscopy. With SEM, high resolution can be obtained and the large depth of field gives the specimen a three dimensional appearance (Goldstein and Yakowitz, 1975). The magnification available to the SEM is reported as being between 10 to 100,000 times (Heywood, 1971). Finally, SEM has large spaces, such as a 125 mm x 100 mm area with the JEOL JSM-6390 SEM (JEOL Ltd, Akishima, Japan)) available for carrying out dynamic experiments on the specimen (Hearle et al., 1972).

Disadvantages of the SEM include its cost; the need to evacuate the vacuum chamber, which can remove important features of the specimen; the inability to show internal detail, which is possible with optical microscopes; and the lack of colour response (Hearle et al., 1972).

More detailed methods on SEM are given by Hearle et al. (1972), and Kim et al. (2002) and Nijdam and Langrish (2006) specifically for the SEM analysis of milk powders.

2.5.2. Particle Size Analysis

Particle size distributions presented in this thesis were determined using the laser diffraction method because it is the most common type of particle size analysis used industrially (Rhodes, 1998). The method is based on the fact that light passing through a suspension diffracts at an angle inversely proportional to particle size (Rhodes, 1998). Advantages of the laser diffraction method include: a wide measuring range (from 0.02 μm to 2 mm); rapid data acquisition; high repeatability such that instrument to instrument variation is less than 1 %; and flexibility enabling the particle size of sprays, dry powders, suspensions and emulsions to be measured (Kippax, Unknown). This technique and others such as sieving, sedimentation and microscopy are discussed in detail by Allen (1997).

2.5.3. Electron Spectroscopy for Chemical Analysis

Electron Spectroscopy for Chemical Analysis (ESCA), also know as X-ray Photoelectron Spectroscopy, was developed in the mid-1960s for surface analysis (Moulder et al., 1992). The technique involves irradiating a solid with monoenergetic soft x-rays and analyzing the energy of the emitted electrons (Moulder et al., 1992). Each element has a unique spectrum, and a spectrum from a mixture of elements can be approximated by the sum of the peaks of the individual constituents (Moulder et al., 1992). The photons usually used, Mg Kα or Al Kα, are limited to penetrating approximately 1 – 10 μm into solids (Moulder et al., 1992). Thus, ESCA detects electrons that have originated only from the first few atomic layers of the sample and is therefore, a unique surface sensitive technique (Moulder et al., 1992). This technique is discussed in more detail by Moulder et al. (1992).

A method was developed for measuring the surface composition of food powders with ESCA by Fa¨ldt et al. (1993). This method has been used by several other authors to measure the surface composition of food powders (Fa¨ldt and Bergenstahl, 1996a; Fa¨ldt and Bergenstahl, 1996b; Millqvist-Fureby et al., 2001) including milk powders (Fa¨ldt and Sjo¨holm, 1996; Kim et al., 2002; Nijdam and Langrish, 2006).

3. Historical Data Investigation

There is a large amount of reported evidence that baghouse performance is a function of a number of operating parameters. For this reason, the influence of a number of spray dryer operating parameters on the CD2 main washable baghouses is investigated here.

3.1. Introduction

Despite the advantages of the new washable baghouse system, high differential pressures, significant caking and excessive bag damage have been common to all Fonterra milk powder plants using washable baghouses. These have caused interruptions to the dryer operation which totalled 66 hours in downtime during the 2002/2003 season for the Clandeboye Dryer 2 plant.

Because the baghouses have operated at high differential pressures, the baghouse extractor fan speeds have had to be increased to maintain the required chamber vacuum. This has increased electricity costs. Bag life is reduced at high differential pressures due to bag fibres stretching, which results in increased bag replacement costs.

Significant caking around the top of the bags has been observed, particularly when producing skim milk powder. Significant caking combined with high differential pressure (above 200 mm H_2O (Agarwal, 2005; Masters, 1972)) leads to bag blinding: particulate matter becomes trapped inside the bag fabric, adheres and cannot be removed by pulse cleaning (Weigert & Ripperger, 1987). Blinding reduces bag permeability and often cannot be remedied by a CIP. Therefore blinded bags have to be replaced to prevent differential pressures across the bags exceeding the upper limit of 180 mm H_2O. In the Clandeboye plant, if this differential pressure is reached, the dryer will automatically switch from running on product to running on water. If the differential pressure reaches 200 mm H_2O, the dryer will automatically shut down.

Finally, excessive bag damage, which arises from bag movement (Morgan & Walters, 1999), has occurred and added to the high bag replacement costs. Bags are damaged when they rub against each other and against sharp sections of the internal cages that support them (Parker,

1997). The movement causing this rubbing arises not only from the nature of pulse cleaning but also from cage movement caused by the dirty airflow in the baghouse. These high internal air flows can bend cages, resulting in more sharp sections for bags to rub on. Damaged bags have to be replaced because of powder lost through damaged bags: lost powder equals lost profits. Moreover, the resulting higher concentration of powder admitted to the atmosphere within the dryer outlet air stream may violate resource consents.

It is likely that the damage of bags due to bag movement is the more dominant mechanism in reducing bag life when compared to operating a baghouse at high differential pressures. Bag damage is a local phenomenon as it occurs at specific areas of a bag and baghouse. Operating a baghouse at high differentials on the other hand is a global phenomenon occurring all along the length of a bag.

3.1.1. Aims

The aims of this historical operating data investigation were to:

1. Determine the dryer operating parameters that have the greatest influence on the baghouses
2. Obtain a suitable air flow measurement instrument to be installed and connected to the plant PLC
3. Compare the operation of the three major product groups, SMP, MPC and WMP made in CD2 during the 2003/2004 season.

3.2. Theory

3.2.1. Fan Operating Conditions

Fan manufactures often supply a fan curve plotting the fan head and power consumption versus the volumetric flow through the fan for a specific fan speed. If during operation the fan speed is changed, similarity laws can be used to determine the conditions of the fan at the new operating point. For example, given the operating head H [mm H_2O] and speed N [rpm] and knowing the fan speed N_c [rpm] of the fan curve, the equivalent head on the fan curve H_c [mm H_2O] can be determined from Equation 3-1:

$$H_c = H\left(\frac{N_c}{N}\right)^2 \tag{3-1}$$

Using this calculated head, the equivalent flow Q_c [m^3 / s] at the fan speed N_c [rpm] of the fan curve can be found from the fan curve. This flow can then be used in Equation 3-2 to find the flow Q [m^3 / s] at the original operating point:

$$Q = Q_c \frac{N}{N_c} \tag{3-2}$$

Douglas et al. (2001) cover this topic in greater detail.

3.2.2. Total Solids of Milk Concentrate

Hunziker (1949) gives the total solids, TS_c [kg / kg], of milk concentrate as

$$TS_c = \frac{D_4}{D_5} \tag{3-3}$$

The parameters D_4 and D_5 are determined from Equations 3-4 and 3-5 where w_{fat} [kg / kg] is the percentage fat in the dry solids and ρ_c [kg / m^3] the concentrate density:

$$D_4 = \frac{100}{\rho_c / 1000} - \frac{100}{D_2} \tag{3-4}$$

$$D_5 = \frac{1.0 - w_{fat}}{D_1} - \frac{1.0}{D_2} + \frac{w_{fat}}{D_3} \tag{3-5}$$

D_1 [kg / m^3], the lumped density for protein, lactose and minerals, is given by Equation 3-6 where T_c [^oC] is the concentrate temperature and the constant M_1 equals 1.635 for skim and whole milk and 1.530 for MPC:

$$D_1 = M_1 - 0.0026T_c + 0.00002T_c^2 \tag{3-6}$$

D_2 [kg / m^3] and D_3 [kg / m^3] are the water and fat densities respectively, given by Equations 3-7 and 3-8:

$$D_2 = 1.0020825 - 0.000114T_c - 0.000003325T_c^2 \tag{3-7}$$

$$D_3 = 0.966665 - 0.001334T_c \tag{3-8}$$

3.2.3. Milk Powder Sticky Point

Because of the presence of lactose in all milk powders, they have the potential to undergo a transition from a glassy state to a rubbery state at temperatures above the glass transition temperature (Fernandez et al., 2003). This can lead to wall deposition which is undesirable because of the following: a reduction in product yields; the combustion potential of milk powers; and product degradation that will result from the oxidation and browning of these deposits (Ozmen & Langrish, 2002).

Equations 3-9 to 3-11 are sticky point curves for SMP, WMP and MPC respectively, where T [^{o}C] is the temperature and RH [%] the relative humidity. These curves were determined experimentally by Dr David Pearce of Fonterra Palmerston North (Pearce, 2005):

$$T_{SMP} = -164.5RH + 105.6 \quad (3\text{-}9)$$

$$T_{WMP} = -113.5RH + 99.8 \quad (3\text{-}10)$$

$$T_{MPC70} = -182.9RH + 197.9 \quad (3\text{-}11)$$

It should be noted that the sticky point is directly influenced by the powder moisture content. Equations 3-9 to 3-11 indirectly account for the influence of moisture content through the relative humidity of the air.

3.2.4. Filter Cake Porosity and Thickness

The Ergun equation is used to predict pressure drop through porous media, such as filter cakes. This equation gives pressure drop as a function of the cake thickness L [m] and porosity ε, as well as fluid density ρ_f [kg / m^3] and viscosity μ [kg / m / s], particle size d_p [m] and filtration velocity V_f [m / s]. Silva et al. (1999) show that a mass balance around the cake can be rearranged to give the cake thickness as in Equation 3-12 where A_f [m^2] is the filtration area, t [s] the filtration time, ρ_f [kg / m^3] the particle density and m [g / s] the mass flow of particles:

$$L = \frac{mt}{A_f \rho_p (1-\varepsilon)} \quad (3\text{-}12)$$

Substituting Equation 3-12 into the Ergun equation and rearranging gives

$$\frac{\Delta P_c}{t} = \frac{150(1-\varepsilon)}{\varepsilon^3}\frac{\mu m V_f}{A_f \rho_p d_p^2} + \frac{1.75}{\varepsilon^3}\frac{\rho_f m V_f^2}{A_f \rho_p d_p} \qquad (3\text{-}13)$$

Thus, knowing the properties of the fluid and particles that form the filter cake and the filtration characteristics of the system enables the filter cake thickness and porosity to be determined. It should be noted that if the average cake pressure drop during the filtration cycle is used, then the filtration time should be halved to account for the fact that the average pressure drop occurs at half a filtration cycle.

3.3. Assumptions

The majority of this section of work is based on the CD2 plant operating data from the 2003/2004 season. Thus, the key assumption for this exercise is that the plant data recorded by the operators was actual, correct and unless stated, recorded on the hour. With regard to the baghouse extractor fans, it is assumed that they are geometrically identical, operate identically and the characteristic fan curve given by the manufacture is precise.

The correlations, and data from the literature used in this exercise are assumed to be correct. Therefore, the total solids correlation of Hunziker (1949), the sticky point curves from Pearce (2005) and the particle densities given by Matheson (1991) are assumed to be accurate.

Assumptions to test the accuracy of the PLC main and SFB flow meters, as well as determine the flows in the outlet air stacks are: that the DM2 Digital Manometer is accurate; that there are no losses in pressure between any pipework connecting the field instruments, or connecting the installed averaging Pitot tube or the single point Pitot tube to the digital manometer; the plant was at steady state when the measurements were taken; the pitot tube was in the centre of each centroid and parallel to the flow when the measurement was carried out; and finally, the correlation provided by Airflow Instruments (High Wycombe, UK) for their averaging Pitot tubes is accurate.

For the calculation of the baghouse filter cake porosity and thickness, it is assumed that all fines entering the baghouse reach the filter bags and become cake. Further, the particle densities from Matheson (1991) are assumed to apply to baghouse particles.

Finally, the new filter bag permeabilities given by bag suppliers are assumed to be true and correct.

3.4. Methods

3.4.1. Plant Log Book Data

Based on a background understanding of atomisation, spray drying and filtration, a thought flow diagram was created to identify operating parameters that warranted investigation because of their possible influence on baghouse performance.

All hourly recordings of data from the 2003/2004 season standardising, evaporator and dryer log books respectively were entered into Microsoft Excel spreadsheets. The baghouse plenum pressure data, a key parameter not recorded in operator log books, was obtained from the Fonterra Stan Data Extract system.

The total solids of the milk concentrate at each data point were calculated using Equations 3-3 to 3-8. Using sticky point curves (Equations 3-9 – 3-11), the temperature difference of each operating point from the powder sticky point was calculated. Equation 2-6 was used to calculate the average baghouse filter drag caused by the cake and filter bags. The data used for this calculation came from a single production run for each product.

All the collected data was then divided into product groups of SMP, WMP and MPC. For each product group with considerable data, the data was divided again into monthly data sets, and for the case of SMP and MPC, nine daily runs were chosen at random from throughout the season.

For each key parameter in the thought flow diagram, two plots were generated. The first plotted the baghouse differential pressure and the key parameter against time, and the second, the baghouse differential pressure against the key parameter. Time periods used were the whole season, months and days.

Finally, season averages of the key plant parameters for each product group were calculated allowing a comparison of the three product groups.

3.4.2. Air Flow Instrumentation

At a point 1 m below the location of the averaging Pitot tubes, several duct traverses were conducted using a single point Pitot tube and the hand held digital manometer (DM2 Digital Manometer, Airflow Instruments, UK). The locations of the points across the duct were determined using the five point centroids of equal area method (Croom, 1995). At each point, the median value from one minute of data was used to calculate the volumetric flow.

Using the hand held digital manometer, the differential pressure of the installed Torbar 402 averaging Pitot tube was recorded eight times between October 2004 and April 2005. Using Equation 3-14 below, with the Torbar 402 constant of 0.7476 $K^{1/2}$ m / s, the stack volumetric flow was calculated.

3.4.3. Assumptions Tested

3.4.3.1. Main and SFB Air Flow Measurements

To check the accuracy of the main and static fluid bed air flow measurements, the differential pressures given by the field instruments were measured using a digital manometer (DM2 Digital Manometer, Airflow Instruments, UK). The measured differential pressure ΔP [bar] was used in the Torbar averaging Pitot tube correlation (Equation 3-14) obtained from the instrument manufacturer, to calculate the actual volumetric air flow Q [m^3 / s]. These values were compared with those obtained from the plant PLC and the discrepancy determined:

$$Q = \sqrt{\Delta P}\left(\frac{KA\sqrt{T+273}}{4.0323\sqrt{S}\sqrt{P}}\right) \qquad (3\text{-}14)$$

The variables in Equation 3-14 are: K, the Torbar 401 constant of 0.7476 $K^{0.5}$ [m / s]; A [m^2], the cross sectional area of the pipe; T [^oC], the temperature of the air; S, the specific gravity of air equal to 1.0 and P [bar], the static pressure.

3.5. Results

3.5.1. Thought Flow Diagram

The CD2 dryer log sheets contain hourly recordings of a number of plant operating parameters. To identify which of these parameters should be investigated for their impact on

baghouse performance, a thought flow diagram was generated (Figure 3-1). This diagram was adapted for baghouse performance from a similar diagram produced by Dr Tuan Truong (Truong, 2005) for powder bulk densities.

The optimal baghouse could be described as that which produces the highest collection efficiency at the lowest differential pressure and results in the longest bag lifetime. Only the baghouse differential pressure was used for this thought flow diagram for two reasons. Firstly, it is shown in Chapter Eight that over the range of expected baghouse inlet powder concentrations and with poor outlet powder concentrations (20 mg / m^3), the baghouse collection efficiencies range from 99.88 % to 99.95 %. Thus, the baghouse collection efficiency is not sensitive enough to be used in this exercise. Secondly, the aim of the diagram was to represent the dryer operating parameters to which baghouse performance is sensitive over short periods of time, for example hours. As the bag lifetime is influenced over several months, this parameter is not suitable for illustrating how parameters affect baghouse performance over short time periods.

Section 2.3.1 of Chapter Two shows a range of differential pressure models and their sources. It can be summarised from these models that the differential pressure is a function of a bag constant k_b, the filtration velocity V_f, a filter cake constant k_c, the fines concentration c and the filtration cycle time t.

The bag constant k_b is the clean bag resistance (Ellenbecker & Leith, 1980) determined from the pressure drop through the bag at a given flow. The choice of filter medium, although important in determining the baghouse differential pressure, is not affected by the dryer operation. Consequently, this parameter was not explicitly represented in the diagram. It is likely that the value of k_b will be constant over the time periods represented by the diagram. However, the older the bag, the higher the value of k_b as small particles fill the voids in the bag over time. Thus, the bag age is included in the diagram because of its influence on the baghouse differential pressure.

The filtration velocity V_f, also termed the air to cloth ratio, is dependent on the inlet air flow and the filtration area present in the baghouse. The filtration area is fixed, but in the CD2 plant, the exit air flows from the chamber do vary among the products. The filtration velocity

is also influenced by the extractor fan speeds, as the filtration velocity will increase with the fan speed.

The filter cake constant k_c represents the resistance to airflow because of the cake. This parameter is affected by the thickness of the cake and the permeability of the cake. In turn, these parameters are influenced by the fines concentration, particle size distribution of the fines and the adhesion of these fines to the filter bags.

The fines concentration is influenced by the particle size distribution and density of the chamber powder; the smaller both parameters are, the higher the fines loadings. The chamber air flow patterns also influence the fines concentration. As the chamber velocities increase, so does the particle carrying capacity of the air. This leads to an increased entrainment of powder and therefore higher fines loadings in the baghouses. Finally, the fines collected in the baghouses can be returned to one of three destinations: the top of the dryer, the SFB or the external fluid beds. Clearly, returning fines into the chamber will increase the fines loadings of the baghouses, hence the fines destination is included in the diagram.

The particle size distribution of chamber powder is known to be a strong function of the elements of the atomisation process (spray nozzle size, nozzle pressure drop, concentrate flow, concentrate density and viscosity) and the particle drying history. The mean diameter from a nozzle atomiser increases with concentrate flow, concentrate density and viscosity, and it increases as the atomiser energy decreases (Bloore, 2002). In turn, concentrate properties (density, viscosity and total solids) are a strong function of composition and temperature as Equations 3-3 to 3-8 show.

The inlet and outlet temperatures in the chamber, the inlet air humidity and the particle residence time, which is influenced by the chamber air flow patterns, impact on the particle drying history. Several reports (Fernandez et al., 2003; Murti et al., 2006; Ozmen & Langrish, 2002; Ozmen & Langrish, 2003) indicate that stickiness of milk powders is strongly dependent on the composition, the local temperature and relative humidity. The filtration velocity also has an impact because particles are more likely to adhere to the fibres of the bag surface at higher filtration velocities.

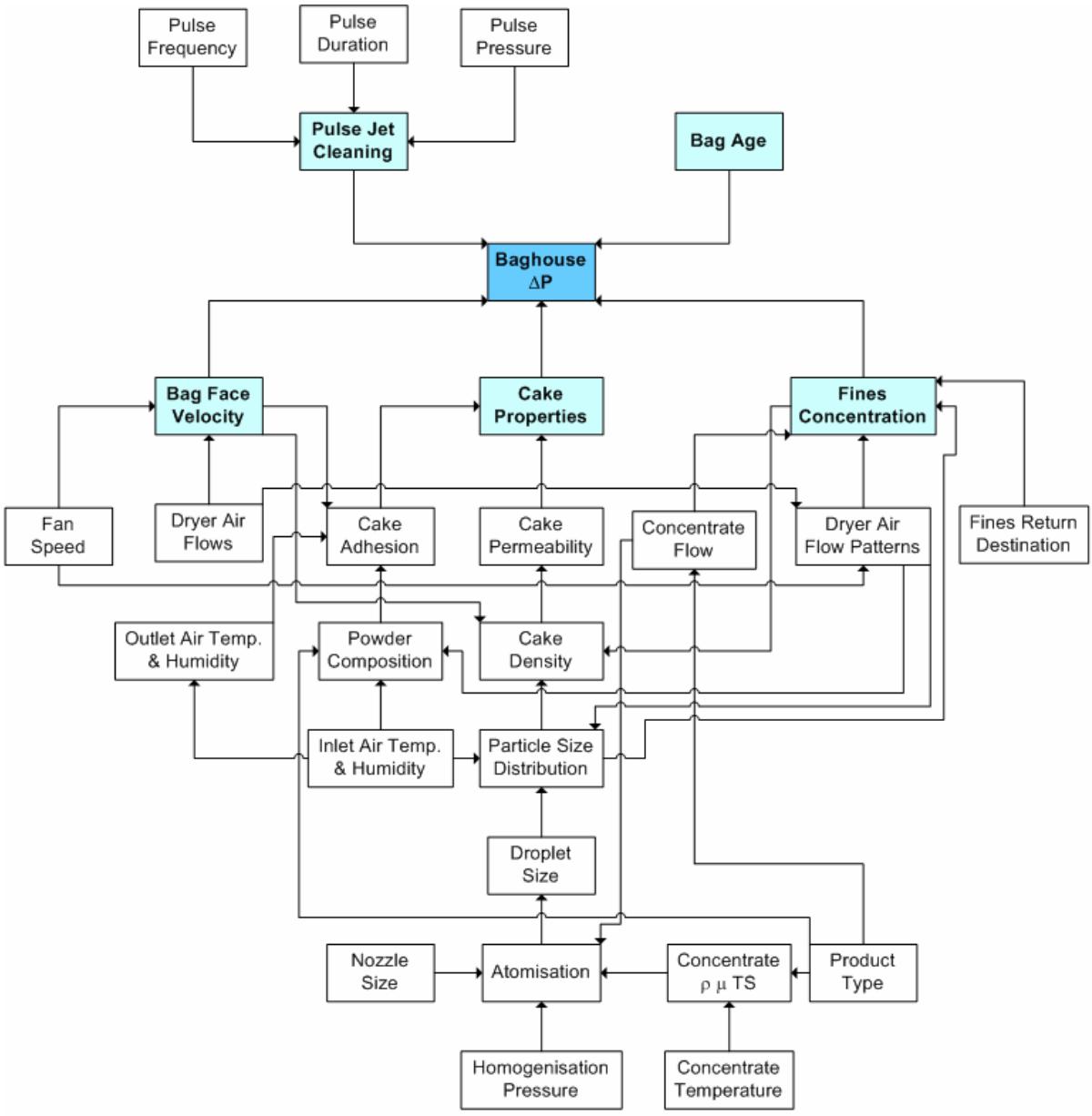

Figure 3-1: Thought flow diagram of parameters affecting baghouse differential pressure

The differential pressure model of Rothwell (1987) indicates that the cleaning frequency is an important parameter. The more frequent a cleaning pulse, the lower the resulting differential pressure, as the cake thickness and therefore the resistance to flow are both reduced. The converse is also true as the less frequent a pulse is, the higher the differential pressure.

Pulse-jet cleaning performance is also a function of the effectiveness of each pulse. An effective pulse is one where the increase in pressure inside the bag is sufficient to accelerate the bag away from its support cage. If the force generated is greater than the adhesion force

between the filter medium and the dust cake, then the cake will be removed (Löffler & Sievert, 1987) and this constitutes an effective pulse. The pulse effectiveness can be manipulated by the volume of air pumped into the bag with each pulse, determined by the pressure of the pulse and its duration.

3.5.2. 2003/2004 Season Trends

Figure 3-2 below shows how the baghouse differential pressure varied during the 2003/2004 season. Important baghouse events can be detected where a sudden change in the differential pressure occurs. Three bag replacements took place during this season on 22 September, 2 February and 1 April. The effect is clearly visible: the differential pressure reduces significantly. This is a result of new bags having a higher permeability than old bags that over time have slowly become blinded.

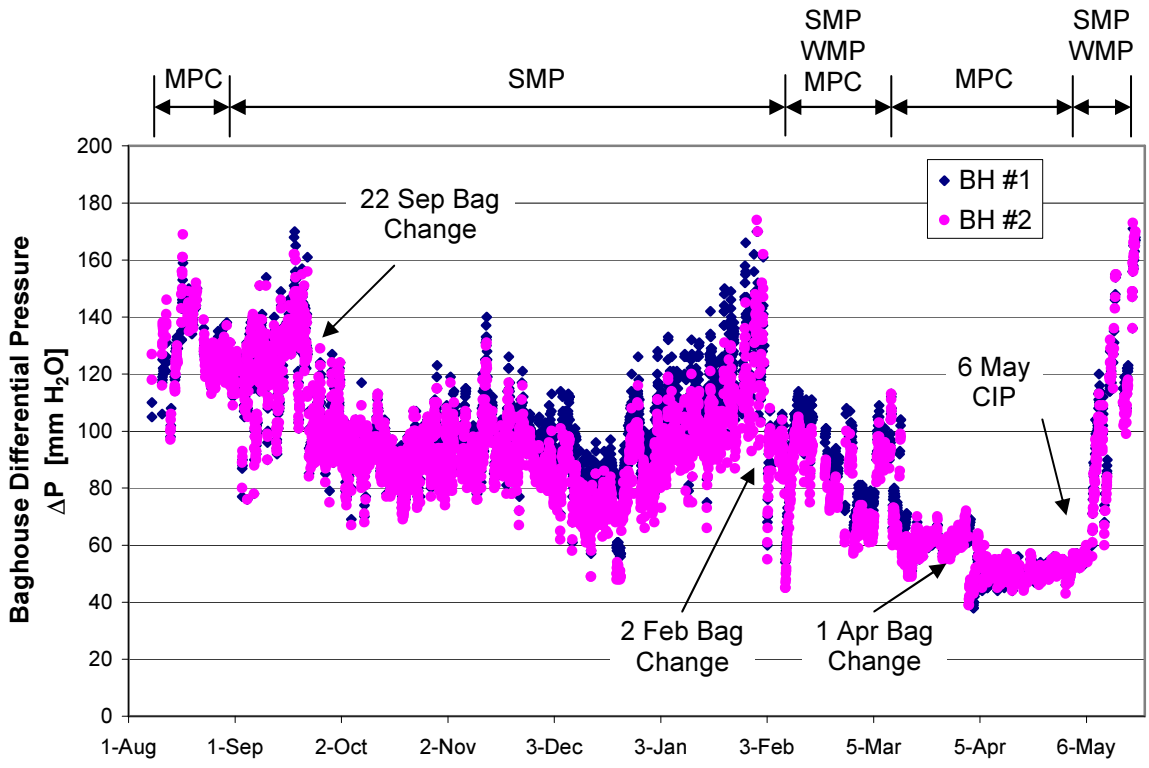

Figure 3-2: Clandeboye Dryer 2 baghouse differential pressures during the 2003/2004 season

Three bag changes in one season is very surprising as bag suppliers claim that bags will last for up to two seasons. The age of the bags that started the season is not known but two life

times that are known are the 19 weeks between September and February, and 8 weeks from February to April. It should be noted that the bags that lasted only 8 weeks were replaced because of a product safety issue, not because of high differential pressures or high emissions: bag fibres were shredding from the bags and thus had the potential to end up in the final product.

The fact that bag life times are well below supplier expectations indicates that the baghouse environment is very harsh on the filter bags. This environment could be due to the baghouse design (high air to cloth ratios and high internal air velocities) or plant operation (high fines loadings). Also, the bag testing conducted by suppliers may not replicate the environment the bags operate in; hence they predict longer than actual life times.

A dramatic increase in differential pressure is observed after 6 May. This was a result of the only baghouse CIP performed during the season, which indicates a poor CIP. Scanning electron microscope images presented in Chapter Five of post CIP filter bags showed a gel-like layer completely covering the surface of these bags that greatly reduced the bag permeability.

The major reason for the variation in baghouse differential pressure in Figure 3-2 is the production schedule: SMP was mainly produced from September through to February, MPC from February to May and short WMP runs were conducted in February and May. Clearly, lower average differential pressures are associated with MPC production. Along with the reasons for this discussed below, shorter run times and increased down time between runs when producing MPC means lower differential pressures.

The three product groups manufactured in the 2003/2004 season are characterised by different feed concentrate flows, feed concentrate total solids and resulting powder bulk densities. Of these three parameters, the bulk density data plotted in Figure 3-3 most clearly distinguishes all three product groups: SMP with bulk densities of around 0.75 g / ml, WMP with bulk densities of around 0.60 g / ml and MPC with bulk densities of around 0.45 g / ml.

It could be suggested from Figure 3-3 that the higher the powder bulk density, the higher the baghouse differential pressure. This is likely to be partly true because the higher the bulk density of a cake, the less void space there is for air flow and hence a greater resistance to

flow. However, because SMP and WMP have much higher concentrate flows and total solids contents than MPC, the differential pressures for these two products will be higher also because the higher fines loadings these products will place on the baghouses (Chapter Four).

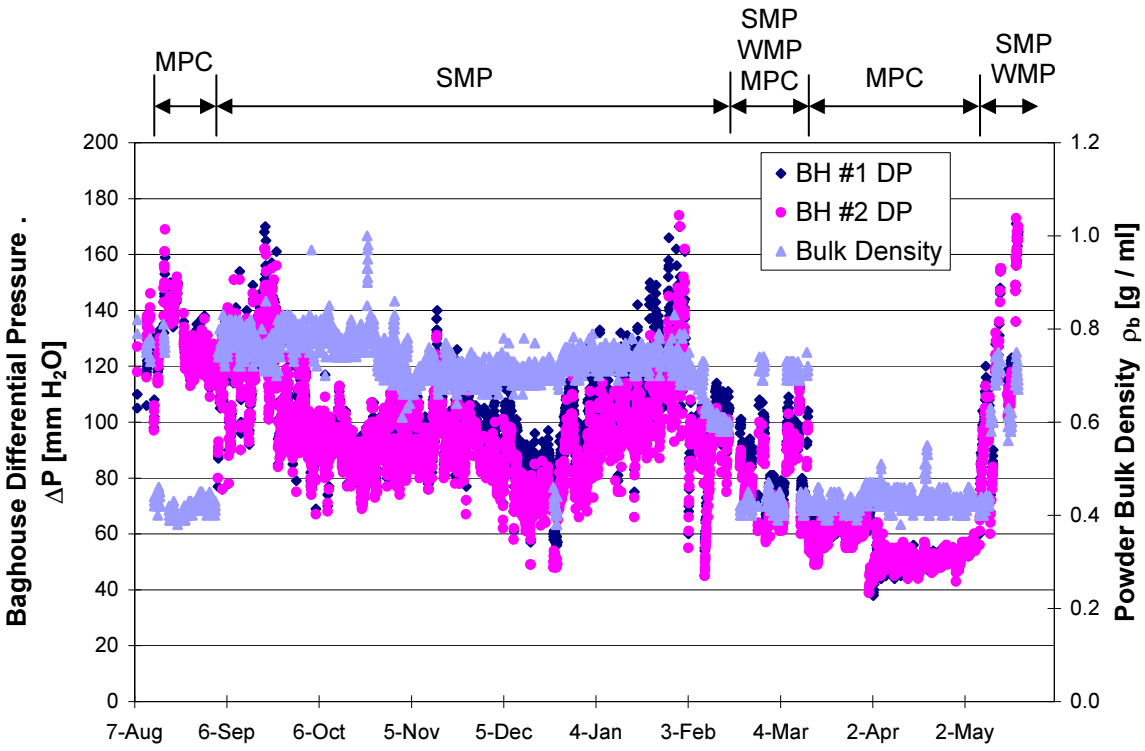

Figure 3-3: Clandeboye Dryer 2 baghouse differential pressures & powder bulk density during the 2003/2004 season

The periods of constant product production in Figure 3-3, January and April, highlight the impact of bag age on the baghouse differential pressure. During these periods the differential pressure increased even though the concentrate flow, total solids and powder bulk density are constant. It is likely that the increase was due to the bag permeability reducing as more particles became trapped in the pores of the bag, thus increasing the differential pressure.

In an attempt to see if changes in the concentrate flow and total solids had an impact on the baghouse differential pressure, Baghouse #1 differential pressure data was plotted against the concentrate flow in different concentrate total solids ranges for each month of the 2003/2004 season. Figure 3-4, which was typical of the 10 plots produced, shows that due to the scatter in the differential pressure, there is no apparent influence of either the concentrate flow or the concentrate total solids on the differential pressure.

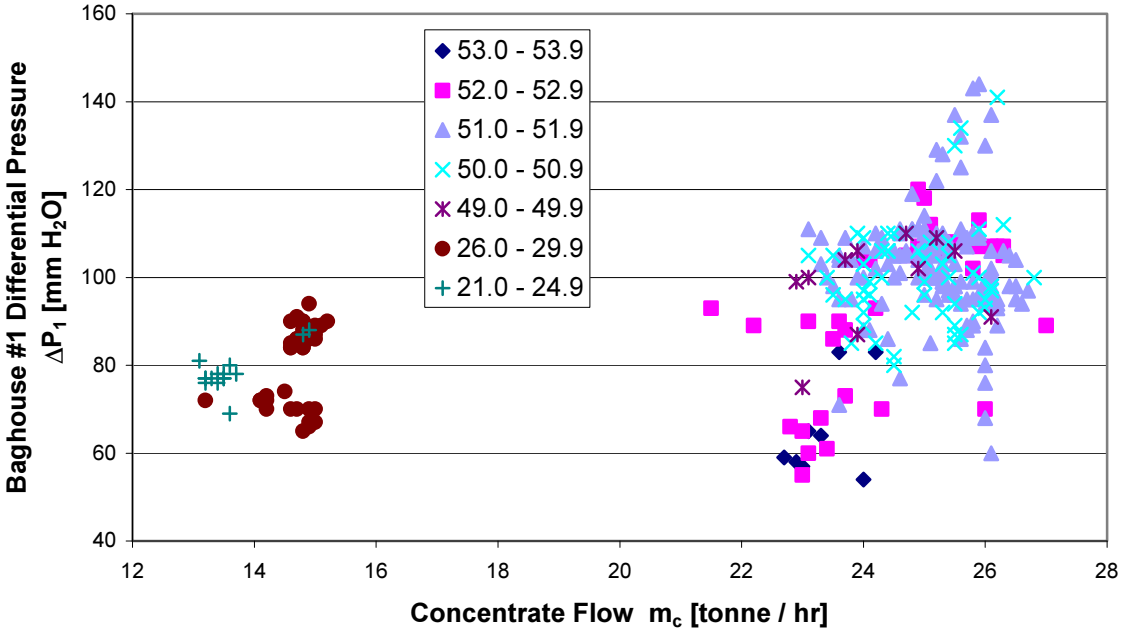

Figure 3-4: Clandeboye Dryer 2 Baghouse #1 differential pressure & concentrate flow for a range of concentrate total solids contents during February 2004

3.5.2.1. Differential Pressure Bias

Figures 3-2 and 3-3 reveal that from December to March there was a clear constant difference in the differential pressure in the two baghouses. This discrepancy was to be expected as it had been evident since the plant began operation, and was also observed in the identical Fonterra Edendale dryers 2 and 3. This suggests that the discrepancy was not due to any measurement error or physical difference between the baghouses as they were the same size, housed the same number of filter bags and had identical inlet ducts on opposite sides of the drying chamber.

The baghouse differential pressure models presented in Chapter Two indicate the pressure drop is a function of the bag constant, the filtration velocity, a cake constant, the concentration of fines and the pulse cleaning frequency. Therefore, one or a number of these parameters must be different between the two baghouses for a constant difference in differential pressure to be observed.

As the bags in the baghouses are always the same age and produced by the same manufacturer, it is unlikely that the bag constant, k_b, is different. It is also highly unlikely that some bags in BH #2 were not installed correctly. Incorrectly installed bags would create gaps between the top of the bag and the cell plate where the air would have a lower flow resistance, thus creating a lower differential pressure. This would also lead to higher stack emissions.

Similarly, a lower differential pressure in one baghouse could be expected if the old bags consistently had more holes than those of the other baghouse. However, this was not the case as the discrepancy was still obvious in February after new bags had been installed.

Properties of the filter cake and the amount of powder present in each baghouse may have differed. For example, one baghouse may have had a thicker filter cake, a more adhesive cake, or a smaller particle size and therefore a less permeable cake. However, Figure 3-5 indicates that, after the September bag change when the plant was running on air, the differential pressure in BH #1 was an average 12 % higher than that in BH #2, hence, the bias was present. Therefore, assuming the bags are identical and they have been installed correctly, the bias cannot be due to powder properties but to an airflow bias; more air must have flowed through BH #1 than BH #2.

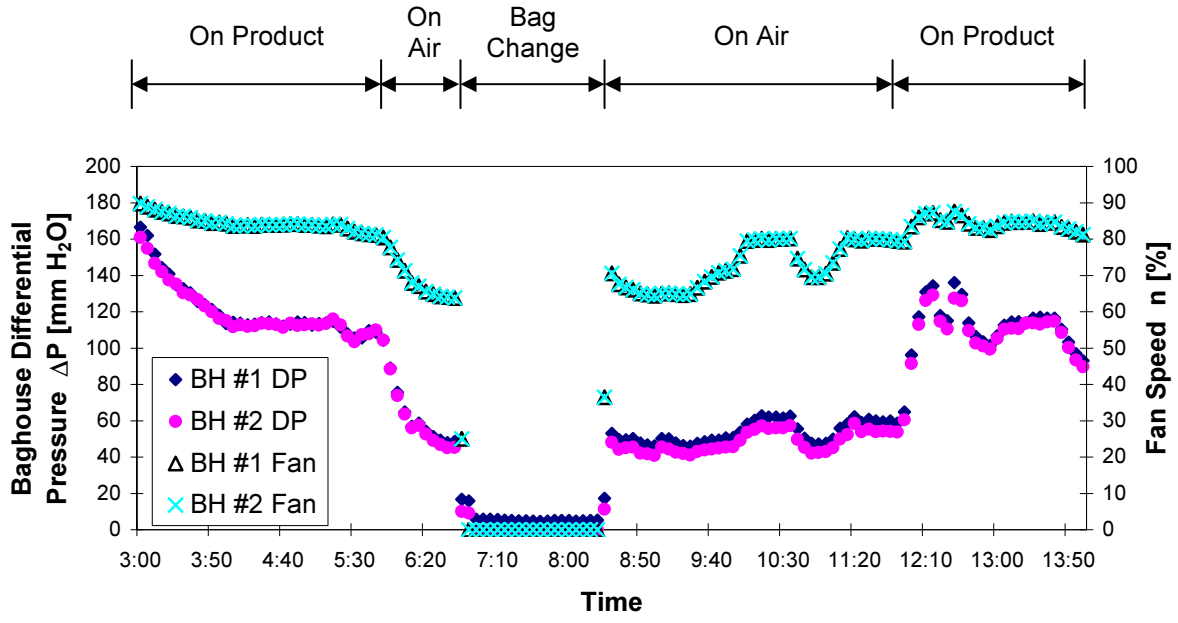

Figure 3-5: Clandeboye Dryer 2 baghouse differential pressure and fan speeds before and after the September 22 2003 bag change

An airflow bias could have been created if the extractor fans drawing air through each baghouse were not running at the same speed. However, Figure 3-5 shows that at the same fan speed, the bias was still obvious. Figure 3-6 also indicates that during the periods when the bias was most evident, the baghouse extractor fan speeds were identical. It is unlikely that the fans were operating differently at identical fan speeds and therefore, they were not the cause of the airflow bias.

Such a bias could be created by a pressure difference across the main drying air inlet. This would cause the flow to tend to the low pressure side and thus not flow evenly down into the chamber but toward one outlet. Such a pressure difference across the main air inlet could be a result of the approach angle of the main inlet air pipe work; the feed pipe approaches the dryer axis running through the centreline of the baghouse inlets at an angle of approximately 34^{o}. This could be an area of future research to determine if this hypothesis is correct.

The periods when a large difference in fan speeds was observed ─ February and during March ─ indicate that plant operators were nursing one of the baghouses. Nursing a baghouse involves reducing the fan speed in an attempt to maintain the differential pressure below 180 mm H_2O. At this differential pressure, the dryer automatically switches to running on water. Operators nurse a baghouse when there is insufficient downtime to CIP or replace the filter bags, so try to run as long as they can before having to come off product. The plant will usually come off product for bag replacement when the differential pressure in the second baghouse nears or reaches 180 mm H_2O.

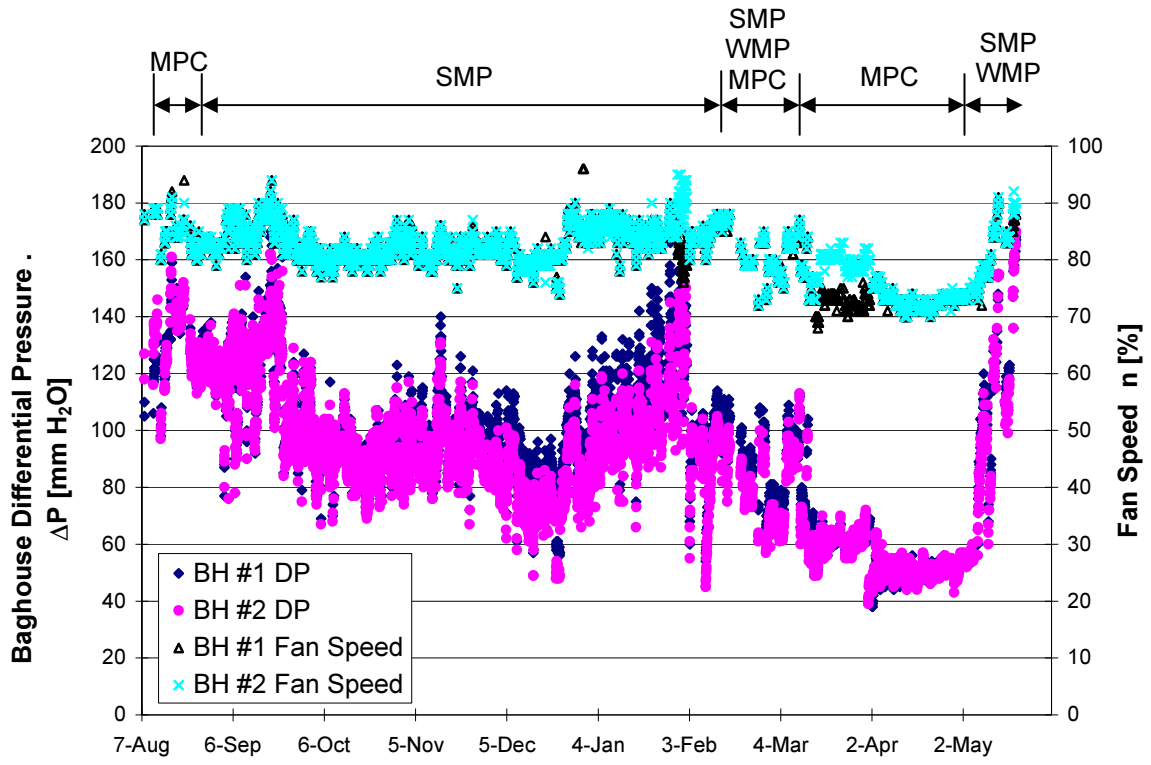

Figure 3-6: Clandeboye Dryer 2 baghouse differential pressures & extractor fan speeds during the 2003/2004 season

The pressure in the fines return lines at the bottom of the baghouses is often used as an indicator of how much powder is entering the baghouses. As Figure 3-7 below shows, there is a significant difference between the fines return lines pressures: those of baghouse #1 were consistently higher than those of baghouse #2. This difference has traditionally been used as evidence to suggest a powder bias, thus creating the difference in baghouse differential pressures observed. This suggestion is not accurate because the two fines return lines are not identical. The two sets of fines return lines are arranged such that they flow from the bottom of their respective baghouses to a point closer to BH #1 on the eastern side of the fourth floor of the CD2 building. From this point, both sets of lines then flow down to the fines return destination, usually the end of the last vibrating fluid bed. Therefore, the BH #2 fines return line is approximately 12 m longer than the BH #1 fines return line.

Despite this difference in length between the two fines return lines, this fines return pressure data can still be used to show that there are significant differences in fines return line pressures between the products as shown in Table 3-1 below.

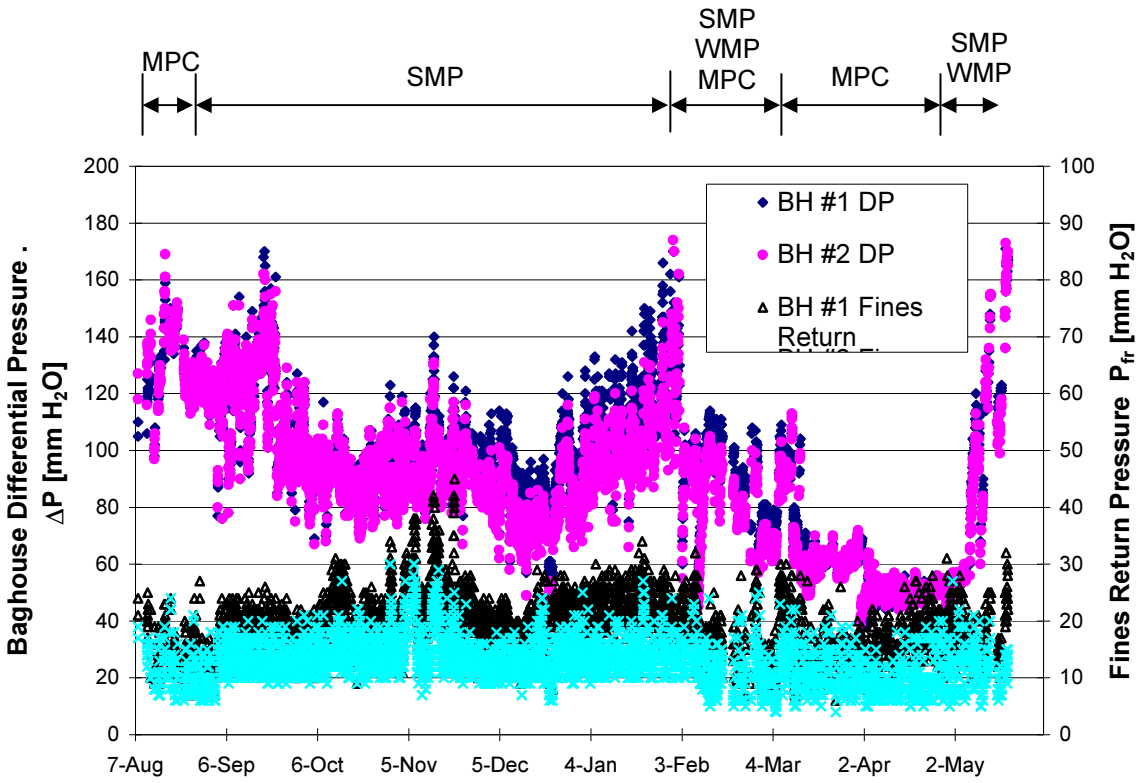

Figure 3-7: Clandeboye Dryer 2 baghouse differential pressures & fines return pressures during the 2003/2004 season

3.5.3. Airflow Instrumentation

An instrument was sourced that was to be connected to the plant PLC to continually monitor the airflow through the two baghouses. If this data could be collected it would prove very useful for plant operators who could use it to balance the air flows and help extend the lifetime of old bags by intentionally creating a bias.

A Torbar 402 averaging Pitot tube (Torbar Flowmeters Ltd, UK) was obtained from Instrumatics Ltd, Auckland. Averaging Pitot tubes produce highly repeatable measurements, are as accurate as other types of insertion flow meters, have a low cost, and are easily installed; moreover, because the flow around the probe produces turbulence, blockage of the ports is virtually eliminated and there is almost no need for purging (Ginesi & Grebe, 1987). Further, this type of flow meter is less sensitive to velocity flow distortions (Ginesi & Grebe, 1987) and therefore the requirements for straight run lengths of pipe are less stringent compared to most other devices (Good & Cisar, 2004).

This model and type of instrument was also chosen because it was consistent with the make and model of other air flow instruments in the CD2 plant. Also, there was no need to calibrate and, with a New Zealand supplier, better after sales support would be available.

One instrument was installed near the base of each of the main exhaust air stacks (Figure 3-8). There were difficulties with this location because it was only one pipe diameter downstream of the angled inlet to the stack, that is, it was well inside the recommended minimum of seven and a half pipe diameters (Croom, 1995). Consequently the accuracy of the instrument was reduced by placing it in this location.

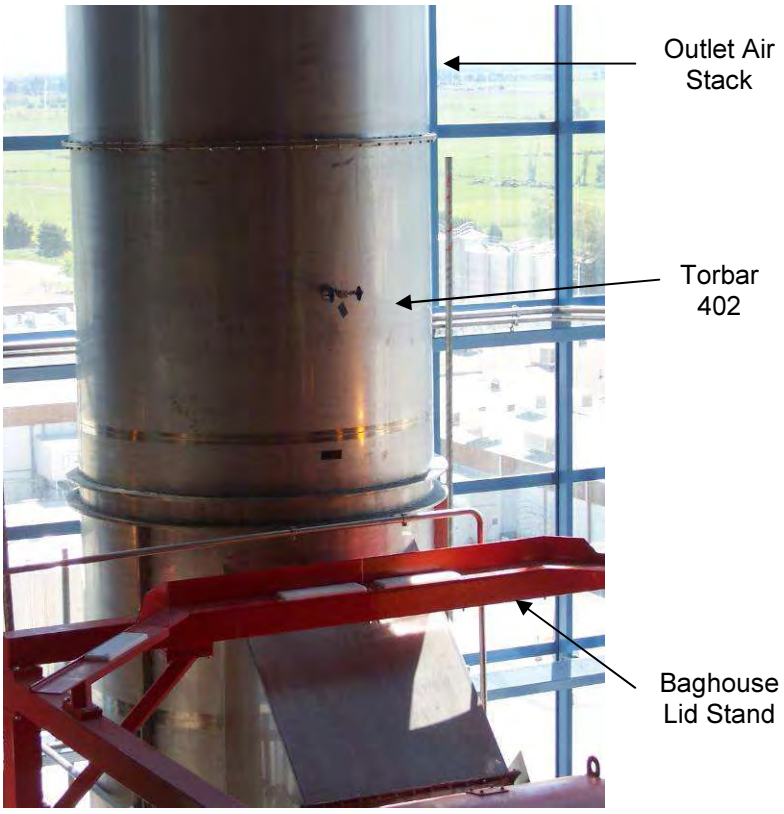

Figure 3-8: Base of Clandeboye Dryer 2 Baghouse #2 outlet air stack showing the installed Torbar 402 and the baghouse lid stand

It was later discovered that this position was not desirable when the baghouse lids were lifted and moved onto their stands next to the outlet stack; the clearance between the end of the averaging Pitot tube and the edge of the baghouse lid en route to their stands is only a few millimetres. So the likelihood of the lids banging into the end of the averaging Pitot tube is very high, and therefore so is the likelihood of damage.

Results from the six traverses of the outlet stacks taken between October and December 2004 are given in Figure 3-9. Five of the six results in Figure 3-9 show a higher air flow through BH #2 than BH #1, the opposite to the perceived direction of the air flow bias. However, in four of these five cases, both baghouse values agree within experimental uncertainty, so no bias can be suggested from these results.

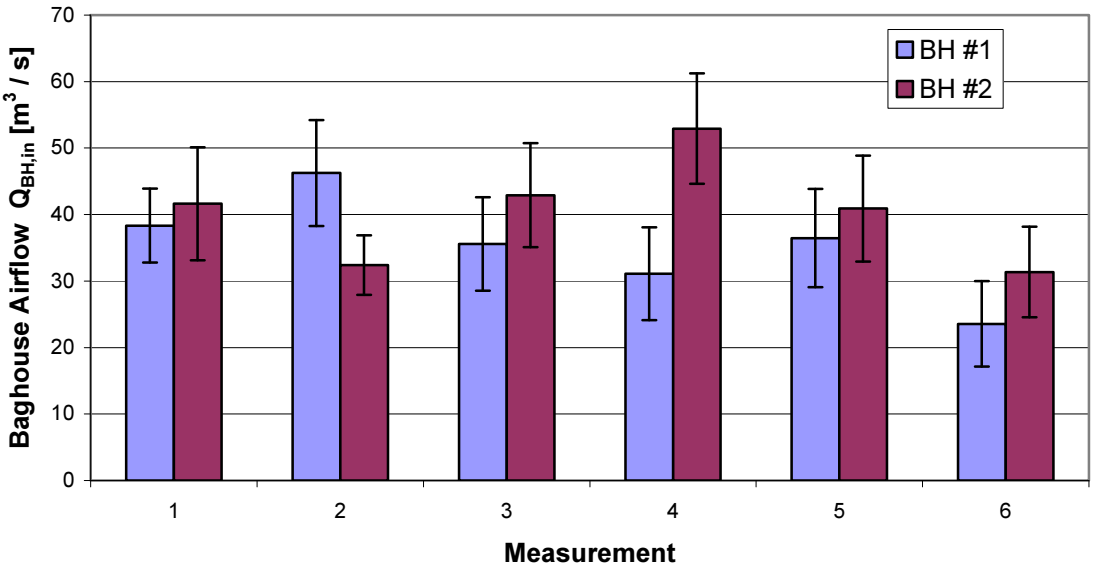

Figure 3-9: Clandeboye Dryer 2 baghouse stack volumetric flows determined from Pitot traverse of the outlet air stacks

The large error, up to 27 % in some cases, is due to the large fluctuation in the differential pressure measured with the manometer. Such large fluctuations could be expected because the measurements were taken so close to the air entry at the base of the stack.

Figure 3-10 shows that, unlike the Pitot traverse results, the majority of the measurements from the installed Torbar 402 averaging Pitot tube show a greater airflow through BH #1 than BH #2. This was the expected trend when considering the discrepancy in baghouse differential pressures. However, again, each pair of values and the majority of all readings agree within experimental uncertainty. The large uncertainty of up to 51 % was due to the fluctuating differential pressure, which, as described above, could be expected because of the location of the instrument.

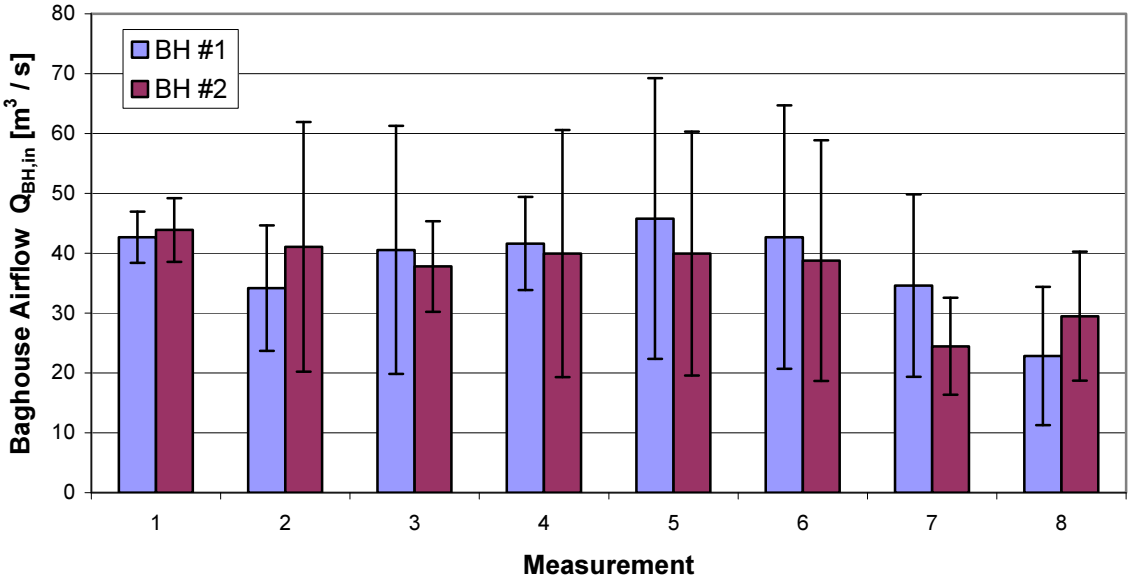

Figure 3-10: Clandeboye Dryer 2 baghouse stack volumetric flows determined from Torbar 402 averaging Pitot tube readings

The original plan was for the differential pressure obtained from the averaging Pitot tube to be measured with installed pressure transmitters that gave 4 – 20 mA outputs. This signal was to be connected to the plant PLC where the flow would be calculated and then displayed on the operators' screens (Appendix B1 provides the information required for this calculation). Despite the fact that quotes were obtained for this instrumentation, electrical and automation support, and a Fonterra CAPEX application written (Appendix B2), the CD2 powder plant staff and Heat Transfer and Drying team technologists deemed this not to be a priority.

Without the connection to the PLC, the averaging Pitot tubes currently sit unused. Therefore, the operators are deprived of the benefits of continually seeing this information. An advantage of having this information in the PLC would be the ability to dampen out the fluctuations in the differential pressure mentioned above, thus giving a more accurate flow rate. If this connection were to go ahead, it is suggested that the instruments be moved from their current location to higher up the stack. This would remove the chance of the end of the averaging Pitot tubes being damaged when the baghouse lids are placed on their stands. Such a move would also increase the accuracy of the readings as the instruments would be located further from the flow disturbance at the base of the stack and would measure a more uniform flow pattern inside the stack.

3.5.4. Individual Product Groups

All parameters presented in the thought flow diagram that are recorded in the operator log books were plotted to view the sensitivity of the baghouse differential pressure to these parameters. Because of the large amount of data, these plots were made on a product group basis. SMP and MPC data sets were broken down further into daily runs and monthly data.

3.5.4.1. Skim Milk Powder Trends

The SMP data were broken into five groups based on the type of heat treatment applied to the concentrate; high, medium – high, medium, regular or low heat. The data were also observed over the course of nine individual runs, each run chosen randomly from each month of the season. Where correlations were found in the plots below, these were checked for all data sets.

Figure 3-11 shows that a relationship exists between the baghouse differential pressure and the extractor fan speed; an increase in the fan speed creates an increase in the baghouse differential pressure. This trend was common for all SMP data observed.

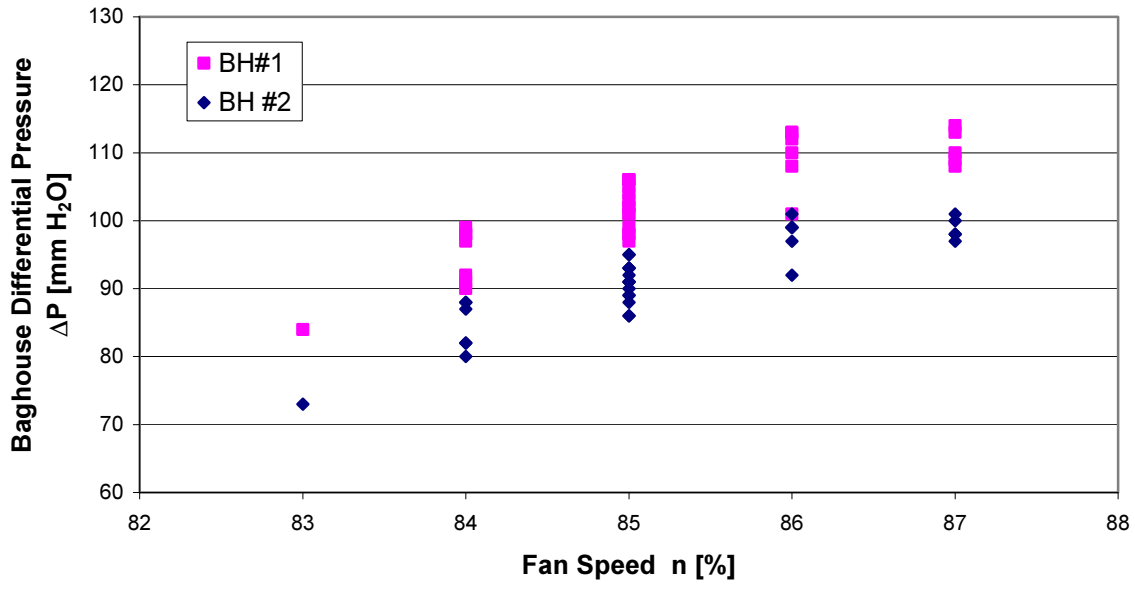

Figure 3-11: Baghouse differential pressures vs. extractor fan speed for skim milk powder produced in Clandeboye Dryer 2 on the 2nd January 2004

A second clear correlation from the SMP data is shown in Figure 3-12; as the amount of fat in the product increases, the baghouse differential pressure decreases. This finding was expected as previous work from CD2 had indicated the correlation existed. All data sets observed in this investigation with sufficient variation in powder fat content showed this to be the case.

Figure 3-12 shows that a change of 0.15 % in the powder fat content creates a 13 % change in the baghouse differential pressure. This finding has significant implications for the operation of milk powder plants with washable baghouses when producing SMP. Only small changes in the powder fat content can create large reductions in the baghouse differential pressure, thus avoiding the issues of operating a baghouse at high differential pressure mentioned in Section 3.1.

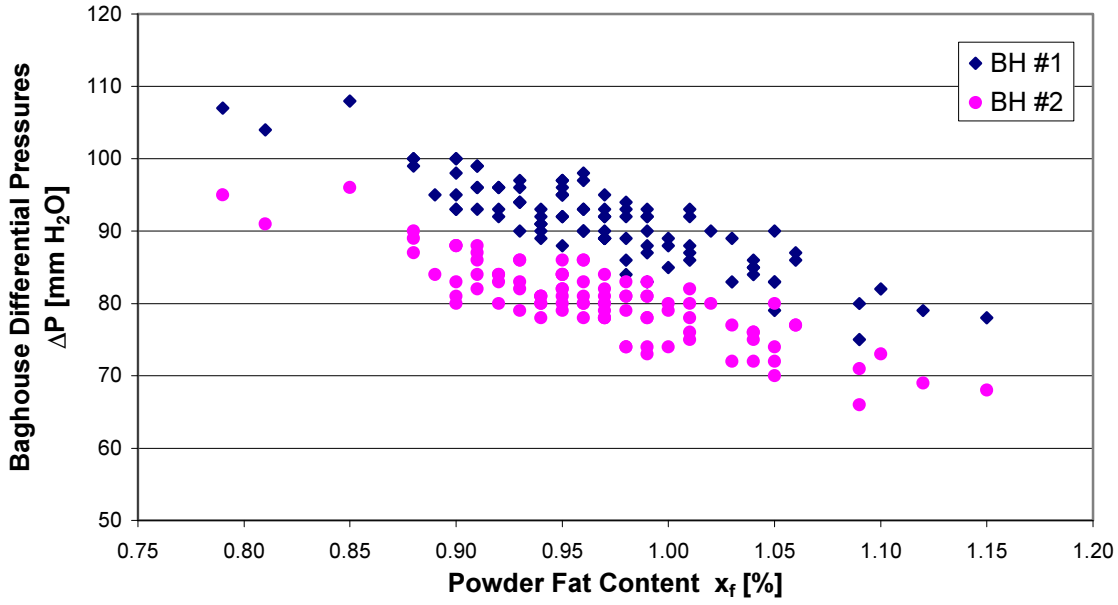

Figure 3-12: Baghouse differential pressures vs. powder fat content for high heat skim milk powder produced in Clandeboye Dryer 2 during the 2003/2004 season

An interesting point to note, however, is that although the powder fat content impacts on the baghouse differential pressure, no trend was observed between the baghouse differential pressure and the flow of standardising fat. This could be due to the mixing that occurs in the standardised milk silos, the tiny ratio of standardising fat flows to the raw milk flows, or the fluctuation in raw milk flows also cause fluctuations in standardising milk flows. None the less, it is clear that the final product fat content makes the difference.

Skim milk powder is the stickiest of the three dairy powders produced in CD2 because of its high lactose content. Therefore it is surprising that there is no apparent correlation between the baghouse differential pressure and the operating point relative to the available SMP sticky point, as it is believed that once operation is above the sticky point, the baghouse differential pressure will increase. Figure 3-13 shows that even for operation beyond the available sticky point there is no change in the baghouse differential pressure.

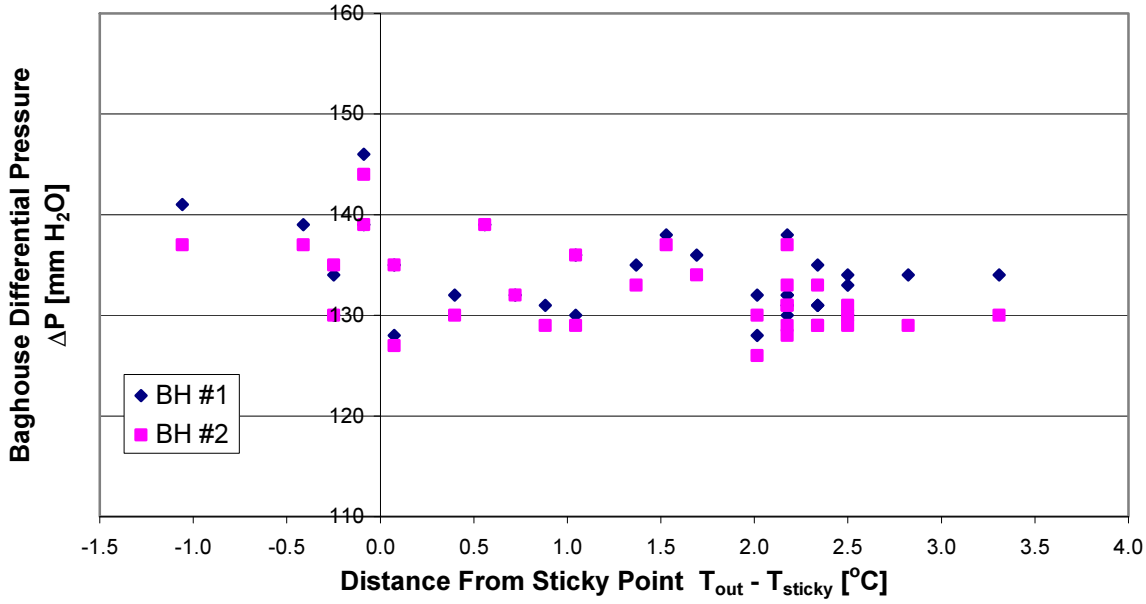

Figure 3-13: Baghouse differential pressures vs. distance from sticky point for skim milk powder produced in Clandeboye Dryer 2 on the 15th September 2003

Figure 3-14 reveals there is no apparent trend between the baghouse differential pressure and the outlet air flow rate; despite the variation of approximately 7 % in the outlet air flow, the baghouse differential pressure is relatively constant.

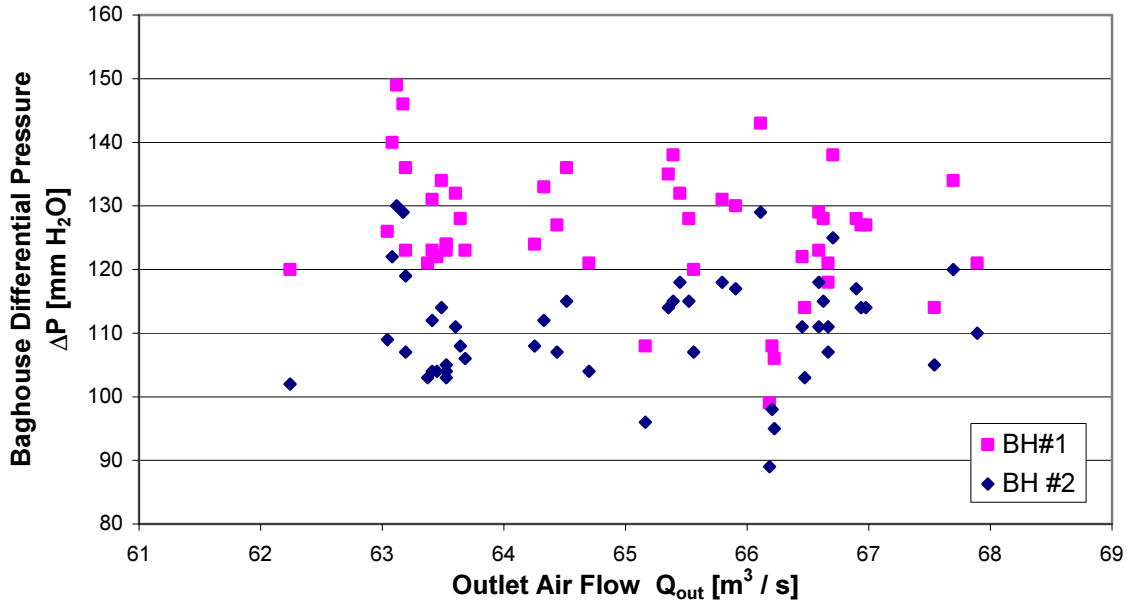

Figure 3-14: Baghouse differential pressures vs. outlet air flow for skim milk powder produced in Clandeboye Dryer 2 on the 22nd January 2004

For all data sets, considerable variation in the feed line pressure was observed. However, as Figure 3-15 illustrates, that had no impact on the baghouse differential pressure.

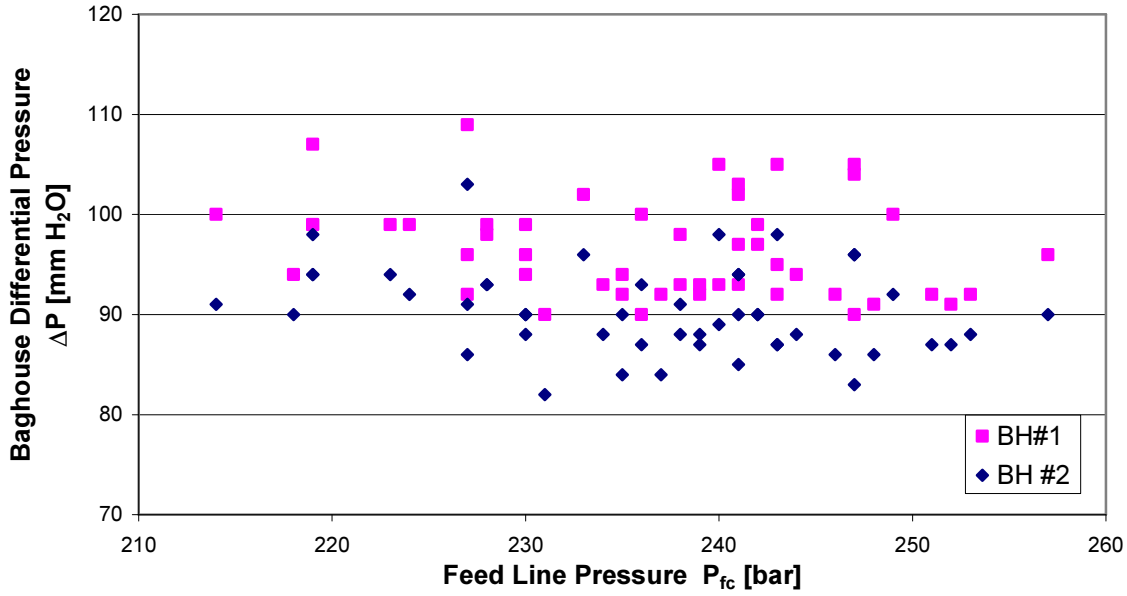

Figure 3-15: Baghouse differential pressures vs. feed line pressure for skim milk powder produced in Clandeboye Dryer 2 on the 5th March 2004

The remaining variables recorded by plant operators shown in the thought flow diagram (flow of standardising fat, flow of standardising lactose, concentrate flow and temperature, concentrate total solids, outlet air temperature, outlet air relative humidity, fines return line pressures, powder moisture content and bulk density) did not show any correlation with the baghouse differential pressure.

3.5.4.2. Whole Milk Powder Trends

Eleven runs of WMP were conducted during the 2003/2004 season, eight runs in February and three in May. Because this generated only 190 data points, single plots using this entire data set were produced rather than daily and monthly plots required for SMP and MPC.

Like SMP, a relationship between baghouse differential pressure and extractor fan speeds exists for WMP. Figure 3-16 shows that an increase in fan speed results in an increase in baghouse differential pressure.

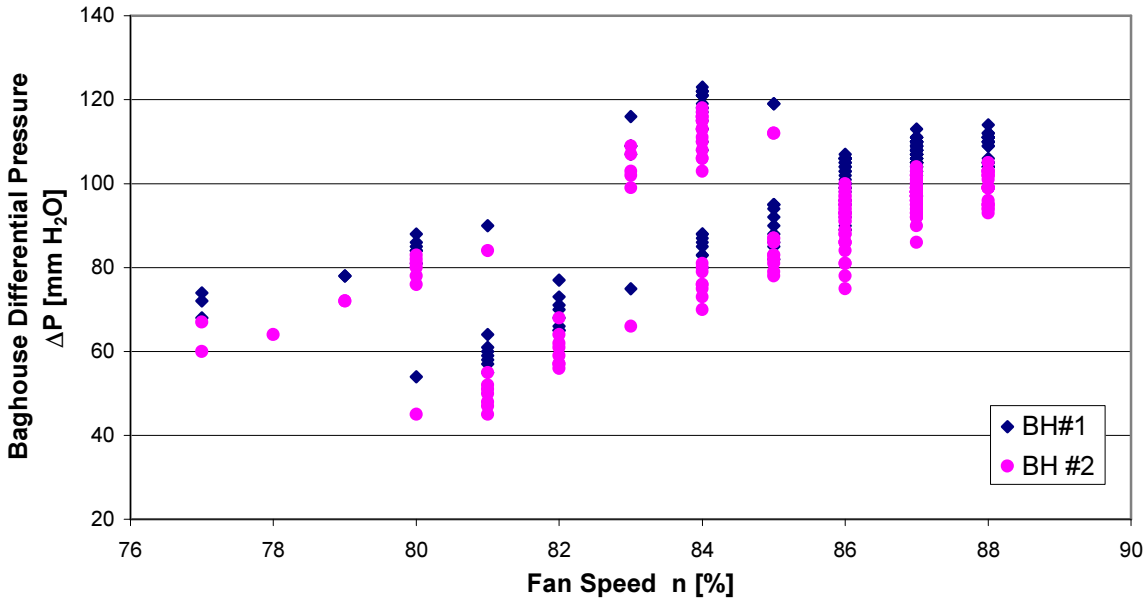

Figure 3-16: Baghouse differential pressures vs. extractor fan speed for whole milk powder operation in Clandeboye Dryer 2 during the 2003/2004 season

For WMP, even though a range of outlet air flows were used in the 11 production runs, no apparent influence on the baghouse differential pressure is observed (Figure 3-17).

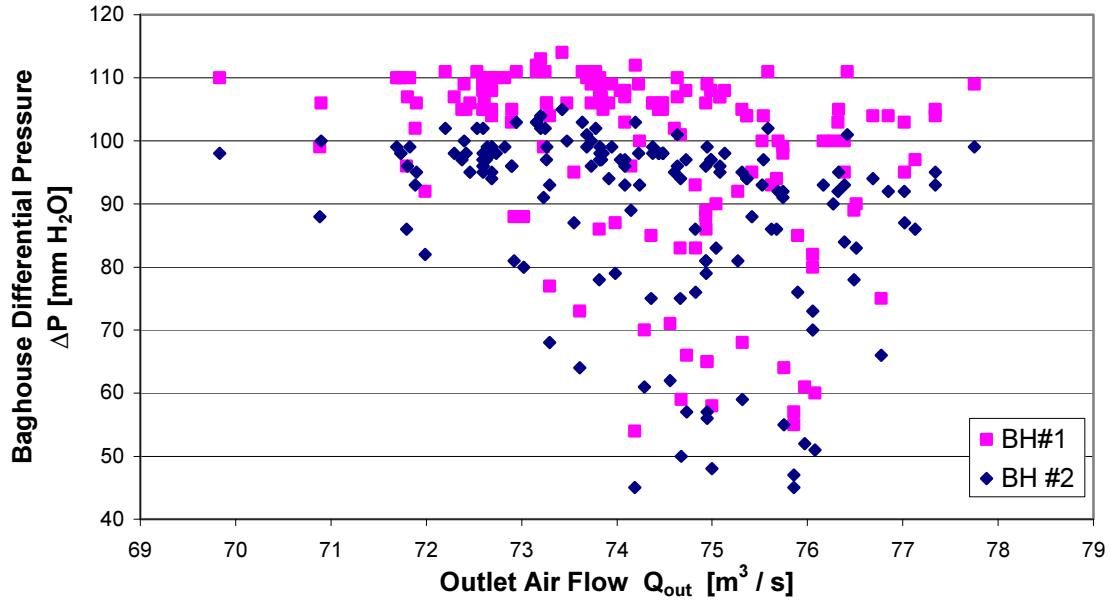

Figure 3-17: Baghouse differential pressures vs. dryer outlet air flow for whole milk powder operation in Clandeboye Dryer 2 during the 2003/2004 season

Figure 3-18 shows that, although there is a 2 tonne / hr range in the concentrate flows, there is no apparent correlation with the baghouse differential pressure.

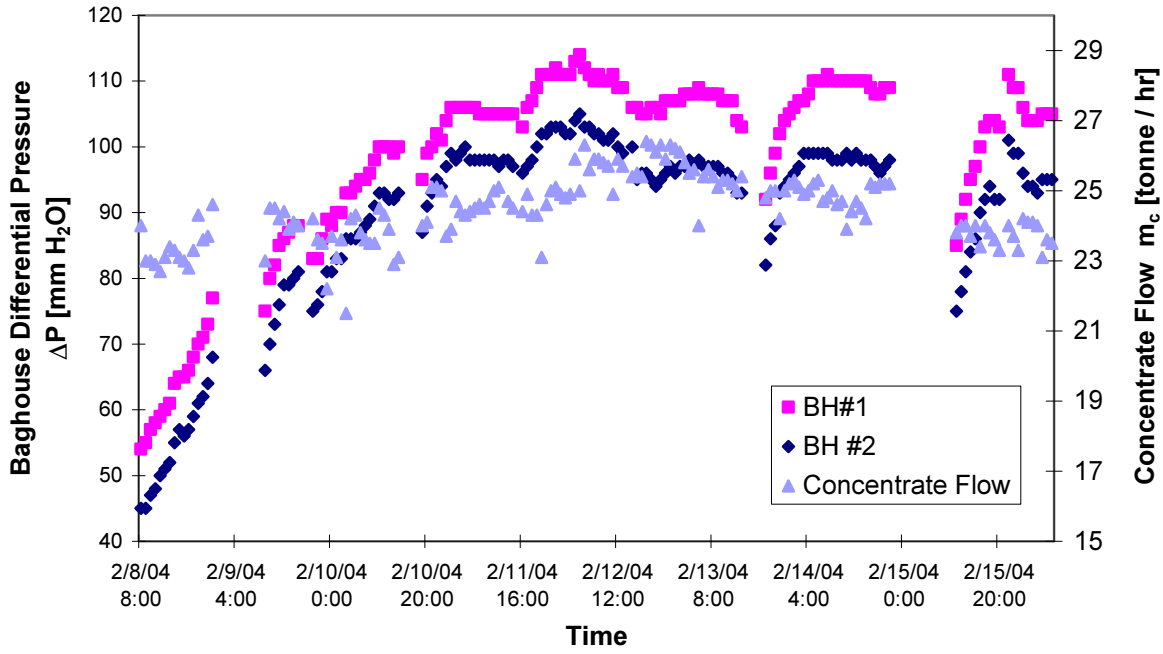

Figure 3-18: Baghouse differential pressures & concentrate flow vs. time for whole milk powder operation in Clandeboye Dryer 2 during the 2003/2004 season

Unlike SMP, as Figure 3-19 shows, small changes in the amount of fat in WMP have no apparent effect on the baghouse differential pressure.

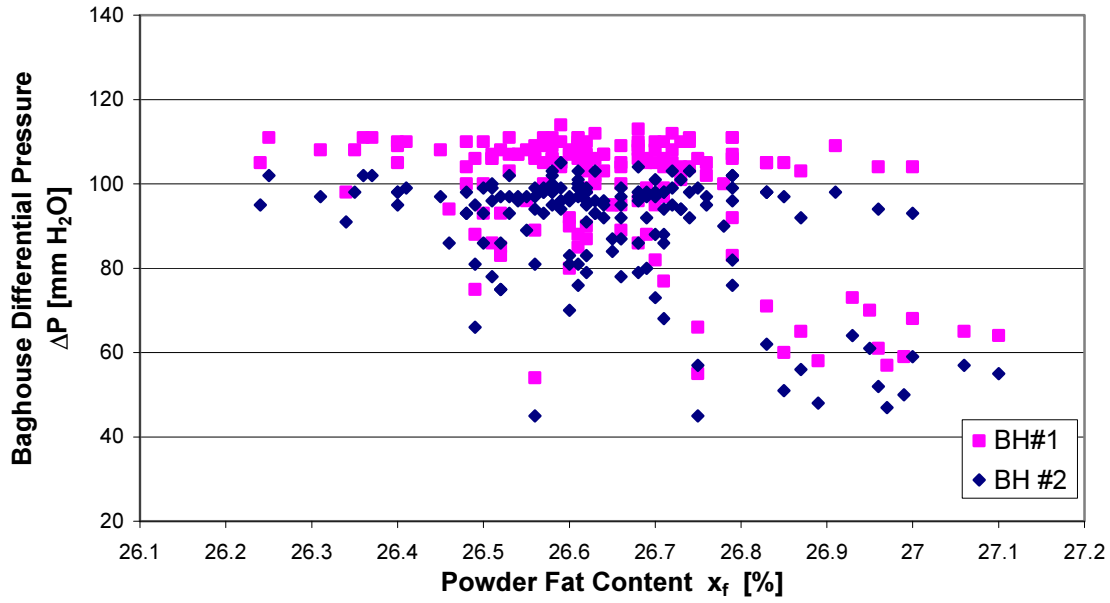

Figure 3-19: Baghouse differential pressures vs. powder fat content for whole milk powder operation in Clandeboye Dryer 2 during the 2003/2004 season

Even though some data points sit on the cusp of the available sticky point, Figure 3-20 shows that there is no trend for baghouse differential pressure as operation approaches the sticky point. Again, this is surprising as it was believed that once operation is above the sticky point, the baghouse differential pressure will increase.

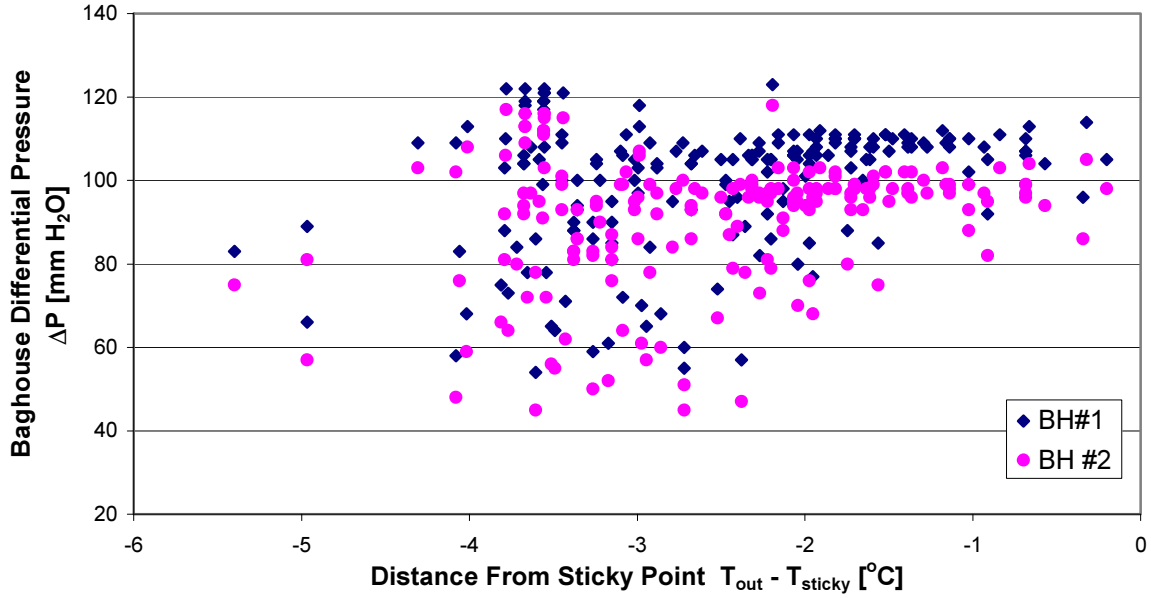

Figure 3-20: Baghouse differential pressures vs. distance from sticky point for whole milk powder operation in Clandeboye Dryer 2 during the 2003/2004 season

All of the other recorded parameters in the thought flow diagram not mentioned here for WMP production (flow of standardising fat, flow of standardising lactose, concentrate temperature, concentrate total solids, feed line pressure, outlet air temperature, outlet air relative humidity, fines return line pressures, powder moisture content and bulk density) showed no apparent correlation with baghouse differential pressure.

3.5.4.3. Milk Protein Concentrate Trends

The MPC data were broken into monthly data and eight individual runs chosen randomly throughout the season. Again, where correlations were found from the plots below, these were checked for all data sets.

As was observed for SMP and WMP, a relationship is shown in Figure 3-21 between the baghouse differential pressure and the extractor fan speed for MPC; an increase in the fan speed creates an increase in the baghouse differential pressure.

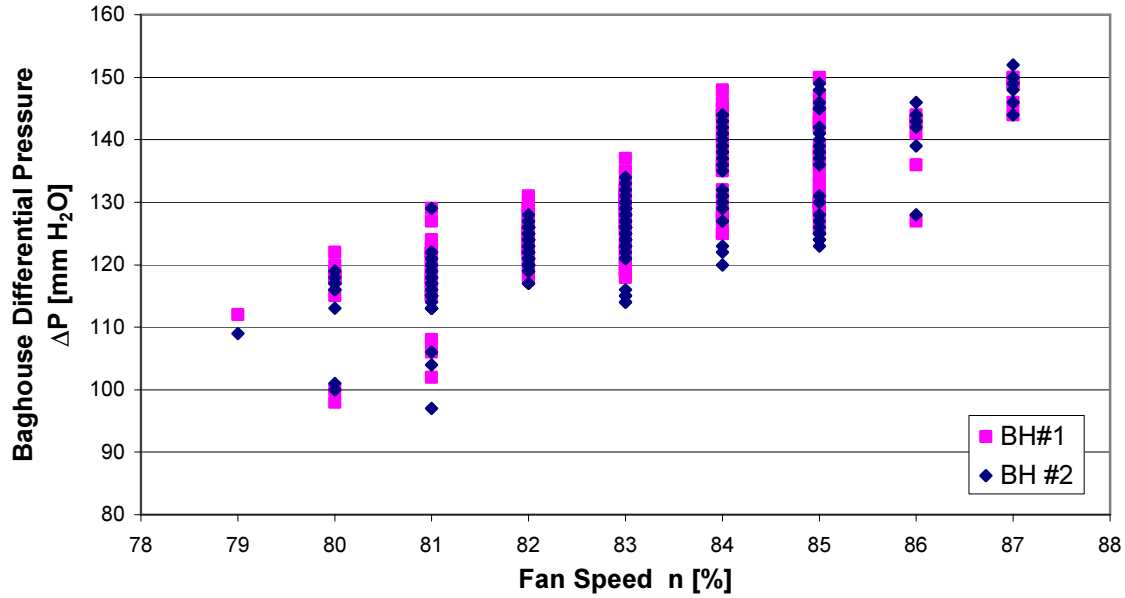

Figure 3-21: Baghouse differential pressures vs. extractor fan speed for milk protein concentrate 70 and 80 powder produced in Clandeboye Dryer 2 during August 2003

Figure 3-22 below indicates that changes in the outlet air flow rate had no immediate influence on the baghouse differential pressure. This observation agrees with the findings from the SMP and WMP data sets.

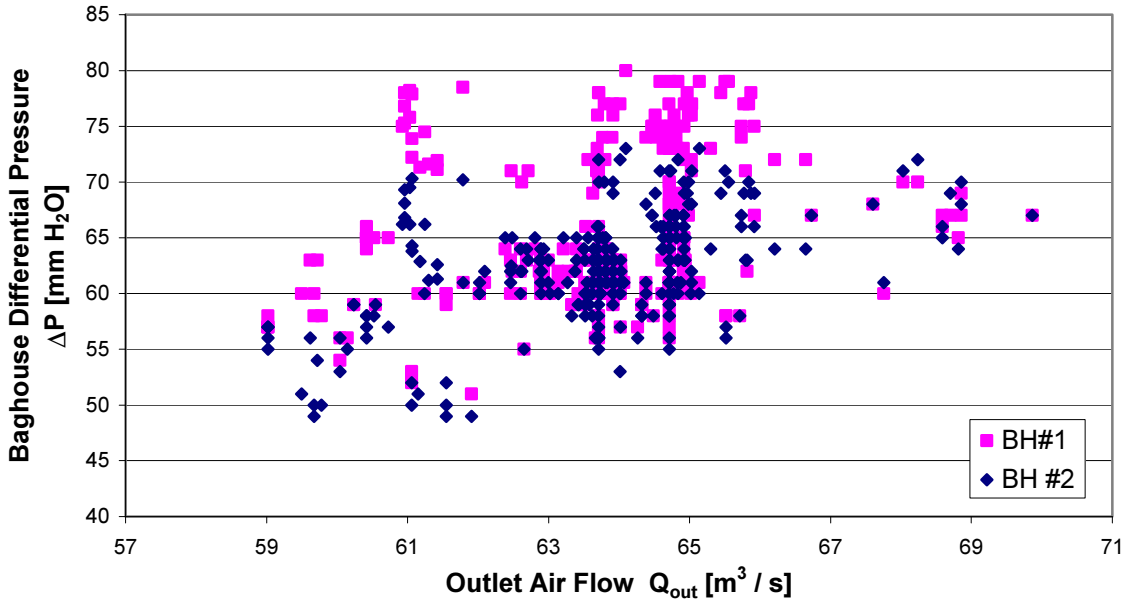

Figure 3-22: Baghouse differential pressures vs. outlet air flow for milk protein concentrate 70 and 80 powder produced in Clandeboye Dryer 2 during March 2004

Unlike SMP, but as for WMP, there was no correlation between the baghouse differential pressure and the powder fat content for MPC. Figure 3-23 shows data for MPC 70 and 80 production from May 2004 when a change in powder fat had no influence on the baghouse differential pressure.

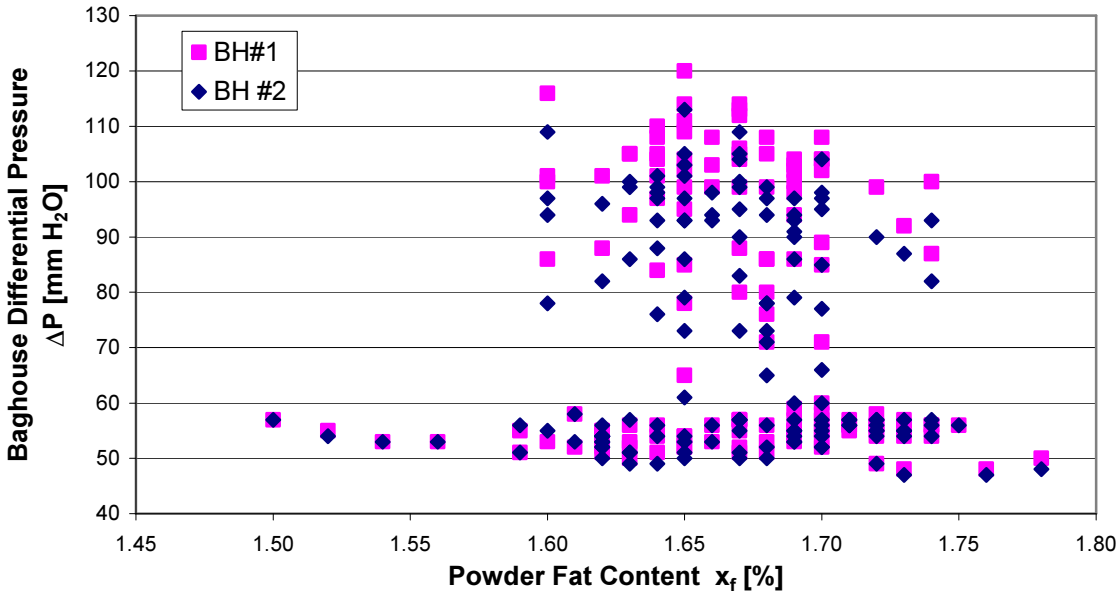

Figure 3-23: Baghouse differential pressures vs. powder fat content for milk protein concentrate 70 and 80 powder produced in Clandeboye Dryer 2 during May 2004

Figure 3-24 below is the sticky point plot for all MPC 70 and 80 produced in CD2 during the 2003/2004 season. The trend line drawn is the sticky point for MPC 70, but the MPC 80 trend line is not included. If operating points are well below the MPC 70 sticky point, as shown, then they will also be below the MPC 80 sticky point; MPC 80 has a lower lactose content than MPC 70, hence this product becomes stickier at combinations of higher air temperatures and humidities.

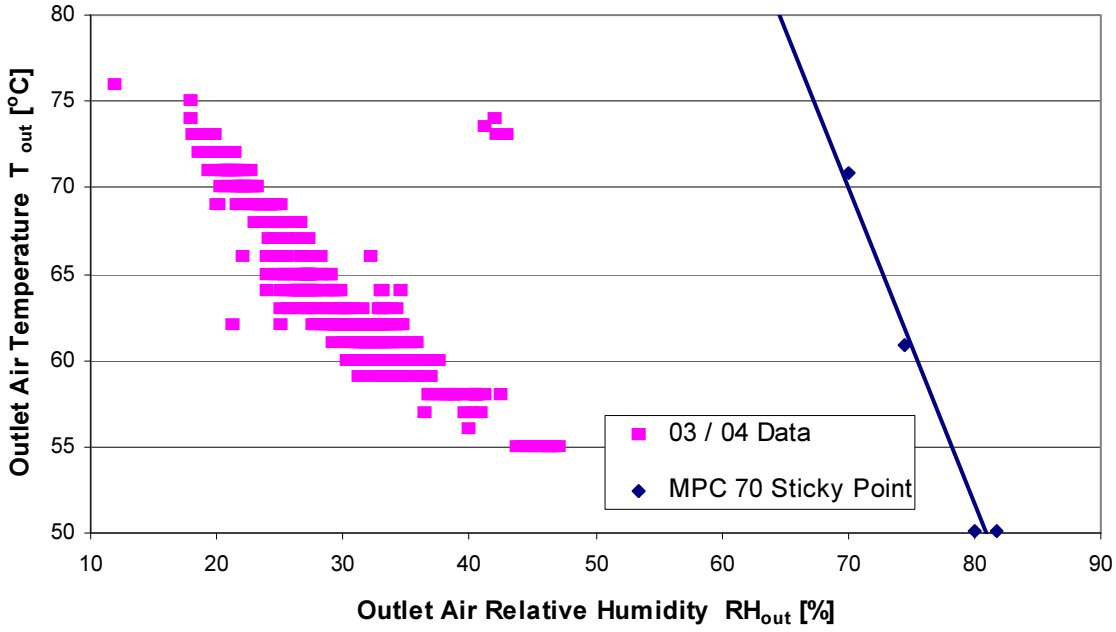

Figure 3-24: Comparison of milk protein concentrate 70 and 80 operating points and milk protein concentrate 70 sticky point for production in Clandeboye Dryer 2 during the 2003/2004 season

Figures 3-2 and 3-3 showed that the baghouse differential pressure was lower for the low total solids concentrate product, MPC. However, Figure 3-25 below shows that, despite the variation in concentrate total solids, there is no apparent change in baghouse differential pressure with concentrate total solids within the MPC product group.

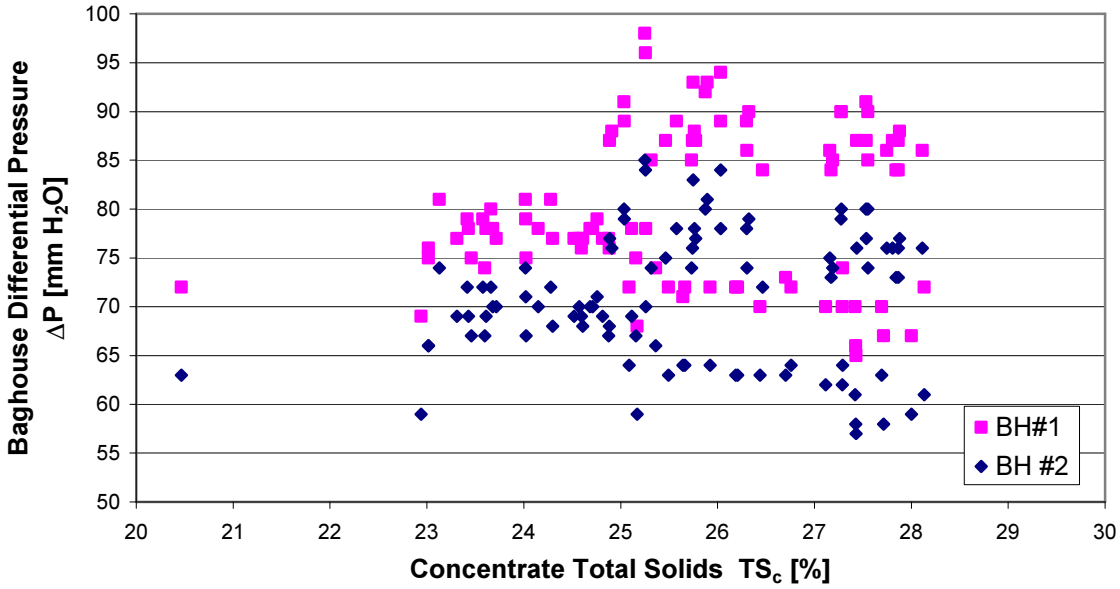

Figure 3-25: Baghouse differential pressures vs. concentrate total solids for milk protein concentrate 70 and 80 powder produced in Clandeboye Dryer 2 during February 2004

Again, the remaining recorded parameters in the thought flow diagram not mentioned here for MPC production (flow of standardising fat, flow of standardising lactose, concentrate flow and temperature, feed line pressure, outlet air temperature, outlet air relative humidity, fines return line pressures, powder moisture content and bulk density) showed no apparent correlation with baghouse differential pressure.

3.5.4.4. Summary of Trends

The analysis of SMP, WMP and MPC operating points above indicates that there are two parameters that have a strong correlation with baghouse differential pressure. Firstly, for all product groups, an increase in fan speed causes an increase in baghouse differential pressure. This is a result of the increase in fan speed reducing the fan suction side pressure, which is the baghouse clean air side pressure. Thus, because the clean air side pressure has been reduced, the pressure drop across the baghouse, the difference between the dirty and clean side pressures, increases.

A change in fan speed will also cause a change in flow through the fan, as Equation 3-2 shows. However, Equation 3-1 shows that a change in fan speed will cause a greater change

in the pressure drop across the fan which in this case, is a reduction in the suction side pressure. For this reason, it is likely that an increase in baghouse differential pressure resulting from an increase in fan speed is due more to the reduction in clean side pressure than to an increased flow.

It should also be noted that fan speeds are changed by operators in response to high baghouse differential pressures. When the dirty side pressure in the baghouse increases, be it due to an increase in fines loadings, more residual powder remaining on the filter bags or to the age of the bags, the fan speed has to be increased to maintain a constant drying chamber vacuum, which is a target for operators. Therefore, some of this data could be more sensibly plotted as fan speed versus baghouse differential pressure, rather than the baghouse differential pressure versus fan speed as plotted here.

The second parameter influencing the baghouse differential pressure for all product groups is the age of the filter bags. As the filter bags age, more and more powder is retained inside the filter bag that is not removed with pulse cleaning and thus, increases the differential pressure. This finding agrees with the work of Machen (2001) who also showed that the bag age has a large impact on the differential pressure.

For SMP operation, a clear trend is observed between the baghouse differential pressure and the powder fat content; as the fat content of the powder increases, the baghouse differential pressure reduces. A change in powder fat content for WMP and MPC however showed no trend. Thus, this phenomenon only occurs for SMP. The reason for these findings is explored in Chapter Seven.

One of two surprising findings was that changes in the outlet air flow had no apparent influence on the baghouse differential pressure in the operating range. This finding cannot be attributed to insufficient variation in the independent variable as a 9 % variation in outlet air flow in SMP caused no variation in the baghouse differential pressure where a 9 % change in differential pressure would be expected. Possibly, the scatter in the data is hiding any trend, thus the baghouse differential pressure shows no sensitivity to the outlet air flow as was thought.

The second surprising finding was that the dryer operating point relative to the available powder sticky point had no influence on the baghouse differential pressure. It has been advised (Pearce, 2005) that the sticky point curves used in this investigation may have a dryer specific component, that would need to be determined in the plant. This statement is possibly based on the fact that individual dryers have velocities, and therefore shear rates, near the chamber walls that are unique to that dryer. Hence, the sticky point curves may have a dryer specific component. Thus, it could be that operation was some distance from the actual sticky point, and hence no trend was obvious.

The baghouse differential pressure did not show sensitivity to the remaining recorded parameters in the thought flow diagram. For parameters such as the concentrate flow and total solids and powder bulk density, the variation in each product group may not be sufficient for any correlation to be evident. Reasonable variation in power moisture content and large variation in the feed line and fines return pressures were observed, but no trend was evident. Thus, it is likely that the baghouse differential pressure is not sensitive to these parameters.

It should be noted that the influence of operation relative to the sticky point and the moisture content of the powder are likely to be long term influences, rather than instantaneous effects which have been studied here. It is more likely that as operation nears the sticky point and as powder moisture contents increase, a gradual increase in the baghouse differential pressure will result. However, the scatter in the differential pressure data, the variation in outlet air flow and powder moisture content during runs, combined with the frequently changing production schedules, makes observing a long term influence very difficult.

3.5.5. Product Averages

To compare the major differences in key plant parameters among the three product groups, averages of the parameters shown in Table 3-1 were calculated for all data points.

SMP requires the highest thermal load of the three products. This product has the greatest feed flow, and thus has the most water in the feed, and although the powder moisture content is not as low as WMP, a total evaporation of 11.7 tonne / hr occurs. This is slightly higher than the 11.0 tonne / hr for WMP and 10.1 tonne / hr for MPC.

Table 3-1: Comparison of plant operating parameters for skim milk powder, whole milk powder and milk protein concentrate in Clandeboye Dryer 2 during the 2003/2004 season

Parameter	Symbol	SMP	WMP	MPC
Concentrate Density	ρ_c [kg / m^3]	1202	1123	1069
Concentrate Flow	m_c [tonne / hr]	25.5	24.1	14.7
Concentrate Total Solids	TS_c [%]	50.6	51.5	25.7
Dry Solids in Feed	m_{ds} [tonne / hr]	12.9	12.4	3.8
Inlet Air Temperature	T_{in} [^oC]	227	216	192
Inlet Air Flow	Q_{in} [m^3 / s]	72	77	67
SFB Air Temperature	T_{SFB} [^oC]	101	97	77
SFB Air Flow	Q_{SFB} [m^3 / s]	15	18	15
Outlet Air Temperature	T_{out} [^oC]	78	78	62
Outlet Air Flow	Q_{out} [m^3 / s]	66	73	63
Outlet Air Humidity	RH_{out} [%]	17.9	16.7	27.6
BH Pressure Drop Due to Cake	ΔP_c [mm H_2O]	49 & 43	45 & 36	20 & 18
Cake Porosity	ε	0.90	0.84	0.80
Cake Thickness	L [mm]	1.63	0.69	0.47
Fines Return Line Pressure Due to Fines	P_{fr} [kPa]	19.5 & 11.5	12.5 & 7.5	12.5 & 7.5
Powder Bulk Density	ρ_b [g / mL]	0.72	0.60	0.43
Powder Fat Content	x_f [%]	0.93	26.65	1.59
Powder Moisture Content	x_{mc} [%]	3.69	2.87	5.58
Filter Drag	S [kPa s / m]	20.8 & 20.3	16.8 & 15.0	10.2 & 10.4

Although the MPC feed flow and therefore the dry solids from the plant, is much lower than for both SMP and WMP, because of the low total solids in the feed (25.7 % c.f. 50.6 % and 51.5 %), evaporation in the same order of magnitude occurs. Milk concentrate viscosity is a strong function of protein content (Bloore & Boag, 1982) hence MPC has a much higher viscosity. Because of this, the MPC total solids are much lower than SMP or WMP to avoid issues such as evaporator tube fouling that would arise because of its high viscosity.

The temperature difference, which is the driving force for evaporation, between the inlet and outlet air streams reflects the amount of evaporation required. SMP has the greatest temperature difference of 149 ^{o}C compared to the 138 ^{o}C for WMP and 130 ^{o}C for MPC. MPC has much lower inlet and outlet temperatures because of the high protein content of this product; proteins denature at high temperatures and because MPC has much more protein than SMP and WMP, lower drying temperatures are required.

The outlet relative humidity is also an indication of the amount of evaporation occurring. The much higher MPC relative humidity is due to the slightly lower air flow and outlet air temperature used for this product. This lower outlet air temperature for MPC reduces the moisture carrying capacity of this air stream, thus the relative humidity is much higher.

As discussed above, the combination of outlet air temperature and relative humidity for SMP and WMP were on the cusp of the sticky point for SMP and WMP, but a long way from the sticky point for MPC because it has a much lower lactose content than the other powders.

The baghouse pressure drop and fines return line pressure values presented in Table 3-1 were calculated as the increase caused by the presence of the milk powder. Baseline values of 55 mm H_2O[1] and 2.5 kPa related to normal values when the plant was running on air. An interesting point to note from the baghouse differential pressure value is that, although WMP has a greater air flow which would lead to a higher baghouse differential pressure, the actual differential pressure is lower than SMP. This is again possibly due to the scatter in the airflow data hiding any trend.

The filter drag calculated using Equation 2-6 show that SMP does provide a greater resistance to airflow than both WMP and MPC. This is due to the SMP cakes being approximately two and half times the thickness of the WMP and MPC cakes, even though the SMP cakes are slightly more porous.

The MPC baghouse differential pressure caused by the presence of the filter cake is much lower than both SMP and WMP. This will be due mostly to the lower level of fines flow for this power (Chapter Four) and consequently the thinnest filter cake.

[1] Fans speed of 77 % and aged bags

It is a little surprising that MPC has the lowest calculated porosity. The bulk density information shown in Table 3-1 suggests that MPC would be the most porous as it has the lowest bulk density. However, because MPC has the larger particle size, it is likely the particles will pack with more order, have less void space and therefore, a lower porosity than SMP and WMP.

Assumptions were made to make the calculation of the filter cake porosities and thicknesses possible. Firstly, it was assumed that all fines entering the baghouse reached the filter bags. However, because of the tangential entry, some powder will be pre-separated in the CD2 baghouses and the possibility of re-entrainment of powder onto the filter bags making it very difficult to quantify the amount of powder making up the filter cake. Secondly, particle density information was obtained from the work of Matheson (1991). These particle densities are likely to be for product powder, not baghouse fines, so it could be expected the baghouse particle density would be slightly lower.

Despite this, the porosities and especially the calculated thickness presented in Table 3-1 look reasonable. Observation of filter bags during operation and once removed from the plant would suggest that the filter cakes are unlikely to exceed 3 - 4 mm. The calculated cake thicknesses for all powder are below this value. Also, it was would be expected that SMP would have a thicker cake and WMP and MPC similar sized cakes, which was the case.

As explained in Section 3.5.2.1, the difference in the two values for the baghouse differential pressures indicates' a consistent bias. Again, because of the physical difference in the fines return lines, these differences in pressures cannot be used to support the idea of a bias.

The average fines return line pressures for SMP are greater than those of WMP and MPC. Surprisingly, the fines return line pressures for WMP and MPC are equal. This would suggest that very similar amounts of powder are flowing. However, these two average particle sizes and densities are markedly different, which may somewhat blur this finding.

GEA Niro A/S have indicated that on WMP, around 2.5 tonne / hr can be expected through each baghouse. If similar amounts of powder were flowing through the baghouse for MPC, this would indicate that all MPC powder is exiting the chamber through the baghouses that is, very little powder is exiting the chamber from the SFB. This agrees with plant observations

supporting the idea that the baghouse fines loadings are approximately 2.5 tonne / hr for WMP and MPC. Fines flows are investigated in greater detail in Chapter Four.

In the process of calculating the bag and cake resistances shown in Table 3-1 above, bag permeabilities for the new bags installed in the CD2 baghouses in April 2004 were calculated. These calculated values are compared with the bag permeabilities provided by bag suppliers in Table 3-2 below.

Table 3-2: Comparison of new bag permeabilites specified by bag suppliers and Clandeboye Dryer 2 plant data

Bag Type	Filter Velocity V_f [m^3 / m^2 / hr]	Permeability [m^3 / m^2 / hr / Pa]
Filtercorp – FM1DRF	540 @ 125 Pa	4.3
Madison – UMT5	960 @ 200 Pa	4.8
Intensiv – PEV511	900 @ 200 Pa	4.5
New Madison UMT5 in CD2	165 @ 149 Pa	1.6

N.B. Data in rows 2 to 4 obtained from bag suppliers, data in row 5 obtained from CD2

Although the data from the plant is of the same order of magnitude as the permeabilites provided by bag suppliers, the supplier permeabilites are still approximately four times those obtained from the plant. Suppliers obtain permeability data by measuring the air flow through a small circular piece of bag fabric at a fixed pressure drop. This method may not be an accurate representation of the permebaility in the plant and hence the difference shown in Table 3-2 results.

3.5.6. Assumptions

The results of the investigation into the main and SFB volumetric air flow rates are shown in Table 3-3 below. It can be seen that for both flows, the PLC is displaying values that are 39% and 48 % respectively below the actual flows. This discrepancy is not due to error associated with the two averaging Pitot tubes, so it is likely that either the differential pressure transmitters are not accurate or an incorrect calculation in the PLC, where the measured

differential pressure is converted into a volumetric flow, is occurring. It should be noted that all flows presented in this report are the actual air flows corrected from the recorded flows.

Table 3-3: Checks on main and SFB volumetric air flow rates in Clandeboye Dryer 2

	Main Air Flow Q_{in} [m^3 / s]	SFB Air Flow Q_{SFB} [m^3 / s]
Actual	39	12
PLC	28	8
Error	39 %	48 %

Figure 3-26 was used to check if the baghouse differential pressure readings were dependent on the pulse-jet cleaning cycle. Clearly the variation between subsequent readings is very small, an average of only 0.5 % and no correlation with the 307 second cleaning cycle is observed. Thus it can safely be assumed that the differential pressures recorded by the operators are accurate and independent of the cleaning cycle.

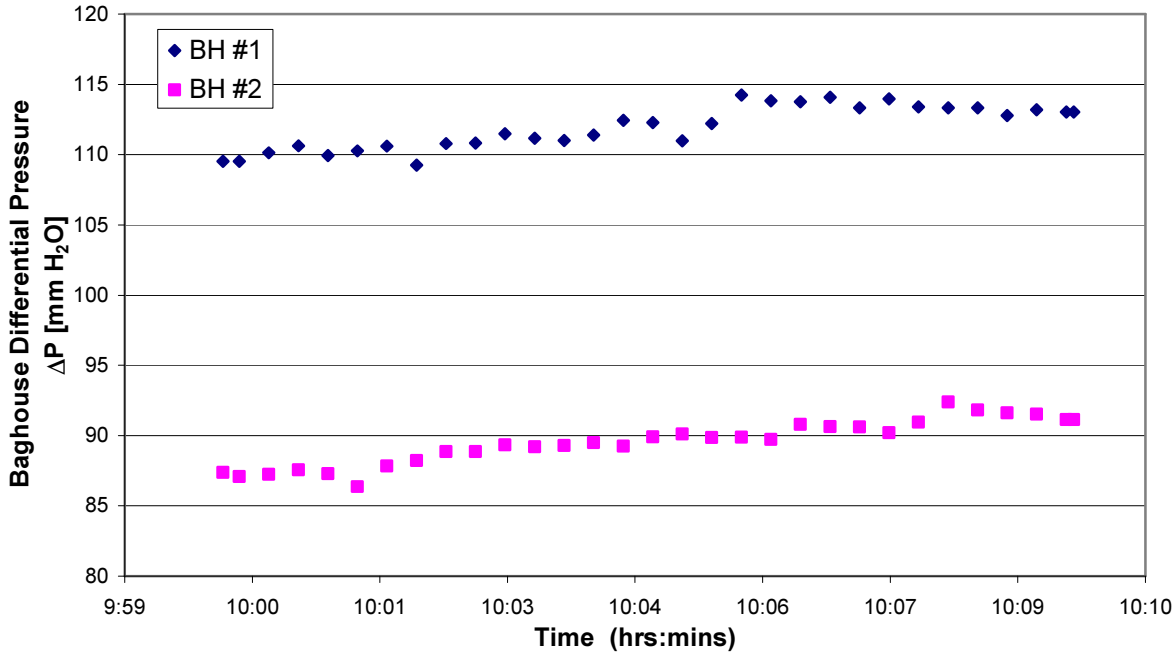

Figure 3-26: Clandeboye Dryer 2 baghouse differential pressure over two pulse cleaning cycles

3.6. Conclusions

A thought flow diagram has been produced to explain how changes in operating parameters influence the baghouse differential pressure. It can be concluded that the major causes for the variation in the baghouse differential pressure during the season are the type of product being made and the age of the bag. SMP and WMP, with higher concentrate flow and total solids contents than MPC operate at higher differential pressure and the differential pressure increases with bag age.

Replacing all bags in the baghouse causes a sudden change in baghouse differential pressure but a poor CIP can have a negative impact by increasing the baghouse differential pressure, rather than having the desired effect of decreasing it.

From the season's historical data it can be concluded that there is a clear bias in differential pressure between the two baghouses. This bias is believed to be result from an airflow bias. Unfortunately, this idea was not supported by a series of Pitot traverses or the use of an installed Torbar 402 averaging Pitot tube; both sets of results had large uncertainty associated with the calculated flows. The use of computational fluid dynamics modelling may be a method for supporting the historical data to show that an air flow bias exists. However, such a model will require the air disperser to be modelled which in turn will require a large computational mesh and therefore long processing times.

A review of the individual product group operating points has shown that two operating parameters have a significant impact on the baghouse differential pressure. For all product groups, the extractor fan speed and the age of the filter bags has an impact on the baghouse differential pressure. The amount of fat in SMP also has a considerable influence. To minimise the baghouse differential pressure, it is advisable to run the extractor fans as low as possible and to have SMP fat contents as high as product specification limits allow.

With regards to operating above the powder sticky point it is concluded that, although this work has not shown operation relative to the sticky point to have an influence, it is recommended that operation remains out of the sticky region.

With respect to the comparison of season averages for the three different product groups, it was observed that SMP has the highest differential pressure owing to the greater resistance

from thicker, denser cakes caused by more, smaller particles. This data also led to the conclusion that the baghouse differential pressure is not as sensitive to the total air flow rate as was first thought.

3.7. Recommendations

Recommendations that can be made from this work are to run the plants with as low a baghouse differential pressure as possible. This will reduce electricity and bag replacement operating costs, and also help reduce plant downtime required for bag changes. For all products, this means running the baghouse extractor fans with as low a speed as possible while still maintaining the chamber vacuum. For SMP it is suggested that the fat in the final product be as high as permitted. Although the sticky point data did not show any apparent relationship with the baghouse differential pressure, it is still recommended that operation be maintained below each products' sticky point.

To gain use from the Torbar 402 averaging Pitot tubes, it is recommended that firstly, the instruments are moved higher up the outlet air stack from their current location. Secondly, it is recommended that differential pressure transmitters be purchased to measure the Torbar 402 differential pressure, connect this reading to the plant PLC and convert the signal to a flow that is displayed on the operators' screens.

Currently the main inlet and SFB air flow rates displayed on the operators' screens are not accurate. Therefore it is recommended that an investigation be carried out to determine whether this error is due to the two differential pressure transmitters, or to an incorrect calculation of these air flows in the PLC.

4. Fines Loadings

The New Zealand dairy industry perceived that up to 20 % of the total dry milk powder flow in a spray dryer was fines. It was believed that this figure was not supported by any plant measurements. Hence, this chapter presents results for fines loadings measured industrially.

Because of the large body of work involved in this fines loading investigation, this chapter requires an outline. After giving the background (Section 4.1), the theory found in Section 4.2 introduces the particle size distribution method and gives the theory behind different solids flow measurement techniques. This section also highlights the available instruments and why the optical scintillation-based CPM 5003 was chosen. The methods used during this investigation are outlined in Section 4.3. Details of the location for the CPM 5003 are given in Section 4.4. The results from the particle size distribution methods and the optical scintillation instrument are presented in Section 4.5 and then discussed in Section 4.6. Plant observations with this instrument and its potential for permanent use in Fonterra plants are covered in Section 4.7. Section 4.8 gives details and results from the use of pneumatic conveying correlations to infer fines loadings. Finally, the conclusions and recommendations are given in Section 4.9.

4.1. Introduction

A key parameter for both the operation and design of baghouses is the inlet powder concentration. In the milk powder plant, the inlet powder concentration of the main washable baghouse is the spray dryer *outlet* air powder concentration. This powder is usually termed fines and thus the inlet powder concentration is known as the fines loading. Currently, the fines loading is not measured in any milk powder plant washable baghouse in New Zealand and it is also believed that this parameter has not been reported in the literature. Consequently, there is great uncertainty about what the fines loadings are for the different milk powder products.

Knowledge of the fines loading may help explain differences in baghouse operation among the different milk powders, as operational data presented in Chapter Three has shown large differences in the baghouse differential pressure among the products. It has been

hypothesised that these differences are largely due to differences in fines loadings because the baghouse differential pressure has been shown to be a strong function of the inlet powder concentration (Caputo & Pelagagge, 2000; Cora & Hung, 2002; Ellenbecker & Leith, 1980; Rothwell, 1987).

Known values of the fines loadings would also allow the baghouse efficiency to be determined. The efficiency could become a useful tool for plant management, using it to deduce when filter bags need to be replaced because of a decrease in efficiency, for example.

Finally, the fines loading is a key parameter required for baghouse design. Air to cloth ratio guidelines require the fines loading as an input to determine suitable values (Chapter Eight). Providing too little filtration area because of low estimates of the fines loadings could have expensive operational consequences.

Masters (1972) presents results from a pilot scale spray dryer showing that up to 35 % of the powder can become fines depending on the powder particle size and the outlet air duct arrangement. It is uncertain how well these results apply to the modern industrial scale spray dryer which, unlike the pilot scale dryer, have internal fluidised beds at the base of the chamber and, in an increasing number of modern spray dryers, outlet air ducts located near the top rather than the bottom of the chamber (Westergaard, 2003). It is likely that these two features will influence the amount of powder that becomes fines.

4.1.1. Aims

The aims of this work were to investigate the feasibility of installing online instrumentation to continually monitor the baghouse fines loadings in the main washable baghouses and to determine the fines loadings of SMP, WMP, MPC and Fat Boy powders produced in milk powder plants with washable baghouses.

4.2. Theory

4.2.1. Particle Size Distribution Method

A typical milk powder process using washable baghouses is shown in Figure 4-1. The dried powder exits the spray drying chamber either through the static fluid bed (SFB) overflow weirs or through the outlet air ducts to the washable baghouses. In the baghouse (BH), the majority of the powder is collected and discharged into the fines return lines and a small fraction is emitted to the atmosphere with the dryer outlet air stream.

Fines from the main baghouses and the powder from the SFB are passed through the vibrating fluid beds (VFs). Here, some powder is elutriated to the vibrating fluid bed baghouse (VF BH), where again some powder is lost to atmosphere while the majority is returned to the end of the second vibrating fluid bed. These fines are reunited with the majority of the powder that has flown through the VFs and is fed to the sifter.

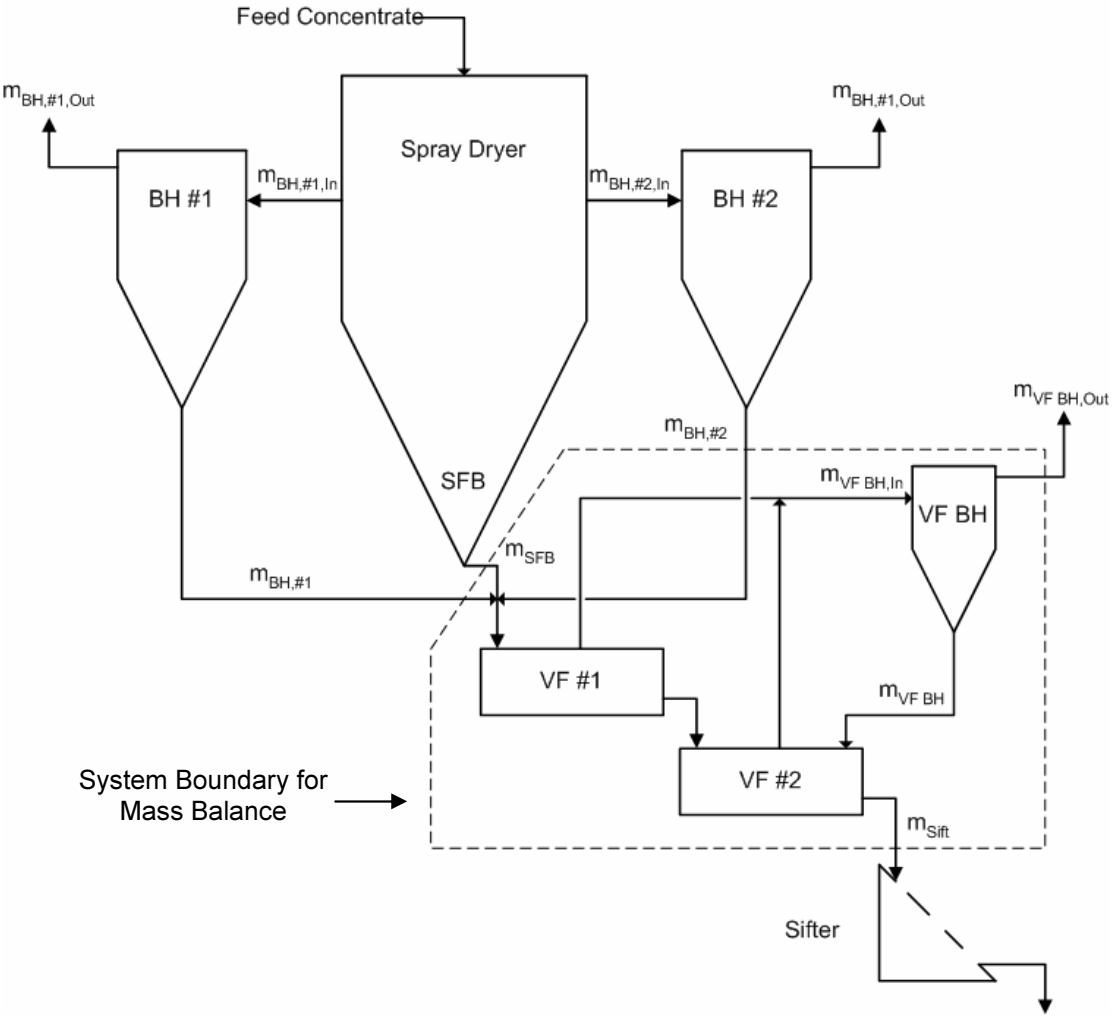

Figure 4-1: Powder flows in typical milk powder plant with washable baghouses

Definitions;

- BH – main baghouse
- SFB – static fluid bed
- VF BH – vibrating fluid bed baghouse
- VF – vibrating fluid bed

If a mass balance is carried out using the system boundary shown, then the flow exiting the spray drying chamber through the SFB and from the base of the main washable baghouses is equal to the powder flowing through the sifter plus the emissions through the VF baghouse as shown by Equation 4-1:

$$m_{BH,\#1} + m_{BH,\#2} + m_{SFB} = m_{Sift} + m_{VFBH,Out} \quad (4\text{-}1)$$

where m [kg / hr] is the mass flow of powder and the subscripts denote;

- BH,#1 – from baghouse #1
- BH,#2 – from baghouse #2
- SFB – from static fluid bed
- Sift – through sifter
- VFBH,Out – emissions from the vibrating fluid bed baghouse

The powder emissions flow [kg / hr] from the main baghouses are represented by;

- $m_{BH,\#1,Out}$ – baghouse #1
- $m_{BH,\#2,Out}$ – baghouse #2

If it is assumed that both the main and VF baghouses have a 100 % collection efficiency, then the emissions from each baghouse equals zero. Therefore, the powder flows to each baghouse equal the powder flows into the fines return system from each baghouse as given by Equations 4-2 to 4-4:

$$m_{BH,\#1,In} = m_{BH,\#1} \quad (4\text{-}2)$$

$$m_{BH,\#2,In} = m_{BH,\#2} \quad (4\text{-}3)$$

$$m_{VFBH,In} = m_{VFBH} \quad (4\text{-}4)$$

where $m_{BH,\#1,In}$ [kg / hr] is the mass flow of powder to baghouse #1, $m_{BHE,\#2,In}$ the mass flow of powder to baghouse #2, $m_{VF\ BH,In}$ the mass flow of powder to the VF baghouse and $m_{VF\ BH}$ the mass flow of powder from the VF baghouse.

If the total powder flow from the chamber to the main baghouses is defined by Equation 4-5

$$m_{BH} = m_{BH,\#1,In} + m_{BH,\#2,In} \tag{4-5}$$

and if the assumptions made above hold, then Equation 4-1 can be simplified to

$$m_{Sift} = m_{SFB} + m_{BH} \tag{4-6}$$

Equation 4-6 indicates that the powder flow through the sifter is equal to the powder that has exited the chamber through the SFB plus the powder that has exited the chamber through the baghouses.

It should be noted that the main baghouse fines can be recycled to one of three locations in the VFs: the start of VF #1 as drawn in Figure 4-1, the start of VF #2 or the end of VF #2. The VF baghouse fines can also be recycled to one of these three locations. However, the location of these return lines to the VFs does not impact on the mass balance above, so Equation 4-6 will always hold.

If it is assumed that a) no breakage or agglomeration of powder occurs in the fines return lines or during the VF process, b) that the flow of powder and particle size distribution of the powder is the same in both the main baghouses, and c) that representative samples of powder have been collected, then the particle size distribution at the sifter should be equal to a combination of the SFB powder particle size distribution and the main baghouse particle size distribution. The amount that the SFB and baghouse particle size distribution contribute to the sifter particle size distribution is determined by the ratio X [%] of the powder flows exiting through the SFB and baghouses respectively to the total powder flow. A mass balance corresponding to Equation 4-6 but for one size interval gives Equation 4-7:

$$\Delta Q_{3,Sift} = \Delta Q_{3,SFB} X_{SFB} + \Delta Q_{3,BH} X_{BH} \tag{4-7}$$

where ΔQ_3 [%] is the volume percent of a sample of powder in the given particle size band, and the subscripts Sift, SFB and baghouse represent the sifter, static fluid bed and baghouse samples respectively. The two remaining terms in Equation 4-7 are X_{SFB} [%], the ratio of SFB powder flow to the total powder flow given by Equation 4-8, and X_{BH} [%], the ratio of baghouse powder flow to the total powder flow given by Equation 4-9:

$$X_{SFB} = \frac{m_{SFB}}{m_{Sift}} \tag{4-8}$$

$$X_{BH} = \frac{m_{BH}}{m_{Sift}} \tag{4-9}$$

X_{BH} is termed the fines fraction, as it gives the percentage of the total powder that exits the spray drying chamber through the baghouses.

Dividing Equation 4-6 by m_{Sift} and substituting Equations 4-8 and 4-9 gives

$$X_{SFB} + X_{BH} = 1 \tag{4-10}$$

Thus, Equation 4-7 can be written as

$$\Delta Q_{3,Sift} = \Delta Q_{3,SFB}\left(1 - X_{BH}\right) + \Delta Q_{3,BH} X_{BH} \tag{4-11}$$

Because the particle size analysis is volume based and the powder flow ratios are mass based, Equation 4-11 assumes that the fines fraction by mass is equal to the fines fraction by volume. This assumption in turn assumes that the density of all particle sizes is the same.

An estimate of the fines loadings can be made by measuring the sifter, SFB and baghouse samples volume percentage in each particle size range i, and determining the value of X_{BH} across all particle size bands that minimises the sum of the squares of the residuals e_i, where

$$e_i = \Delta Q_{3,Sift,i} - \Delta Q_{3,Sift,\Pr ed,i} \tag{4-12}$$

and $\Delta Q_{3,Sift,Pred}$ [%], is calculated from Equation 4-11. A standard optimisation package such as Microsoft Excel Solver can be used to carry out this minimisation.

On some occasions, the production of SMP for example, fines from one of the main baghouses are recycled to the drying chamber. If BH #1 fines were being recycled to the chamber for example, and again assuming that the fines flows from each baghouse are equal, Equation 4-6 would become

$$m_{Sift} = m_{SFB} + \frac{m_{BH}}{2} \tag{4-13}$$

In this situation, Equation 4-10 would become Equation 4-14 as only half of the fines flow is contributing to the sifter flow.

$$X_{SFB} + \frac{X_{BH}}{2} = 1 \tag{4-14}$$

Equation 4-11 would also be modified to account for the smaller contribution from the fines as Equation 4-15 shows

$$\Delta Q_{3,Sift} = \Delta Q_{3,SFB}\left(1 - \frac{X_{BH}}{2}\right) + \Delta Q_{3,BH}\,\frac{X_{BH}}{2} \qquad (4\text{-}15)$$

4.2.1.1. Regression Analysis

To check the accuracy of curve fitting, regression analysis is required. This is achieved by firstly creating an overall plot to see how the predicted values compare with the actual values. Next a plot of the residuals versus the fitted $\Delta Q_{3,Sift}$ value will show more clearly if the key regression fitting assumptions hold true. In this plot, the residuals should show random scatter about zero while any pattern suggests a poor fit. The key regression fitting assumptions are that the model errors are Normally distributed with constant variance and a mean of zero, are uncorrelated, random and independent, and that there is negligible error in the independent variable (Montgomery, 2001).

The third plot required is a standardised residual plot, where the standardised residual d_i is given by Equation 4-16, with the mean square of error MS_E, obtained from Equation 4-17. Standardised residuals should have an expected range of -2 to 2 (Draper & Smith, 1981):

$$d_i = \frac{e_i}{\sqrt{MS_E}} \qquad (4\text{-}16)$$

$$MS_E = \frac{\Sigma e_i^2}{n} \qquad (4\text{-}17)$$

Finally, a Normal probability plot, a plot of the inverse of the normal cumulative probability Q (Equation 4-18) against the residual, is required. Outliers can easily be identified if the point does not lie sufficiently near the linear line running through 25th and 75th percentiles of the Normal probability plot (Draper & Smith, 1981).

$$Q = \frac{i - 0.5}{n} \qquad (4\text{-}18)$$

4.2.2. Particle Flow Measurement Techniques

A short review of three possible particle flow measurement techniques follows: electrostatic, opacity and optical scintillation. Other techniques, which are beta gauge sampling, back

scatter devices and acoustic methods, are not discussed because no such instrument was located for this work.

4.2.2.1. Electrostatic

Electrostatic charge is generated by the movement of particulates in pipes and other elements of a process plant (Yan & Stewart, 2001). The charge can be detected by an insulated electrode in conjunction with a charge detection circuit, which can measure fluctuations in the electric field caused by the passage of charged particles (Yan & Stewart, 2001). The current produced is proportional to the particle concentration, thus it can be calibrated using isokinetic testing (Manuell and Bardsley, 2000). To use an electrostatic instrument, it is assumed that each particle has a constant charge.

If there is no direct contact between the probe and the particles, the sensing interaction is achieved by electrostatic induction (Yan & Stewart, 2001). Alternatively, if there is direct contact between the probe and the particles, interaction is direct charge transfer.

The charge detection circuit uses the a.c. method if the magnitude of the alternating components of the charge signal wihtin a defined bandwidth is measured, or the d.c. method if the overall magnitude of the signal is measured without concern for frequency (Yan & Stewart, 2001). The a.c. method gives more repeatable results (Yan & Stewart, 2001).

Two common trade names appear for instruments that use the electrostatic techniques: triboelectric and electrodynamic. A triboelectric sensor relies on the direct charge transfer mechanism (Croom, 1995), whereas the electrodynamic instrument relies on electrostatic induction (Yan & Stewart, 2001).

Advantages of both methods are that the instruments are easy to install compared with other methods (Clarke, 1998), have lower operating maintenance and calibration requirements (Croom, 1995) and are cheap relative to other options (Clarke, 1998). These instruments can also measure low dust concentrations (Manuell and Bardsley, 2000).

The limitation of both sensing techniques is that the measured signal is affected by particle and environmental factors such as particle size, velocity and precharge, and gas humidity and

temperature (Yan & Stewart, 2001). Also, when the particle properties differ from those at the time of calibration, the electrical signal cannot be related to powder concentration, thus, only a relative solids concentration can be given (Yan & Stewart, 2001). Finally, these probes are not suitable for large ducts (Clarke, 1998).

4.2.2.2. Opacity

Opacity monitors consist of a light beam projected from an optical head to a second optical head located either inside or on the opposite side of the duct (Croom, 1995). Particulates in the beam absorb and scatter the light causing changes in the intensity of the received light (Clarke, 1998).

As shown in Equation 4-19, the opacity Op [%] is determined in the optical head by comparing the measured intensity of light received I [cd], with that transmitted I_o [cd]:

$$Op = 100\left(1 - \frac{I}{I_o}\right) \tag{4-19}$$

The average concentration of powder in the air stream c [g / m^3] across the path length l [m] can be determined from Equation 4-20, where K_1 [m^3 / m^2] is the plume parameter and ρ_p [g / m^3] the particle density:

$$c = K_1 \frac{\rho_p}{l} \log(1 - Op) \tag{4-20}$$

Equation 4-20 is based on the Beer-Lambert law which states if light with an initial light intensity I_0 travels a path length l, then the final light intensity I is given by Equation 4-21 where b [m^{-1}] is the extinction coefficient:

$$I = I_0 \exp(-bl) \tag{4-21}$$

The extinction coefficient includes contributions from both scattering and absorption of the light caused by the particles (Clarke, 1996), and is generally assumed to be proportional to the mass concentration of powder.

Air purge systems can be used to prevent build up of powder on the head units (Clarke, 1998) and also keep the temperature of the head surfaces sufficiently cool. This is required as

opacity monitors cannot differentiate between particles in the gas stream and particles on the optical heads (Clarke, 1998).

An improvement to the simple opacity monitor is the double pass system, where the light source and receiver are mounted on the same side of the duct (Clarke, 1998). Doubling the path of the light effectively doubles the sensitivity of the instrument (Clarke, 1998).

Opacity instruments are suitable for large diameter ducts and are not affected by velocity variations (Clarke, 1998). Also, they provide an average across the entire duct (Clarke, 1998), unlike the electrostatic techniques, and variations in dust composition and moisture content have little effect on the output (Yan & Stewart, 2001).

Limitations to opacity meters are that they are not accurate for dust levels below 10 mg / m^3 (Manuell and Bardsley, 2000) and the light beam is susceptible to misalignment (Clarke, 1998). Further disadvantages are that calibration is affected by particle size, density, shape and refractive index (Manuell and Bardsley, 2000) and dust build up on the optical heads can lead to false high readings (Yan & Stewart, 2001).

4.2.2.3. Optical Scintillation

Optical scintillation, also known as developed opacity or optical flicker, is a variation of the opacity meter. Instead of measuring the intensity of the received light, the optical scintillation instrument measures the short term fluctuations in transmitted light intensity, that is, small changes in the extinction coefficient relative to its average value (Clarke, 1996) as Equation 4-22 shows:

$$\frac{\delta I}{I_{av}} = -l\delta b \tag{4-22}$$

Fluctuations in the extinction coefficient are given by Equation 4-23:

$$\delta b(t) = b(t) - b_{av} \tag{4-23}$$

A key assumption in using this instrument is that the fluctuations in the extinction coefficient are solely caused by changes in concentration and not other effects such as incomplete mixing

due to upstream influences, turbulence or density fluctuations (Clarke, 1996). It is also assumed that the fluctuations in concentration are proportional to the mean concentration.

If the extinction coefficient b is made proportional to concentration c as in Equation 4-24,

$$b = ac \tag{4-24}$$

and the root mean square concentration fluctuation made proportional to concentration as in Equation 4-25,

$$\delta c_{rms} = gc \tag{4-25}$$

then taking the root mean square values of both sides, Equation 4-22 becomes:

$$\frac{\delta I_{rms}}{I_{av}} = -l(ag)c \tag{4-26}$$

The product (a g) is a constant that is determined by calibration.

The major advantage of the optical scintillation instrument is that because $\delta I/I_{av}$ is measured then the actual initial light intensity is irrelevant. Thus, the instrument is not affected by drift or fouling of the optical lenses. Like the opacity instrument, the optical scintillation instrument is suitable for large diameter ducts, is not affected by velocity variations and provides an average across the entire duct (Clarke, 1998). It is claimed that this instrument can measure dust concentrations as low as 2.5 mg / m^3 (Hill, 1999).

Disadvantages of optical scintillation are again similar to those of the opacity meter. That is, calibration is affected by the particle size and shape (Manuell and Bardsley, 2000) and the light beam is susceptible to misalignment (Clarke, 1998). Also the maintenance requirements are higher than other options (Hill, 1999).

4.2.2.4. Available Instruments

Four potential solids flow instruments were found for this application. The companies, the supplier location, the instrument technique and the unit cost are shown in Table 4-1 below.

The most expensive option found was the PCME StackMasster 2, which uses the electrodynamic technique. PCME instruments are currently used in most Fonterra milk powder plants to measure emissions in the outlet air stacks that follow the baghouses or

cyclones. Therefore, a good relationship with the Auckland supplier existed which would have led to good after sales support. However, this instrument was not investigated further because it was too expensive, a trial offer was not available and the instrument does not measure across the entire duct.

Table 4-1: Potential solids concentration instruments

Company	Nearest Supplier	Technique	Unit Cost
PCME	Auckland	Electrodynamic	$38,886
Sintrol	Finland	Triboelectric	$5,500
BHA Group	Australia	Scintillation	$22,924
SICK Ltd	Australia	Opacity	$12,674

The cheapest instrument found was a triboelectric-based instrument supplied by Sintrol of Finland. Because of the supplier location, after sales support for this instrument would be problematic. Although no trial was available for this instrument, Sintrol would have been willing to give a full refund if the instrument did not work. Other factors against using this instrument were that this technique also gave a point rather than cross duct measurement and the limitations of electrostatic based instruments outlined in Section 4.2.2.1 above.

SICK Ltd was able to supply an opacity-based instrument. The major benefit of this instrument was the cross duct sampling. The price for each unit was relatively cheap and support would have been possible because the supplier is based in Australia. However, this instrument was not selected as a trial offer was not available; the instrument output was only a low, medium or high level because of the high expected powder concentrations and the potential false high readings opacity instruments suffer.

The BHA Group CPM 5003 was chosen because of the availability of an instrument for trial, the advantages of the optical scintillation technique over electrostatic and opacity techniques and the good after sales support that came from the Australian supplier. Two additional features of this instrument that supported its selection were the 30 day on-board storage capability and the multiple calibration feature (the instrument could be calibrated for up to three different operating conditions and automatically switch between the correlations when a

different operating condition was detected). Finally the suppliers claimed that the instrument would operate at powder concentrations of up to 50 g / m^3.

4.2.3. Pneumatic Conveying Correlations

Section 2.3.2 in Chapter Two revealed that the pressure drop in a pneumatic conveying system is a function of several parameters including the mass flow of solids. This section also highlighted the procedures available for calculating the pressure drop caused by solids and gas in a pneumatic conveying line. If sufficient data about the carrier gas, the solids and the pipe system were known, using procedures such as those of the Klinzing (1997), Maynard (2006), Mills (2004) and Molerus and Wellman (1981), one could determine the influence of the amount of solids present on the system pressure drop, and hence the solids flow.

4.3. Methods

4.3.1. Particle Size Distribution Method

This method was used for MPC, SMP, WMP and Fat Boy (a high fat protein powder) in CD2, WMP in CD3, WMP in ED2 and SMP in ED3. In each case, sets of samples were obtained from the SFB overflow weir, the inspection hatch above the baghouse hopper and from the sample point at the start of the sifter.

Particle size distributions were measured using a Microtrac X-100 (Leeds & Northrup, North Wales, USA) with the samples suspended in an air flow. With this configuration, the available range of measure was 1 – 700 μm. Analysis involved using a Microsoft Excel Solver routine to calculate the baghouse fines loading.

To test the assumption of no breakage or clumping occurring between the SFB/ baghouse and the sifter, SEM images of each type of milk from the three locations were generated using a JEOL JSM-6100 scanning electron microscope (JEOL Ltd, Tokyo, Japan).

4.3.2. Online Instrument

The only location for the online instrument could be the dryer outlet duct, which is a short 1.7 m by 1.9 m rectangular duct 3.3 m in length. The conditions at the location were obtained by estimating the air velocities, size and location of the vena contracta, air temperatures and humidities, and powder particle sizes and concentrations. Duct dimensions were measured and location of exterior features on the duct (CIP and fire system spray balls, inspection hatches, welds, bracing) that would influence the location of the instrument were detailed.

Specifications of potential instruments were obtained from both national and international suppliers. These details included costs of instruments, features, measurement range, instrument output, ease of installation, after sales support and availability of a trial.

A scintillation based instrument from the BHA Group was selected, installed and the instrument trialled for several months. Plant operating data for the evaporators and spray dryer, along with readings from the instrument were taken every six minutes. This data was analysed by comparing the differences between products, and key operating periods such as evaporator and feed line swaps.

4.3.2.1. Thimble Filter Isokinetic Sampling

An assembly was designed so that an existing thimble filter casing shown in Figure 4-2 could be mounted on to the side of the CD2 BH #1 inlet duct. The thimble casing consisted of a cylindrical stainless steel housing with a small outlet pipe at the back end, and a cover plate that was screwed on to the front end of the cylinder. In the middle of the cover plate a swagelock nut tightened a chosen nozzle into place. A glass fibre thimble filter was placed over the lip on the underside of the cover plate and held in place with an O-ring over the outside of the thimble.

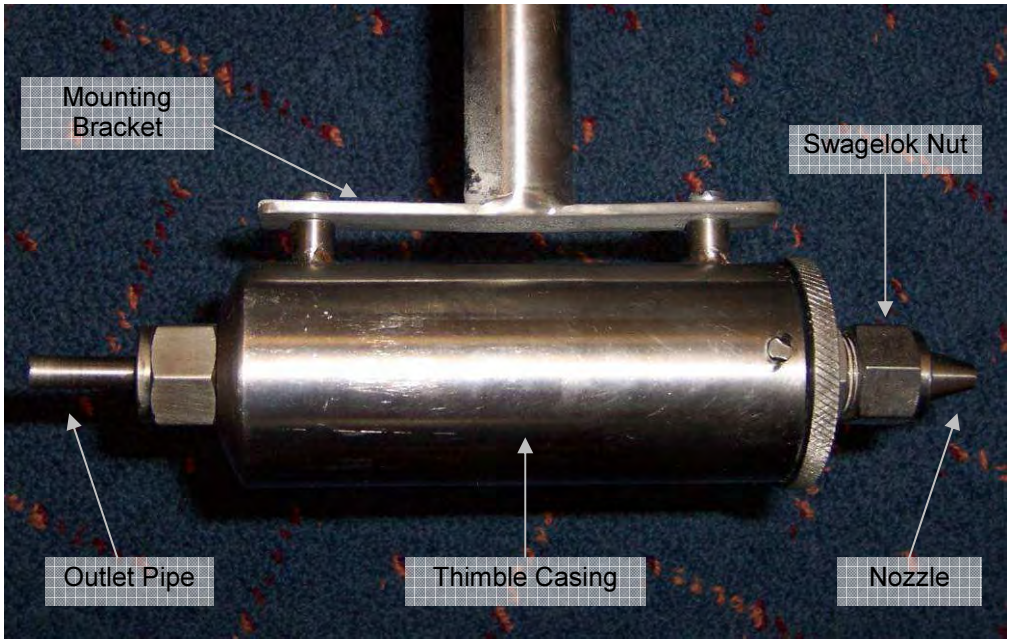

Figure 4-2: Thimble filter casing

The assembly consisted of a 335 mm diameter circular stainless mounting, through the centre of which ran a 1200 mm long stainless pole with a handle at one end and a bracket at the other. The thimble casing was bolted to the bracket and the rubber air hosing from the back of the thimble fed through the middle of the pole and out near the handle (Figure 4-3).

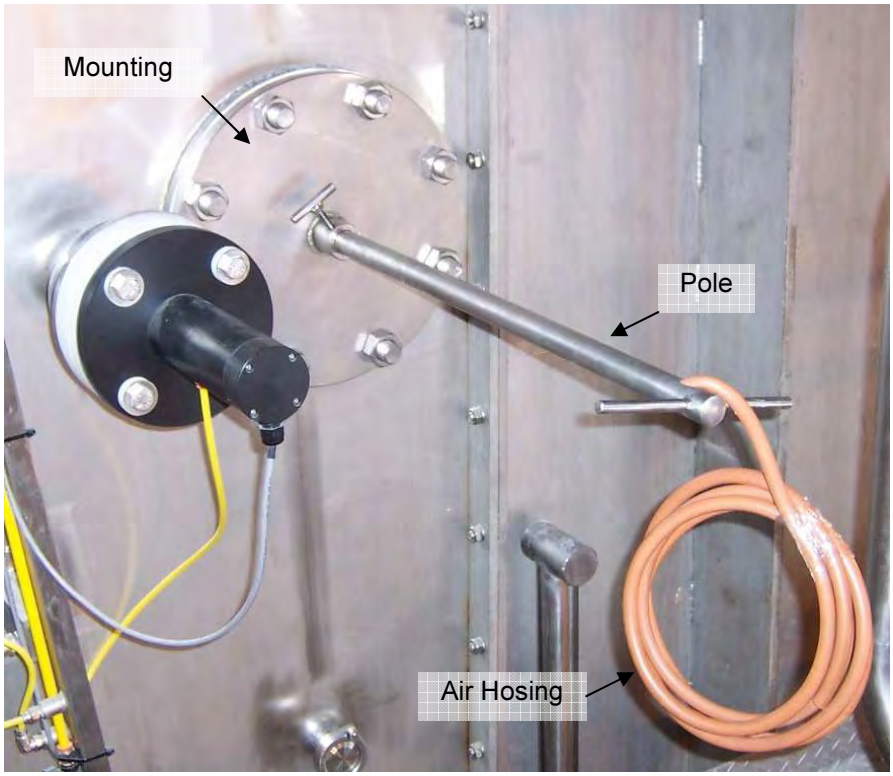

Figure 4-3: Thimble filter assembly mounted on Clandeboye Dryer 2 Baghouse #1 inlet duct

The air stream was sampled following a standard isokinetic sampling method such as those outlined in Method 5 - United States Environmental Protection Agency, (1977); Clarke (1998); and Manuell & Bardsley (2000). The mass flow of air in the duct was determined from a mass balance of the spray dryer. These main inlet and SFB air flows, along with the temperature in the duct, were taken from the operators' screens, allowing the volumetric flow and then the average velocity in the duct to be calculated. The water vapour in the duct air stream was determined using psychometric charts. It was assumed that a) the ratio of air flow through each outlet duct was equal to the ratio of the two extractor fan speeds, b) because of the small size of the duct relative to the size of the dryer chamber, and the close proximity of the sampling station to the chamber exit, the velocity in the duct was uniform over its cross section.

An appropriately sized nozzle was fixed to the end of the thimble housing, and the pump flow was adjusted to maintain isokinetic sampling. The thimble was pre weighed after being stored in a desiccator for several days. A sample was obtained by mounting the thimble filter assembly on the duct. The thimble casing was pushed to the centre of the duct, the nozzle pointed into the flow and the pump was run for five minutes. The thimble and collected powder were removed from the casing, placed in a 104 ^{o}C oven for three hours and then stored in a desiccator until they reached ambient temperature. The thimble with its collected powder was then weighed, the collected powder weight determined and the fines concentration calculated.

4.3.3. Pneumatic Conveying Correlations

Operating data for SMP, WMP and MPC produced in CD2 during the 2003/2004 season has been investigated and is discussed in Chapter Three. This included calculating the average fines return line pressure drops because of the solids from the main CD2 baghouses for each product.

The pipe diameter, length, number of elbows and change in elevation were either measured in the plant or taken from the plant layout drawings. The airflow was assumed to be that displayed by the blower manufacturer on the blower specification plate and the air temperature assumed to be 20 ^{o}C. Average particle sizes were taken from samples obtained to estimate fines loadings using the particle size distribution method. Particle densities for SMP

and WMP were obtained from the work of Matheson (1991), and the particle density of MPC was estimated based on the bulk density of the final product. The slip velocity was determined using correlations from Molerus and Wellman (1981).

Using this gathered information, the procedures of Molerus and Wellman (1981); Maynard (2006) and Williams et al. (2004) were used in an attempt to determine the fines loading on the baghouses from the plant pneumatic conveying pressure drop caused by solids.

4.4. Instrument Location

The solids flow instrument could be placed only in the short dryer outlet ducts shown in Figure 4-4 below. The dimensions of these ducts are given in Table 4-2.

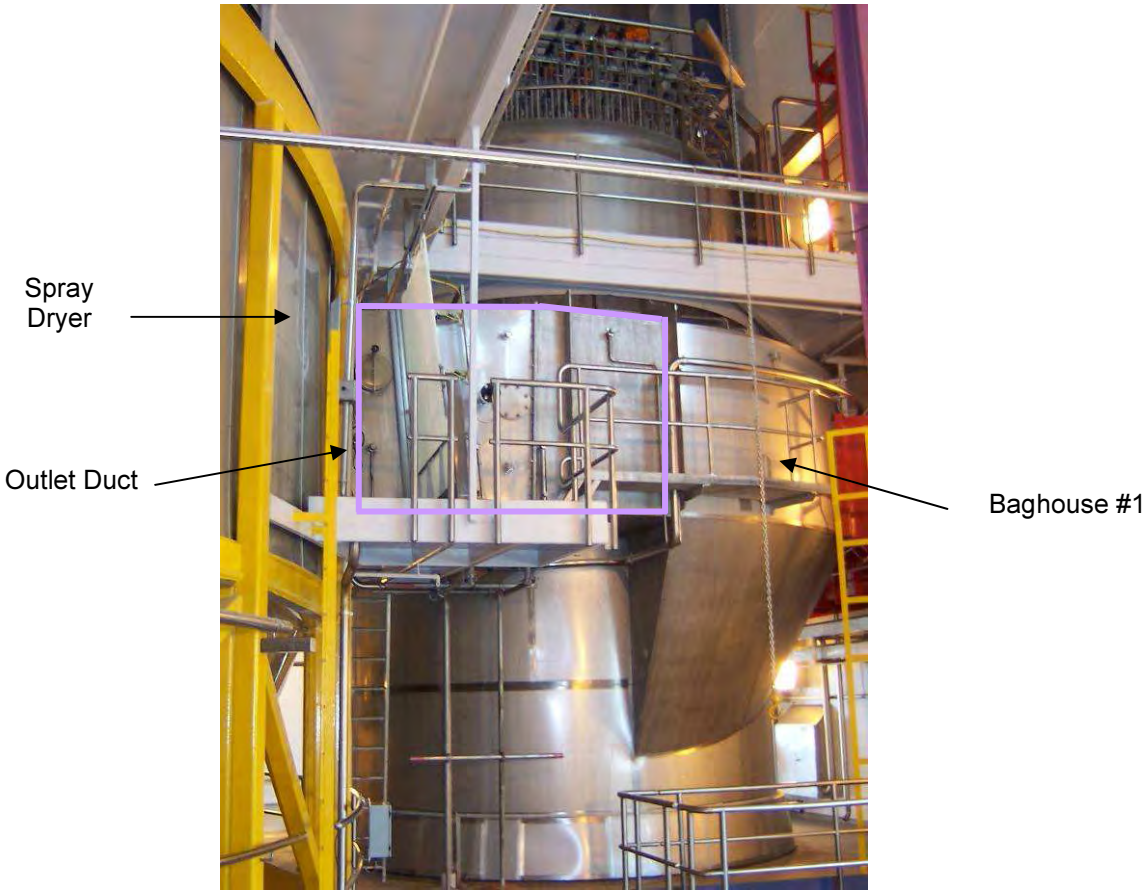

Figure 4-4: Clandeboye Dryer 2 Baghouse #1 inlet duct

Table 4-2: Dimensions of Clandeboye Dryer 2 outlet ducts

Outlet Duct Height [m]	Outlet Duct Width [m]	Duct Length [m]
1.9	1.3	3.3

Table 4-3 shows the properties of the air stream in the dryer outlet duct. The variation in air temperature, relative humidity and air velocity are due to differences in operating parameters among the products.

Table 4-3: Clandeboye Dryer 2 air conditions in dryer outlet ducts

Air Temperature [^{o}C]	Pressure [mm H_2O]	Relative Humidity [%]	Velocity [m / s]	Ideal Instrument Location from Duct Inlet [m]
60 - 80	- 30	20 - 35	12.3 – 12.9	5.7 m

Wight (1994) defines the ideal instrument location as that where no flow disturbance, such as a bend or change in cross-section, is less than eight duct diameters downstream or two duct diameters upstream. This was not physically possible in the baghouse #1 inlet duct because the total length of the duct was just over two duct diameters. This would suggest that entrance effects from the dryer would not be dissipated before the air stream entered the baghouse, hence a uniform flow pattern would be unlikely.

It was thought that a vena contracta would develop in the outlet duct because of the small duct cross sectional area relative to the size of the dryer chamber. Three different correlations for the flow coefficient of a sudden contraction in pipe diameter were used to estimate the size of the vena contracta. The upstream size of the sudden contraction, w_1 in Figure 4-5, was varied because the air flow from the dryer was confined by walls at different angles, and it was unknown how this would impact on the potential vena contracta area.

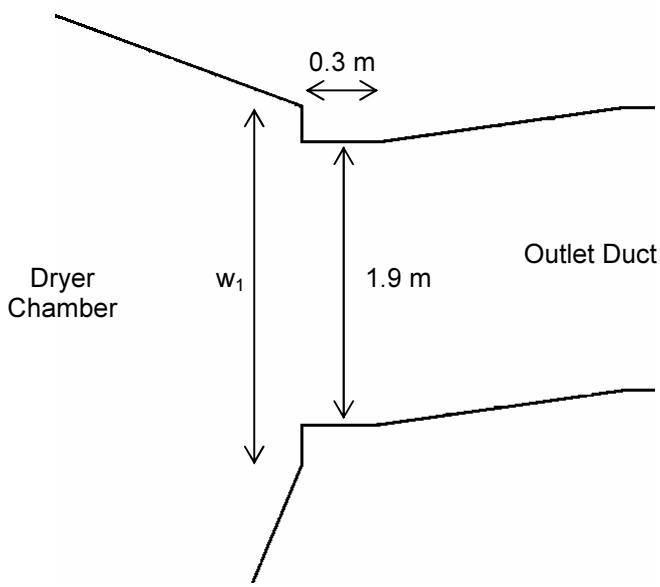

Figure 4-5: Elevation view of Clandeboye Dryer 2 Baghouse #1 inlet duct

The results are shown in Table 4-4 below. The theoretical results show that the vena contracta area would range between 61 % and 86 % of the duct area, depending on how the airflow entered the duct.

Table 4-4: Clandeboye Dryer 2 outlet air duct theoretical vena contracta area

Correlation	Vena Contracta Range [m^2]	Percentage of Duct Area [%]
Graebel (2001)	1.55 to 1.73	61 to 68
Oertel (2004)	1.62 to 1.70	63 to 66
White (1999)	1.64 to 2.21	64 to 86

To estimate the position of the vena contracta relative to the start of the duct, the correlations of Liou and Hwang (1992) and Sparrow and Cur (1982) were used. Both correlations are for air flow in rectangular ducts where the entrance is a sudden contraction. As the results in Table 4-5 show, both correlations gave similar results, suggesting that the centre of the vena contract is located approximately 0.17 m from the start of the duct.

Table 4-5: Clandeboye Dryer 2 outlet air duct theoretical vena contracta location from start of duct

Correlation	Vena Contracta Position [m]
Liou & Hwang (1992)	0.14 – 0.21
Sparrow & Cur (1982)	0.16

Because of the short length of the duct, it was decided to install the instrument at the location of the vena contracta. However, as Figure 4-6 shows, this was not possible because of the presence of an inspection hatch at this location. The CPM 5003 was installed as close to this point as was possible, approximately 1 m along the duct because of the presences of the vapour barrier and its hydraulic arm supports.

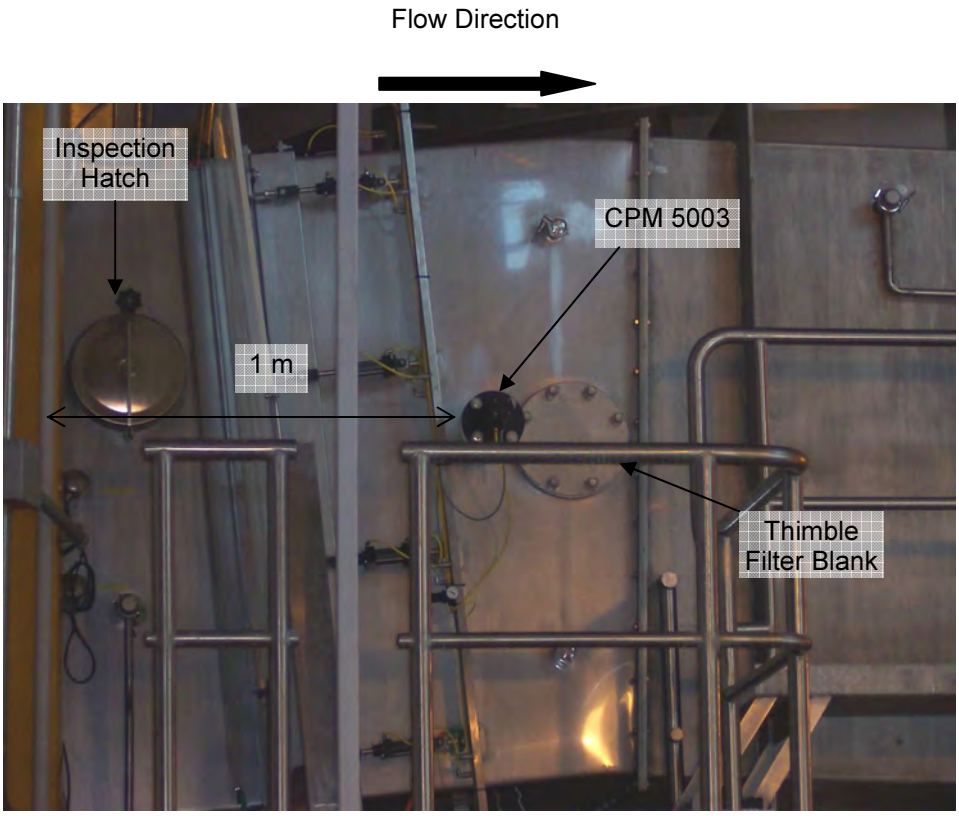

Figure 4-6: Features of the Clandeboye Dryer 2 Baghouse #1 inlet duct

4.4.1. Instrument Measurement Range

Figure 4-7 shows estimates of the likely baghouse inlet solids concentrations for a range of fines fractions for each product. SMP had the greatest calculated concentration of fines and

MPC 80 the lowest, thus the maximum required by the instrument would be determined from the maximum SMP fines fraction.

It was suggested by GEA Niro A/S that during normal operation, 10 tonne / hour of SMP is fines, thus giving a baghouse inlet powder concentration of 39 g / m^3. If the SMP fines fraction varied by ± 10 %, then an expected maximum inlet powder concentration would be 45 g / m^3. Any powder concentrations greater than this would indicate serious operational issues within the spray dryer. As stated above in Section 4.2.2.4, the CPM 5003 suppliers claimed the instrument was capable of measuring at powder concentration up to 50 g / m^3, that is, greater than the expected SMP maximum.

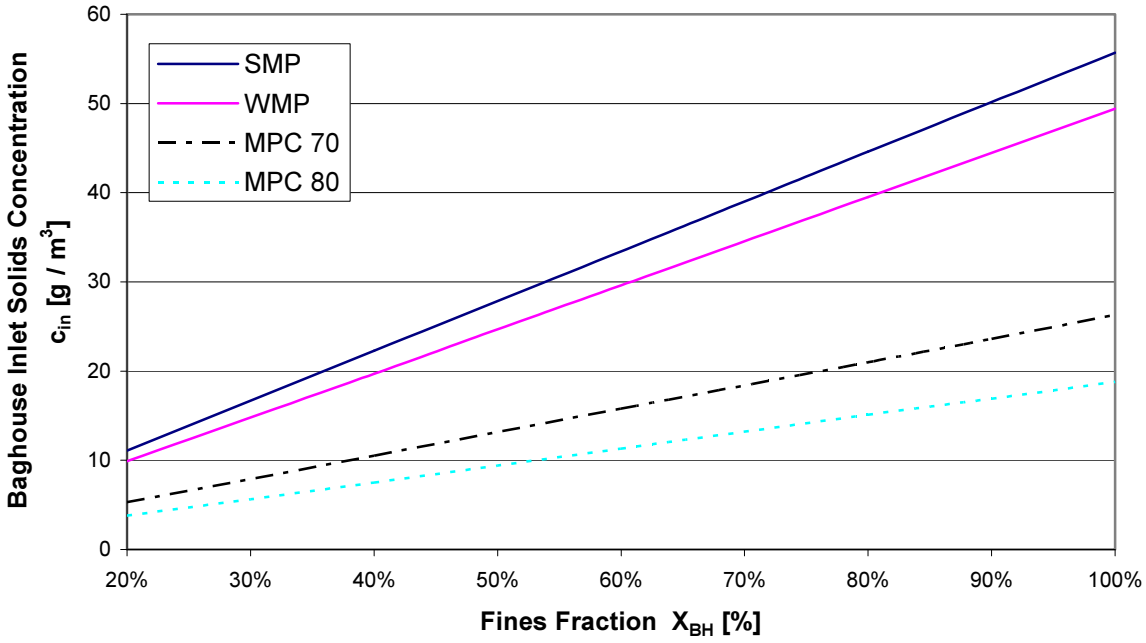

Figure 4-7: Estimated solids concentration in Clandeboye Dryer 2 dryer outlet ducts as a function of entrainment

4.4.2. Installation

The CPM 5003 was installed during plant downtime in late February 2005. This involved an industrial abseiler climbing from the static fluid bed up the inside of the chamber wall and positioning himself on the inside of the outlet duct to control any foreign matter generated.

The CPM 5003 consisted of a transmitter head emitting light at a wavelength of 660 nm from an LED light source. On the opposite side of the duct, the 50 mm receiver head was located. This head was approximately half the diameter of the emitted light beam. Therefore, supposedly a greater target for the transmitter was provided allowing for greater tolerance in alignment of the transmitter and receiver heads. Both the transmitter and receiver surfaces were flushed with approximately 96.5 kPa plant compressed air to prevent excessive build up of powder and over temperature. The LED light sensor of the receiver was connected to a microprocessor which had 30 day data storage capability.

During installation, it was noticed that the maximum readout on the display (Figure 4-8) was 10,000 mg / m^3. Upon further investigation, it was clarified by the instrument suppliers that this was in fact the supposed maximum concentration the instrument would operate at, even though the suppliers had stated that it would measure up to 50 g / m^3. However, the trial continued and as shown in Section 4.5.2 below, the instrument did give sensible results at concentrations beyond the suppliers' specifications. Thus, the instrument has outperformed the suppliers' expectations.

Figure 4-8: Installed CPM 5003 control panel and display

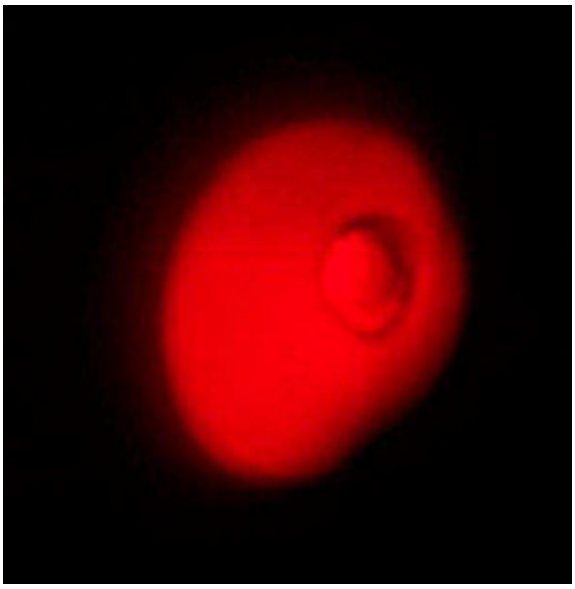

Figure 4-9: Installed CPM 5003 transmitter light shinning onto receiver lens and duct wall

4.5. Results

4.5.1. Particle Size Distribution Method

4.5.1.1. SMP Results

Table 4-6 shows the results of the SMP fines fractions, the ratio of the fines flow to the total powder flow, in CD2 and ED3. The bracketed numbers following the plant name indicate operating condition one or operating condition two. The average of the single CD2 and ED3 samples at operating condition one is 86 %, which equates to a fines mass flow of approximately 10.2 tonne / hr. The average of the three ED3 samples at operating condition two is much lower at 53 %, a fines mass flow of approximately 6.5 tonne / hr.

Table 4-6: Fines fraction estimates for Skim Milk Powder using the particle size distribution method in Clandeboye Dryer 2 and Edendale Dryer 3

Plant	Number of Samples	Average	Range
CD2 (1)	1	84 %	-
ED3 (1)	1	88 %	-
ED3 (2)	3	53 %	30 - 76 %

With an average value of greater than 50 %, the sifter particle size distribution should lie closer to the baghouse particle size distribution than the SFB particle size distribution. As Figure 4-10 shows, this is the case for particle sizes less than approximately 150 μm but above this size, the sifter distribution lies closer to the SFB distribution.

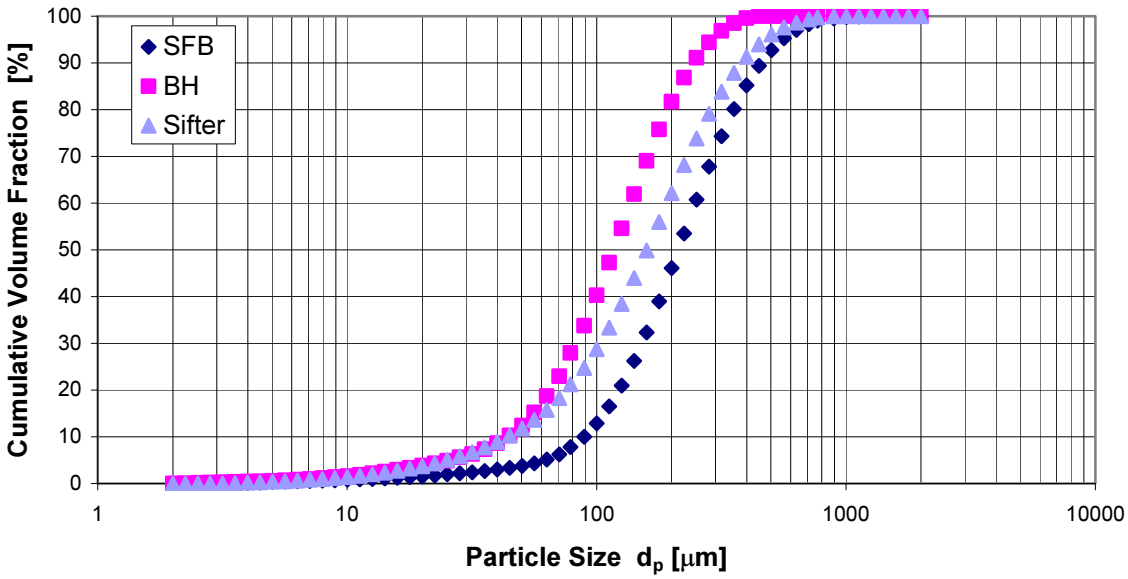

Figure 4-10: Cumulative Volume Particle size distribution for Skim Milk Powder samples obtained from Clandeboye Dryer 2 March 2005

4.5.1.2. WMP Results

The results for the WMP fines fractions determined using the particle size distribution method are given in Table 4-7 below. The averages from the identical GEA Niro A/S MSD dryers (CD2 and ED2) show very good agreement, with average values of 48 % and 49 % respectively. This indicates good repeatability.

The CD3 average of 42 % is slightly lower than the CD2 and ED2 values, but it should be noted that the CD3 Stork design drying chamber and attached Intensiv washable baghouses are markedly different to the CD2 and ED2 design.

Table 4-7: Fines fraction estimates for Whole Milk Powder using the particle size distribution method in Clandeboye Dryer 2, Clandeboye Dryer 3 and Edendale Dryer 2

Plant	Number of Samples	Average	Range
CD2	4	48 %	42 – 54 %
ED2	3	49 %	43 - 59 %
CD3	5	42 %	27 - 64 %

As it has an average value of roughly 50 %, it would be expected that the WMP sifter particle size distribution would be midway between the baghouse and SFB particle size distributions. Figure 4-11 below shows this is the case.

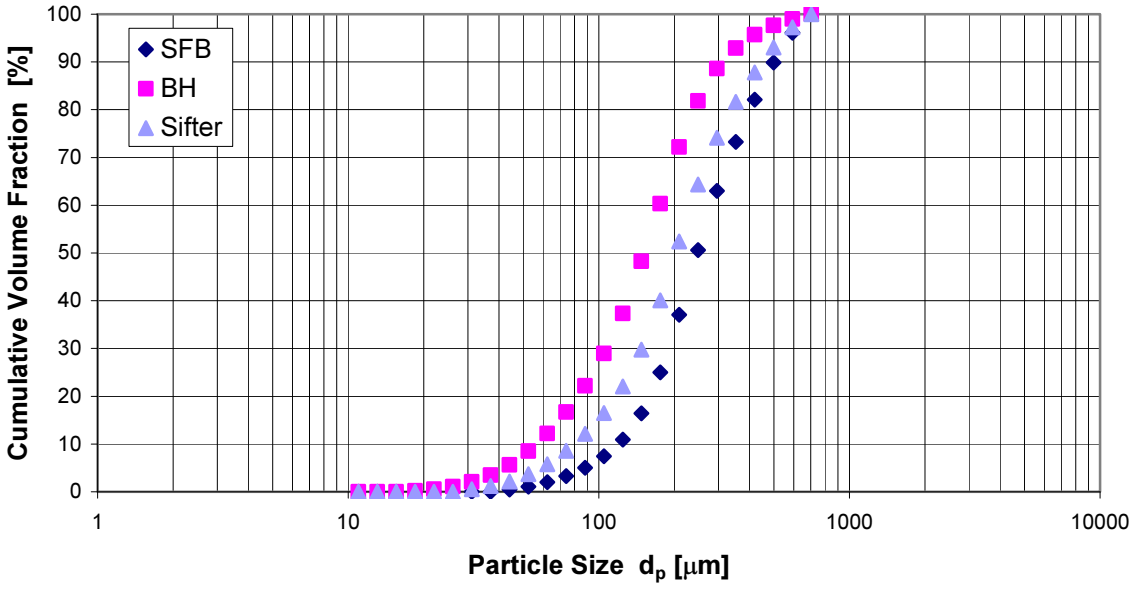

Figure 4-11: Cumulative Volume Particle size distribution for Whole Milk Powder samples obtained from Edendale Dryer 2 February 2006

4.5.1.3. MPC Results

The results for the MPC fines fractions in CD2 are given in Table 4-3 below. The average value of 96 %, which equates to approximately 6.7 tonne / hr, indicates that almost all of the powder is exiting the chamber through the baghouses. The sifter and baghouse particle size distributions would be expected to be almost identical. As Figure 4-12 below shows, this is the case.

Table 4-8: Milk Protein Concentrate fines fraction estimates using the particle size distribution method in Clandeboye Dryer 2

Plant	Number of Samples	Average	Range
CD2	4	96 %	90 – 98 %

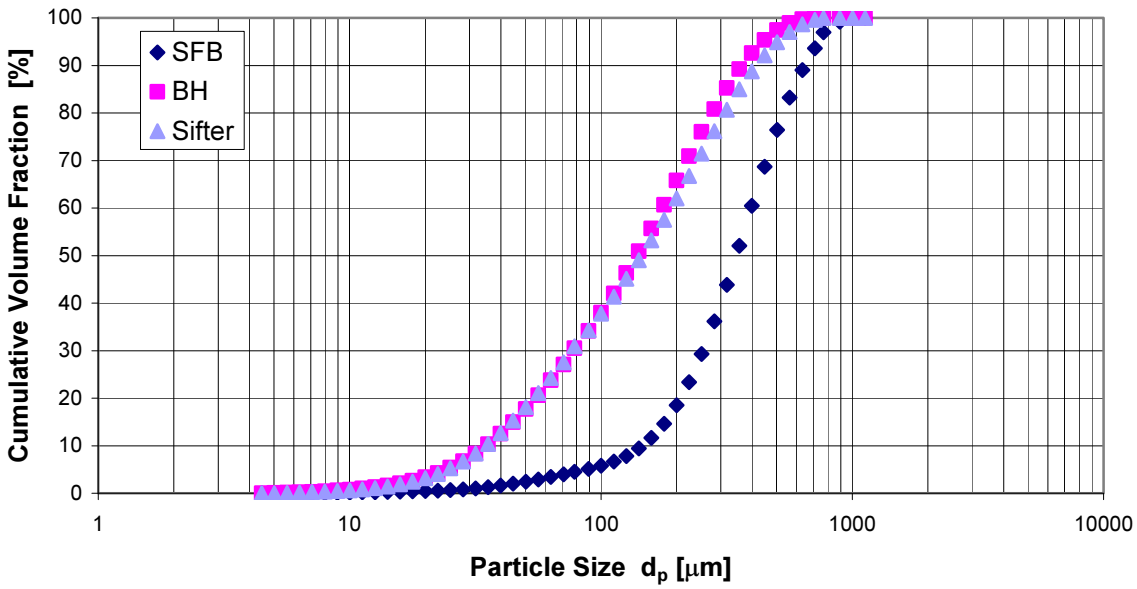

Figure 4-12: Cumulative Volume Particle size distribution for Milk Protein Concentrate samples obtained from Clandeboye Dryer 2 October 2005

4.5.1.4. Fat Boy Results

The Fat Boy fines fractions in CD2 determined using the particle size distribution method are shown in Table 4-9 below. Again, the bracketed number following the plant name indicates a different plant operating condition. An average value of 64 % was calculated and a range of 60 % to 71 % found at operating condition one. As a mass flow, this 64 % equates to 6.7 tonne / hr. At operating condition two an average value of 83 % or approximately 8.7 tonne / hour was found.

Table 4-9: Fines fraction estimates for Fat Boy powder using the particle size distribution method in Clandeboye Dryer 2

Plant	Number of Samples	Average	Range
CD2 (1)	3	64 %	60 – 71 %
CD2 (2)	3	83 %	82 – 84 %

Because 74 % of the total powder is fines, the sifter particle size distribution should lie more closely to the baghouse particle size distribution than the SFB particle size distribution. Figure 4-13 below indicates this is the case.

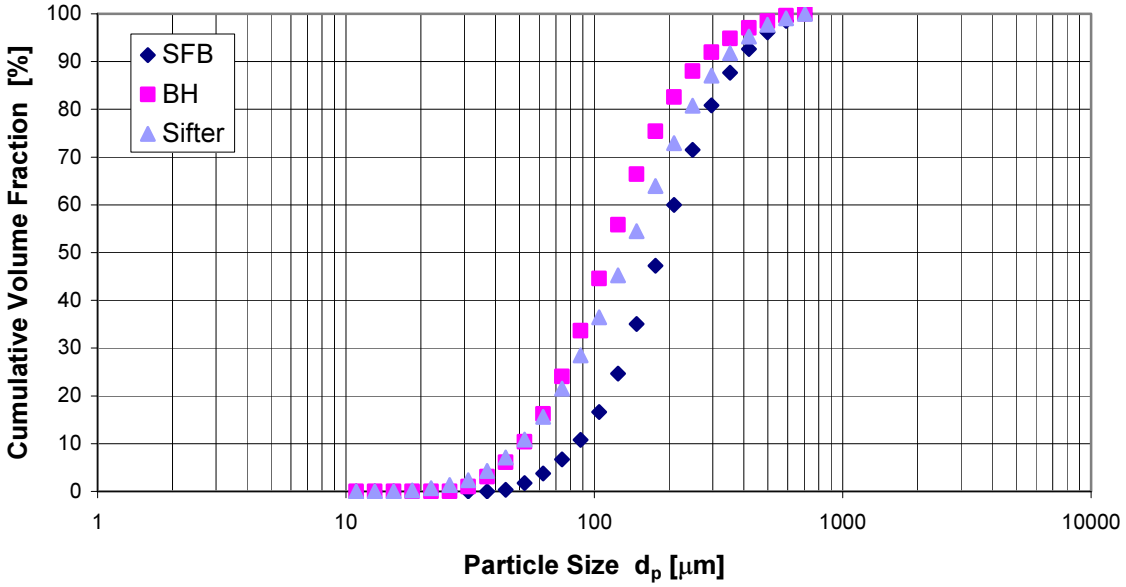

Figure 4-13: Cumulative Volume Particle size distribution for Fat Boy samples obtained from Clandeboye Dryer 2 October 2006

4.5.2. Online Instrument

During the CPM 5003 trial period, five different products were produced in CD2; SMP, MPC 70, MPC 80, Fat Boy and WMP. Figure 4-17 shows the average scintillation values for each product. The scintillation values plotted are an indication of the level of powder entering the baghouse; the higher the scintillation value, the higher the level of fines. The error included in Figure 4-14 is plus or minus half the difference between the observed upper and lower

scintillation values for each product. Therefore, these error bars are larger than the expected random error.

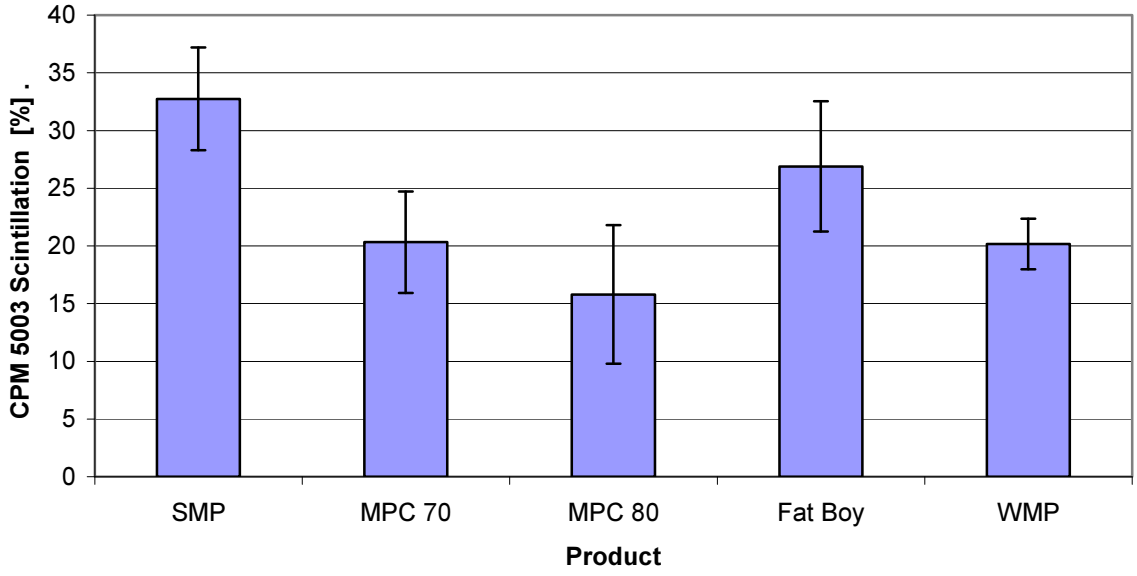

Figure 4-14: Average CPM 5003 scintillation values for powders produced in Clandeboye Dryer 2

4.5.2.1. Isokinetic Sampling

Isokinetic sampling of Fat Boy and MPC 80 powders was carried out in an attempt to calibrate the CPM 5003. The results are shown in Table 4-10 below. Unfortunately, the thimble filter assembly was not constructed in time for sampling of SMP in March 2005, and time constraints meant that no WMP or MPC 70 was sampled using this method.

Table 4-10: Fines fraction (ratio of baghouse powder flow to total powder flow) estimates for Fat Boy and Milk Protein Concentrate 80 powders using the isokinetic sampling method in Clandeboye Dryer 2

Product	Number of Samples	Powder Concentrations c_{in} [g / m^3]	Fines Fraction Average X_{BH}	Fines Fraction Range X_{BH}
Fat Boy	3	35.1, 37.0, 38.0	76 %	74 - 78 %
MPC 80	4	13.3, 13.5, 14.8, 14.8	85 %	83 - 92 %

The Fat Boy fines fractions showed excellent agreement among themselves giving an average value of 76 % and a range of 74 – 78 %. These values also showed excellent agreement with the fines fraction of 74 % obtained using the particle size distribution method. An average value of 85 % was obtained for MPC 80. This value was approximately 10 % lower than the fines fraction of 96 % obtained using the particle size distribution method.

4.5.2.2. Calibration Curve

A difficulty in calibrating the CPM 5003 was that it was very hard to influence the level of fines loadings on the baghouses for each product. As discussed in Section 4.7.1 below, a change in fines loadings does occur with an evaporator swap, but this period of operation is not at steady state so measuring a constant fines level is not possible. A consistent level of different fines loadings was observed because of a change in atomisation equipment (Section 4.7.2). However, no isokinetic sampling was carried out during this period. Finally, the concentrate total solids content has been seen to influence the fines fraction. However, this parameter cannot be easily manipulated.

In an attempt to increase the fines loadings for MPC 80 production, the speed of one of the two extractor fans drawing air through the baghouses was increased. Although this increased the mass flux of fines, the fines concentration as measured by the thimble filter was constant; changing the fan speed increased the air flow to the baghouse in question and therefore more powder entered the baghouse, but the change in fan speed did not alter the fines concentration as measured by the CPM 5003.

Therefore, the calibration curve for the CPM 5003 was created using fines loadings per baghouse determined using the particle size distribution method, isokinetic sampling and the estimates obtained from GEA Niro A/S. These were plotted against the average scintillation values or the scintillation values during the sampling period for the isokinetic sampling results (Figure 4-15). This calibration curve is based on the assumption that the extinction coefficient has the same value for the different milk powders at a given concentration.

The errors in the fines flows were obtained by taking half the difference between the maximum and minimum fines fractions of each product for the particle size distribution method. The isokinetic sampling fines fraction errors reflect the error values in powder

concentration, which are the calculated contribution of errors associated with each measurement required to calculate the concentration. The scintillation value errors were again obtained by calculating half the difference between the maximum and minimum observed scintillation values for each product.

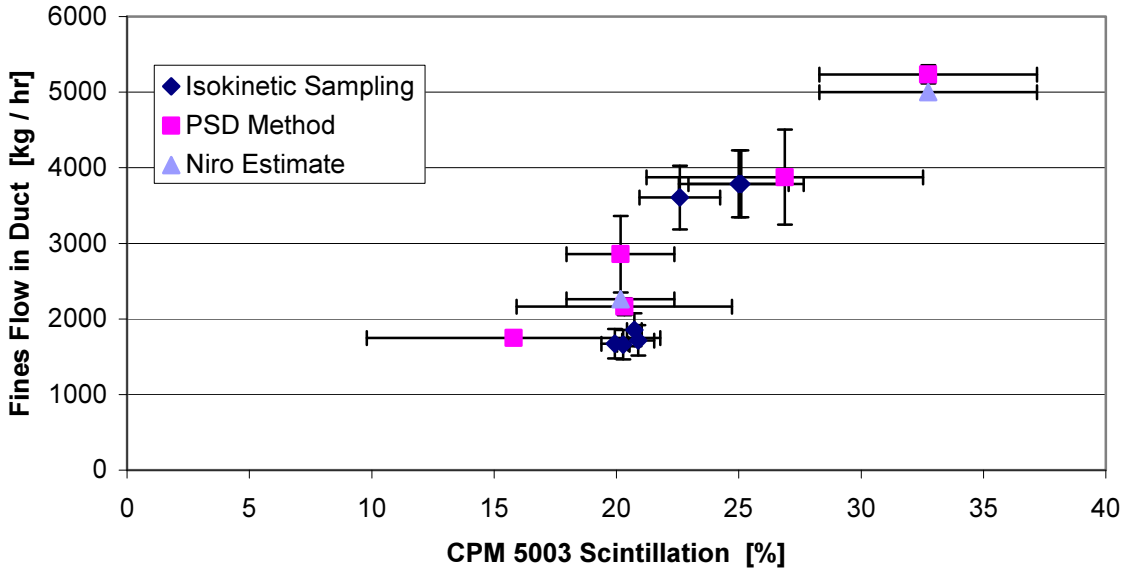

Figure 4-15: CPM 5003 calibration curve for all milk powder flows in Clandeboye Dryer 2 Baghouse #1 inlet duct

4.6. Fines Loadings Discussion

Results from the particle size distribution method and the optical scintillation instrument show very good agreement. Both methods showed that SMP, at operating condition one, has the highest fines loading of all products at approximately 10.2 tonne / hr. Fat Boy at operating condition two was shown to be the powder with the second highest fines loading at 8.7 tonne / hr. This fines loading is some 1.5 tonne / hr less than SMP at operating condition one, and Fat Boy was shown to have a lower optical scintillation of roughly 6 %. The average scintillation for WMP and MPC 70 was approximately 20 % and the fines flows of 5.7 and 4.3 tonne / hr obtained from the particle size distribution method were different. Both methods showed that MPC 80 had the lowest fines loading (3.5 tonne / hr) and scintillation (15.8 %) of all products.

The SMP at operating condition one and WMP fines loading values obtained from the PSD method show good agreement with design values from GEA Niro A/S. These estimates were made based on plant measurements on a MSD style dryer smaller than the 2000 series CD2 design (Moran, 2006). It has been indicated that GEA Niro A/S (Moran, 2005) would expect 10 tonne / hr of SMP and 5 tonne / hr of WMP to be fines. These fines flows equate to fines fractions of 82 % for SMP, which is almost identical to the CD2 (1) value obtained using the particle size distribution method, and 42 % for WMP. This WMP value is 7 % lower than the results found using the particle size distribution method.

A fines fraction of 42 % for WMP gives a fines flow of 5.0 tonne hr^{-1}. This fines flow is approximately equal to the MPC fines flow and supports the scintillation results of WMP and MPC having equal fines flows. This suggests that the WMP fines fractions from the particle size distribution method are slightly higher than the actual, although the two estimates agree within experimental uncertainty. This could be possible if the samples clumped during storage, thus giving a larger particle size distribution than the actual; WMP has the greater tendency for clumping because of the higher percentage of fat in the powder.

The particle size distribution method was used for Fat Boy at two different operating conditions. The first three samples obtained in September 2006, operating point one, had an average value of 69 %. However, after a reduction in the total solids of the concentrate fed to the dryer by approximately 4 % of the original (41.5 % to 40 %) in late September, the remaining three samples taken at the beginning of November 2006 (operating point two) had an average value of 83 %. This result is supported by the fact that a reduction in static fluid bed height was observed, indicating that less powder is at the base of the chamber and more powder was exiting the dryer as fines in the outlet air ducts. Therefore, it is clear that the reduction in total solids caused an increase in fines loading. This indicates that the particle size distribution method is sensitive enough to detect changes in fines loadings caused by key changes in plant operating conditions.

The particle size distribution method was also used for SMP at two different operating conditions. Under the second operating condition (ED3 (2)), fines from one baghouse were returned to the top of the spray drying chamber. Operating condition one (CD2 (1) and ED3 (1)) had no fines return. It is likely that increased agglomeration occurred under the second operating condition and because the agglomeration process is difficult to control (Williams et

al., 2006), the large range in fines fractions observed is a result of varying rates of agglomeration. There is also a possibility that the large range in fines fractions for ED3 (2) is a result of a much larger mass of powder in the chamber: when fines are recycled to the chamber, fines fractions of the recycled stream can exceed 100 % (Bloore, 2005). The increased agglomeration is also the likely reason for the fines fractions at operating condition two being significantly lower than those at operating condition one: increased agglomeration would increase the average particle size of the sifter sample and therefore reduce the amount of fines present.

The particle size distribution and optical scintillation findings are supported by average baghouse differential pressure and fines return line pressure plant operating data (Chapter Three). This operating data shows that SMP has the highest baghouse differential pressure and fines return line pressure for all products, and the MPC products the lowest baghouse differential pressures of all products. Although the baghouse differential pressure (Equation 2-2) and fines return line pressures are functions of more than just the fines loadings, the significant difference observed in these parameters among the products are likely to be mostly due to the large difference in fines loadings.

Plant observations also support the particle size distribution and optical scintillation results above. The plant operators struggle to retain powder on the SFB when producing MPC, and the time required to obtain a sufficient sample of MPC powder from the SFB overflow weir is much longer than for SMP, WMP and Fat Boy. This indicates that most of the MPC powder exits the chamber through the baghouses. The time required to obtain a WMP SFB sample was the shortest of all powders. This suggests that compared with the other powders, more WMP is flowing through the SFB and, therefore, less powder flows through the baghouses.

The finding of WMP and MPC 70 have similar levels of fines agrees with the findings in Chapter Three where it was postulated that these two powders have a similar level of fines because the fines return line pressures were approximately equal. The particle size distribution method and scintillation result above shows this to be true, even though the powders are significantly different in terms of particle size and density.

Table 4-11 shows some of the key difference in powder properties among the five products produced during this investigation. It would be expected that SMP has the highest fines

loading because it has the higher powder flow (12.2 tonne / hr) and therefore the greatest quantity of powder that can become fines. At the other extreme, MPC 80 would be expected to have the lowest fines loading because it has the lowest powder flow of all products (3.7 tonne / hr). However, Fat Boy (11.1 tonne / hr) has a slightly lower powder flow than WMP (11.9 tonne / hr) but a much higher fines loading, and, WMP and MPC 70 (4.5 tonne / hr) have similar fines loadings even though they have very different powder flows. This indicates that the fines loadings are a function of more than just the total powder flow.

Table 4-11: Comparison of parameters influencing fines loadings for products made in Clandeboye Dryer 2

Product	Powder Flow m_{ds} [tonne / hr]	Concentrate Total Solids TS_c [%]	Baghouse Particle Size $M_{1,3}$ [μm]	Powder Bulk Density ρ_b [g / mL]
SMP	12.2	50.6	133	0.71
WMP	11.9	51.5	144	0.55
Fat Boy	11.1	41.8	143	0.51
MPC 70	4.5	27.3	162	0.50
MPC 80	3.7	25.2	159	0.40

Table 4-11 shows that WMP and Fat Boy have a similar mean particle diameter based on volume from the baghouse samples, but a slight difference in powder bulk density. It is likely that, because Fat Boy has the lower bulk density, the lighter particles are more easily entrained in the outlet air stream and hence, Fat Boy has a higher fines loading than WMP. Also, because Fat Boy has a mass flow much greater than the MPC powders, it places a higher fines loading on the baghouse.

Although the MPC powders have one of the larger particle sizes, the fact that these particles are likely to have lower particle densities than the majority of the other powders potentially indicates that this powder will have a greater percentage of fines. Therefore, although MPC 70 has a much lower powder flow rate than WMP, because of the differences in powder density, these two powders have a similar level of fines.

4.6.1. CPM 5003 Calibration Curve

Figure 4-15 shows that a reasonably good straight line fit can be drawn through the data including the origin. This calibration curve means that the optical scintillation values obtained from the CPM 5003 could with some confidence be converted to fines flows and displayed as an additional operating parameter on the operators' screens. This would give operators another tool to help minimise baghouse differential pressures as running conditions that minimised the fines flows to the baghouses could be obtained.

This calibration curve is a very good result considering the instrument is operating at powder concentrations above the supposed maximum: the supposed limit was stated as 10 g m^{-3} but these results indicate the instrument has responded to concentrations as high as 42 g m^{-3}. Also, the data is obtained from the industrial scale, where there is very little control when compared with that at the laboratory scale.

It can be seen from Figure 4-15 that for Fat Boy (fines flows between 3000 – 4000 kg / hr) and MPC 80 (fines flows between 1000 – 2000 kg / hr), the particle size distribution and isokinetic sampling method results agree respectively within experimental uncertainty. This indicates that both methods can be used to give accurate predictions of the fines flow rates.

Two possible sources of experimental error during the isokinetic sampling exist. Firstly, the thimble assembly may not have been perfectly aligned in the horizontal position during sampling. This would mean that the effective cross sectional area of the nozzle perpendicular to the flow would be reduced and a smaller mass of powder than expected was collected.

Secondly, there may have been errors in determining the velocity for isokinetic sampling. This velocity was calculated by carrying out a mass balance on the air flow in the dryer and accounting for the moisture in the outlet air stream. Slight variation in the values taken from the operators' screens to achieve this was observed and these values may have changed during the time it took to calculate the pump flow and carry out the sampling. This same velocity was used to calculate the required sampling flow, and therefore, this may not have been truly isokinetic.

4.6.2. Particle Size Distribution Method Assumptions

A key assumption that makes the particle size distribution method possible is that there is no change in individual particle size of the SFB or baghouse powder between the sample locations at the SFB overflow weir and the BH hopper, and the sifter. To test whether agglomeration or break-up of particles occurred between these locations, scanning electron microscope images were produced for a set (SFB, baghouse, sifter) of SMP, WMP and MPC samples. The SMP set of samples are shown in Figure 4-16 below.

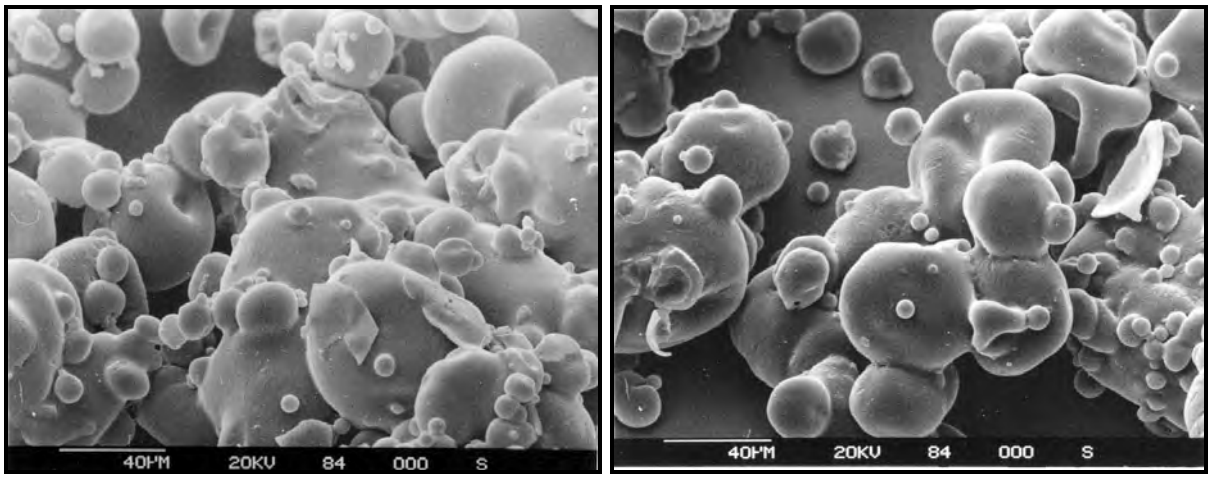

Figure 4-16: Scanning electron microscope images of skim milk powder obtained from Clandeboye Dryer 2 baghouse (left) and sifter (right) in March 2005

Figure 4-16, and those images for the other powders, showed that at all sample locations, the powders were highly agglomerated as at least 95 % of the particles were adhering to other particles. The SFB samples appeared to be more highly agglomerated than the baghouse and Sifter samples, thus it appeared that no further agglomeration of the powder occurred in the vibrating fluid beds. Broken particles constituted less than 1 % of each sample, suggesting that pneumatic transport of the powder from the SFB and BH Hopper to the Sifter did not cause any further break up of the powder. Therefore, it was concluded that the assumption of no change in particle size was correct.

The particle size distribution method assumes that the main and VF baghouses have collection efficiencies of 100%. It is shown in Chapter Eight that over the range of expected baghouse inlet power concentrations the CD2 main baghouses have efficiencies of 99.88 % and above. Although this means the assumption of 100 % collection efficiency is not correct, the

maximum difference is only 0.12 % and therefore the influence on the results presented above is negligible.

A final assumption made to simplify the particle size distribution method was that the particle size distributions in the main baghouses were equal. In most cases this was not true as there was a slight difference as Figure 4-17 shows. The difference in baghouse particle size could be real, because one baghouse collects slightly larger particles, or perceived, because the samples were taken approximately 10 minutes apart. To minimise this effect, the average of the two main baghouse particle size distributions was used.

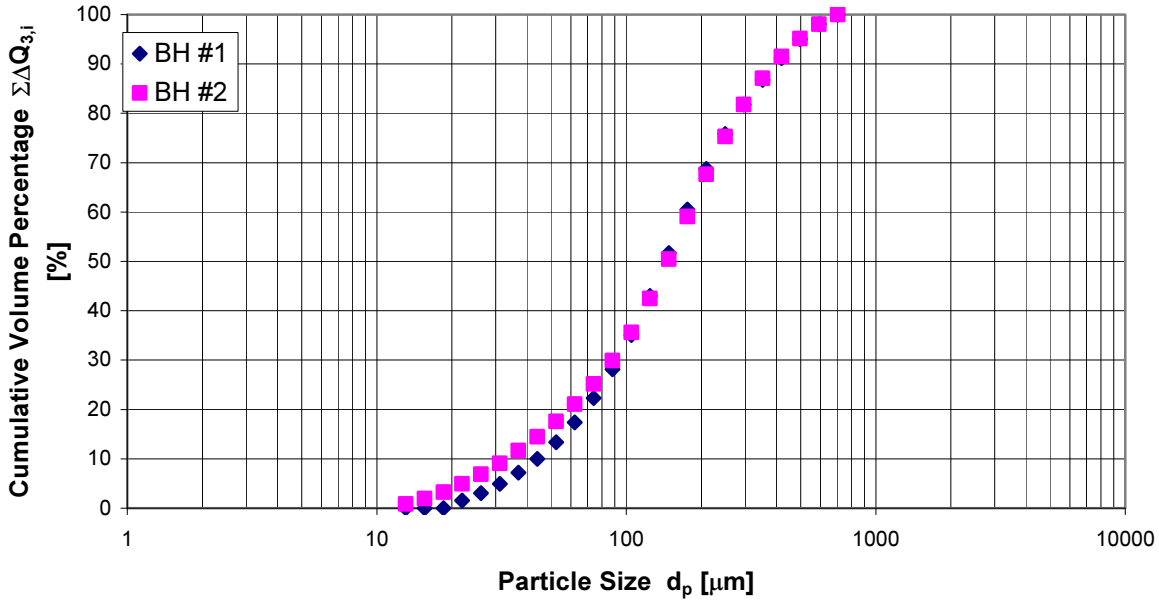

Figure 4-17: Clandeboye Dryer 2 Baghouse 1 & 2 cumulative volume particle size distributions for Milk Protein Concentrate produced on the 8th of December 2005

4.6.3. Accuracy of Particle Size Distribution Method Curve Fitting

As explained in Section 4.2.1.1 above, regression analysis is required to determine the accuracy of a fit of experimental data to a model. The fit of predicted to actual data in Figure 4-18 was typical for particle size distribution method data sets; a very good fit occurred with only a small discrepancy observed at the peak of the distribution where the actual volume percentage has a higher peak than that predicted.

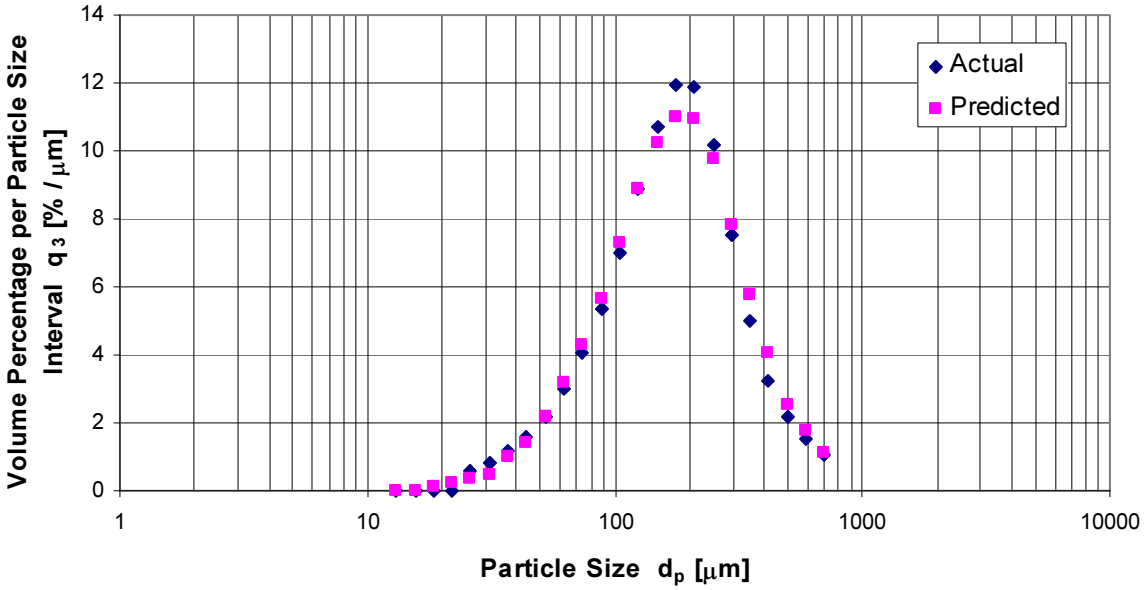

Figure 4-18: Actual and predicted sifter volume percentage particle size distribution for Whole Milk Powder from Clandeboye Dryer 2 3.45 pm 31 August 2006

The standardised residual plots, such as that of Figure 4-19, show a mild trend and the largest residuals were found, as expected, at the peak of the distribution.

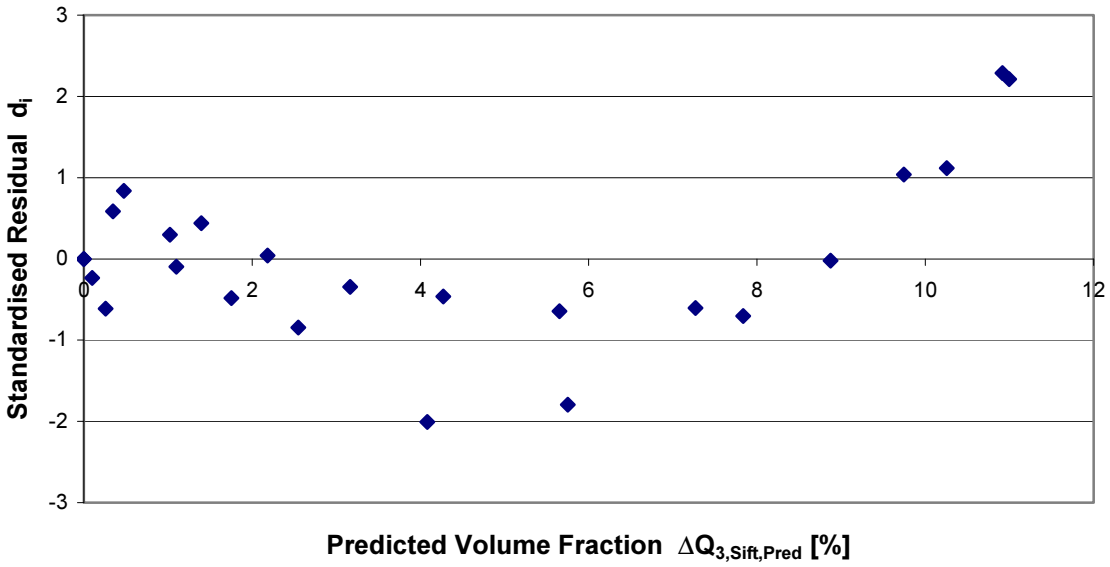

Figure 4-19: Standardised residual plot for Whole Milk Powder from Clandeboye Dryer 2 3.45 pm 31 August 2006

The normal probability plot in Figure 4-20 shows that most data points fall on the line running through the 25th and 75th percentiles. This was the case for all data sets. Therefore it can be stated that the fit is accurate and the key assumptions for fitting data in this manner have held.

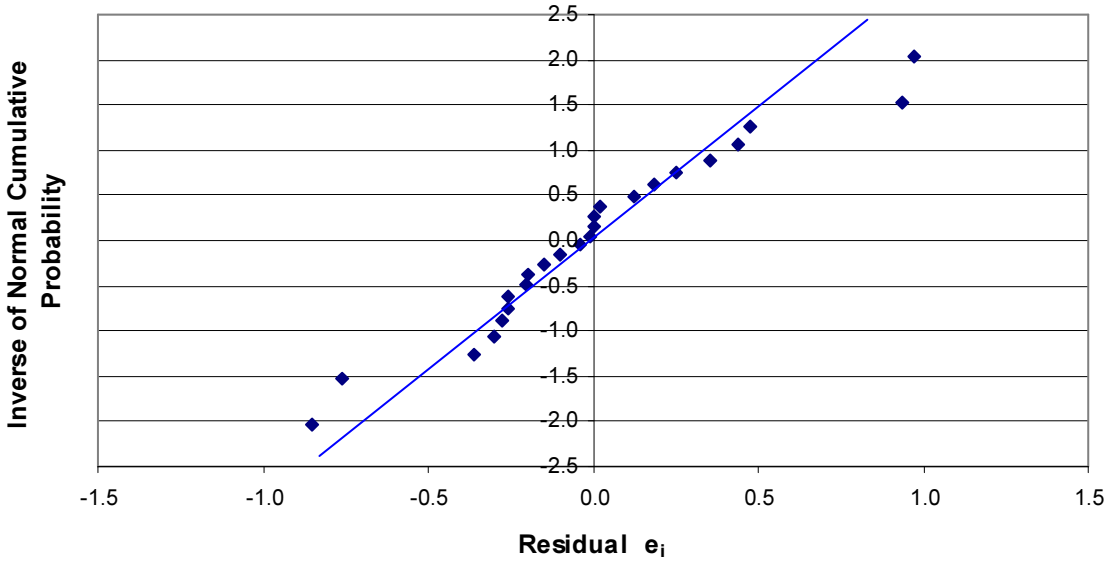

Figure 4-20: Normal probability plot for Whole Milk Powder from Clandeboye Dryer 2 3.45 pm 31 August 2006

4.7. Use of Optical Scintillation Instrument

During the CPM trial, various plant operations occurred. The CPM was used during these periods in an attempt to understand how these plant operations affected the fines loadings.

4.7.1. Evaporator Swaps

Evaporators are changed approximately every 8 hours for SMP and WMP, and 10 to 12 hours for MPC as they require a CIP. The responses of the baghouse differential pressure and fines level to the evaporator change are shown in Figures 4-21 and 4-22. These were typical for MPC; the baghouse differential pressure (Figure 4-21) would peak approximately 20 to 30 minutes after the evaporator change and a small reduction in fines level (Figure 4-22) would be observed at the time of the evaporator change.

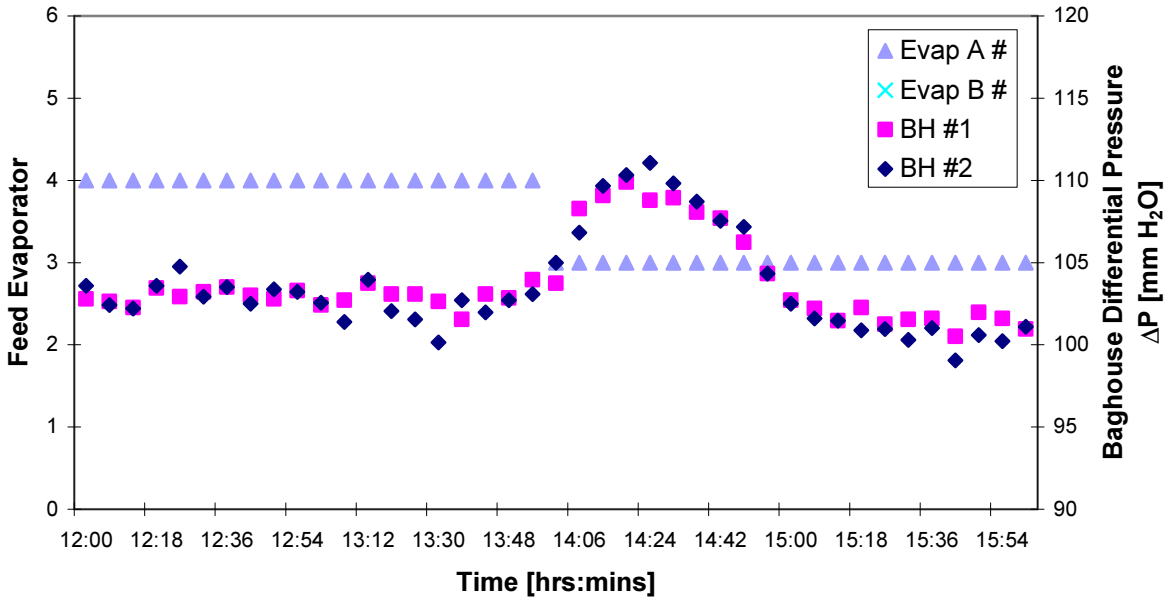

Figure 4-21: Influence of feed evaporator change on baghouse differential pressure - Clandeboye Dryer 2 Milk Protein Concentrate production 20/3/05

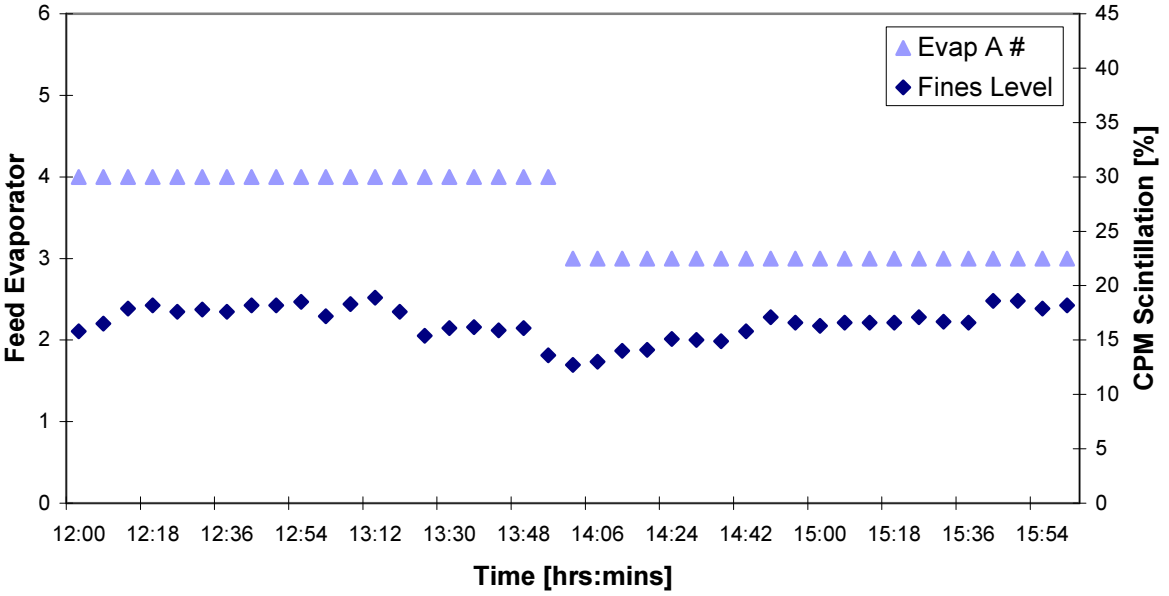

Figure 4-22: Influence of feed evaporator change on fines level - Clandeboye Dryer 2 Milk Protein Concentrate production 20/3/05

The increase in baghouse differential pressure while the fines levels reduce appears initially to be counter intuitive. Several reports (Caputo & Pelagagge, 2000; Cora & Hung, 2002; Ellenbecker & Leith, 1980; Rothwell, 1987) show that the differential pressure in a bag filter is a function of the concentration of powder in the inlet gas stream. Therefore, a reduction in

fines level should create a reduction in the baghouse differential pressure. A slight reduction in concentrate flow occurs at an evaporator swap, and hence a reduction in fines level, but a second mechanism must be occurring for the baghouse differential pressure to increase.

At the end of an evaporator run, water is used to flush the concentrate through the evaporator. Low solids are created by the dilution that occurs at the interface between the water and concentrate. However, because of the large volumes of concentrate involved, operators do not flush this low solids concentrate to drain, and oddly, have not being using the low solids recovery tank in CD2. When a new evaporator comes on line it is initially purged with water before concentrate is fed through the evaporator. Again, dilution of the concentrate occurs at the interface and again, this low solid concentrate is retained because of the large volumes involved. Therefore, during an evaporator swap, a significant amount of low solids concentrate is generated that is fed to the dryer.

It is well known (Bloore, 2002) that a reduction in concentrate flow and total solids reduces the particle size in a spray dryer. It is likely that when these smaller sized fines reach the baghouse, a more tightly packed filter cake will develop, even though there are fewer fines to form the filter cake. This more tightly packed filter cake increases the resistance to air flow and hence, increases the baghouse differential pressure. It should be noted that this hypothesis has not been tested because of the inability to perform measurements on the filter cake at the industrial scale. However, in the first instance, this hypothesis appears to be correct: the baghouse differential pressure data (Chapter 3) combined with the particle size distribution measurements for each product carried out here, appears to indicate that the differential pressure increases as the particle size decreases.

The effect shown in Figures 4-20 and 4-21 above is not so evident for SMP and WMP production. In these cases, two evaporators are used to feed the dryer so that when an evaporator swap occurs, the reduction in concentrate flow and amount of low solids concentrate produced is not as marked because of the continual supply of concentrate from a second evaporator.

4.7.2. Feed Line Swaps

Feed line swaps occur roughly every 20 hours, to allow for the feed line to be CIPed. Initially, water is used to purge the new line before concentrate is recirculated through the feed line using one of the three feed concentrate tanks. As the pressure in the new feed line increases, operators slowly open the flow to a spray nozzle of the new line and close the flow to a nozzle from the old line. When half of the spray nozzles in the new line are in production (half of the spray nozzles of the old line no longer in production), the homogenisers of the new feed line ramp up and the homogenisers in the old line ramp down. The increase in pressure in the new line allows for all bar two of the spray nozzles in the new line to be activated. Once all the spray nozzles from the old feed line have been removed from production, recirculation of concentrate through the old feed line is stopped. Water then flushes the concentrate from this line, which is returned to the concentrate feed tank.

During this feed line swap, two opportunities for dilution of the concentrate and therefore generation of low solids exist. The first is at the interface between the water filling the new feed line and the concentrate that follows the water. The second is at the interface between the concentrate coming from the old line and the water used to purge the line. However, any low solids concentrate created in both instances are buffered in the concentrate feed tank, which is usually above 50 % full during a swap, so very little change in the total solids of the concentrate being fed to the dryer occurs.

In most cases there was no apparent change in the fines level with a change in feed line. On the odd occasion as Figure 4-23 shows, a slight reduction at the change occurred, followed by a quick return to the original level within five to ten minutes.

The fines levels during a feed line swap are likely to follow the same pattern as the concentrate flow. Because recirculation takes place in the feed lines, the concentrate flow data (Figure 4-23) shows a sudden reduction for only approximately five minutes at the change then a quick return to the pre change flow. However, because the number of spray nozzles being used during a swap changes, the powder flow in the spray dryer is likely to reduce slightly, as is seen in Figure 4-23, and then returns to normal levels once all spray nozzles of the new feed line are in production. Therefore, a slight reduction in fines level could be expected.

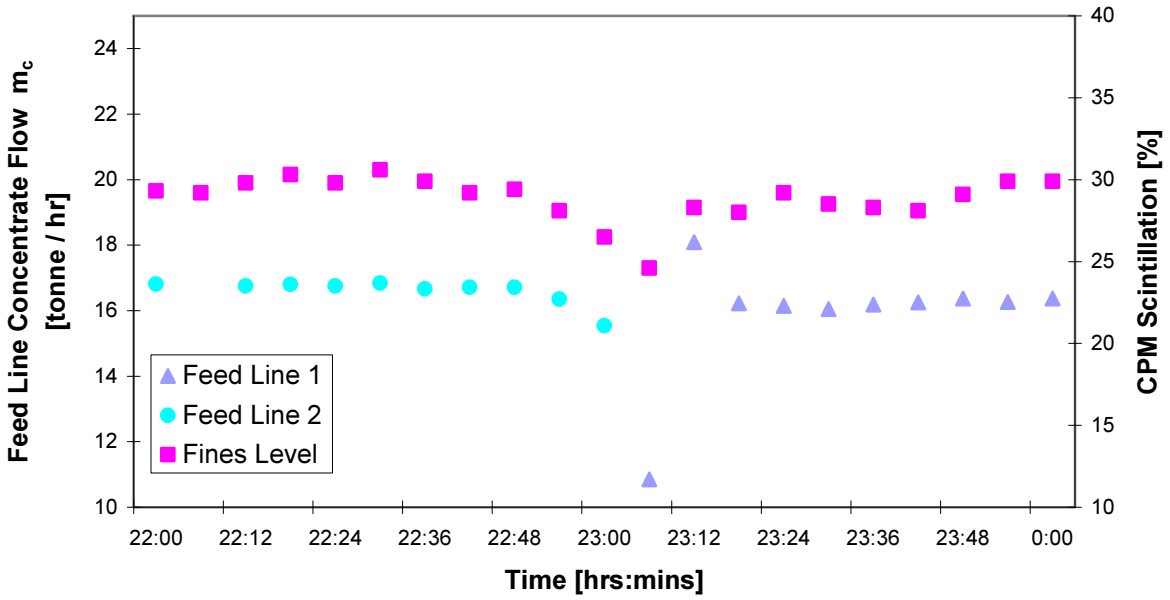

Figure 4-23: Influence of feed line change on fines level - Clandeboye Dryer 2 Skim Milk Powder production 15/3/05

As Figure 4-24 shows, a slight reduction in the baghouse differential pressure occurred at the time of feed line change. However, this reduction was always relatively small, especially when compared with the impact an evaporator swap has the on baghouse differential pressure.

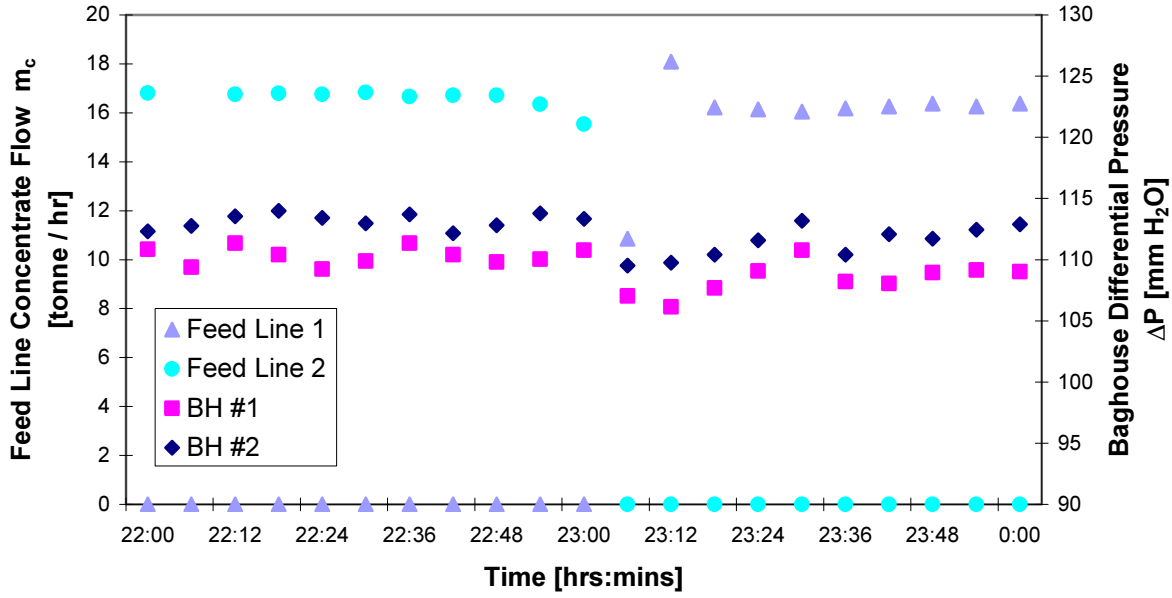

Figure 4-23: Influence of feed line change on baghouse differential pressure - Clandeboye Dryer 2 Skim Milk Powder production 15/3/05

Unlike an evaporator swap where large volumes of low solids concentrate are produced, it could be expected that a change in feed line has little impact on the baghouse differential pressure; the volumes of low solids concentrate produced is much lower because of the mixing that occurs in the concentrate feed tank. Therefore, it is likely that very little, if any change in particle size occurs, and hence the slight reduction in baghouse differential pressure is due to the small temporary decrease in concentrate flow to the dryer.

4.7.3. Changes in Atomisation Equipment

During August 2006, Fat Boy production was trialled in CD2. Over the course of three runs, the powder flow rates were increased from around 9.5 tonne / hr to 11.0 tonne / hr. For the first of the three runs, the atomisation nozzle orifice used was the Delavan SDX-3 118, which has a diameter of 3.00 mm. The final two runs used the Delavan SDX-3 125, which has a 3.20 mm diameter.

Figure 4-25 shows that during this period the fines level decreased slightly, even though the total powder flow increased. Thus it is likely that the larger orifice diameter and higher concentrate flows produced larger, denser particles which were less likely to become entrained in the outlet air stream, consequently a reduction in fines occurred.

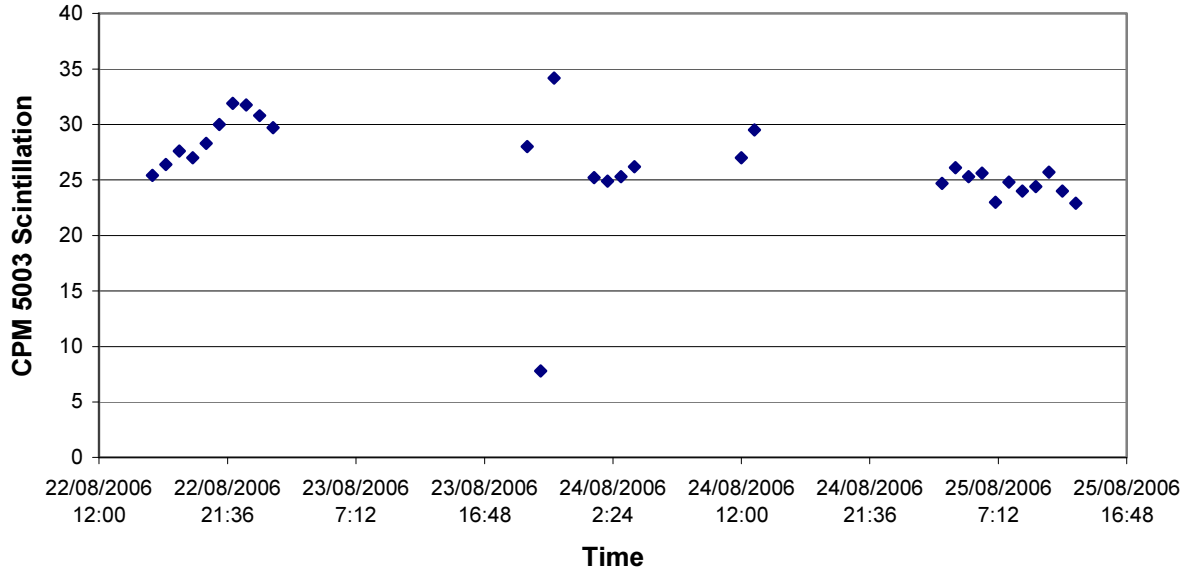

Figure 4-25: CPM 5003 scintillation for Fat Boy production in Clandeboye Dryer 2 August 2006

The fines return line pressures plotted in Figure 4-26 support this idea of a reduction in fines level; they also reduced over the three days, particularly the BH #1 fines return line, indicating fewer fines were flowing through the baghouses.

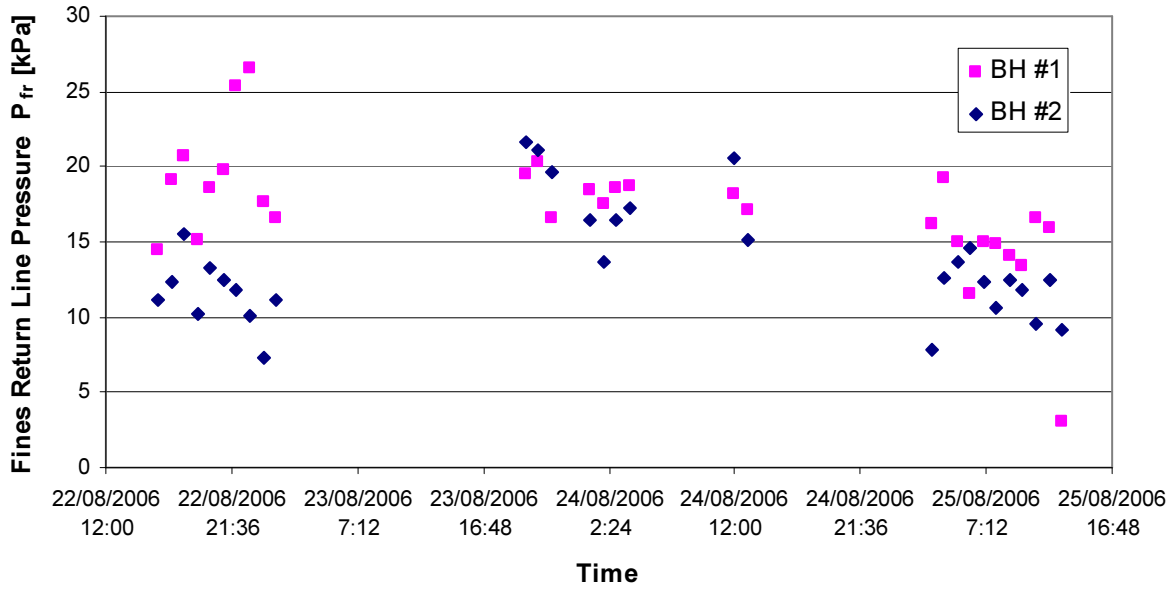

Figure 4-26: Baghouse fines return line pressures for Fat Boy production in Clandeboye Dryer 2 August 2006

The baghouse differential pressures cannot be used to support the idea of a reduction in fines levels because they increased over this period (Figure 4-27). Because the filter bags were brand new, the baghouse differential pressure increased each run because depth filtration was occurring; the pores of the new bags were slowly filling with powder that was not being removed with pulse cleaning, hence the baghouse differential pressure increased. The onset of cake filtration, characterised by a constant differential pressure, had not yet occurred.

These findings show that the CPM 5003 is sensitive and stable enough to detect changes in fines levels within a product group. Thus, a measurement technique has been found that will observe the effect of changes in atomisation equipment on fines loadings. This instrument could therefore be used to deduce the most appropriate atomisation equipment for each powder that produces the required bulk density with as few fines as possible. Reducing the fines loadings will have positive influences in the baghouses; a reduction in electricity requirements, and possibly reduced compressed air usage. This is because the baghouse

could operate at a lower differential pressure, with longer bag life, have fewer baghouse CIPs and hence, less plant downtime.

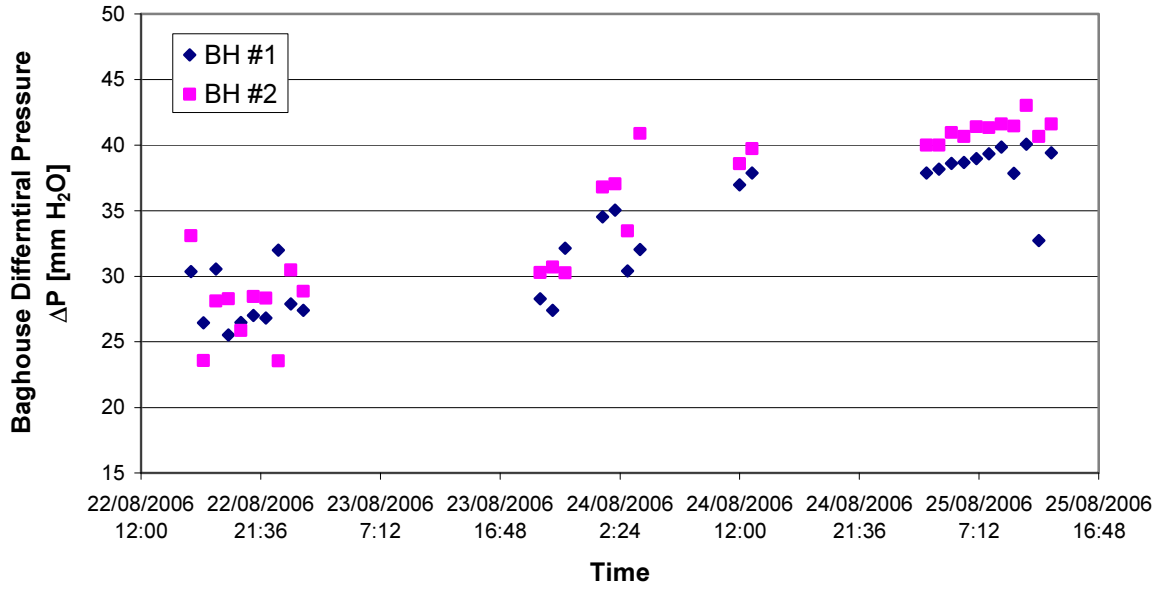

Figure 4-27: Baghouse differential pressures for Fat Boy production in Clandeboye Dryer 2 August 2006

If the instrument was to be installed permanently, it would be advantageous for the scintillation value to be converted to a fines flow and connected to the operators' screens rather than recording the data manually from the instruments' 30 day data logger. Displaying this information on the operators' screens will show during operation when changes in fines levels are occurring.

4.7.4. Suitability of the Trialled Instrument

The trialled CPM 5003 has provided very valuable information that has improved the fundamental understanding of milk powder plant washable baghouse operation. It has been shown that the CPM 5003 has the potential to be used to deduce fines levels for different products, detect changes in fines levels caused by changes in plant operating conditions and see the influence of different atomisation equipment on the fines levels. This is possibly the area for greatest potential use; the instrument could be used to deduce which set of lance angles and spray nozzle orifice sizes produce the required powder properties and limit the fines loadings on the baghouses.

A major problem deduced from the trial was that, after long periods of operation such as a season, the CPM 5003 optical lenses became covered with powder. This powder was not being removed even though the instrument was equipped with compressed air blowing across the lenses to prevent fouling. Manually resetting the window value on the control panel often enabled the instrument to resume successful operation but in some cases, the blockage of the lenses was so bad that the lenses had to be removed, this powder cleared away and the lenses reinstalled for the CPM 5003 to continue operating successfully. There is potential here for the lenses to be reinstalled out of alignment every time this task is performed. Also, if the blocked lens is not in a very accessible position, as was the case with the CPM 5003 receiver in CD2, scaffolding may be required to access the lens. Manually resetting the window value, although not a difficult task, will often be needed if the instrument is installed permanently. Therefore the potential for long term use in Fonterra plants is low because of this high and difficult maintenance requirement.

The location of the instrument is an issue; because of the short duct length, entrance and exit effects are likely to occur, which reduce the repeatability of the measurements. This is the likely reason for the scatter in the scintillation values of each product. However it appears that because the instrument is located close to the entrance of the duct, it is measuring and responding to changes in the concentration of powder entering the baghouse quite well.

The cost of the instrument is moderate compared with the other suitable instruments found. However, if both baghouses in CD2 were to be monitored, for example, then the cost will easily exceed $50,000 once an instrument in each duct is purchased, installed and the output connected to the operators' screens.

To obtain actual fines flows from the instrument, it has to be calibrated in each location it is installed in. This can be a difficult and time consuming task. However, the good fit of the calibration curve (Figure 4-15), and the fact that the extinction coefficient appears to be independent of milk powder composition, implies that no further calibration may be possible if the instrument was moved to a new location.

4.8. Pneumatic Conveying Correlations

Three different pneumatic conveying correlations were used in an attempt to calculate the fines flows through the main baghouses in CD2 for SMP, WMP and MPC.

4.8.1. Molerus and Wellman

Initially, the correlation of Molerus and Wellman (1981) was used. These relationships, represented in the form of non-dimensional groups such as the Galileo, Reynolds and Froude numbers, are applicable for all ranges of concentrations, particle size and pipe diameter for hydraulic transport.

A solver routine was used to minimise the difference between the observed and calculated pressure drop by changing L [m], the equivalent length of horizontal straight pipe. This was done separately for both fines return lines. An estimate of the fines loadings for each product was required, obtained from the particle size distribution method results, and assumed to be evenly split between the two main baghouses. The results obtained are shown in Table 4-12 below.

Table 4-12: Equivalent horizontal pipe lengths for baghouse fines return lines from Molerus and Wellman for product s produced in Clandeboye Dryer 2

Product	Baghouse #1 Fines Return Line Equivalent Length L_1 [m]	Baghouse #2 Fines Return Line Equivalent Length L_2 [m]
SMP	205	121
WMP	175	105
MPC	358	215

Table 4-12 shows that MPC has the longest equivalent pipe length, twice that of WMP and approximately one and a half times longer than SMP. It is likely that this is due to MPC having lower solids flow and also a much smaller density ratio than SMP and WMP.

The original idea was to use the calculated equivalent pipe lengths with the known air and powder properties, to deduce the change in fines flow when there are changes in the fines

return line pressures. However, as the sensitivity analysis results (Tables 4-13 and 4-14) for SMP in the BH #1 fines return line results show, the pressure drop is sensitive to changes in particle size and density. Therefore, one would not be able to attribute a change in fines return line pressure solely to a change in fines flow, as a change in particle size or density could have created the change in pressure.

Table 4-13: Sensitivity of Clandeboye Dryer 2 Baghouse #1 fines return line pneumatic conveying pressure drop to changes in skim milk powder particle size

Particle Size d_p [μm]	Particle Size as Percentage of Normal Value $d_p / d_{p,norm}$	Pressure Drop due to Solids ΔP_s [Pa]	Pressure Drop due to Solids as Percentage of Normal Value $\Delta P_s / \Delta P_{s,norm}$
99	90 %	33,463	104 %
105	95 %	32,719	102 %
110	100 %	32,040	100 %
116	105 %	31,417	98 %
121	110 %	30,844	96 %

Table 4-14: Sensitivity of Clandeboye Dryer 2 Baghouse #1 fines return line pneumatic conveying pressure drop to changes in skim milk powder particle density

Particle Density ρ_p [kg / m^3]	Particle Density as Percentage of Normal Value $\rho_p / \rho_{p,norm}$	Pressure Drop due to Solids ΔP_s [Pa]	Pressure Drop due to Solids as Percentage of Normal Value $\Delta P_s / \Delta P_{s,norm}$
1215	90 %	22,213	84 %
1283	95 %	23,402	88 %
1350	100 %	26,537	100 %
1418	105 %	28,871	109 %
1485	110 %	31,322	118 %

4.8.2. Maynard

Maynard (2006) outlines a design method for pneumatic conveying systems. Here, the pressure drop caused by solids is the sum of four terms that account for the acceleration of solids, friction of solids with the pipe walls, the vertical lifting of solids and the pressure drop caused by solids flowing around elbows. Surprisingly, this method does not account for any particle properties, other than those that are inferred by the slip velocity.

The pressure drop caused by friction between the solids and the pipe wall requires a friction factor. In this case a milk powder – stainless steel friction factor is needed. Unfortunately, no such friction factor was found in the open literature, within Fonterra or from their contractors GEA Process Engineering, or pneumatic conveying design companies Colby Powder Systems and MAC Equipment Inc. Therefore, friction factors of various authors given in Klinzing (1997) were used.

For SMP, WMP and MPC a spreadsheet was set up calculating the total pressure drop caused by solids. A solver routine was used to minimise the difference between this calculated pressure drop and the actual pressure drop caused by solids by changing the mass flow of solids. The range of fines fractions calculated using the different friction factors available in Klinzing (1997) are shown in Table 4-15 below.

Table 4-15: Range of fines fractions calculated for powders produced in Clandeboye Dryer 2 using the pneumatic conveying methodology of Maynard (2006)

	SMP	WMP	MPC
Fines Fraction X_{BH}	95 – 443 %	63 – 294 %	186 – 874 %

In all three cases, the majority of the friction factors used gave fines fractions greater than 100%. For SMP and WMP, the friction factor of van Swaail et al. (1970) gave fines fractions of less than 100 % but much larger than fines fractions determined for these products by the methods discussed above. Therefore, the friction factors used here are not accurate for milk powder and hence give unrealistic fines fractions for all three powders.

4.8.3. Williams

Williams et al. (2004) attempted to use the fines return line pressure drop in a milk powder plant to estimate the fines flow rates. SMP was fed into the transport line at a range of controlled rates and the resulting pressure drop recorded. It was concluded that complex pipework gave an experimental friction factor much higher than the literature, that fluctuation in pressure readings was due to poor delivery of fines to the rotary value and that in the future, a more reliable method is needed to estimate fines flow rates.

The procedure outlined by Williams et al. (2004) was used to estimate the fines loadings in CD2. The friction coefficients determined experimentally by Williams et al. (2004) and those from the correlation of Yang cited in Williams et al. (2004) were used.

It should be noted that the procedure of Williams et al. (2004) uses the actual length of pipe between two points, which in the plant is the length of pipe between two pressure transducers, rather than an equivalent length of straight pipe as is the case with the Molerus and Wellman (1981) correlations (Section 4.8.1). Therefore, the application to an industrial plant is severely limited because the deceleration and acceleration of solids at pipe elbows is not accounted for.

Results from the friction coefficient of Yang gave physically impossible fines flows for MPC and SMP, as in both cases a fines flow greater than the total powder flow in the chamber were calculated. For the case of WMP, a total fines flow of 8.8 tonne / hr was calculated which equates to a fines fraction of approximately 69 %. This value is much higher than the values obtained using the particle size distribution method, information provided by GEA Niro A/S and using the CPM 5003 calibration curve.

It can be summarised from the use of the procedure outlined by Williams et al. (2004) that the friction coefficient of Yang cannot be applied to milk powder systems. This work agrees with the work of Williams et al. (2004) as the actual friction coefficients are likely to be higher that the values calculated from the Yang correlation because of the high fines loadings calculated here.

Using the friction coefficient of approximately 0.05 experimentally determined by Williams et al. (2004) for SMP gave a total fines flow of 3.9 tonne / hr. This equates to a fines fraction

of approximately 30 %, much lower than the expected value based on the results in Section 4.4 above. Thus, it is likely that as Williams et al. (2004) state, the method outlined can only be used with system calibration because of complex pipework of milk powder baghouse fines return lines.

Williams et al.'s (2004) experimentally determined friction coefficient for SMP was not used for WMP and MPC in CD2 as these powders have different properties and thus will have different friction coefficients with the stainless steel pipe walls.

4.8.4. Future Development

Despite the difficulties experienced, the use of pneumatic conveying line pressure data is an attractive option for monitoring fines flows in baghouses. The method is simple and the majority of the data required is available. An area of potential future research which would greatly assist in making the use of pneumatic conveying correlations more possible is determining the friction factors for SMP, WMP and MPC with stainless steel. This could be achieved in an experiment where the pressure drop in a pipe system because of a known solids loading, pipe length, and accurately determined powder properties is measured. This information would reduce the unknowns experienced during this work and thus make it possible to use pneumatic conveying correlations to determine fines flow rates from a baghouse system.

4.9. Conclusions and Recommendations

This investigation has established a new method for determining the fines loadings in milk powder plants with washable baghouses. The method is based on a comparison of the particle size distributions of powder samples obtained from the SFB, the baghouse and the sifter and determining the percentage of sifter powder from the SFB and the baghouses.

The particle size distribution method results led to the conclusion that the fines fraction is 82% for SMP, 48 % for WMP, 96 % for MPC and 74 % for Fat Boy powder. These fines fractions are much higher than what was traditionally thought (10 % to 20 %). It can be

concluded from this work that the particle size distribution method developed is a relatively simple, but accurate method for estimating fines flows.

Because this method is sensitive enough to detect changes in Fat Boy fines fraction caused by changes in concentrate total solids, it is recommended that this method be used to determine fines fractions for any new milk powders produced by Fonterra, or to determine the fines fractions in any new milk powder plants with washable baghouses.

It is also concluded that a CPM 5003 optical scintillation instrument available from the BHA Group can be used to measure fines concentrations in milk powder plants. This was despite the powder concentrations experienced in CD2 being higher than the upper limits of the instrument stated by the supplier.

It is clear from the trial of this instrument that SMP has the highest fines level of all powders and MPC 80 the lowest. Fat Boy was shown to have the second highest level of fines among the powders. It was also concluded that WMP and MPC 70 have approximately the same level of fines. Thus it was concluded that the level of fines is a function of the total dry powder flow rate, the concentrate total solids, the powder particle size and density, and the atomisation nozzle size.

With regard to evaporator swaps it was concluded that the resulting rise and fall in baghouse differential pressure is not due to an increase in fines. It was postulated this mechanism is due to a change in powder particle size arising from a reduction in concentrate total solids and probably therefore, a reduction in concentrate viscosity in the atomisers. It is recommended that powder samples be obtained before, during and after an evaporator swap to determine if this hypothesis is correct. It is also recommended that the number of evaporator swaps during production runs be minimised to limit this undesirable increase in differential pressure. For feed line swaps, because a small reduction in baghouse differential pressure occurs with a slight change in fines level, it was concluded that because of a hypothesised constant concentrate total solids, baghouse powder properties are relatively unaffected by a feed line change.

Regarding the use of pneumatic conveying correlations to infer fines flows, it was concluded that the Molerus and Wellman (1981) correlations are sensitivity to changes in particle size

and density, as well as powder mass flow. Therefore, using this correlation to deduce and display fines flows on the operators' screens would not be accurate because changes in fines return line pressures could be a result of changes in particle size, particle density and or fines flow. A further conclusion from the pneumatic conveying correlations work was that use of the methods of Maynard (2006) and Williams (2004) were not accurate for milk powder fines return lines as the friction factors used are not accurate for milk powders.

Finally, it is recommended that laboratory experiments be conducted to experimentally determine friction factors for milk powder and stainless steel. These factors will then enable the pneumatic conveying methods of Maynard (2006) and Williams et al. (2004) to infer fines flow rates from the fines return line pressure drop data if the methods are sufficiently insensitive to changes in particle size and density.

5. Filter Bag Scanning Electron Microscopy

There is sufficient evidence to suggest that the type of filter bag has a large bearing on its performance inside a baghouse. Industry experience would also suggest that different processes during milk powder plant operation also have an influence on the performance of filter bags. A scanning electron microscopy investigation of new, used and CIPed filter bags follows.

5.1. Introduction

Filter bags are rightly or wrongly identified as the weak link in baghouse systems because faults, such as blinding or penetration, are attributed to the filter material (Rothwell, 1987). Several other authors indicate that the ability of a baghouse to have collection efficiencies around 99.99 % is strongly dependant on the filter bag (Croom, 1995; Löffler et al., 1988).

To date, all filter bags used in the main CD2 baghouses have had to be replaced well before the one to two season life time claimed by bag suppliers because the bags have either blinded or been damaged. Several different suppliers of filter bags have been used in an attempt to improve bag longevity. Filtercorp International Ltd bags, Madison bags (supplied by Canterbury Filters), and Intensiv Filter bags have all been trialled with limited success. A lot of filter bag technical information provided by these companies has been sourced from other baghouse applications, so has little relevance to the dairy industry. For this reason, a fair comparison based on this information among the different bags has not been possible.

During plant operation, bags are subjected to a variety of conditions: filtration of sticky powder during production; caustic solutions during a CIP; and hot air during bag dry-out post CIP. The result of these processes on bag performance and lifetime is not well known, particularly the influence of a CIP.

The idea behind a washable baghouse is that the CIP will rejuvenate bags to a near new state. However, industry experience suggests that CIPs are detrimental to bag quality and may even reduce bag life: a plant visit to Fonterra Edendale revealed CIPed bags vastly different to

CIPed bags from Clandeboye. Therefore, information to give a better understanding of the effect of a CIP on filter bags is valuable.

5.1.1. Aims

There were three aims for this section of work. Firstly, it was aimed to deduce if there is a difference in surface condition of bags supplied from Filtercorp International Ltd, Madison Filters and Intensiv Filter. Secondly, it was aimed to view how much powder penetration occurs in used bags. Finally, the investigation aimed to discover the effect of a CIP on the condition of the filter bags.

5.2. Assumptions

As only one of the batch of new bags, and one bag from a main baghouse have was used to produce these SEM images, it is assumed that representative samples of each has been used. With regard to the used and CIPed filter bags, it is further assumed that removal of the bags from the plant and transportation to the SEM facilities has not changed the characteristic of the bag. This is particularly poignant for the new bag as the potential for cake to be removed from the surface of the bag is high.

The data supplied for use in this is investigation is assumed to be correct. Therefore, the bag specifications provided by suppliers and the plant operating data recorded by the plant operators and Fonterra database are assumed to be accurate.

5.3. Methods

HortResearch Palmerston North generated the SEM images of the bags presented here. Three types of bags were used for this comparison. Filtercorp International Ltd, Madison Filters (courtesy of Canterbury Filter Services Ltd) and Intensiv Filter supplied the new bags. A used Madison Filter bag that had not been CIPed, was taken from CD2 in May 2004. The CIPed bags were a Madison bag removed from CD2 on June 2 2004 and a Filtercorp bag removed from ED3 at the end of the 2003/2004 season.

The samples from the new bags were taken 100 mm from the snap band at the top of the bag. Two samples were taken from each of the used and CIPed bags, 20 mm from the snap band and from the bottom of the bag (6000 mm from the snap band).

For each sample magnifications of 50, 200 and 1000 times were used. For the first two magnifications, images in the horizontal (surface of bag) and vertical plane (within the bag fabric) were generated.

5.4. Results

5.4.1. New Bags

Surface images of the three new filter bags are shown below in Figures 5-1 to 5-3. Surprisingly, each bag surface is very non-uniform, with large amounts of resin-like globules sticking to the fibres that make up the bag surface. This resin like structure on the surface of the bag was also observed by Machen (2001). The Figures below show that this surface coverage is more pronounced on the Filtercorp International Ltd (Filtercorp) and Intensiv Filter (Intensiv) bags (see Figures 5-1 and 5-3) than on the Madison Filters (Madison) bag (Figure 5-2).

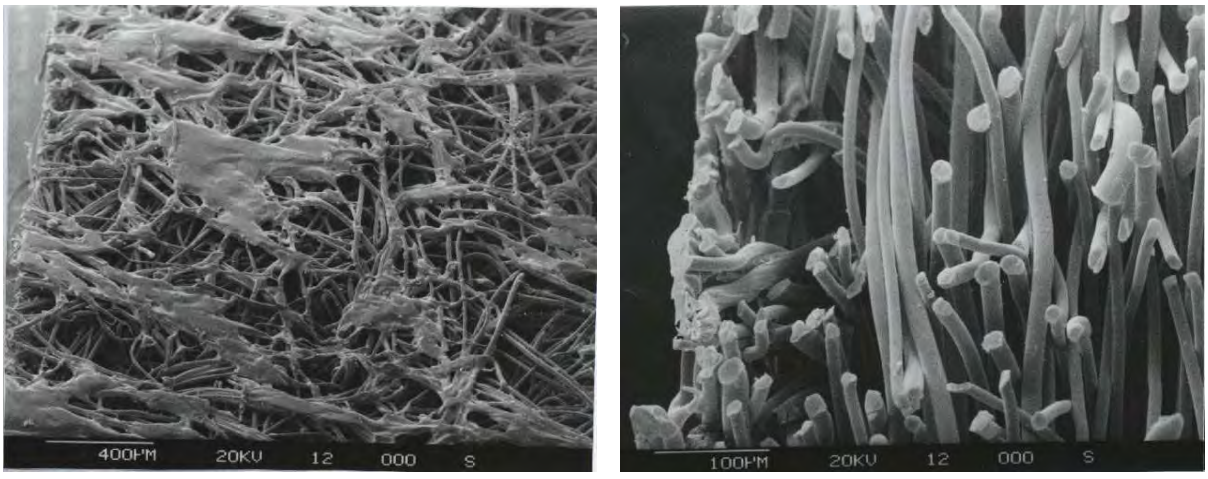

Figure 5-1: Surface and cross section of new Filtercorp FM1DRF filter bag

Observation of the three bags with the naked eye revealed that the Filtercorp and Intensiv bags are much shinier than the Madison bag and that these shiny sections occur in small random patches on all bags. These observations support two ideas. Firstly, the resin-like

globules shown above are likely to be the cause of the surface shine. It would then be expected that the Filtercorp and Intensiv bags, having more 'globules', would be shinier than the Madison bag, which is the case. Secondly, because these images are only very small sections of the filter bag, approximately 0.0001 % of the total surface area, it could be argued that the patchy nature of the three surfaces is localised. However, the naked eye observation rejects this because the shiny patches are observed over the entire surface of each bag.

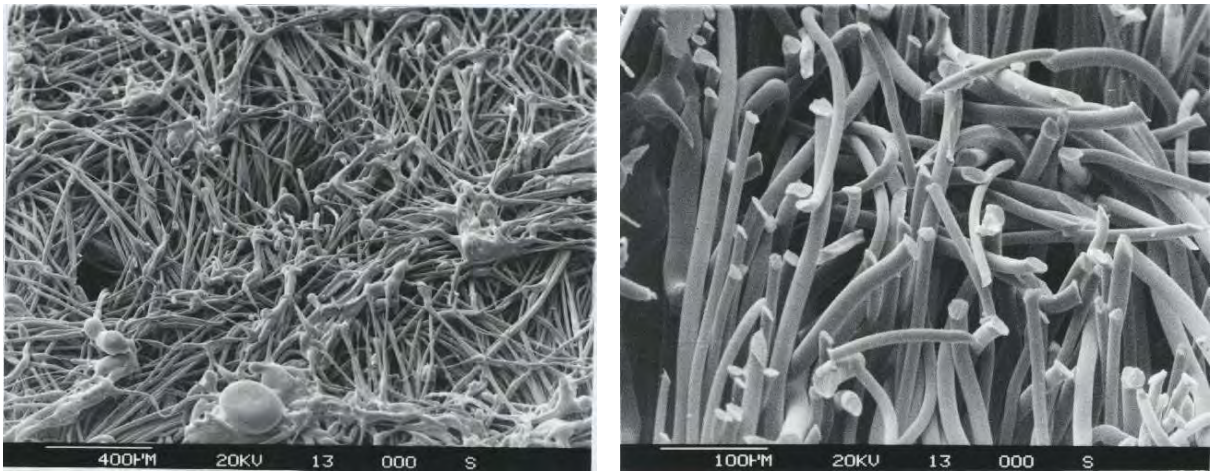

Figure 5-2: Surface and cross section of new Madison UMT5 filter bag

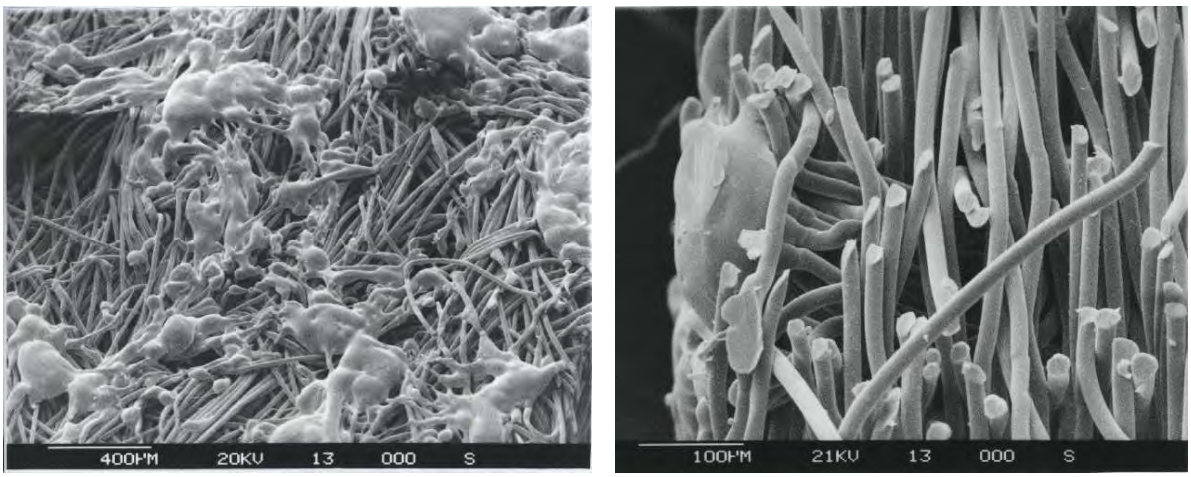

Figure 5-3: Surface and cross section of new Intensiv filter bag

The likely cause of these surface globules is the heat treatment or surface finish that is applied to each bag. Surface modifications are conducted to ensure fabric quality, modify the surface characteristics and to regulate the fabric's permeability (Lydon, 2004). Rothwell (1987) explains that needlefelts possess geometrical discontinuities due to needle punches and that surface finishes are used to make these discontinuities less obvious. Therefore, it is

interesting that the surface finish, applied to help develop a uniform surface, may actually add to the heterogeneous nature of the fabric.

Table 5-1 below lists the properties of the three bags, each of which is a polyester needlefelt bag. All data was obtained from the specification sheets published by each supplier.

Table 5-1: Properties of the filter bags viewed by Scanning Electron Microscopy

	Filtercorp FM1DRF	Madison UMT5	Intensiv PEV511
Composition	Polyester needlefelt	Polyester needlefelt	Polyester needlefelt
Surface Finish	Infa-red heat treatment	Heat set and singed	Note 1
Air Permeability [m^3 / m^2 / hr]	540 @ 125 Pa [Note 2]	960 @ 200 Pa	900 @ 200 Pa
Bag Weight [g / m^2]	550	540	500
Bag Thickness [mm]	1.9	1.7	1.5

1. Due to intellectual property issues, Intensiv Filter would not disclose the surface treatment used on their bags
2. Using linear interpolation, the permeability @ 200 Pa is 864 m^3 / m^2 / hr

The Madison bag has the highest permeability at 960 m^3 / m^2 / hr at a pressure drop of 200 Pa. This is not surprising when looking at Figures 5-1 to 5-3: the Madison bag has the least amount of surface finish, which, if is a result of calendaring, decreases bag permeability (Humphries, 1981; Lydon, 2004; Weigert and Ripperger, 1987). There is a difference in permeability between the Filtercorp and Intensiv bags, despite the similar amount of surface finish. Potentially, bag thickness is an important factor in bag permeability, hence the thicker Filtercorp bag is less permeable than the Intensiv bag. Wiryawan and Trinh (2003b) found that Filtercorp filter bags had a scrim structure supporting the needlefelt that had a much tighter weave made from a finer yarn than the Intensiv filter bags. Thus, this difference in bag structure is also a likely to cause the difference in permeability.

Since each of the bags was made from needlefelt and has the same surface area, it is not surprising that the bag weight is a function of bag thickness. The 1.9 mm thick Filtercorp bag is the heaviest of the three at 550 g / m^2. This is slightly heavier than the 1.7 mm thick Madison bag weighing 540 g / m^2, and 50 g / m^2 heavier than the 1.5 mm thick Intensiv bag.

The similarity of the bags, as shown by the properties in Table 5-1, does not explain the large difference in the cost of each bag. The Intensiv bags are the most expensive at $110 each, the Filtercorp bags are $40 each and the Madison bags are $57 each. It is surprising that the amount of needlefelt used is not the dominant factor in the bag cost, as the cheapest bag (Filtercorp) uses the most material and the most expensive bag (Intensiv) uses the least amount of material. It could be that the type of surface finish is the dominant factor in the total cost: the Intensiv bag has an undisclosed surface treatment, which is the probable reason for its expense.

5.4.2. Used Bags

Comparison of the new and used bags shows that an appreciable powder cake remains on the surface of the used bags, as shown in Figure 5-4. Very few polyester fibres can be seen in between the powder on the bag surfaces. Differences are also observed between the samples taken from the top and bottom of the bags. Samples taken 20 mm from the top of the bag collected particles much smaller in size than those from the sample taken at the bottom of the bag: Figure 5-4a shows a large amount of very fine material and a wider range of particle sizes than Figure 5-4b. Vertical separation of coarse particles could be occurring before the dirty gas reaches the top of the bag, thus only fine particles remain and are collected at the top of the bag.

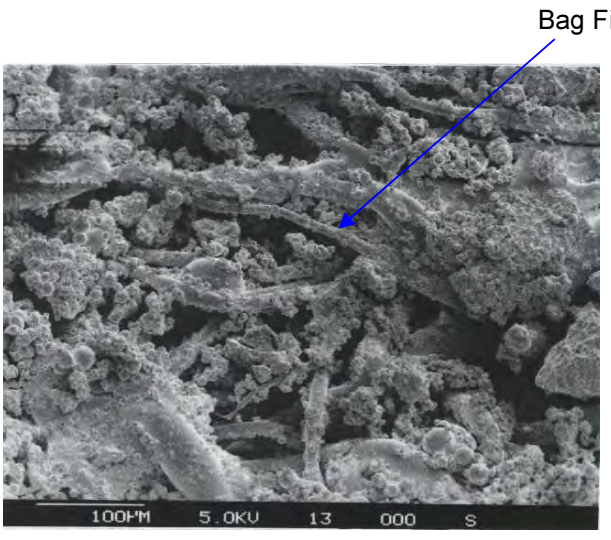

Figure 5-4a: Surface of Clandeboye Dryer 2 20 mm used bag

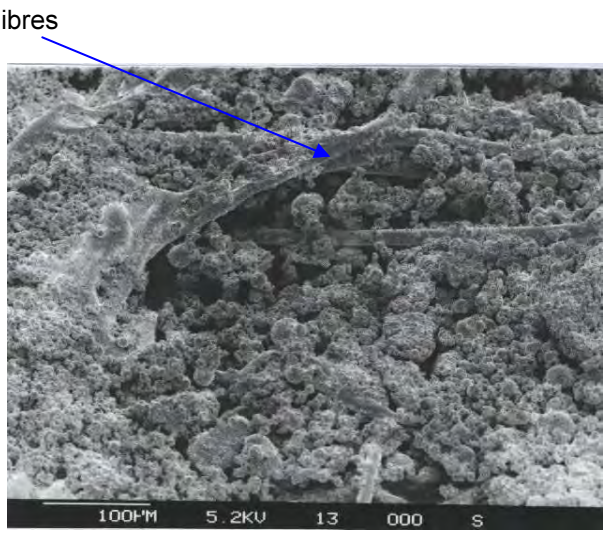

Figure 5-4b: Surface of Clandeboye Dryer 2 6000 mm used bag

The cross sectional images of the samples show that penetration of powder into the bag fabric is more pronounced at the top of the bag. As Figure 5-5 shows, a thicker layer of powder develops at the surface, and just below the surface at the top of the bag. Also, a greater presence of powder can be seen under the bag surface of this top section. There is almost no penetration in the bottom section of the bag as only a few very small particles can be seen clinging to fibres in the interior[1] of the bottom section of the bag (c.f. Figures 5-1 to 5-3).

Klingle and Löffler (1984) found from single bag experiments using a 2.5 m long polyester needlefelt bag, that before pulse cleaning, the very bottom of the bag had the highest dust density and the very top of the bag the lowest dust density. These findings conflict with those of Ellenbecker and Leith (1980) who conducted similar experiments with three 2.4 m long polyester needlefelt bags in a pilot scale baghouse. These authors found the greatest dust density to be at the top of the bags, not the bottom. Both research groups used X-ray adsorption techniques to measure the dust density inside and on the surface of the bag, thus it is surprising that such different results were obtained.

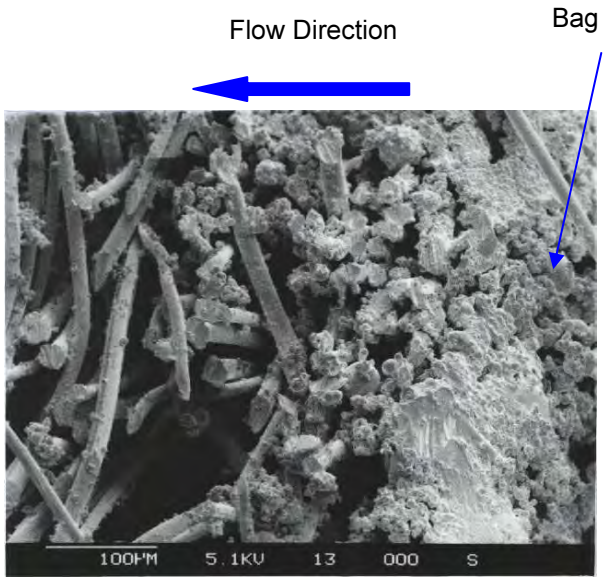

Figure 5-5a: Cross section of Clandeboye Dryer 2 20 mm used bag

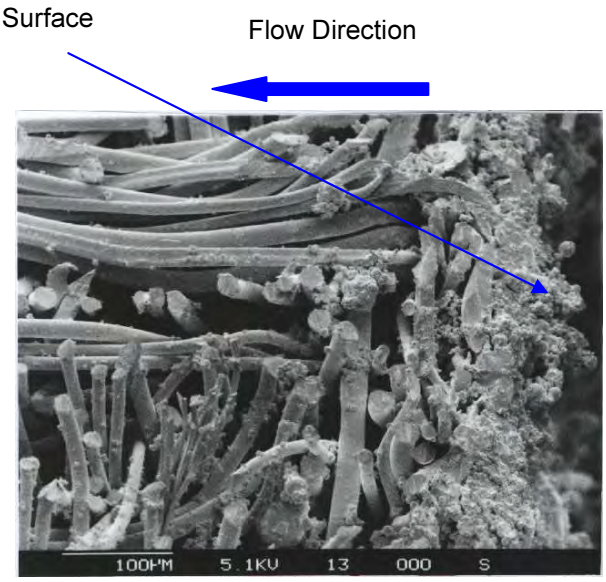

Figure 5-5b: Cross section of Clandeboye Dryer 2 6000 mm used bag

[1] The interior of the bag referred to here is defined as the area of fibres between the front surface of the bag, where filtration occurs, and the back surface on the inside of the bags. The interior is not to be confused with the inside of the bag, which refers to the open space contained within the circumference of the bag fibres.

The main reason for the different results is likely to be the inlet location for the dirty air stream. Although Ellenbecker and Leith (1980) do not state if they used a top or bottom entry baghouse, the bottom entry used by Klingle and Löffler (1984) is believed to have lead to the localised higher dust density at the bottom of the bags. A second major cause for this difference could be the type of pulse jet cleaning system used. However, neither researchers' mention the type of jet ejector, its position above the bag, the flow of compressed air nor the pulse length and frequency used for pulse cleaning.

Potentially the difference in dusts used could also have led to the different findings. Limestone was the dust used by Klingle and Löffler (1984), which has a larger average particle size than the fly ash used by Ellenbecker and Leith (1980). Although Ellenbecker and Leith (1980) used a wider range of filtration velocities, 50 to 150 mm / s compared to the 42 to 83 mm / s, because the velocities overlap, it is believed that this difference in experimental conditions is not the cause of the dissimilar findings.

Figures 5-4 and 5-5 support the findings of Klingle and Löffler (1984). Few bag fibres can be seen on the surface in Figure 5-4b as the surface is mostly covered in powder. In Figure 5-4a however, a number of bag fibres are observed, indicating a smaller powder density on the surface at the top of the bag than at the bottom. It should be noted that removal of the bags from the plant and transportation to the SEM facilities might have changed the dust densities.

With such a large dust density on the surface of the bottom of the bag, it could safely be assumed that cake filtration is occurring here, and the particles already collected within and on the bag surface collect incoming powder, causing the filter cake to grow. This assumption would not hold for the top of the bag owing to the very small dust density right at the surface. Depth filtration would be the more likely particulate collection mechanism in this section of the bag.

In terms of penetration, it would be expected that this would be more prominent in the section of the bag where depth filtration is occurring. A small surface layer of powder would not stop finer material from penetrating and then migrating into the interior of the bag. At the bottom of the bag, the large cake would collect this fine material, preventing it from penetrating into the bag interior.

Adding to the greater penetration at the top of the bag is the effectiveness of the pulse jet cleaning. Again performing single bag experiments using a 2.5 m long bag, Löffler and Sievert (1987) found that the cleaning efficiency at the very top of the bag was almost zero compared to approximately 90 % at the bottom of the bag. Negative pressures recorded in the top section of the bag when the compressed air jet initiated the bag cleaning resulted in dust and the filter bag being sucked onto the supporting cage instead of being accelerated away from the cage and the collected cake being released.

There is a difference between the pulse jet cleaning system used by Löffler and Sievert (1987) and that used in CD2. The Löffler and Sievert (1987) apparatus consisted of a compressed air pulse of 0.2 s flowing through a venturi situated at the top of the bag. The CD2 pulse system does not have a venturi, but an annulus jet located 500 mm above the bag. Each pulse is 0.25s in duration.

Fonterra Clandeboye powder plant staff have observed a build up of powder at the top of the bags (Clandeboye Milk Powder Plant Operators, 2004), suggesting that, despite the difference in pulse jet cleaning systems, the industrial bags also have a near zero cleaning efficiency in this section. Obviously, if the top of the bag is not cleaned, and the pulse jet cleaning is actually drawing more powder onto the bags, then there is greater potential for penetration to occur at the top of the bags, as is seen in the SEM images above.

5.4.3. CIPed Bags

One of the main reasons for performing a CIP on a washable baghouse is to restore the filter bags to a state as near to new as possible, thereby prolonging the bag life and reducing operating costs. However, the SEM images for the CIPed bags from the Clandeboye and Edendale factories suggest that a baghouse CIP is detrimental to the state of the filter bags and that the CIP does not rejuvenate the bags to a state as near to new as would be expected.

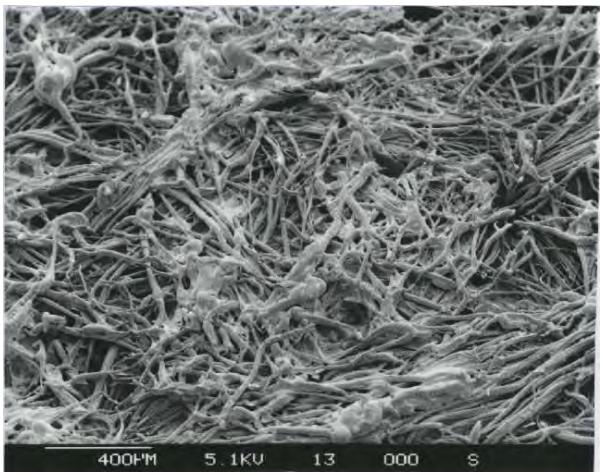

Figure 5-6a: Surface of Clandeboye Dryer 2 20 mm CIPed bag

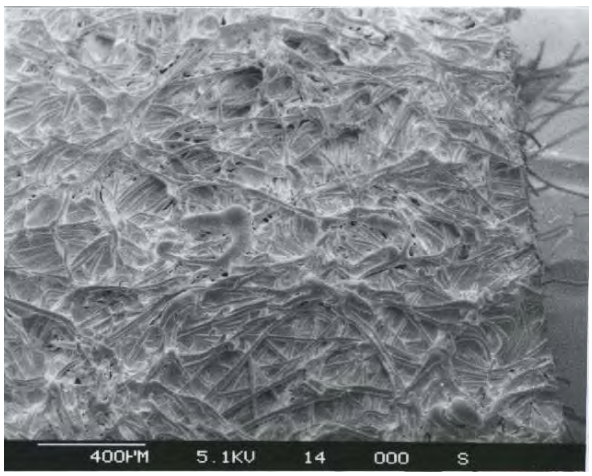

Figure 5-6b: Surface of Clandeboye Dryer 2 6000 mm CIPed bag

Figures 5-6 and 5-7 show large patches of what looks like milk powder that has not been removed from the surface of both the Clandeboye and Edendale bags during a CIP. The 6000 mm surface sample from CD2 is completely covered in this powder layer. This layer is the likely cause of the difference in feel between the soft Edendale and very rigid, sandpaper like Clandeboye bags.

From Figure 5-6b, it could be suggested that the bottom of the bag develops a larger layer of the unremoved powder due to the nature of CIP fluid application. During the CIP, liquid is sprayed on to all bags from above and only on to the side of bags in the exterior of the bag bundle. This fluid runs down the length of the bag, potentially carrying solids and forming a gel that deposits on the bottom of the bag. However, the Edendale surface images in Figure 5-7 do not show any difference in surface coverage between the top and bottom of the bag, indicating that the extensive layer in Figure 5-6b is not due to this mechanism.

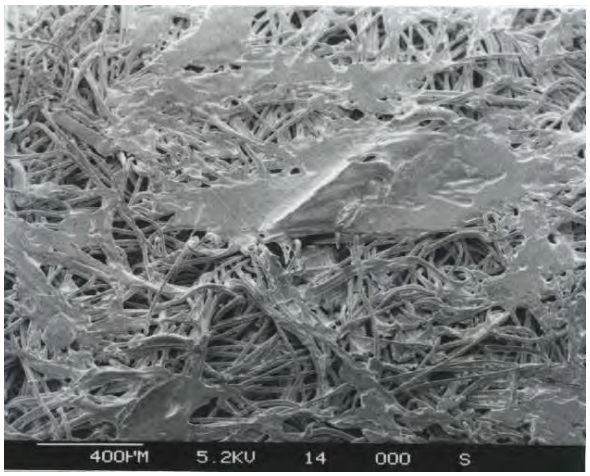

Figure 5-7a: Surface of Edendale Dryer 3 20 mm CIPed bag

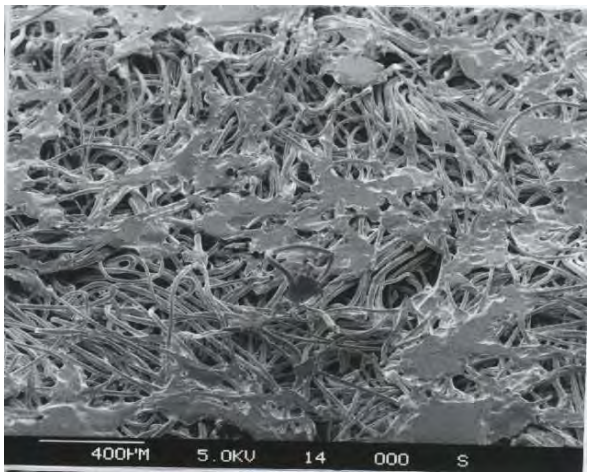

Figure 5-7b: Surface of Edendale Dryer 3 6000 mm CIPed bag

The formation of a gel layer was identified by Machen (2001) during the initial Whareroa Powder 2 washable baghouse CIPs. It was postulated that this gel layer formed because of low rinse temperatures. The images above also suggest a gel layer formed in the CD2 and ED2 washable baghouses. It is likely that the stiff CD2 bag is a result of a larger gel layer forming that was then baked when the plant was run on hot air at the end of the CIP to dry the filter bags.

Stapper et al. (1976) warned that the cleaning sequence needed to be carefully monitored because of potential bag damage: these authors observed bag deterioration after brushing the filter bags and soaking them in water. Because of this point and the large difference in state of the CD2 and ED3 bags, the performance of the individual CIP sets is called into question. The CD2 baghouse CIP had been ineffective since the plant was commissioned, hence plant management were extremely reluctant to perform a CIP. Two major factors contributed to this. Firstly, plant operators had little experience setting up and running an effective CIP. Secondly, issues with the CIP set and sequence programming meant the sequence was frequently interrupted (the CIP return pump low level switch was broken and continually stopped the pump and the sequence, and all CIP pumps stopped during hot water recirculation while waiting for the water to reach the desired temperature). It is believed that because of these interruptions, the filter bags were cleaned poorly as shown in Figure 5-6.

Production schedules could be a factor in the larger layer on the CD2 bag. The CD2 bag was removed in May 2004 after a CIP that followed a period of milk protein concentrate (MPC) production; whereas the ED3 bag was removed after a CIP that followed skim milk powder (SMP) production. MPC has approximately two and a half times the amount of protein as SMP. It is known that when protein contacts caustic solutions, such as the liquid used in the second step of the baghouse CIP, the milk powder forms a gel. Consequently, the large layer shown in Figure 5-6b could also be a result of caustic interacting with a high protein powder. If this were the case, cleaning with an enzyme based cleaner or even acid might help prevent this layer from forming.

The baked gel layer observed above could be expected to increase bag resistance and consequently increase baghouse differential pressures after the CIP. Also, it has been found that filter bag material shrinks after a CIP (Wiryawan, 2005). Bag shrinkage would reduce bag permeability and therefore increase the differential pressure. Therefore, an increase in baghouse differential pressure after a CIP could be expected. Figure 5-8 shows that even though MPC was being produced before and after the CIP, and key plant variables that influence baghouse differential pressures (dryer air flows, concentrate flows and extractor fan speeds) were constant, this was exactly what happened after the May 2004 CIP at Clandeboye: the differential pressures increased by 50 % in baghouse #1 and 70 % in baghouse #2 because the filter drag increased by 57 % in BH #1 and 76 % in BH #2.

The larger increase in filter drag, and thus a larger increase in differential pressure in BH #1 is a surprising result. Two possible explanations exist. Firstly on average, a thicker layer of powder could have remained on the BH #1 bags after the CIP because of either a more substantial original cake, or a non uniformity in washing between the baghouses. Alternatively, this greater difference could be due to the air flow bias that exists in the CD2 chamber. This bias has been shown to appear after bag replacement (and now CIPs), and decreases over time, hence no bias is obvious before the CIP.

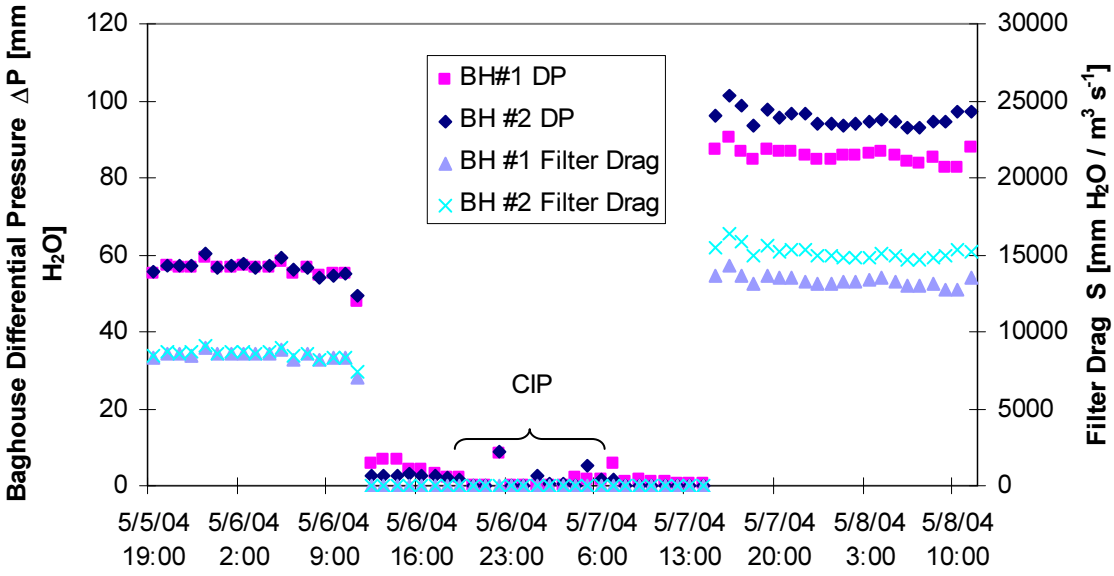

Figure 5-8: May 2004 Clandeboye Dryer 2 baghouse CIP influence on baghouse differential pressures and bag and filter drag

As mentioned above, the May 2004 CIP was performed when the CIP sequence was far from optimal for effective bag cleaning. The sequence was recommissioned at the end of the 2003/2004 season. Figure 5-9 below shows that, after the late September 2004 CIP, the baghouse differential pressure dropped significantly. Although no fan speed data is shown, to reduce the differential pressure by the observed 50 %, the fan speed would also need to be reduced by approximately 50 %. This would not occur because the fans would have to run well above 50 % to maintain the dryer chamber vacuum and draw the required volumes of air through the dryer and baghouse. Also, the production runs before and after the CIP were MPC, so it can be concluded that the reduction in differential pressure was due to an effective CIP and consequently, improvements to the CIP sequence prevented the large gel layer seen in Figure 5-6b from forming.

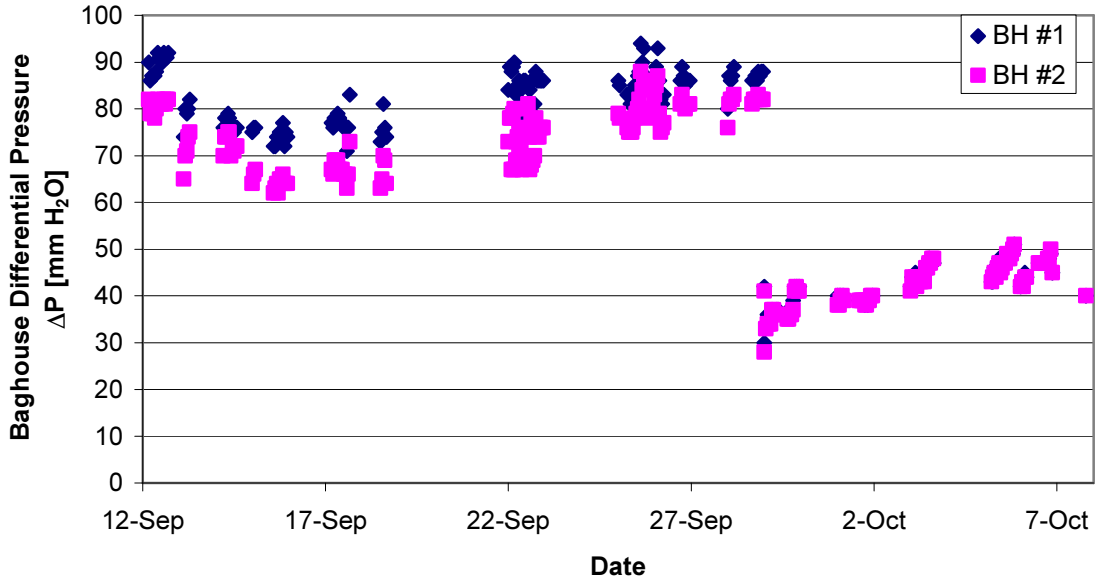

Figure 5-9: September 04 Clandeboye Dryer 2 baghouse CIP influence on baghouse differential pressures

Figure 5-7 shows that, although the Edendale CIP does a better job in removing collected powder from the surface of the bag, a reasonable amount of powder still remains on the bag surface. However, it would be expected that the CIP would reduce the differential pressure: the area of bag fibres exposed after the CIP (Figure 5-7) is much greater when compared to a used bag that has not been CIPed (Figure 5-4). Again, it is likely that the protein in the Edendale powder is creating a similar effect to that observed at Clandeboye, but because of a better CIP sequence and the lower protein concentrations, the effect is not as marked.

The baghouse CIP does clean the interior of the filter bags well. When compared with the used filter bag cross-sections in Figure 5-5, Figure 5-10 below shows that the majority of the interior particles have been removed by the CIP. It is believed that a gel layer did not develop within the bag because of the low concentrations of powder found here despite the fact that a fine mist of CIP solution was pulsed down the inside[2] of, and would have passed into the fibres of the bag.

[2] Pulsing of the CIP solution down the inside of the filter bags no longer occurs at Clandeboye

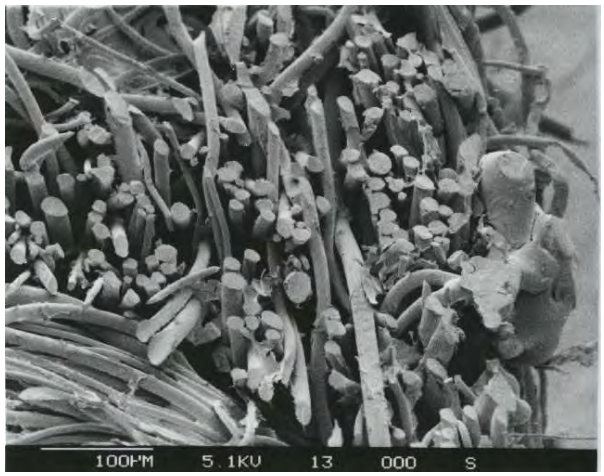

Figure 5-10: Cross section of Clandeboye Dryer 2 20 mm, CIPed bag

5.5. Conclusions

From the discussion above it can be concluded that new filter bags have non uniform surfaces. The degree of non uniformity varies among the suppliers and is believed to be a result of the surface finish applied to each bag. Further, it is the type of surface finish and the method of its application that appears to determine the bag cost. In terms of bag properties, it can be concluded that bag permeability is a function of surface finish and bag thickness.

It is clear that from a combination of plant experience and these SEM images support is found for the findings of Klingle and Löffler (1984): a zero cleaning efficiency occurs near the top of pulse-jet cleaned filter bags because a negative pressure arises due to entrainment of surrounding air on initiation of the pulse. In turn, powder is not removed from the surface of the bag and can gradually migrate to the bag interior. The generated images also lead to the conclusion that the bag surface collects and retains a large amount of powder that is not removed after long periods of operation.

Regarding the CD2 baghouse CIP, it has been demonstrated that the poor sequence encountered since the plant was commissioned was detrimental to the state of the filter bags. It appeared that a milk powder gel was formed during the CIP that was then baked during the dry out phase of the CIP. However, it can be concluded that recommissioning the CIP set at the end of the 2003/2004 season has improved the CIP so much that blinding does not result and baghouse differential pressures now decrease after the CIP. Finally, it can be concluded

that as the amount of protein in milk powders increases, so does the likelihood of the formation of the observed gel layer blinding bags during a CIP.

6. Single Cell Baghouse

A large number of fundamental unknowns were discovered throughout this project that could only be investigated further using a pilot scale baghouse. However, as no suitable laboratory scale baghouses were available in New Zealand, a single cell baghouse was installed at the University of Canterbury. This chapter details the design, construction and potential future use of this rig.

6.1. Introduction

In the original scope of this research, the pressure drop characteristics of a single bag were to be studied using a laboratory scale baghouse belonging to the Institute of Food, Nutrition and Human Health at Massey University in Palmerston North. However, access to this equipment was not granted nor was a copy of the design made available. Filtercorp International Ltd, Auckland, was contacted in an attempt to find a second existing laboratory scale baghouse. However, they had recently disposed of their piece of equipment.

Because of the large number of unknown fundamentals associated with washable baghouse operation and design in the dairy industry, and the lack of any available suitable equipment, it was decided to design and construct a single cell baghouse at the University of Canterbury. Additional funding was supplied by Fonterra as they were very keen to establish such a facility to solve a number of problems. This funding was received after a proposal found in Appendix D was submitted to the Fonterra Heat Transfer and Drying process technology team.

Interest was also shown by Canterbury Filters (Mr Darren Herd, June 2005, 33 Watts Rd, Christchurch) who saw the potential to use the rig as a bag testing facility. Orica Chemnet (Ms Trinh Greener, January 2005, Oricia Chemnet Office, Fonterra Clandeboye), was also keen to use the rig for testing different baghouse CIP chemicals. Dairy plant designers GEA Niro A/S (Mr David Bower, October 2006, 356 Church St, Auckland) also showed interest in the rig.

6.2. Design Idea

The major driver in the design of this laboratory scale baghouse was to replicate as closely as possible, the environment experienced by a bag in the Fonterra Niro Sanicip baghouses. However, because of limitations of space, there were two significant differences between the laboratory and industrial scale baghouses. Firstly, it was not possible to build a rig to hold a 6 m long bag, thus a 3 m long bag was chosen. Secondly, it was much easier to use a bottom entry rather than a tangential entry dirty air inlet.

The CD2 baghouse conditions were characterised as shown in Table 6-1 below. Using these values, the equivalent conditions for a single 3 m long bag to be housed in the CAPE single cell baghouse were determined. These resulting values are shown in column three of Table 6-1. The variation in values on both scales is due to the difference in operating conditions between SMP, WMP and MPC.

Table 6-1: Industrial and Laboratory Scale Bag Information

Parameter	Symbol	CD2	CAPE
Filtration Area	A_f [m^2]	941	1.9
Baghouse Footprint	A_{BH} [m^2]	19.6	0.1
Temperature	T_{out} [^oC]	62 – 78	62 – 78
Humidity	RH_{out} [%]	16 – 28	16 – 28
Filtration Velocity	V_f [m^3 / m^2 / min]	2.2 – 2.4	2.2 – 2.4
Volumetric Air Flow	Q_{in} [m^3 / s]	32.7 – 36.3	0.068 – 0.076
Solids Flow to Filtration Area Ratio	m_{in} / A_f [kg / hr / m^2]	2.7 – 5.7	2.7 – 5.7
Elutriation Velocity	V_e [m / s]	2.7 – 3.0	1.0 – 1.1

One key difference between the industrial and laboratory scale is the elutriation velocity. Because the single cell baghouse had an internal diameter of 360 mm, giving a bag to wall distance of 76 mm, the area around the outside of the bag is much greater than the area around the outside of a bag on the industrial scale. Consequently, the elutriation velocity on the laboratory scale is approximately one third of that on the industrial scale.

The basic process description used for the laboratory scale baghouse is shown in Figure 6-1. Hot, humid air from the laboratory scale spray dryer was fed to the base of the baghouse. Also at the base of the baghouse, powder was fed up onto the bag using a powder ejector. An extractor fan drew air through the system which was connected to the top of the baghouse. Compressed air was supplied from the laboratory mains supply through a regulator, a reservoir and solenoid valve and pulsed periodically down into the bag. Because of the small size of the clean air plenum, an ambient air reservoir was connected to the top of the baghouse to ensure it would not collapse from the entrainment of air caused by the cleaning pulse.

The CAPE Particle Technology Special Purposes Laboratory was the chosen location for two reasons. Firstly, the CAPE laboratory scale spray dryer (Mobile Minor 2000 Model E type from GEA Niro A/S, Denmark), located in this laboratory, was to be used as the humidifier for the air stream fed to the baghouse. Secondly, this laboratory had sufficient space, both vertically and horizontally, to house such a large piece of laboratory equipment.

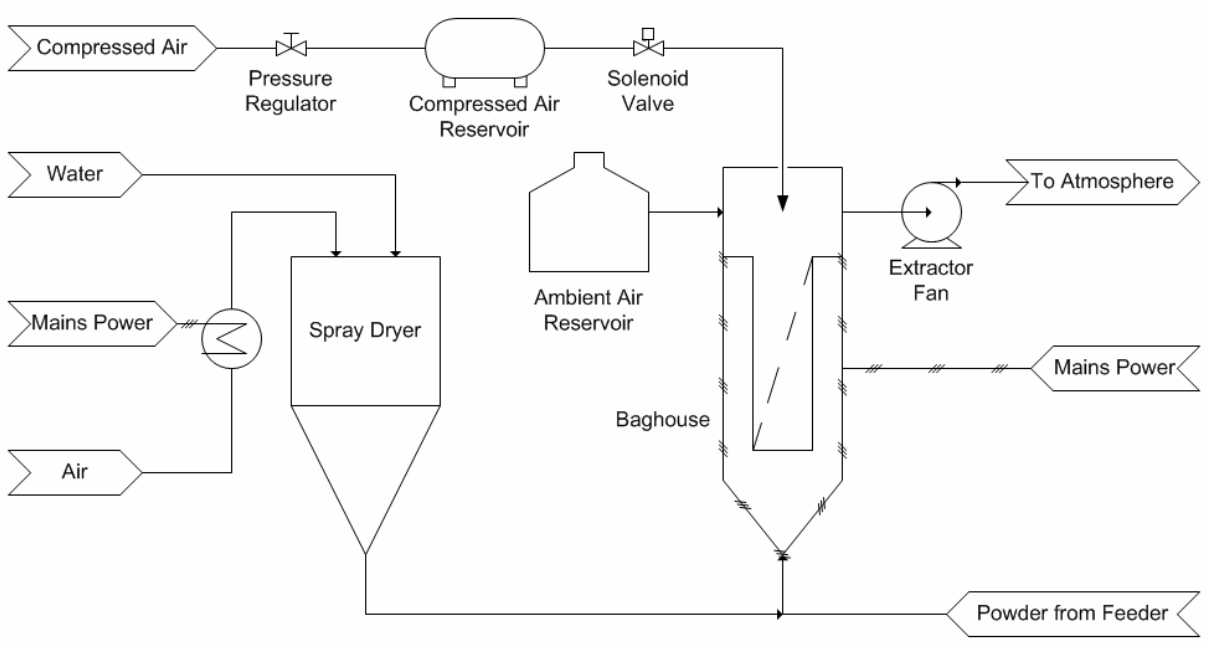

Figure 6-1: Process flow diagram of single cell baghouse

The baghouse design also took into account how best to leave a soiled filter bag in situ after a run. Leaving the filter bag in situ after a run, rather than removing the bag and hence disturbing the developed filter cake, would make possible accurate measurements and

observations of the filter cake. Therefore the shell of the baghouse was designed in such a way that it could be removed without disturbing the filter bag.

6.3. Construction

6.3.1. Structure

The structure was designed to fit against the alcove in the southern wall of the Particle Technology laboratory. The section of the structure holding the baghouse had to be located beneath the highest point of the laboratory so that the 3 m long bag support cage could be removed from the top of the baghouse. Therefore, the structure design had to account for the change in ceiling height at this location.

One slight difficulty with this location was the services pipe work running around the side of the laboratory between 3.3 and 4.6 m above the floor. This meant that the structure had to have a clear space at this location to avoid these service pipes. Other clear spaces were required on the western face at the 3.3 m level and the southern face at the 2.0, 3.3, 4.6 and 5.5 m levels to go around the other services and electrical conduits running around the wall of the laboratory.

As Figure 6-2 shows, the structure consisted of two sections. The first had a rectangular footprint that would sit up against the two walls. The second had a square footprint attached to the eastern edge of the northern face of the rectangular section. This is where the baghouse would hang. Two landings were included at the 2.0 m and 4.6 m levels. These landings gave access to the top of the baghouse as well as the majority of the bag hanging in situ.

The structure was made from 3 mm thick 50 by 50 Rolled Hollow Sections. Adjustable feet were installed at the base of the seven members contacting the ground. The two landings were made from galvanised grating. Access to these landings was achieved via 5.4 m and 3.0m single pole ladders attached to the eastern and northern face of the structure respectively. Both ladders and mounting brackets were obtained from R&S Trade Centre, Christchurch. Because the upper landing was lower than 6.0 m above the ground, the ladder to this landing did not require a ladder enclosure. At the edges of the two landings, the

structure was anchored into the concrete block southern wall of the laboratory using Dynabolts.

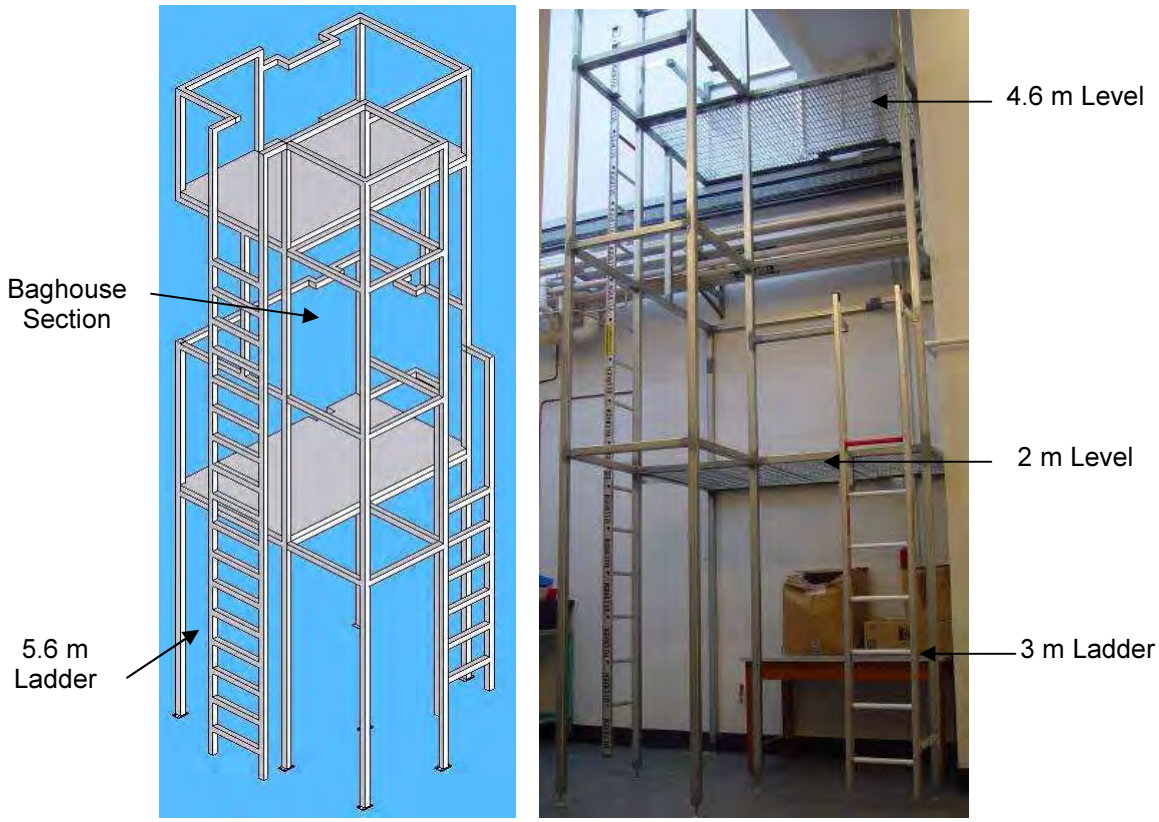

Figure 6-2: Solidworks drawing and installed baghouse structure in the Particle Technology laboratory

The structural design was checked by Mr Kieran McCall of Lewis Bradford Consulting Engineers Ltd, Christchurch. The structure was constructed and installed by Canterbury Metal Work Ltd, Christchurch.

Once installed, CAPE mechanical workshop technician Mr Frank Weerts welded 5mm GMS50 woven wire mesh, obtained from Advanced Engineering Group Ltd, Christchurch, across three vertical sections of the structure for safety reasons. Mr Weerts also installed two PA300A MAHO1000 electric hoists supplied by Topmaq, Christchurch (Figure 6-3). These hoists had a combined rating of 300 kg and were used to lift and lower Sections A to D of the baghouse shell (see section 6.3.2), a maximum load of approximately 120 kg. With these sections removed, access to the bag in situ was possible.

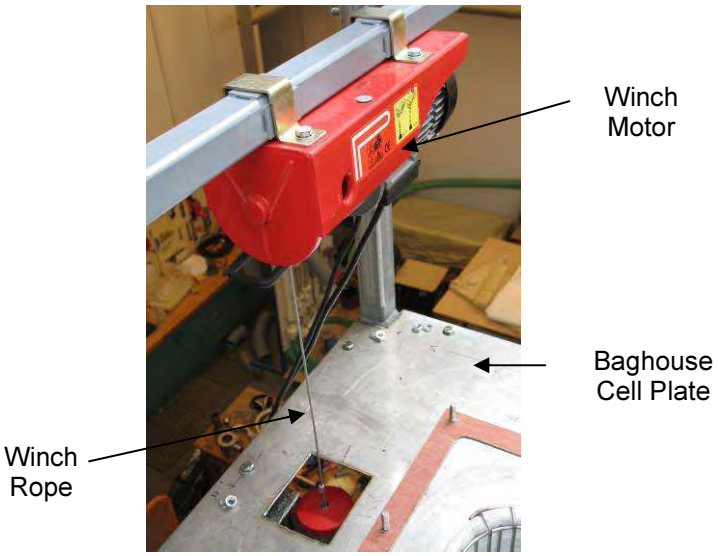

Figure 6-3: Western side electric hoist installed above the cell plate of the single cell baghouse

6.3.2. Baghouse Shell

The baghouse shell shown in Figure 6-4 consisted of a hopper (Section A), three cylindrical sections (B – D) and a fourth cylindrical section containing the cell plate (Section E). Two rectangular sections (F and G) and a 5 mm thick rectangular plate made up the clean air plenum. Each circular section was made from 2 mm thick stainless steel but the rectangular sections were made from 3 mm thick stainless steel.

Sections A-B, B-C, C-D and D-E were linked using 5 mm thick, 35 mm circular flanges. Both Sections F and G had 5 mm thick, 35 mm rectangular flanges top and bottom. The flanges were sealed by 3 mm thick CA fibre gaskets, supplied by Shuk Engineering Distributors Ltd, Christchurch. The flanges were bolted together with six 10 mm bolts evenly distributed around the flange.

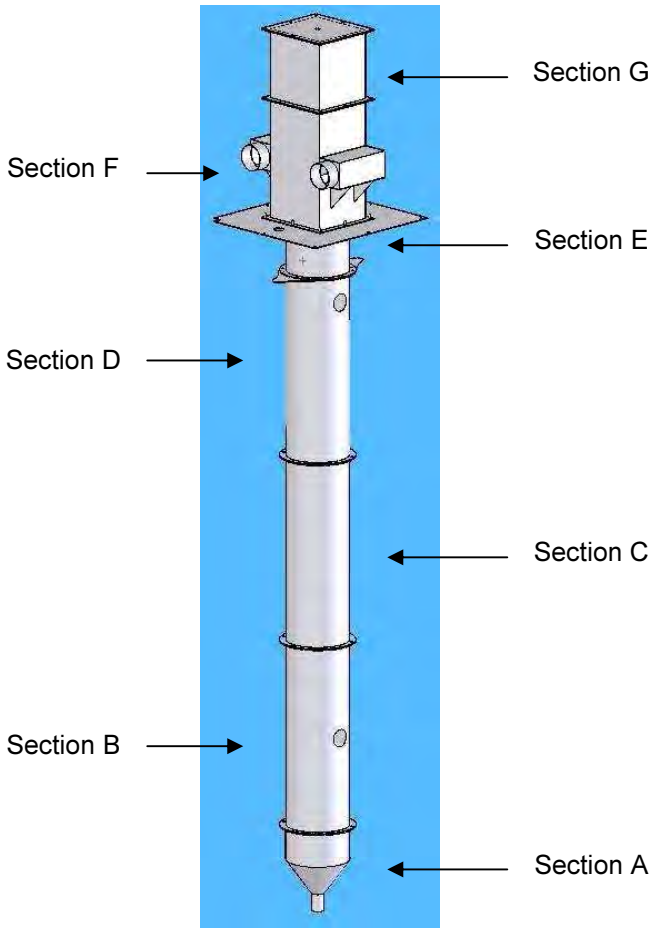

Figure 6-4: Solidworks drawing of the single cell baghouse shell

The baghouse sections and the entrained air supply reservoir were fabricated by Priest Sheetmetal and Plate Ltd, Christchurch. CAPE mechanical technician Mr Frank Weerts, and Mr Richard Snoek, a 2006/2007 Fonterra summer student, installed the majority of the remaining parts of the baghouse.

Three pieces were assembled to complete Section A shown in Figure 6-5. Initially, the hopper section was made. This piece comprised a 5 mm thick, 35 mm flange at the top, a 195 mm length of the 360 mm ID cylindrical section, a 200 mm high hopper with wall angles of 50^{o} and a 100 mm length of a 70 mm ID cylindrical section. Finally, 95 mm from the base of the 70 mm ID inlet pipe, a 5 mm thick, 6" circular flange was welded to the outside of this section. This flange had six holes and a rubber gasket to seal when the assembly below was attached.

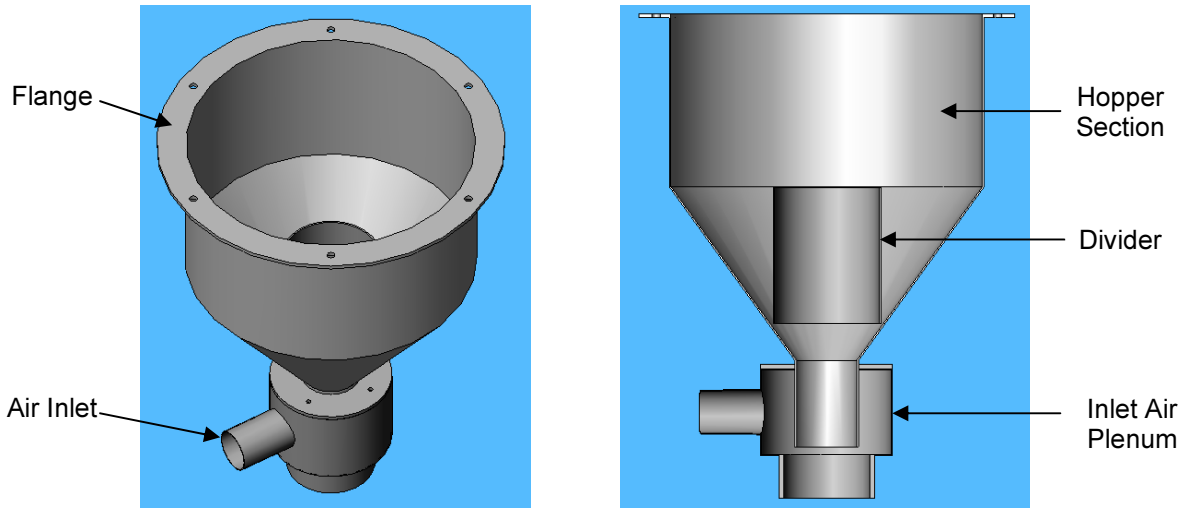

Figure 6-5: Solidworks isometric and section drawings of the single cell baghouse hopper assembly

The second piece of the assembly was a 156 mm length of 121 mm ID 2 mm thick stainless steel pipe. This pipe was designed to divide the powder falling into the hopper from the humid air and powder flowing up this pipe from below. It was envisaged that powder falling off the bag would be collected between the outside of this pipe and the hopper walls. This collected powder could be weighed and compared with the known amount of powder fed to the column to give an estimate of the residual powder on the bag.

The dimensions of the divider were such that the top of the divider was horizontally in line with the top of the angled section of the hopper. The pipe was fixed in place with two support rods welded to the hopper walls and the side of the pipe. A seal was created between the internal face of the hopper and the bottom edge of the pipe by gluing a strip of Styrofoam around the contact area and filling any gaps with RTV.

The third piece of this assembly was the inlet air plenum. This comprised a 70 mm length of 51 mm OD stainless steel pipe entering radially into the middle of a 100 mm high 6" circular section. The top of this section was covered with a 5 mm thick plate that had a 94 mm OD hole in the centre and six 5 mm threaded holes. These threaded holes enabled this third piece of Section A to be bolted onto the 6" flange of the hopper section. At the base of this third piece, a second 5 mm thick plate was welded with a 110 mm central hole. Welded into this hole was a 50 mm length of 110 mm OD stainless steel pipe. The bottom 28 mm of this pipe

was threaded so the powder ejector unit could be screwed onto the bottom of this section, sealing it.

Sections B – D were each 360 mm ID by 1005 mm high cylindrical sections including flanges at each end of the cylinder. Two sets of sight glasses were fixed to the middle of Section B and near the top of Section D (Figure 6-6). To house the inspection ports, two 101 mm holes were cut into the side of the shell. A 60 mm length of 101 mm OD stainless steel pipe was welded into the cut holes. On the end of the stainless steel pipe, a 30 mm, 5 mm thick circular flange was welded. On each flange a rubber gasket was placed between the flange and the 5 mm thick, 161 mm diameter Perspex cover. These site glasses would enable the bag movement at the base of the bag and any build up of powder around the top of the bag to be viewed.

The top flange of Section D was almost elliptical in shape. It consisted of a 35 mm, 5 mm thick circular flange with six 10 mm bolt holes but also had two additional pieces on the eastern and western sides (Figure 6-6). These additional pieces were a 65 mm circle located 309 mm from the centre of the section joined to the circular flange with two arcs. In the centre of each additional piece, a 35 mm diameter hole was drilled, through which the hooks of the hoists would be located. Each additional piece was supported by a 3 mm thick, 90 mm long by 40 mm wide gusset welded to the flange and the cylindrical part of the section.

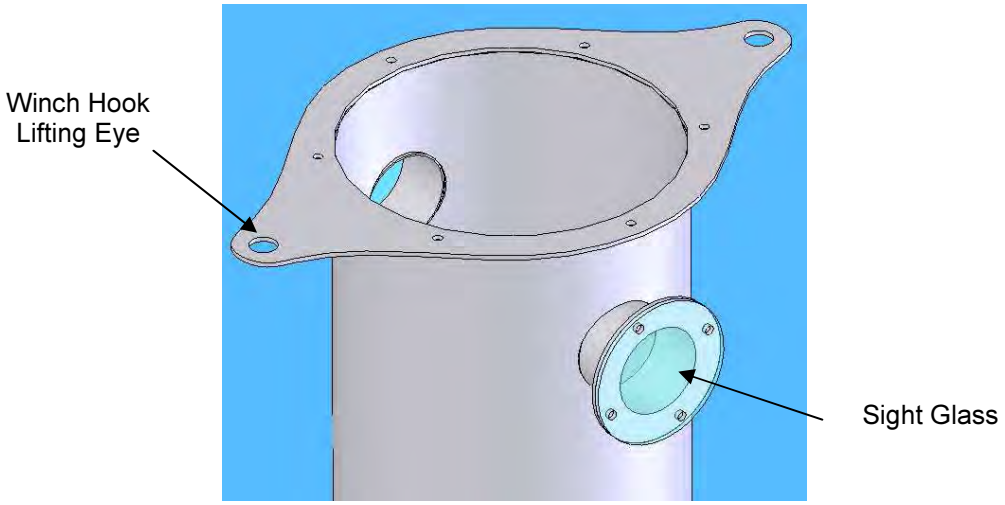

Figure 6-6: Solidworks drawing of the top flange and holes for the inspection ports of Section D of the single cell baghouse shell

Section E (Figure 6-4) consisted of a circular flange at the bottom, a 290 mm high cylindrical section and the cell plate acting as the top flange. Two 3 mm thick, 200 mm long by 250 mm wide support gussets were welded to the cell plate and the side of the cylindrical section.

The cell plate was a 900 by 800 mm rectangular plate, 5 mm thick. Two 50 by 50 mm corners were cut out on the northern edge so the plate could fit around the RHS members of the structure at the 5.5 m level. In the centre of the cell plate, a 208 mm hole was cut out to fit the filter bag. Two 100 by 120 mm rectangles were cut out of the plate centred approximately 420 mm from the northern edge and 135 mm from the eastern and western edges of the cell plate respectively. These holes enabled the hooks and guide bobble of each hoist to pass down from the hoists mounted above.

The cell plate had eight 10 mm bolts facing upward welded in a rectangular pattern around the centre of the cell plate. These bolts enabled the bottom flange of Section F to be bolted down onto the cell plate. The cell plate itself was fixed with three bolts into each of the four RHS member supports of the structure below using 10 mm bolts.

The two rectangular sections that made up the clean air plenum (Figure 6-7) had inside dimensions of 364 by 395 mm. Sections F and G were 700 and 405 mm high respectively including the flanges. A 5 mm thick, 434 by 465 mm stainless steel plate formed the lid that sat on top of Section G. Again, 3 mm thick CA fibre gaskets from Shuk Engineering Distributors Ltd, Christchurch, were used to seal the flanges.

On the northern and southern faces of Section F, a 50 mm high by 430 mm wide slit was cut 325 mm from the base of the flange. Over the outside of each slit, a rectangular air supply box (364 mm long by 177 mm high by 155 mm wide) made from 3 mm stainless steel was welded. Two 155 mm wide by 155 mm long support gussets were welded to the base of the air box and to the side of Section F. A 6” hose barb was welded onto the western end of each (Figure 6-7) so the hosing from the entrained air reservoir could be connected.

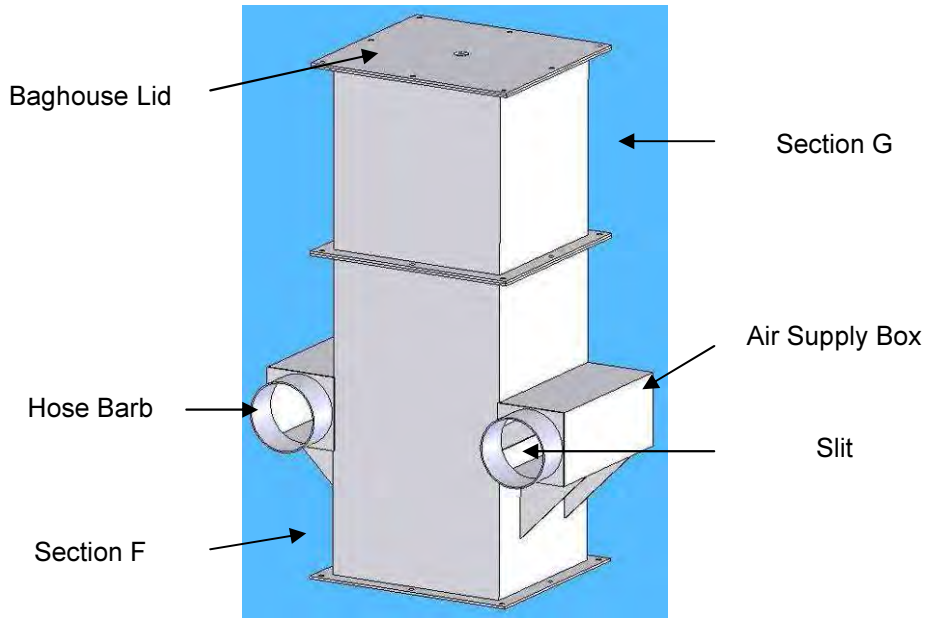

Figure 6-7: Solidworks drawing of Section E and F along with the lid that made up the clean air plenum of the single cell baghouse shell

During pulse cleaning of compressed air in a baghouse, a significant amount of surrounding stagnant air is entrained. The entrained volume for each pulse was estimated to be 139 L, which is almost the volume of the clean air plenum (156 L). Therefore, a 595 L entrained air reservoir was attached to the clean air plenum using two 6" Volcano ducting hoses supplied by HCD Flow Technology, Christchurch (Figure 6-8). The air in this reservoir ensured that the reduction in pressure inside the clean air plenum caused by the pulse and entrainment of stagnant air, did not create a significant vacuum that would alter the action of the pulsed ejector from that in the industrial size baghouse. This also prevented any chance of collapse of the clean air plenum. The reservoir, made from 3 mm thick stainless steel, was a 700 by 1000 by 850 rectangular stainless steel box with two 6" hose barbs fixed in the middle of the front panel.

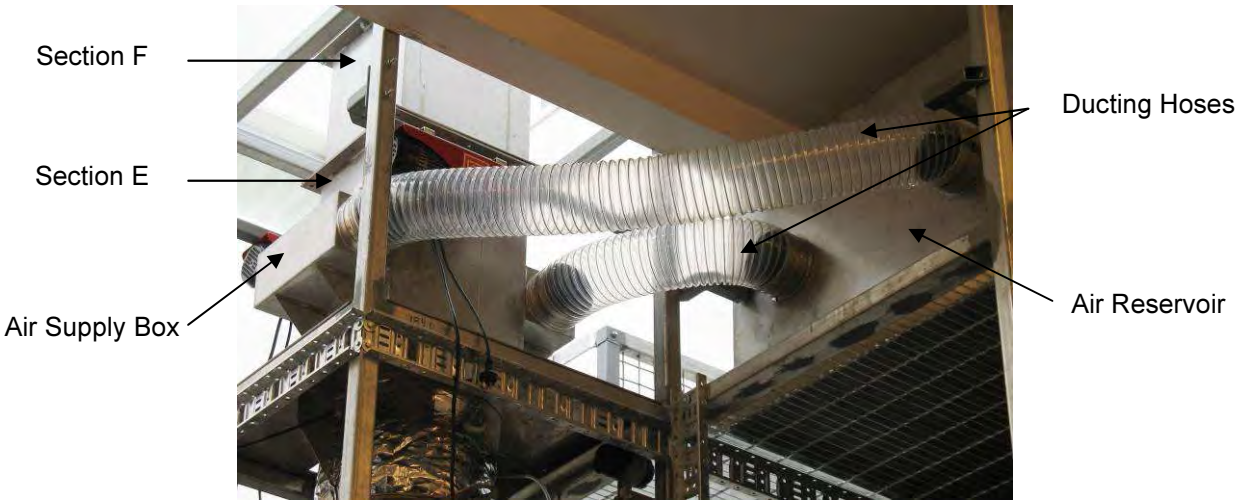

Figure 6-8: Ducting linking the entrained air reservoir to Section F

6.3.3. Instrumentation & Pipe work

The GEA Niro A/S laboratory scale Mobile Minor 2000 Model E type spray dryer was used to supply the humid air to the baghouse. The usual cyclone and associated pipe work on the dryer was removed to reduce the overall system pressure drop. A different 50.8 mm stainless steel outlet air pipe was made so that it could easily be removed from the dryer by undoing the RJT coupling. The pipe was 450 mm in length and contained a tap for the dryer outlet air thermocouple 100 mm from the end of the pipe. At the end of the outlet pipe a 50.8 mm to 76.2 mm stainless steel expansion (supplied by Steel and Tube, Christchurch) was welded.

A 2 m length of 75 mm OD Emair rubber hosing supplied by HCD Flow Technology, Christchurch, was used to connect the spray dryer outlet to the baghouse inlet. At the baghouse entry point, this tubing fitted onto a 76.2 mm to 50.8 mm stainless steel reducer also supplied by Steel and Tube, Christchurch. Hose clamps were installed over the tubing at both ends to prevent it from coming off the stainless steel fittings.

To measure air temperature and humidity at the baghouse entry, an 11 mm diameter hole was made in the stainless steel pipe of the inlet air plenum. This hole allowed the handheld Vaisala HM34C Pocket Size Relative Humidity Meter (Vaisala, Finland) to be inserted into the air stream to carry out this measurement. When not in use, this hole was covered with tape (Figure 6-9), to prevent cooling of the inlet air stream.

The powder ejector (Figure 6-9) was screwed onto the bottom of Section A. The length of the ejector meant that its downstream tip was located flush with the bottom of the 6" section of the inlet air plenum. Powder was fed into the injector feed pipe using a vibrating hopper (VFB2 type from Vibco Equipment Ltd, Te Kuiti). Compressed air to drive the ejector was obtained from the laboratory mains supply.

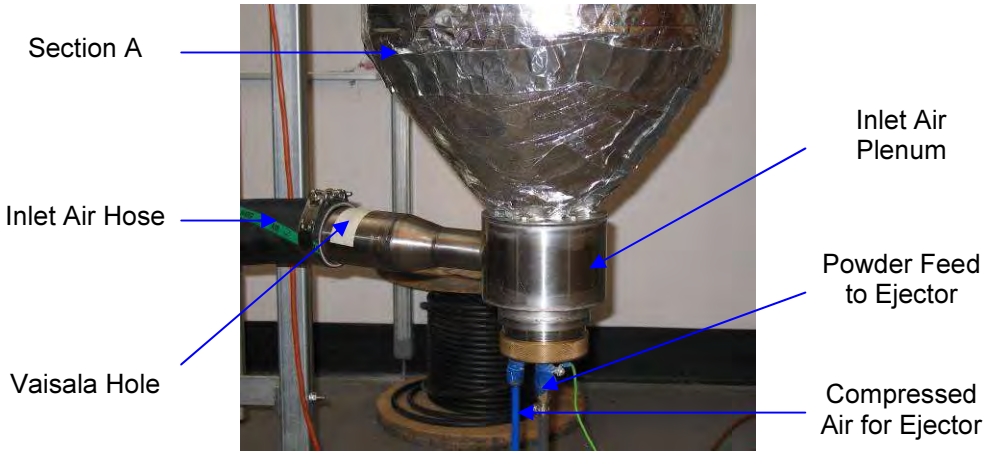

Figure 6-9: Powder ejector used at the base of the single cell baghouse

It was assumed that the jet from the powder ejector would behave as a turbulent circular jet with a total expansion angle of 15°. To check that a diverging plug was not required, the jet profile from its entry point at the base of the baghouse was plotted, along with the dimensions of the baghouse wall and position of the filter bag. As seen in Figure 6-10, the total jet diameter is initially 10 mm at the ejector and does not contact any part of Section A. The jet expands to contact the walls of the baghouse approximately 1350 mm from the ejector. This point is some 200 mm above the bottom of the bag, therefore it appeared that there was no need for a diverging plug to increase the angle of the jet.

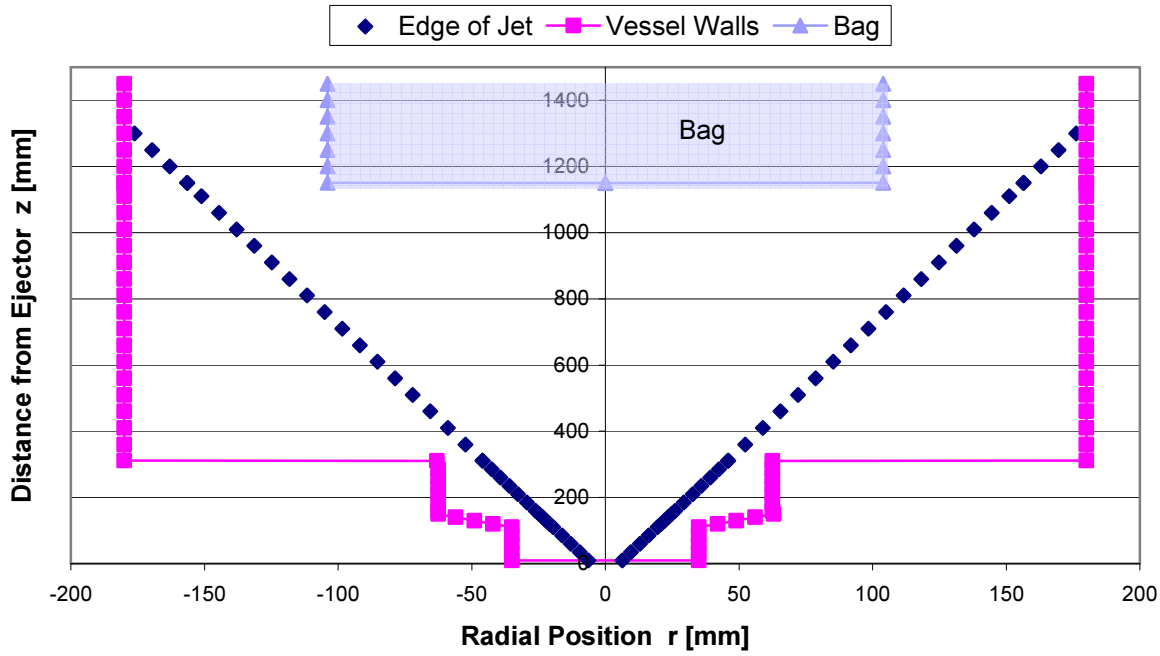

Figure 6-10: Edge of powder ejector jet inside the baghouse from the ejector inlet

The vibrating hopper shown in Figure 6-11 was a VFB2 type from Vibco Equipment Ltd, Te Kuiti. Powder flowed from the vibrating hopper, down the feed chute and through the clear plastic tubing to the powder ejector.

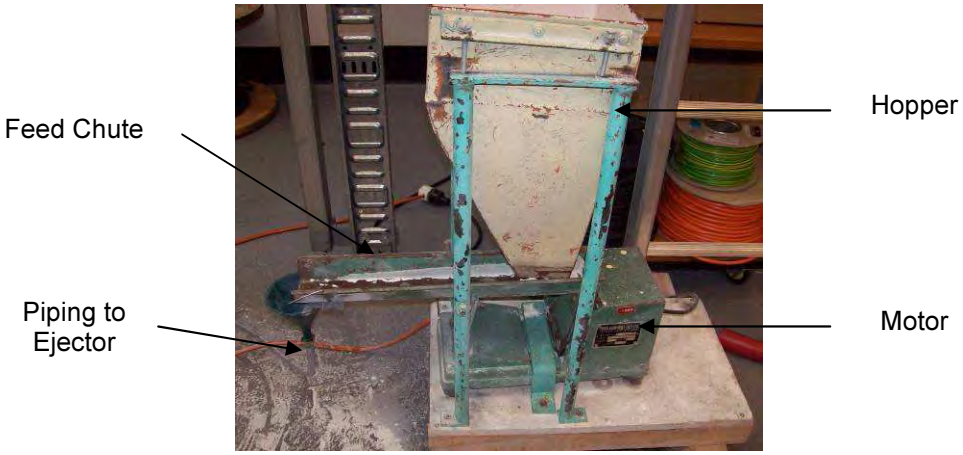

Figure 6-11: Vibrating hopper powder feeder

Each section on the dirty side of the baghouse was covered with a 230 V foil heating element (supplied by Argus Heating Ltd, Christchurch). Each heating element was supplied with mains electricity. Installed on top of the foil elements was 50 mm thick Lightweight Equipment Insulation sourced from Forman Building Systems, Christchurch (Figure 6-12). A

thermocouple was attached to the external wall in the middle of Section C to be connected to a control circuit, installed to maintain an external wall temperature of 26 ^{o}C.

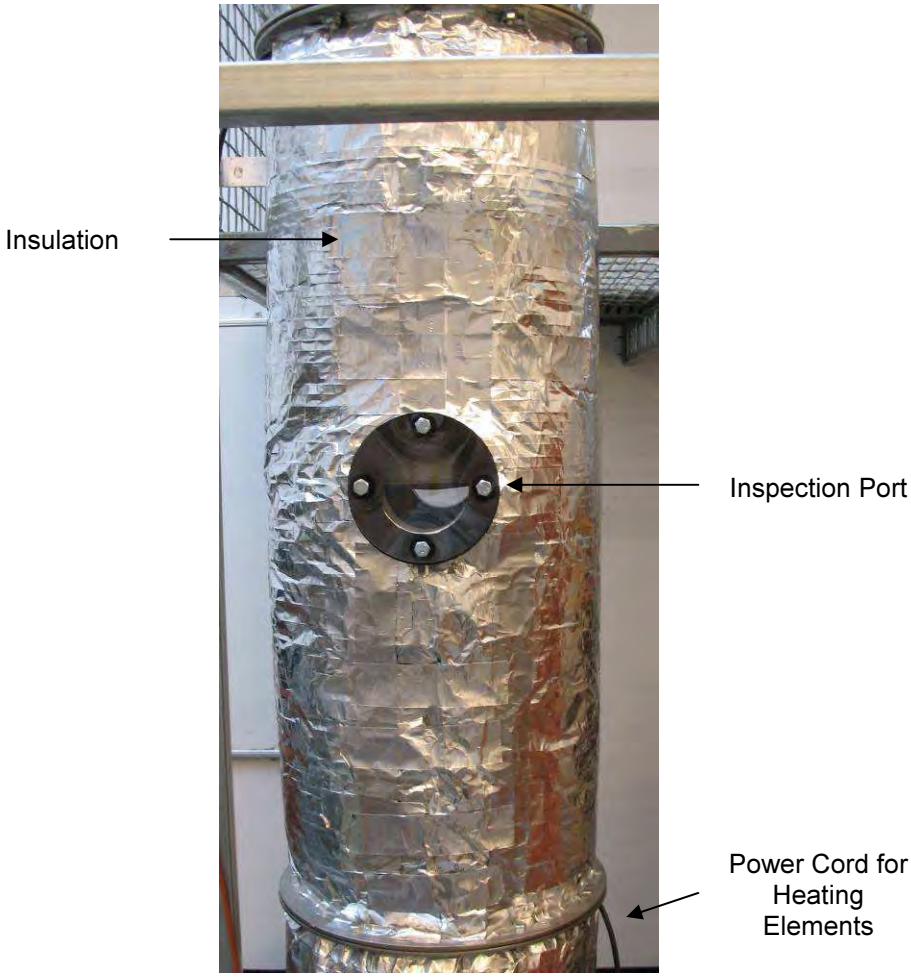

Figure 6-12: Installed Section B of the single cell baghouse showing the inspection port and LEI insulation covering the heating elements

The baghouse differential pressure was measured using two pressure taps, one into each of the dirty and clean sides of the baghouse close to the cell plate. The taps were connected using 6 mm clear hosing to a JUMO p02 pressure transmitter (JUMO GmbH & Co, Germany) obtained from Intech, Christchurch, that was mounted onto the structure (Figure 6-13).

Figure 6-13: Baghouse differential pressure transmitter and dirty side pressure tap

The 3 m long filter bags were obtained from both Canterbury Filters and Filtercorp International Ltd. The support cage was made from two sections of an old CD2 support cage where the base plate from the bottom 3 m section was welded to the bottom of the top 3 m section. The cage was held in place at the cell plate by two lugs bolted down onto the top of the cage (Figure 6-14). Each lug was made from a flat piece of stainless steel and had a 10 mm screw welded to the cell plate and facing up, running through an off centre hole. This allowed a nut to be screwed down onto the lug.

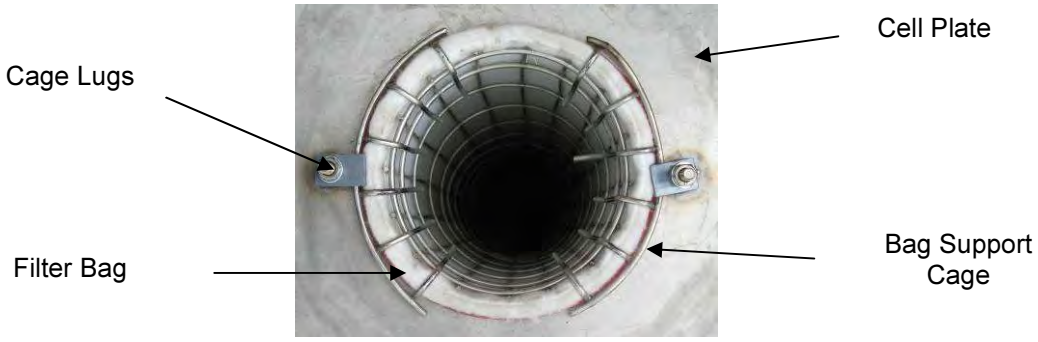

Figure 6-14: Top of bag and support cage supports

Running through the centre of the lid of the baghouse was the compressed air pulsing lance. This lance comprised a 1 m length of 32 mm diameter stainless steel tube with the GEA Niro A/S pulse cleaning ejector welded to the bottom (Figure 6-15). This ejector was provided free of charge from GEA Niro A/S, Denmark.

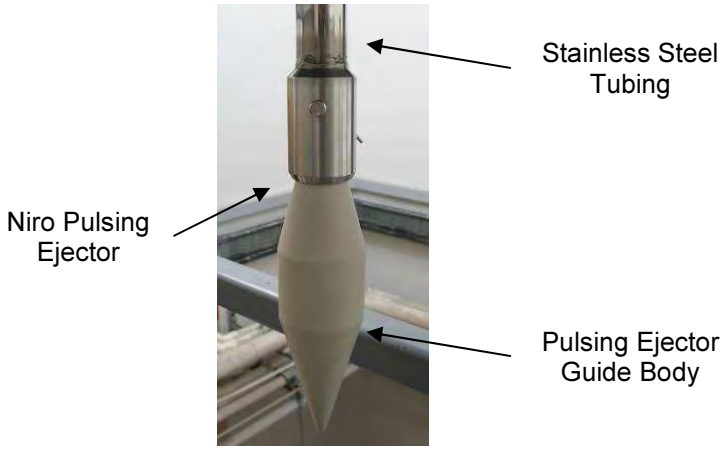

Figure 6-15: GEA Niro A/S compressed air pulse jet ejector

A 15 mm high, 80 mm OD stainless steel circular boss was screwed onto the lid of the baghouse. Inside the boss, two grooves were cut and each filled with an O-ring. One O-ring near the base of the boss created a seal between the lance tubing and the baghouse lid. The second O-ring situated near the top of the boss, created a seal between the boss and the lance tubing.

The tube was fixed in place using a Valu guide bracket obtained from Engineering Plastics Ltd, Christchurch, which was mounted onto the top of the baghouse. A plastic sleeve in the centre of the mounting was tightened with two bolts when the ejector was at the correct height above the bag. The design of this bracket was such that the tip of the ejector could be moved between 400 and 1000 mm from the top of the bag.

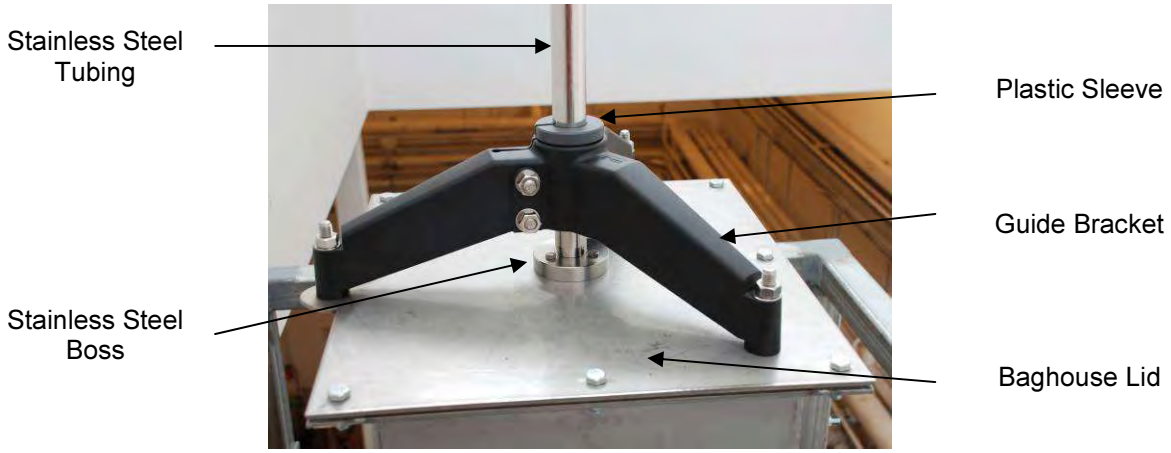

Figure 6-16: Compressed air tubing location guide and boss

The laboratory mains compressed air, supplied at a pressure of around 7.5 to 8.5 bar, was piped using 10 mm flexi compressed air hosing through a pressure regulator (Wilkinson R08-C2-F000 ¼" Relieving Regulator). The pressure was set at a supply pressure of 6 bar, but this could be easily adjusted. Both the hosing and the regulator were supplied by Engineering & Compressor Services Ltd, Christchurch. From the regulator, the compressed air was fed into a 55 L reservoir which ensured that the required pulse volume of air (5 L) could be supplied in the very short pulse durations. This reservoir was originally from a portable air compressor obtained from Engineering and Compressor Services Ltd, Christchurch.

From the reservoir the air was piped, using 1 ¼" diameter flexi fuel line hosing supplied by HCD Flow Technology, Christchurch, through a solenoid valve to the top of the stainless tube at the top of the baghouse. The 2" diameter fast acting DC solenoid valve was a CA50T Goyen type (Goyen Valve Corporation, Los Angeles, USA) supplied by Pneumatic Services Ltd, Christchurch. This valve was operated by a Trumeter 7931 programmable predetermining timer (Trumeter Company Ltd, Manchester, UK) supplied by Intech Instruments Ltd, Christchurch. The timer was initially set at 0.15 s to replicate the Fonterra CD2 main baghouse pulse durations, but could be adjusted to any multiple of 0.01 s.

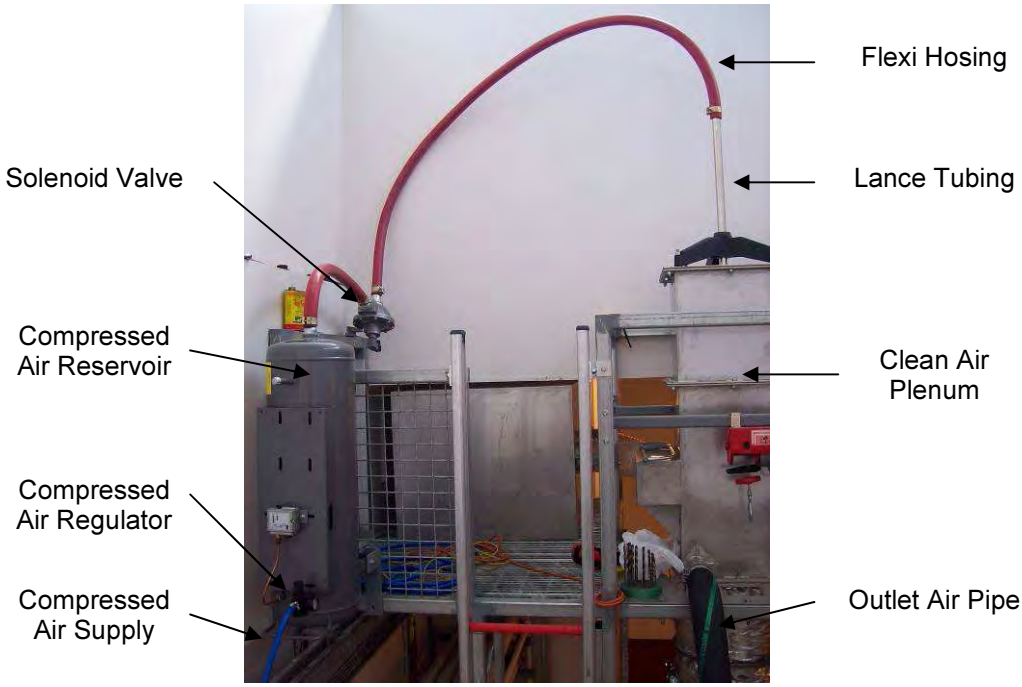

Figure 6-17: Compressed air supply system for pulse jet ejector (source: Richard Snoek)

A 5 m length of 75 mm OD Emair rubber hosing supplied by HCD Flow Technology Ltd, Christchurch, was used to connect the clean air plenum outlet to the fan inlet. At the clean air

plenum outlet, the hosing was clamped onto a 50.8 to 76.2 mm stainless steel expansion. At the fan inlet, the hose was also clamped onto a 76.2 to 50.8 mm stainless steel reducer. The reducer and expander were supplied by Steel and Tube, Christchurch.

The fan used to draw air through the system was the existing spray dryer extractor fan (HN2500-1800 type from B.Bille Ingeniorfirma, Denmark) shown in Figure 6-18. Using a known air velocity of 15 m / s in the fan outlet pipe, the volumetric flow through the fan was determined and hence the expected fan operating point when supplying air to the baghouse. This required the estimation of difference in pressure drop allowing for the addition of the baghouse rig and removal of the spray dryer cyclone.

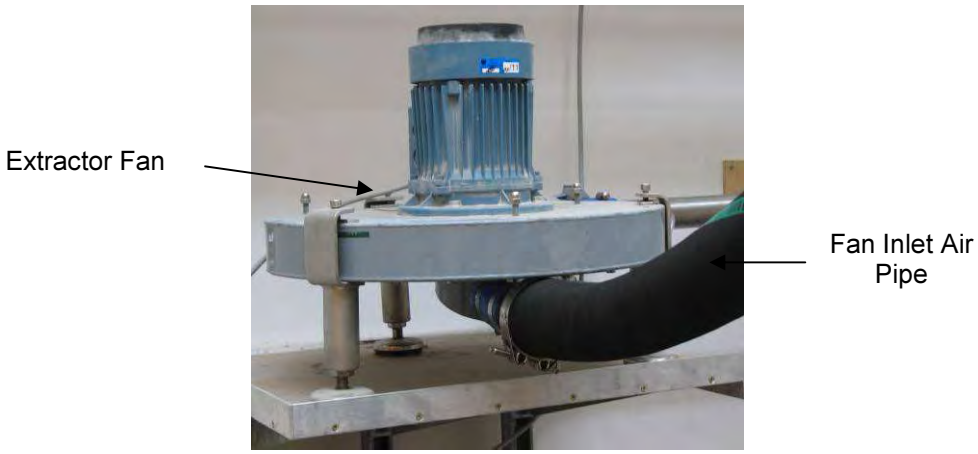

Figure 6-18: Spray dryer extractor fan and inlet air pipe

The baghouse flow was to be measured using a correlation to be developed for the pressure drop between the pressure tap in the fan outlet pipe and atmospheric pressure (Figure 6-19). A pressure tap was placed in this fan outlet pipe and a second was made through the laboratory wall to atmosphere. Again 6 mm clear hosing was used to connect the taps to a second JUMO p02 pressure transmitter.

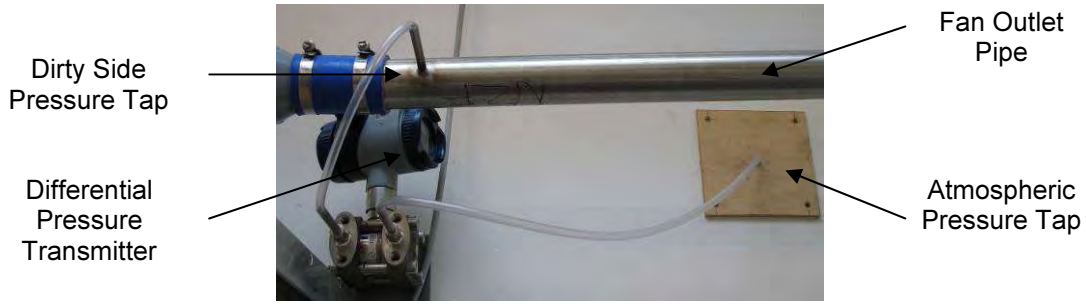

Figure 6-19: Baghouse airflow differential pressure transmitter with pipe and atmospheric pressure taps

6.4. Commissioning

Mr Richard Snoek ran the extractor fan, while no humidification of the air was occurring in the spray dryer, and measured the velocity of air in the fan outlet pipe with a Pitot tube and at the outlet of this pipe with a vane anemometer. Both measurements showed good agreement and gave a volumetric flow through the fan of 176 m^3 / hr. At an air temperature of 75 ^oC, and therefore a decrease in density of approximately 18 % from the density of ambient air, this volumetric flow would be expected to increase to around 208 m^3 / hr. This flow is well below the volumetric flows of 245 m^3 / hr, 258 m^3 / hr and 273 m^3 / hr required to mimic industrial MPC, SMP and WMP operation. Thus, the fan speed will need to be increased to achieve these desired flows.

During this experiment it was noticed that air was being sucked into the baghouse between the flanges. This was not surprising considering the uneven surfaces of these stainless steel flanges and the hard and unforgiving nature of the CA fibre gaskets. Therefore, additional filling between the flanges, such as rubber gaskets, is required to prevent any additional air entering the baghouse.

A second set of experiments were carried out by Mr Richard Snoek to characterise the flow rates of powder possible from the vibrating hopper powder feeder. The hopper was filled with MPC powder and at the maximum vibrating speed the discharged mass of powder was collected every minute and weighed until the hopper was empty. The average mass flow during the experiment was calculated to be 85 kg / hr. This maximum flow is well above the required feed rates of powder to replicate the industrial situation of 10.8 kg / hr for SMP, 7.8 kg / hr for WMP and 5.2 kg / hr for MPC. However, as the minimum feed rate has not been determined, it cannot be ascertained whether the vibrating hopper powder feeder may be used.

6.5. Further Work

Although the rig structure, baghouse shell and majority of the instrumentation have been installed, none of the instrumentation has been supplied with power. A CAPE electrical technician is required to supply power to the two differential pressure transmitters, the heating elements and the solenoid valve. The solenoid valve also requires connection to the programmable predetermining timer.

Installation of two control circuits is required. Firstly, the thermocouple measuring the external wall temperature on Section C needs to be connected to a control circuit supplying power to the heating elements to ensure this external wall temperature remains at 26 ^{o}C. Secondly, to maintain a constant air flow through the bag, a variable speed drive and control circuit is needed on the extractor fan. As the filter cake grows during the filtration cycle, the bag pressure drop will also increase. To ensure a constant filtration velocity, the fan speed must also be increased. This can be achieved by increasing the power and frequency supplied to the fan motor.

Finally, to make the rig more user friendly, the winch controls need to be made accessible from the ground level. This could be possible if the cables connecting the winch controls to the winch motor were extended by approximately two metres.

A significant amount of further commissioning is required before any more experimental work can be carried out on the rig. The spray dryer operation needs to be characterised so that the desired baghouse inlet air temperature and humidity can be achieved from a known combination of spray dryer feed water rate and outlet air temperature.

The pulse jet cleaning behaviour of the single cell baghouse will also have to be characterised. Checks will need to be made to ensure that the set up installed provides a sufficient volume of air in the required time to mimic the industrial Fonterra baghouse cleaning, that the pulse is directed down the inside of the bag and that sufficient air is stored in the ambient air reservoir to prevent the baghouse clean air plenum from collapsing. Finally, the chosen pulse duration, frequency and pressure will need to be checked to ensure the industrial situation is replicated as closely as possible.

After a filtration run without pulse cleaning, the distribution of powder up the bag will need to be measured to see if the powder ejector distributes powder to all parts of the filter bag. If not, the height of the position of the ejector below the bag or the angle of the nozzle from the horizontal can be manipulated. Associated with this, the minimum powder flow possible from the vibrating hopper powder feeder will need to be measured.

To determine the baghouse air flow, a calibration curve needs to be created. This could be achieved by noting the differential pressure reading and measuring the velocity of air in the

fan outlet pipe with a Pitot tube at a range of fan speeds. The volumetric air flow could then be calculated and the calibration curve plotted as the air flow versus the differential pressure reading.

6.6. Future Use of Rig

Once commissioned, there are several experiments that could be conducted that are likely to significantly improve the understanding of washable baghouse operation in milk powder plants.

As mentioned in Chapter Three, there is a significant difference in the filtration characteristics of the various milk powder products made in CD2. However, it has not been possible to physically measure filter cake properties such as thickness, porosity, permeability and adhesion. Therefore, to compare more accurately the filter cake produced by different milk powders, the same quantity of the various powders could be fed at the same temperature, humidity and air flow rates and the resulting pressure drop profiles, thickness, adhesion and permeability of the filter cakes could be measured, and the amount of powder that is collected on the filter bag could be determined.

Chapter Eight discusses an investigation into why the addition of fat in SMP has a beneficial influence on the baghouse differential pressure. However, this investigation does not clearly identify this mechanism. This laboratory scale baghouse would provide information that may identify this mechanism as the thickness, mass, permeability and adhesion of filter cakes produced by SMP at different fat contents could be compared. Obviously, work of this nature could not be carried out on an industrial scale.

The findings on the industrial plant in Chapter Three are rather surprising in that it was shown that changes within the operating limits in process variables such as air flow rate, humidity and temperature had virtually no impact on the baghouse differential pressure. Also, it was not possible during this PhD study to ascertain how changes in powder loadings on the baghouse impact on the baghouse differential pressure. Therefore, experiments investigating how changes in each of these parameters impacts on the baghouse differential pressure could easily be carried out using the single cell baghouse.

As it currently stands, the compressed air pulsing sequence used in CD2 is constant for all products. This sequence is that a pair of bags experience a 0.15 s pulse of compressed air, there is a 2.40 s hold before the next pair of bags is pulsed and finally a 1.0 s reset delay occurs at the end of the cycle after all 120 pairs of bags have been pulse cleaned. This sequence gives a total cycle time of 307 s. This sequence is significantly different to that used in the identical ED2 and ED3 plants. In February 2005, ED2 was using a 0.25 s pulse, a 2.0 s hold and a 5.0 s reset delay giving a cycle time of 275 s whereas ED3 was using a 0.28 s pulse, a 1.8 s hold and a 5.0 s reset delay giving a cycle time of approximately 255 s.

These findings indicate that the best pulse cleaning sequence is for the GEA Niro A/S Sanicip designed washable baghouses is uncertain, and that potential optimisation of compressed air use by changing the cycle time for different products is possible. The CD2 plant management is very reluctant to trial different pulse cleaning sequences in CD2, so experiments using the single cell baghouse could provide more solid evidence on how changes to the pulse cleaning cycle times will impact on the baghouses.

Chapter One highlighted that an early observation when producing SMP in CD2 was that a large amount of powder builds up around the top of the filter bag. This finding was supported by SEM evidence discussed in Chapter Five where powder penetration into the interior of the bag fabric was more pronounced at the top of the bag than at the bottom, and this was attributed to the nature of pulse cleaning. This single cell baghouse could be used to investigate whether the position of the ejector above the bag can be manipulated to prevent this mechanism from occurring.

A final use of the single cell baghouse could be as a bag filter testing facility. New filter bags from suppliers could be compared in this rig at conditions very similar to those that bags would experience in the plant. These would be better tests to carry out than the traditional tests conducted by suppliers as these have often been with dusts other than milk powder and using only small sections of bag material rather than complete filter bags.

6.7. Conclusions and Recommendations

A 3 m long single bag baghouse that, as far as is possible, replicates the conditions of a 6 m long industrial bag found in the GEA Niro A/S designed CD2, ED2 and ED3 Sanicip CIPable baghouses has been designed and installed within the department of Chemical and Process Engineering at the University of Canterbury. Because of this, it can be concluded that a pilot sale baghouse is now available that can be used to greatly enhance the understanding of milk powder plant washable baghouses.

It is recommended that the electrical support be provided so that power is provided to all the instrumentation, control circuits are installed for the heating elements and extractor fan, and the timing devices is connected to the compressed air solenoid valve.

Finally, it is concluded that owing to the large number of unknown fundamentals associated with washable baghouses used for milk powder collection, a large amount of future research can be carried out using this rig. Some topics for investigation include the optimisation of the pulse cleaning pulse duration, frequency and pressure; why the addition of fat to SMP helps reduce baghouse differential pressures; if the position of the pulse cleaning ejector can be changed to prevent powder build up around the top of the bag; and what impact dryer operating parameters have on the baghouse differential pressure.

7. Fat in Skim Milk Powder

Chapter Three showed that the composition of skim milk powder has a strong influence on the baghouse differential pressure. Because this mechanism was a mystery to Fonterra, it was investigated here.

7.1. Introduction

During the early seasons of CD2's operation (2000 – 2003), SMP was commonly produced and several operational issues already discussed arose during these production runs. However, it was also observed that as the amount of bulk fat in the powder increased, the baghouse differential decreased as Figure 7-1 shows. This led to a Fonterra CAPEX being approved which allowed a cream dosing system to be installed in the CD2 standardising area to control the level of fat in SMP. The Fonterra CAPEX for the cream dosing system was approved even though the mechanism behind this phenomenon was unknown.

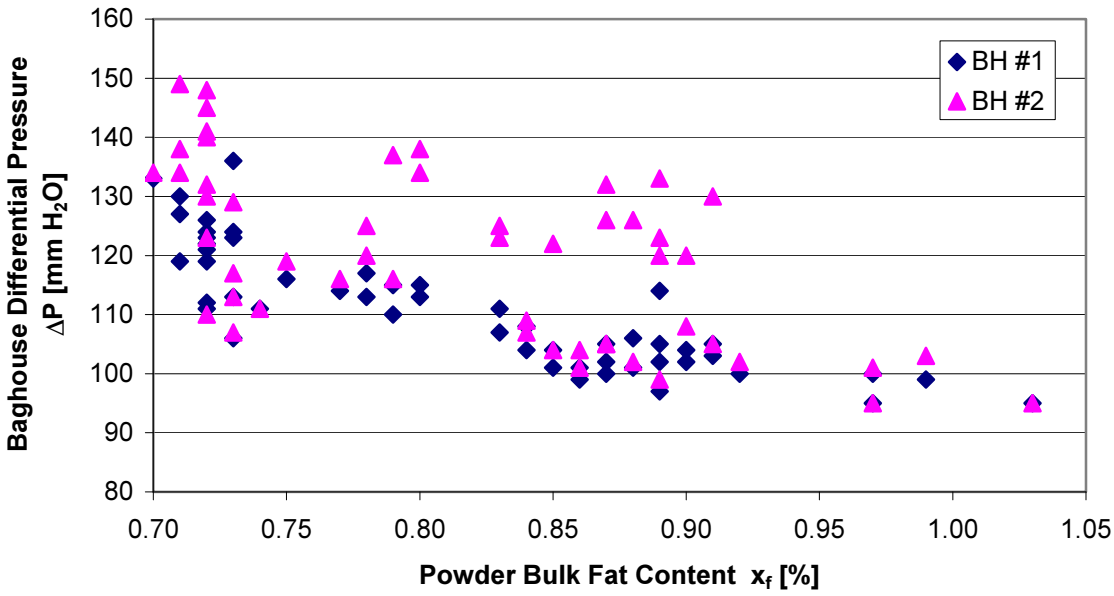

Figure 7-1: Clandeboye Dryer #2 baghouse differential pressure data as a function of skim milk powder bulk fat content

The historical data investigation discussed in Chapter Three shows that the trend of Figure 7-1 was common for all SMP production runs where a sufficient variation in dry powder bulk fat content occurred. This section of work also shows that changes in dry WMP or MPC bulk fat

content had no apparent influence on the baghouse differential pressures of these products. Therefore, it is likely that this mechanism only applies to SMP production.

It has been shown by several authors (Fäldt and Sjöholm, 1996; Kim et al., 2002; Nijdam and Langrish, 2006) that fat in milk powder is over represented on the surface of the particles (Figure 7-2). A relatively new measurement technique known as electron spectroscopy for chemical analysis or X-ray photoelectron spectroscopy is used to measure the relative atomic concentrations of carbon, oxygen and nitrogen at the surface layer (approximately 10 nm) of the powder. The ratios are then converted to a surface coverage ratio of lactose, protein and fat by assuming a linear relationship between the elemental surface composition and the elemental composition of pure lactose, protein and fat. This method is described in more detail by (Fäldt et al., 1993).

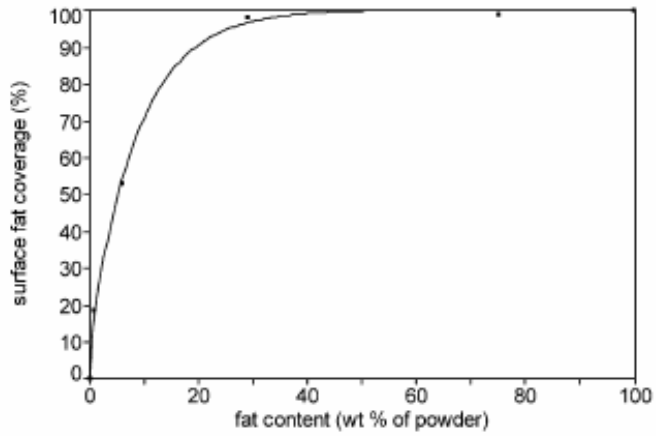

Figure 7-2: Surface fat coverage of milk powders as a function of bulk fat (source: Kim et al., 2002)

Figure 7-2 shows that the surface coverage of fat far exceeds the bulk fat content of the milk powder. For example, SMP with a powder bulk fat content of 1.0 % is likely to have a surface fat coverage of approximately 18 %, which is an order of magnitude of surface coverage higher than in the bulk. Figure 7-2 also suggests that, owing to the steep gradient in the range of allowable SMP fat contents (0.5 % to 1.2 %), any small change in the bulk fat content will cause a large change in the surface fat coverage.

WMP typically has a bulk powder fat content of approximately 27 % and therefore, a surface fat coverage of approximately 90 %. Figure 7-2 suggests that unlike SMP, any small change

in the bulk fat content of WMP, 0.5 % for example, will result in very little change in the surface fat coverage because the surface is already almost completely covered in fat. This is the likely reason why the trend of Figure 7-1 is SMP specific and does not occur during WMP production.

There is uncertainty about the mechanism that causes fat being over represented on the surface of milk powder particles. Nijdam and Langrish (2006) propose that the surface affinity of protein causes it to accumulate at the surface of the milk droplet. However, because of the formation of a skin, which is more rapid at higher drying temperatures, this process is hindered. These authors believe that, because fat will be in liquid form throughout the drying process, and hence not hindered by the skin formation, it is readily transported to the surface of the droplet/particle.

This suggested mechanism differs from that proposed by Kim et al. (2003). These authors postulate that, owing to the presence of moisture gradients, the milk solids concentrate at the surface of the particles where the moisture content is lowest, causing Fickian diffusion of the solids towards the core of the milk particle. Apparently, the lower molecular weight solutes, such as lactose, diffuse inwards more rapidly than the higher molecular weight solutes protein and fat, which consequently concentrate at the surface.

Several reports (Foster et al., 2005; Nijdam and Langrish, 2006; Özkan et al., 2002; Rennie et al., 1999) indicate that the presence of fat in milk powders helps to increase their ability to cake. Two possible mechanisms have been postulated: that fatty liquid bridges between particles solidify thus increasing bonding strength (Foster et al., 2005; Rennie et al., 1999); or that liquid fat may soften the powder, deforming the particles and creating an increased contact area between particles for attractive forces (Rennie et al., 1999).

Özkan et al. (2002) have postulated that the presence of fat on the surface of particles forms weak bridges between the particles which helps them to bind together and form larger agglomerates. The caking index results of Nijdam and Langrish (2006) are consistent with this, as these authors observed a significant increase in the caking index of milk powders with bulk fat contents between 1.1 % and 3.4 %, suggesting that the presence of fat on the surface has a strong influence on the caking ability of the powders.

Stapper et al. (1976) carried out experiments on the laboratory scale, on a bag filter attached to a spray dryer producing SMP, WMP and sodium caseinates. Because the drop in baghouse differential pressure after a cleaning pulse was more distinct for WMP than for SMP, it was postulated that the stickiness of WMP caused powder to fall from the bags as clumps after a pulse, thus preventing fines from becoming re-entrained onto the filter bags. The discussion above would suggest that it was the greater proportion of fat in WMP causing the powder to cake and, according to Calle et al. (2002), the greater the cohesion within the cake, the larger the size of cake fragments dislodged during cleaning.

The recommended air to cloth ratios for milk powders given by Löffler et al. (1988) (Chapter Eight) are adjusted for the stated fat content of milk powders. Fonterra industrial experience would suggest that the lower the fat content, the lower the air to cloth ratio required. Despite this design suggestion, Löffler et al. (1988) do not detail any putative mechanism behind their recommendation.

Several reports present particle size information for different groups of spray-dried milk powders from the industrial scale (Fitzpatrick et al., 2004; McKenna et al., 1999; Nijdam and Langrish, 2005; Teunou et al., 1999) and pilot scale (Buma, 1971; Keogh et al., 2003; Nijdam and Langrish, 2005; Nijdam and Langrish, 2006). However, no reports have been found that investigate changes in spray-dried milk powder particle size caused by a change in composition within a product group.

The closest anyone has come to investigating this phenomenon was Nijdam and Langrish (2006). They showed that, as the bulk fat content of pilot scale milk powders produced at 200^{o}C increased from 1.1 % to 29.8 %, the average particle size reduced from approximately 30 μm to 18 μm. These findings are opposite to industrial experience: it is commonly known that WMP (27 % fat) has a larger particle size than SMP (1 % fat).

7.1.1. Aim

The aim of this investigation was to determine the mechanism that causes baghouse differential pressures to increase when the fat content of SMP is reduced.

7.2. Theory

The pressure drop models presented in Section 2.3.1 of Chapter Two express the differential pressure in a baghouse as the sum of the pressure drop caused by the filter bag and the pressure drop caused by the filter cake (Equation 2-1). Equation 2-2 from Billings and Wilder (1970) expressed the total pressure drop as a function of the filter bag resistance k_b [Pa s / m], the filtration velocity V_f [m / s], the filter cake resistance k_c [s^{-1}], the fines concentration c [g / s] and the filtration cycle time t [s]. This implies that a change in the amount of bulk fat in SMP causes a change in one of the parameters on the right hand side of Equation 2-2 and therefore, a change in the total pressure drop.

The filtration velocity is a function of the air flow through the baghouse and the filtration area in the baghouse, which is obviously constant. The results in Chapter Three showed this airflow to vary slightly, but these small changes are a result of fluctuations in the main dryer inlet air mass flow rate and the dryer outlet air temperature, not changes in the composition of SMP. Therefore, the filtration velocity can be considered a constant. The filtration cycle time is also a constant because the plant operators have never changed this value from the original setting of 307 s.

Fonterra Clandeboye milk powder plant operators have observed the change in SMP fat content to have an almost instantaneous impact on the baghouse differential pressure. For this reason, it is likely that the nature of the filter cake, which will be filtering incoming particles by cake filtration, changes with the amount of bulk fat in SMP. Therefore, because of the almost immediate response to such changes and the nature of the filtration regime, slow changes in the bag resistance k_b can neglected in the first instance.

With the filter bag resistance, the filtration or face velocity and the filtration cycle time as constants, it can be seen from Equation 2-2 that the change in the total pressure drop due to changes in SMP composition is a result of changes in the cake pressure drop. The cake pressure drop from Billings and Wilder (1970) is expressed by Equation 7-1:

$$\Delta P_c = k_c c V_f^2 t \qquad (7\text{-}1)$$

Therefore changes in the cake pressure drop due to changes in the amount of bulk fat in SMP can be due to a) changes in the filter cake resistance, b) changes in the fines concentration, or c) changes in both the filter cake resistance and the fines concentration.

The filter cake resistance represents properties such as the particle size distribution of the dust and the structure and porosity of the filter cake (Löffler et al., 1988). Therefore, changes in the amount of bulk fat in SMP could be changing the powder particle size distribution or the nature of the filter cake: if the powder became more adhesive for example, it is likely that a greater residual mass of powder will remain on the filter bags after pulse cleaning. It is possible that two mechanisms could create a different fines concentration because of a change in the amount of bulk fat in SMP. Firstly, a different powder particle size distribution could be created because of different amounts of fat in the SMP concentrate altering the atomisation conditions. This would lead to a different fines fraction entering the baghouse. Secondly, if the particle densities changed then the separation of powder within the chamber could also be altered and hence, a different fines concentration would result. This latter possibility seems less likely. Changes in the fines concentration would also influence the filter cake structure.

Because the filtration velocity and the filtration cycle time are constant, Equation 7-1 can be rearranged giving the ratio of the cake pressure drop at two different operating points 1 and 2, as the ratio of the product of the filter cake resistance and the fines concentration as Equation 7-2 shows:

$$\frac{\Delta P_{c,1}}{\Delta P_{c,2}} = \frac{k_{c,1} c_1}{k_{c,2} c_2} \tag{7-2}$$

Equation 7-2 shows that if the filter cake resistance is constant, then the filter cake pressure drop varies linearly with the fines concentration. Therefore, if the change in baghouse differential pressure relative to the amount of bulk fat in SMP is due solely to a change in fines concentration rather than a change in cake structure, then the ratio of the filter cake pressure drop at the two operating points is equal to the ratio of the inlet powder concentrations as shown by Equation 7-3:

$$\frac{\Delta P_{c,1}}{\Delta P_{c,2}} = \frac{c_1}{c_2} \tag{7-3}$$

If this were the case, then Equation 7-3 allows the inlet powder concentration to be calculated if the cake pressure drop at two different operating points and the original inlet powder concentration are known.

7.3. Assumptions

The baghouse differential pressure model of Billings and Wilder (1970) forms the basis of this work and hence is assumed to be accurate and to apply to industrial scale baghouses. The filter bag resistance is assumed to be constant because of the almost immediate change in baghouse differential pressure with a change in bulk SMP fat content, and because cake filtration is likely to capture all particles before they reach the filter bag surface and interior. This filter bag resistance is assumed to be equal to 15803 kg / m^2 / s. This value was calculated by dividing the baghouse pressure drop obtained when the plant was running on particle-free air with used filter bags in place, by the baghouse filtration velocity. Also, the plant operating data recorded by the plant operators and presented here is assumed to be correct.

With regard to the collected powder samples, it is assumed that all samples are representative and that the plant was operating at steady state during sampling. The CD2 powder process laboratory FOSS InfraXact NIR spectrometer (FOSS, Hillerød, Denmark) is assumed to be accurate, which is a safe assumption as the instrument is calibrated daily by Clandeboye calibration technologist Mr Mark Fauth. As discussed below, this instrument was used to measure the bulk composition of the powder.

The electron spectroscopy for chemical analysis technique applied to milk powder assumes that milk powder is composed of three main components; lactose, protein and fat. The technique converts the measured relative atomic concentrations of carbon, oxygen and nitrogen at the surface of the sample, to a surface coverage ratio of lactose, protein and fat. This is made possible by assuming that the elemental composition of the sample is a simple combination of the elemental composition of pure lactose, pure protein and pure fat. This work is based on the elemental composition for lactose, protein and fat determined by Nijdam and Langrish (2006) and these compositions are assumed to be correct. Finally, because there is only a small difference in the molecular mass of carbon, oxygen and nitrogen, it may be assumed that the molecular based relative surface coverage of the sample closely approximates the mass based coverage (Kim et al., 2002).

7.4. Methods

Two trials were carried out in CD2 to produce SMP at different dry powder bulk fat contents. The first was carried out over November 11 and 12, 2004 and the second over March 9 and 10, 2005. During each trial at a given bulk fat content, samples were obtained from the locations detailed below. The standardising operator would then slowly reduce the flow of standardising cream until a reduction in sifter powder bulk fat content was observed. After approximately an hour, when the plant had reached a steady state, samples at the lower powder bulk fat content were taken.

The target sifter powder bulk fat contents mentioned in this chapter refer to the desired sifter powder bulk fat content at the time of sampling. The sifter powder bulk fat content was chosen as the sample location to reflect changes in composition because the bulk fat content of this powder is measured and recorded hourly by plant operators. The desired sifter powder bulk fat content is termed a target because during sampling, fluctuations in powder bulk fat content in all samples were observed. Therefore the actual powder bulk fat contents were often not equal to the target value.

During the November trial, samples were taken from the SFB overflow weir and baghouse hopper at target sifter powder bulk fat contents of 1.0 % and 0.8 %, and a SFB sample was obtained at a target sifter powder bulk fat content of 0.5 %. Unfortunately, no baghouse hopper sample was obtained at the lowest powder bulk fat content because high baghouse differential pressure caused the plant to automatically shut down while the samples were being collected. This sampling was carried out at the end of the production run. Therefore, because there was a very small amount of SMP concentrate remaining to be processed, the plant did not start up after it had automatically shut down and hence, no baghouse hopper sample was obtained at the lowest powder fat content.

Samples during the March trial were obtained from the SFB overflow weir, the baghouse hopper and the sifter at target sifter powder bulk fat contents of 1.1 % and 0.9 %. A SFB sample and a baghouse hopper sample were obtained for a target sifter powder bulk fat content of 0.7 %. However, again high baghouse differential pressures caused the dryer to automatically shut down, and because this sampling was conducted at the end of the production run, the plant did not start up again on SMP. Therefore, again no sifter sample was obtained at the 0.7 % target bulk fat content.

It should be noted that during normal plant operation, operators would ensure the bulk fat content of SMP (allowable range is 0.5 % to 1.2 %) was such that the high baghouse differential pressures that caused the plant to automatically shut down during these trials, did not occur: it was the desire to produce SMP at low bulk fat contents for this research that caused the high baghouse differential pressures.

The bulk fat, bulk protein, bulk moisture content and the bulk density of each sample were measured using the FOSS InfraXact NIR spectrometer (FOSS, Hillerød, Denmark) located in the CD2 powder process laboratory. The average from three lots of powder from each sample was reported to ensure accuracy. The bulk lactose content of each sample was determined by the Clandeboye Chemistry laboratory using the standard ChloramineT test for milk powder (NZTM3; 5.1, Issue 7.0, June 2000). Finally, the bulk minerals content of each sample was determined by difference.

For each of the collected samples, particle size distribution analysis was carried out by Mrs Guan Truong of Fonterra Palmerston North using a Malvern Mastersizer 2000 (Malvern Instruments Ltd, Malvern, UK). The powder was fed to the analyser as a suspension in air. Repeats of each measurement were made to ensure the results were reproducible.

All samples from both trials were viewed by SEM. The images were produced by Ms Robyn Hirst of Fonterra Palmerston North. The samples were mounted on double-sided tape on an aluminium stub, sputter coated with gold to a thickness of approximately 20 nm using a Polaron E5100 sputter coater (Polaron Instruments Inc, Haffield, USA) and viewed using a Cambridge 250/3 scanning electron microscope (Cambridge Scientific Instruments Ltd, Witchford, UK).

The surface composition of all samples from the November trial, and the SFB and baghouse samples at target sifter powder bulk fat contents of 1.1 % and 0.7 % from the March trial were determined using electron spectroscopy for chemical analysis. The SFB and baghouse samples at target sifter powder bulk fat contents of 0.9 % from March were not analysed as they had almost identical powder bulk fat contents to the 1.1 % bulk fat set of samples.

The November group of samples was analysed at the University of Sydney using a monochromatic Al Ka source on an ESCALAB220i-XL instrument (VG Scientific, UK). The

X-ray source was operated at 120 W, using a pass energy and step-size of 100 eV and 0.5 eV respectively. The take-off angle of the photoelectrons was perpendicular to the sample, and the area analysed was a circular region of 0.5 mm in diameter. The pressure in the vacuum chamber during the analysis was less than $1x10^{-9}$ mbar.

The March 2005 samples were analysed at the University of Auckland, again using a monochromatic Al Ka source but on a Kratos Axis Ultra DLD instrument (Kratos Analytial, Japan) operated at 150 W power. A pass energy of 160eV, step size of 1 eV and a take off angle perpendicular to the sample were set. The sample area analysed was a 300 μm x 500 μm rectangle and the pressure in the analysis chamber was around $1x10^{-7}$ mbar.

SMP samples were obtained from the CD1 SFB during October and November 2006. Again, the bulk fat, bulk protein, bulk moisture content and the bulk density of each sample were measured using the FOSS InfraXact NIR spectrometer (FOSS, Hillerød, Denmark). The average of three repeats for each sample was reported. The particle size of these samples was analysed using a Microtrac X-100 (Leeds & Northrup, North Wales, USA) at the University of Canterbury, set up so that the powder was fed as a suspension in air.

7.5. Results

7.5.1. Differential Pressure

During both trials, a clear correlation between the amount of bulk fat in the dry SMP and the baghouse differential pressure was observed. Figure 7-3 below shows that, during the November 2004 trial, the change in dry SMP bulk fat content from 0.63 % to 1.10 % caused a change in the differential pressure from roughly 145 mm H_20 to 95 mm H_2O in BH #1, and approximately 160 mm H_20 to 125 mm H_20 in BH #2.

It could be postulated from Figure 7-3 that the major change in baghouse differential pressure occurs in the lower range of fat content. This would appear to be consistent with the surface fat coverage trend of Figure 7-2, which changed much more rapidly with low bulk fat values. However, the reason for the much greater increase in BH #1 compared to the BH #2 differential pressures at bulk SMP fat contents of less than 0.7 % is a difference in fan speeds. The BH #2 fan speed was approximately constant throughout the trial, but at these low fat

contents the BH #1 fan speed was increased by 9 %. This was done by the operators to increase the air and powder flow through BH #1, thereby preventing the BH #2 differential pressure exceeding 180 mm H_2O and causing the dryer to shut down. Had the fan speeds in both baghouse remained the same, it is likely that the gradients in Figure 7-3 would have been the same for both baghouses.

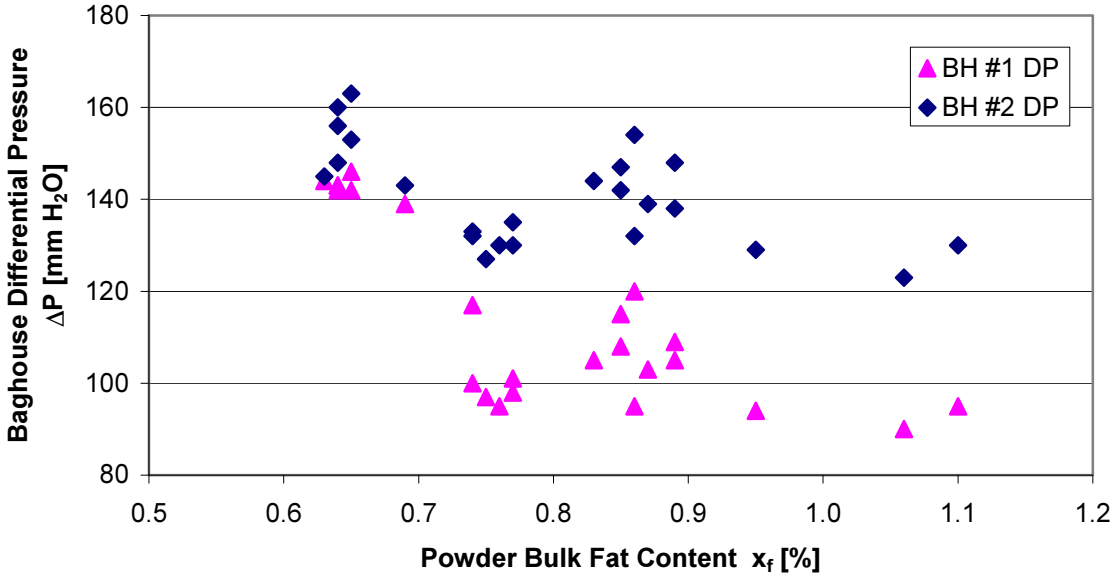

Figure 7-3: Influence of dry skim milk powder bulk fat content on the Clandeboye Dryer 2 baghouse differential pressures – November 2004 trial (60 hour period)

Figure 7-4 below shows that, during the March 2005 trial, there was a much smaller range in dry SMP bulk fat contents, between 0.96 % and 1.13 %, compared with the 0.63 % to 1.10 % range experienced during the November 2004 trial. The reason for a smaller range in March was that the differential pressures were higher because the bags were much older (approximately seven months old compared to approximately three months old in November) and therefore more heavily blinded compared with the bags in November. Also, the bags in the March trial had experienced four CIPs compared with just two CIPs experienced by the November bags. It should also be noted that the fan speeds in the March trial were approximately constant and hence, no difference in baghouse differential pressure between the baghouses at the lower fat contents occurred.

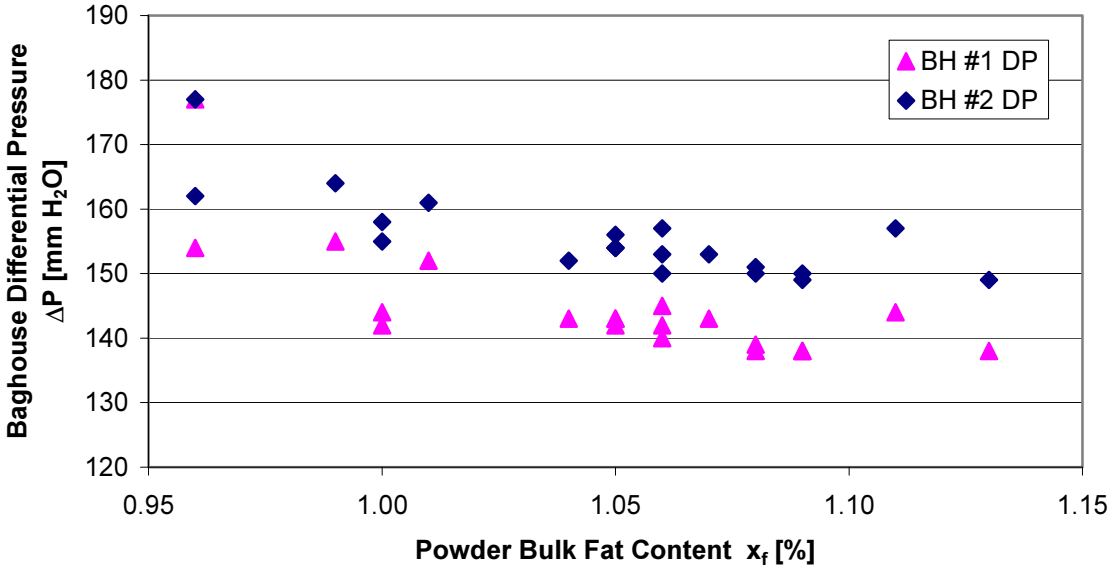

Figure 7-4: Influence of dry skim milk powder bulk fat content on Clandeboye Dryer 2 baghouse differential pressures – March 2005 trial (20 hour period)

These factors combined meant that, because the March baghouse differential pressures were much higher, the SMP bulk fat contents could not be lowered without the upper baghouse differential pressure limit of 180 mm H_2O being breached. This actually occurred at the end of the March trial: as the powder bulk fat content dropped below 0.95 %, the baghouse differential pressures exceeded 180 mm H_2O; therefore the dryer automatically came off product and ran on water.

The fact that the dryer automatically came off product because of the high differential pressures shows how sensitive the baghouse differential pressures are to the composition of SMP. This result also highlights the importance of standardisation of fat levels by cream dosing in SMP plants with washable baghouses to control the dry SMP bulk fat content.

There are several advantages of running a baghouse at lower differential pressures. Firstly, electricity requirements for the extractor fans are reduced as the fan speeds can be lowered as the baghouse differential pressure is reduced. Secondly, longer bag life times result, which in turn reduces bag replacement costs and plant downtime for bag replacement. Finally, a reduction in pulse cleaning frequency may be possible which would save on compressed air usage and reduce bag wear. The advantages of running a baghouse at lower differential

pressures mentioned above was supplied to support the generation of Fonterra Edendale's CAPEX to install a cream dosing system in the ED2 and ED3 plants. The information supplied contributed to the approval of this CAPEX and therefore the cream dosing system was installed.

7.5.2. Filtration Velocity

The differential pressure models discussed in Section 2.3.1 of Chapter Two predict that the differential pressure in a baghouse is a strong function of the filtration velocity. Because the filtration area is the same in both CD2 baghouses, the differential pressure is therefore expected to be a function of the baghouse air flow. However, it is shown in Chapter Three that there was no apparent change in the baghouse differential pressure with the change in baghouse air flow.

To check that this finding was the case during this SMP fat investigation, for both trials the baghouse differential pressures were plotted against the total dryer outlet air flow. As Figure 7-5 (the line included is the expected slope from theory) below shows, there was no apparent change, which was also the case in the March 2005 trial. This finding agrees with the results reported in Chapter Three, but also because the changes in total dryer outlet air flow were less than 5 %. Finally, this is also to be expected as the bulk fat content of the dry SMP has no influence on the dryer air flow. Therefore, it can be stated that the change in baghouse differential pressure when there is a change in dry SMP bulk fat content is not due to changes in the baghouse air flow.

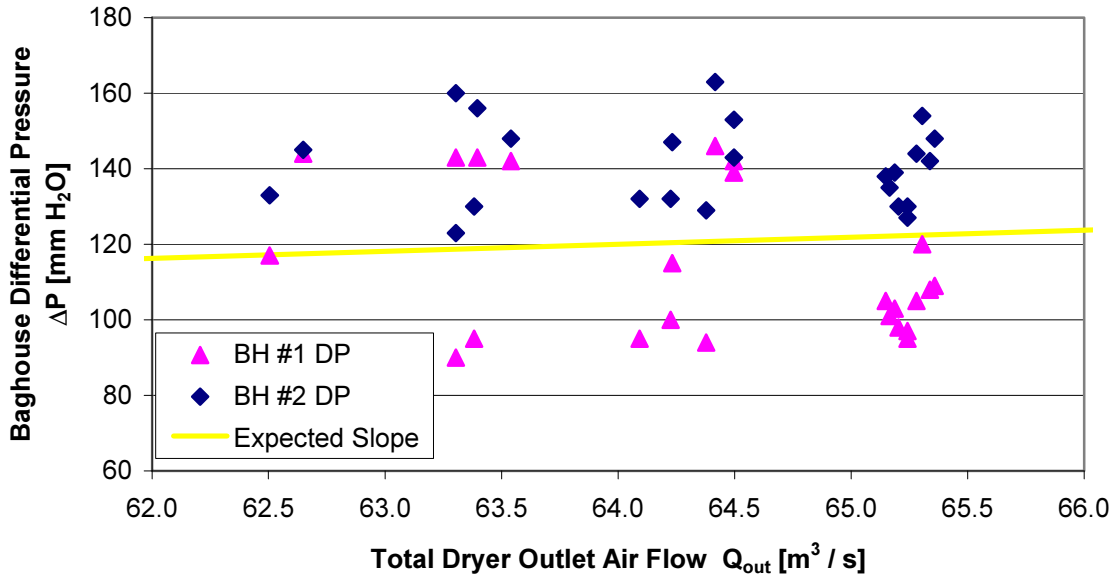

Figure 7-5: Influence of total outlet air flow on the Clandeboye Dryer 2 baghouse differential pressures – November 2004 trial (60 hour period)

7.5.3. Fines Concentration

The CPM 5003 optical scintillation instrument discussed in Chapter Four was used to measure the fines concentration during the March 2005 SMP trial. Figure 7-6 shows that, despite the change in bulk fat content and resulting change in baghouse differential pressure (Figure 7-3), no apparent change in fines concentration occurred.

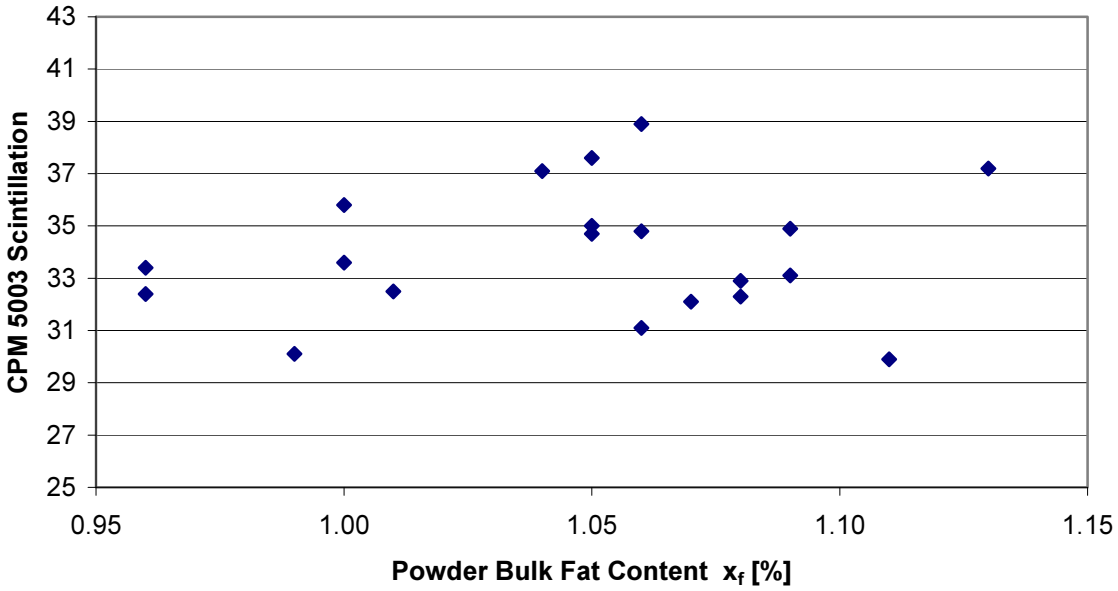

Figure 7-6: Influence of dry skim milk powder bulk fat content on CPM 5003 optical scintillation in Clandeboye Dryer 2 – March 2005 trial (20 hour period)

It is shown in Chapter Four that the CPM 5003 could easily detect the differences in fines loadings amongst the various milk powders, and was sensitive enough to detect small changes in fines loadings caused by an evaporator swap and different spray nozzle sizes. So, if a change in fines loading occurred because of changes in SMP bulk fat content, it would be expected that the optical scintillation instrument would detect this. Therefore, it can be stated with confidence that the mechanism causing baghouse differential pressures to increase when there is a reduction in dry SMP bulk fat content is not due to changes in fines loadings.

Chapter Four also discusses the pressure drop in a pneumatic conveying line being a function of the amount of solids present. Therefore, if there was a change in the fines loading, a change in the fines return line pressure would also result. Figure 7-7 below shows that the fines return line pressures were relatively constant during the March 2005 trial. The November 2004 trial fines return line pressures were also relatively constant, providing further evidence to suggest that there is no change in fines concentration when there is a change in dry SMP bulk fat content.

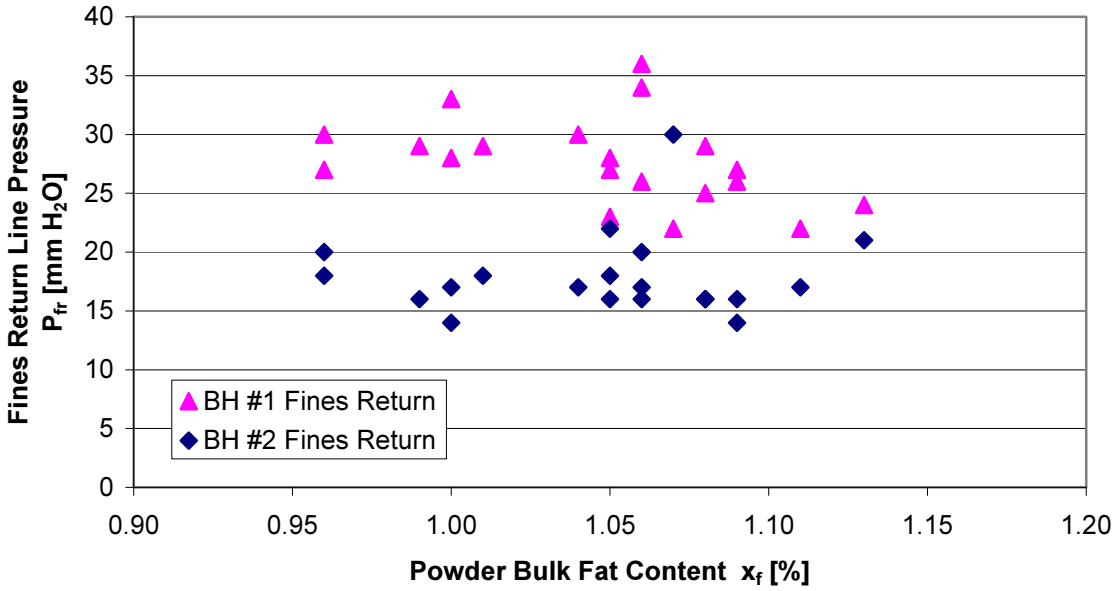

Figure 7-7: Influence of dry skim milk powder bulk fat content on the Clandeboye Dryer 2 baghouse fines return line pressures – March 2005 trial (20 hour period)

Additional analysis of the differential pressure data was carried out to further investigate whether a change in fines loadings occurs when there is a change in dry SMP bulk fat content. From Figure 7-4 above, at a dry powder bulk fat content of 1.13 %, BH #1 had a differential pressure of 138 mm H_2O. Assuming that filter bags running on air, that is, without the presence of power, have a pressure drop of 55 mm H_2O (Chapter Three), then the baghouse differential pressure of 138 mm H_2O equates to a filter cake pressure drop of 83 mm H_2O. Also assuming that, as Chapter Four showed, 82 % of the total SMP flow of 12.2 tonne / hr becomes fines, and that these fines are evenly split between the two baghouses, the baghouse inlet fines flow is 5 tonne / hr. Using Equation 7-1, these parameters give a filter cake resistance of 52606 s^{-1}.

At a lower dry powder bulk fat content of 0.99 %, the BH #1 differential pressure from Figure 7-4 is 155 mm H_2O and using the same filter bag pressure drop, this equates to a filter cake pressure drop of 100 mm H_2O; an increase of 17 mm H_2O or 20 %. Assuming the filter cake resistance is constant, then from Equation 7-3, the fines flow per baghouse at this lower dry powder bulk fat content must be 6.0 tonne / hr. This is an increase in the baghouse inlet fines loadings by 1.0 tonne / hr which increases the overall fines fraction by 20 %. Such a large change in the fines loadings is well beyond the error in the CPM 5003 and scatter in the fines

return line pressures, both of which appeared to be constant. Therefore, there is clear evidence to suggest that a change in dry SMP bulk fat content does not change the baghouse fines loadings and hence from Equation 7-2, the change must be in the filter cake resistance.

7.5.4. Filter Cake Resistance

The final parameter in Equation 2-2 that is most likely to be influenced by a change in dry SMP bulk fat content is the filter cake resistance. It is agreed that the filter cake resistance is a function of the particle size distribution, structure and porosity of the filter cake (Calle et al., 2002; Cora and Hung, 2002; Löffler et al., 1988). This parameter is also influenced by the filtration velocity, as higher filtration velocities result in increased cake compaction and therefore higher resistance coefficients (Calle et al., 2002; Ellenbecker and Leith, 1980).

It has already been shown that the filtration velocity was constant during this investigation. Thus, a change in particle properties, such as size or density, causing changes to the filter cake structure must be related to a change in the amount of bulk fat in SMP.

7.5.4.1. Particle Size

The average particle size results from both CD2 trials are shown in Figure 7-8 below. The data is split into three groups representing the SFB, baghouse and sifter samples.

Figure 7-8 suggests that, as the powder bulk fat content increases, there is an increase in the SFB particle size: the average particle size at a bulk fat content of 1.03 % is 249 μm, but this particle size reduces to 206 μm at a powder bulk fat content of 0.60 %, and to 170 μm at a bulk fat content of 0.48 %. The baghouse hopper particle size distribution appears to be constant as the bulk fat content increases. The five samples have a range in bulk fat content of 0.72 % to 1.09 % and a range of particle sizes from 89 μm to 133 μm. There is insufficient sifter data to give a trend but these particle sizes, as expected, lie between the SFB and baghouse sizes: this powder, as discussed in Chapter Four, is a made up of a combination of powder from the SFB and baghouses.

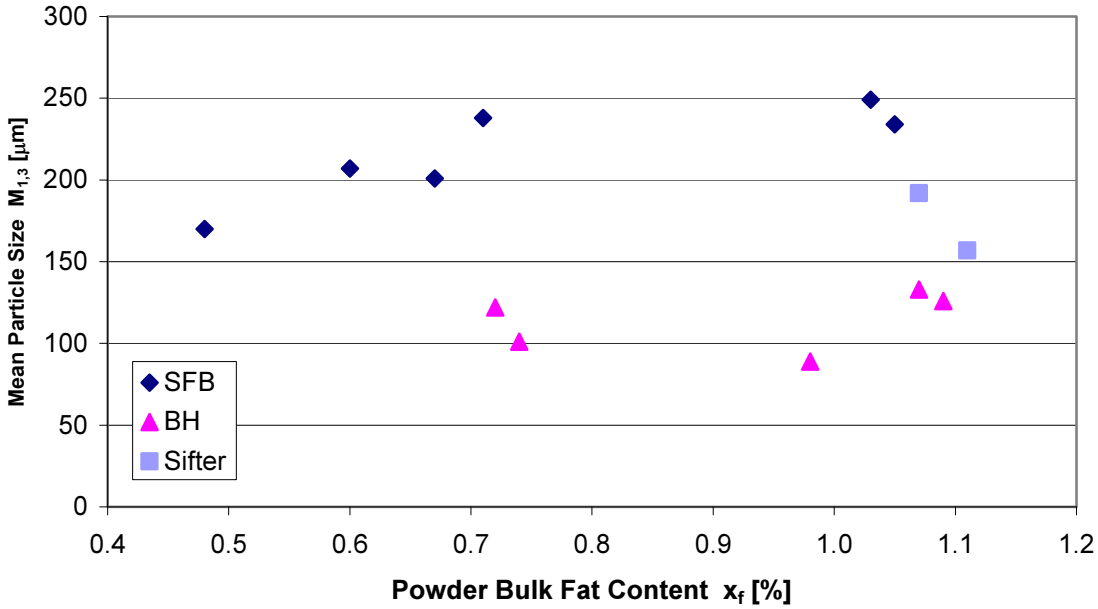

Figure 7-8: Combined mean particle size results for skim milk powder obtained from Clandeboye Dryer 2 in November 2004 and March 2005 from the static fluid bed, baghouse and sifter

Section 2.3.2 of Chapter Two highlights that the fines return line pressures are a function of particle size. If a particle size change results from a change in SMP bulk fat content, then the fines return line pressures would also change. Fines return line pressures (Figure 7-7) for both trials did not show any variation when the dry SMP bulk fat content changed. This indicates that there was no change in baghouse hopper particle size distribution and hence, supports the baghouse hopper particle size results.

The average particle sizes for SMP obtained from the CD1 SFB at different bulk fat contents are shown in Table 1 below. These average particle sizes are smaller than those from the CD2 SFB because CD1 is a Niro compact dryer that uses a rotary disc atomiser, whereas CD2 is a Niro MSD 2000 dryer which uses pressure nozzle atomisation.

Unlike the SFB particle size data obtained from CD2, the CD1 values show no apparent trend in relation to the powder bulk fat content. However, the bulk fat content of the CD1 samples is in a much smaller range of 0.66 % to 0.93 % compared with the range of 0.48 % to 1.05 % of the CD2 samples. In the 0.66 % to 0.93 % range, the CD2 samples also show no apparent

trend, so if the CD1 results included samples at higher and lower fat contents, then the two sets of results could possibly agree.

Table 7-1: Influence of dry skim milk powder bulk fat content on the Clandeboye Dryer 1 static fluid bed particle size

Powder Bulk Fat Content x_f [%]	Mean Particle Size $M_{1,3}$ [μm]
0.66	138
0.71	107
0.88	158
0.93	129

If the baghouse particle size distribution is constant and the SFB particle size is changing, then, because the SFB powder flow contributes approximately 20 % to the sifter powder flow, it would be expected that a change in powder bulk density caused by changes in dry SMP bulk fat content would also occur. However, as Figure 7-9 shows, there is no correlation between bulk fat content and bulk density for the November 2004 trial data. The same is also true for the March 2005 trial.

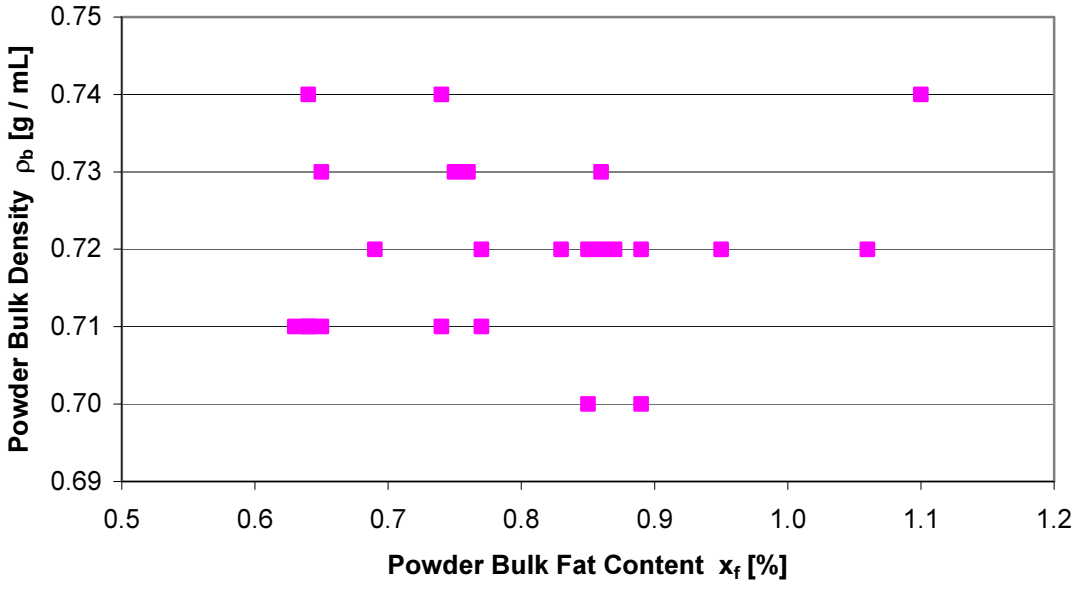

Figure 7-9: Influence of dry skim milk powder bulk fat content on the Clandeboye Dryer 2 sifter powder bulk density – November 2004 trial (60 hour period)

For a change in SFB particle size to occur, a change in atomisation conditions must also occur. It is highly unlikely that a change in concentrate viscosity or total solids occurs when there are such small changes in SMP composition. A change of 0.4 % in the bulk fat content of the dry powder equates to roughly a 0.2 % change in the fat content of the concentrate. Therefore the total solids of the concentrate is virtually constant.

It is well known (Bloore and Boag, 1982; Snoeren et al., 1982) that the viscosity of milk concentrates are a strong function of the protein content. Because the protein content of all samples varied by a maximum of 2 % during both trials, and because such small changes in the fat content of the concentrate will have no impact on the viscosity, it is safe to assume that the concentrate viscosity was constant.

Finally, the same spray nozzle sizes were used during the two CD2 trials. These points support a conclusion that no change in particle size occurred because of a change in bulk composition and therefore, the change in baghouse differential pressure when there was a change in dry SMP bulk fat content was not due to changes in particle size.

These results were obtained from trials on an industrial scale where it is very difficult to control all other parameters that may influence the particle size distribution. For example, the concentrate flows during both trials varied by an average of 5 % and the atomisation pressures varied by an average of approximately 15 %. Also, because of the transient nature of the air flow within a spray dryer (Chapter Ten), the drying histories of the droplets could have easily been different even though the same inlet air flow rates and temperatures were used. For these reasons, it is likely that the apparent trend in the CD2 SFB particle size results (Figure 7-8) and the scatter in CD1 SFB particle sizes (Table 7-1), was merely part of the natural fluctuation in these process parameters, that is, within the expected error. Therefore, it appears changes in the dry SMP bulk fat content do not influence SMP particle size.

The best way to provide evidence suggesting that a change in the particle size of the powder entering the baghouses is not caused by a change in SMP bulk fat content would be to measure the particle size distribution of this powder. Unfortunately, this was not possible during both trials as the isokinetic sampling apparatus mentioned in Chapter Four was not ready for use during either trial. Also, because of changes in Fonterra production schedules SMP was, and is never likely to be produced again in CD2. Therefore, measurement of the

baghouse inlet particle size distribution for SMP would only be possible on either ED2 or ED3 once a hole was cut into one of the baghouse inlet ducts and a thimble filter mounting installed.

7.5.4.2. Surface Composition

The influence of surface fat on the caking ability of milk powders and the flow-on influence on baghouse cleaning have been discussed above. To see if a change in surface composition was affected by the small changes in bulk fat content, the surface composition of samples were analysed using ESCA. All samples from the November trial and the SFB and baghouse samples at target sifter powder bulk fat contents of 1.1 % and 0.7 % from the March trial were analysed. The results for these samples from both trials, along with the trend of Kim et al. (2002) (Figure 7-2) are presented in Figure 7-10 below.

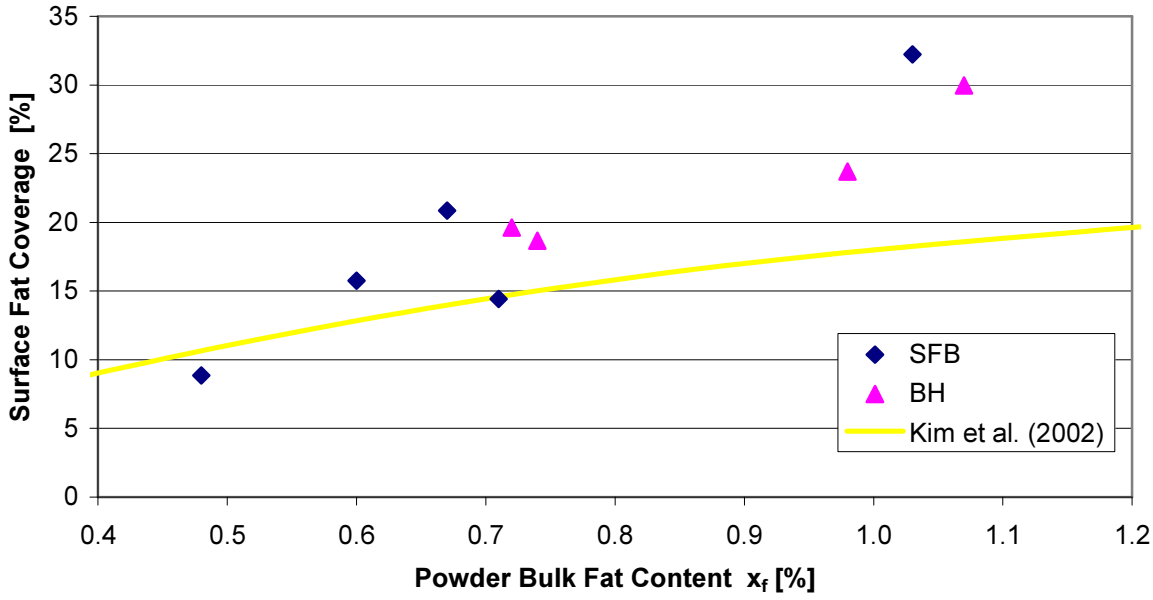

Figure 7-10: Combined surface composition results for skim milk powder obtained from Clandeboye Dryer 2 in November 2004 and March 2005

Figure 7-10 shows that, as expected, the representation of fat on the surface of all the samples was much greater than the amount of fat in the bulk. For example, at a powder bulk fat content of 0.60 %, 16 % of the surface was covered with fat, that is, there were two orders of magnitude more fat on the surface of particles than in the bulk.

Kim et al. (2002) found that industrial SMP with a powder bulk fat content of 1.0 % had a surface fat coverage of 18 %. As Figure 7-10 shows, this point is slightly lower than the data obtained during this investigation, but the trends from both data sets agree; fat is over-represented on the surface of the powder and increases significantly with small changes in the bulk fat content.

It appears the scatter in Figure 7-10 is the reason for the slightly higher surface fat readings obtained here compared to that of Kim et al. (2002) and therefore, the higher surface fat readings are not significant. However, there are two possible reasons for the slightly higher surface fat readings obtained above. First a difference may result from the powder samples of this work being obtained from within the milk powder plant and not obtained from packaged powder. Second, the plant where Kim et al. (2002) obtained their powder from was a different design from CD2 and operated with different process parameters. Nijdam and Langrish (2006) have shown these parameters to have an influence on the surface fat coverage.

Nijdam and Langrish (2006) produced milk powders with bulk fat contents ranging from 1.1% (SMP) to 29.8 % on a pilot scale dryer. These authors also found that fat was over-represented on the surface of the powder and small changes in bulk fat content resulted in much larger changes in the surface fat coverage. For the powder with a bulk fat content of 1.1% produced with an inlet air temperature of 120 ^{o}C, corresponding to an outlet air temperature of 80 ^{o}C, Nijdam and Langrish (2006) measured a surface fat coverage of 7 %. The same bulk fat content powder but produced with an inlet air temperature of 200 ^{o}C (outlet air temperature of 125 ^{o}C) had a surface fat coverage of 16 %. Both of these surface fat coverage values are below the surface fat values obtained during this work and by Kim et al. (2002).

The majority of the fats in milk powder are in the liquid phase at the outlet air temperatures used to produce SMP industrially ($\approx$ 78 ^{o}C) and those used by Nijdam and Langrish (2006). It is likely that the industrial scale powder analysed in this work and by Kim et al. (2002), had longer residence times than the laboratory scale powder produced by Nijdam and Langrish (2006). Therefore, it appears that because of the increased residence times at the industrial scale, fat had more time to migrate to the surface of the powder and hence, the industrial scale surface fat coverage was higher than the laboratory scale surface fat coverage.

It is interesting to note that all the baghouse samples have a higher powder bulk fat and consequently surface fat content than the SFB samples obtained at approximately the same time. It is likely that this is again a result of differences in powder residence time: baghouse powder has longer residence times within the milk powder plant than SFB powder and therefore, more time for fat to migrate to the surface of the powder.

It is clear from the results that a small change in the powder bulk fat content causes a significant change in the surface fat coverage. A change in powder bulk fat content from 0.48% to 0.67 %, an increase of approximately 40 %, results in a change in the surface coverage from 8.86 % to 21 %, a change of approximately 135 %. This finding agrees with the trend in Figure 7-2 and the trend of Nijdam and Langrish (2006). Also, these findings suggest that it is this significant change in surface fat coverage caused by small changes in the bulk fat content that is causing the significant change in baghouse differential pressures.

7.5.5. SEM Images

The SEM images produced were generated in an attempt to observe any obvious difference among the powders produced at different fat contents. In general, all three groups of images showed a range of particle sizes clumped together forming medium to large scale agglomerates.

Hollow particles were present in several samples (Figure 7-11), which agrees with the observations of Buma and Henstra (1971), Nijdam and Langrish (2005), and Nijdam and Langrish (2006). According to Nijdam and Langrish (2006), hollow particles are formed as follows: a vapour bubble (vacuole) forms within a particle soon after a skin develops on the surface; the bubble inflates once the particle temperature exceeds the local ambient boiling point; the vapour pressure within the vacuole rises above the local ambient pressure; and finally, the vapour condenses within the vacuole as the particle moves into cooler regions of the dryer. Therefore, milk powders are expected to be spherical and hollow.

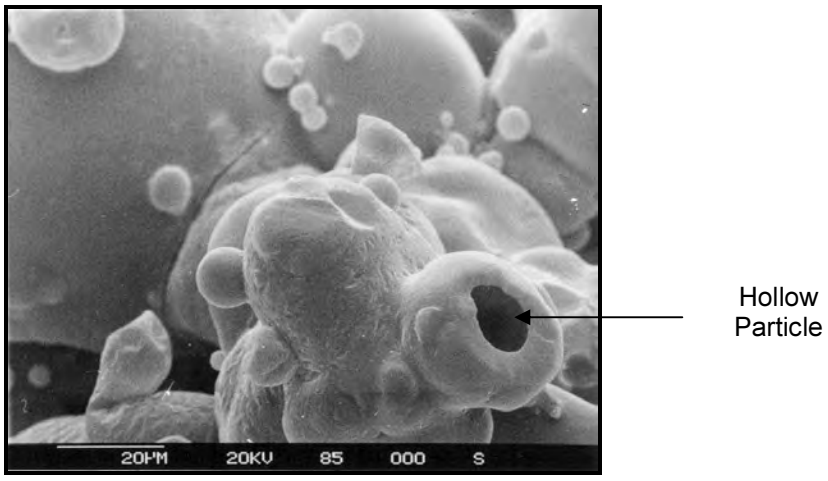

Figure 7-11: Skim milk powder obtained from Clandeboye Dryer 2 static fluid bed in March 2005

Although the majority of the particles were spherical, there were also some broken shells and collapsed particles (Figure 7-12). Broken particles arise when the drying of the droplet is fast, so the surface skin becomes dry and hard (Nijdam and Langrish, 2006), and smashes when it impacts with other particles, the spray dryer wall or because of pneumatic transport. Collapsed particles are likely to be caused by much slower drying of the particle. Lower temperatures mean that the skin of the droplet remains moist and supple for longer so the hollow particle deflates and shrivels as it cools (Nijdam and Langrish, 2006).

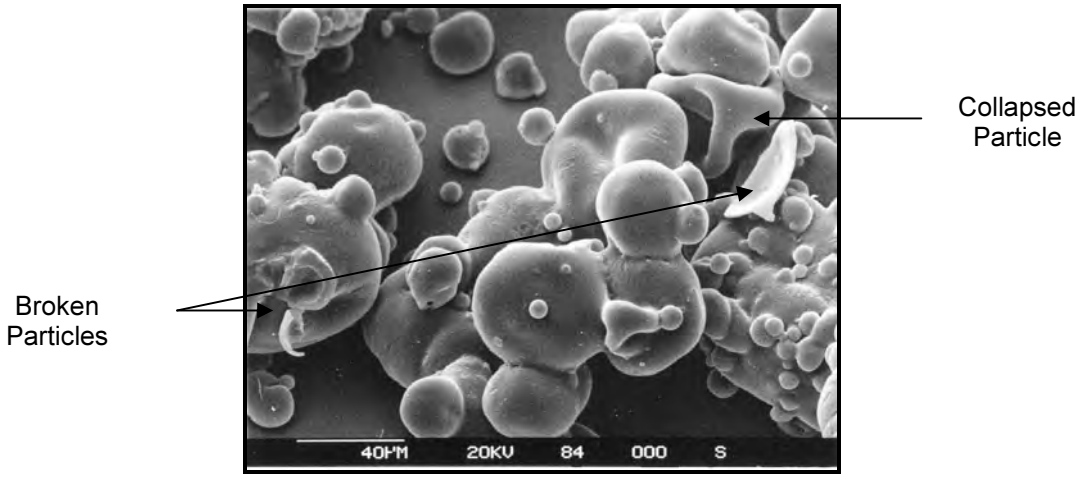

Figure 7-12: Skim milk powder obtained from Clandeboye Dryer 2 sifter in March 2005

The surface morphology of the particles was either fairly smooth or showed some degree of wrinkling. As Figures 7-13 and 7-14 below show, it was evident that as the powder bulk fat content increased, and therefore so did the surface fat coverage, the surface morphology

became smoother. These observations were common for all samples with a sufficient difference in bulk fat content. In general, the March samples, which had higher average fat contents, had smoother surfaces than the November samples.

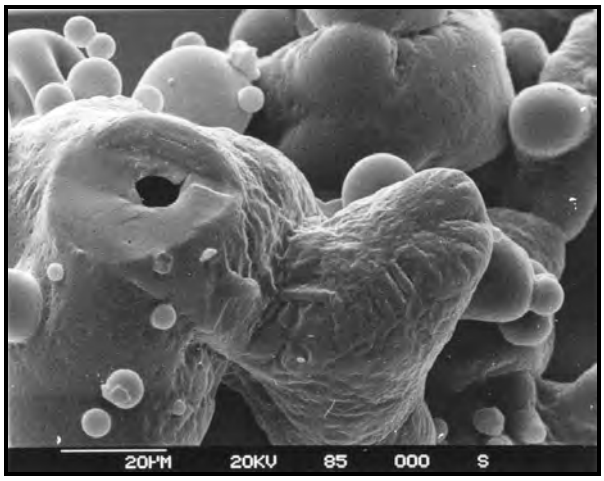

Figure 7-13a: Skim milk powder obtained from Clandeboye Dryer 2 baghouse in March 2005 – bulk fat of 0.7 %, surface fat of 19.6 %

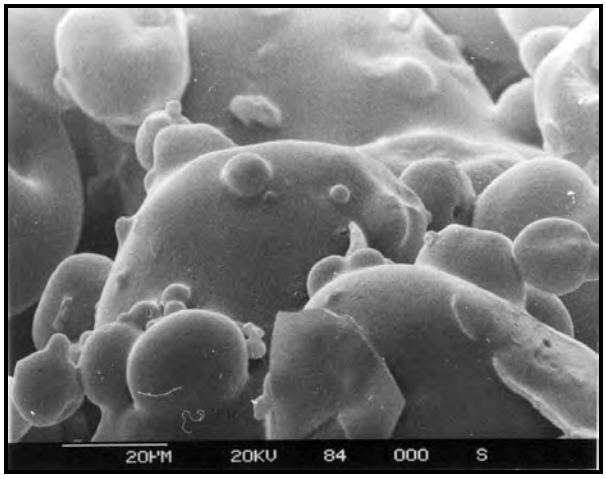

Figure 7-13b: Skim milk powder obtained from Clandeboye Dryer 2 baghouse in March 2005 – bulk fat of 1.1 %, surface fat of 30.0 %

Figure 7-14a: Skim milk powder obtained from Clandeboye Dryer 2 static fluid bed in November 2004 – bulk fat of 0.6 %, surface fat of 15.8 %

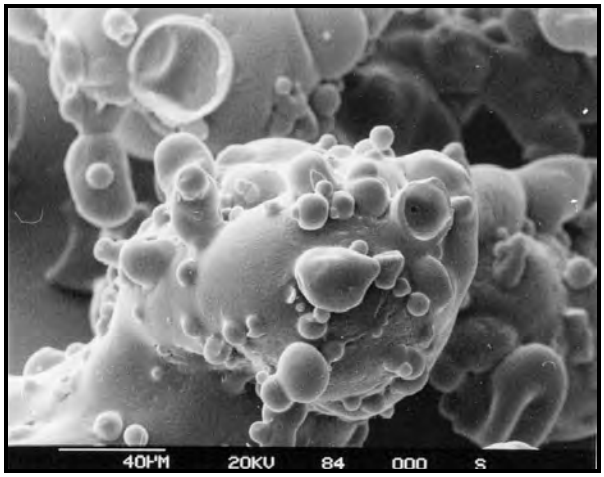

Figure 7-14b: Skim milk powder obtained from Clandeboye Dryer 2 static fluid bed in March 2005 – bulk fat of 1.0 %, surface fat of 32.2 %

This pattern of the particle morphology becoming smoother as the powder fat content increases is to be expected for general classifications of milk powders. SMP has a characteristics wrinkly surface compared with WMP which has a relatively smooth surface

because the increased fat of this powder fills the surface voids and smoothes it out (Hirst, 2005). Therefore, these SEM observations support the ESCA results that showed that an increase in the powder bulk fat content significantly increases the surface fat content of the powder. Also, both the SEM observations and the ESCA results are consistent with surface fat being the cause of the smooth surface appearance and thus, fat being in liquid form throughout the drying process.

7.5.6. Proposed Mechanisms

It has been highlighted above that several authors have found the presence of fat and more specifically, the surface coverage of fat on milk powders increases the likelihood of particles caking and forming clumps. It may therefore be suggested that a potential mechanism that causes the baghouse differential pressures to decrease as the bulk fat in SMP increases is as follows.

Small increases in the bulk fat of SMP cause a large increase in the surface fat coverage of the powder. This increased surface coverage of fat increases the caking ability of the powder as liquid bridges of fat form between the particles. Alternatively, the surface irregularities are covered over by the increased liquid fat, enhancing the surface contacts and therefore higher Van der Waals forces may result. Consequently, powder approaching the surface of the filter bags is more likely to adhere to other particles and form clumps, and the cake formed is possibly more porous. Because of these clumps cake filtration rather than depth filtration will occur. Consequently, and because there are fewer individual particles as a result of the clumping, the penetration of powder into the interior of the filter bag will reduce.

When the filter bag is pulse cleaned, the clumps are more easily pulsed from the bag compared with individual particles. Hence, less residual powder remains on the bag after the pulse. Also, because of the clumping, powder falling from the filter bags will have a higher settling velocity and is therefore, more likely to reach the hopper at the bottom of the baghouse than become re-entrained and re-deposited on neighbouring bags.

Therefore, because there is less penetration into the interior of the bags, less powder remaining on the surface of the bags after the cleaning pulse, and less re-entrainment of

powder after pulse cleaning, the cake pressure drop and hence the baghouse differential pressure, is reduced.

7.6. Future Work

Because the mechanism behind the change in baghouse differential pressure related to changes in SMP bulk fat content is not yet fully understood, considerable future research could be carried out in this area. The aim should be to determine whether the hypothesis stated above is correct. To achieve this, SMP at different bulk fat contents should be fed to the CAPE pilot scale baghouse (Chapter Six) and the properties of the resulting filter cakes investigated. These properties should include the thickness, porosity, filter drag and adhesion of the cake to the filter bag as well as the amount of powder remaining on the bag at the completion of a run. Also, the location particles are deposited, either on the surface or within the filter bag, should be determined, which is likely to require SEM analysis.

The cake thickness could easily be measured and the filter drag calculated from knowledge of the baghouse differential pressure and the volumetric air flow through the bag. The residual mass of powder on the bag could be determined from the difference between the original bag weight before the run and the bag and powder weight at the end of the run.

A small apparatus could be made up to give estimates of the relative cake adhesion. At a fixed flow through a sampling pump, a nozzle and filter assembly, such as that mentioned in Chapter Four, could be placed against the filter cake for a given time period. At the end of this time, the collected powder could be weighed. To allow comparison with other runs, which would use the same pump flow and collection time, the collected mass of powder would need to be normalised by dividing the collected powder by the total residual powder remaining on the bag at the end of the run. This would give the percentage of the total residual powder collected by the sampler. A small local suction pad could be loaded up with SMP to produce the required filter cakes, or alternatively, cakes produced on the single cell baghouse could be used.

A measure of the cohesiveness of the SMP produced at different bulk fat contents could be obtained by using a Jenike Shear cell or a cohesive tester. To make these tests more relevant

to the industrial setting, the powder could be sheared against filter bag material. If these experiments are carried out, it is recommended that they are done at constant humidity and temperature. This could be achieved if the samples are stored in an oven at the same temperature as that in the industrial baghouses for SMP production, before the runs are quickly conducted at ambient conditions.

To clarify that no change in baghouse inlet particle size distribution occurs in relation to the amount of bulk fat in SMP, the isokinetic sampling method mentioned in Chapter Four could be used at either ED2 or ED3. This would require a hole to be cut into one of the baghouse inlet ducts and a flange mounted to house the sampling unit.

7.7. Conclusions and Recommendations

From the results and discussion above it is concluded that the baghouse differential pressure is very sensitive to the amount of bulk fat present in SMP. Furthermore, a lack of bulk fat in SMP has the ability to cause the entire spray dryer plant to automatically shut down. Therefore, strict control of the SMP bulk fat content is recommended. This can be achieved by cream dosing in the milk standardising area.

With regard to the mechanism behind this phenomenon, this investigation showed that the change in baghouse differential pressure was not due to changes in the baghouse filtration velocity. There was also no apparent change in fines concentration as measured by an optical scintillation instrument and no apparent correlation discernible between the powder bulk fat content and the baghouse fines return line pressure. It can therefore be concluded that a change in SMP bulk fat content does not change the amount of SMP fines and through that, the baghouse differential pressure. It was also concluded that no apparent change in particle size occurs, which is to be expected as such small changes in the composition of the milk concentrate are likely to have little influence on the atomisation process, and thus, changes in baghouse differential pressure are not due to this mechanism.

ESCA measurements and SEM images showed that fat is over-represented on the surface of milk powder particles, and only small changes in the bulk fat content are required to see large changes in surface coverage for SMP. It is hypothesised that an increase in surface fat

coverage causes clumping of powder on the filter bags. These clumps are thought to have two consequences a) the cake is more porous and b) the cake is deposited on the surface of rather than the interior of the filter fabric, and is more easily removed during pulse cleaning. Therefore, the baghouse differential pressure is expected to be reduced with an increase in SMP bulk fat content.

It is recommended that further research be carried out in this area to fully understand this mechanism. This research should be carried out at the pilot scale so it will be possible to investigate properties such as the structure, porosity, thickness and permeability of filter cakes produced from SMP at different bulk fat contents.

8. Design of Pulse-Jet Baghouses

Due to operational issues and significantly different designs of washable baghouses in the New Zealand dairy industry, uncertainty surrounded the suitability of these designs. Therefore, this chapter investigates the design of pulse-jet baghouses with a specific focus on milk powder collection.

8.1. Background

Despite the numerous advantages of the washable baghouse system over the traditional cyclone system, as already highlighted, high differential pressures, some blinding and bag damage due to bag movement have caused frequent interruptions to the dryer operation across all Fonterra milk powder plants with washable baghouses. Consequently, the suitability of these baghouse designs is brought into question.

Fonterra currently operates milk powder plants with three different types of washable baghouse designs. WP2 has a Lubbers design; CD2, ED2 and ED3 a GEA Niro A/S Sanicip design; and CD2 and TA Dryers A and B, are all Intensive designed washable baghouses. There is uncertainty within the industry if one of these three designs is a better design than the others. In addition to this, because these units of process equipment are in their infancy, there is very little industry knowledge on how to and what is a suitable design for a milk powder plant washable baghouse.

8.1.1. Aim

The aim of this work was to examine the design of pulse-jet baghouses applied to milk powder production. The key design parameters available from the open literature were to be explored, a design procedure determined and the most suitable of the available air to cloth ratio guidelines for milk powder collection from the open literature established from Fonterra industrial experience.

8.2. General Pulse-Jet Baghouse Design

8.2.1. Baghouse Design Parameters

8.2.1.1. Air to Cloth Ratio

One of the most important aspects of filter selection is the air to cloth ratio (V_f [m^3 / m^2 / min]) (Morgan & Walters, 1999). It is the ratio of the inlet gas flow $Q_{BH,in}$ [m^3 / min] to the required filtration area A_f [m^2] as shown in Equation 8-1. This gives the air velocity at the external surface of the filters, that is, the filtration velocity (Agarwal, 2005):

$$V_f = \frac{Q_{BH,in}}{A_f} \tag{8-1}$$

where A_f is given by

$$A_f = nA_b \tag{8-2}$$

n is the total number of bags and A_b the filtration area [m^2] of a single bag (ignoring the end area) given by

$$A_b = \pi D_b L_b \tag{8-3}$$

where D_b [m] and L_b [m] are the bag diameter and length.

The choice of the air to cloth ratio is based on tests or knowledge of past experiences with similar dusts (Croom, 1995). Factors that affect this ratio are the dust loadings, the fineness of dust and the type of filter medium used (Agarwal, 2005). Also, the particle shape, cohesiveness of the deposited dusts and the stickiness of the particles' impact on the air to cloth ratio (Turner et al., 1998).

A number of authors (Agarwal, 2005; Moore et al., 1996; Morgan & Walters, 1999; Vidmar, 1990) state that the effects of operating at high air to cloth ratios are that particles become imbedded in the pores of the filter medium and cannot be removed by cleaning. Thus the bags become blinded and a higher differential pressure results, which increases operating costs and shortens bag life. Morgan and Walters (1999) also state that the higher the air to cloth ratio, the greater the re-entrainment of dust. This has the effect of an overall increase in dust loadings.

According to Vidmar (1990), an acceptable air to cloth ratio range is between 6 to 8 ft^3 / min / ft^2 (1.83 to 2.44 m^3 / m^2 / min). Agarwal (2005) states that the air to cloth ratio should never exceed 12 ft^3 / min / ft^2 (3.66 m^3 / m^2 / min) and that the ratio should be reduced as the

particle size decreases; 0.31 to 1.53 m^3 / m^2 / min for powder less than 200 µm in diameter, 1.53 to 2.14 m^3 / m^2 / min for granular material and 2.14 to 2.75 m^3 / m^2 / min for pelleted materials. Masters (1972) states that pulse jet baghouses can operate effectively up to 15 ft / min (4.6 m^3 / m^2 / min) on particle sizes in the exhaust air from spray dryers.

Moore et al. (1996) indicate that the air to cloth ratio should be reduced as the bag length increases: 2.44 m^3 / m^2 / min for 2.44 m long bags, 1.98 m^3 / m^2 / min for 3.05 m long bags and 1.68 m^3 / m^2 / min for 3.66 m long bags.[1] Their reasoning is that these air to cloth ratios will maintain a suitable elutriation velocity in the baghouse of 6 ft / s (1.8 m / s). Löffler et al. (1988) propose that for applications with more than 200 bags, the maximum air to cloth ratio can be increased by 10 %.

These suggested maximum values for pulse-jet baghouses are shown with their sources in Figure 8-1. It can be seen that they vary by approximately 90 %, from a value of 2.4 m^3 / m^2 / min (Moore et al., 1996; Vidmar, 1990) to 4.6 m^3 / m^2 / min (Masters, 1972). Löffler et al. (1988) mentions that conservative air to cloth ratios should be used to avoid the potential problems mentioned above. However, a downside of this is that the filter will be more expensive due to the increased size (Morgan & Walters, 1999) and that the baghouse will contain unused filter capacity (Löffler et al., 1988).

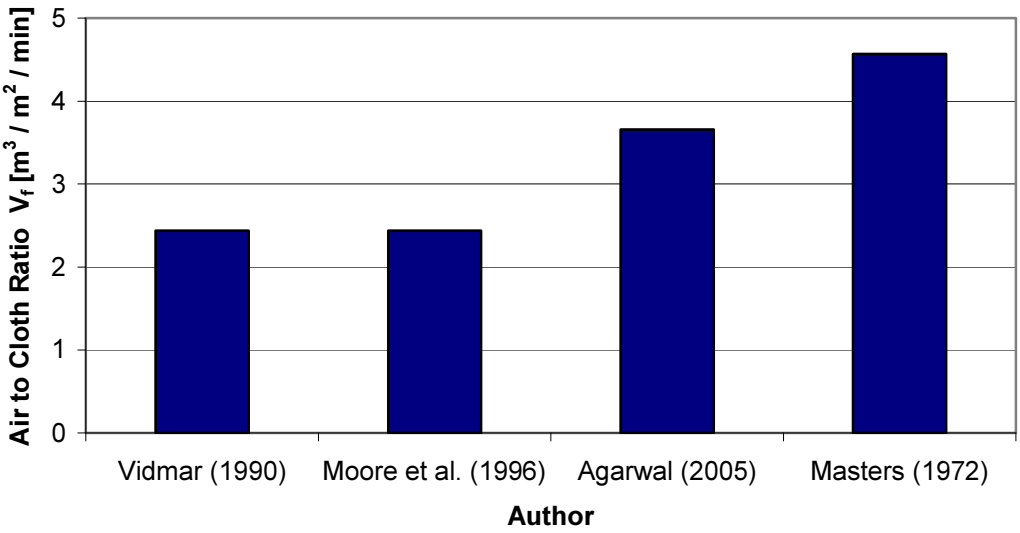

Figure 8-1: Maximum pulse-cleaned baghouse air to cloth ratios recommended by various authors

[1] A linear extrapolation gives 1.06 m^3 / m^2 / min for a 6.0 m long bag

8.2.1.2. Elutriation Velocity

The elutriation velocity V_e [m / s] is determined by dividing the gas flow Q_{in} by the cross-sectional area of the vessel minus that of the bags (Equation 8-4). This parameter is termed the can velocity by a number of authors (Croom, 1995; Moore et al., 1996; Agarwal, 2005).

$$V_e = \frac{Q_{BH,in}}{A_{BH} - A_{Bags}} \tag{8-4}$$

For a circular baghouse the footprint A_{BH} [m^2] is given by Equation 8-5 where D_{BH} [m] is the baghouse diameter.

$$A_{BH} = \pi\left(\frac{D_{BH}}{2}\right)^2 \tag{8-5}$$

A_{Bags} [m^2] is the total cross sectional area of the bags given by

$$A_{Bags} = n\pi\left(\frac{D_b}{2}\right)^2 \tag{8-6}$$

Although the definition of Equation 8-4 uses the total plan baghouse area, a more accurate definition would use the bag bundle area as the re-entrainment of dust removed from the bags during cleaning within the bag bundle is of more interest (see Figure 8-2).

Equation 8-4 assumes that the gas flow within the bag bundle is uniform, both between the bags and along the length of each bag. This is believed to be an extreme case as not all gas flow down the annular area outside of the bag bundle from a top entry inlet, or across the bag bundle for a bottom entry inlet, is evenly distributed; there will have been some radial flow into the bag bundle and into the clean side of the bags.

The elutriation velocity is important because if it is too high, it will inhibit dust falling off the bag surface into the hopper and promote recirculation of the dust (Agarwal, 2005). This will have the same effect as increasing the inlet dust loadings (Morgan & Walters, 1999). If the elutriation velocity is too low, a larger housing than necessary will result, increasing the original capital cost (Croom, 1995).

The upper limits of the elutriation velocity, again with their sources, are given in Table 8-1. The basis for the elutriation velocities is a single particle terminal velocity in the baghouse (Agarwal, 2005). However, the terminal velocity is strongly dependant on particle size, and it is unclear which size should represent the powder falling off the bags. It is reported that the

elutriation velocity should be evaluated by tests or deduced from experience but that any value above 250 ft / min (1.27 m / s) is unacceptable (Croom, 1995). Moore et al. (1996) indicate from their field experience a limiting value of 6 ft / s (1.83 m / s) should be used to avoid the dust remaining in suspension. However, these authors do point out that this value can be exceeded with light duty applications or when capturing heavy dusts. The Agarwal (2005) guideline values include particle size limitations of 150 ft / min (0.76 m / s) for fine powders, 250 ft / min (1.27 m / s) for granular materials and 300 ft / min (1.52 m / s) for pelleted materials.

Table 8-1: Recommended maximum elutriation velocities

Author	V_e [m / s]
Croom (1995)	1.27
Agarwal (2005)	1.52
Moore et al. (1996)	1.83

The bag spacing (X_b [m]) is defined as the perimeter-to-perimeter distance between neighbouring bags. By increasing this parameter, the elutriation velocity can be decreased. Alternatively, the elutriation velocity can be decreased with constant bag spacing, by reducing the bag diameter. Hence Bergmann (2001) suggests the following bag spacing to achieve adequate elutriation velocities: 2 inch for 11.5 inch diameter bags (17 % of the bag diameter); 1.5 inch for 8 inch diameter bags (19 % of the bag diameter); 1 inch for 5 (20 % of the bag diameter); and 6 inch (17 % of the bag diameter) diameter bags. Löffler et al. (1988) gives a minimum bag spacing of 50 to 80 mm for jet filters to ensure that dust removed by pulse cleaning is not pulsed onto neighbouring bags.

It is surprising that no source mentions a relationship between bag spacing and bag length. One would expect that the longer the bag, the greater the bag spacing required to prevent the long bags rubbing and abrading near the base of the bags.

8.2.1.3. Choice of Filter Medium

Although not investigated in this PhD project, the choice of filter media is a key design parameter. Croom (1995) again indicates that selection should be based on experience as well

as testing and performance guarantees. Factors that must be considered are bag permeability, filtration velocity, filter drag and the bag properties such as weight, thickness and surface treatment. For a greater coverage of this topic refer to Löffler et al. (1988), Cora and Hung (2002), or Barnett (2000).

8.2.1.4. Operating Differential Pressure

Cora and Hung (2002) indicate that the airflow resistance causes the baghouse differential pressure when the air passes through the cake and the bag. Croom (1995) states that the following parameters affect the differential pressure; air to cloth ratio, media type, dust loadings, particle size distribution, elutriation velocity, cleaning efficiency and the porosity of filter cake. Fonterra industrial experience shows that the age of the bag also has a large impact on the baghouse differential pressure, as the older the bags, the more blinded they become.

Agarwal (2005) states the operating differential pressure in a baghouse should be 4 – 8 inches of water (100 – 200 mm H_2O). When this pressure rises to 10 in H_2O (250 mm H_2O), these authors suggest that the bags should be replaced.[2] Finally, Agarwal (2005) indicates when the plant is running on air with clean bags, the operating pressure should be approximately 1 in H_2O (25 mm H_2O). However, if the plant is running with dirty air and this differential pressure is found, there will be holes in the bags (Agarwal, 2005). Masters (1972) states the pressure drop for a baghouse on a spray drying plant ranges between 1.5 – 8 in H_2O (38 – 200 mm H_2O).

The baghouse differential pressure needs to be considered in the design because of its influence on operating costs. The higher the differential pressure, the higher the energy costs for running the fans that suck or blow the air through the baghouse (Cora & Hung, 2002; Caputo & Pelagagge, 2000). Cleaning too frequently, thus maintaining a low differential pressure, will increase compressed air costs, accelerate bag wear, that is, induce higher operating costs, and higher dust emissions also result (Caputo & Pelagagge, 2000).

[2] The Fonterra GEA Niro A/S Sanicip plants will automatically switch to water if the baghouse differential exceeds 180 mm H_2O and automatically shut down if the differential exceeds 200 mm H_2O. Bags are typically replaced when the differential pressure exceeds 150 mm H_2O.

The cleaning efficiency is important to maintain a suitable differential pressure, as determined by operating costs. According to Cora and Hung (2002), the frequency of the cleaning cycle is strongly dependent on the particle size of the dust. Agarwal (2005) shows that pulse frequencies can vary between 30 seconds and 2 minutes, and the pulse durations between 0.05 and 0.1 s. Masters (1972) states that for single bag cleaning the pulse duration can be 0.1 – 0.2 s and occur every 10 – 15 s. Turner et al. (1998) and Masters (1972) warn that the larger the interval between bag cleaning, the lower the air to cloth ratio must be.

Agarwal (2005) also states that an alternative to a timed control is an automatic system based on differential pressure; the pulse is initiated once an upper limit is reached, then stopped when the lower limit is achieved. This can increase bag life and save on compressed air usage.

Moore et al. (1996) state that a poor venturi design may cause bags to rupture or abrade as they are snapped back by the shock wave of the cleaning pulse. Further, these authors warn that high energy pulse jets can be highly destructive if bags are not designed to withstand the additional force. The pressure of the pulse can be reduced if this is the case, depending on dust loadings (Agarwal, 2005).

8.2.1.5. Bag Dimensions

The required air to cloth ratio can be accomplished by a number of different combinations of bag length and diameter. Agarwal (2005) states that the pulse jet cleaning efficiency drops as the bag length increases because of the energy decay in the pulse from the top to bottom of the bag. Löffler et al. (1988) suggest bag length is limited by the type and location of the pulse jet nozzle. These authors recommended that the air to cloth ratio be decreased for bags in excess of 3 m, as bags longer than this are likely to touch and abrade near the bottom.

Löffler et al. (1988) indicate that the bag diameter is the largest influence on space requirements and therefore the installation cost; narrow bags require larger numbers but wider bags can tend to be spaced too closely resulting in poor cleaning, presumably because powder pulsed from one bag is thrown onto neighbouring bags. Hence, these authors recommend careful consideration of bag length and diameter but state a 200 mm diameter as the upper limit and that 120 - 150 mm is optimal for pulse jet filters.

Again, there are several guidelines available on what is a suitable combination of bag length and diameter. Bergmann (2001) suggests a length to diameter ratio of 33 be used. Agarwal (2005) advises the maximum bag diameter should be limited to 5 or 6 inches (0.127 or 0.152 m) and the length should generally be 6 to 8 feet (1.83 to 2.44 m). Moore et al. (1996) state that the bag length also affects the vessel height, the area required to house the filter medium and the overall baghouse footprint, that is, the capital cost. Thus, these authors recommend bags 10 ft (3.0 m) in length because of price, efficiency and size ratio but 12 ft (3.7 m) for applications where floor space is limited. For bag diameters Moore et al. (1996) believe the standard 4.5 inch bag be replaced with a 6 inch bag due to cost efficiencies. These recommended optimal and maximum bag dimensions are summarised in Table 8-2.

Table 8-2: Recommended bag dimensions

Author	Diameter D_b [mm]		Length L_b [m]		Ratio L_b / D_b	
	Optimal	Max	Optimal	Max	Optimal	Max
Agarwal (2005)	127 – 152	152	1.8 – 2.4	3.7	14.2 – 15.8	24.3
Moore et al. (1996)	152	-	3.0	3.7	19.7	-
Löffler et al. (1988)	120 – 150	200	-	-	-	-

8.2.1.6. Baghouse Footprint

The space requirement for a baghouse has a large bearing on the cost of the installation; the larger the filtration area, the more bags, cages, valves and control equipment needed which all takes up space (Löffler et al., 1988). Vidmar (1990) states that larger collectors will cost more initially, but yield longer bag life and reduce maintenance costs. Further from Vidmar (1990) 'if space or funds are limited smaller collection systems with slightly higher air to cloth ratio may be necessary, but such systems result in shorter bag life and higher operating pressures'.

Two authors give guidelines for the optimal footprint of the baghouse, that is, the diameter of the vessel. The optimum of Löffler et al. (1988) is based on the bag diameter and spacing;

the larger the bag diameter and the greater the spacing, the fewer bags that should be housed per square meter of floor area. Löffler et al. (1988) do not say what the driver for this optimum is but a sound guess would be to ensure suitable elutriation velocities are maintained.

Croom (1995) explains that a reduced floor area will permit fitting the collector into a smaller plant layout, which can be critical. The optimal footprint from these guidelines is chosen such that the air to cloth ratio and elutriation velocity limits for the chosen bag length and bag spacing are maintained.

If the baghouse is located indoors with other process equipment, careful consideration of the use of available building space is required. In milk powder plants for example, the height of the building is determined by the height of the spray dryer, which will always be greater then the height of the baghouse. Therefore, a tall, thin baghouse makes better use of the building volume than a shorter, squatter design.

The baghouse footprint A_{BH} [m^2] consists of the area of the bag bundle A_{BB} [m^2] and the area between the edge of the bag bundle and the baghouse walls. Equation 8-7 gives the bag bundle area, where N [m^{-2}] is the bag density (number of bags per unit area of A_{BB}).

$$A_{BB} = \frac{n}{N} \tag{8-7}$$

For bags arranged in a square matrix spaced perimeter-to-perimeter distance X_b apart, the bag density N [m^{-2}] is given by

$$N = \frac{1}{\left(D_b + X_b\right)^2} \tag{8-8}$$

Therefore, for a circular baghouse, the diameter of the bag bundle D_{BB} [m] is given by Equation 8-9

$$D_{BB} = 2\left(D_b + X_b\right)\sqrt{\frac{n}{\pi}} \tag{8-9}$$

It is often more convenient to state the baghouse diameter instead of the baghouse footprint. The baghouse diameter is the sum of the bag bundle diameter and twice the gap G [m] from the edge of the bag bundle to the baghouse wall as shown in Figure 8-2 and given by Equation 8-10.

$$D_{BH} = D_{BB} + 2G \tag{8-10}$$

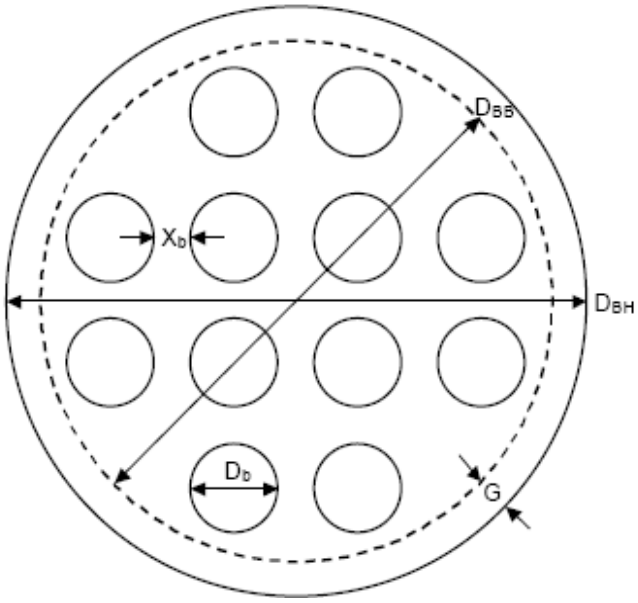

Figure 8-2: Definition of parameters required to determine baghouse footprint in a circular baghouse

8.2.1.7. Inlet Arrangement

The design of the dirty air inlet is critical to good baghouse performance. According to Agarwal (2005) a properly designed inlet can reduce the dust loadings on bags. A uniform distribution of the inlet air across the full cross section of the baghouse is needed (Croom, 1995) which will give minimum drag and improve the separation efficiency (Löffler et al., 1988). Löffler et al. (1988) suggest as large an inlet cross section as possible be used to achieve this.

High inlet velocities cause problems with bag abrasion and can impart significant swinging motions on the bags (Parker, 1997; Morgan & Walters, 1999; Moore et al., 1996) both of which lead to a reduced bag life. Moore et al. (1996) state that the inlet air stream should be taken from around 3500 ft / min (17.8 m / s) and slowed to 350 ft / min (1.78 m / s) in a short distance. Croom (1995) recommends reducing the velocity in the inlet duct to below 10 m / s. Löffler et al. (1988) imply that gas velocities in the inlet duct should be kept low, as these authors suggest avoiding small inlet ducts. These authors also state that potential turbulence in the baghouse is to be avoided as it could interfere with the cake build up and therefore, reduce separation efficiency.

There are a number of different options available for the dirty air inlet. The most common type is a radial entry fitted with a baffle plate. Moore et al. (1996) state that a full-length baffle plate was common in older designs but was costly. Fitting gas flow correction baffles will eliminate bag abrasion, and surprisingly, reduce emissions (Parker, 1997).

Several authors (Croom, 1995; Moore et al., 1996; Agarwal, 2005) suggest the use of an angled baffle plate to direct the dust down to the hopper and distribute the inlet gas. However, Croom (1995) warns that this is not suitable for very fine powders. Other baffle options to help improve inlet gas distribution include a perforated baffle, which can block with dust, or the use of a diffuser, a series of deflector plates across the inlet (Croom, 1995).

Löffler et al. (1988) recommend for aspiration type filters a tangential entry. Croom (1995) states that this type of entry is used for larger particle sizes, which could reduce the dust loadings to an acceptable level for filtration. Moreover, Croom (1995) mentions a tangential entry needs a high inlet velocity for good cyclonic separation and at best, the collection efficiency is similar to a cyclone, between 75 and 90 %. Agarwal (2005) states that a tangential entry is seldom used because it can result in the smearing of solids on the vessel walls, particularly when they are soft or sticky, and that the high tangential velocity can cause erosion of the vessel walls.

8.2.1.8. Other

A number of other factors need to be considered for a successful baghouse design. According to Moore et al. (1996) the baghouse hopper design is important because if it is too short, dust levels can rise too high leading to re-entrainment. Agarwal (2005) suggests the hopper angle be at least 60^{o} from the horizontal. Other choices for the design include a cylindrical versus rectangular baghouse (Agarwal, 2005) and top or side bag removal (Moore et al., 1996).

8.2.1.9. Collection Efficiency

The baghouse collection efficiency is a key parameter used to assess the performance of a baghouse. Löffler et al. (1988) state the overall collection efficiency ϕ of a baghouse can be determined from Equation 8-11 where m_{col} [g / s] is the mass flow of collected powder and m_{in} [g / s] the mass flow of powder in the feed stream:

$$\phi = \frac{m_{col}}{m_{in}} \tag{8-11}$$

Equation 8-11 can be rewritten in terms of the outlet air powder flow m_{out} [g / s] as shown in Equation 8-12:

$$\phi = 1 - \frac{m_{out}}{m_{in}} \tag{8-12}$$

More frequently the inlet air and outlet air stream powder concentrations are known because of online monitoring. If the total feed air flow is equivalent to the outlet air flow then Equation 8-12 can be rewritten as Equation 8-13 where c_{in} [g / m^3] and c_{out} [g / m^3] are in the inlet and outlet air powder concentrations respectively:

$$\phi = 1 - \frac{c_{out}}{c_{in}} \tag{8-13}$$

It has been shown (Schmidt, 1995) that between 60 % and 90 % of emissions are due to pulse cleaning; once the filter cake has been removed from the filter bag, particles pass more easily through the bag polluting the clean air. The emissions then decrease because as the filter cake grows, its collection efficiency increases. Therefore, the emissions peak immediately after the cleaning pulse, and decrease with time until the next cleaning pulse (Löffler et al., 1988).

8.2.2. Design Procedures

The key baghouse design parameters have been covered in section 8.2.1 above. This section presents baghouse design procedures.

The best baghouse design is one that takes both the air to cloth ratio and the elutriation velocity into account and strikes a delicate balance between the two (Moore et al., 1996). According to Löffler et al. (1988) a baghouse design can never be too large, but because of cost aspects, the optimum design is obtained by considering the space needed for the installation, the plant capital cost and operating expenses.

The design philosophy of Morgan and Walters (1999) is to size the dust collector to capture the sub micron particulates while designing the inlet to drop out the larger particles. Thus their method is to choose the appropriate filter type and medium, determine optimum air to

cloth ratio, calculate a suitable elutriation velocity which fixes the collector size, select the appropriate inlet configuration and finally design the hopper for dust removal.

Croom (1995) reports that consideration of the velocity limits and associated performance benefits should drive the design. His velocities to consider are the inlet duct conveying velocity, the baghouse inlet velocity and entry loss reduction, the elutriation velocity, the filtration velocity and the tube sheet or filter outlet velocity (the velocity of the gas as it flows from the top of the bag into the clean air plenum), which becomes more important for longer bags. Thus Croom's method for optimal sizing is to obtain the appropriate filtration velocity, determine the bag length given the air to cloth ratio and the elutriation velocity, calculate the number of bags from a chosen length and diameter combination and ascertain the baghouse foot print area from the number of bags and their spacing to maintain a suitable elutriation velocity.

The method covered by Turner et al. (1998) is slightly different from those mentioned above as the design is driven by a limitation on the baghouse pressure drop. Once this parameter has been specified, the cleaning parameters of cleaning frequency and energy are determined. From field, pilot plant or laboratory measurements, the values of coefficients such as cake resistance, clean bag resistance and cleaning efficiency must be obtained. A value is estimated for the air to cloth ratio and the average pressure drop is calculated. If this value matches the specified value, the design is complete. If not, the air to cloth ratio must be readjusted and the procedure repeated until the specified and calculated pressure drops are equal.

8.2.2.1. Design Procedures Rationalized

There exist nine baghouse design parameters (previously defined): $Q_{BH,in}$, V_f, V_e, n, L_b, D_b, X_b, G and D_{BH}. Rearranging Equations 8-1, 8-4 and 8-10 with respect to these parameters gives Equations 8-14, 8-15 and 8-16:

$$V_f = \frac{Q_{BH,in}}{n\pi L_b D_b} \tag{8-14}$$

$$V_e = \frac{4Q_{BH,in}}{\pi\left(D_{BH}^2 - nD_b^2\right)} \tag{8-15}$$

$$D_{BH} = 2G + \sqrt{\frac{4n}{\pi}\left(D_b + X_b\right)^2} \qquad (8\text{-}16)$$

Because there are nine parameters and three equations, six parameters must be specified. The inlet air flow $Q_{BH,in}$ is specific to the application and determined from the upstream process feeding the baghouse. Upper limits for air to cloth ratio V_f, elutriation velocity V_e, bag length L_b and bag spacing X_b are discussed above and can be used as the specified values for the initial stage of the design. The gap G, between the edge of the bag bundle and the baghouse walls may be chosen such that it is greater than the between-bag distance. In the interest of distributing the incoming airflow evenly to the bag bundle, a baffle to deflect a radial inflow, or a tangential inflow may be used, both in conjunction with a sufficiently large annular flow area. Initial annular velocities V_{Anl} [m / s], defined by Equation 8-17, should be no larger than the inlet velocity, meaning that the area (GL_b) should be no less than the inflow area. This is normally set so that the inlet duct velocity is larger than the minimum particle carrying velocity, generally around 15 m / s. Thus all six parameters have been specified.

$$V_{Anl} = \frac{Q_{in}}{GL_b} \qquad (8\text{-}17)$$

The system of equations can easily be solved using standard optimisation packages, for example Microsoft Excel Solver. A spreadsheet can be created listing the values of the six specified parameters, initial guesses for the three remaining unknowns (n, D_b and D_{BH}) and calculated values of the air to cloth ratio, the elutriation velocity and the baghouse diameter. The solver target cell is calculated as the squared difference between the repeatedly guessed baghouse diameter and that calculated from Equation 8-16. The solver is run to minimise this target cell by changing the values of the three guessed unknowns with constraints placed on the maximum air to cloth ratio, elutriation velocity and bag diameter.

Although this process generates one optimal design, a cost optimisation may be the next step for example, Caputo and Pelagagge (2000) who deal with some of the above parameters. The cost of accessories (bags, cages, solenoid valves, air ejectors) will feature in this optimisation.

By including the area between the edge of the bag bundle and the baghouse walls, which is significant in practice, this sequence differs slightly from those found in the literature. Löffler et al. (1988) list seven design parameters ($Q_{BH,in}$, V_f, L_b, D_b, n, X_b, D_{BH}), specify five values ($Q_{BH,in}$, V_f, L_b, D_b and X_b) and solve two equations (n, D_{BH}) based on a square bag matrix.

Löffler et al. (1988) vary the bag diameter and bag spacing to minimise the capital cost within the recommended limits of the parameters above (as long as cleaning performance and bag life are not compromised).

Croom (1995) lists eight design parameters ($Q_{BH,in}$, V_f, V_e, L_b, D_b, n, X_b, D_{BH}) as he also includes the elutriation velocity, specifies six values ($Q_{BH,in}$, V_f, V_e L_b, D_b and X_b) and solves two equations (n, D_{BH}) based on a square bag matrix. From the resulting numbers, the elutriation velocity is checked. To suit design standards and supplier templates, and to minimise the capital cost related to number of bags and the baghouse footprint (while maintaining velocity limits), the bag diameter or length is varied.

The procedure developed here may be illustrated by using a baghouse application where the inlet air flow is 1000 m^3 / min. The value of the six parameters requiring specification are set at: an air to cloth ratio of 1.6 m^3 / m^2 / min; a maximum elutriation velocity of 68.4 m / min; a bag length of 3.0 m; a bag spacing of 0.08 m; and a distance between the bag bundle and the baghouse wall of 0.35 m. Solving using Microsoft Excel Solver from an initial guess of n = 380, D_b = 0.15 m and D_{BH} = 7 m gives the values shown in column two of Table 8-3.

Table 8-3: Results of baghouse design procedure example

Parameter	Solver	Option 1*	Option 2*
$Q_{BH,in}$ [m^3 / min]	1000	1000	1000
X_b [m]	0.08	0.08	0.08
L_b [m]	3.0	3.0	3.0
G [m]	0.35	0.35	0.35
V_f [m^3 / m^2 / min]	1.6	1.6	1.6
V_e [m / min]	45.3	45.5	44.9
n [-]	380	442	332
D_b [m]	0.17	0.15	0.20
D_{BH} [m]	6.3	6.2	6.5

* These options correspond to commercially available bag diameters

The range of bag diameters available from bag suppliers affects the chosen bag diameter. In the example above, if 0.17 m bags are not available, a choice is made between 0.15 m and

0.20 m bags. The results of calculations run using these values are shown in columns three and four of Table 8-3. Using 0.20 m rather than 0.15 m diameter bags requires 110 fewer bags. Although the baghouse diameter increases from 6.2 to 6.5 m and will therefore have a higher material cost than the first option, it is likely that having 110 fewer bags, support cages, solenoid valves and compressed air ejectors will make the second option cheaper.

Another point to note is that the total number of bags required may need to be adjusted. Bags are arranged in a uniform manner, so if 442 or 332 bags do not produce a uniform pattern, extra bags will need to be added until the arrangement is uniform. The number of bags should never be rounded down to create a uniform pattern, as this would cause the desired air to cloth ratios to be exceeded.

8.2.3. Milk Powder Collection

Clearly, the air to cloth ratio is one of the key baghouse design parameters. Several authors have a separate design procedure to establish suitable values for air to cloth ratios for milk powder collection. Each is based on applying a number of factors that take account of gas and dust properties when estimating an initial air to cloth ratio for milk powder.

Croom (1995) applies correction factors as shown in Equation 8-18, where a nominal filtration velocity V_{fn} [m^3 / m^2 / min] is modified by correction factors for the application type (B), gas temperature (T), particle size (P) and dust load (D) to give a final filtration velocity V_{fe} [m^3 / m^2 / min]. For pulse-jet cleaning milk powder with a resting bulk density of 0.24 – 0.48 g /m^3 (15 – 30 lb / ft^3), V_{fn} is 2.44 m^3 / m^2 / min (8.0 ft / min). The application factor B is based on the collection situation: oily moist or agglomeration dusts, product collection or nuisance collection.

$$V_{fe} = V_{fn} \times B \times T \times P \times D \qquad (8\text{-}18)$$

Löffler et al. (1988) determine the effective air to cloth ratio V_{fe} m^3 / m^2 / min] from Equation 8-19:

$$V_{fe} = V_{fn} \times A_n \times B \times P \times D \times T \times F \times I \times H \qquad (8\text{-}19)$$

Like Croom (1995), factors are applied for application type (B), gas temperature (T), particle size (P) and dust load (D). Additional factors are:

- bulk flow behaviour (F), for dusts with bulk densities less than 600 kg / m^3

- flue gas flow (I), for online cleaning and upwards gas flow past the bags
- tropical climate factor (H), applicable for food production and dusts with hygroscopic tendencies
- filter system factor (A_n), distinguishing between single bag or group pulsing, and on-line or offline cleaning.

Löffler et al. (1988) vary the base air to cloth ratio V_{fn} between 1.6 – 2.5 m^3 / m^2 / min, depending on the fat content of the milk powder. This author also lists base values of 2.6 - 3.0 m^3 / m^2 / min for spray dried protein and 2.2 - 2.6 m^3 / m^2 / min for whey powder. Thus, Löffler et al. (1988) are the first authors to allude to the influence of milk powder composition on the air to cloth ratio.

Turner et al. (1998) published a design procedure for the United States Environmental Protection Agency (USEPA) in 1998, with a specific method for pulse-jet baghouses. Again, factors for application type (B), gas temperature (T [^oF]), dust loadings (D_T [gr / ft^3]) and particle size (P [μm]) are applied. The USEPA guideline uses the material factor, A_T, instead of a base air to cloth ratio used by Croom (1995) and Löffler et al. (1988), to distinguish between different dusts. Once these five factors are determined, the recommended air to cloth ratio, V_{fe} [ft / min], is calculated using Equation 8-20:

$$V_{fe} = 2.878 A_T B T^{-0.2335} D_T^{-0.06021} \left(0.7471 + 0.0853 \ln P\right) \qquad (8\text{-}20)$$

Milk powder is listed under the material factor category with solids that are unstable in their physical or chemical state due to hygroscopic nature, sublimation, and/or polymerization.

The Intensiv-Filter (1999) guideline is presented in tabulated form. The suggested air to cloth ratio is based on dust size and then a chosen combination of gas temperature, application type and dust loadings. Factors are then applied for dust loadings, if different from those initially chosen, and bag length, both of which inversely affect the air to cloth ratio. Only the Intensiv-Filter (1999) guideline applies a factor for bag length.

8.3. Fonterra Washable Baghouse Designs

This section lists the values of the key baghouse design parameters for the Fonterra milk powder plant washable baghouses. Also, the recommended milk powder air to cloth ratios are calculated for the products made in each plant using the four guidelines of Croom (1995),

Intensiv-Filter (1999), Löffler et al. (1988) and Turner et al. (1998) and are compared to the current Fonterra values.

It has been mentioned several times that the information required to use the factorial methods above is most often derived from past experiences or from product testing. Particle size distributions, particle densities and outlet gas temperatures for spray dryers in the New Zealand Dairy Industry are well known. However, the key factor of fines loadings is not easily obtainable as this parameter is not measured industrially or published in the open literature. However, the work presented in Chapter Four has determined the fines loadings for several powders in three Fonterra milk powder plants.

To apply these guidelines to the current Fonterra plants, it is assumed that the fines fractions shown in Chapter Four apply to the main washable baghouses across all sites. Cream powder (CP) is assumed to have a similar percentage of fines as WMP, that is, 49 %. The fines loadings in the vibrating fluid bed baghouses are assumed to be less than 20 g / m^3.

The second assumption made is for the base air to cloth ratios of Löffler et al. (1988). It is assumed that these authors suggest an air to cloth ratio of 1.6 m^3 / m^2 / min for SMP, 1.9 m^3 / m^2 / min for buttermilk powder (BMP), 2.2 m^3 / m^2 / min for WMP and 2.5 m^3 / m^2 / min for CP, as discussed previously in this report.

8.3.1. Main Washable Baghouses

The key baghouse parameters for the main washable baghouses are shown in Table 8-4 below. Also included is the bag number density in the bag bundle and the annular velocity, the velocity of the air in the area outside the bag bundle. Although some of these parameters vary with different products, those presented in the table are for the most common products made in the plant.

Table 8-4: Fonterra main washable baghouse design parameters

Design Parameter	WP2	CD2 / ED2 / ED3	CD3
Inlet Air Flow $Q_{BH,in}$ [m^3 / s]	36.7	34.5	32.2
Air to Cloth Ratio V_f [m^3 / m^2 / min]	3.3	2.2	2.6
Elutriation Velocity V_e [m / s]	4.5	3.0	1.7 - 3.3 [3]
Number of Bags n	177	240	260
Bag Length L_b [m]	6.0	6.0	5.6
Bag Diameter D_b [mm]	208	208	165
Bag Spacing X_b [mm]	55	60	50
Outer Spacing G [mm]	150	160	270
Baghouse Diameter D_{BH} [m^2]	4.25	5.0	4.4
Bag Number Density N [m^{-2}]	14.5	13.9	21.6
Annular Velocity V_{Anl} [m / s]	40.5	36.5	21.2
SMP Operating Issues?	Yes	Yes	N / A
WMP Operating Issues?	No	No	No
MPC Operating Issues?	N / A	No	N / A

8.3.1.1. Whareroa Powder 2

Whareroa Powder 2 is one of five milk powder plants located on the Whareroa site, south of Hawera. A retrofit prior to the start of the 2000/2001 season saw the original cyclone system replaced with a Leubbers designed washable baghouse, the first washable baghouse installed in New Zealand.

As Table 8-4 above shows, this baghouse has the highest air to cloth ratio (3.3 m^3 / m^2 / min), elutriation velocity (4.5 m / s) and annular velocity (40.5 m / s) of all Fonterra washable

[3] See Section 8.3.1.4

baghouses. The high inlet velocity enters the baghouse by a tangential scroll so bags at the front of the baghouse bear the brunt of this impact.

WP2 is used to produce SMP, WMP and CP. As Table 8-5 below shows, the current air to cloth ratio is higher than all guideline values for SMP, WMP and CP. This plant has historically had operational issues when producing SMP, but has performed soundly with the high fat powders of WMP and CP. This suggests that the guideline values from all authors are suitable with respect to operational difficulties, but there would be a large difference in capital costs based on the guidelines used.

Table 8-5: Comparison of actual and suggested air to cloth ratios (V_f [m^3 / m^2 / min]) for powders produced in Whareroa Powder 2

Product	Actual	Croom (1995)	Intensiv-Filter (1999)	Löffler et al. (1988)	Turner et al. (1998)
SMP	3.3	2.6	2.4	1.7	0.8
WMP	3.2	2.8	2.4	2.4	0.9
CP	4.2	2.8	2.4	2.5	0.6

The extremely high annular velocity in the WP2 baghouse would mean that very little powder will fall from the inlet air stream but rather be carried to the surface of the filter bags. To achieve a reduction in this annular velocity to a suitable value of 15 m / s, the outer gap G would need to be increased from 150 to 430 mm.

The developed procedure has been used to find an optimal WP2 SMP design for WP2 using an air to cloth ratio of 1.7 m^3 / m^2 / min, a maximum elutriation velocity of 1.14 m / s (recommended by Croom (1995) for milk powder), the current bag dimensions, bag spacing and an outer spacing of 0.43 m. Using these parameters, the required number of bags would be 345, 165 more than currently used, and a baghouse diameter of 7.6 m, over 3 m larger than the current design. Clearly this is a dramatically different design, but one that is likely to perform with lower baghouse differential pressures, require fewer CIPs and increase bag life.

It should be noted that a large difference between the iterative and calculated baghouse diameters results from this solution, that is, the solution has a high value of the solver target

cell. The calculated number of bags with the specified bag diameter, bag spacing and outer spacing gives a calculated baghouse diameter of 4.9 m. However, this baghouse diameter gives insufficient cross sectional area between the bags to reduce the elutriation velocity below the desired maximum. Therefore, a final iterative guessed baghouse diameter of 7.1 m is chosen because it does give sufficient cross sectional area between the bags to reduce the elutriation velocity below the desired maximum. Because this large baghouse diameter is chosen, it means that the specified values for the bag and outer spacing could be increased, which would aid baghouse performance.

8.3.1.2. Clandeboye Dryer 2

GEA Niro A/S installed an MSD 2000 designed dryer with Sanicip washable baghouses at the Clandeboye site for the start of the 2000/2001 season. This plant has two main baghouses for the dryer exhaust air and a smaller baghouse for the VF air. It should be noted that slight variations in dryer air flows due to production of different powders will see the air to cloth ratio listed in Table 8-2 vary between 2.1 and 2.3 m^3 / m^2 / min.

Like the WP2 inlet, the CD2 baghouses have a tangential entry. The annular velocity is much lower, 28.6 m / s compared to 40.5 m / s but is almost double the acceptable 15 m / s. The air to cloth ratio and elutriation velocity is also lower.

CD2 produces SMP, MPC and WMP. A comparison of the actual and the air to cloth ratios recommended by the literature guidelines for these powders are found in Table 8-6 below.

Table 8-6: Suggested air to cloth ratios (V_f [m^3 / m^2 / min]) for powders produced in Clandeboye Dryer 2

Product	Actual	Croom (1995)	Intensiv-Filter (1999)	Löffler et al. (1988)	Turner et al. (1998)
SMP	2.2	2.8	1.8	1.6	0.8
MPC	2.1	2.8	2.4	3.1	0.9
WMP	2.2	2.8	2.4	2.3	0.8

One can see that the current CD2 SMP air to cloth ratio of 2.2 m^3 / m^2 / min is greater than that recommended by all but Croom (1995) for SMP. Traditionally, this plant has had operational issues (high differential pressures, short bag life) when producing SMP. This would suggest that the Croom (1995) value is not suitable but those of the other authors are, again with respect to operational performance.

If baghouse capital cost is directly proportional to the amount of required filtration area, a baghouse based on the Turner et al. (1998) guideline would cost twice as much as the Löffler et al. (1988) or Intensiv-Filter (1999) based plant because it would require twice the filtration area. This extra cost of Turner's extreme values would probably be unacceptable to Fonterra and therefore, the Turner et al. (1998) guideline can be rejected.

There have been no baghouse issues with the production of MPC in CD2. This allows one to conclude that there is more filtration area than required for the production of MPC as Croom (1995), Intensiv-Filter (1999) and Löffler et al. (1988) all recommend air to cloth ratios well above the current CD2 value.

For WMP, the current value is less than those recommended by Croom (1995), Intensiv-Filter (1999) and Löffler et al. (1988). CD2 has operated well on WMP, which implies these guideline values are suitable for WMP.

Like WP2, the CD2 annular velocity is well above the suggested 15 m / s because of the high air flow around the small annular area. An outer spacing of 380 mm would be required to meet the suggested velocity.

The design procedure presented in section 8.2.2.1 has been used to produce an optimal CD2 SMP design using an air to cloth ratio of 1.6 m^3 / m^2 / min, a maximum elutriation velocity of 1.14 m / s, the current bag dimensions, bag spacing and an outer spacing of 380 mm. Using these parameters, the required number of bags would be 330, 90 more than currently used, and a baghouse diameter of 7.3 m, over 2 m larger than the current design. Again, this is a dramatically different design, but one that is likely to perform with fewer operational difficulties.

In the Canterbury region, the regional council (Environment Canterbury) states that particulate emission concentrations must not exceed 20 mg / Nm^3 (O'Brien, 2004). The outlet air stream concentrations are continually monitored and also checked annually by contractors to the regional council (O'Brien, 2004). Washable baghouses operated by Fonterra Co-operative Group Ltd normally meet this regulation as outlet air stream powder concentrations usually range between 6 – 10 mg / Nm^3.

Figure 8-3 below shows for a range of inlet powder concentrations the baghouse efficiency. Over the range of expected inlet powder concentrations, the Fonterra CD2 washable baghouses have very high collection efficiencies; for inlet powder concentrations ranging from 16.3 – 40.8 g / m^3 with a poor outlet powder concentration of 20 mg / m^3, the overall collection efficiency ranges from 99.88 % to 99.95 %. Such high collection efficiencies are to be expected, as one of the main advantages of baghouses over other forms of particulate collection equipment is their high collection efficiencies, which can often be beyond 99 % (Ruthven, 1997).

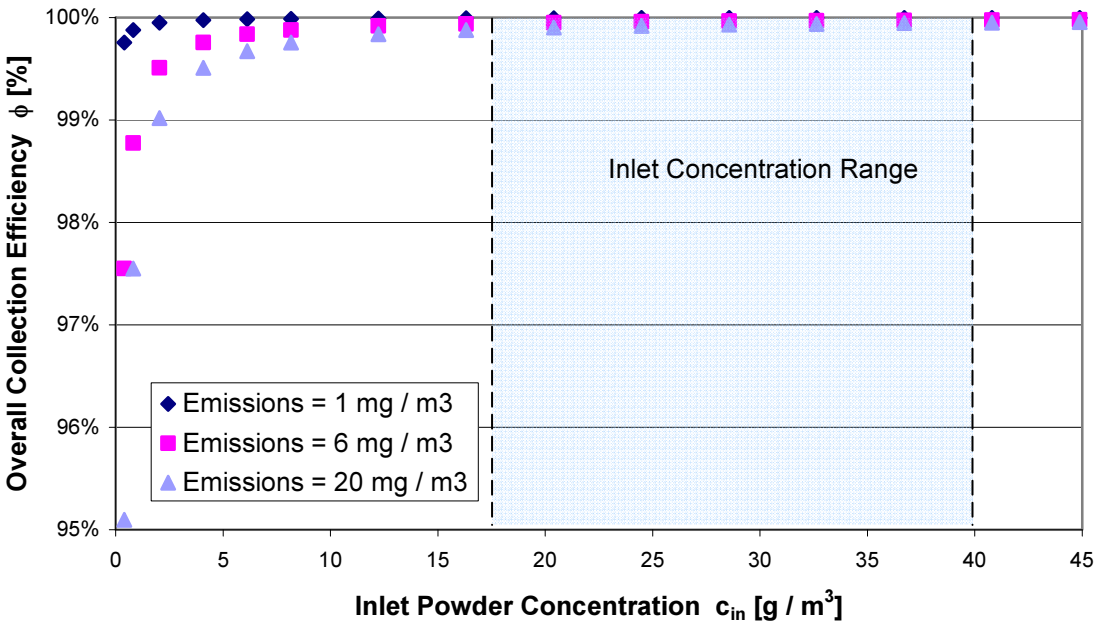

Figure 8-3: Fonterra Clandeboye Dryer #2 main baghouse collection efficiencies and expected range of inlet powder concentrations

8.3.1.3. Edendale Dryers 2 and 3

ED2 and ED3 are also GEA Niro A/S MSD 2000 designs. These plants, installed for the start of the 2001/2002 and 2002/2003 seasons respectively, have subtle differences from the CD2 plant (see Appendix A4). However, for the purpose of this exercise the main Sanicip baghouses can be considered identical, hence the CD2 design parameters mentioned above also apply to the ED2 and ED3 main baghouses.

ED2 and ED3 are used to produce SMP and WMP and like CD2, these plants have had few operational issues with WMP, but several with SMP. Therefore, the comparison of the guideline values for these powders to the current air to cloth ratio in section 8.3.1.2 above also applies here.

8.3.1.4. Clandeboye Dryer 3

The most recent milk powder plant to be built in the South Island is Clandeboye Dryer 3, the world's largest. This Stork designed dryer has four Intensiv-Filter designed washable baghouses off the main chamber, and a fifth washable baghouse filters the vibrating fluid bed air.

The dirty air inlet to each baghouse is radial, hence the inlet air flows straight into a large deflector plate. Because of this type of inlet, the inlet velocity is slowed very quickly. The elutriation velocity of 3.3 m / s at the bottom of the bags is similar to the 3.0 m / s in the CD2, ED2 and ED3 baghouses. However, because these baghouses have tapered dirty side plenums, the elutriation velocity at the top of the bags is 1.7 m / s.

The CD3 baghouses have slightly shorter (5.6 c.f. 6.0 m) and narrower (165 c.f. 208 mm) bags. This will allow these baghouses to operate at slightly higher air to cloth ratios than the bags found in the other Fonterra washable baghouses because the narrower, shorter bags are more easily pulse cleaned (Löffler et al., 1988).

CD3 is a WMP plant. As Table 8-7 shows, the current air to cloth ratio of 2.6 m^3 / m^2 / min lies between the guideline values of Croom (1995) and Löffler et al. (1988), and agrees with the Intensiv-Filter (1999) guideline value. There have been no operational issues associated with the CD3 washable baghouses, indicating all bar the guideline values of Croom (1995)

are appropriate when considering operational performance. The Croom (1995) value is very close to the current and Intensiv-Filter (1999) value. However, because it is larger than the current value, it would be risky to suggest that an increase in the air to cloth ratio would not impact on the baghouse performance.

Table 8-7: Suggested air to cloth ratios (V_f [m^3 / m^2 / min]) for powders produced in Clandeboye Dryer 3

Product	Actual	Croom (1995)	Intensiv-Filter (1999)	Löffler et al. (1988)	Turner et al. (1998)
WMP	2.6	2.8	2.6	2.4	0.9

The CD3 annular velocity of 21 m / s is the closest of all main Fonterra washable baghouses to the suggested 15 m / s. This is because these baghouses have an annular area almost twice those found in the CD2 and Edendale baghouses. An outer spacing of 380 mm would be required to meet the suggested velocity.

An optimal CD3 WMP design has been produced using the developed procedure where the design parameters used were an air to cloth ratio of 2.4 m^3 / m^2 / min, a maximum elutriation velocity of 1.14 m / s, the current bag dimensions, bag spacing and an outer spacing of 380 mm. Using these parameters, the required number of bags would increase slightly to 278 bags and a baghouse diameter of 6.6 m, over 2.2 m larger than the current design. Unlike the optimum designs for the other Fonterra plants, the current CD3 design is much closer to this optimal, suggesting the Intensiv-Filter designed baghouse is a better design than the GEA Niro A/S design.

8.3.2. Vibrating Fluid Bed Washable Baghouses

The key baghouse parameters for the VF washable baghouses are shown in Table 8-8 below.

Although the CD2, ED2 and ED3 main washable baghouses are virtually identical, there are significant differences between the VF washable baghouses (see Appendix A4). The main point of difference is that the Edendale vibrating fluid beds are much smaller than those in CD2.

Consequently, the Edendale fluid beds require less fluidisation air, which leads to less filtration area in the VF baghouse, because the superficial velocities in both the CD2 and ED2/ED3 fluid beds are approximately the same.

Table 8-8: Fonterra vibrating fluid bed washable baghouse design parameters

Design Parameter	CD2	ED2 / ED3	CD3
Inlet Air Flow $Q_{BH,in}$ [m^3 / s]	16.5	15.0	31.4
Air to Cloth Ratio V_f [m^3 / m^2 / min]	1.5	1.7	2.5
Elutriation Velocity V_e [m / s]	1.7	1.4	3.3
Number of Bags n	164	136	260
Bag Length L_b [m]	6.0	6.0	5.6
Bag Diameter D_b [mm]	208	208	165
Bag Spacing X_b [mm]	60	60	40
Outer Spacing G [mm]	260	440	500
Baghouse Diameter D_{BH} [m^2]	4.4	4.4	4.4
Bag Number Density N [m^{-2}]	13.9	13.9	21.6
Annular Velocity V_{Anl} [m / s]	10.5	5.9	20.7
Operating Issues?	No	No	No

8.3.2.1. Clandeboye Dryer 2 Vibrating Fluid Bed Baghouse

The comparison of the guideline air to cloth ratios with the actual values used in the CD2 VF baghouse are shown in Table 8-9 below. Excluding the ultra conservative values of Turner et al. (1998), it is clear that for all milk powders produced, the current air to cloth ratios are less than those recommended by the remaining three guidelines. This would suggest that this baghouse has more filtration area than required, therefore one would expect there to have been no operational issues with this baghouse, which has been the case.

It is difficult to deduce using the VF baghouse values, which of the Croom (1995), Intensiv-Filter (1999) or Löffler et al. (1988) values are suitable because all are much larger than the current value. However, it seems that the Löffler et al. (1988) values are more product sensitive, so following these guidelines may well be acceptable.

Table 8-9: Suggested vibrating fluid bed baghouse air to cloth ratios (V_f [m^3 / m^2 / min]) for powders produced in Clandeboye Dryer 2

Product	Actual	Croom (1995)	Intensiv-Filter (1999)	Löffler et al. (1988)	Turner et al. (1998)
SMP	1.5	2.4	2.1	2.2	1.0
MPC	1.5	2.4	2.1	2.8	1.0
WMP	1.5	2.6	2.5	3.4	1.0

Note: the guideline values for the VF baghouses are different to those for the main baghouses because of different fines concentrations, air temperatures, particle sizes, bulk densities and application type.

The CD2 annular velocity is 10.5 m / s. This is a very good value as it will allow powder to fall from this air stream, which will reduce the effective loadings on the filter bags. The value is because of the lower inlet airflow and the larger outer spacing.

Note that the bag density in the VF baghouse bag bundle is the same as in the main baghouses. However, the elutriation velocity in the CD2 VF baghouse is much closer to the limit of 1.14 m / s recommended by Croom (1995). This will mean more power will fall to the hopper on entry to this baghouse than in the main baghouses. Combine this with the lower inlet powder concentrations means the effective loadings on these filter bags will be reduced.

The developed procedure has been used to produce an optimal CD2 VF design for SMP production. Parameters were set as follows; an air to cloth ratio of 2.2 m^3 / m^2 / min, a maximum elutriation velocity of 1.14 m / s, the current bag dimensions, bag spacing and outer spacing. Using these parameters, the required number of bags would be 115, approximately 50 fewer than the current design, and a baghouse diameter of 4.8 m, only 0.4 m larger than the current design. The current CD2 VF design is very close to the calculated optimum as it has

more filtration area than required and annular velocities much lower than the suggested 15 m/s. These are likely reasons why these baghouses have had almost no operational difficulties.

8.3.2.2. Edendale Dryers 2 and 3 Vibrating Fluid Bed Baghouses

Like the CD2 VF baghouse, the current ED2 and ED3 VF baghouse air to cloth ratios are less than those suggested by Croom (1995), Intensiv-Filter (1999) and Löffler et al. (1988), as the values in Table 8-10 show. Again, these three guidelines propose air to cloth ratios greater than those currently used, suggesting these baghouses have more filtration area than required. Only the guideline of Löffler et al. (1988) shows sensitivity to product type.

Table 8-10: Suggested vibrating fluid bed baghouse air to cloth ratios (V_f [m^3 / m^2 / min]) for powders produced in Edendale Dryers 2 and 3

Product	Actual	Croom (1995)	Intensiv-Filter (1999)	Löffler et al. (1988)	Turner et al. (1998)
SMP	1.6	2.4	2.1	2.2	1.1
WMP	1.8	2.4	2.1	2.8	1.1

The ED2/ED3 annular velocity is very low at 5.9 m / s, an order of magnitude lower than those in the main baghouses. At such a low velocity, the particle carrying capacity of the air stream is significantly reduced, so a lot of the entrained powder will be preseparated, reducing the overall loadings on the filter bags.

The ED2/ED3 elutriation velocity is almost equal to the upper limit of Croom (1995). Like in the CD2 VF baghouse, this will have the effect of reducing the overall loadings on the bags compared to baghouses with higher elutriation velocities, as more powder will be able to fall to the dust hopper.

Again, the developed procedure has been used to produce an optimal ED2/ED3 VF design for SMP production. Parameters were set as follows; an air to cloth ratio of 2.2 m^3 / m^2 / min, a maximum elutriation velocity of 1.14 m / s, the current bag dimensions, bag spacing and outer spacing. Using these parameters, 105 bags would be required, 31 fewer than currently used

and the baghouse diameter would need to be increased by only 0.2 m to 4.6 m. This shows that the current ED2/ED3 VF baghouse design is the closest of all Fonterra baghouses to optimal, indicating why these baghouses have had no operational difficulties.

8.3.2.3. Clandeboye Dryer 3 Vibrating Fluid Bed Baghouse

The current and guideline air to cloth ratios for the CD3 VF baghouse are shown in Table 8-11. Again, the current value is less than that suggested by Croom (1995), Intensiv-Filter (1999) and Löffler et al. (1988) indicating this baghouse has more filtration area than is required.

Table 8-11: Suggested vibrating fluid bed baghouse air to cloth ratios (V_f [m^3 / m^2 / min]) for powders produced in Clandeboye Dryer 3

Product	Actual	Croom (1995)	Intensiv-Filter (1999)	Löffler et al. (1988)	Turner et al. (1998)
WMP	2.5	2.8	3.5	3.3	1.0

It must be noted that using the Intensiv-Filter (1999) guideline for the CD3 VF baghouse gave a different value from the actual, which is in fact an Intensiv-Filter design. The designers have used the air to cloth ratio associated with loadings less than 20 g / m^3, air temperature between 20 and 80 ^oC and milk powder, which sits in the 50 – 100 μm particle size category. However, the actual average particle size for WMP in the CD3 VF baghouse is 157 μm. The air to cloth ratio from the guideline for these same conditions and this particle size is 3.5 m^3 / m^2 / min.

The design procedure presented above has been used to produce an optimal CD3 VF design for WMP production. Parameters were set as follows; an air to cloth ratio of 3.3 m^3 / m^2 / min, a maximum elutriation velocity of 1.14 m / s, the current bag dimensions, bag spacing and an outer spacing of 370 mm. Using these parameters, 197 bags would be required, approximately 60 fewer than currently used but the baghouse diameter would need to be increased by 2 m to 6.4 m.

8.3.3. Discussion

8.3.3.1. Comparison of the Air to Cloth Ratio Guidelines

From the work above, it can be seen that there is significant variation among the air to cloth ratio guidelines

8.3.3.1.1. Turner et al. (1998)

The air to cloth ratios from the design guidelines of Turner et al. (1998) are much lower than those used by Fonterra. These recommended air to cloth ratios are too conservative and thus capital costs would be extremely high because of the need for large filtration areas. The operating costs resulting from these designs would be low, but the combination of capital plus operating costs would not be a minimum with such a conservative design.

The Turner et al. (1998) guideline is very insensitive to the influence of different types of milk powders on baghouse performance. Although factors for fines loadings and particle size, which vary between the milk powders, are included, the influence of these factors is insufficient to vary the recommended air to cloth ratio for milk powders, that is, this method suggests one air to cloth ratio will suffice for all milk powder types, which contradicts industry experience.

8.3.3.1.2. Croom (1995)

The air to cloth ratios from Croom (1995) are greater than those used by Fonterra. Firstly, the GEA Niro A/S Sanicip designs (CD2, ED2 and ED3) on SMP have struggled to perform adequately with an air to cloth ratio of 2.2 m^3 / m^2 / min, but the Croom (1995) guideline recommends a higher value of 2.6 m^3 / m^2 / min. Secondly, the recommended value for WMP in CD2 and CD3 is greater than the current value. Although the Croom (1995) WMP value may perform adequately, it would be risky to increase the air to cloth ratio as negative side effects may be experienced. Finally, although this guideline recommends reducing the WP2 air to cloth ratio for SMP, the value is the highest of the four guidelines so may not be suitable.

A second point against the use of the Croom (1995) guideline is the fact that, although this method applies factors to account for the influence of particle size and fines loadings, the guideline does not distinguish between the different milk powders for the base air to cloth

ratios. For these reasons, it is likely the Croom (1995) guideline would compound the operational difficulties Fonterra has experienced.

8.3.3.1.3. Intensiv Filter (1999)

The design guideline provided by Intensiv-Filter (1999) suggests air to cloth ratios that are more conservative than the Croom (1995) guideline, thus would experience higher capital costs but are likely to result in lower operating costs. The Intensiv-Filter (1999) guide is the simplest to apply but one must be careful in correctly selecting the particle size and application factor categories. This method does not suggest any difference between powder types outside of the factors applied for fines loadings and particle size.

The suggested Intensiv-Filter (1999) values agree well with industry experience. In CD2, the guideline suggests the same air to cloth ratio as the current value for WMP where no issues have occurred historically, and reducing the air to cloth ratio for SMP, where a number of issues have arisen with the current value. In WP2, a lower value for SMP is suggested, which may eliminate some of the operational issues experienced here, and also a slightly reduced air to cloth ratio for WMP production.

CD3 is an Intensiv-Filter (1999) design. Because the design value in the main baghouse is the same as the calculated guideline value, it can be concluded that the Intensiv-Filter (1999) guideline has been correctly used in this exercise and that this recommended air to cloth ratio works well. Therefore, the Intensiv-Filter (1999) design guide is an accurate guideline.

8.3.3.1.4. Löffler et al. (1988)

The base air to cloth ratio for milk powders in the Löffler et al. (1988) method vary depending on composition. This agrees with industry experience: the higher the fat content of the powder, the better the baghouse performance.

The recommended air to cloth ratios from this guideline are very similar to those of the Intensiv-Filter (1999) guideline for WMP, but quite different for MPC and SMP in the main baghouses. The Löffler et al. (1988) values are lower than those from the Croom (1995) guideline for SMP, CP and WMP in the VF baghouses, but greater than the Croom (1995) values for MPC and WMP in the main baghouses. These values tend to agree with industry

experience, indicating that following this guideline would reduce the current high industry operating costs.

The suggested Löffler et al. (1988) guideline value for WMP in CD2 agrees with the current value that has generated no operational issues when producing WMP. The guideline value is lower than the current CD2 value for SMP, which has historically caused problems. The CD3 value is approximately the same as the current value that has had no operational issues. Finally, this guideline recommends reducing the air to cloth ratio in WP2 for SMP, where production has traditionally had problems. Therefore, the guidelines of Löffler et al. (1988) are clearly the best of the four found guidelines tested for this application.

8.3.3.2. Comparison of Main and VF Baghouses

The Fonterra VF baghouses have traditionally had no operational issues even when the plants have been producing products such as SMP that have caused problems in the main baghouses. Key differences between the main and VF baghouses such as lower inlet air temperature and humidity, fines loadings and powder moisture contents, indicate an environment that will have fewer operational difficulties. The differences in design are that the VF baghouses operate with lower air to cloth ratios, lower elutriation velocities and have larger outer spacings leading to lower annular velocities.

From consideration of these differences, the Fonterra VF baghouses would be expected to have fewer operational issues than the main baghouses, which has been the case. This indicates that a well designed baghouse will perform with few operational difficulties and the developed design procedure will provide such designs.

8.3.3.3. General Comments on Fonterra Washable Baghouses

The main baghouse designs of Fonterra are aggressive designs; air to cloth ratios are at the high end of those recommended, the elutriation velocities are above the suggested maximum, the bag lengths are very long and the outer spacings lead to very high annular velocities. It is highly likely that the current designs are causing the majority of the operational problems experienced. Thus the designs have not struck the balance required between capital costs and operating expenses.

The nature of the spray dryers, and the relative unfamiliarity of the washable baghouse systems in the New Zealand dairy industry are two reasons for seeking cautious designs. These spray dryers are some of the largest in the world, and the baghouses attached are also very big, housing filtration areas of up to 940 m^2. Secondly, these washable baghouse systems are a recent innovation with the first installed in New Zealand for the 2000/2001 season. Therefore, designers have no past experience at this scale on which to base their designs.

Milk powder production schedules are often changing in the New Zealand dairy industry to accommodate changes in commodity prices or to meet customer orders. The industry must be cautious when dealing with a washable baghouse system as the baghouse designed for one product may not perform adequately with a second product. As can be seen from the guidelines above, different milk powder products require more or less filtration area; this is likely to be because of differences in fines loadings, particle sizes or other powder characteristics such as stickiness. For example, the baghouse would certainly become a limitation if the CD3 designed whole milk powder plant produced skim milk powder.

8.4. Recommended Design Changes

Three design changes are recommended for future washable baghouses. Firstly as is discussed in Chapter Nine, inspection hatches are strongly recommended for improved bag inspection and reduced bag dry out times, which have both seen CIP times reduce by approximately two hours.

Secondly as discussed above, the gap between the baghouse wall and the bag on the edge of the bag bundle should be set such that the annular velocity is approximately 15 m / s, which is likely to be the minimum particle carrying velocity. It is postulated this design change will reduce the effective loadings on the filter bags as more powder is likely to fall to the hopper than currently at these lower annular velocities.

Finally, industry experience shows that baghouse designs where the entire clean air plenum can be removed, such as the GEA Niro A/S Sanicip design (Figure 8-4), allows for easier and therefore quicker bag replacement. The alternative design currently used in some Fonterra

plants is the Leubbers (WP2) and Intensiv Filter (CD3, TA Dryer A, TA Dryer B) designs where the access to the clean air plenum is through a large door. To remove bags and cages in these baghouses, the cages must be disconnected in three places and passed out through the door (Figure 8-5), rather than being able to pull the entire cage out as is the case in the GEA Niro A/S design. Clearly this is a much more difficult and time consuming task. Therefore, it is recommended that future washable baghouse designs, particularly in SMP plants where greater bag replacement is likely to occur, be such that the entire clean air plenum can be removed.

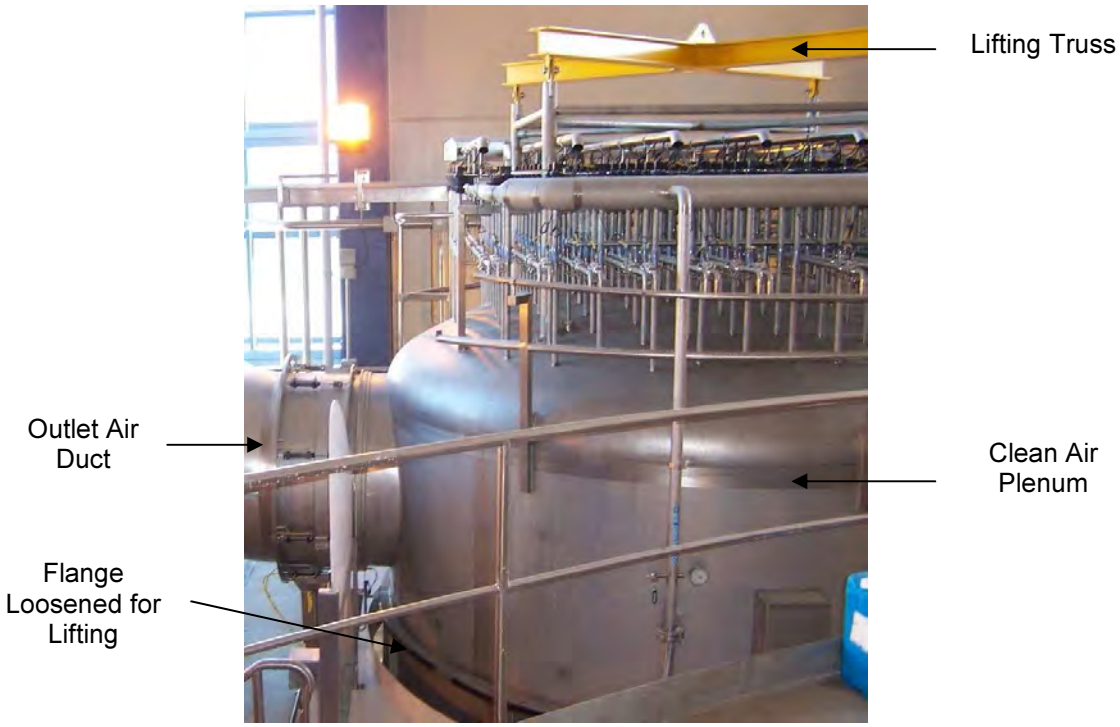

Figure 8-4: GEA Niro A/S Sanicip designed Clandeboye Dryer #2 Vibrating Fluid bed baghouse clean air plenum

Figure 8-5: Leubbers designed Whareroa Powder 2 baghouse clean air plenum

8.5. Future Research

A key design parameter highlighted above is the elutriation velocity. Here large variation in the recommended maximum values was reported. For this reason, it is recommended that elutriation velocities for milk powders be determined experimentally. The use of the UC CAPE pulsed diode laser and high speed camera could be used to determine the velocities of different sized milk powder particles falling under gravity, that is, the settling velocities. These values could be compared with the recommended maximums in Table 8-1 above and used to determine suitable annular velocities for milk powders. This information could then be used to give more milk power specific washable baghouse designs.

8.6. Conclusions and Recommendations

This investigation has established that there is a large variation in the recommended baghouse design parameters of air to cloth ratio, elutriation velocity, bag spacing and bag dimensions. Other key design parameters that must be considered are the type of filter medium, operating differential pressure and baghouse footprint. The choice for an optimal design relies heavily on past experience and or laboratory experiments with the dust under consideration, or if not available, similar dusts.

It is clear that the procedure for baghouse design which has been developed differs from previous work in that it includes the area outside the bag bundle as a key design parameter and uses an optimisation routine to solve the system of equations. Using this procedure provided evidence that the majority of the Fonterra main washable baghouse designs are far from optimal because of high air to cloth ratios, long bags and high elutriation and annular velocities. The VF washable baghouses, however, are much closer to the optimum calculated using the procedure, which is likely to be the reason these units have provided almost no operational issues.

Regarding the procedures found to determine air to cloth ratios for baghouses collecting milk powder, it was concluded that significant variation exists among the four available guidelines. It appears that the methods of Löffler et al. (1988) and Intensiv-Filter (1999) are both reasonable in light of industrial experience. However, the method of Löffler et al. (1988) is more specific for fines collection in milk powder plants because of its sensitivity to the milk powder type and is therefore recommended as the procedure to follow to determine air to cloth ratios in future washable baghouse designs.

Future design recommendations are that inspection hatches at the bag level be installed into the side of all washable baghouses, the annular velocity in the baghouse be reduced to around 15 m / s by increasing the outer spacing, and ensure the baghouse clean air plenum can be removed for easier bag replacement.

9. Bag Movement

The previous chapter identified that the bags used in the Fonterra washable baghouses are very long. It was believed a lage amount of the bag damage experienced by Fonterra is because of the movement of these long bags. Consequently, bag movement was examined in this chapter.

9.1. Introduction

During the first few seasons of operation, the CD2 washable baghouses had very short bag lives. These bag life times of less than a season were much shorter than the one to two season lifetime suggested by bag suppliers.

A major reason for the short bag lifetimes was mechanical failure. Holes were being created in the bags, which meant powder was flowing into the clean side of the baghouse and consequently, this led to high outlet air emissions. It was believed that significant bag movement was occurring because several bag support cages were being bent out of shape.

Bag movement causes the mechanical failure of filter bags (Morgan & Walters, 1999) and this was thought to be the case within the Fonterra baghouses. Because the bags could swing and rub against each other, bag abrasion was likely to occur. Also, the bent support cages were creating sharp sections, which the bags could rub on (Parker, 1997) and not surprisingly, they were being punctured.

Each support cage used in CD2 consists of two three-metre sections. Originally, the two sections were joined with a finger joint and held in place with two clips around the horizontal struts of the cage (Figure 9-1). In the 2004 winter, overlapping wires of the two sections of the cages were spot welded together, which is believed to have reduced the bag and support cage damage since.

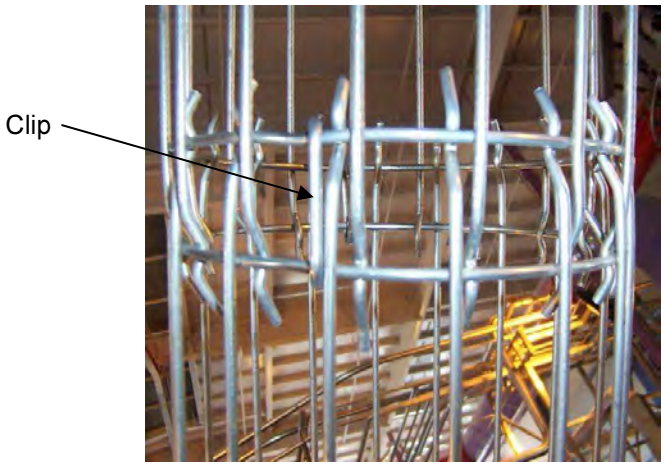

Figure 9-1: Finger joint of support cages used in Clandeboye Dryer #2

Bags 5.6 m in length are used in the Intensiv designed Fonterra washable baghouses and 6.0 m bags are used in the Niro Sanicip washable baghouses. These are long bags and (Löffler et al., 1988) warns that bags greater than 3.0 m in length are likely to touch and abrade near the bottom which leads to premature wear. Therefore, it is safe to assume that bag movement was causing the majority of the Fonterra bag damage.

The Fonterra Baghouse User Group identified in the Niro Sanicip design (CD2, ED2 and ED3) an area of common bag damage. This common bag damage zone, shown in Figure 9-2, was the inlet area where the dirty air from the tangential scroll enters the baghouse. Zielinksi (2003) suggests that if bags two to three metres away from this zone were not damaged, the bag damage is due to mechanical failure.

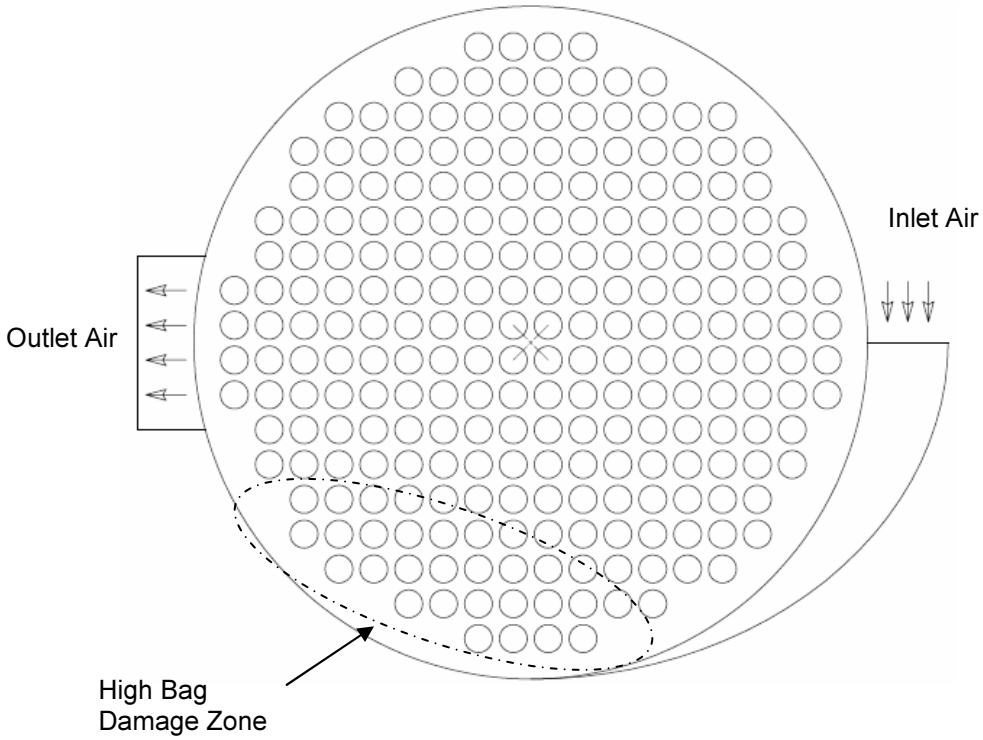

Figure 9-2: Identified zone of high bag damage in the Niro Sanicip washable baghouse (original drawing sourced from Fonterra)

9.1.1. Aims

The aims of this bag movement investigation comprised three parts. The first aim was to deduce the cause of the high bag damage zone at the baghouse inlet. Secondly, the investigation aimed to determine the natural and operational frequencies of bag movement at the industrial scale and the natural frequency of bag movement at the laboratory scale, and apply a simple cantilever beam model to the findings. Finally, observations of the industrial cleaning pulse aimed to deduce its effectiveness.

9.2. Theory

The filter bag and support cage could be considered as a cantilever beam fixed at the cell plate and free to move at the bottom. Hrouzek et al. (1995) give the circular frequency ω [Hz] of a free cantilever by Equation 9-1 where α is a numerical constant equal to 1.875, E [Pa] the

Young's modulus, I [m^4] the cross-sectional area moment of inertia, $\overline{m}$ [kg / m] the mass per unit length of beam and L [m] the length of the beam:

$$\omega = \alpha^2 \sqrt{\frac{EI}{\overline{m}L^4}} \tag{9-1}$$

Rearranging Equation 9-1 for the product of the Young's modulus and the moment of inertia gives Equation 9-2:

$$EI = \left(\frac{\omega}{\alpha^2}\right)^2 \overline{m}L^4 \tag{9-2}$$

Alternatively, the filter bag and support cage could be considered a simple pendulum of Length L [m], with frequency ω [Hz] related as shown in Equation 9-3 where g [m / s^2] is the acceleration due to gravity:

$$\omega = \frac{1}{2\pi}\sqrt{\frac{g}{L}} \tag{9-3}$$

Equation 9-3 shows that the frequency of a pendulum is inversely proportional to the square root of the pendulum length. Therefore, the ratio of the frequencies for two pendulums, 1 and 2, with lengths L_1 an L_2 is given by Equation 9-4:

$$\frac{\omega_1}{\omega_2} = \sqrt{\frac{L_2}{L_1}} \tag{9-4}$$

9.3. Assumptions

With regard to the observations of bag movement from below (see Method in section 9.4), it is assumed that the motion observed replicates what occurs when the plant is running on product. This assumption is made because the main inlet air flow and therefore velocities within the plant provided by the main inlet air fan at ambient temperature, are lower than those that occur when the plant is running on product.

The cantilever beam model given by Equation 9-1 is assumed to be accurate and apply to the filter bag and support cage situation. The model assumes that at the fixed end of the beam, the deflection is zero. Therefore, it is assumed here that there is no movement in the support cage at the cell plate. The model also assumes that the properties of the beam are constant

along its length, hence it is assumed that the properties of the bag and support cage are also constant along its length. Finally, the product EI from Equation 9-2 is assumed to give adequate detail about the bag and cage, without the need to detail the structure of the bag and cage any further. Thus, it is assumed that the filter cake does not add appreciably to EI.

9.4. Methods

During the 2006 winter, CD2 was run on ambient air without product. The bag movement of the bag bundle in BH #1 was observed from below by eye and recorded using a video camera (Sony Mini DV Digital Handycam, Sony Corporation, Tokyo, Japan). These observations were sufficient to draw conclusions about the cause of the high bag damage zone in the baghouse inlet.

To view the amount of bag movement occurring in the main baghouses, inspection hatches were installed near the base of the bags in the high bag damage zone. As Figure 9-3 shows, the hatches to be permanently in place were made from stainless steel, hinged and opened into the baghouse.

Figure 9-3: Stainless steel inspection hatches installed in the main Clandeboye Dryer #2 baghouses

To view the bag movement, a single Perspex hatch replaced the stainless steel hatch as Figure 9-4 shows. This hatch had to be installed when the plant was running on air, allowing the hatch time to warm up before powder began flowing around the hatch during production. If

not, the hatch at ambient temperature would provide a cool surface for powder to stick to which would then block the view through the hatch.

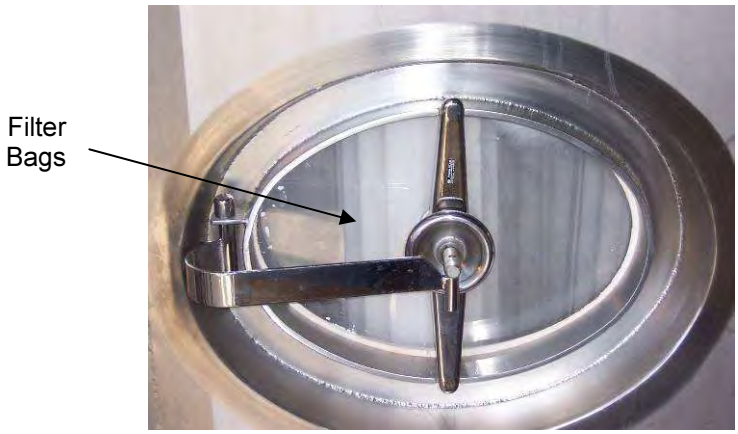

Figure 9-4: Perspex inspection hatch used in the main Clandeboye Dryer #2 main baghouses

To determine the natural and operational periods of the industrial scale bags, and the natural period of the laboratory scale bag, bag movement was recorded using the hand held video camera at a rate of 25 frames per second. For the natural period at the industrial scale, this bag movement was generated during plant downtime. The stainless steel inspection hatch was removed, the bag in the centre of the inspection cavity pushed to its point of maximum displacement and released. The component of bag movement in the plane perpendicular to that viewed by the video camera was recorded from the time of release until the oscillations ceased and the bag returned to its rest position (17 s).

The operational movement of the same bag used to determine the natural period of the industrial scale bag was recorded through the Perspex hatch for 30 s while the plant was producing MPC 80. Again, the component of bag movement in the plane perpendicular to that viewed by the video camera was observed.

The movement required for the natural period of the *laboratory* scale bag was achieved by removing the baghouse shell, pushing the bag to its point of maximum displacement and releasing the bag. Again, the movement was recorded from the time of release until the oscillations ceased and the bag returned to its rest position (3.5 s). Like the industrial scale observations, it was the component of bag movement in the plane perpendicular to that viewed by the video camera that was observed.

From each video file, still images of the bag at its point of maximum displacement for each oscillation were created using Ulead VideoStudio 6 (Ulead Systems Inc., Taipei, Taiwan). The time of each image was also noted. Each still image was then opened in SigmaScan Pro 5.0 (SPSS Science, Chicago, USA) and the bag displacement from its rest position measured. The period of oscillation was determined by calculating the power spectrum of the data set of maximum displacement measurements. This was achieved through the Fast Fourier Transform, calculated with Matlab 7.0.

It should be noted that because the video footage recorded the intermediate as well as the maximum bag displacements for each oscillation, still images and therefore measurements of the intermediate bag displacement could have been made. However, only the still images and measurements of the maximum bag displacements were generated. Therefore, the data sets for the industrial bag natural and operational movement, and the laboratory bag natural movement, only contained measurements of the extreme values for each oscillation

During MPC 80 operation with the Perspex inspection hatch removed, the change in bag diameter during a cleaning pulse was recorded using the video camera. Still images from each frame of the video footage were created and the diameter of the bag throughout the duration of the pulse measured.

9.5. Results

9.5.1. Observations From Below Bag Bundle

Observations from below the bag bundle in the CD2 main baghouses showed the bags in the centre of the bag bundle gently swaying in the same direction, and the majority of the bags touching at least one of their neighbours at the base. Around the edge of the bag bundle, there was significantly more bag movement. This was despite the support cages of bags in the two outer most rings of the bag bundle being heavier than those in the middle of the bag bundle in an attempt to dampen the movement of these bags (Moran, 2005). The movement increased in intensity the closer the bags were positioned to the air inlet. Approximately one dozen bags closest to the air inlet moved much more violently than the others. This supports the idea that the reason for this area of the baghouse being one of high bag damage is the large amount of bag movement occurring here.

It has been suggested to Fonterra by GEA Niro A/S that a matrix of rods could be installed into the baghouses to hold the base of the bags to prevent bag movement. However, this option is seen as unfeasible because of the ability of powder to build up on the rod matrix and become a fire and explosion risk. This option is also seen as unfeasible because the difficultly it would create in replacing the filter bags and therefore, increase the downtime required to replace all filter bags in a baghouse.

An alternative option to dampen out the bag movement could be to redesign the inlet air tangential scroll. A baffle plate in the inlet could be used to slow and deflect the inlet velocity away from the high bag damage zone (Zielinski, 2003), but this may suffer from a heavy build up of powder. A larger inlet duct would also reduce the inlet velocity but the duct velocity must remain above the minimum particle carrying velocity of the powder.

Slowing the annular velocity around the outside of the bag bundle would potentially reduce the amount of bag movement occurring in the inlet region. This could be achieved by increasing the outer gap, the distance from the edge of the bag bundle to the baghouse wall.

The use of heavier support cages may dampen out the bag movement. The cages currently used around the edge of the bag bundle may be suitable in the middle of the bag bundle, but heavier cages than are currently used around the edge of the bag bundle will be required. However, heavier support cages will make removing the cages for bag replacement more difficult and also increase the health and safety risk for operators.

To prevent bags from rubbing against each other in future designs two options are available, both of which however, would increase the capital cost of the baghouse. The first would be to reduce the length of bag used. Obviously shorter bags would have less contact with their neighbours but require a greater number of bags to maintain the current filtration area. The second option would be to increase the bag spacing (Bergmann, 2001). Spacing the bags further apart would reduce the amount of bag to bag contact and possibly reduce the amount of bag damage, but also increase the baghouse diameter.

9.5.2. Inspection Hatches

Fonterra capital expenditure was approved for the installation of the inspection hatches because of the written application found in Appendix F. The expenditure was justified by three benefits. Firstly, improved access to the bags would reduce CIP downtime as operators could more quickly inspect the cleanliness of the bags. Secondly, CIP effectiveness would be improved as operators would be able to view the CIP and be able to make more accurate decisions about the state of the bags. An increased CIP effectiveness should also reduce the number of CIP's required, decreasing further the downtime associated with CIP's. Finally, the inspection hatches would allow for more proactive decisions to be made on when bags should be replaced.

Once installed, an added benefit of the inspection hatches was discovered. CIP times were reduced further because opening the hatches during the bag dry out stage decreased the amount of time required to dry the filter bags. Adding this benefit to those mentioned above in total reduced the average CIP time by approximately two hours (20 %). For this reason, it is strongly recommended that all current and future washable baghouses install equivalent inspection hatches at the bag level.

9.5.3. Periods of Industrial Scale Bag Movement

9.5.3.1. Natural Period

The first three still images created from the video footage of the industrial scale natural bag period are shown in Figure 9-5 below. The 49 extreme displacement and time data points measured from all such still images is plotted in Figure 9-6 below.

Figure 9-5: Position of Clandeboye Dryer #2 baghouse #2 filter bag 1.36 s, 1.72 s and 2.08 s after release from maximum displacement

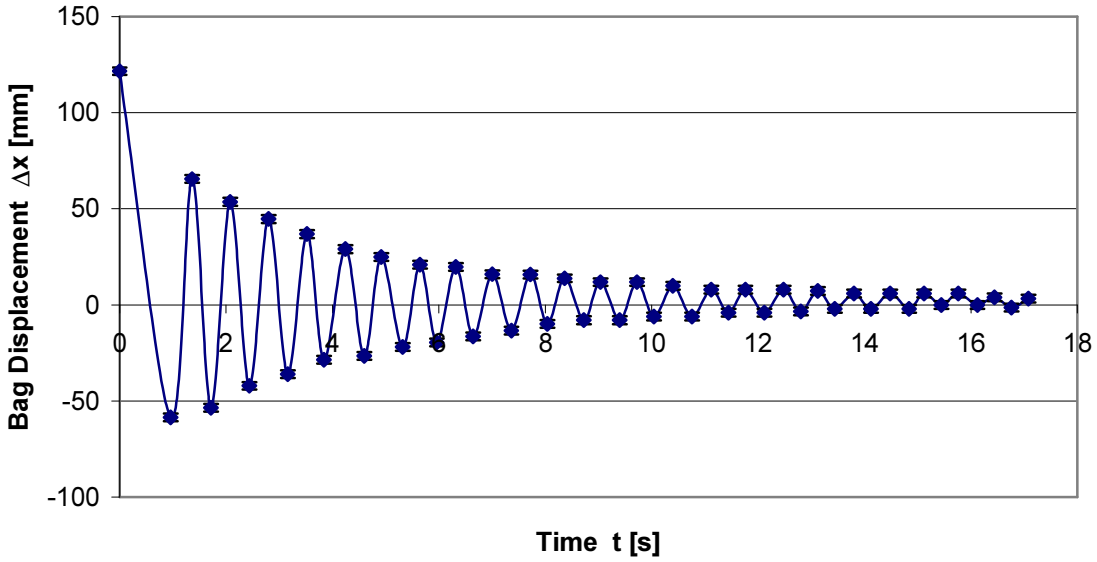

Figure 9-6: Natural bag displacement of Clandeboye Dryer #2 baghouse #2 filter bag

Figure 9-6 shows that it takes approximately 17 s for the bag to return to its initial rest position. During this time, the bag has oscillated 24 times. The bag displacement during the first seven oscillations reduces considerably and much smaller oscillations are observed after 10 s. An average decay ratio (the ratio of successive maximum or minimum displacement values) of 85 % is obtained from the data plotted in Figure 9-6.

Figure 9-7, the power spectrum plot for the industrial scale natural bag period, clearly shows the dominant frequency was 1.4 Hz. This equates to a period of roughly 0.7 s.

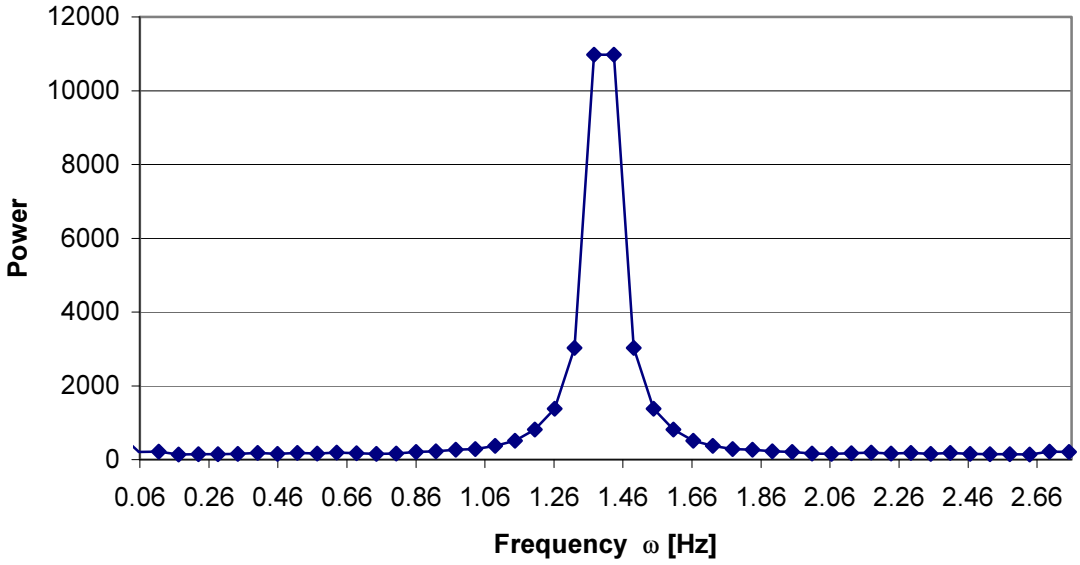

Figure 9-7: Power spectrum based on 49 data points for natural bag movement of Clandeboye Dryer #2 baghouse #2 filter bag

9.5.3.2. Operational Period

Figure 9-8 shows the 93 extreme operational displacement values of the filter bag during a 30s period. The displacement seems to average at around 10 mm, but there are some extreme displacements of up to 20 mm and some minium displacements of approximately 1 mm.

It should be noted that the degree of operational bag movement shown in Figure 9-8 is an extreme case. The filter bag used for this experiment and the natural period of the industrial bag experiment is located on the edge of the bag bundle in the high bag damage zone. The movement of this bag was hardly hindered by neighbouring bags which is very rare inside these baghouses. As discussed above in Section 9.5.1, most bags contact at least one of their neighbours when they move which dampens out their movement. This is not the case for the bag whose results are shown, because its position on the edge of the bag bundle means it has fewer neighbouring bags and therefore, its movement is not dampened as much as the other bags.

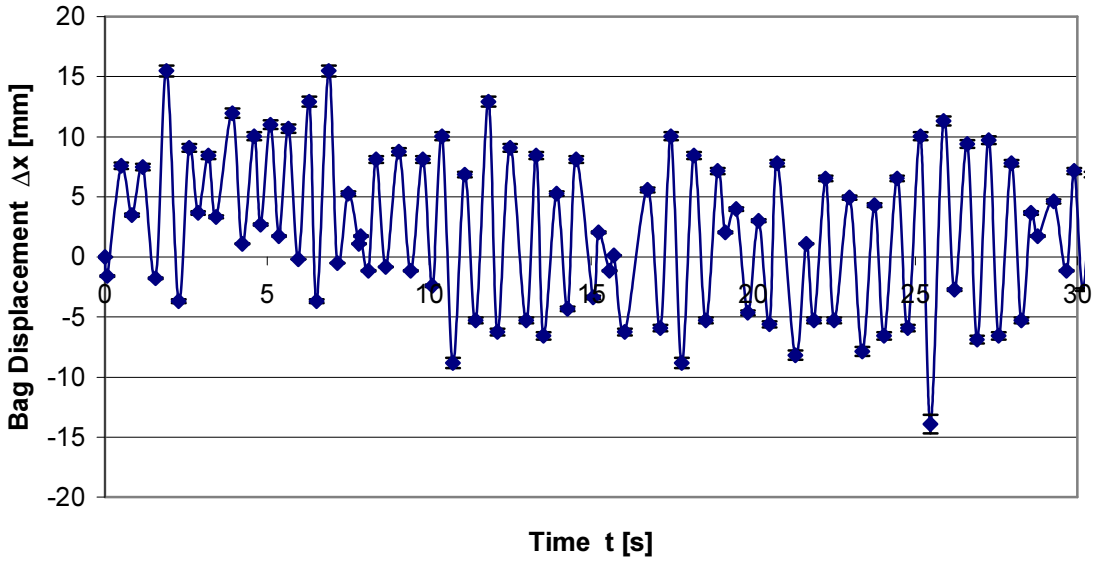

Figure 9-8: Operational bag displacement of Clandeboye Dryer #2 baghouse #2 filter bag

As Figure 9-9 shows, the operational frequency was approximately 1.5 Hz giving a period of 0.66 s. The operational frequency is more distinct than the natural industrial scale frequency because of the greater number of data points (93 c.f. 49) in this data set. However, comparing this operational period with the natural period for the identical bag, it can be seen that these two periods are approximately the same. This indicates that the presence of powder on the filter bags and the dirty airflow during operation do not have an impact on the oscillation of the filter bags, and also indicates that the assumption made about bag movement observed while running on ambient air replicating that which occurs when the plant is running on product was correct.

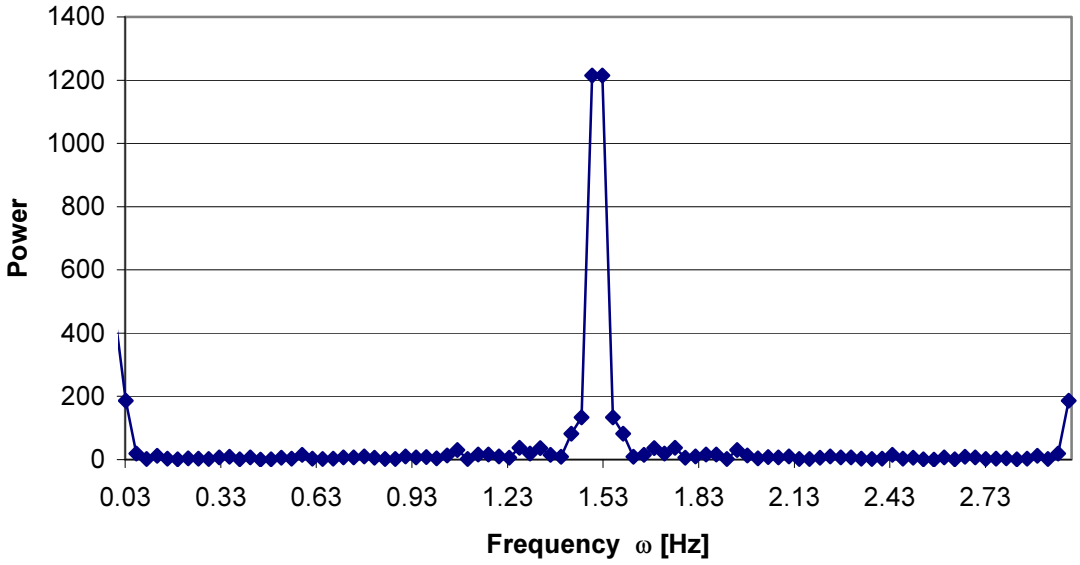

Figure 9-9: Power spectrum based on 93 data points for operational bag movement of Clandeboye Dryer #2 baghouse #2 filter bag

9.5.4. Natural Period of Laboratory Scale Bag

Three of the still images produced from the laboratory scale natural bag movement period video footage are shown in Figure 9-10 below.

Figure 9-10: Position of Chemical and Process Engineering baghouse filter bag 0.40 s, 0.64 s and 0.92 s after release from maximum displacement

As Figure 9-11 shows, the maximum displacement and time for the oscillations to die out for the 3 m bag are much less than for the natural period of the 6 m bag. Only seven oscillations are required before the bag returns to its rest position compared to 24 for the industrial scale. Therefore the average decay ratio of 52 % is much smaller than that of the industrial scale bag.

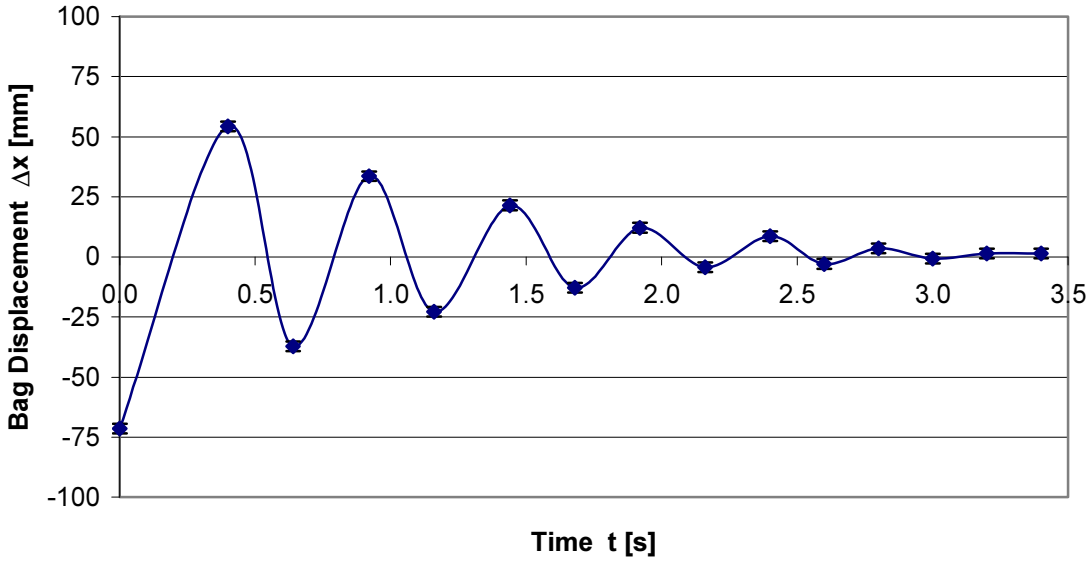

Figure 9-11: Natural bag displacement of Chemical and Process Engineering baghouse filter bag

The power spectrum from the displacement data of Figure 9-11 is plotted in Figure 9-12. It is apparent from this figure that the natural period of the 3 m bags is approximately 2.2 Hz, giving a period of 0.45 s. As expected, this is a much shorter period and higher frequency than for the 6 m industrial bag.

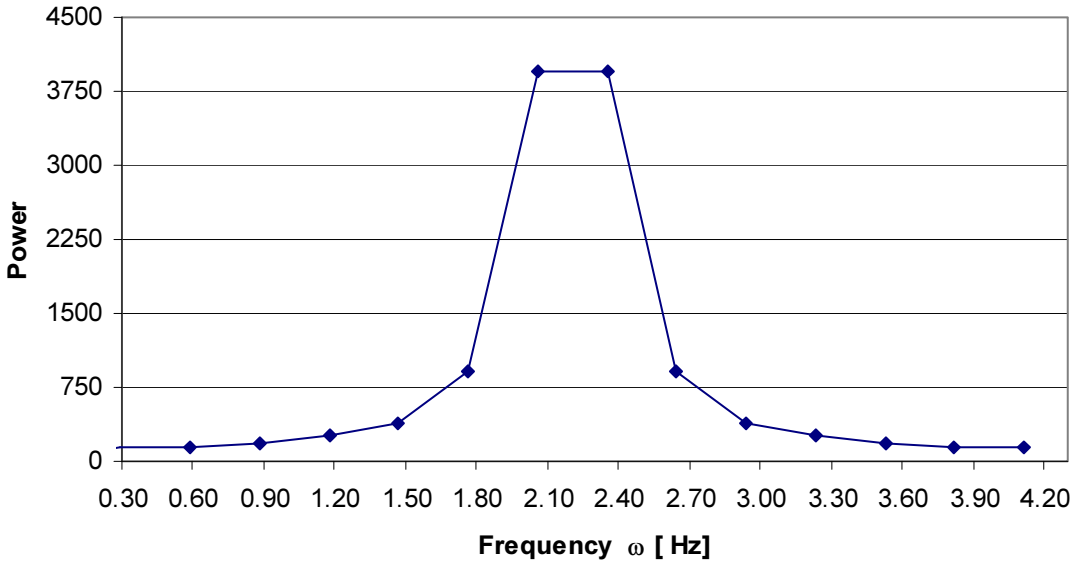

Figure 9-12: Power spectrum based on 15 data points for natural bag movement of Chemical and Process Engineering baghouse filter bag

9.5.5. Bag Movement Modelling

The filter bag and cage have an outer diameter of 208 mm and an inner diameter of 201 mm. For a 6 m long bag when the bag and cage weigh 14.7 kg and the oscillating frequency as determined above is 1.5 Hz, then applying a cantilever beam model, the product EI from Equation 9-2 equals 504 Nm^2. The same diameter bag and cage but 3 m in length with a combined bag and cage weight of 7.9 kg, where the oscillating frequency determined above is 2.2 Hz, has an EI value of 83 Nm^2.

It would be expected that the 6 and 3 m bags would have the same EI value if length was the only difference between the two scales. However, the model results indicate that there is a difference of approximately 600 % suggesting either there is a difference in behaviour of the bags at the different scales, or that the cantilever model does not apply to the cage and filter bag situation.

It should be noted that the mass per unit length is not a constant (2.5 kg / m for the 6 m bag c.f. 2.6 kg / m for the 3 m bag). This is due to the 3 m cage weight of 6.8 kg being greater than half the weight of the 6 m cage that weighs 12.6 kg. The 3 m cage contains both the lip at the top of the cage to help hold the bag at the cell plate and the flat disc covering the bottom of the cage. This makes the 3 m cage heavier than the first three meters of the 6 m cage and hence, the difference in mass per unit length between the scales. However, this slight difference would be insufficient to create the observed 600 % difference in EI values.

Three assumptions made for the cantilever model may have been violated here. Firstly, the model assumes that at the fixed end, the deflection is zero. In the case of the filter bags and cages though, there may be a small degree of movement at the cell plate. The degree of this movement may differ between the industrial and laboratory scales because of the slight difference in cell plate holes: the laboratory scale cell plate hole is not as uniform as that of the industrial scale because it was not laser cut; and, because a rubber seal was placed on the lip of the hole at the laboratory scale and formed a firm seal (Figure 9-13).

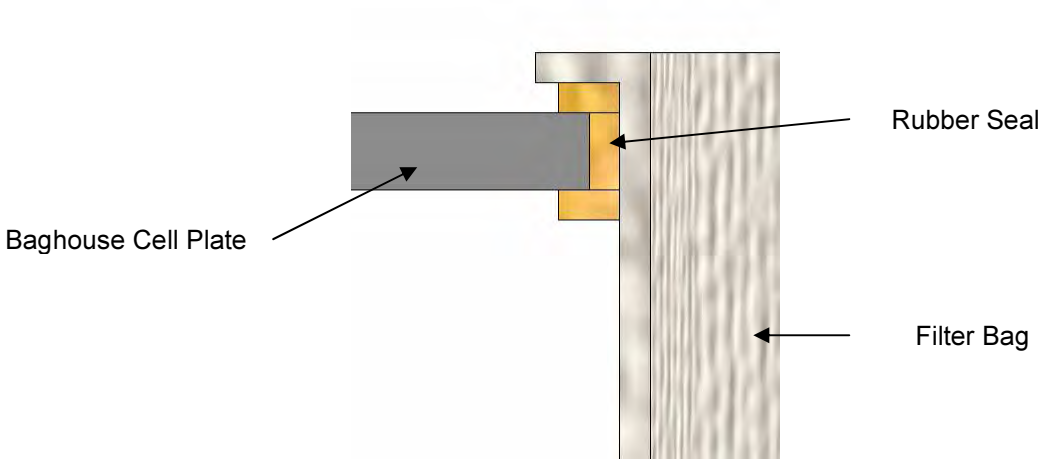

Figure 9-13: Left hand side cross section of laboratory scale baghouse cell plate showing rubber seal and filter bag

Secondly, the model assumes that the properties of the beam are constant along its length. The 6 m support cage was made by spot welding the overlapping rods of two 3 m sections. Therefore, at this point, the cage is likely to be more rigid compared to the rest of the bag thus violating this assumption slightly. At the mid point of the 3 m cage, there is no such additional strength, therefore creating a difference between the two scales.

Thirdly, the model assumes that the mass is evenly distributed throughout the cross section of the beam. However as shown in Figure 9-14, if the cross section of the bag was discretised into horizontal bands of even widths, then the two bands on the edge of the matrix have a greater mass than the remaining bands. Therefore, the assumption of the mass being evenly distributed throughout the cross section of the beam is not correct in this case.

These sources of error are unlikely to explain the larger difference in EI values and thus, it is most likely that the cantilever beam model used is not applicable in this situation. Also, the cantilever model does not account for the influence of gravity which clearly is important with the bag hanging vertically.

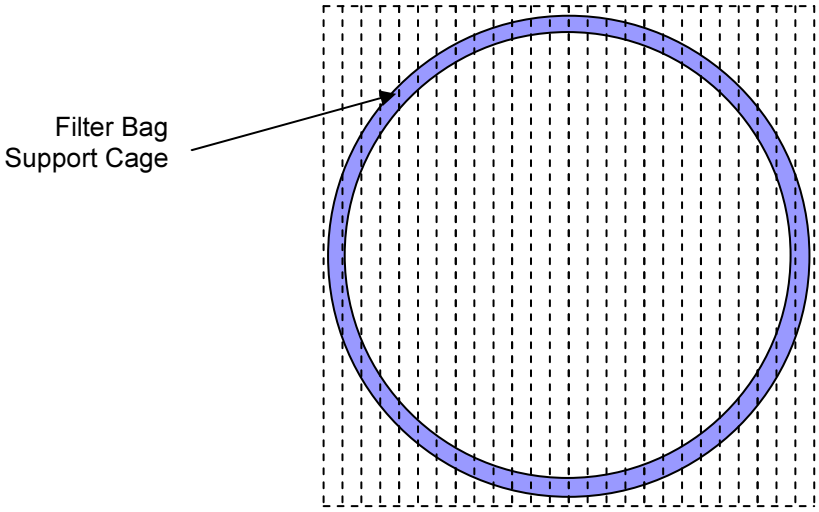

Figure 9-14: Discretisation of filter bag and cage showing that the mass is not evenly distributed throughout the cross section

If a simple pendulum model applies to the bag and cage movement, then Equation 9-4 shows that the ratio of the frequencies for two different length bags should equal the square root of the inverse ratio of bag lengths. The ratio of the 3 m bag frequency to the 6 m bag frequency is 1.47. The square root of the ratio of the 6 m bag length to the 3 m bag length is 1.41. These results show a difference of only 4 % which indicates that the bag and cage behaves very much like a simple pendulum rather than a cantilever beam. This good agreement also suggests that the rubber seal included at the laboratory scale but not present at the industrial scale, has no influence on the movement of the filter bags.

It appears there are some relatively simple solutions available to increase the stiffness of the industrial scale bags, which in turn, should decrease the bag displacement, reduce the likely hood of bag to bag contact, and therefore increase bag lifetimes. Firstly, the use of two additional support lugs (four in total) to fix each cage to the cell plate could be an option. This should decrease any movement of the cage at the cell plate. However, the time taken to install and remove support cages will be increased. A second option could be the use of heavier cages or cages made from a stiffer grade material. However, as mentioned above, the use of heavier cages will become a health and safety risk to plant operators installing or removing these cages. Therefore, it seems that use of additional support lugs at the cell plate is the most logical option.

9.5.6. Observation of Cleaning Pulse

The first three still images from the pulse cleaning video footage are shown in Figure 9-15 below. In the first image, the filter bag is wrapped tightly onto the filter cage as the cleaning pulse has not yet reached this location near the bottom of the bag. The second and third images show that the bag has moved away from the support cage due to both the reverse flow of pulse cleaning air and the resulting stretching of the filter bag.

Figure 9-15: Clandeboye Dryer #2 baghouse #2 filter bag diameter 0.0 s, 0.08 s and 0.12 s after initiation of the compressed air cleaning pulse

The measurements of bag diameter at each frame during the cleaning pulse plotted in Figure 9-16 below indicates that the cleaning pulse causes the diameter of the filter bag to suddenly increase from the normal diameter of 208 mm to a value around 220 mm. This change occurs within 0.12 s. For the next 0.25 s, the bag diameter remains constant. Therefore, between 0.12 s and 0.16 s from the initiation of the cleaning pulse, the bag has decelerated from a constant velocity of approximately 0.06 m / s each side to rest. This equates to an average deceleration each side of roughly 1.44 m / s^2. The bag diameter remains constant until a second increase in diameter to 225 mm occurs around 0.40 s. Finally, the bag diameter reduces over the remaining 0.15 s back to the original 208 mm.

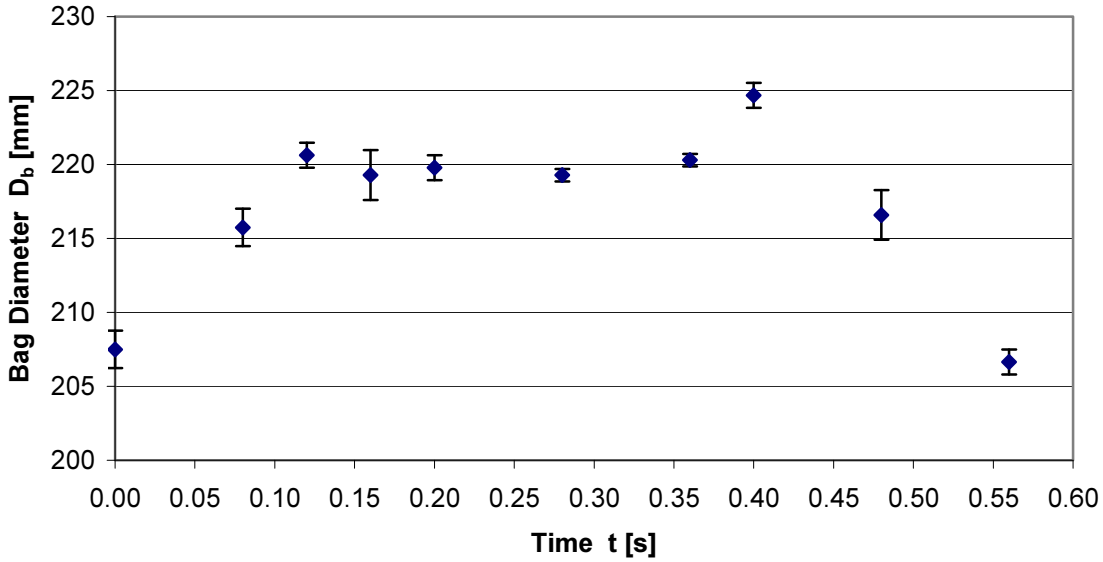

Figure 9-16: Clandeboye Dryer #2 baghouse #2 bag diameter during cleaning pulse

Ignoring the second peak at around 0.40 s, the profile plotted in Figure 9-16 is typical of the pulse cleaned filter bag. It is agreed (Leith et al., 1978; Löffler and Sievert, 1987; Morris et al., 1991) that there are three stages to a conventional pulse. Initially, the compressed air enters the bag and rapidly pushes it outward. At full inflation, the bag decelerates rapidly to a state of metastable rest. At the end of the pulse, the compressed air flow stops, normal filtration resumes and the bag accelerates back to the support cage.

The second peak observed at the 0.40 s mark is somewhat surprising. This peak cannot be attributed to experimental uncertainty so it suggests that a modified type of cleaning pulse from the typical one described above occurs. This second increase in bag diameter is possibly due to a second pressure peak inside the bag. Such a pressure rise could result from a second wave travelling down the bag: a significant amount of air entrained with the initial pulse could increase the pressure in the bag above the initial pressure rise. Alternatively, the second peak could be caused by reflection of the initial pressure wave off the stainless steel disc at the bottom of the support cage. A much more extensive experimental investigation would be required to deduce which of these mechanisms was causing the second peak.

Because of the time between data points in Figure 9-16, two phenomena associated with the change in bag behaviour as a result of the cleaning pulse are not well shown. Firstly, the bag

diameter will initially accelerate on the initiation of the pulse. If the front of the compressed air pulse travels at the speed of sound, 350 m / s, then, the initial acceleration of the filter bag 5.6 m from the top of the bag will occur approximately 16 ms from the initiation of the pulse. Clearly, to observe any phenomenon at this time scale, a camera operating at a much faster frame rate than the 25 per second used here would be required.

Secondly, the bag deceleration between 0.12 s and 0.16 s is likely to not be a simple linear deceleration. It has been shown by several authors, that the cleaning pulse has a wave like motion (Allen et al., 1999; Leith and Allen, 1986; Löffler and Sievert, 1987). At the point of maximum bag displacement, this wave causes the bag diameter to behave in an oscillatory manor and hence, experience a number of deceleration and acceleration cycles before coming to rest. Therefore, the magnitude of the deceleration will be much greater than the 1.44 m / s^2 calculated here and hence, this value should be considered a minimum. Again, observing this phenomenon will require a camera capable of operating at much faster frame rates than was used here.

It was observed with the naked eye using the inspection hatches that powder on the surface of the bags at this location, approximately 5.4 m from the top of the bag, was pulsed off. This occurs because the forces acting on the filter cake because of the cleaning action are greater than the adhesion force between the filter bag and the cake (Löffler and Sievert, 1987). Thus, the cleaning pulse is effective at removing powder at this position on the bag. This is a positive result for such long filter bags as it is difficult to effectively clean long bags (Orr, 1977) because cleaning performance decreases as the bag length increases (Löffler et al., 1988).

Löffler and Sievert (1987) found from pilot scale baghouse experiments with a 2.4 m long filer bag that during cleaning, there is less bag acceleration and deceleration in the lower bag regions compared with the upper bag regions. These authors showed that the inertia forces in the upper bag regions caused the filter cake to be removed during cleaning, but that the reduced inertia forces in the lower bag regions were insufficient to remove the dust cake. Löffler and Sievert (1987) postulated that the cake in the lower bag regions is mainly removed by pressure forces caused by the reverse air flow, which is the likely mechanism that caused the powder observed to be pulsed off 0.6 m from the bottom of the CD2 filter bags.

It can be seen from the images of Figure 9-15 that in the centre of the bag, a vertical hole in the fabric is present. As the pulse progresses and the bag diameter increases, this hole grows in size. Holes such as this reduce the efficiency of the baghouse as powder can escape through this hole and be emitted to atmosphere. Over time, as the bag is subjected to numerous cleaning pulses, this hole will grow in size and this effect will become more pronounced. Eventually, when the outlet powder concentration is too high, bags such as this will have to be replaced.

9.6. Future Research

As the number of milk powder plants using the washable baghouse system increases, the ability to reduce bag damage, increase bag life times and therefore decrease operating costs for bag replacement will become much more financially important to Fonterra. This area of bag movement and the resulting bag damage is a key area requiring further research.

A large part of this research should involve Computational Fluid Dynamics (CFD) studies into the air flow patterns in the baghouses. Studies of this nature could investigate the flow patterns in the inlet region, which are likely to be causing the bag movement documented here. These CFD studies could also investigate different designs such as different inlet air arrangements, perhaps including a baffle plate, larger bag spacings and larger outer gaps.

Further experimental work is recommended exploring bag movement at the laboratory and industrial scales. The EI value at the laboratory scale could be easily determined as follows: the bag could be laid horizontally and supported at each end by a fulcrum; a load could be applied in the middle of the bag/cage and the resulting deflection measured; the maximum deflection will be a function of the applied load, the bag/cage length and the bag/cage EI value; hence, the bag EI value can be determined. The laboratory scale rig should also be used to further investigate the ideas suggested above of increasing the bag stiffness through use of additional support lugs to fix the cage to the cell plate and use of heavier support cages.

Experimental studies could also be conducted into the pulse cleaning. Capturing a greater number of frames with a high speed camera would enable more accurate measurement of the change in bag diameter during the cleaning pulse. This could be carried out at either the

laboratory or industrial scale. A high speed camera should also be used with a mirror arrangement so that cake removal during pulse cleaning can be observed from the front and the side of the bag at the same time. This would enable the mechanisms causing cake removal to be investigated and estimates made of the adhesion forces the particles had to overcome to be removed from the surface of the filter bag.

A potential topic which could be investigated to help increase the bag life time is the compressed air pressure used for pulse cleaning. If studies show that the current compressed air pressure of 6.0 bar combined with the current pulse cleaning cycle times provide sufficient cleaning, it could be possible that a reduction in compressed air pressure and/or a decrease in the cleaning frequency is possible. A reduction in pressure is likely to reduce the acceleration of the filter bag during a cleaning pulse. Combined with a decrease in cleaning frequency, the long term filter bag wear will decrease and thus, increase the bag life time.

To check the pressure profile that develops inside a filter bag during the cleaning pulse, a fast acting pressure transducer could measure this profile. Such measurement would indicate whether a second rise in pressure occurs inside the bag that causes a second increase in bag diameter.

9.7. Conclusions & Recommendations

From this section of work it can be concluded that the use of stainless steel inspection hatches located near the base of the filter bags in the inlet air region has reduced the CIP times because of improved access to observe the filter bags and reduced baghouse dry-out times. It is strongly recommended that these stainless steel inspection hatches be installed in all current and future milk powder plant washable baghouses to also reduce CIP times and aid in decisions to be made about the state of the bags.

From the operational observations of the bag movement from below, it can be concluded that the reason for there being a high bag damage zone in the dirty air inlet region is because of the large amount of bag movement occurring here. These observations also led to the conclusion that the bag movement around the edge of the bag bundle reduces the further the bags are

from the inlet region, and the bag movement in the middle of the bag bundle is almost negligible.

It was concluded that the operational and natural periods of oscillation of the industrial filter bag are approximately the same at 1.4 – 1.5 Hz. This indicates that there is no influence on the period of oscillation from either the dirty air flow or presence of filter cake on the bags during operation. From the 3 m long pilot scale filter bag movement experiment, it was concluded that this bag had a period of oscillation of 2.2 Hz.

Use of a cantilever beam model to determine the Young's modulus of the bag and cage at both the industrial and laboratory scales allowed it to be concluded that this model does not describe the filter bag and cage situation well. However, it was concluded that a simple pendulum model accurately described the filter bag and cage movement.

It is recommended that the topic of bag movement and resulting bag damage be the subject of future research, with the aim of further reducing bag damage. This should involve experimental studies investigating the possibility of using additional support lugs or heavier support cages to reduce bag movement. Also, CFD studies looking at alternative baghouse designs may prove useful in helping to reduce bag damage.

With regard to the observations of the industrial cleaning pulse, it can be concluded that the current cleaning pulse is effective even near the base of these long bags because the cake at this location of the bag is visibly pulsed off. It can also be concluded that the cleaning pulse is probably a modified type because of a second change in bag diameter occurring near the end of the pulse likely to be due to a second rise in pressure within the bag. This pulse could possibly be a result of the shape of the pulse-cleaning ejector.

Further research into the pulse cleaning behaviour of the filter bags is also an option. These studies could investigate the use of reduced compressed air pressure and increased pulse cleaning cycle times to optimise the use of compressed air. Finally, use of a high speed video camera would enable the mechanisms causing cake removal during pulse cleaning to be explored in greater detail.

10. Spray Dryer CFD Modelling

Computational fluid dynamics (CFD) studies of spray dryers have been reported extensively. However, the majority of these studies have been on the pilot scale and may not be representative of the industrial situation. In this chapter a CFD study of an industrial scale spray dryer investigates the transient nature of the air flow and includes some steady state particle tracking.

10.1 Computational Fluid Dynamics

Versteeg and Malalasekera (1995) define CFD as "the analysis of systems involving fluid flow, heat transfer and associated phenomena such as chemical reactions by means of computer based simulation". The technique works by solving equations of fluid flow over a region of interest with specified boundary conditions (ANSYS, 2005a). The technique is very powerful and has been applied in a wide range of industries including aerodynamics of aircraft, hydrodynamics of ships, turbomachinery, chemical process engineering, environmental engineering and biomedical engineering (Versteeg and Malalasekera, 1995).

CFD packages contain three main elements (Figure 10-1); a pre-processor, a solver and a post-processor (Versteeg and Malalasekera, 1995). This work was carried out using the commercial CFD package ANSYS CFX 10.0 (ANSYS Europe Ltd, Riseley, UK).

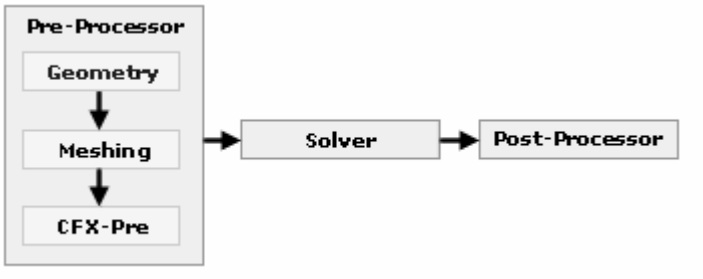

Figure 10-1: The main elements of CFD simulation packages (source: ANSYS CFX website)

According to Versteeg and Malalasekera (1995), the user activities in the pre-processing stage involve definition of the geometry (the computational domain); generation of the grid or mesh; selection of the physical and chemical phenomena that are to be modelled; definition of

fluid properties; and specification of appropriate boundary conditions. It should also be noted that the solver parameters are specified in the pre-processing stage (ANSYS, 2005a). Within the ANYSYS Workbench environment that was used for this work, the problem geometry can be created in either ANSYS DesignModeler 10.0 (SAS IP Inc, Canonsburg, USA) or imported from an external CAD package such as Solidworks. The geometry is then meshed using either ANSYS ICEM CFD 10.0 (SAS IP Inc, Canonsburg, USA) or CFX Mesh 10.0 (ANSYS Europe Ltd, Riseley, UK).

The solver is the component of the CFD code that solves the problem (ANSYS, 2005a). The Solver algorithm consists of three processes (ANSYS, 2005a; Versteeg and Malalasekera, 1995):

1. The partial differential governing equations of fluid flow are integrated over all control volumes that form the flow domain
2. These integral equations are discretised to a system of algebraic equations. This step involves the substitution of a variety of finite difference approximations for the terms in the integral equations.
3. Because of the non linear nature of the equations, the system of algebraic equations is solved by an iterative method.

The ANSYS CFX 10.0 Solver uses a coupled solver where the hydrodynamic equations are solved as a single system (ANSYS, 2005a). This coupled solver is faster than the traditional segregated solver and hence, fewer iterations are required to obtain a converged solution (ANSYS, 2005a).

The majority of the simulations carried out during this project were solved using parallel processing on the University of Canterbury Super Computer. This super computer is composed of eight IBM p5-575 high-end compute nodes, where each node contains 16 IBM Power 5, 1.9 Giga Hertz processors and 32 GigaBytes (GB) of memory. Because all nodes have a high speed, low latency interconnect, the CFD simulations of this project were solved using a single complete node, that is, 16 dual core processors in parallel.

The post-processor is used to analyse, visualise and present the results generated by the Solver (ANSYS, 2005a). Post-processors allow results to be presented using vector, line and surface plots; particles to be tracked; the mesh to be displayed; quantitative calculations to be

performed; and charts showing graphical plots generated. In more recent times, post-processors have included animation features for display of dynamic results (Versteeg and Malalasekera, 1995).

Modelling complex physical processes such as combustion and turbulence is often achieved using empirical relationships (ANSYS, 2005a). Consequently, the approximations inherent in these models contribute to differences between the CFD solution and the real solution (ANSYS, 2005a). How close the CFD solution is to the exact solution also depends on a number of factors, including the size and shape of the control volumes of the mesh (ANSYS, 2005a). Therefore, validation of the CFD solution is essential. Validation can be achieved by comparing CFD results with experimental data such as point flow velocity measurements (Versteeg and Malalasekera, 1995). If comparison with experimental data is not possible, a CFD user must rely on previous experience, comparison with analytical solutions of similar but simpler flows or comparison with high quality data from closely related problems published in the literature (Versteeg and Malalasekera, 1995).

10.1.1 Governing Equations

The governing equations of fluid flow are mathematical statements of the conservation laws of physics (Versteeg and Malalasekera, 1995). Thus, the Navier-Stokes equations, which represent the conservation of mass, momentum and energy, are the governing equations of CFD. For a compressible Newtonian fluid, the Navier-Stokes equations in Cartesian coordinates are represented as Equations 10-1 to 10-5 (Versteeg and Malalasekera, 1995) where Equation 10-1 is the mass or continuity equation, Equations 10-2 to 10-4 the momentum equation in each direction and Equation 10-5 the internal energy equation:

$$\frac{\delta\rho}{\delta t} + div(\rho U) = 0 \qquad (10\text{-}1)$$

$$\frac{\delta(\rho u)}{\delta t} + div(\rho u U) = -\frac{\delta\rho}{\delta x} + div(\mu \ grad \ u) + S_{Mx} \qquad (10\text{-}2)$$

$$\frac{\delta(\rho v)}{\delta t} + div(\rho v U) = -\frac{\delta\rho}{\delta y} + div(\mu \ grad \ v) + S_{My} \qquad (10\text{-}3)$$

$$\frac{\delta(\rho w)}{\delta t} + div(\rho w U) = -\frac{\delta\rho}{\delta z} + div(\mu \ grad \ w) + S_{Mz} \qquad (10\text{-}4)$$

$$\frac{\delta(\rho h)}{\delta t} - \frac{\delta p}{\delta t} + div(\rho h U) = div(\lambda \ grad \ T) + \Phi + S_E \qquad (10\text{-}5)$$

The parameters in Equations 10-1 to 10-5 are ρ [kg / m^3] fluid density; U [m / s] velocity vector; u [m / s] velocity component in the x direction; v [m / s] velocity component in the y direction; w [m / s] velocity component in the z direction; p [Pa] pressure; μ [Pa s] dynamic viscosity; S_M [N / m^3] momentum source terms in the x, y, or z directions; h [J / kg] internal energy; λ [W m / K] thermal conductivity; T [K] temperature; Φ [W / m^3] a dissipation function accounting for the effects of viscous shear; S_E [W / m^3] internal energy source term.

For an incompressible fluid the density is constant. Therefore, Equation 10-1 can be simplified to

$$div(U) = 0 \qquad (10\text{-}6)$$

Equations describing other processes, such as combustion, can also be solved in conjunction with the Navier-Stokes equations (ANSYS, 2005a).

10.1.2 Turbulence Modelling

Most flows of interest to engineers are turbulent (Versteeg and Malalasekera, 1995). Turbulence is a result of inertia forces in the fluid becoming more significant than the viscous forces (ANSYS, 2005a), and hence, is indicated by high Reynolds numbers. Turbulence is a complex process because it is diffusive (mass and momentum are transported) and dissipative (energy is cascaded from larger to smaller eddies where it is removed by viscous resistance). It is also unsteady, three dimensional and consists of many turbulent length and time scales. To numerically solve the Navier-Stokes equations directly for a fully turbulent flow requires extremely large computing power (Versteeg and Malalasekera, 1995). Consequently, several approximating turbulence models have been developed.

Turbulent flow could be considered to exhibit an average characteristic, with an additional fluctuating component. Most turbulence models modify the original unsteady Navier-Stokes equations by introducing these averaged and fluctuating quantities to produce the Reynolds Averaged Navier-Stokes (RANS) equations (ANSYS, 2005a). RANS turbulence modelling represents the mean flow quantities only, while concurrently modelling turbulence effects

without a need for the resolution of the turbulent fluctuations (ANSYS, 2005a). More advanced turbulence models such as Large Eddy Simulation (LES), Direct Eddy Simulation (DES) and Scale-Adaptive Simulation (SAS) are available and are becoming more common in CFD packages. However, these models require very fine computational grids and very small timesteps to capture the large and small eddies (Wesseling, 2001). Further information on LES, DES and SAS models are given by Menter (2006) and the ANSYS CFX Release 10.0 (2005).

Turbulence models based on the RANS equations are known as Statistical Turbulence Models because of the statistical averaging procedure employed to obtain the equations (ANSYS, 2005a). The averaging procedure introduces additional unknown terms containing products of the fluctuating quantities (ANSYS, 2005a). Turbulence models close the RANS equations by providing models for the summation of the products of the Reynolds stresses and Reynolds fluxes (ANSYS, 2005a).

RANS based turbulence models can be divided into two classes; Eddy-viscosity models and Second Order Closure models (Collie et al., 2001). Linear Eddy-viscosity models are further categorized based on the number of partial differential equations (Zero- to Two- equations). Two-equation models solve a transport equation for the turbulent kinetic energy per unit mass k [m^2 / s^2], and another transport equation determining length or time scales. Two-equation models are more dominant in CFD codes because they are more complete, have been more widely validated and offer a good compromise between numerical effort and computational accuracy (ANSYS, 2005a).

There are numerous Two-equation turbulence models available in CFX 10.0 such as the k-ε model, the RNG k-ε model, the k-ω model and the Baseline (BSL) k-ω model (ANSYS, 2005a). The majority of these standard Two-equation models over-predict shear stress in adverse pressure gradient flows and therefore they miss the separation and predict attached flow even from strong pressure gradient flows (Menter, 2006). The Shear Stress Transport (SST) model, which was used for this work, is one of the most accurate Two-equation models for separation prediction (ANSYS, 2005a).

10.1.2.1 Shear Stress Transport Model

The SST model consists of the same equations as the BSL k-ω model. Therefore, it combines the advantages of the k-ε and k-ω models by using a blending function F_1 to switch between the k-ω model and the k-ε model. $F_1 = 1$ in the sub- and log-layer and $F_1 = 0$ in the wake region of the boundary layer, so both the BSL k-ω model and the SST model switch from the k-ω model near the wall to the k-ε model away from the wall (Menter, 2006). The SST model differs from the BSL k-ω model in that a second blending function F_2 is introduced in the eddy-viscosity equation to account for the transport of the turbulent shear stress.

The SST model was chosen for this work because it is regarded as the most advanced Two-equation model as it combines the strengths of the k-ε and k-ω models and overcomes the weaknesses of the k-ε, k-ω and BSL k-ω models. Also, the SST model has been reported as being numerically stable in complex applications and the increased computational requirements are seen as insignificant compared with the k-ω model (Menter, 1994).

The additional equations and coefficients required for the SST turbulence model can be found in Menter (1994) and the ANSYS CFX Release 10.0 (2005).

10.1.2.2 Near Wall Treatment

The turbulent boundary layer near a solid surface is composed of an inner and outer region (Versteeg and Malalasekera, 1995). The inner region comprises three zones. Firstly, the innermost layer is the viscous sub-layer where the flow is predominantly laminar and viscous forces dominate. For straight boundaries, further away from the wall is the logarithmic layer where turbulence dominates (ANSYS, 2005a). The region between these two layers is known as the buffer layer, where viscous and turbulent stresses are of similar magnitude (Versteeg and Malalasekera, 1995). The outer region, far from the wall, is inertia dominated and hence free from direct viscous effects (Versteeg and Malalasekera, 1995).

The logarithmic region can be represented by a logarithmic relation between u^+, the dimensionless near wall velocity (Equation 10-8) and y^+, the dimensionless distance from the wall (Equation 10-9) as Equation 10-7 shows:

$$u^+ = \frac{1}{\kappa}\ln\left(y^+\right) + C \tag{10-7}$$

$$u^+ = \frac{U_t}{u_\tau} \tag{10-8}$$

$$y^+ = \frac{\rho \Delta y u_\tau}{\mu} \tag{10-9}$$

κ is the von Karman constant equal to 0.4187 (Versteeg and Malalasekera, 1995), C a logarithmic layer constant depending on wall roughness, U_t [m / s] the tangential velocity a distance Δy [m] from the wall and u_τ [m / s] the friction velocity given by Equation 10-10 where τ_w [kg / m / s^2] the wall shear stress.

$$u_\tau = \sqrt{\frac{\tau_w}{\rho}} \tag{10-10}$$

There are three approaches to modelling the flow in the near-wall region in CFX 10.0: standard wall functions, scalable wall functions and automatic near-wall treatment (ANSYS, 2005a). Standard wall functions use empirical formulae to impose suitable conditions near to the wall without resolving the boundary layer (ANSYS, 2005a). However, if the value of y^+ falls below 11.067 (the intersection between the logarithmic and viscous sub-layer near wall profile), the standard wall function is no longer applicable because the profile is linear, not logarithmic. Hence, this is the major drawback of the wall-function approach as the predictions depend on the location of the point nearest to the wall and are sensitive to the near-wall meshing (ANSYS, 2005a).

To overcome this fine grid inconsistency, scalable wall functions and automatic near-wall treatments have been developed. Scalable wall functions limit the value of y^+ to a minimum value of 11.067 (ANSYS, 2005a), hence, it is assumed that the first node from the wall is at the boundary of the viscous sub-layer and the logarithmic region. Therefore, scalable wall functions can be applied on arbitrarily fine meshes and allows consistent mesh refinement independent of the Reynolds number (ANSYS, 2005a).

Automatic near-wall treatment is the default for all ω-based turbulence models, including the SST model in CFX 10.0 (ANSYS, 2005a). This approach considers the viscous sub-layer because it automatically allows for a smooth shift from a low-Reynolds number formulation if

the near wall resolution is high, to a wall function formulation if the near wall resolution is insufficient (ANSYS, 2005a). Therefore, integration through to the wall will occur using the low-Reynolds number formulation, whereas, when the first node away from the wall is assumed to be outside the viscous sub-layer, the wall function formulation will be used. A y^+ value of up to 200 is acceptable if the automatic wall treatment is being used (ANSYS, 2005a).

10.1.3 Particle Tracking Theory

The flow of solid particles in a gas stream can be considered a multiphase flow situation where the particles are a dispersed phase in the gas stream. There are two models available in CFX 10.0 that can be used to model such a situation: an Eulerian-Eulerian multiphase model and a Lagrangian Particle Tracking model (ANSYS, 2005a).

In the Eulerian-Eulerian approach, both the gas and particle flows are treated as continua and mathematically as two interacting fluids (Tu and Fletcher, 1995). This model is the preferred modelling approach for moderate to dense particulate flows or when the volume fraction of the particles is more than 10 % (Ranade, 2002). The Eulerian-Eulerian model has the advantages of providing complete global information, being relatively cheap computationally for one additional set of equations and automatically including interphase turbulent dispersion forces (ANSYS, 2005a). However, the Eulerian-Eulerian model can be computationally expensive if a number of sets of equations are used, where for example, a range of particle sizes are included (ANSYS, 2005a).

The Lagrangian Particle Tracking model was used for this work. In this approach, the fluid phase is treated as a continuum and solved using the Eulerian approach, whereas the particles are explicitly calculated using a Lagrangian framework (ANSYS, 2005a). Several individual particles are tracked through the flow field from their injection point until they escape the domain or some integration limit criterion is met (ANSYS, 2005a). Each particle represents a sample of particles that follow an identical path (ANSYS, 2005a). The behaviour of the tracked particles is used to describe the average behaviour of the dispersed phase and generate source terms for the fluid mass, momentum and energy equations (ANSYS, 2005a).

The motion and position of each particle in the flow field is determined using Newton's Law, that is, the inertial force of a particle is equal to the total forces acting on the particle

$$m_p \frac{dU_p}{dt} = F_D\left(U_g - U_p\right) + F_g + \Sigma F_o \qquad (10\text{-}11)$$

where m_p [kg] is the mass of the particle; U_p [m / s] and U_g [m / s] the particle and gas velocity vectors; t [s] time; F_D [N] the drag force and F_g [N] the gravitational force. F_o [N] refers to other forces such as the force to accelerate the virtual mass of the fluid, the force applied on the particle because there is a pressure gradient in the fluid surrounding the particle caused by fluid acceleration, and the turbulent dispersion forces (ANSYS, 2005a). The integration of the force balance (Equation 10-11) gives the motion and trajectory of the particle as Equation 10-12 shows:

$$\frac{dx_p}{dt} = U_p \qquad (10\text{-}12)$$

where x_p [m] is the particle location.

Particles can be either fully coupled to the continuous fluid or are one-way coupled. When fully-coupled, the particles exchange momentum with the continuous phase and thus the particles affect the fluid behaviour (ANSYS, 2005a). When using one-way coupling there is no such exchange of momentum so the gas flow influences the particle trajectories but the converse does not occur. The choice of coupling is dependent on the powder mass loading. One-way coupling may be an acceptable approximation in flows with low mass loadings but if the particles influence the fluid flow significantly, then full coupling should be used (ANSYS, 2005a).

The Lagrangian technique is recommended when the dispersed phase volume fraction is less than 10 % (Ranade, 2002). The Lagrangian Particle Tracking model has three advantages over the Eulerian-Eulerian approach: complete information on behaviour and residence time of individual particles is available; the approach is relatively cheaper computationally for a wide range of particle sizes; and this approach is more flexible when there is a significant size distribution leading to different particle velocities (ANSYS, 2005a). The disadvantage of the Lagrangian Particle Tracking model is that it can be computationally expensive if a large number of particles have to be tracked and if turbulence is included (ANSYS, 2005a).

10.2 Introduction to Spray Dryer CFD Modelling

CFD methods have been used to carry out spray dryer studies such as comparing the performance of rotary disc and pressure nozzle atomisation (Huang et al., 2006), assessing chamber design alternatives (Huang et al., 2003b; Southwell et al., 2001) and predicting drying performance (Li and Zbicinski, 2005; Southwell et al., 1999). The air flow patterns in spray dryers have been the subject of numerous experimental and CFD studies. Langrish et al. (1992) give a review of flow visualisations and the results from numerous CFD simulations have been published (Fletcher et al., 2003; Guo et al., 2003; Harvie et al., 2002; Kieviet et al., 1997; Langrish, 1993; Langrish et al., 2004; LeBarbier et al., 2001; Oakley and Bahu, 1990; Stafford et al., 1996; Straatsma et al., 1999). This literature is discussed in more detail in Appendix G.

The general consensus from the previous spray dryer CFD studies mentioned above is that the main air jet flows at high velocity down the centre of the chamber and there are large recirculation zones between this central jet and the walls of the chamber. Several authors have shown the flow field is transient as the main jet moves or precesses slightly around the central axis. Therefore, simulations have to be 3D and transient to fully capture the flow field within a spray dryer.

The majority of spray dryer studies have been conducted on laboratory or pilot scale equipment because these simulations are not as computationally demanding as industrial scale simulations. Also, measurement of flow properties, and therefore simulation validation, is much easier at the pilot scale. However, these studies do not truly represent the industrial situation as modern spray dryers are two-stage stage dryers with internal fluidised beds at the base of the chamber. Also, in an increasing number of modern spray dryers, the outlet air passes through ducts located near the top of the chamber rather than through a single outlet near the bottom of the chamber. Finally, the outlet boundary conditions applied in most previous CFD studies has been an average static pressure, but the outlet air stream experiences additional pressure drop through the fines collection equipment before the constant pressure condition is reached at the point where the air is discharged to atmosphere. Thus, it is possible that the resistance to flow because of the downstream unit operations will have an impact on the flow field in the spray dryer.

Simulations including particle tracking have been carried out by a number of authors including Harvie et al. (2002), Huang et al. (2003a), Huang et al. (2003b), Huang et al. (2006), Kieviet and Kerkhof (1996), Southwell et al. (1999), Straatsma et al. (1999) and Ullum (2006). These simulations have modelled spray dryers with pressure nozzle atomisation (Harvie et al., 2002; Southwell et al., 1999), rotary disc atomisers (Kieviet and Kerkhof, 1996; Ullum, 2006) or both (Huang et al., 2006; Straatsma et al., 1999). These authors have performed particle tracking to investigate evaporation rates within the chamber and the likely locations of chamber fouling caused by particle contact with the chamber walls.

The Lagrangian approach has traditionally been used to model particle transport with two-way coupling because of the significant heat, mass and momentum exchanged between the two phases. The initial droplet distributions were represented using a Rosin Rammler distribution (Huang et al., 2003a; Huang et al., 2003b; Huang et al., 2006; Kieviet and Kerkhof, 1996; Ullum, 2006), specifying a mean diameter (Southwell et al., 1999; Straatsma et al., 1999) or using a user specified relationship between initial droplet size and final particle diameter (Harvie et al., 2002). The droplet velocities from pressure nozzles have usually been specified axial and radial components (Huang et al., 2003a; Huang et al., 2003b; Kieviet and Kerkhof, 1996; Southwell et al., 1999), although a total velocity has also been specified (Huang et al., 2006; Straatsma et al., 1999). The spray angles have ranged from 60^{o} (Huang et al., 2003b) to 90^{o} (Straatsma et al., 1999).

The area of spray dryer CFD modelling that is probably causing the most hindrance to accurate modelling is the condition given to define the droplet behaviour when droplets impact the walls. Most previous authors have used a coefficient of restitution equal to zero (Huang et al., 2003a; Huang et al., 2003b) or very near to zero (Southwell et al., 1999). A value of zero causes the particles to become trapped at the wall and the momentum of the particles is transferred to the wall as a force (ANSYS, 2005a). Using a coefficient of restitution equal to unity implies that particles will rebound from the walls and retain their normal or tangential momentum (Huang et al., 2003b).

Harvie et al.'s (2002) is the most advanced approach to wall behaviour for milk powders. These authors used a 'sticky-point' curve, a plot of particle temperature versus particle moisture content, to determine whether the droplet rebounded elastically from the wall or remained near the wall; particles rebounded when the particle temperature was below the

sticky point temperature (a coefficient of restitution of 1.0) or remained near the wall when the particle temperature was above the sticky point temperature (a coefficient of restitution of 0).

It is somewhat surprising that none of the mentioned previous spray dryer CFD studies that performed particle tracking has investigated the chamber collection efficiency. This is possibly because of the uncertainty regarding appropriate values of the coefficient of restitution, but as Chapters Four and Eight highlight, this information would be very useful for industrial operators and plant designers.

10.2.1 Aims

The first aim of this work was to determine the transient behaviour of the CD2 flow field and investigate the influence of different SFB air flows and a more representative outlet boundary condition on the chamber flow field. The second aim was to investigate the amount of fines entrained in the outlet air ducts by steady state particle tracking. Thirdly, the aim was to validate the simulations by comparing the simulation results against data collected from the industrial scale.

10.3 Model Description

10.3.1 Geometry

The CD2 spray dryer geometry was used for this model. CD2 is a GEA Niro A/S MSD 2000 design which is a modified conical type of chamber. The chamber is approximately 22 m at the highest point and 18 m wide at the widest point. These dimensions mean that the geometry simulated is larger than that reported by Straatsma et al. (1999).

The main airflow enters the chamber between the pressure nozzle lances and external recycle fines return holes. This CFD model has simplified the actual inlet arrangement because the size of the main inlet boundary includes the open area available for the inlet air stream, as well as the area of the fines recycle holes and the pressure nozzles. The main inlet is the very top of the chamber drawn in Figure 10-2. The fluid bed air enters a plenum chamber then flows up through the perforated plate, inducing some swirl. This plate is the base of the

chamber in Figure 10-2. Both air streams are drawn out through the two identical ducts located across a diameter near the top of the chamber by extractor fans, and hence the chamber and ducts are under slight vacuum.

The geometry was drawn using Solidworks 2005 SP3.1 (Solidworks Corporation, Conrod, USA) and imported into ANSYS DesignModeler 10.0. In DesignModeler, the geometry check option was run which checks the geometry for short edges and faces that may create a poor mesh or even prevent the mesh from being generated (ANSYS, 2005b).

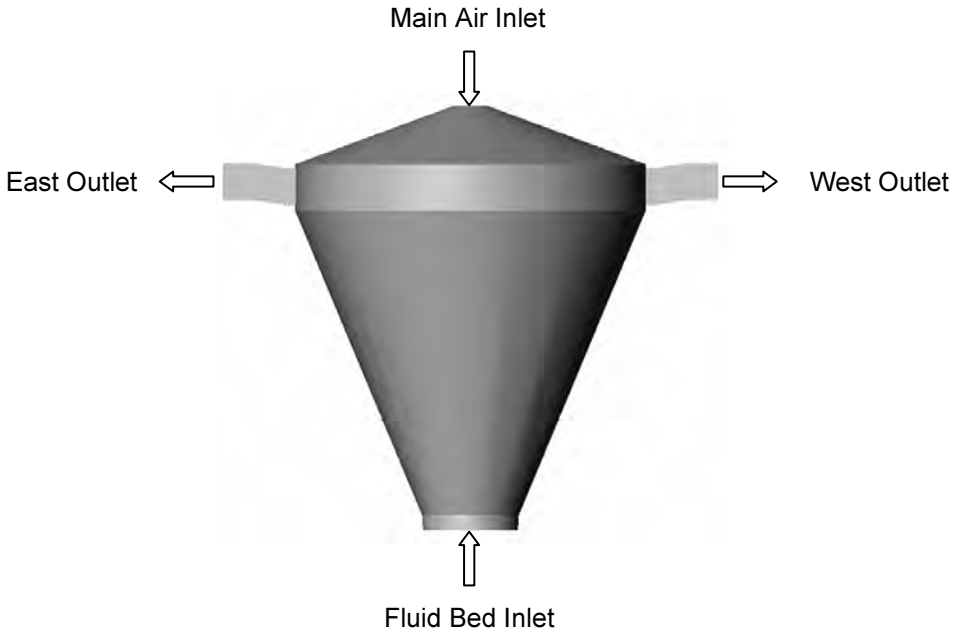

Figure 10-2: Solidworks drawing of Fonterra Clandeboye Dryer #2 used for CFD simulations

10.3.2 Mesh

The geometry was meshed using CFX Mesh 10.0. An unstructured mesh was generated in the volume of the chamber using tetrahedral elements. The default CFX Mesh 10.0 surface mesh, meshing strategies and volume mesh of Delaunay, Advancing Front & Inflation 3D, and Advancing Front were used. With this approach, boundary nodes are triangulated according to the Delaunay criterion and then the prismatic inflation layers and then tetrahedral volume elements are built progressively inward from the surface.

Edge proximity was applied so that mesh elements were automatically modified in regions where curved and flat surfaces were in close proximity; in this mesh these elements were near the entrance of the outlet air ducts. A resulting surface mesh is shown in Figure 10-3.

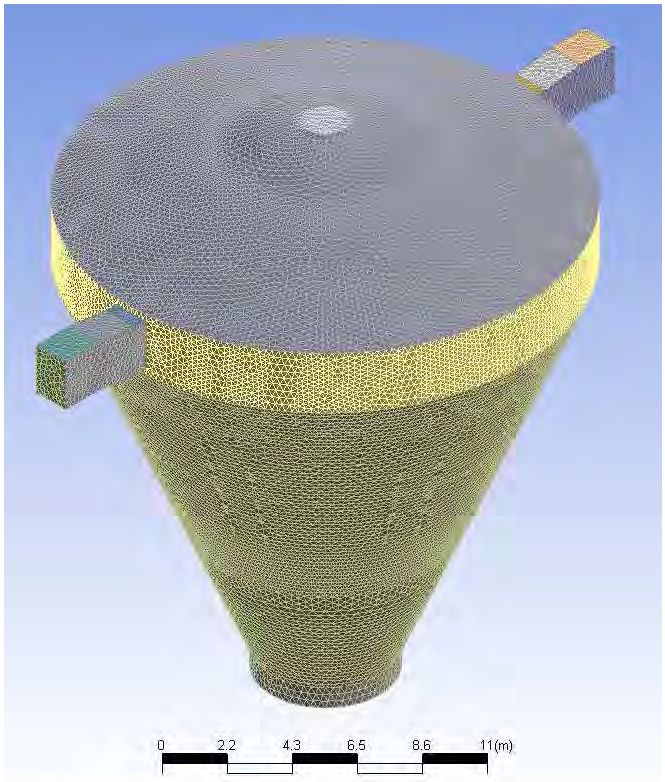

Figure 10-3: Surface of fine mesh used for CFD simulations

An inflation layer consisting of three prismatic elements was used at the walls to ensure boundary layer effects were captured. Although it is recommended that the boundary layer should contain a minimum of 10 nodes (ANSYS, 2005a), because these simulations were more interested in the flow away from the wall, and to reduce computational requirements, only three nodes were included in the boundary layer. A maximum inflation layer thickness of 0.012m and an inflation layer expansion factor of 1.2 were chosen. This ensured that the position of the first node away from the wall gave a y^+ value of less than 200.

Using initial steady state runs, three iterations of mesh adaptation based on velocity were used to increase the mesh density in the regions of high velocity gradients. As Figure 10-4 shows, these areas were down the centreline of the chamber from the main air inlet, and in the outlet air ducts.

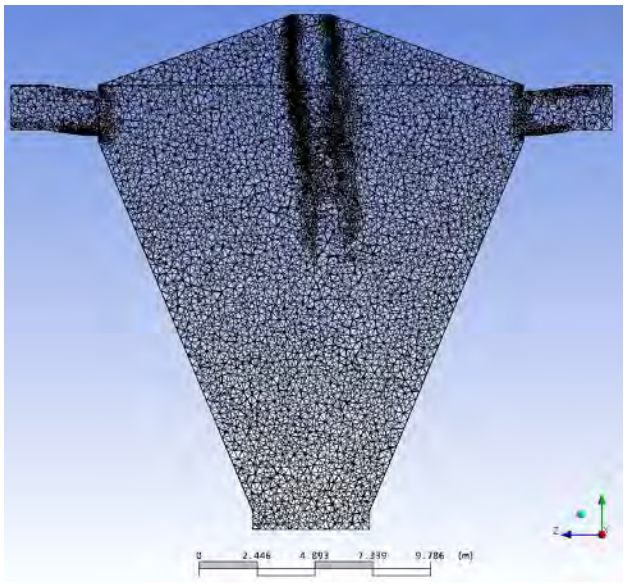

Figure 10-4: ZY plane through centre of drying chamber showing medium mesh used for CFD simulations

Three different meshes were produced and the simulations repeated on each (see Section 10.4.3 below). The number of elements and nodes in each of these meshes is shown in Table 10-1 below.

Table 10-1: Number of nodes and elements in the three meshes used for mesh independence study

Mesh	Coarse	Medium	Fine
Elements	532,035	1,598,227	3,377,845
Nodes	128,868	325,595	669,753

10.3.3 Transient Air Flow Simulation

10.3.3.1 Boundary Conditions

The air flow in this simulation was assumed to be incompressible and isothermal at 25 ^{o}C. Ambient air temperature was used to allow the validation experiments discussed in Section 10.4.4 below to be carried out.

The inlet velocity was set at 17.5 m / s with a turbulent intensity of 3.7 % and a turbulent length scale based on the inlet diameter. This inlet turbulence approach is identical to that of

a number of studies (Guo et al., 2003; Harvie et al., 2001; Harvie et al., 2002; LeBarbier et al., 2001). In the industrial plant, this main inlet air flow has passed through an air disperser designed to ensure a uniform flow pattern, therefore it was assumed that there is no swirl in the inlet.

The fluid bed air inlet is modelled as a circular inlet where the velocity was initially set at 0.77 m / s. Again it was assumed there was no swirl with this flow and a turbulence intensity of 3.7 % was used with a turbulent length scale based on the fluid bed inlet diameter. The value of this turbulent length scale is not expected to be critical. Simulations were also run with SFB air flows giving velocities at this inlet of 0 m / s and 0.38 m / s to investigate the influence of the fluid bed flow on the overall flow field.

The main inlet air velocities used in these air flow simulations are much lower (17.5 m / s c.f. ≈ 30 m / s) than those experienced during production. This occurred because validating the simulations using an ambient air case meant that the air density was much lower than that during production, and hence the inlet air fan was not large enough to supply the equivalent production air flow.

Initially, average static pressures of – 60 Pa were specified in the two outlet air ducts as the chamber is operated under vacuum to prevent the loss of product. To model the effects of the downstream resistance that the flow experiences upon exit of the chamber, the outlet boundary condition was changed to an opening, and a loss coefficient f given by Equation 10-13 was set. The value of the loss coefficient was determined using an average outlet duct air density and velocity, and average pressure drop through the baghouse with no milk powder present from CD2.

$$\Delta P = f \frac{\rho u^2}{2} \qquad (10\text{-}13)$$

The chamber walls were treated with the default CFX 10.0 boundary conditions of no slip, with smooth, adiabatic walls. Automatic wall functions were used to model the near wall flow.

10.3.3.2 Simulation Procedure

3D simulations were carried out using the commercial CFD package CFX 10.0. The transient Reynolds Averaged Navier-Stokes equations and the Shear Stress Transport (SST) turbulence model were used to account for the effects of turbulence. Second order discretization schemes were used in both time and space.

A convergence criterion of a root mean square residual of 1 x 10^{-4} was used to terminate the coefficient iterations. Using this scheme, convergence was not possible for steady state simulations, indicating, as expected, that the simulations needed to be run in transient mode. The unconverged steady state results were used as an initial guess for the transient simulations.

Adaptive time stepping was used where the timestep could range between 0.008 and 0.1 s and start from an initial value of 0.05 s. Usually only two or three iterations at each timestep were required. A total real simulated time of 100 s was specified.

Velocity components in the x, y and z directions, along with the pressure at four fixed points, were recorded for each timestep. The first of these four points was located on the dryer centreline 1 m above the SFB. Figure 10-5 shows that the remaining three points were located 2 m from the start, and in the middle of the east outlet duct.

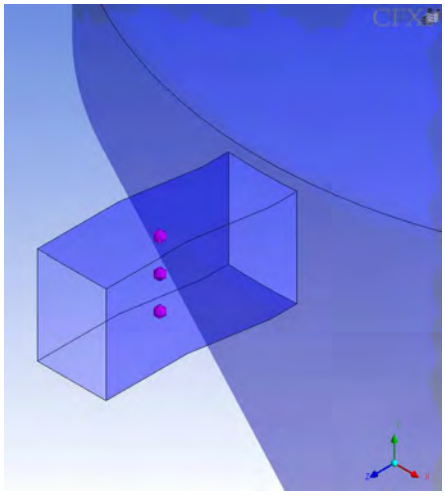

Figure 10-5: Location of three points in middle of east outlet duct where velocity components and pressure data were obtained at each timestep

10.4 Transient Air Flow Results

The major flow feature in the drying chamber is the main axial jet entering the top of the chamber (Figure 10-6). It diverges slightly as it moves into the chamber but it generally retains a flat profile that does not grow much larger than the diameter of the inlet. The jet slows as it moves further into the dryer and moves about the central axis with time. There is very little flow normal to the dryer axis (Figure 10-7) with the axial flows dominating.

Figure 10-8, a series of velocity contour snapshots on a plane in the middle of the dryer, shows that the low velocity fluid bed air flows up and creates a stagnation point with the main jet approximately 1 m above the fluid bed. At this point, the flow is radial, but the flow switches from being split to both walls or all favouring one wall or the other because of the movement of the main jet (Figure 10-7). The position of the stagnation point moves closer to and further from the SFB with time.

Between the main jet and the walls of the chamber, slow recirculation zones are evident (Figure 10-7). The sizes of these zones swell and compress as the main jet changes in size and moves about the central axis. This movement of the jet also increases the velocities near the walls; they increase when the jet is on the opposite side and decrease when it moves close to the wall.

According to Guo et al. (2003), the driving force for the jet movement is the pressure difference between the recirculation zones across the jet which is consistent with the interaction between the jet and the recirculation zones observed here. However, these authors do not indicate what causes the fluctuations in pressure in the recirculation zones. The spray dyer system is inertially dominated because the velocities in the main inlet air jet are much greater than those in the recirculation zones. Therefore, it is more likely that it is small instabilities in the jet and also in this case, the destabilising influence of the SFB flow, that causes the movement of the main inlet air jet.

The air velocities in the outlet ducts are high. As expected, they are much higher in magnitude than the majority of velocities in the chamber, as these ducts are quite small in cross sectional area when compared with the cross sectional area of the chamber. The velocity profiles across the ducts are quite uniform which is likely to be because of the small size of the duct relative to the size of the spray dryer chamber, and also because of the short

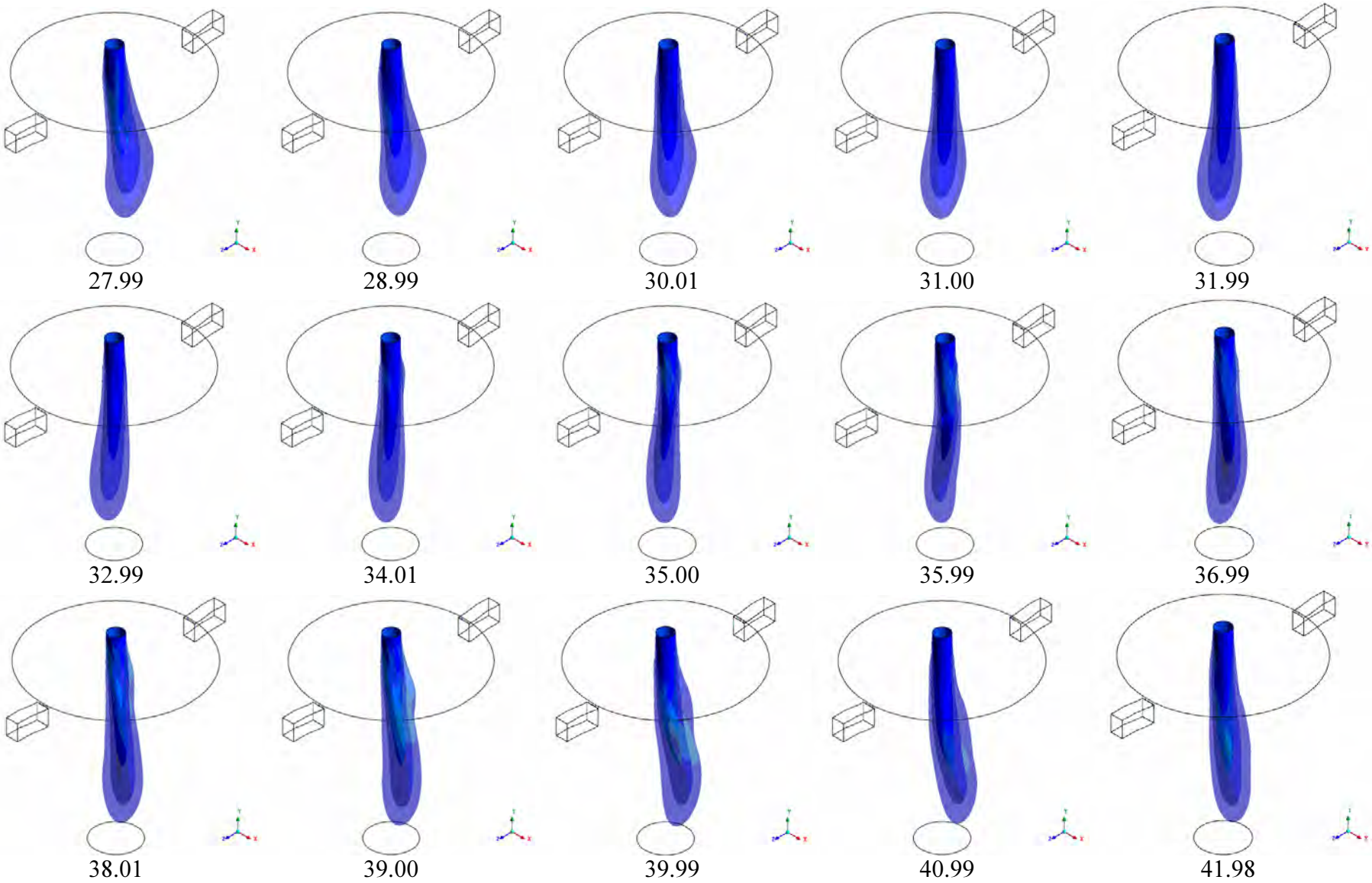

Figure 10-6: 3D axial velocity contour plot of main jet where the times shown are seconds from the beginning of the simulation

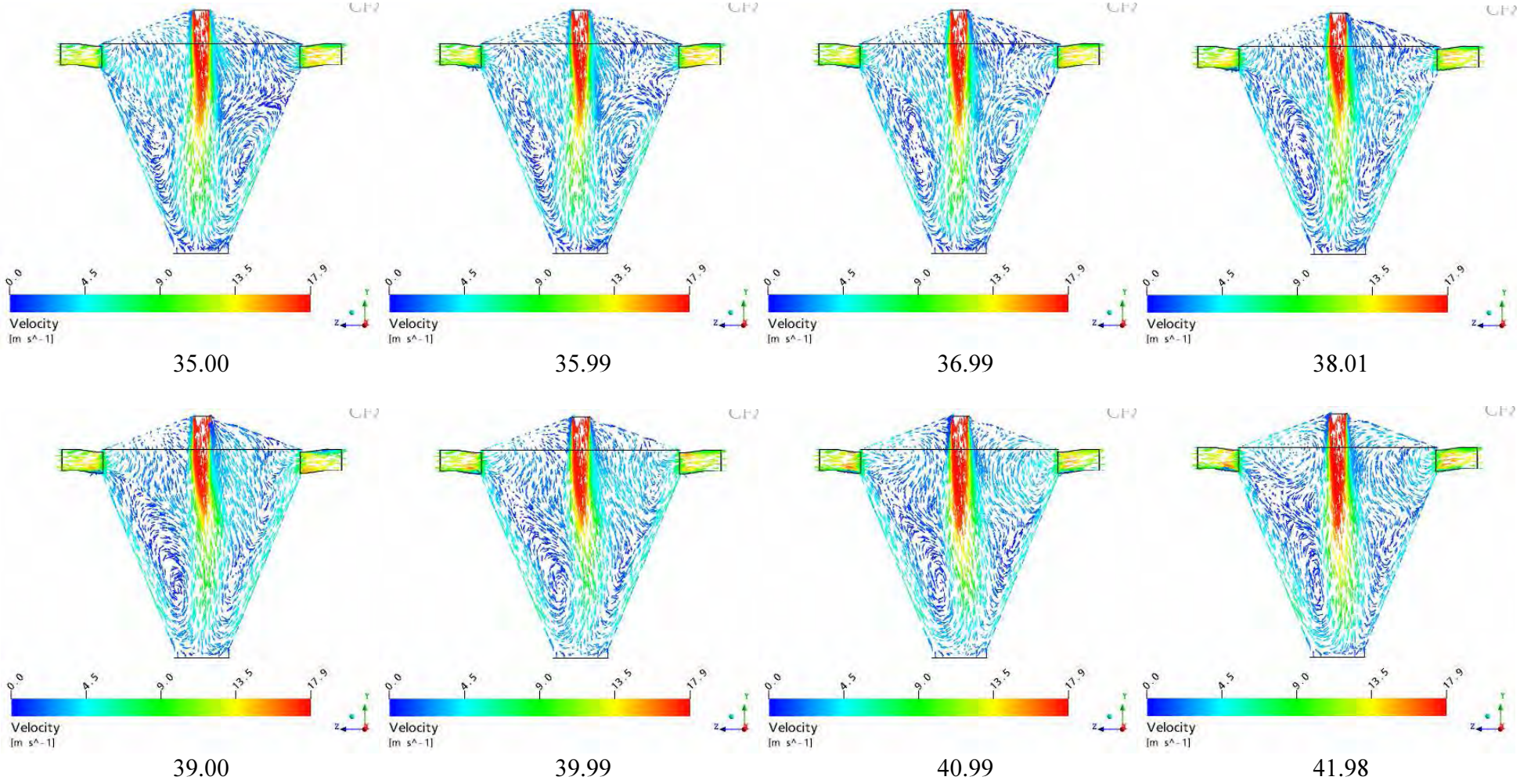

Figure 10-7: Velocity vector plots on a vertical plane running through the centre of the dryer where the times shown are seconds from the beginning of the simulation

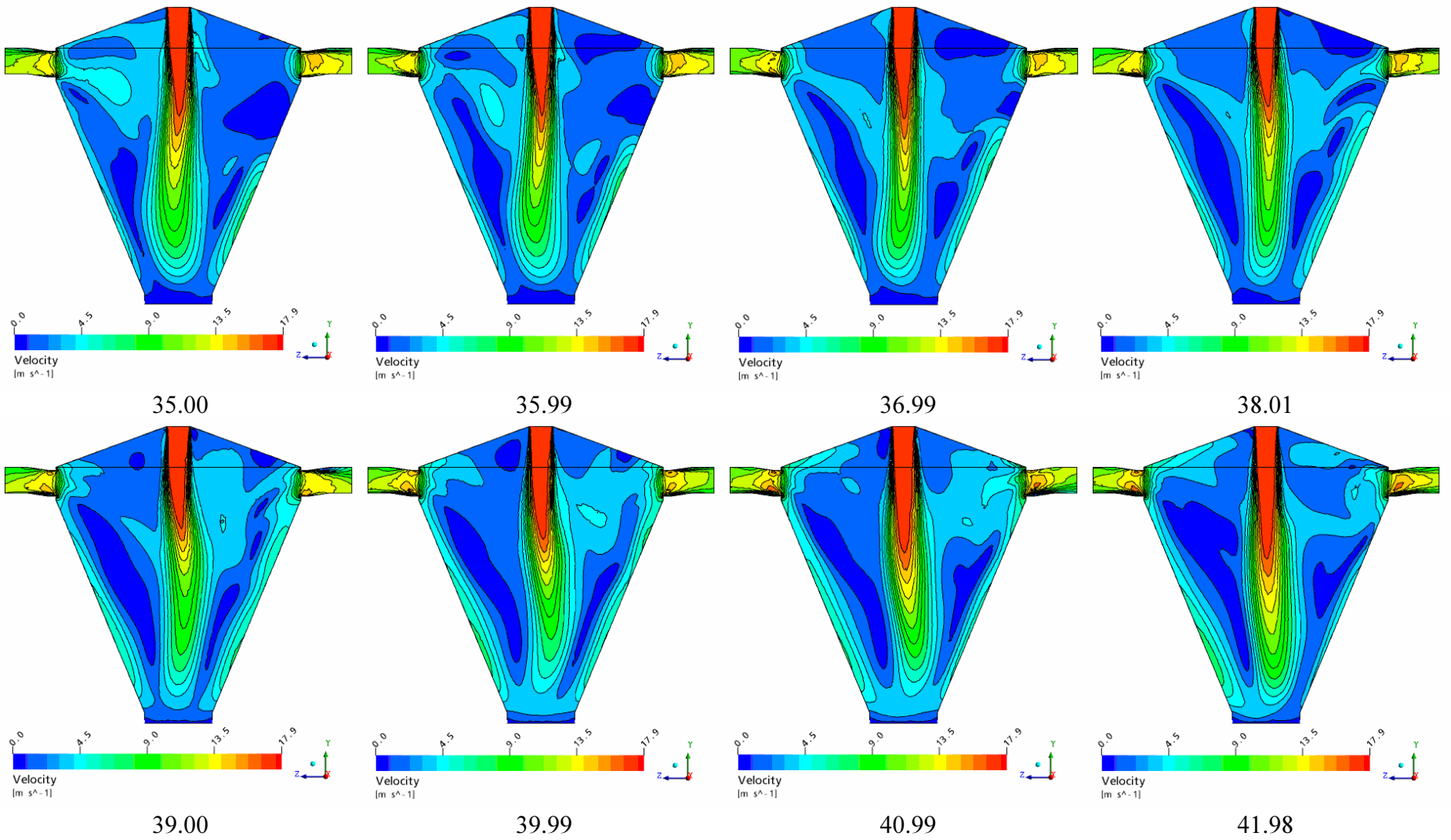

Figure 10-8: Velocity contour plot on a vertical plane running through the centre of the dryer where the times shown are seconds from the beginning of the simulation

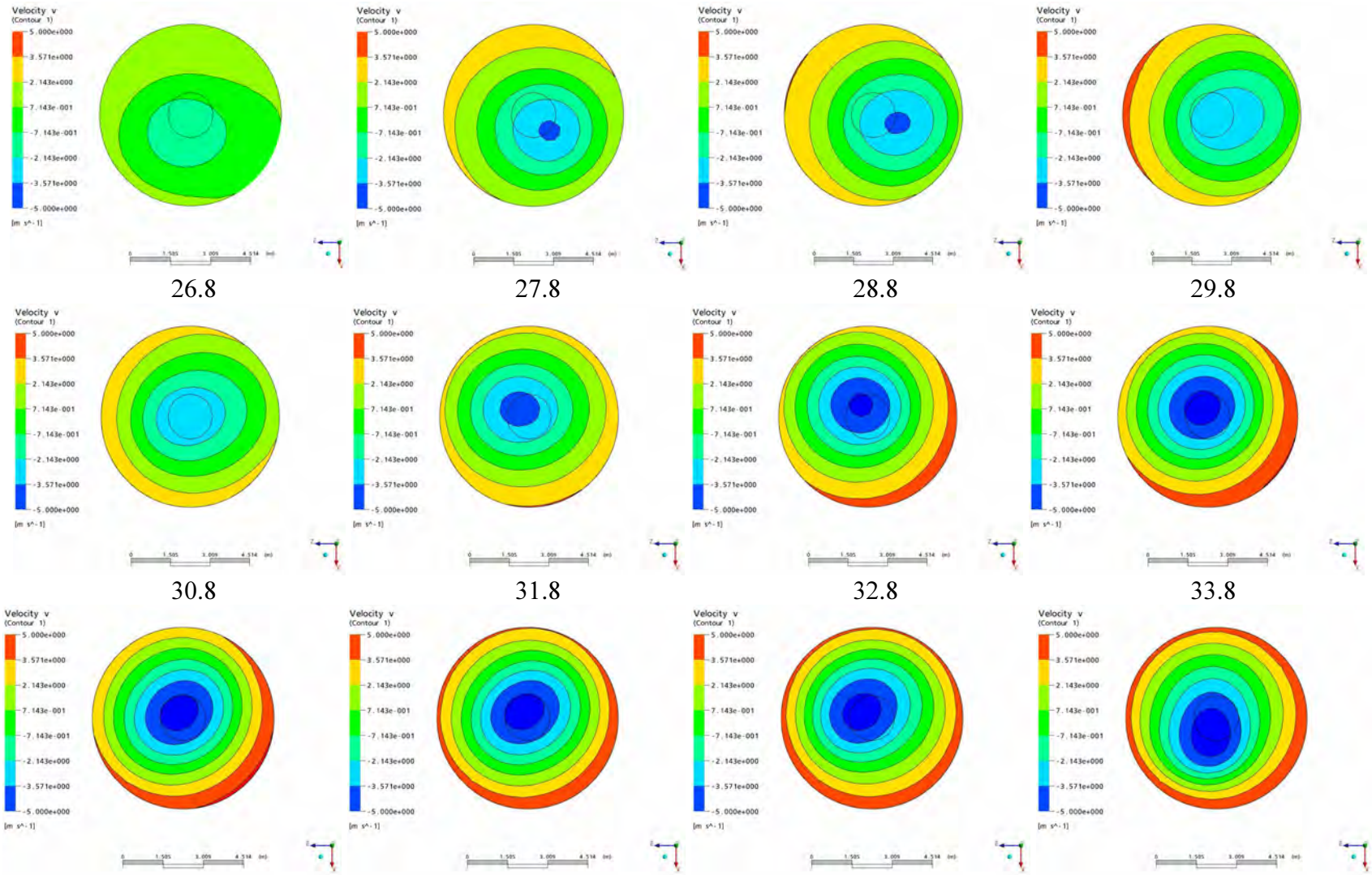

Figure 10-9: Axial velocity contour plot through a horizontal plane 2 m above the SFB where the times shown are seconds from the beginning of the simulation

length of the duct. The uniform velocity profiles across the duct are to be expected because the entry into the outlet duct is similar to any entry from a large plenum.

The flow in the ducts is seen to surge slightly with the movement of the main jet in the chamber. The surging flow in the outlet ducts could be the possible explanation of the slow pulsing sound industrial operators hear and term ‘breathing’.

The movement of the tip of the main jet is likely to be more pronounced in these simulations than the majority of those published in the literature. Figure 10-9, a series of axial velocity contour snapshots on a horizontal plane 2 m above the SFB, clearly demonstrates the movement of the jet around the central axis with time. This figure also highlights the movement of the stagnation point of the main jet and the SFB air flow: the magnitude of the velocities increases in the downward direction at the centre of the plane and in the upward direction at the edge of the plane, that is, up the walls of the dryer.

It is likely that there are two reasons for this increased movement of the main jet compared to previous publications. Firstly, because the outlet air ducts are located at the top of the chamber, the tip of the main jet is not fixed by the outlet boundary condition. This is the case for spray dryer geometries where the outlet air duct is located near the base of the chamber, and hence near the tip of the main jet. Secondly, these simulations were performed on a large industrial geometry, thus the length of the main jet and the space available for movement is proportionally larger than in most previous studies.

Excessive movement of the main jet can become a problem if the jet moves close to the chamber walls and leads to significant powder deposition on the wall. Figure 10-10 shows that 63 s from the beginning of the simulation, the main jet did move very close to the chamber walls. Thus, it is possible that droplets entrained in the main air jet will impact on the wall. It is mentioned in section 10.5 below that wall deposition is dependent on the stickiness of the particles, which in turn is a function of the particle moisture content and the local temperature and relative humidity. Therefore, particle tracking simulations that also model evaporation will be required to find out whether particles would adhere. However, if they do, the particles can brown and therefore this has a negative impact on product quality as well as becoming a fire and explosion risk. It should be noted that chamber fouling or heavy wall deposition has not been a problem in the CD2 chamber.

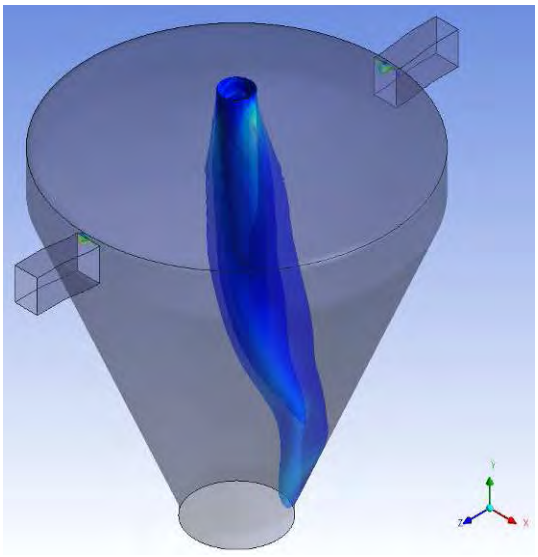

Figure 10-10: Axial velocity contour plot of main jet 63 s from beginning of simulation

Figure 10-11 shows the absolute velocity for a 100 s period at the point in the middle of the east outlet duct. The absolute velocities for this same period at the points above and below the point in the middle of the east outlet duct showed very similar patterns, and the fluctuating nature of this velocity highlights the transient nature of this flow field.

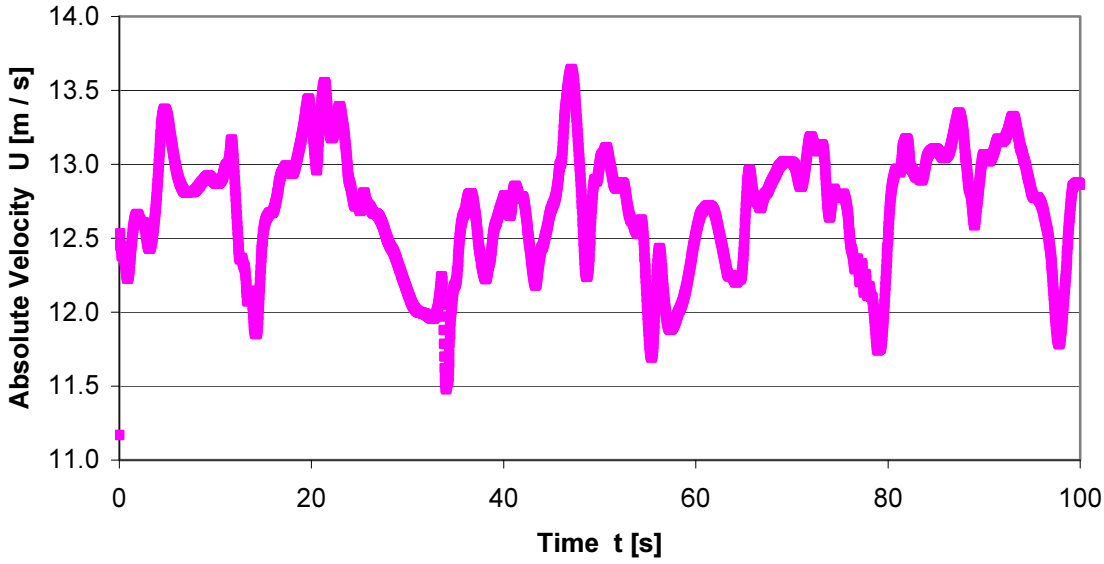

Figure 10-11: Absolute velocity for a 100 s simulated period from a point in the centre of the east outlet duct

The power spectrum (Equation 2-9) of the absolute velocity data series for the SFB point and the mid point of the east outlet duct were determined and are plotted in Figure 10-12. The spectra for both data series show that a number of frequencies are present and there is a peak

at approximately 0.04 Hz. However, because of the range of frequencies, it appears that there is no distinct frequency for the movement of the main jet.

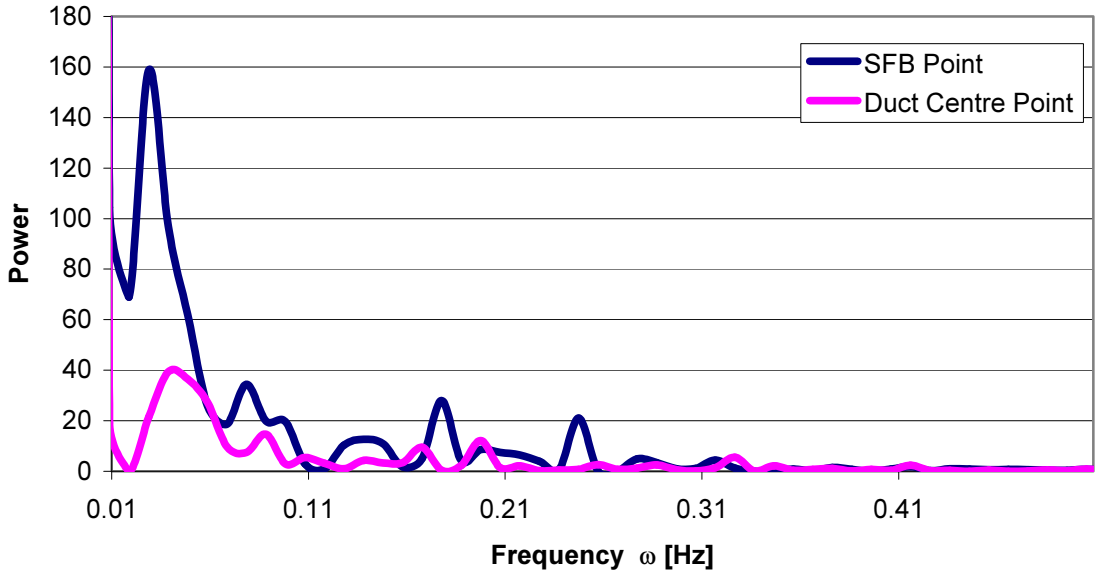

Figure 10-12: Power spectrum for absolute velocity data from a point 1 m above the static fluid bed and in the centre of the east outlet duct

From experimental observations on a pilot scale spray dryer, LeBarbier et al. (2001) found that the power associated with the movement of the main jet was contained within the low frequency (0 – 0.5 Hz) part of the spectrum. This is also true for these simulations as Figure 10-12 shows. For the case of no inlet swirl LeBarbier et al. (2001) found average frequencies of 0.065 and 0.155 Hz and stated that the absence of a single frequency peak was because the precession of the main jet was not always regular. These authors also simulated this case and found good agreement with the experimental observations as a frequency of 0.17 ± 0.03 Hz was obtained from the simulations. Langrish et al. (2004) found from experimental and simulations on a pilot scale spray dryer that in the case of no inlet swirl, there was no distinct frequency but there was a dominant frequency of about 0.05 Hz. From simulations of an industrial scale spray dryer, Fletcher et al. (2003) found that the main jet had a frequency of approximately 1 Hz, but stated the presence of higher frequencies were evident. Therefore, it is to be expected that no apparent frequency exists, which the simulations have shown. It also appears that the results presented here are in good agreement with previous studies (Langrish et al., 2004; LeBarbier et al., 2001), even though they were conducted at the pilot scale, because the peak in Figure 10-12 is at approximately 0.04 Hz.

In an inertially dominated system a geometrically similar behaviour at the laboratory and pilot scales would be expected. Therefore, the dimensionless Strouhal number St, given by Equation 10-14, should be similar.

$$St = \frac{2}{\sqrt{\pi}} E^2 \frac{\omega D}{U_o} \qquad (10\text{-}14)$$

The parameters in Equation 10-14 are: E, the expansion ratio (ratio of the chamber diameter D [m] to the inlet diameter d [m]); ω [Hz], the precession frequency; and U_0 [m / s], the inlet velocity. The Strouhal numbers from a number of pilot scale CFD studies published in the literature and the Strouhal number from this study on the CD2 dryer are given in Table 10-2 below. It can be seen that the industrial scale CD2 chamber diameter is two orders of magnitude higher and the inlet velocity one order of magnitude higher than those used in the pilot scale studies.

Table 20-2: Strouhal number calculation from a range of spray dryer studies with no inlet swirl

Parameter	Guo et al. (2003)	LeBarbier et al. (2001)		Langrish et al. (2004)	CD2
Source	Simulated	Experimental	Simulated	Simulated	Simulated
Expansion Ratio E	3.8	8.1	8.1	14.5	10.6
Frequency w [Hz]	0.22	0.16	0.17	0.05	0.04
Chamber Diameter D [m]	0.94	0.29	0.29	0.8	18
Inlet Velocity U_0 [m / s]	7.55	4.32	4.32	8.38	17.5
Strouhal Number St (Equation 10-14)	0.12	0.09	0.10	0.05	0.49

The very good agreement between the experimental and simulated work of LeBarbier et al. (2001) and the very good agreement obtained during this work (section 10.4.4) indicates that CFD simulations of spray dryers give good predictions at both scales. The results in Table 10-2 also indicate that the frequency of the main jet movement does not appear to scale well

using the Strouhal number because the industrial scale Strouhal number from this work (0.49) is much larger than the Strouhal numbers from the pilot scale studies (0.05 – 0.12). Therefore, it is likely that another mechanism is determining the movement of the main jet at the industrial scale and hence, an additional dimensionless number is required.

10.4.1 Influence of SFB Flow

The results discussed above were for a SFB inlet velocity of 0.77 m / s. Because none of the authors highlighted above modelled a dryer with a SFB flow, simulations were also run with SFB inlet velocities of 0 m / s and 0.38 m / s to investigate the influence of the fluid bed flow on the overall flow field.

Figure 10-13 shows a velocity contour plot on a plane running through the centre of the dryer for three different fluid bed flow rates: no flow (0 m / s); a medium flow (0.38 m / s); and a high flow (0.77 m / s). The three images were taken 72.7 s, 68.9 s and 64.1 s respectively from the beginning of each simulation. Figure 10-13 and the series of snapshots from each case showed that the three different SFB air velocities had very little effect on the flow field compared to the general unsteadiness. Hence, the flow fields observed were very similar to that described above. For all three cases the main inlet air jet expanded slightly and slowed as it proceeded into the chamber. The jet flapped and precessed around the central axis as expected. Between the jet and the chamber walls slow recirculation zones swelled and compressed along with the movement of the main jet. The movement of the jet influenced the direction of the SFB flow when it was present, switching the flow from left to right.

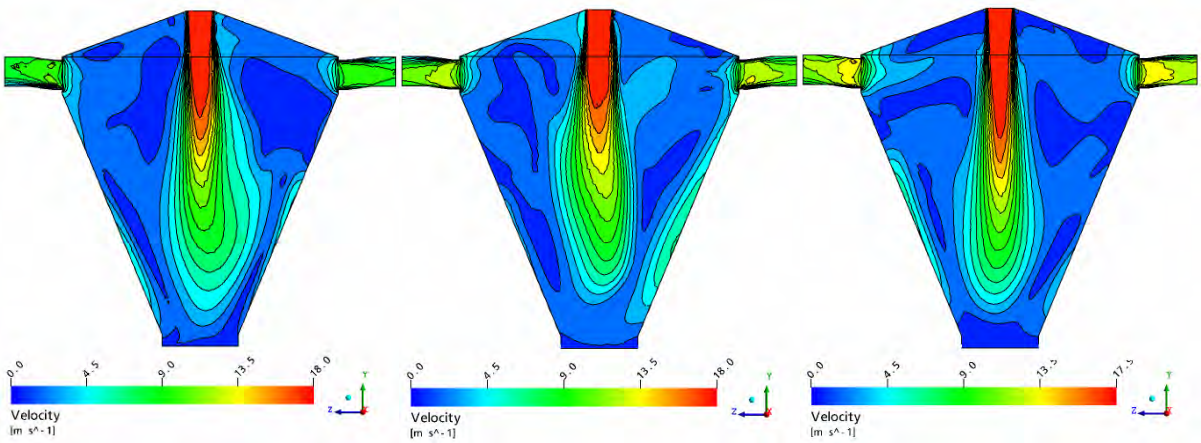

Figure 10-13: Velocity contour plot on a vertical plane running through the centre of the dryer for static fluid bed inlet air velocities of 0, 0.38 and 0.77 m / s

There were two subtle effects of the different fluid bed velocities on the flow field. Firstly, the velocities in the outlet air ducts increased with the fluid bed velocity (Figure 10-13). This is to be expected because, as the total mass flow of air entering the dryer increases, the total mass flow of air exiting the dryer increases because of continuity; a greater mass flow or air in the outlet duct at a constant air density translates to an increase in velocity. Secondly, as the SFB air velocity increased, the length of the main jet decreased slightly as the very base of the chamber was dominated by the low velocity SFB flow.

Figure 10-14 below shows the simulated absolute velocity at a point 1 m above the SFB for the three different SFB air flow cases over a 100 s period. Clearly, the flow is highly transient because the velocities are changing significantly with time for each data set. The average velocity at this point decreases as the SFB air velocity increases, which supports the point made above that the tip of the main inlet air jet moves closer to the SFB as the SFB air velocity decreases.

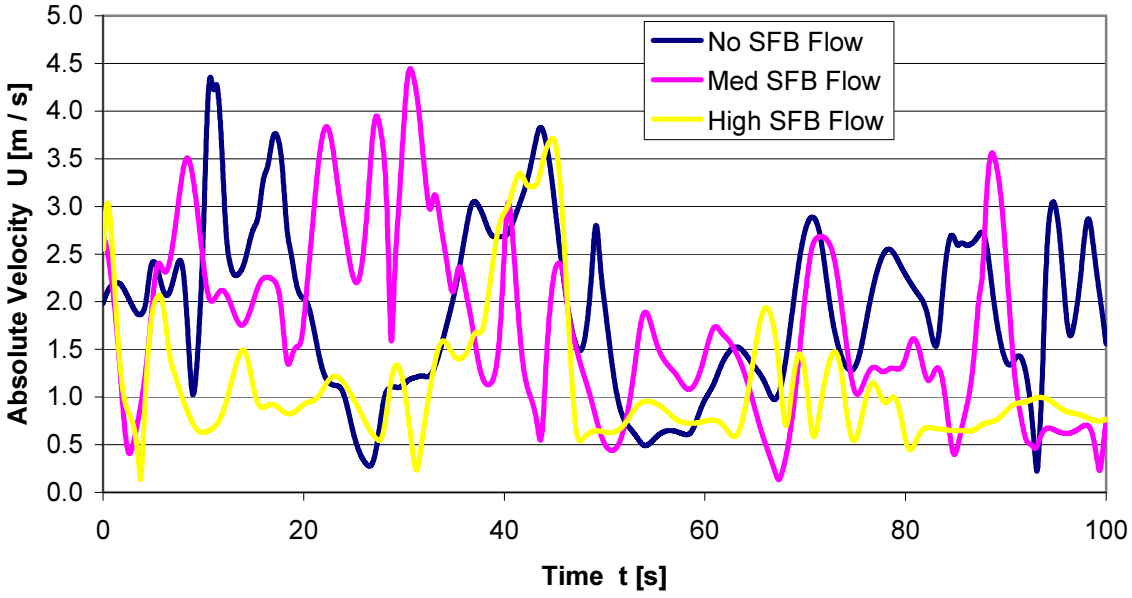

Figure 10-14: Absolute velocity for a 100 s simulated period from a point 1 m above the static fluid bed at three different static fluid bed flows

For the three SFB flows, the average, maximum and minimum periods, defined as the time between peak or trough absolute velocity values, are summarised in Table 10-3 below. The three average periods are 5.1 s, 4.6 s and 5.0 s respectively which implies that there is very little, if any, influence of the different SFB air inlet velocities on the movement of the main jet. Interestingly, the minimum period increases with the fluid bed velocity. Possibly, the

increased interaction between the SFB flow and the tip of the main jet with an increasing SFB velocity increases the period of the main jet.

Table 10-3: Simulated average, maximum and minimum periods for absolute peak and trough velocities at a point 1 m above the static fluid bed

SFB Velocity U_{SFB} [m / s]	Average Period [s]	Maximum Period [s]	Minimum Period [s]
0.00 (Low)	5.1	13.3	0.9
0.36 (Medium)	4.6	10.5	1.5
0.77 (High)	5.0	13.0	2.0

The power spectrum for each data series plotted in Figure 10-14 was determined and is shown in Figure 10-15 below. It appears from Figure 10-15 that the different SFB air velocities have little influence on the movement of the main jet because the three spectra are very similar; all the power is contained in the low frequency range (0 – 0.5 Hz), a number of frequencies are present, and a peak occurs at approximately 0.04 Hz. Thus, it seems that the SFB flow has only a local influence in the area above the fluid bed. This is not surprising as the main inlet air velocities are two orders of magnitude higher than the SFB air velocities and therefore more dominating. It should be noted that the difference in velocity between the main inlet air and SFB inlet air streams will be greater on production (heated air containing some water vapour) than the velocities used here, so it is likely that the SFB flow will have even less of an effect on the flow field. Therefore, the flow field in a spray dryer is dominated by the main inlet air flow and the recirculation zones that are generated between the main inlet air jet and the dryer walls.

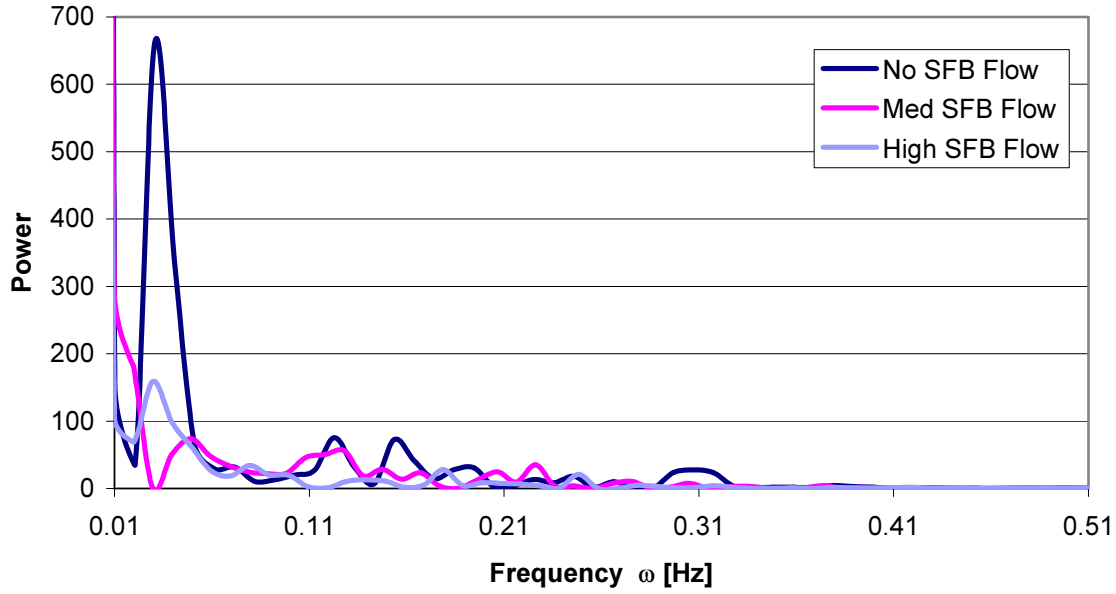

Figure 10-15: Power spectra for absolute velocity data from a point 1 m above the static fluid bed at three different static fluid bed flows

10.4.2 Influence of Outlet Boundary Condition

The outlet boundary conditions applied in most previous CFD studies has been an average static pressure. However, the outlet air stream experiences a pressure drop across the fines collection equipment before the constant pressure condition is reached at the discharge point to atmosphere. To investigate the influence of this on the flow field, the outlet boundary condition was changed to an opening, and a loss coefficient given by Equation 10-13 was specified: an outlet duct velocity of 12.8 m / s and baghouse differential pressure of 970 Pa were assumed giving a value of 11.6 for the loss coefficient. The SFB inlet air velocity was set at 0.77 m / s.

To maintain convergence, the adaptive timestep was limited to 0.003 s at the lower end and 0.1 s at the upper end. The initial timestep was set at 0.003 s. It was to be expected that the timestep would have to be reduced because changing the outlet boundary to an opening with a specified loss coefficient changes the boundary conditions from the most robust combination of an inlet velocity or mass flow and a static pressure at the outlet (ANSYS, 2005a).

As Figure 10-16 shows, the flow field obtained using an opening with a loss coefficient as the outlet boundary condition was similar to that described in section 10.4 above with a specified

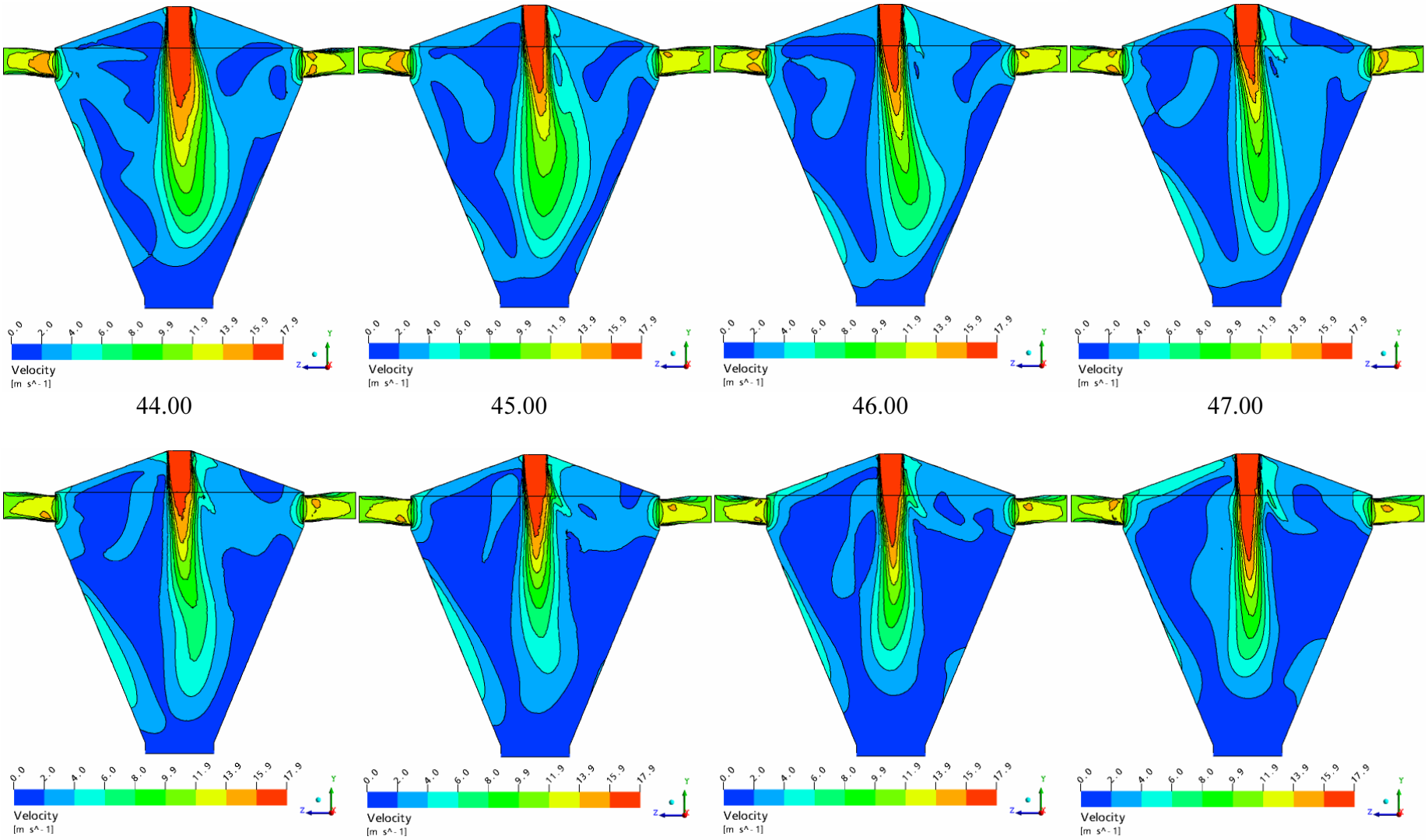

Figure 10-16: Outlet boundary condition reflecting the baghouse pressure drop with a SFB velocity of 0.77 m / s - Velocity contour plot on a vertical plane running through the centre of the dryer where the times shown are seconds from the beginning of the simulation

pressure at the outlet. The main inlet air jet retained a flat profile, the jet length changed with time and recirculation zones between this jet and the chamber walls swelled and compressed with time. The velocities in the slow recirculation zones between the main jet and the walls of the spray dryer were possibly slightly more uniform than those shown in Figure 10-8.

In the outlet air ducts, the velocities were more uniform with respect to time when the opening boundary condition was used. This is presumably because the opening condition dampens out the fluctuations in air flow observed in the outlet air ducts with the average static pressure boundary condition. Despite this difference, the average velocity in the centre of the east outlet duct was 12.7 m / s for both the opening and static pressure outlet boundary conditions. This was to be expected because the total inlet and therefore outlet mass flow was the same for both simulations.

It appeared that the length of the main inlet air jet was not as long as had been observed when the outlet boundary condition was specified as an average static pressure. Consequently, the SFB inlet air flow was not directed toward the chamber walls until several metres above the SFB where the stagnation point with the tip of the main jet occurred. Also, at times, the width of the base of this jet appeared to be larger than had been seen previously.

The absolute velocity over a 100 s period at a point 1 m above the SFB for the opening outlet boundary condition is shown in Figure 10-17. This figure is similar to those for the different SFB velocities with a static pressure outlet boundary condition (Figure 10-14). The average period (time between peak or trough absolute velocity values) from Figure 10-17 is 5.0 s. This average is identical to that for the same SFB velocity (0.77 m / s) with the static pressure boundary condition shown in Table 10-3. The ranges for these average periods are also very similar (1.4 s – 13.5 s c.f. 2.0 s – 13.0 s).

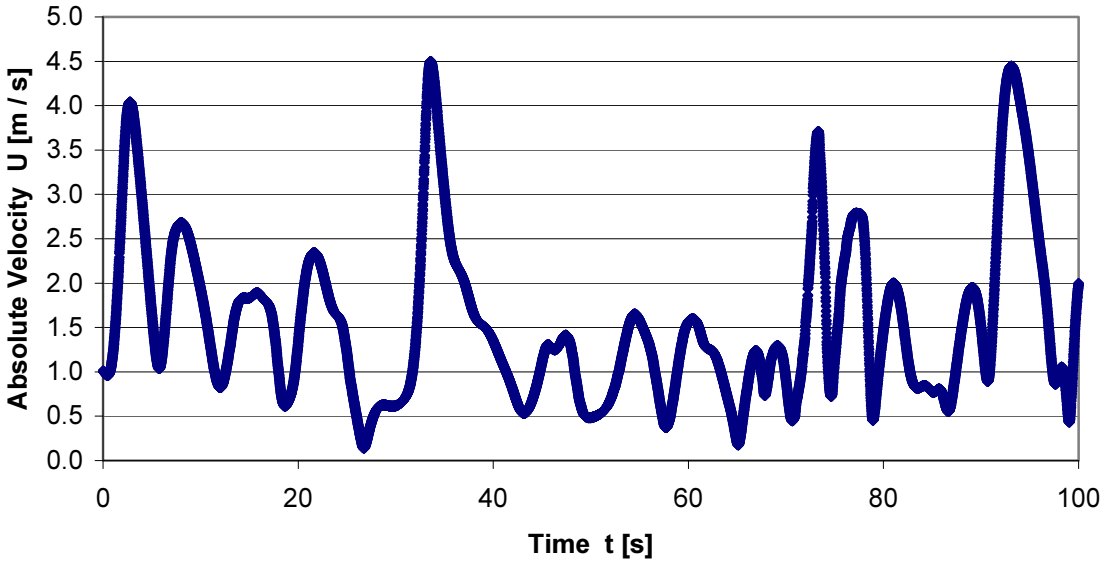

Figure 10-17: Absolute velocity for a 100 s simulated period from a point 1 m above the static fluid bed for an opening with specified loss coefficient outlet boundary condition and SFB velocity of 0.77 m / s

Consequently, the power spectrum from 100 s of absolute velocity data at a point 1 m above the SFB for the opening outlet boundary condition (Figure 10-18) is similar to those of the different SFB flow cases; all the power is contained in the low frequency range (0 – 0.5 Ha) and a large range of frequencies are present. However, although there is a dominant peak at around 0.05 Hz, the magnitude of the other peaks is much greater than those observed for the different SFB flow cases where the outlet boundary condition was specified as a static pressure. This suggests that the main inlet air jet fluctuates more because of the different outlet boundary condition.

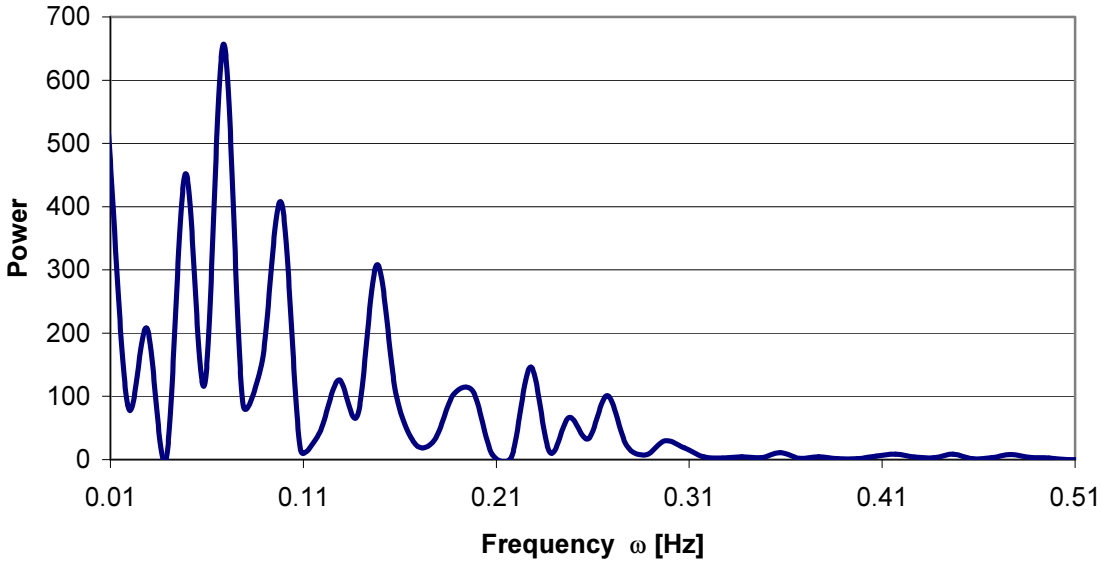

Figure 10-18: Power spectra for absolute velocity data from a point 1 m above the static fluid bed for an opening with specified loss coefficient outlet boundary condition and SFB velocity of 0.77 m / s

As mentioned above, it appeared from Figure 10-16 that use of the opening boundary condition reduced the length of the main inlet air jet. To quantitatively confirm this finding, the average absolute velocity at each time step at the point on the chamber axis 1 m above the SFB for the two different boundary conditions were compared. As Figure 10-19 shows, there is a significant difference of approximately 0.4 m / s between the two averages after 100 s. The gradients of both lines at this point also suggest that this difference will increase if the simulations are run for longer. Therefore, use of an opening boundary condition with a specified loss coefficient has two distinctly different features when compared to the simulations with a static pressure boundary condition: the length of the main inlet air jet is shorter and this jet has a wider spread of frequencies.

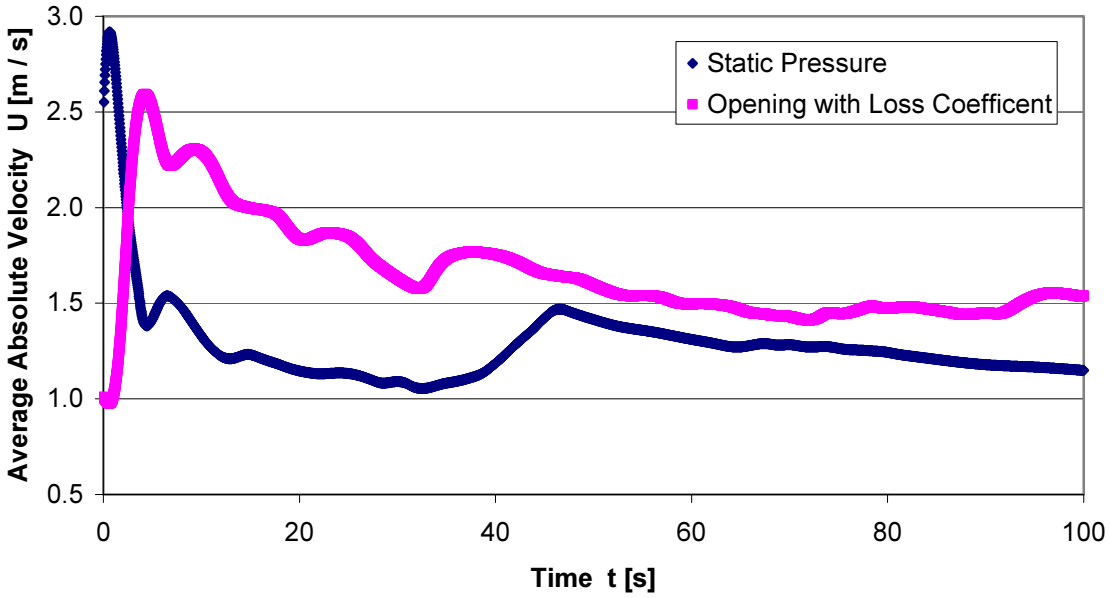

Figure 10-19: Comparison of average absolute velocity during a 100 s simulated period from a point 1 m above the SFB for the static pressure and opening with loss coefficient boundary conditions with an SFB velocity of 0.77 m / s

Although it has not been investigated here, it is highly likely that the main inlet velocity profile will have a more dominant influence on the flow patterns within the dryer. A simplifying assumption was made here that the main inlet air stream had no swirl at the inlet. However, this air stream has flowed through an air radiator, turned a 90^{o} bend, moved into a larger diameter pipe via an expansion, passed through a fine mesh screen, entered a symmetrical plenum chamber and then flowed down through the air disperser into the drying chamber. Therefore, it is likely that each of these stages will influence the flow profile on entry to the chamber and hence, the flow field within the spray dryer.

It is interesting to note that the fine mesh screen was installed in the main inlet air duct to collect and thus, prevent any metal shavings entering the drying chamber. If the pressure drop across this screen is greater than the kinetic head of the air stream, then any non uniformity in the air stream should be cancelled out. Therefore, installing the mesh screen may have had the added benefit of stabilising the main inlet jet within the drying chamber.

10.4.3 Air Flow Patterns Mesh Independence

To check that the solutions obtained were independent of the mesh size, the simulations were repeated using the three meshes which had the number of nodes and elements shown in Table 10-1. It is difficult to compare results from transient simulations because the value of a variable at a fixed location will vary with time because of the transient nature of the flow field. Because of this difficulty, steady state simulations were run. The boundary conditions used were the high SFB inlet velocity and static pressure outlet boundary conditions mentioned in section 10.3.3 above, but using a timestep of 0.01 s and a root mean square convergence criterion of 1×10^{-3}. The same initial conditions were specified for each run. Absolute velocities along the axis of the dryer and through a line running from wall to wall of the chamber along a central plane 8 m above the base of the dryer (Figure 10-20) were compared.

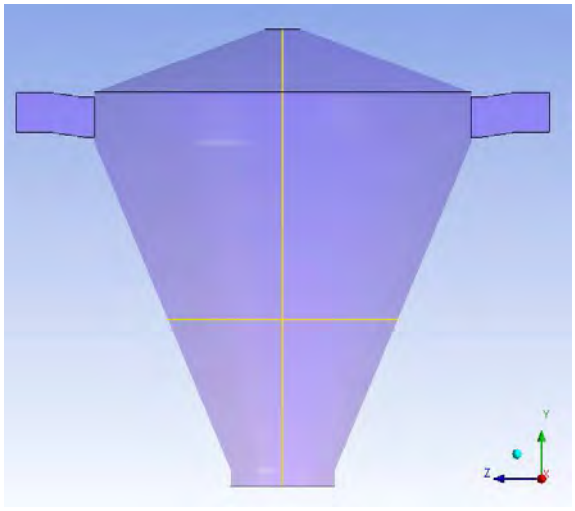

Figure 10-20: Location of the two lines used to compare steady state velocity magnitude data from the coarse, medium and fine mesh

Figure 10-21 shows that a very similar velocity profile along the dryer axis was obtained from all three meshes, and that the velocity magnitudes from the medium and fine mesh are very similar. The average absolute discrepancy between the medium and fine mesh as a percentage of the fine mesh velocity magnitude was only 0.8 % and ranged from 0.1 % to 5.3%.

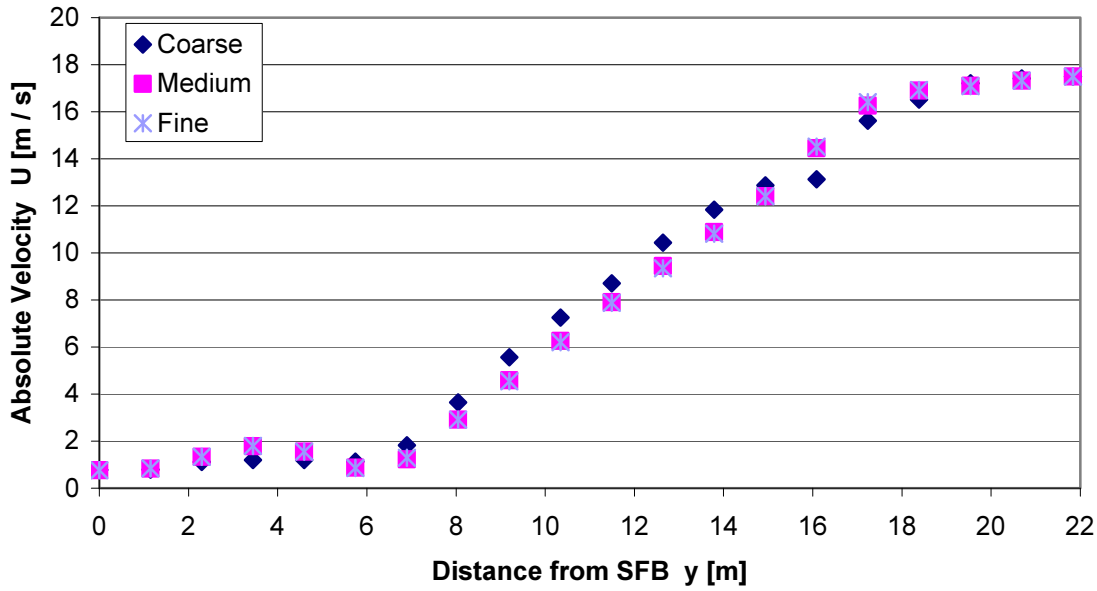

Figure 10-21: Comparison of absolute velocities along chamber axis using the coarse, medium and fine mesh

Figure 10-22 shows that the velocity profile and magnitudes from the line running across the chamber were again very similar for the medium and fine mesh. It is to be expected that the velocity profile across the chamber is not symmetrical because the profile is a steady state solution to a transient flow field. The results from the coarse mesh gave a velocity profile and velocity magnitudes quite different to those from the medium and fine mesh. The average absolute discrepancy between the medium and fine mesh as a percentage of the fine mesh velocity magnitude of 2.5 % was higher than that from the centreline velocity magnitudes, but had a similar range from 0.1 % to 5.8 %.

These steady state mesh independence results suggest that, because of the small discrepancy between the results from the medium and fine mesh, which has approximately 2 x 10^6 more elements, the medium mesh results are mesh independent. However, because of the reduced convergence criteria in these steady state simulations, transient results from each of the mesh also needed to be compared before it could be concluded that the medium mesh results were independent of the mesh.

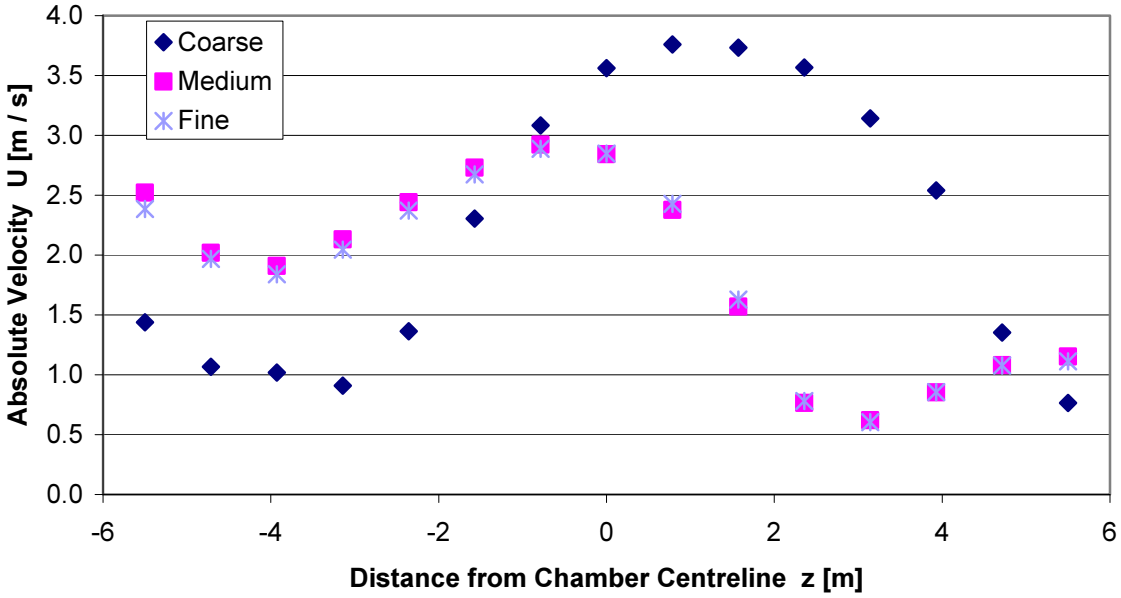

Figure 10-22: Comparison of absolute velocities from a line on the central plane of the chamber running between the walls and 8 m above the SFB for the coarse, medium and fine mesh

The transient simulations with a high SFB inlet velocity and average pressure outlet boundary condition described in section 10.3.3 above were run on the coarse, medium and fine mesh to support the steady state mesh independence results above. Because of the difficulty in quantitatively comparing results from transient simulations, the transient mesh independence was determined qualitatively by comparing the flow features produced from each mesh. Mesh independence was also determined quantitatively by comparing the average absolute velocity at each time step at the point on the chamber axis 1 m above the SFB, and comparing the absolute velocity power spectrum at this point and the point in the centre of the east outlet duct shown in Figure 10-5.

Qualitatively, all three mesh produced flow fields as described in section 10.4 above: the main inlet air jet retained a flat profile, the jet length changed with time and there was no distinct frequency of the main jet; recirculation zones between this jet and the chamber walls swelled and compressed with time; the velocities in the outlet ducts were higher than the velocities of the majority of the gas in the chamber; and the low velocity fluid bed flow direction changed with the movement of the main jet.

Quantitatively, the average absolute velocity during the simulation at the point 1m above the SFB on the central axis shown in Figure 10-23, converged to very similar values. After 80 s of simulated time, the average value from each of the coarse, medium and fine mesh were 1.18 m / s, 1.24 m / s and 1.30 m / s respectively. This gives a discrepancy between the fine and medium mesh and the coarse and medium mesh as a percentage of the medium mesh of only 4.8 %. The gradient at the 80 s point for each mesh indicates that if each simulation were run for longer, then the results from each mesh will converge even closer and hence, the discrepancy reduce.

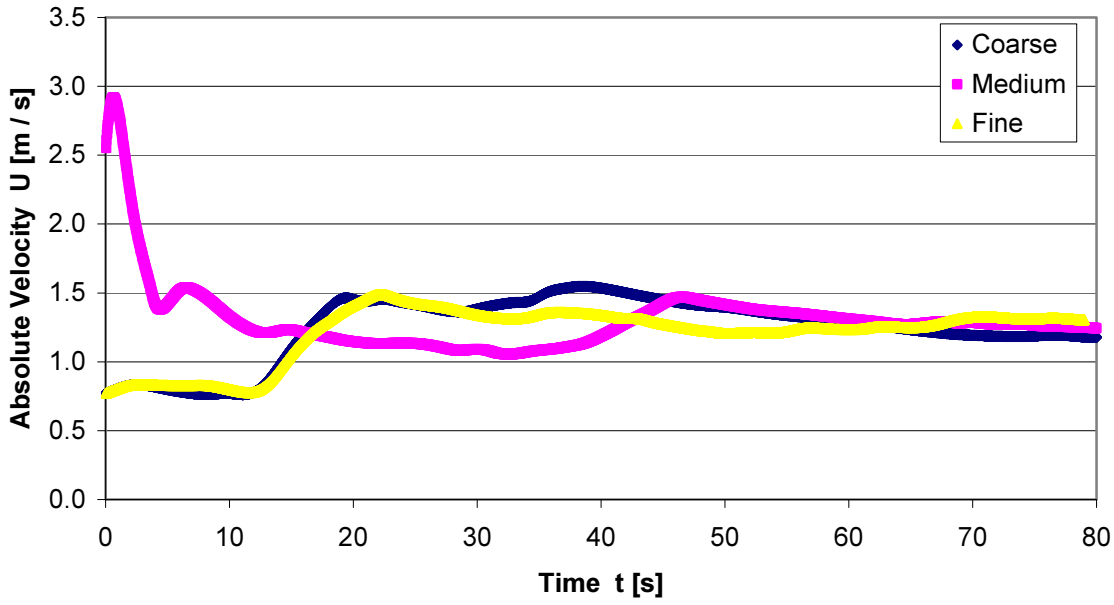

Figure 10-23: Comparison of average absolute velocity during the simulation at a point 1m above the SFB on the central axis for the coarse, medium and fine mesh

The power spectra from each mesh at both monitoring points were similar. Figure 10-24, the power spectra for the absolute velocity at a point 1 m above the SFB, shows that the results from each mesh indicated that all the power is contained in the low frequency range (0 – 0.5 Hz), a number of frequencies are present, and a peak occurs at approximately 0.05 Hz. The average periods for the absolute velocity at the point 1 m above the SFB on the central axis were 6.0 s, 5.0 s and 5.2 s for the coarse, medium and fine mesh respectively. Clearly there is good agreement in this period, especially between the medium and fine mesh where the difference is only 4 % of the medium mesh value. Therefore, based on both the steady state and transient results from the three different meshes, the medium mesh results were

determined to be mesh independent. Thus the medium sized mesh with 326,000 nodes was used for the results presented here.

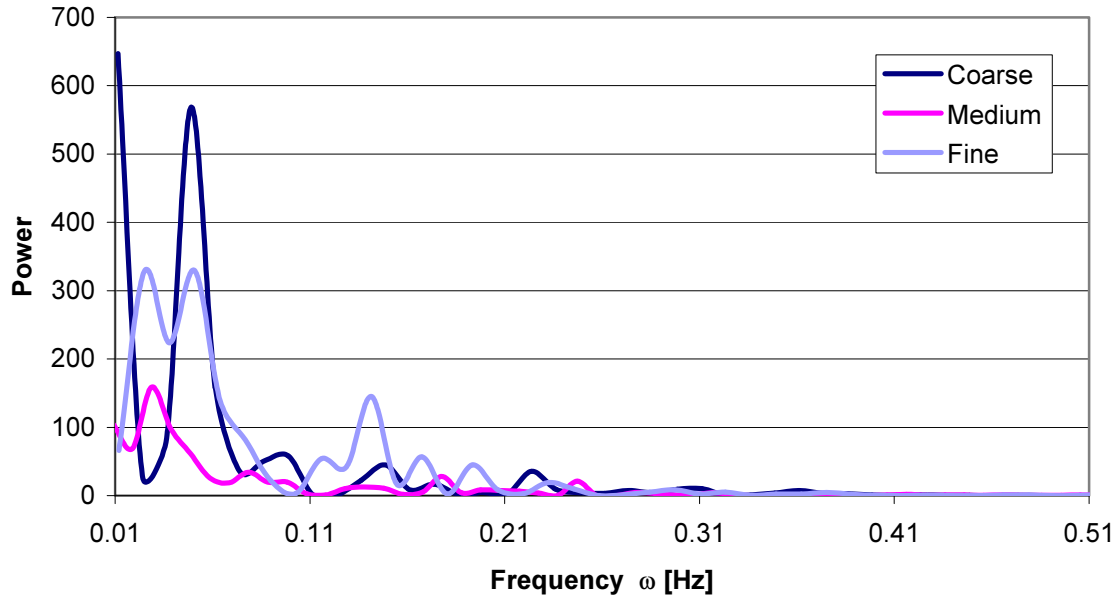

Figure 10-24: Comparison of power spectra from absolute velocities from a point 1m above the static fluid bed for coarse, medium and fine mesh

10.4.4 Air Flow Patterns Validation

The transient air flow results were validated by measuring the period of oscillation of the main air jet using the telltale pole shown Figure 10-25. The 3 m stainless steel pole had fabric tufts placed at 200 mm intervals up the pole, was mounted to a stainless steel base plate and supported by four guy wires anchored to the base plate.

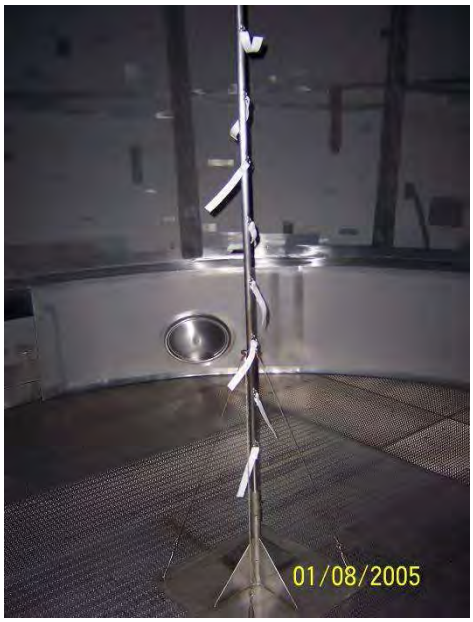

Figure 10-25: Telltale pole located at centre of dryer static fluid bed for observing the movement of the main air jet

The spray dryer was run on ambient air with a main inlet air flow giving an inlet velocity of 18.4 m / s and three fluid bed flows that gave measured velocities of 0, 0.38 and 0.77 m / s. The main inlet velocity was slightly higher than that simulated (17.5 m / s). The telltale rig was placed in the centre of the fluid bed and 180 s of the motion of the jet at each SFB flow was recorded with a video camera (Sony Mini DV Digital Handycam, Sony Corporation, Japan).

The telltale tuft observations showed a reasonably consistent behaviour: the tufts would flap in one direction; the flapping would die away as the tails pointed toward the fluid bed at the bottom of the chamber; and then flap again but in the opposite direction. The period of oscillation was estimated by determining the time between directional changes of the tails. The average, maximum and minimum periods at the three different fluid bed flows is shown in Table 10-4 below.

The results in Table 10-4 indicate that there is no distinct period of the main jet because a range of periods is present. Also, because the average, maximum and minimum telltale periods at each SFB velocity are approximately the same, the telltale results suggest that the SFB flow has very little, if any influence on the period of the main jet. Both of these points agree with the simulation observations.

Table 10-4: Average, maximum and minimum telltale periods from telltale validation experiment

SFB Velocity U_{SFB} [m / s]	Average Telltale Period [s]	Maximum Telltale Period [s]	Minimum Telltale Period [s]
0.00 (Low)	4.7 (5.1)	10.9 (13.3)	1.6 (0.9)
0.36 (Medium)	5.0 (4.6)	10.2 (10.5)	0.5 (1.5)
0.77 (High)	4.4 (5.0)	10.0 (13.0)	1.6 (2.0)

N.B. Values in brackets are simulated absolute velocity periods at a point 1 m above the static fluid bed from Table 10-3

The telltale pole observations recorded the movement of the main jet in an area of the dryer that included the point 1 m above the SFB where the absolute velocities from the simulations were obtained. It can be seen from a comparison of the simulated results (Table 10-3) with the experimental results (Table 10-4) for the three different SFB inlet air velocities, that the average, maximum and minimum absolute velocity and telltale periods are very similar. The average periods show very good agreement because the difference between the simulated and experimental values as a percentage of the experimental values are 8.5 %, 8.0 % and 13.6 % respectively for each of the three SFB inlet air velocities. The maximum and minimum values do not show such good agreement. This should be expected because these values are single points in the data series, and are extreme values in a transient flow field.

The simulated flow field described here for the CD2 dryer shows the major features expected for a spray dryer based on the simulations of several previous authors (Fletcher et al., 2003; Guo et al., 2003; Huang et al., 2006; Langrish et al., 2004; LeBarbier et al., 2001; Straatsma et al., 1999). This point supports the validation findings above; therefore it can be concluded that these simulations are an accurate representation of the air flow patterns within an industrial spray dryer.

10.5Steady State Particle Tracking Simulation Details

The steady state particle tracking simulations were mainly to ascertain the amount of powder that exits the chamber through the outlet air ducts. Therefore, the evaporation of moisture

from liquid droplets was not simulated and the particles were injected into the chamber as solid dry particles.

Several authors (Harvie et al., 2002; Huang et al., 2003a; Huang et al., 2006; Straatsma et al., 1999; Ullum, 2006) have shown that outside of the atomisation area of the chamber, the air temperature is relatively constant. Hence, like the air only cases, these simulations were isothermal. The air temperature within the chamber was assumed to be equal to the dryer outlet air temperature for each product.

To account for the momentum of the moisture evaporated from the liquid droplets that would be exchanged with the gas stream under normal operation, the momentum of this moisture was added to the momentum of the main inlet air stream. Therefore, the velocity of the main inlet air stream represented the momentum flux of the drying air stream plus the momentum flux of moisture evaporated from the liquid droplets. The expected velocities of the liquid droplets in the spray nozzles for each product were obtained from Fonterra. It was assumed that the velocity of the liquid within the nozzle is equal to the velocity of the liquid film jet sprayed from the nozzle, hence the nozzle velocities obtained from Fonterra were used to specify the initial particle velocities.

Like the air-only simulations, the Shear Stress Transport model was used to account for the effects of turbulence. Second order discretization schemes were used in both time and space and the Reynolds Averaged Navier-Stokes equations were solved.

The drag force on the particles was represented using the Schiller Naumann model. This model was applied in this case because of the low solids loading relative to the gas flow (approximately 5 % and less). The Schiller Naumann model assumes that the particles are spherical, hence the CFX 10.0 default particle shape factors were used. Despite the large difference in density between the air and the particles, buoyancy forces were applied because of the importance of settling of the particles. The reference density was set as that of air. Turbulent dispersion forces were also applied because the size of some of the milk powder particles was less than 100 μm. Finally, because the particle densities were two to three orders of magnitude greater than the air density, the virtual mass force and pressure gradient forces were assumed to be negligible.

The particle size distribution used to simulate the powder injected at the top of the dryer was assumed to be equal to the sifter powder particle size distributions for each product obtained from the plant (Chapter Four). The sifter powder is the combination of powder that has exited the chamber through the SFB and the powder that has exited the chamber through the baghouses. Consequently, it was assumed that there was no change in particle size caused by particle-particle collisions or particle-wall collisions, hence no particle break up was modelled.

The particle size distributions for the four products were represented by a Rossin Rammler distribution (Equation 10-15).

$$R = \exp\left[-\left(\frac{d_p}{d_e}\right)^{\gamma}\right] \qquad (10\text{-}15)$$

The terms in Equation 10-15 are: R, the mass fraction of powder above a given particle diameter d_p [μm]; d_e [μm], the measure of fineness (the particle diameter where R equals 0.368); and γ, the spread parameter (a measure of size dispersion). The values of the measure of fineness and the spread parameter for each powder are shown in Table 10-5. The particle densities specified for each product are also given in Table 10-5. The values for SMP, WMP and MPC are the same as those used in Chapter Four and the value for Fat Boy was assumed to be equal to that of WMP.

Table 10-5: Rossin Rammler distribution parameters and particle densities for different milk powders simulated

Powder	Measure of Fineness d_e [μm]	Spread Parameter γ	Particle Density ρ_p [kg / m^3]
SMP	208	1.44	1350
WMP	196	1.91	1250
MPC	162	1.27	900
Fat Boy	223	1.63	1250

Despite previous spray dryer CFD studies showing the need for two-way coupling between the gas and droplets, one way coupling was used for these simulations for three reasons. Firstly, because no evaporation was being modelled, there was no mass or internal energy to

exchange between the phases. The momentum from the mass of water vapour exchanged between the phases was accounted for by specifying an inlet air velocity equivalent to the momentum of the air and water vapour. Secondly, the dry solids flow for the four products was approximately 5 % or less of the air flow and thus, was at a mass loading ratio where one-way coupling is believed to give an adequate prediction. Thirdly, the most significant result from the simulations was the location where the particles exited the drying chamber. Because the SFB and the outlet air ducts are some distance away from the atomisation zone, where the majority of the mass and momentum exchange would occur, one-way coupling was sufficient to predict where the particles exited the dryer chamber.

10.5.1.1 Boundary Conditions

The boundary conditions specified for the simulation of each product is shown in Table 10-6 below. Also included is the average dryer outlet air temperature, that is, the isothermal temperature used for each product.

Table 10-6: Summary of boundary conditions used for the particle tracking simulations of each product

Parameter	SMP	WMP	MPC	Fat Boy
Domain Temperature T [^{o}C]	78	78	62	58
Total Main Inlet Air Velocity U_{in} [m / s]	39.9	38.7	36.9	40.6
Total Inlet Particle Velocity U_p [m / s]	145	145	152	145
Mass Flow of Powder m_p [kg / s]	3.39	3.31	1.11	3.08
Total SFB Velocity U_{SFB} [m / s]	0.92	0.89	0.91	0.64

Both the air and particle velocities were specified as normal speeds. To model the effect of the CD2 having 15 pressure nozzles spaced throughout the main inlet, the particles were injected uniformly at locations equally spaced around the main inlet. Section 10.6.4 below

shows that for the SMP case, it appeared that the fines *fraction* exiting the two outlets became independent of the number of injected particles at around 2750 particles. The results from the three other powder types were assumed to also be independent of the number of injected particles at around 2750, hence, for all four powder types 2750 particles were injected.

A turbulent intensity of 3.7 % and length scale based on the diameter of the inlet were specified at the two inlets. The outlet boundary conditions were specified as average static pressures of – 60 Pa.

Close observations on small accessible areas within the CD2 dryer and a more general view of the remainder of the chamber were made on completion of a production run. From these observations it was estimated that the amount of powder remaining on the chamber walls compared with the amount of powder that had flowed through the chamber, was less than 1 %. Also, Hennings et al. (2001) states that cold dry milk particles tend to rebound when they hit the chamber walls compared with hot, moist particles that tend to stick. Therefore, as these simulations used dry particles, and because the interest in these simulations lay in where the particles exited the chamber, the coefficient of restitution in both the perpendicular and parallel directions was set to 1.0. Again the walls were treated with the default CFX 10.0 conditions to create no slip, smooth, adiabatic walls. Automatic wall functions were used to model the near wall flow.

10.5.1.2 Simulation Procedure

As mentioned above, these 3D particle tracking simulations were carried out at steady state despite the flow field being strongly periodic, as the air only simulations above showed. Consequently, the root mean square residual target was decreased to 1×10^{-3} so convergence could be obtained at steady state. A physical timescale of 0.01 s was used and a maximum number of iterations of 250 specified. However, convergence was reached usually after approximately 150 iterations.

Initially, the flow field was solved without the presence of particles for each product's operating conditions. These values were then used as the initial values for the particle tracking simulations. Particles were tracked until they exited the domain, had been tracked for 200 s or had been tracked for 250 m. This meant that the particles exited the domain

through either the outlet air ducts or, if they reached the SFB, assumed to exit through the SFB overflow weirs.

10.6 Steady State Particle Tracking Results

10.6.1 Particle Trajectories

Figure 10-26 shows 40 of the 2750 particle tracks for each of the four powders produced in CD2. The different colours represent different particle diameters. The diagrams show the particles that enter the chamber from the main air inlet and exit the chamber at either the SFB or the outlet air ducts.

For all four powders, the particles follow the gas streamlines down the centre of the chamber faithfully. Just above the SFB, the larger particle sizes flow perpendicularly into the fluid bed. Those particles at the edge of the main inlet air jet are influenced by the fluid bed flow and have an angled approach to the fluid bed. The smaller size fraction particles follow the gas streamlines that take the particles away from the SFB into the recirculation zones between the main inlet air jet and the chamber walls. The majority of these particles flow to the outlet air ducts and exit the chamber. Some of the particles from the SFB flow back to the atomisation area at the top of the dryer and follow the main inlet air gas stream back down to the SFB.

In the CD2 type of spray dryer, it is expected that powder returns to the atomisation area at the top of the chamber, which these simulations show. This mechanism is known as spontaneous secondary agglomeration (Westergaard, 2003). The fraction of powder returning to the atomisation zone is important for predicting agglomeration rates and is therefore of importance to plant designers.

There is a difference in the size of particles that flow straight into the SFB and those that exit the chamber as fines. The particle size at each outlet also depends on powder type because of the differences in particle size and density among the four different powders. As Table 10-7 shows, the SFB particle size for SMP, WMP and Fat Boy is approximately 50 μm to 700 μm. The momentum of these particles is sufficient to overcome the momentum of the SFB air flow and therefore these particles reach the fluid bed. MPC has a much larger range in the

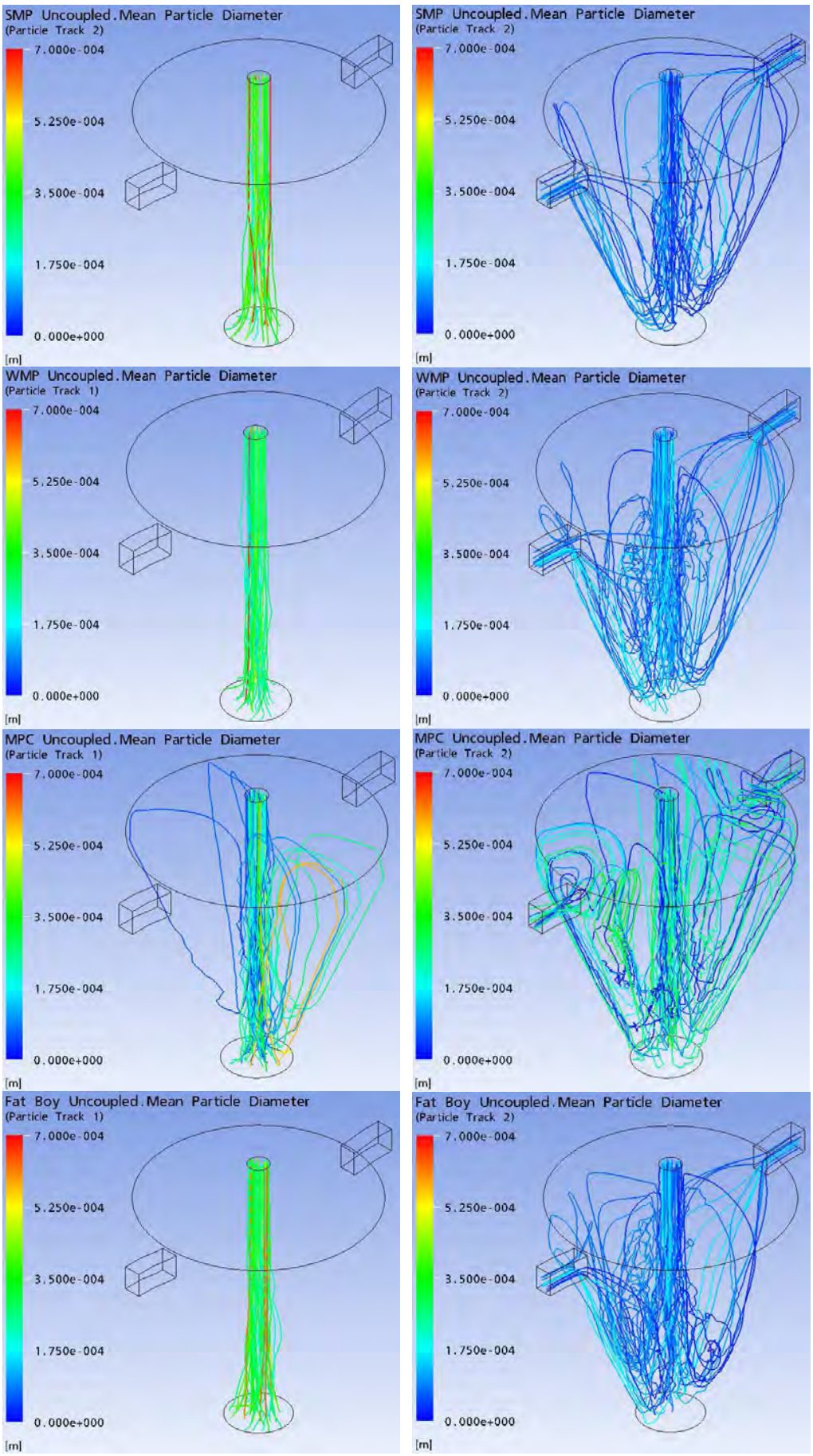

Figure 10-26: 40 particle tracks of four different milk powers (top to bottom – SMP, WMP, MPC Fat Boy) exiting the drying chamber through the static fluid bed or the outlet air ducts

particle sizes (0 μm to 630 μm) that reach the SFB, hence there is less classification with this product. This is because the MPC particles have a lower particle density than the other three powders. Some of these MPC particles are initially elutriated and flow in the recirculation zones back to the main inlet. Here, they follow the main inlet air streamlines a second time until they reach the fluid bed.

The particle tracks of those particles that exit the chamber as fines are much longer and more random than the particle tracks of the majority of those particles that exit the chamber through the SFB. Again, at the main inlet, these particles follow the streamlines of the main inlet air stream. However, at the SFB, because these particles have insufficient inertia to overcome the momentum of the SFB air flow and reach the fluid bed, these particles flow into the recirculation zones. It appears that those particles that flow up the chamber close to the walls exit the chamber through the outlet air ducts. Those particles that flow in the middle of the recirculation zones or in the quarters of the chamber where the outlet air ducts are not, appear to flow back to the main inlet and follow the main inlet air streamlines a second time.

Table 10-7: Simulated particle size range exiting the Clandeboye dryer 2 chamber at the static fluid bed or the outlet air ducts for different milk powders

Product	SFB Particle Size Range $d_{p,SFB}$ [μm]	Fines Particle Size Range $d_{p,BH}$ [μm]
SMP	150 – 700	0 – 200
WMP	50 – 700	0 – 200
MPC	0 – 630	0 – 360
Fat Boy	130 – 700	0 – 190

It can be seen from Table 10-7 that there is an overlap in particle sizes that exit the chamber through the SFB and those that exit the chamber as fines. This overlap is a result of the track these particles follow in the main inlet air jet. If the particle is located on the edge of the main inlet air jet, it is most likely it will become fines. However, if the same size particle flows down the middle of the main inlet air jet, it often has insufficient inertia to escape this track and therefore exits the chamber through the SFB.

The fines particle tracks are affected by turbulent dispersion: particles smaller than 400 μm in diameter that exit the chamber as fines have wiggly particle tracks, particularly in the recirculation zones. Only a few particles on the edge of the main inlet air jet show some influence of turbulent dispersion. It should be noted that these predictions are from steady state solutions – transient solutions are expected to show larger changes in direction and increased mixing.

It was expected from previous research that the particle trajectories largely follow the gas streamlines. Harvie et al. (2002) found from simulations on a pilot scale tall-form dryer that the smallest particles faithfully follow the gas streamlines and stay close to chamber centreline because of their small momentum. Furthermore, the flow patterns in the recirculation zones were complex and these authors also found highly variable particle residence times. Although these times were not determined from these particle tracking simulations, it can be seen in Figure 10-26 that in all cases, similar sized particles have very different particle tracks. These different particle tracks would also lead to highly variable residence times.

10.6.2 Fines Fractions

The fines fractions from the simulations were estimated by dividing the mass flow of powder exiting through the outlet air ducts by the total powder flow exiting the dryer, that is, the powder flow through the outlet air ducts and the SFB (Simulated Fines Fraction 1). Table 10-8 shows that, except for the MPC case, the predicted fines fractions were much smaller than those measured in the plant (Chapter Four).

Table 10-8: Experimental and simulated fines fractions for different milk powders

Product	Experimental Fines Fraction X_{BH} [%]	Simulated Fines Fraction 1 X_{BH} [%]	Simulated Fines Fraction 2 $1 - X_{SFB}$ [%]	Simulated Particles Exiting Chamber [%]
SMP	86 ± 2	24	65	50.3
WMP	49 ± 8	26	63	51.4
MPC	96 ± 4	91	93	97.6
Fat Boy	74 ± 12	16	53	57.0

Table 10-8 also shows that for the SMP, WMP and Fat Boy cases, the percentage of the particles injected at the main air inlet that exited the domain through one of the outlet air ducts or the SFB was approximately 50 %. Therefore, a significant amount of the injected powder mass did not exit the chamber. These particles either did not reach an outlet boundary or were permanently trapped in recirculation zones (ANSYS, 2005a) and therefore tracking of these particles was stopped because they had exceeded the maximum number of integration steps. In an attempt to reduce the number of particles not exiting the chamber, the number of integration steps for the SMP, WMP and Fat Boy simulations was increased from the CFX 10.0 default value of 10,000 (ANSYS, 2005a) to 60,000. However, this only reduced the percentage of particles remaining within the chamber by approximately 10 %, which in turn only changed the fines fractions by roughly 2 %, and thus had little effect.

The simulation results showed that the particles that did not exit the chamber through an outlet or were trapped in the recirculation zones were generally less than 400 μm in size and appeared to be heading for the outlet air ducts rather than the SFB because of their size. Therefore, the fines flows are reduced. If the fines fractions are determined from unity minus the ratio of mass flow of powder through the SFB to the injected mass flow of powder (Simulated Fines Fraction 2 in Table 10-7), fines fractions of 65 % for SMP, 63 % for WMP, 93 % for MPC and 53 % for Fat Boy are obtained. Again however, the SMP and Fat Boy fines fraction estimates are much lower than those determined experimentally for these two products. The WMP estimate is slightly larger than that determined experimentally but the MPC estimate agrees very well with both the simulated fines fraction 1 and the experimental MPC fines fraction.

It would be expected that MPC has the highest fines fraction of the four powders because as mentioned above, MPC has the lowest particle density. Also, the SFB inlet air velocity for MPC is approximately the same as that for SMP and WMP. Hence, the lighter MPC particles have less inertia than SMP and WMP particles above the SFB, and therefore are more easily entrained with the air stream taking the powder away from the SFB. As is shown in Figure 10-26, because more MPC flows away from the SFB, more powder becomes fines and exits the dryer through the outlet air ducts.

The most likely reason for the large discrepancies among the simulated and experimental fines fractions is the particle density values used in the simulations. The simulations used a

constant particle density for each product, but it is likely that each particle size band for each product has a different particle density. If the simulated particle density is higher than the actual, it would be expected that the fines flow would be reduced because of less entrainment of powder in the outlet air stream.

The average particle density used for each product may not exactly replicate the CD2 values. It is possible that the SMP and WMP density values obtained from Matheson (1991) were slightly different to those in the CD2 plant because of differences in atomisation conditions and plant design between CD2 and the plant from which Matheson (1991) obtained his powder. The MPC and Fat Boy particle densities were estimated from CD2 bulk density data. Because of the good agreement between the simulated and experimental fines fractions for MPC, it appears this estimate was accurate. However, the large difference between the simulated and experimental fines fractions for Fat Boy suggests that the average particle density of 1250 kg / m^3 was too large.

Also adding to the discrepancy is the difference in actual and simulated particle shapes. The simulated particles were assumed to be spherical. However, it is well known (Buma and Henstra, 1971; Nijdam and Langrish, 2005; Nijdam and Langrish, 2006) that milk powder particles are usually clumped together as medium to large scale agglomerates, particles can be hollow or collapsed and some broken particles can be present. This idea is supported by the SEM images in Chapters Four and Seven.

Hollow particles, particle fragments and collapsed particles will have particle densities less than the equivalent diameter particles simulated here. Consequently, the simulated particles will be more likely to settle at the bottom of the drying chamber rather than become entrained with the outlet air stream and exit the chamber as fines. Therefore, the simulated fines flow would be expected to be less than the actual, as indeed they are.

These simulations also did not truly replicate the concentrated milk droplet spray conditions. In the plant, milk concentrate enters the chamber through one of 15 lances spaced around the main inlet. The angle and direction of the spray from the nozzle in each of the lances is unique, and set such that a well-formed spray cloud results. The simulations did not account for this lance arrangement as particles were injected from random locations around the main inlet. The angle of the spray cloud was also not accounted for because the same absolute

velocity was given to all injected particles rather than specifying the unique velocity components and spray angle at each nozzle.

The simulation of the inlet gas stream and injected particles momentum was also not a true replication of the industrial situation. The momentum of the water vapour evaporated from the droplets was accounted for by adding this momentum to the inlet gas stream. Hence, the inlet gas stream had slightly more momentum as it entered the chamber than in the plant. However, this momentum flow should have been accurate very soon after the main air jet entered the chamber. Also, because dry particles rather than liquid droplets were injected, the injected particles had less momentum than the atomised droplets because of the reduced mass. These two factors combined with the fact that the axial and radial components of the injected particles were not accounted for, meant that the injected particles followed the inlet gas streamlines more closely than expected. Hence, it was more likely that these particles reached and exited the chamber at the SFB than as fines with the outlet air stream.

If atomised liquid droplets had been simulated, it would be expected that some of these droplets would have sufficient inertia to move in the radial direction away from the main inlet air jet. Here, the droplets would probably follow the streamlines of the recirculation zones between the main air jet and the walls of the chamber. If the droplets remained in these areas of the chamber and dried, it is likely they would have exited the chamber as fines: it appeared from the particle tracking simulations that most of the particles in the recirculation zones exited the chamber through the outlet air ducts. Therefore, it is likely that the simulated fines fractions were lower than the experimental because of the inlet boundary conditions specified for the main inlet air stream and the injected particles.

Particles landing on the SFB were assumed to exit the chamber through the SFB overflow weirs. However, because of the presence of powder in the fluid bed in the plant, it is possible that some powder collected on the SFB could be elutriated with the SFB air flow and therefore, become entrained in the air flow above the SFB and carried to the outlet air ducts – powder is often spurted up to 1 m above the top of a fluid bed because of bubbling. If so, a slight increase in the fines flow and therefore the fines fractions would occur. Because the behaviour of powder on the internal fluid bed was not modelled, this mechanism was not accounted for in the particle tracking simulations.

Finally, the simulation procedure employed for these particle tracking simulations could have added to the discrepancy in fines fractions. The particle tracking simulations were steady state, but as Section 10.4 showed, the flow field within a spray dryer is highly transient. Consequently, a reduced convergence criterion was used for these particle tracking simulations. The movement of the main jet and most likely, the change in length of the main jet may influence the fines fractions: particles would not flow as far down the axis of chamber, become influenced by the SFB flow sooner, and possibly more powder would follow gas streamlines to the outlet air ducts.

Figure 10-27 shows the experimental chamber collection efficiency plotted against the simulated chamber collection efficiency for the four different milk powders, and a one to one trend line. Included with each data point are the total powder mass flow (m_p [kg / s]) and the average particle terminal velocity (U_T [m / s]) for that powder. As expected, three of the four data points are far from the one to one trend line because of the reasons discussed above. However, the plot shows that the chamber collection efficiency appears not to be correlated with the average particle terminal velocity, but possibly correlated with total mass flow of powder in the chamber. Therefore, it is likely some other mechanism determines the amount of power that becomes fines in a spray drying chamber.

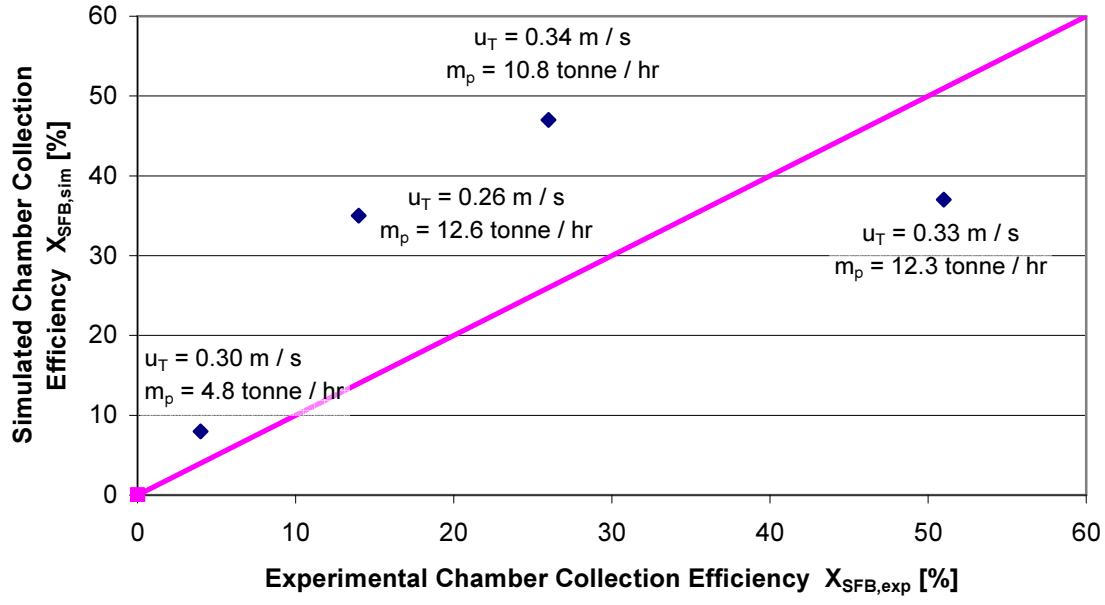

Figure 10-27: Experimental versus simulated chamber collection efficiencies for different milk powders

10.6.3 Particle Tracking Mesh Independence

Because the main inlet air velocities in the particle tacking simulations were greater than twice those used in the transient air flow simulations, the particle tracking gas flow fields also needed to be shown to be independent of the mesh. The three meshes used to prove mesh independence of the transient air flow results were used to check the particle tracking mesh independence.

It was assumed that if the SMP particle tracking results were mesh independent, then the flow fields of the three other powders would also be mesh independent because of the similar boundary conditions. Hence, the SMP boundary conditions given in Table 10-6 were used. Like the transient air flow mesh independence study, absolute velocities along the axis of the dryer and through a line running from wall to wall of the chamber were compared. The slight difference for the particle tracking mesh independence was that the line running from wall to wall of the chamber, was along a central plane 6 m rather than 8 m above the base of the dryer.

Figure 10-28 shows that a very similar velocity profile along the dryer axis was obtained from all three meshes, and that the velocity magnitudes from the medium and fine mesh are similar. The average absolute discrepancy between the medium and fine mesh as a percentage of the medium mesh velocity magnitude was 5.2 % and ranged from 0 % to 50 %, the latter of which occurred just above the SFB.

The velocity profiles from the line running across the chamber were again similar for all three meshes. However, the velocity magnitudes were again not as close as the centreline comparison. The average absolute discrepancy between the medium and fine mesh as a percentage of the medium mesh velocity magnitude was 9.8 % and had a range from 2.0 % to 23.7 %.

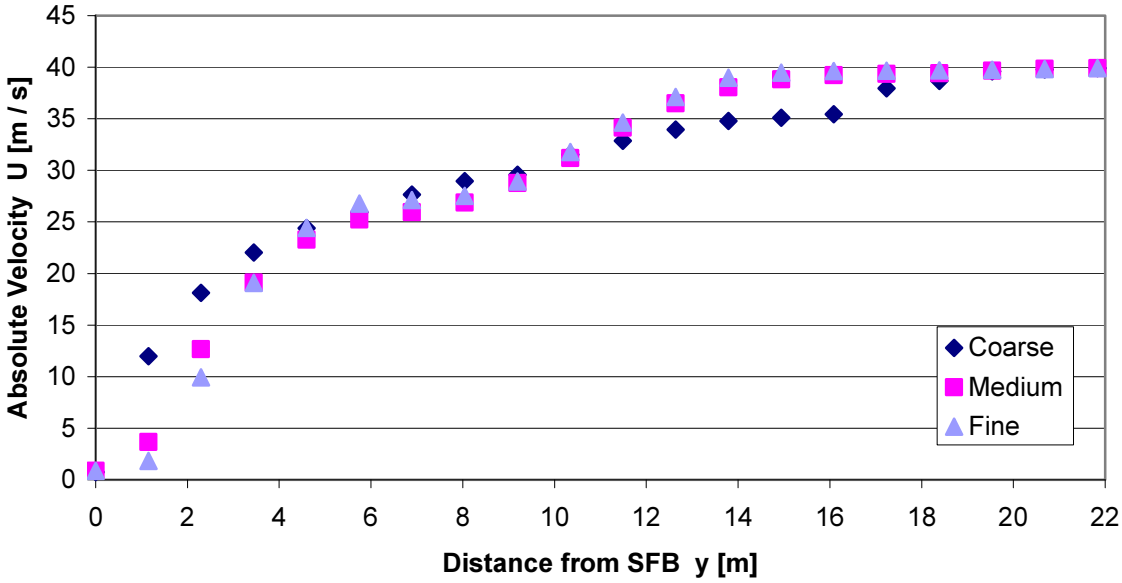

Figure 10-28: Comparison of absolute gas velocities along chamber axis using the coarse, medium and fine mesh for the skim milk powder particle tracking simulations

These discrepancies between the results from the medium and fine mesh from the particle tracking gas flow field are greater than those from the transient air flow gas flow field. However, it was deemed that this discrepancy was sufficiently small to conclude that the particle tracking gas flow field results were mesh independent.

10.6.4 Particle Independence Study

A different number of particles were injected at the main inlet for the SMP case to determine when the fines fractions calculated from the results became independent of the number of injected particles. As Figure 10-29 shows, it appeared that the fines fraction was independent of the number of injected particles at around 2500 particles as a relatively constant fines fraction of approximately 23 % was obtained. It was assumed that the simulations of the remaining three powders (WMP, MPC and Fat Boy) were also independent of the number of injected particles at around 2500. Hence, for all four powders, 2750 particles were used to represent the powder flows.

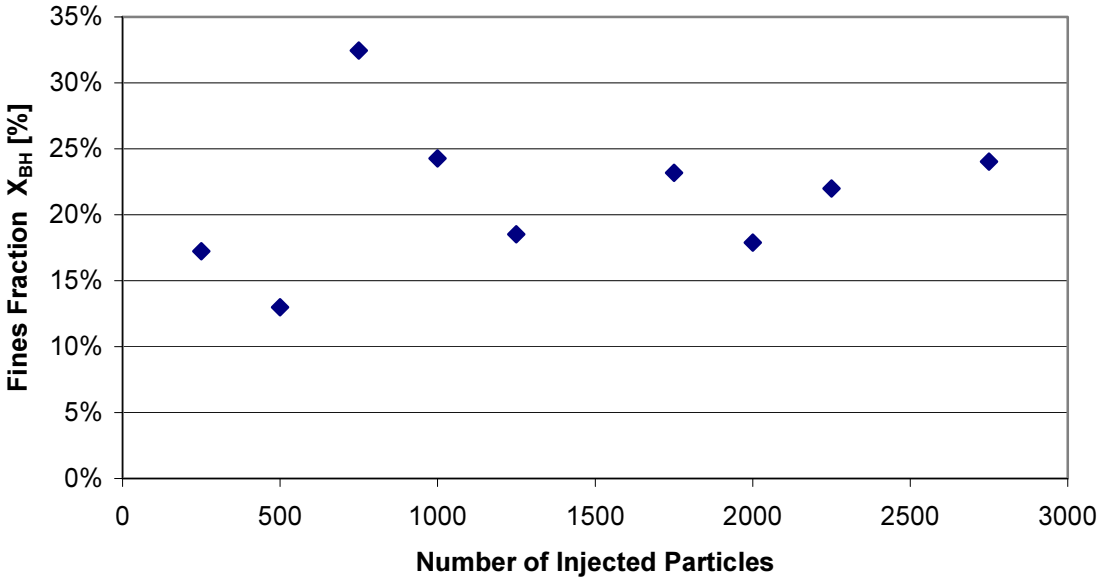

Figure 10-29: Fines fractions at different number of injected particles for skim milk powder particle tracking simulations

10.7 Future Work

There are several improvements that could be made to the CFD simulations reported here that would increase the understanding of the CD2 dryer and baghouse system. Using an order of magnitude more particles would show if the particle tracking simulations performed were truly independent of the number of injected particles. Also, these particle tracking simulations could be conducted on a finer mesh to further prove that the results are mesh independent.

The particle tracking simulations could be repeated using the Eulerian-Eulerian model (two-way coupling) to investigate the influence the particles have on the gas flow field. Also, transient rather than steady state simulations could be performed. The most accurate model of the dryer would require adding the simulation of drying of the liquid droplets. Although not impossible, simulating evaporation of liquid droplets for a transient industrial scale case would be very computationally demanding.

Additional data obtained from the industrial scale may improve the validity of these simulations. For the air only situation, velocity measurements with a Pitot tube or a hot wire

anemometer could relatively easily be carried out in the east outlet air duct or above the SFB. These experimental values could then be compared with the simulated values from the same locations. Validating the particle tracking simulations using Particle Image Velocimetry or Laser Doppler Anemometry would prove almost impossible at the industrial scale because of the large turbulent movements and because the geometry would severely limit the ability to create a well illuminated light sheet.

As mentioned in Chapter 9, the CFD modelling of the main baghouses attached to the CD2 drying chamber would be very interesting. This modelling could investigate alternative designs such as different inlet air configurations, bag spacing and outer spacing in an attempt to improve bag life. Frey (2001) modelled different pilot scale baghouses using CFD with the aim of deducing the best inlet air configuration for pre-separation of powder, that is, removal of powder from the air stream before it reaches the filter bags. A tangential entry located at the top of the dirty side chamber was concluded to be the most efficient because of the strong downward swirl induced. Surprisingly, Frey (2001) also concluded that the baghouse diameter had no influence on the pre-separation of powder: it was discussed in Chapter Eight that a reduction in the annular velocity is likely to reduce the particle carrying capacity of the air stream via a longer time for settling and therefore, increase the pre-separation of powder.

It appears that GEA Niro A/S based their Sanicip washable baghouse design on the conclusions drawn by Frey (2001). However, what Frey (2001) modelled and what GEA Niro A/S built in CD2 is quite different. As Table 10-9 shows, the annular velocities at the industrial scale are two orders of magnitude higher that those simulated by Frey (2001). Therefore, the pre-separation of powder caused by the tangential scroll at the industrial scale may not be as high as is claimed. CFD modelling at the industrial scale could deduce if this is the case.

Table 10-9: Comparison of baghouse design parameters used by Frey (2001) and those implemented in the Clandeboye Dryer 2 washable baghouses

Parameter	Frey Models	Main CD2 Baghouses	VF CD2 Baghouses
Air to Cloth Ratio V_f [m^3 / m^2 / min]	1.4 – 2.9	2.2	1.5
Bag Diameter D_b [mm]	150	208	208
Bag Spacing X_b [mm]	50	60	60
Outer Spacing G [mm]	100 – 400	160	260
Bag Number Density N [m^{-2}]	25.0	13.9	13.9
Annular Velocity V_{Anl} [m / s]	0.25 – 0.73	36.5	10.5

One difficulty in attempting to simulate the industrial scale baghouses is the development of a suitable calculation mesh. The high aspect ratio of the filter bags (6 m in length and 0.208 m in diameter) and their very close spacing (Figure 10-30) will mean that getting a sufficient number of nodes between each bag without generating an excessively large mesh will be a challenge. The geometry could be simplified if the bag bundle, the area encompassing the filter bags and the space between them, was modelled as a porous media, thus enabling the influence of different inlet air arrangements and outer spacing to be investigated.

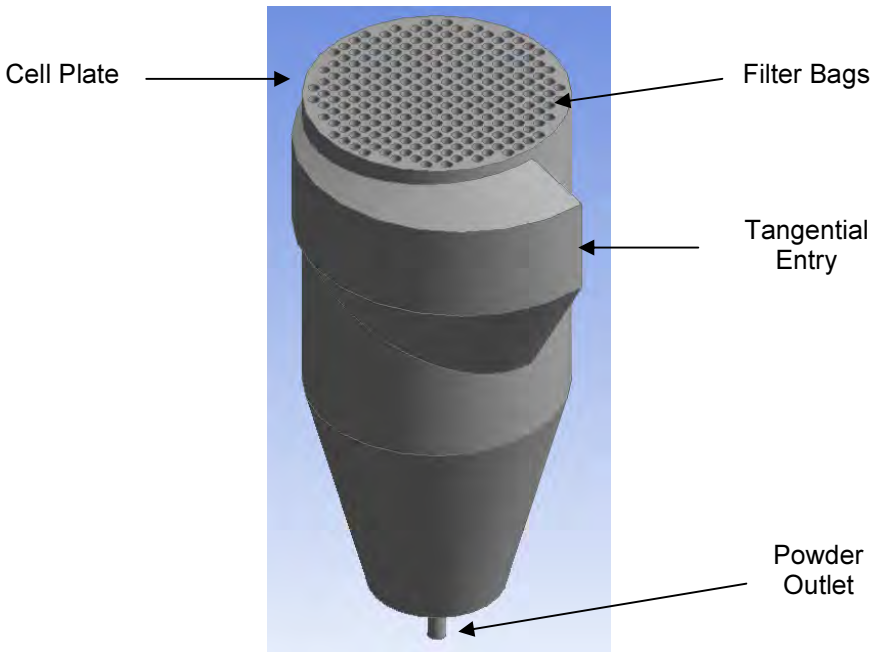

Figure 10-30: Solidworks drawing of Clandeboye Dryer 2 main washable baghouse dirty air side flow domain.

10.8 Conclusions and Recommendations

From this section of work it can be concluded that the main axial jet in a spray dryer retains a flat profile and moves about the central axis of the dryer with time. Recirculation zones are present between this jet and the dryer walls that change in size and interact with the motion of the main jet. Spectral analysis allowed it to be concluded that the main jet has no apparent distinct frequency because of the presence of a range of frequencies. These simulation observations reiterate the conclusions of previous authors that transient, 3D simulations are required to fully capture the flow features of spray dryers.

The movement of the tip of the main jet in these simulations was concluded to be more pronounced than in the majority of previous spray dryer CFD studies published in the literature. It was believed that the location of the outlet air ducts near the top of the chamber and the use of an industrial scale geometry meant the tip of the jet was not fixed by the outlet boundary condition, and had a large space available for movement.

This is possibly the first work to include the influence of a spray dryer's internal fluid bed airflow on the flow patterns within a spray dryer. The results showed that the flow field and period of the main jet were very similar for different SFB inlet air velocities. The SFB flow had only a local influence in the area above the SFB and consequently, reduced the length of the main jet slightly. Thus it was concluded that because the SFB inlet air velocity was two orders of magnitude less than the main inlet air jet, the gas flow field of a spray dryer is dominated by the main inlet air flow.

It was concluded that use of an opening with specified loss coefficient as the outlet boundary condition to simulate the downstream pressure drop the air stream experiences after leaving the spray dryer chamber had little influence on the overall flow field. The simulations showed that the stagnation point between the main and SFB air flows was further from the SFB than had been observed in previous simulations and consequently, the length of the main inlet air jet was slightly shorter. Also, the movement of the main inlet air jet had a wider range of frequencies. Finally, velocities in the slow recirculation zones were possibly slightly more uniform than the case with an average static pressure outlet boundary condition but in general, the flow field within the dryer and the period of the main jet was the same.

Results from visualisation of the main jet movement by use of a telltale rig located in the dryer confirmed the transient nature of the main jet. Because the measured periods ranged from approximately 1 s to 11 s it was concluded that no apparent distinct frequency exists. Also, because the average telltale periods for different SFB flows were similar, it was concluded that the SFB flow had very little influence on the overall gas flow field, which agreed well with the simulated results. Finally, the very good agreement between the average telltale periods and the simulated SFB absolute velocity periods at a point 1 m above the SFB also enabled it to be concluded that the simulated results are an accurate representation of the air flow patterns within an industrial spray dryer.

The investigations into different SFB flow rates and use of an opening boundary condition showed only a local influence in the area above the SFB. However, it is possible that these different flow patterns above the SFB will impact on elutriation of powder from the fluid bed and hence, the amount of powder that becomes fines. The steady state particle tracking simulations performed did not alter the SFB flow for a given product and thus, the importance of the SFB flow on particle tracking was not studied.

With regard to the steady state particle tracking simulations using the Lagrangian framework, the results showed the smaller size fractions followed the main inlet air streamlines until they reached the SFB and then followed the air flow into the recirculation zones and eventually the outlet air ducts. The larger size fractions were observed to follow the main inlet air streamlines to the SFB. Particles approximately 150 μm and above exited the chamber through the SFB, and particles between 0 μm and approximately 250 μm exited the chamber as fines. These particle sizes were dependant on the powder type and hence, the assumed particle density.

The poor agreement between the simulated and experimental fines fractions was concluded to be a result of a number of factors. The major source of the discrepancy was believed to be the average particle density value used for each product. It is likely that each particle size band will have a unique particle density associated with it, but this was not accounted for in the simulations. Also, it is unclear how well the estimates and literature particle density values used match the actual particle density for powders produced in the CD2 plant.

The differences between the simulated and actual plant were believed to also add to the discrepancy between simulated and experimental fines fractions. The particle tracking simulations were steady state but the flow pattern within a spray dryer is strongly transient. The main inlet air and particle injection region did not match the industrial situation because absolute rather than the Cartesian components of the velocities were specified for the injected particles. Also, the hydrodynamics of powder in the internal fluid bed was not accounted for in this model.

It is recommended that future CFD modelling of the CD2 dryer be carried out to improve on the work conducted here. These simulations should be transient rather than steady state, use also the Eulerian-Eulerian as well as the Lagrangian model and ensure that the particle tracking results are independent of the mesh and number of injected particles. The most complete model of the CD2 spray dryer would require modelling of droplet drying, which is a possibility for future work.

It is also recommended that CFD studies modelling the flow within the main washable baghouses attached to the CD2 dryer be conducted. These studies should investigate different baghouse designs such as different inlet air configurations, different bag spacing and different outer spacing. Also, baghouse CFD modelling should deduce if the pre-separation of powder caused by the tangential scroll at the industrial scale is as is high as is claimed by GEA Niro A/S based on the pilot scale modelling work of Frey (2001).

Conclusions and Recommendations

The main aims of this study were to increase the fundamental understanding of both operation and design of washable baghouses, particularly for application in milk powder plants. The author considers that these aims were achieved. Other factors indicating that this project was a success are reduced downtime in the Fonterra Clandeboye Dryer 2 plant associated with the washable baghouses (from 66 to 10 hours per annum), and the increase of life time of filter bags in this plant (from approximately 4 months to 12 months). It should be noted that this reduction in downtime and improvement in bag life are a result of both the work carried out in this project and changes in the Clandeboye Dryer 2 production schedule.

11.1 Conclusions

11.1.1 Historical Data Investigation

The major causes of variation in the baghouse differential pressure during the milk processing season were shown to be the type of product being made and the age of the filter bags. For all product groups, the baghouse differential pressure increased with the extractor fan speeds, and the amount of fat in SMP also had a considerable influence. Surprisingly, the baghouse differential pressure was shown not to be sensitive to the total air flow rate. It was observed that replacement of all filter bags in a baghouse caused a sudden drop in baghouse differential pressure. However, it was also concluded that a poor CIP can actually increase rather than have the desired effect of decreasing the baghouse differential pressure.

It was concluded that SMP has the highest differential pressure because of a greater flow resistance from thicker, denser cakes caused by smaller average particles. The converse was true for MPC, which had the smallest filter cake and therefore least resistance because of the lowest powder flow and largest average particle size.

11.1.2 Fines Loadings

The fines loadings investigation established a new (and first) method for determining the fines loadings in spray dryer plants, applying it to a milk powder plant with washable baghouses. The method is based on a comparison of the particle size distributions of powder samples

obtained from the bottom of the dryer (SFB in this plant), the collector (baghouse in this plant) and the mixed product stream (here through the sifter). These size distributions allowed a determination of the percentages of sifter powder flowing from the SFB and also from the baghouses. It was concluded that despite the particle size distribution method being relatively simple, it is sensitive enough to detect changes in plant operating conditions and can accurately estimate fines flows.

The CPM 5003 optical scintillation instrument available from the BHA Group was trialled for this study, and was able to measure fines concentrations in an outlet air duct of the CD2 spray dryer. This was despite the powder concentrations experienced being higher than the supposed upper limits of the instrument stated by the supplier. Because a calibration curve for the instrument was developed using particle size distribution method estimates and isokinetic sampling results, it was concluded that this instrument is suitable to measure fines flow rates experienced in milk powder plants, and this can be carried out online.

Results from this fines loadings investigation led to the conclusion that the fines fractions in milk powder plants are significantly higher than what was traditionally thought (10 % to 20 %). Fines fractions were found to be 48 ± 8 % for WMP, 96 ± 4 % for MPC and either 86 ± 2 % or 53 ± 23 % for SMP and 64 ± 5 % or 83 ± 1 % for Fat Boy powder depending on the operating conditions. In terms of mass flow of fines, it was shown that SMP has the highest fines level of all powders, Fat Boy the second highest level, MPC 80 the lowest and WMP and MPC 70 approximately the same level of fines. Thus, it was concluded that the level of fines is a function of the feed milk concentrate flow and total solids, the powder particle size and density, and the atomisation nozzle size.

With regard to evaporator swaps, the resulting rise in baghouse differential pressure was concluded to not be caused by any increase in fines loading. It was postulated that this mechanism is due to a decrease in powder particle size arising from a reduction in concentrate total solids and probably therefore, a reduction in concentrate viscosity in the atomisers. Because a small reduction in baghouse differential pressure resulting from a slight decrease in fines level occurs with feed line swaps, it was concluded that baghouse powder properties are relatively unaffected by a feed line change. Hence, the concentrate total solids was hypothesised to be constant during a feed line swap.

An attempt to use pneumatic conveying correlations to infer fines flows showed that the Molerus and Wellman (1981) correlations are sensitivity to changes in particle size and density, as well as powder mass flow. Therefore, using this correlation to deduce and display fines flows on the operators' screens would not be reliable because changes in fines return line pressures could be a result of changes in particle size, particle density and or fines flow. Use of the methods of Maynard (2006) and Williams (2004) appeared to be inaccurate for milk powder fines return lines because the friction factors used are not accurate for milk powders.

11.1.3 Filter Bag Scanning Electron Microscopy

From scanning electron microscopy of industrial bags, it was concluded that new filter bags have non-uniform surfaces and the degree of non-uniformity varies among the suppliers, which is believed to be a result of the surface treatment applied to each bag. Further, the type of surface finish and its method of application appeared to determine the bag cost. The surface finishes, as well as the bag thickness, appeared to be parameters strongly influencing the bag permeability.

From a combination of plant experience and the SEM images produced during this project, it was concluded that a zero cleaning efficiency occurs near the top of the Clandeboye Dryer 2 pulse-jet cleaned filter bags. It was reasoned using the work of Löffler and Sievert (1987) that because a local negative pressure pulse arises from entrainment of surrounding air on initiation of the pulse at the top of the bag, powder is not removed from the surface of the bag and can gradually migrate to the bag interior. The generated images also lead to the conclusion that the bag surface at the top of the bag collects and retains a large amount of powder that is not removed after long periods of operation.

With regard to the CD2 baghouse CIP, it was demonstrated that the poor sequence encountered since the plant was commissioned was detrimental to the state of the filter bags; a milk powder gel appeared to form during the CIP that was then baked during the dry-out phase of the CIP and caused the baghouse differential pressure to be higher after the CIP than it had been before the CIP. Recommissioning the CIP settings at the end of the 2003/2004 season improved the CIP to avoid blinding and the baghouse differential pressures now

decrease after a CIP. Finally, it was concluded that higher protein levels in milk powders encourages gel layer formation and therefore blinding of bags during a CIP.

11.1.4 Single Cell Baghouse

The 3 m long single bag baghouse installed within the department of Chemical and Process Engineering at the University of Canterbury was designed and built to replicate as far as is possible the conditions of a 6 m long industrial bag found in the GEA Niro A/S Sanicip CIPable baghouses. Therefore, it was concluded that a pilot scale baghouse is now available in New Zealand that can be used to greatly enhance the understanding of milk powder plant washable baghouses, including the cleaning pulse behaviour, and potentially even CIP behaviour.

11.1.5 Fat in Skim Milk Powder

The investigation into the amount of fat in SMP showed that the baghouse differential pressure is very sensitive to the amount of bulk fat present in SMP. Furthermore, experiments for this thesis showed that a lack of bulk fat in SMP has the ability to cause the entire spray dryer plant to automatically shut down. It was concluded that the mechanism behind this phenomenon is not a result of changes in fines concentration as fines concentration measured by the optical scintillation instrument were constant and also, no apparent correlation was established between the powder bulk fat content and the baghouse fines return line pressure. There was also no apparent change in particle size, which was to be expected as such small changes in the composition of the milk concentrate are unlikely to have much influence on the atomisation process. Therefore, changes in baghouse differential pressure were concluded to not be due to this mechanism.

ESCA measurements and SEM images allowed it to be concluded that fat is over-represented on the surface of milk powder particles. The ESCA measurements also showed that only small changes in the bulk fat content are required to see large changes in surface coverage for SMP. It is hypothesised that an increase in surface fat coverage increases the clumping of SMP before reaching the bag. This clumping is thought to create more porous filter cakes. Also, it is believed that clumping causes the cake to deposit closer to the surface of the filter

bags and is therefore more easily removed during pulse cleaning, rather than if individual particles penetrated into the interior of the filter bag as may happen with lower fat contents.

11.1.6 Design of Pulse-Jet Baghouses

It was concluded from the design investigation of pulse-jet baghouses that there is a large variation in the recommended baghouse design parameters of air-to-cloth ratio, elutriation velocity, bag spacing and bag dimensions. Other key design parameters that must also be considered are the type of filter medium, operating differential pressure and baghouse footprint. Because of the variation in recommended baghouse design parameters, it was concluded that the choice of an optimal design relies heavily on past experience and or laboratory experiments with the dust under consideration, or if this is not available, similar dusts.

The procedure for baghouse design developed during this work differs from previous work in that it includes the area outside the bag bundle (between the bags and the baghouse wall) as a key design parameter and uses an optimisation routine to solve the system of equations. Using this procedure showed that the majority of the Fonterra main washable baghouse designs are far from optimal because of high air to cloth ratios, long bags and high elutriation and annular velocities. Also, it was concluded that the Fonterra VF washable baghouses are much closer to the optimum calculated using the procedure, which is the likely reason these units have had almost no operational issues.

Regarding the procedures found to determine air-to-cloth ratios for baghouses collecting milk powder, it was concluded that significant variation exists among the four available guidelines. The methods of Löffler et al. (1988) and Intensiv-Filter (1999) appeared reasonable in light of Fonterra industrial experience. However, because the method of Löffler et al. (1988) is also more sensitive to the milk powder type, it was concluded that this method was the most appropriate for fines collection in milk powder plants.

11.1.7 Bag Movement

Observations from below the bag bundle of bag movement during air flow showed large bag movements near the dirty air inlet. This correlated with the observed high bag damage in this zone. These observations also led to the conclusions that the bag movement around the edge of the bag bundle reduces the further the bags are from the inlet region, and that the bag movement in the middle of the bag bundle is almost negligible. It was also concluded that the installation and use of stainless steel inspection hatches located near the base of the filter bags in the inlet air region allowed easy observation of the filter bags and reduced baghouse dry-out times. Consequently, the overall CIP turnaround times were reduced by approximately 20 %.

The periods of oscillation of a 6 m long industrial bag located just inside the inspection hatch were measured at two different conditions: a) a clean filter bag with no air flow and b) a bag and cake in the presence of the dirty air flow. There was insignificant change from a value of 1.4 Hz to 1.5 Hz for these conditions. It was found that a 3 m long pilot scale filter bag had a natural period of oscillation of 2.2 Hz. Modelling the bag and cage movement using a cantilever beam model was thought to be inappropriate because of a 600 % discrepancy in EI values between the industrial and laboratory scales. However, it was concluded that a simple pendulum model described the filter bag and cage movement reasonably; only a 4 % discrepancy between the actual and modelled ratio of laboratory to industrial scale periods of oscillation was obtained.

From observations of cleaning pulses acting on the industrial bags, it was concluded that the pulses derived from current plant settings are effective even near the base of these long bags because the cake at this location was visibly pulsed off. It was also noted that a second change in bag diameter occurred near the end of the pulse, indicating a second rise in bag pressure. The cleaning pulse appears to be complex.

11.1.8 Spray Dryer CFD Modelling

CFD simulations of the air flow patterns within an industrial spray dryer showed that the main axial jet retains a flat profile and moves about the central axis of the dryer with time. Recirculation zones between this jet and the dryer walls are present that change in size in

accordance with the motion of the main jet. For the CD2 case, spectral analysis showed that the main jet has no apparent distinct frequency because of the presence of a range of frequencies. Hence, these simulation observations reiterate the conclusions of previous authors that transient, 3D simulations are required to fully capture the flow features of spray dryers.

It was concluded that the movement of the tip of the main jet in these simulations was proportionately greater than those in the majority of previous spray dryer CFD studies. The location of the outlet air ducts near the top of the chamber rather than at the bottom as in smaller pilot-scale dryers, along with use of an industrial scale geometry, were believed to allow the tip of the jet to be more mobile.

This work is possibly the first simulation to study the influence of a spray dryer's internal fluid bed airflow on the flow patterns within a spray dryer. The results from simulations using internal fluid bed airflow rates ranging between the current plant levels and zero showed that the flow field and period of the main jet were very similar over the range, and that the effect of different SFB flows, was confined to a somewhat reduced length of the main jet. This could have a significant effect on elutriation of powder from the fluid bed.

An opening with a specified loss coefficient was used as the outlet boundary condition to simulate the downstream pressure drop the air stream experiences after leaving the spray dryer chamber. This new boundary condition was concluded to have little influence on the overall flow field. However, it was observed that the stagnation point between the main and SFB air flows was further from the SFB than had been observed in previous simulations and consequently, the length of the main inlet air jet was slightly shorter. This finding implies that a greater amount of powder would be elutriated from the SFB and thus, become fines entrained in the outlet air stream.

Some validation of the simulations was achieved by observing the movement of telltales above the fluid bed, indicating local effects of movement of the main jet. These visualisations confirmed the transient nature of the main jet, showing that the main jet has no apparent distinct frequency. Very good agreement between the average telltale periods (movement) and the simulated fluid bed periods (absolute velocity) at a point 1 m above the fluid bed was found.

Steady state particle tracking simulations using the Lagrangian framework showed the smaller size fractions of powder following the main inlet air streamlines until they reached the SFB, and then following the air flow into the recirculation zones and eventually through the outlet air ducts. The larger size fractions were observed to follow the main inlet air streamlines to the SFB, being captured there. Particles approximately 150 μm and above left the chamber through the SFB, and particles up to approximately 250 μm in size left the chamber as fines, depending on the powder type.

The results from these steady state particle tracking simulations using the Lagrangian framework showed poor agreement with the experimental fines fractions. It is believed that the average particle density values used for each product in the simulations contributed to the discrepancy; it is possible each particle size band will have a unique particle density. Differences between the simulated and actual plant were likely to also add to the discrepancy between simulated and experimental fines fractions. These discrepancies included steady state rather than transient simulations being carried out and hydrodynamics of powder in the internal fluid bed not being accounted for.

11.2 Recommendations

To prolong filter bag life, reduce electricity costs associated with the extractor fans and reduce plant downtime required for bag changes, it is recommended that the baghouse differential pressures be maintained as low as possible. This can be achieved as follows: a) running the extractor fans at minimum speeds consistent with maintaining the chamber vacuum; b) continuing to operate the dryer outlet air humidity and temperature so that each product remains below its sticky point; c) minimising the number of swaps between supplying evaporators that occur during production runs; and d) producing SMP with a final powder fat content as high as is possible. To achieve SMP with the highest possible final powder fat content, it is recommended that cream dosing systems be installed in the milk standardising area of all current and future SMP-making plants with washable baghouses.

It is recommended that to minimise the amount of powder that becomes fines, the total solids of the milk concentrate fed to the dryer be as high as possible. Also, the appropriate choice of spray nozzle orifice size and spray nozzle lance angles that minimise fines loadings should be

determined using the particle size distribution method developed here and/or the optical scintillation instrument. Finally, for any new milk powders produced or any new milk powder plants with washable baghouses built by Fonterra, it is recommended that the particle size distribution method be used to check the fines fractions of these powders or in these new plants.

For washable baghouse design, it is recommended that the design procedure developed here and the air to cloth ratio guidelines of Löffler et al. (1988) be the procedure followed to determine suitable designs. It should be noted that the design must be for the product that requires the lowest air to cloth ratio because a one-size-fits-all approach will lead to operational difficulties if a range of products are made in the plant. It is strongly recommended that stainless steel inspection hatches at the bag level be installed in all current and future milk powder plant washable baghouses to reduce CIP times and to aid in decisions made about the state of the bags. Finally, it is recommended that in future designs of washable baghouses, the annular velocity be reduced to around 15 m / s by increasing the annular gap outside the bag bundle, and that the baghouse clean air plenum is removable to enable easier bag replacement.

With regard to the single cell baghouse built in the Department of Chemical and Process Engineering at the University of Canterbury, it is recommended that electrical technical support be provided so this rig can be used for experimental work. For the installation to be completed all the instrumentation needs to be supplied with power, the control circuits associated with the heating elements and extractor fan must be installed and the timing device needs to be connected to the compressed air solenoid valve.

To fully understand the mechanism causing the baghouse differential pressure to change with the amount of bulk fat in SMP, it is recommended that further research be carried out. This research should use the single cell baghouse to investigate any differences in deposition location on the surface or interior of the filter bag fabric, for SMP with different bulk fat contents. Also studied should be any corresponding differences in porosity, thickness and permeability of the resulting filter cakes.

It is recommended also that bag movement and resulting bag damage be investigated. This work should aim to reduce bag damage through experimental studies investigating the

possibility of using additional support lugs, use of heavier support cages or other options to reduce bag movement.

Further CFD modelling of the CD2 dryer is recommended to improve on the work conducted during this project. Transient rather than steady state simulations that use the two-phase Eulerian-Eulerian as well as the Lagrangian particle tracking models are recommended. A complete model of the CD2 spray dryer is possible if droplet drying was also modelled.

The use of CFD modelling is also recommended to study the flow patterns within the main washable baghouses attached to the CD2 dryer. Baghouse designs with different inlet air configurations, different bag spacings and different outer gaps should be investigated in an attempt to further reduce bag movement. It is also recommended that CFD modelling of the baghouse be performed to assess the claim of GEA Niro A/S of appreciable pre-separation of powder caused by the tangential scroll at the industrial scale.

Once completed, it is recommended that a significant amount of additional research be carried out using the single cell baghouse. These studies could optimise the filter bag pulse cleaning for each product, which would save on compressed air usage and increase bag life times. Also, changing the position of the pulse cleaning ejector may prevent powder build up around the top of the bag. Finally, it is recommended that experiments be conducted on what impact dryer operating parameters have on the filter bag differential pressure.

The final recommendation from this work is to better use the Torbar 402 averaging Pitot tubes installed in the CD2 dryer outlet air stacks. It is recommended that the instruments be moved higher up the outlet air stacks from their current location. It is also recommended that differential pressure transmitters be purchased so that the Torbar 402 differential pressure can be measured, connected to the plant PLC and hence, the air flow through the outlet air stacks routinely displayed on the operators' screens.

References

Agarwal, A.T., 2005. Design guide for dust collectors. Chemical Engineering, 112(2): 42-49.

Allen, R.W.K., Goyder, H.G.D. and Morris, K., 1999. Modelling media movement during cleaning of pulse-jet fabric filters. Chemical Engineering Research and Design, 77(A3): 223-230.

Allen, T., 1997. Particle size measurement - volume 1. Powder sampling and particle size measurement. Chapman & Hall, London.

ANSYS, 2005a. ANSYS CFX Release 10.0. ANSYS Europe Ltd, Riseley.

ANSYS, 2005b. Release 10.0 Documentation for ANSYS Workbench. SAS IP Inc, Canonsburg.

Barnett, T., 2000. Improving the performance of fabric filter dry dust collection equipment. Filtration & Separation, 37(2): 28-32.

Berbner, S. and Löffler, F., 1994. Influence of high temperatures on particle adhesion. Powder Technology, 78(3): 273-280.

Bergmann, L., 2001. Beating the baghouse blues. Chemical Engineering, 108(1): 65-67.

Bethea, R.M., 1978. Air pollution control technology: an engineering analysis point of view. Van Nostrand Reinhold, New York.

Billings, C.E., 1974. Aerosol filtration technology for source emission control. AIChE Symposium Series, 70(137): 341-350.

Billings, C.E. and Wilder, J., 1970. Handbook of fabric filter technology - fabric filter systems study, 1. GCA Corporation, Bedford.

Bloore, C.G., 2005. Personal Communications.

Bloore, C.G., 2002. Spray drying course. Dairy Industry Systems, Dunedin.

Bloore, C.G. and Boag, I.F., 1982. The effect of processing variables on spray dried milk powder. New Zealand Journal of Dairy Science and Technology, 17: 103-120.

Buma, T.J., 1971. Free fat in spray dried-whole milk. 3. Particle size. Its estimation, influence of processing parameters and its relation to free-fat content. Netherlands Milk and Dairy Journal, 25: 53-72.

Buma, T.J. and Henstra, S., 1971. Particle structure of spray-dried milk products as observed by a scanning electron microscope. Netherlands Milk and Dairy Journal, 25: 75-80.

Bylund, G., 2003. Dairy processing handbook. Tetra Pak Processing Systems, Lund.

Calle, S., Contal, P., Thomas, D., Bemer, D. and Leclerc, D., 2002. Description of the clogging and cleaning cycles of filter media. Powder Technology, 123(1): 40-52.

Caputo, A.C. and Pelagagge, P.M., 2000. Baghouse system design based on economic optimization. Environmental Progress, 19(4): 238-245.

Clandeboye Milk Powder Plant Operators, 2004. Personal Communications.

Clarke, A.G., 1996. Cross-duct monitoring of particulate emissions by opacity fluctuations. Environmental Technology, 17: 101-106.

Clarke, A.G., 1998. Industrial air pollution monitoring. Environmental management series 8. Chapman & Hall, London.

Collie, S.J., Gerritsen, M. and Jackson, P.S., 2001. A review of turbulence modelling for use in sail flow analysis. Department of Engineering Science, University of Auckland, Auckland.

Cora, M.G. and Hung, Y., 2002. Controlling industrial particulate emissions: a practical overview of baghouse technology. Environmental Quality Management, 11(4): 53-64.

Croom, M.L., 1995. Filter dust collectors: design and application. McGraw-Hill, New York.

Dickenson, C., 1992. Filters and filtration handbook. Elsevier Advanced Technology, Oxford.

Douglas, J.F., Gasiorek, J.M. and Swaffield, J.A., 2001. Fluid mechanics. Prentice Hall, Upper Saddle River.

Draper, N.R. and Smith, H., 1981. Applied regression analysis. John Wiley & Sons, New York.

Ellenbecker, M.J. and Leith, D., 1980. The effect of dust retention on pressure drop in a high velocity pulse-jet fabric filter. Powder Technology, 25(2): 147-154.

Ellenbecker, M.J. and Leith, D., 1983. Dust removal characteristics of fabrics used in pulse-jet filters. Powder Technology, 36(1): 13-19.

Fäldt, P., Bergenstahl, B. and Carlsson, G., 1993. The surface coverage of fat on food powders analyzed by ESCA (electron spectroscopy for chemical analysis). Food Structure, 12: 225–234.

Fäldt, P. and Bergenstahl, B., 1996a. Changes in surface composition of spray-dried food powders due to lactose crystallization. LWT - Food Science and Technology, 29(5): 438–446.

Fäldt, P. and Bergenstahl, B., 1996b. Spray-dried whey protein/lactose/soybean oil emulsions. 1. surface composition and particle structure. Food Hydrocolloids, 10(4): 421–429.

Fäldt, P. and Sjöholm, I., 1996. Characterization of spray-dried whole milk. Milchwissenschaft, 51(2): 88–92.

Fernandez, E., Schebor, C. and Chirife, J., 2003. Glass transition temperature of regular and lactose hydrolyzed milk powders. Food Science and Technology, 36(5): 547-551.

Fitzpatrick, J.J., Iqbal, T., Delaney, C., Twomey, T. and Keogh, M.K., 2004. Effect of powder properties and storage conditions on the flowability of milk powders with different fat contents. Journal of Food Engineering, 64: 435–444.

Fletcher, D F., Guo, B., Harvie, D J E., Langrish, T A G., Nijdam, J J. and Williams, J., 2003. What is important in the simulation of spray dryer performance and how do current CFD models perform? Third International Conference on CFD in the Minerals and Process Industries, Melbourne, pp. 357-363.

Foster, K.D., Bronlund, J.E. and Paterson, A.H.J., 2005. The contribution of milk fat towards the caking of dairy powders. International Dairy Journal, 15(1): 85-91.

Frey, M.G., 2001. Product recovery from spray dryers. Technical University of Denmark, Lyngby.

Ginesi, D. and Grebe, G., 1987. Flowmeters a performance review. Chemical Engineering, 94(9): 102-118.

Goldstein, J. and Yakowitz, H., 1975. Practical scanning electron microscopy: electron and ion microprobe analysis. Plenum Press, New York.

Good, J. and Cisar, V., 2004. Averaging pitot tubes: six steps to successful installation. Veris Inc., Niwot.

Graebel, W.P., 2001. Engineering fluid mechanics – the international student edition. Taylor and Francis, New York.

Guo, B., Langrish, T.A.G. and Fletcher, D.F., 2003. Simulation of gas flow instability in a spray dryer. Chemical Engineering Research and Design, 81(A6): 631-638.

Halliday, D., Resnick, R. and Walker, J., 2005. Fundamentals of physics. Hoboken, New York.

Harvie, D.J.E., Langrish, T.A.G. and Fletcher, D.F., 2001. Numerical simulations of gas flow patterns within a tall-from spray dryer. Chemical Engineering Research and Design, 79(A3): 235-248.

Harvie, D.J.E., Langrish, T.A.G. and Fletcher, D.F., 2002. A computational fluid dynamics study of a tall-from spray dryer. Food and Bioproducts Processing, 80(C3): 163-175.

Hearle, J.W.S., Sparrow, J.T. and Cross, P.M., 1972. The use of the scanning electron microscope. Pergamon Press, Oxford.

Hennings, C., Kockel, T.K. and Langrish, T.A.G., 2001. New measurement of the sticky behaviour of skim milk powder. Drying Technology, 19(3): 471-484.

Heywood, V.H., 1971. Scanning electron microscopy: systematic and evolutionary applications. Academic Press, London

Hill, M., 1999. Particulate monitoring solutions technology. PCME Ltd, St Ives.

Hirst, R., 2005. Personal Communications.

Hrouzek, M., Voda, A., Stark, M. and Chevrier, J., 1995. Model of the cantilever used as a weak force sensor in atomic force microscopy, 16th IFAC World Congress, Prague.

Huang, L., Kumar, K. and Mujumdar, A.S., 2003a. A parametric study of the gas flow patterns and drying performance of co-current spray dryer: results of a computational fluid dynamics study. Drying Technology, 21(6): 957-978.

Huang, L., Kumar, K. and Mujumdar, A.S., 2003b. Use of computational fluid dynamics to evaluate alternative spray dryer chamber configurations. Drying Technology, 21(3): 385-412.

Huang, L., Kumar, K. and Mujumdar, A.S., 2006. A comparative study of a spray dryer with rotary disc atomizer and pressure nozzle using computational fluid dynamic simulations. Chemical Engineering and Processing, 45(6): 461-470.

Humphries, W., 1981. Influence of cloth structure on dust dislodgement from fabric filters. Powder Technology, 28(2): 189-194.

Hunziker, 1949. Condensed milk and milk powder. La Grange, Illinois.

Intensiv-Filter, 1999. Dedusting technology filter media. Intensiv-Filter GmbH & Co, Langenberg.

Kavouras, A. and Krammer, G., 2003. Distributions of age, thickness and gas velocity in the cake of jet pulsed filters - application and validation of a generations filter model. Chemical Engineering Science, 58(1): 223-238.

Keogh, M.K., Murray, C.A. and O'Kennedy, B.T., 2003. Effects of ultrafiltration of whole milk on some properties of spray-dried milk powders. International Dairy Journal, 13(12): 995–1002.

Kieviet, F.G. and Kerkhof, P.J.A.M., 1996. Using computational fluid dynamics to model product quality in spray drying: air flow, temperature and humidity patterns. 10th International Drying Symposium, Krakow, pp. 259-266.

Kieviet, F.G., van Raaij, J., de Moor, P.P.E.A. and Kerkhof, P.J.A.M., 1997. Measurement and modelling of the air low pattern in a pilot-plant spray dryer. Chemical Engineering Research and Design, 75(A3): 321-328.

Kim, E.H.J., Chen, X.D. and Pearce, D.L., 2002. Surface characterization of four industrial spray-dried dairy powders in relation to chemical composition, structure and wetting property. Colloids and Surfaces B: Biointerfaces, 26: 197-212.

Kim, E.H.J., Chen, X.D. and Pearce, D.L., 2003. On the mechanisms of surface formation and the surface compositions of industrial milk powders. Drying Technology, 21(2): 265-278.

Kippax, P., Unknown. Measuring particle size using modern laser diffraction techniques. Malvern Instruments Ltd, Malvern.

Klingel, R. and Löffler, F., 1984. Investigations on optimal cleaning conditions for bag filters with pulse jet cleaning. Chemical Engineering and Processing, 18(4): 189-198.

Klinzing, G.E., 1997. Pneumatic conveying of solids. Chapman & Hall, London.

Koch, D., Seville, J. and Clift, R., 1996. Dusk cake detachment from gas filters. Powder Technology, 86(1): 21-29.

Langrish, T.A.G., 1993. The flow patterns of gas and particles in spray dryers. Chemical Engineering in Australia, 18(4): 16-20.

Langrish, T.A.G., Keey, R.B. and Hutchinson, C.A., 1992. Flow visualization in a spray dryer fitted with a vaned-wheel atomizer. Chemical Engineering Research and Design, 70(A5): 385-394.

Langrish, T.A.G., Williams, J. and Fletcher, D.F., 2004. Simulation of the effects of inlet swirl on gas flow patterns in a pilot-scale spray dryer. Chemical Engineering Research and Design, 82(A7): 821-833.

LeBarbier, C., Kockel, T.K., Fletcher, D.F. and Langrish, T.A.G., 2001. Experimental measurement and numerical simulation of the effect of swirl on flow stability in spray dryers. Chemical Engineering Research and Design, 79(A3): 260-268.

Leith, D.S. and First, M.W., 1977a. Performance of a pulse-jet filter at high filtration velocity, 3. Penetration by fault processes. Journal of Air Pollution Control Association 27(8): 754-762.

Leith, D.S. and First, M.W., 1977b. Pressure drop in a pulse-jet fabric filter. Filtration & Separation, 14(6): 473-474.

Leith, D.S., First, M.W. and Gibson, D.D., 1978. Effect of modified cleaning pulses on pulse jet filter performance. Filtration & Separation, 15(5): 400-406.

Leith, D. and Allen, R.W.K., 1986. Dust filtration by fabric filters. Progress in Filtration and Separation. Elsevier, Oxford, UK.

Li, X. and Zbicinski, I., 2005. A sensitivity study on CFD modelling of cocurrent spray-drying process. Drying Technology, 23(8): 1681-1691.

Liou, T. and Hwang, J., 1992. Developing heat transfer and friction in a ribbed rectangular duct with flow separation at inlet. Journal of Heat Transfer, 114(August): 565-573.

Löffler, F., Dietrich, H. and Flatt, W., 1988. Dust collection with bag filters and envelope filters. Wiley, Chichester, U.K.

Löffler, F. and Sievert, J., 1987. Cleaning mechanisms in pulse-jet fabric filters. Filtration & Separation, 24(2): 110-113.

Lydon, R., 2004. Filter media surface modification technology: state of the art. Filtration & Seperation, 41(9): 20-21.

Machen, K., 2001. Characterisation of a washable baghouse in a milk powder manufacturing plant. Dissertation Thesis, Massey University, Palmerston North.

Manuell, D. and Bardsley, T., 2000. Air pollution measurement manual: Volume two: a practical guide to sampling and analysis. Clean Air Society of Australia and New Zealand, Mitcham.

Masters, K., 1972. Spray drying: an introduction to principles, operational practice and applications. Leonard Hill, London.

Matheson, K., 1991. Investigation into relationships between physical and functional properties of milk powder. DT91R01, New Zealand Dairy Research Institute, Palmerston North.

MathWorks, 2004. Matlab 7.0 Release 14. MathWorks Inc, Natick.

Maynard, E., 2006. Designing pneumatic conveying systems. Chemical Engineering Progress, 102(5): 23-33.

McKenna, A.B., Lloyd, R.J., Munro, P.A. and Singh, H., 1999. Microstructure of whole milk powder and of insolubles detected by powder functional testing. Scanning, 21: 305–315.

Menter, F.R., 1994. Two-equation eddy-viscosity turbulence models. American Institute of Aeronautics and Astronautics Journal, 32(8): 1598-1605.

Menter, F.R., 2006. Introduction to turbulence modelling. ANSYS Germany, Otterfing.

Millqvist-Fureby, A., Elofsson, U. and Bergenstahl, B., 2001. Surface composition of spray-dried milk protein-stabilised emulsions in relation to pre-heat treatment of proteins. Colloids and Surfaces B: Biointerfaces, 21: 47-58.

Mills, D., 2004. Pneumatic conveying design guide. Elsevier/Butterworth-Heinemann, Oxford.

Molerus, O. and Wellman, P., 1981. A new concept for the calculation of pressure drop with hydraulic transport of solids in horizontal pipes. Chemical Engineering Science, 36(10): 1623-1632.

Montgomery, D.C., 2001. Design and analysis of experiments. John Wiley & Sons, New York.

Moore, S., Rubak, J. and Jolin, M., 1996. Selecting baghouse dust collectors. Plant Engineering, 50(11): 58-62.

Moran, C.P., 2005. Personal Communications.

Moran, C.P., 2006. Personal Communications.

Morgan, L. and Walters, M., 1999. Test your dust - getting dust collection right. Ceramic Industry, 149(7): 24-29.

Morris, K. and Allen, R.W.K., 1996. The influence of dust and gas properties on cake adhesion in fabric filters. Filtration & Separation, 33(4): 339-343.

Morris, K., Cursley, C.J. and Allen, R.W.K., 1991. The role of venturis in pulse-jet filters. Filtration & Separation, 28(1): 33-36.

Moulder, J.F., Stickle, W.F., Sobol, P.T. and Bomben, K.D., 1992. Handbook of x-ray photoelectron spectroscopy. Perkin-Elmer Corporation, Minnesota.

Murti, R.A., Paterson, A.H.J., Pearce, D.L. and Bronlund, J.E., 2006. Characterisation of the sticky point of skim milk powder using the particle gun technique. 5th World Congress on Particle Technology, Orlando.

Neiva, A. and Goldstein, L., 2003. A procedure for calculating pressure drop during the build-up of dust filter cakes. Chemical Engineering and Processing, 42(6): 495-501.

Nijdam, J.J. and Langrish, T.A.G., 2005. An investigation of milk powders produced by a laboratory-scale spray dryer. Drying Technology, 23: 1043–1056.

Nijdam, J.J. and Langrish, T.A.G., 2006. The effect of surface composition on the functional properties of milk powders. Journal of Food Engineering, 77: 919–925.

NZTM3; 5.1, Issue 7.0, June 2000

Oakley, D.E. and Bahu, R.E., 1990. Computational modelling of spray dryers. European Symposium on Computer Aided Process Engineering - 2, Toulouse, pp. 493-498.

O'Brien, J., 2004. Personal Communications.

Oertel, H., 2004. Prandtl's essentials of fluid mechanics. Springer, New York.

Orr, C., 1977. Filtration - principles and practices part 1. Marcel Dekker, New York.

Ozkan, N., Withy, B. and Chen, X.D., 2003. Effects of time, temperature and pressure on the cake formation of milk powders. Journal of Food Engineering, 58: 355-361.

Ozkan, N., Walisinghe, N. and Chen, X.D., 2002. Characterisation of stickiness and cake formation in whole and skim milk powders. Journal of Food Engineering, 55: 293-303.

Ozmen, L. and Langrish, T.A.G., 2002. Comparison of glass transition temperature and sticky point temperature for skim milk powder. Drying Technology, 20(6): 1177-1192.

Ozmen, L. and Langrish, T.A.G., 2003. An experimental investigation of the wall deposition of milk powder in a pilot-scale spray dryer. Drying Technology, 21(7): 1253-1272.

Parker, K.R., 1997. Technological advances in high-efficiency particulate collection. Proceedings of the Institution of Mechanical Engineers, 211(1): 53-65.

Pearce, D.L., 2005. Personal Communications.

Press, W.H., Flannery, B.P., Teukolsky, S.A. and Vetterling, W.T., 1989. Numerical recipes. Cambridge University Press, Cambridge.

Ranade, V.V., 2002. Computational flow modelling for chemical reactor engineering. Academic Press, San Diego.

Rennie, P.R., Chen, X.D., Hargreaves, C. and Mackereth, A.R., 1999. A study of the cohesion of dairy powders. Journal of Food Engineering, 39: 277-284.

Rhodes, M.J., 1998. Introduction to particle technology. John Wiley & Sons, New York.

Richardson, J.F., Harker, J.H. and Backhurst, J.R., 2002. Coulson & Richardson's chemical engineering - volume 2. Particle technology & separation processes. Butterworth-Heinemann, Oxford.

Rothwell, E., 1987. Who needs better filter media? Filtration & Separation, 24(2): 104-108.

Ruthven, D.M., 1997. Encyclopaedia of separation technology, 2. John Wiley & Sons, New York.

Schmidt, E., 1995. Experimental investigation into the compression of dust cakes deposited on filter media. Filtration & Separation, 32(8): 789-793.

Schmidt, E. and Löffler, F., 1990. Preparation of dust cakes for microscopic examination. Powder Technology, 60(2): 173-177.

Schweers, E. and Löffler, F., 1994. Realistic modelling of the behaviour of fibrous filters through consideration of filter structure. Powder Technology, 80(3): 191-206.

Silva, C.R.N., Negrini, V.S., Aguiar, M.L. and Coury, J.R., 1999. Influence of gas velocity on cake formation and detachment. Powder Technology, 101(2): 165-172.

Snoeren, T.H.M., Damman, A.J. and Klok, H.J., 1982. The viscosity of skim-milk concentrates. Netherlands Milk and Dairy Journal, 36: 305-316.

Southwell, D.B., Langrish, T.A.G. and Fletcher, D.F., 1999. Process intensification in spray dryers by turbulence enhancement. Chemical Engineering Research and Design, 77(A3): 189-205.

Southwell, D.B., Langrish, T.A.G. and Fletcher, D.F., 2001. Use of computational fluid dynamics techniques to assess design alternatives for the plenum chamber of a small spray dryer. Drying Technology, 19(2): 257-268.

Sparrow, E.M. and Cur, N., 1982. Turbulent heat transfer in a symmetrically or asymmetrically heated flat rectangular duct with flow separation at inlet. Journal of Heat Transfer, 104(February): 82-89.

Spreer, E., 1998. Milk and dairy product technology. Marcel Dekker Inc, New York.

Stafford, R.A., Fauroux, O. and Glass, D.H., 1996. Flow visualisation and instantaneous velocity measurements of spray dryer gas and spray flows using particle image velocimetry. 10th International Drying Symposium, Krakow, pp. 555-562.

Stapper, H.L.C.M., Baldwin, A.J., Boniface, H.A. and Ward, D.E.J., 1976. The collection of milk powders with a reverse pulse bag filter. New Zealand Journal of Dairy Science and Technology, 11: 267-272.

Straatsma, J., Van Houwelingen, G., Steenbergen, A.E. and De Jong, P., 1999. Spray drying of food products: 1. simulation model. Journal of Food Engineering, 42: 67-72.

Teunou, E., Fitzpatrick, J.J. and Synnott, E.C., 1999. Characterisation of food powder flowability. Journal of Food Engineering 39: 31–37.

Truong, H.T., 2005. Personal Communications.

Tsai, C., Tsai, M. and Lu, H., 2000. Effect of filtration velocity and filtration pressure drop on the bag-cleaning performance of a pulse-jet baghouse. Separation Science and Technology, 35(2): 211-226.

Tu, J.Y. and Fletcher, C.A.J., 1995. Continuum hypothesis in the computation of gas-solid flows. Computational Fluid Dynamics. Springer-Verlag, Berlin.

Turner, J.H., McKenna, J.D., Mycock, J.C., Nunn, A.B. and Vatavuk, W.M., 1998. Section 6: particulate matter controls - chapter 1: baghouses and filters, USEPA/452/B-02-001. United States Environmental Protection Agency, Research Triangle Park.

Ullum, T., 2006. Simulation of a spray dryer with a rotary atomizer: the appearance of vortex breakdown. 15th International Drying Symposium, Budapest.

USEPA Emissions Measurement Centre, 1977, Method 5 – determination of particulate matter emissions from stationary sources. United States Environmental Protection Agency, Research Triangle Park.

van Swaail, W.P.M., Buurman, C. and van Breugel, I.W., 1970. Shear stresses on the wall of a dense gas - solids riser. Chemical Engineering Science, 25(11): 1818-1820.

Versteeg, H.K. and Malalasekera, W., 1995. An introduction to computational fluid dynamics - the finite volume method. Pearson Education Ltd, Harlow.

Vidmar, T.J., 1990. Selecting a dust collection system. Plant Engineering, 44(8): 70-73.

Weigert, T. and Ripperger, S., 1997. Effect of filter fabric blinding on cake filtration. Filtration & Separation, 24(3): 507-510.

Wesseling, P., 2001. Principles of computational fluid dynamics. Springer-Verlag, Berlin.

Westergaard, V., 2003. Sanitary bag filter - SANICIP. Niro A/S, Gladsaxevej.

White, F.M., 1999. Fluid mechanics. McGraw-Hill, Boston.

Wight, G.D., 1994. Fundamentals of air sampling. CRC Press Inc, Boca Raton.

Williams, A.M., Jones, J.R., Paterson, A.H.J. and Pearce, D.L., 2004, Fines flowrate estimation using pressure drop. Society of Chemical Engineers New Zealand Conference, Christchurch, New Zealand.

Williams, A.M., Jones, J.R., Paterson, A.H.J. and Pearce, D.L., 2006, Agglomeration in the spray zone of a spray drier: determining an agglomeration index. Proceedings of 5th World Congress on Particle Technology., Orlando.

Wiryawan, I., 2005. Personal Communications.

Wiryawan, I. and Trinh, T., 2003a. Mechanical strength comparison of filter bag materials. Massey University, Palmerston North.

Wiryawan, I. and Trinh, T., 2003b. Tensile strength of baghouse filter materials. Massey University, Palmerston North.

Wiryawan, I. and Trinh, T., 2003c. Accelerated abrasion test by water blasting. Massey University, Palmerston North.

Wiryawan, I. and Trinh, T., 2003d. Characterisation of washable baghouses. Massey University, Palmerston North.

Yan, Y. and Stewart, D., 2001. Guide to the flow measurement of particulate solids in pipelines. Institute of Measurement and Control, London.

Zielinski, R.S., 2003. Keep pulse-jet baghouses running well. Chemical Engineering, 110(6): 58-61.

Appendix A – Background Information on Milk Powder Plants

A1 – Fonterra Clandeboye Dryer 2 Process Description..... A2

A2 – Fonterra Whareroa Powder 2 Process Description A15

A3 – Fonterra Clandeboye Dryer 2 Process Block Diagram A24

A4 – Fonterra Edendale Dryers 2 and 3 Visit Report A28

John Gabites
Department of Chemical and Process Engineering
University of Canterbury
Christchurch, New Zealand

Clandeboye Dryer 2 Process Description

March 2004

Prepared for:

James Winchester

1. Milk Reception and Treatment

Raw milk is unloaded from tankers, stored and then chilled on route to either the cheese hall or the four powder milk treatment modules. Each powder milk treatment module filters, pasteurises and separates the milk into cream, skim and solids. The skim is standardised using cream for fat levels and permeate for protein levels.

2. Evaporation

The supply to each evaporator is from a feed balance tank. The standardised milk is pre-heated in a plate heat exchanger using condensate, it passes through the first and second stage calandria of the chosen evaporator and in the case of high heat products, is fed through the top of two flash vessels. The feed is then heat treated firstly by direct steam injection with 1.1 bar steam and then held for 10 seconds in holding tubes at approximately 84 ^{o}C.

The process is designed for vitamin addition with one line dosing after the feed balance tank and three lines dosing after the pasteurisation section. However, the majority of the products produced do not require vitamin addition.

Heat is recovered from the milk, firstly by reverse passage through the pre-heat plate heat exchanger mentioned above and then through the bottom of the flash vessels (if the product is high heat).

Five evaporators are available for concentration of the milk. All are four-effect evaporators with two mechanical vapour recompression (MVR) effects and two thermal vapour recompression (TVR) effects. There are two Dryer 1 (D1) evaporators (#1 and #2) and three Dryer 2 (D2) evaporators (#3, #4 and #5) which can supply either the D1 or D2 dryers. Evaporators one and two were built with the original powder plant D1, whereas evaporators three, four and five were built at the same time as D2.

3. Spray Drying

The D2 dryer was designed by GEA Niro A/S and built in 2001. The dryer was designed to produce agglomerated powders, but the majority of powders produced (skim milk, whole milk and milk protein concentrate powders (MPC)) are not agglomerated powders.

3.1. Feed

There are two identical feed lines for the supply of concentrate to the top of the dryer. The feed lines are changed approximately every 24 hours allowing a continuous flow of concentrate to the dryer while one line is cleaned.

Each feed line is supplied from one of two feed silos, each holding 8 m^3 of concentrate in the range of 48 – 50 % total solids. The feed is swapped between these two silos every eight hours. The flow rate of concentrate is product dependant, MPC is fed at roughly 15 tonne / hr, skim and whole milk at 25 tonne / hr.

A control loop exists to divert any low solids concentrate, which has an adverse effect on baghouse performance, to the 30 m^3 low solids silo. This low solids product is slowly blended back into concentrate at the correct total solids on route to the dryer.

3.2. Preheat

Concentrate is heated in two stages to obtain the appropriate viscosity required for the specific powder properties, droplet size, bulk density and solubility for example.

3.2.1. Spiral Flow Shell and Tube Heat Exchanger

Using 80 ^{o}C hot water, the concentrate from the feed tank is heated to roughly 60 ^{o}C in the spiral flow shell and tube heat exchanger shown in Figure 1 below.

Figure 1: Spiral flow heat exchanger and supply pumps

3.2.2. Lenient Steam Injection

The second stage of concentrate heating is achieved by lenient steam injection (LSI). Here, 6 bar steam is dynamically mixed with the concentrate increasing the concentrate temperature to around 70 ^{o}C. The LSI shown in Figure 2 provides minimal heat damage to the concentrate.

Figure 2: Lenient steam injector

3.3. Filter

Concentrate is pumped through two 200-micron filters working in parallel to remove large milk globules and scale from the evaporators. Another parallel set of filters is sitting idle for use when the first set becomes blocked (Figure 3). Filter lines are changed either every eight hours or when the pressure differential across the filters exceeds 1.0 to 1.5 bar.

Figure 3: Inline filters and a removed filter

3.4. Homogenisers

Two-stage homogenisation is used to achieve two goals. Firstly, the free fat content of the milk is reduced thus improving the keeping quality of the final product. Secondly, the homogeniser pump increases the pressure of the feed to that required for atomisation at the lances.

The homogenisation occurs in two stages in two homogenisers working in parallel (Figure 4). In the first stage, large fat globules are forced through an orifice reducing their size, thus stabilising the emulsion. In the second stage, concentrate is forced through a second orifice breaking up any reagglomerated fat.

Figure 4: Feed line two stage homogenisers

3.5. Lances

Atomisation occurs at the nozzles located on the end of the lances by forcing the concentrate through an orifice at high pressure. This greatly increases the surface area of the milk, hence enhancing the drying rate in the main drying chamber.

The two feed lines have a series of 15 separate lances. This significantly reduces the downtime required for a change in feed line; only lances from the first line have to be manually removed from the dryer and replaced by those of the second line for this to be accomplished. Figure 5 below shows the blue feed line one lances inserted into the drying chamber.

To ensure the temperature of each lance inside the dryer does not become excessively high, ambient air is fed to each lance from a blower situated on top of the drying chamber. This cooling is only sufficient if concentrate is flowing through the nozzles, hence lances must be removed if there is no concentrate flow.

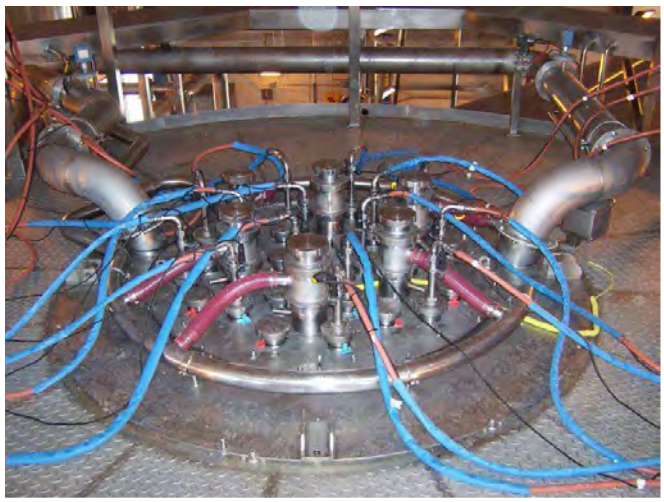

Figure 5: Lance inlets, fines return and cooling lines on top of dryer

3.5.1. Nozzles

The atomiser nozzles used are the Delavan SDX SG. Concentrate is supplied from the homogenisers into the nozzles. Here, the liquid is accelerated centrifugally in the swirl chamber, passes through an orifice and enters the drying chamber in a thin film at high velocity.

The two orifice sizes used are 2.4 mm diameter for MPC and 3.0 mm diameter for skim and whole milk. The larger orifice size for skim and whole milk maintains the flow required through the limited number of available lances.

The nozzles are individually angled to obtain an optimum spray angle. A poor spray angle can lead to powder build up on the chamber walls and excessive entrainment of powder in the dryer exhausts. Spray angles from the orifices are 65 degrees for the 2.4 mm orifice and 70 degrees for the 3.0 mm orifice. Spray angles also increase as the size of the swirl chamber decreases and as the fluid viscosity decreases.

Throughout a run, the number of lances in use changes due to fluctuations in the pressure at the nozzles. On start up, lances come on line one by one as this pressure reaches and exceeds

the set point of 250 bar. Blocked nozzles arise during production, increasing the nozzle pressure beyond this set point. To compensate, additional lances are used to reduce the nozzle pressure.

3.6. Drying Air

Around 60 kg / s of approximately 200 ^{o}C air is supplied to the top of the dryer chamber through the duct shown in Figure 6. The air is indirectly heated in a tube bank steam radiator using 34 bar steam. A damper on the feed line partially controls the inlet air flow rate to the top of the drying chamber.

The dryer air passes through a filtration screen and then an air disperser on entry to the chamber. The disperser is a baffle that imparts the required air flow patterns on the inlet air. Poor velocities have negative effects, influencing the rate and drying pattern in the chamber and deposits on the chamber walls. A blower located on the top of the dryer cools the disperser itself to prevent damage due to overheating.

Figure 6: Dryer air inlet duct

3.7. Drying Chamber

The dryer is a Niro MSD 2000 design. This is a mixed air flow chamber with a small cylindrical section at the top of the dryer and a large conical section tapering towards the powder outlet at the bottom of the chamber.

The atomised concentrate and dryer air are forced down the centre of the dryer cone. Moisture evaporates from the concentrate and particles of milk powder fall to the bottom of the cone. The temperature of the drying air decreases due to the energy removed during evaporation.

The dryer air flows up the side of the chamber shown in Figure 7 to two outlet ducts on the eastern and western sides of the chamber, hence the mixed air flow. These air flows are controlled by the blowers at the bottom of each baghouse stack and are typically 70 ^{o}C in temperature on skim milk production and 60 ^{o}C when producing MPC. Up to 40% of skim milk powder and 90% of the MPC powder produced is believed to become entrained in this air flow and pass into the main baghouses. Other factors affecting the solids concentrations of

these air flows are particle size and density; entrainment is inversely proportional to these two properties. The maximum solids' loading to each baghouse is believed to be 20 kg / s.

Two rings of 12 pneumatic hammers are located about half way up the conical section of the dryer. These hammers are pulsed in groups of four while the dryer is on product, banging the chamber walls in an attempt to prevent powder build up.

The main chamber pressure is maintained slightly below atmospheric. This enables easy access for inspection by operators during production and prevents product losses due to leaks.

The dryer is designed to produce agglomerated powders. The fines collected in the three baghouses can be returned to the top of the dryer. Here, dry powder sticks to the finely dispersed concentrate helping to form agglomerated powders. Returning fines to the top of the dryer is supposed to reduce the loadings on the main baghouses. This effect has not been observed at Clandeboye.

Figure 7: Drying chamber walls and static fluid bed

3.7.1. Static Fluid Bed

The dryer has an internal fluid bed mounted at the bottom of the main chamber (Figure 7). The presence of a static fluid bed (SFB) allows for higher chamber moistures, increases the capacity of the dryer and more lenient drying (i.e. less likely occurrence of heat damaged powder).

The 16 kg / s of air supplied to the SFB is heated between 80 to 120 ^{o}C using 34 bar steam. This maintains a powder temperature in the vicinity of 60 to 80 ^{o}C, drying the powder to a total solids of 96 to 97.5. Both temperatures are product dependant. The inlet air passes through a distributor before flowing up through a specially designed perforated plate. The

plate is such that the air flow prevents powder dead spots developing, which have been a problem in some Niro designed dryers in the industry.

Two weirs located on the northern and southern sides of the dryer are the powder outlets from the SFB. The height of the weirs can be adjusted according to the desired moisture content of the powder exiting the bed. An increase in weir height increases the powder residence time in the bed and therefore decreases the moisture content. No moisture contents are measured routinely at the SFB.

The air velocity in the main chamber affects the performance of the SFB. If the air flow above the bed is too high, powder can be forced into and foul the perforated plate. If the velocity is too low, excessive powder on the SFB can be entrained in the air flow out of the chamber ducts. This can also occur if the air flow through the perforated plate is too high. The chamber plenum pressure is used as an indicator of an appropriate SFB air flow.

Fines collected in the three baghouses can also be returned to the SFB. This helps to build up the fluid bed, preventing fouling of the perforated plate and assisting in the formation of agglomerated powders if required.

3.8. Vibrating Fluid Beds

The total powder exiting the SFB is split into two and fed to the first series of vibrating fluid beds, VF 1a and VF 1b (Figure 8). Fluid bed drying is used for further drying of the product and ensures uniform temperature and moisture content powders are produced. The vibrating fluid beds are slightly angled. Air flow through the perforated plate is also angled, and combined with the vibration, moves the powder from one end of the bed to the other. The air supply to each bed is at 5 m^3 / s and in the vicinity of 80 ^oC.

The powder from VF 1a and 1b are combined on entry to VF 2. This fluid bed is also vibrated but is split into two sections. In the first section, 4 m^3 / s of hot air at roughly 40 ^oC passes through the powder. The second section is used to cool the powder to approximately 35 ^oC. For this, 2.5 m^3 / s of 25 ^oC dehumidified air is used.

The cooling section temperature control is not currently used due to the adverse effects dehumidification can cause. Running the dehumidifier causes a serious risk of microbiological contamination. Also, collected condensate can entrain in the supply air, causing fouling of the fluid bed on contact with the powder.

Fines recovered from baghouse 1 can be returned to VF 1a or VF 2 and fines from baghouse 2 can be returned to VF 1b or VF 2. Typically the fines are returned to the first of the VF beds. This allows the fines to dry to the required moisture content as otherwise they would have higher moisture content than powders that overflowed from the SFB and did not pass through the baghouses. The fines from the VF baghouse are typically returned to the end of the last VF bed.

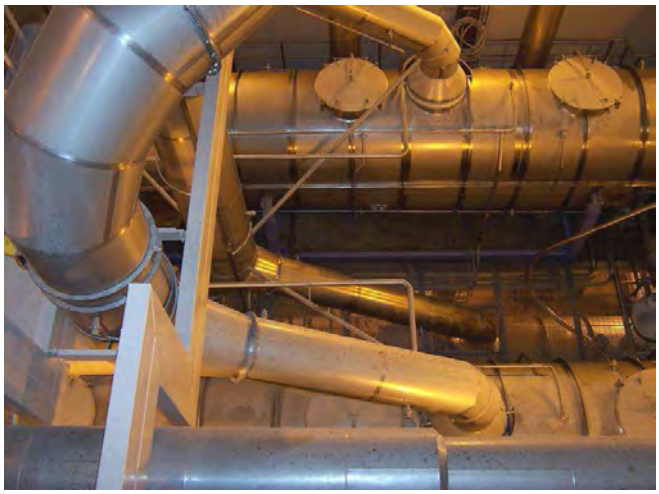

Figure 8: Vibrating fluid beds 1a, 1b and 2

3.9. Lecithin Dosing

A lecithin dosing system exists to coat the powder on transfer between the first and second fluid beds. Lecithin is oil containing anhydrous milk fat (AMF) and soya bean oil that improves powder solubility. This system is designed to aid in the production of agglomerated powders, which the dryer does not do. Hence, this system is not used.

3.10. Powder Packing

The cooled powder from VF 2 is sifted to break up any lumps or remove any foreign objects from the powder. Three mills are then used to mill the powder to a uniform size that is then passed to a surge hopper. The hopper ensures a constant supply of powder to the AVAPAC and SAPAC systems. Skim milk can be packed in 25 or 100 kg bags, whole milk in 25 or 800 kg bags and MPC in 20 kg bags.

3.11. Main Baghouses

Baghouses (BH) 1 and 2 are used to filter the powder entrained in the dryer air. These baghouses sit at the north east and north west of the drying hall.

As mentioned above, the loading on each baghouse is dependant on product type, lance angle and particle size. Smaller particles are more easily drawn straight out of the chamber ducts to BH 1 and 2.

The inlet to each BH from the dryer is tangential. It is believed that this imparts significant motion on the bags in the baghouse, which may lead to excessive bag wear. The weight of the supporting bag cages is much heavier for those bags on the circumference of the bag bundle in an attempt to limit the impact of the tangential entry.

Pressures are measured on the dirty air and clean air sides of the bags. This allows calculation of the all important pressure differentials. Operators typically try to run the baghouses with a differential pressure of 60 mm of water gauge when producing MPC 80 and 90 mm of water gauge when producing skim milk. The ratio between blower speeds on the main stacks is manipulated to ensure both baghouses run at these values. Operating in this fashion prolongs

the life of damaged bags in the first baghouse and forces the second baghouse to operate with higher loadings.

Other measurements made on the BH 2 stack are the air temperature, relative and absolute humidity. These measurements are used for plant mass and energy balances.

A systematic drop in differential pressure indicates bag failure. This can be supported by emission measurements taken on both stacks. Stack emission metres measure powder concentrations between 0 and 25 mg / Nm^3, milligrams per normal cubic meter of air. Emission levels are slightly higher at the start of a run, presumably before the cake required for effective filtration develops on the bags.

Air cleaning of the bags occurs as follows: a 0.15s pulse of compressed air into two socks, a 2.40 s hold, then a 0.15 s pulse in two new socks. At the end of the cycle (120 pulses and holds) there is a reset delay of 1 s. Therefore the cycle time is 307 s, much larger than the 180 s suggested in the Niro instruction manual.

Figure 9: Baghouse #2 cone heating system

The cone of each baghouse is heated to prevent formation of condensation that would lead to powder sticking to the baghouse walls. Air is circulated through a 10 bar steam heater exiting at 65 ^oC. This air circulates around the jacketed cone of the baghouse and merges with the blower inlet air supply. Air is drawn off this loop downstream of the blower, then through the perforated conical bottom of the baghouse. The plenum pressure here must be such that powder does not fall through the plate or be blown off the plate. It is to be gently bubbled to the powder outlet.

Figure 10: Baghouse #2 perforated cone

As in the main dryer chamber, pneumatic hammers are pulsed periodically to move any caked powder from the chamber walls. Four such hammers are placed in a ring in the bottom section of each baghouse.

The baghouses are designed and built for CIP cleaning. A CIP manifold sits on top of the baghouse supplying the five turbine nozzles to clean the outlet chamber and each of the 240 compressed air jets which in turn clean the inside of each bag. The cell plate, where the bags are supported, has a series of nozzles for cleaning purposes. These nozzles are purged with compressed air during production to prevent powder deposits. Eight retractable CIP spray nozzles are located in the main chamber and four in the plenum chamber. On completion of the CIP and loss of pressure, the nozzle heads withdraw from the chamber ready for production.

The long down time required for the bags to dry out means CIPs are very rarely done; only one CIP was performed in the 2003/2004 season. The six to seven hours required to manually remove and replace all bags is quicker than the baghouse CIP, hence it is the preferred ‘cleaning’ option.

Figure 11: Main chamber of VF and #2 baghouses

3.12. VF Baghouse

The drying air from the three vibrating fluid beds is combined in one feed line and sent to the VF baghouse. As Figure 11 shows, this baghouse is physically smaller than baghouses 1 and 2, containing 164 filter socks. Again, these socks are cleaned in pairs as above except that the hold between pulses is 3.99 s giving a total cleaning cycle of 340 s. Even with fewer bags this cycle time is almost twice the 180 s suggested in the Niro instruction manual.

The VF baghouse has the same features of the main baghouses, i.e. loaded air entry is tangential, pressures are measured in the plenum, the clean air and the dirty air side of the bags, emission levels are measured in the VF baghouse stack, hammers are present on the chamber and the plenum cone is heated.

The loadings on the VF baghouse are much less than the main baghouses; the differential pressures are only approximately 30 - 50 mm of water gauge pressure compared to 80 – 110 mm H_2O in BH 1 and 2.

The CIP set up of this baghouse is identical to the main baghouses. The only differences are that fewer compressed air jet feeds are required (Figure 12) and the number of chamber nozzles is four.

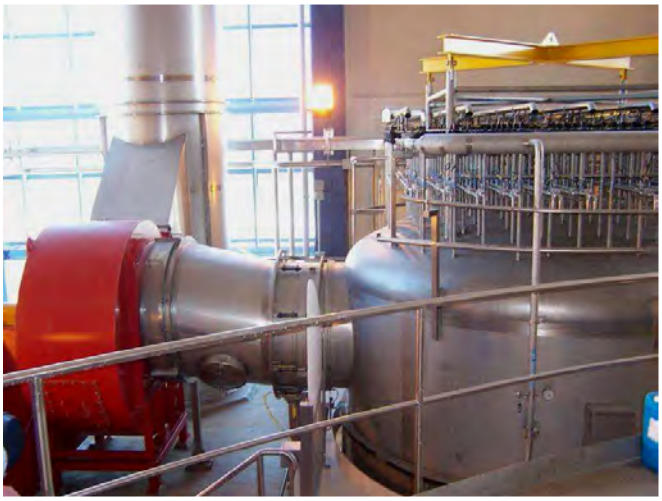

Figure 12: VF baghouse clean air outlet

This page is intentionally left blank

John Gabites
Department of Chemical and Process Engineering
University of Canterbury
Christchurch, New Zealand

Whareroa Powder 2 Process Description

June 2005

Prepared for:

James Winchester

1. Background

Whareroa Powder 2 is one of five milk powder plants located on the Whareroa site, south of Hawera. The plant was first located in Midhurst but was moved to the Whareroa site in 1983. A rotary disc was originally used for concentrate atomisation, a cyclone system for fines collection and four vibrating fluid (VF) beds for powder drying after leaving the drying chamber.

Prior to the start of the 2000/2001 season, a major retrofit of the plant was undertaken so the plant met regulatory requirements for stack emissions and noise levels. The retrofit saw the disc atomiser replaced with six nozzle lances, one metre added to the drying chamber body, the cyclones replaced with a single Leubbers designed washable baghouse, the first washable baghouse installed in New Zealand, and two of the VF beds removed.

The number 2 dryer now has a capacity of 3.4 tonnes per hour. Products produced are instant and agglomerated skim milk powders, whole milk powder and cream powder.

2. Concentrate Handling

Approximately 5.7 tonnes / hr of 46 – 47 % total solids concentrate comes off the single evaporator and feeds the single feed line. The concentrate passes through a shell and tube heat exchanger, exiting at 60 ^{o}C before being drawn through the concentrate filters, which are changed every 6 hours during production. The feed line pressure is maintained at a pressure of 6 bar. Two stage homogenisation occurs after passing through the concentrate filter if the product is whole milk or cream powders. For all powders, the homogenisation stage also acts as a high pressure pump.

A recent change in the concentrate handling has been the addition of a CO_2 dosing point after the homogenisers. The injection of this CO_2 has helped to control the final product's bulk density.

3. Drying Chamber

The Whareroa Powder 2 dryer is a Niro compact design. Atomisation of the concentrate occurs via one of six lances inserted into the drying chamber (black hoses in Figure 1). Inlet air enters the chamber via the air disperser. Figure 1 below shows that the inlet air enters the air disperser via a tangential scroll before passing into the chamber. The inlet air flow is 90 tonnes / hr at a temperature of 210 ^{o}C.

Figure 13: Dryer inlet air and lancer feed lines

Figure 2 shows the lances, inlet air and the central fines return line from the inside of the chamber. The fines return is used to assist in the agglomeration of powders where dry powder is partly coated with wet concentrate, which helps agglomerates to form.

Figure 14: Concentrate lances and inlet air disperser inside chamber

At the bottom of the chamber the static fluid bed collects and dries the powder further. The powder flows off the SFB via an overflow weir, the height of which can be adjusted to manipulate the powder temperature exiting the drying chamber. The air flow to the SFB is 30 tonnes / hr at a temperature of 90 ^{o}C. As Figure 3 shows, the outlet air ducting is located in the middle of the SFB. The temperature of this exiting air is typically 73 ^{o}C.

Figure 15: Chamber static fluid bed and outlet air duct

4. Fluid Beds

Further drying of the powder occurs in two vibrating fluid beds. The first bed uses 8.7 tonnes / hr of 30 ^{o}C air and the second, also operating with 30 ^{o}C air has an air flow of 8.0 tonnes / hr. Like the SFB, adjustment of the weir height manipulates the moisture content of the powder exiting the fluid bed.

Figure 16: Vibrating fluid bed #1

Lecithin can be dosed to help form agglomerates when producing agglomerated SMP. The dosing point is the duct between the SFB and the first VF. However, it is very rare that Lecithin is dosed.

The distance between the last VF and the sifter is at least 20 meters, so a long transport line carries the powder to be fed into the sifter. A bucket elevator is used to feed the two powder

bins as shown in Figure 5 after the sifter. Powder is packed in either 25 kg or 520 kg bulk bins.

Figure 17: Powder transport line, sifter, bucket elevator and packing bins

5. Baghouse

All fines from the dryer, and two vibrating fluid beds are fed to a single Leubbers designed washable baghouse. The baghouse contains 177 filter bags, 6 m in length and 0.208 m in diameter, which equates to 694 m^2 of filtration area. The vessel is 4.3 m in diameter and bags are spaced approximately 0.26 m apart centre to centre. These dimensions give a elutriation velocity of 4.0 m / s.

Figure 6 shows the outside of the clean air plenum, the ducting to the extractor fan and the bottom of the outlet air stack. The extractor fan typically runs at 90 % of its maximum speed. Interestingly, the outlet air stack does not have any emissions instrumentation. The line connecting to the top of the clean air plenum feeds a CIP spray ball but the clean air plenum is not CIPed as cleaning is done manually with a vacuum cleaner.

Figure 18: Baghouse clean air plenum and extractor fan

5.1. Dirty Air Inlet

The inlet to the baghouse is tangential, as Figure 7 shows. The air temperature here is 70 ^{o}C due to mixing of the colder VF air with the 73 ^{o}C air exiting the chamber. Relative humidity is roughly 21 – 22 %, which varies with ambient humidity and evaporation rates. Plant operators adhere strictly to sticky point data for powders, hence the outlet humidity is monitored closely.

Figure 7: Baghouse dirty air chamber and inlet air duct

The cross sectional area of the inlet air duct is 1.7 m^2 giving an inlet velocity of 19.5 m / s. As Figure 8 shows, the edge of the bag bundle is in the direct path of the inlet air. It is this area of the baghouse that experiences greater bag wear. Based on a total volumetric flow of 1948 m^3 / min to the baghouse that has a filtration area of 694 m^2, the Whareroa Powder 2 baghouse has a high air to cloth ratio of 2.8 m^3 / m^2 / min. This value is the highest of the five Fonterra milk powder plants with washable baghouses.

Figure 8: Baghouse inlet scroll and edge of bag bundle

5.2. Baghouse Hopper

Powder removed from the filter bags collects on the baghouse hopper. As Figure 9 shows, this is an angled perforated plate. Air at 65 ^{o}C flows up through this plate to help transport powder to the hopper outlet. A large deflector cone is placed above the hopper outlet. This

cone prevents large wads of powder falling straight down the outlet and blocking the rotary valve and also prevents powder bridges forming across the outlet that would cause it to block.

Figure 9: Baghouse hopper and deflector cone

The conical section of the baghouse has a warm air jacket. Air at 65 ^{o}C is circulated within the jacket to prevent condensation occurring on the baghouse walls that would result in powder sticking to these moist spots.

The rotary valve shown in Figure 10 removes powder from the baghouse hopper and feeds the fines return lines. These fines can either be returned to the top of the dryer or to the first of the vibrating fluid beds. Typical fines return line pressure is 17 to 19 kPa.

Figure 10: Baghouse rotary valve

5.3. Pulse Jet Cleaning

The pulse jet cleaning of the bags is achieved through the Intensiv annulus with a two stage coanda system shown in Figures 11 and 12. Compressed air is fed into the annular gap at the top of the trumpet and ejected through a narrow slit into the trumpet venturi. This flow induces air from above the trumpet down the central guide body. As this combined air stream flows down into the throat of the bag, further air below the guide body is entrained down into the bag, thus creating the two stage effect.

Figure 11: Coanda two stage trumpet above filter bag

Bags are pulsed in pairs, except for a single bag pulse to end the sequence. A pulse lasts for 0.12 s, with a 0.8 s hold between pairs of bags. Therefore, the total cycle time is 82 s. The pulse pressure is 6 bar. Typical baghouse differential pressures are 30 – 40 mm H_2O for cream powder, 40 mm H_2O for whole milk powder and between 85 – 150 mm H_2O for skim milk powders.

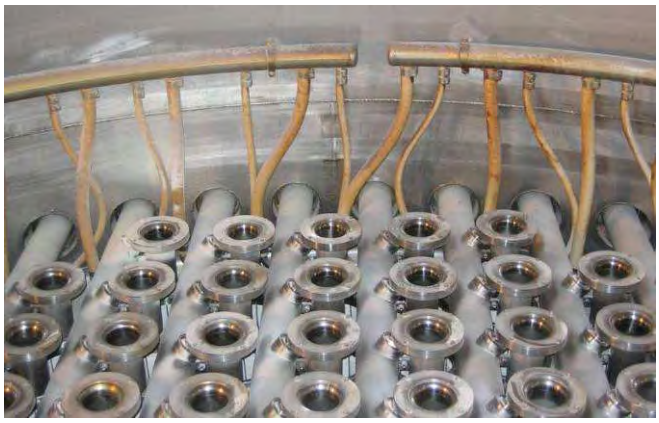

Figure 12: Coanda trumpets, compressed air supply and CIP supply to the cell plate

Compressed air flow to the trumpets is not measured or recorded. Operators have to continually check the solenoid field box to check whether there is a faulty solenoid valve. Figure 13 shows the compressed air headers feeding the trumpets.

Figure 13: Coanda two stage trumpet compressed air solenoids

6. CIP Regime

The full dryer and baghouse CIP at Whareroa Powder 2 is quite different to that used by other Fonterra sites with washable baghouses because there is an acid rinse in the sequence. Also the frequency of wash at Whareroa is much higher: fortnightly compared with two or three a season at the other sites. The CIP sequence at Whareroa is as follows:

1. Warm rinse @ 55 ^{o}C
2. Caustic rinse @ 75 ^{o}C
3. Warm rinse @ 55 ^{o}C
4. Acid rinse @ 65 ^{o}C
5. Warm rinse @ 55 ^{o}C

Plant operators use visual turbidity at the CIP drain to determine whether a rinse step has been successful and hence the next step in the sequence can begin. Pulsing of the filter bags does not occur during the CIP in an attempt to prevent bag damage.

Figure 12 above shows the ring main and flexi hosing supplying CIP fluid to the pressurised nozzles below the cell plate. There are two nozzles per bag that operate at a pressure of 1.5 to 2 bar.

Plant management use the principle that once the baghouse differential pressure exceeds 150 mm H_2O, a CIP should be carried out. This principle is based on information obtained from Filtercorp International; pulse pressures of 6 bar will not generate sufficient force to overcome the 150 mm H_2O pressure drop. The Whareroa Powder 2 baghouse CIP is successful in rejuvenating blinded bags.

This page is intentionally left blank

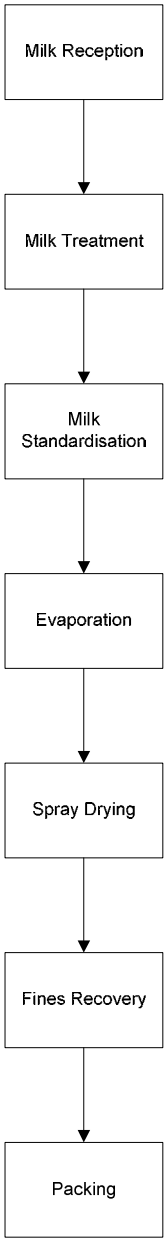
Milk Reception
Milk Treatment
Milk Standardisation
Evaporation
Spray Drying
Fines Recovery
Packing

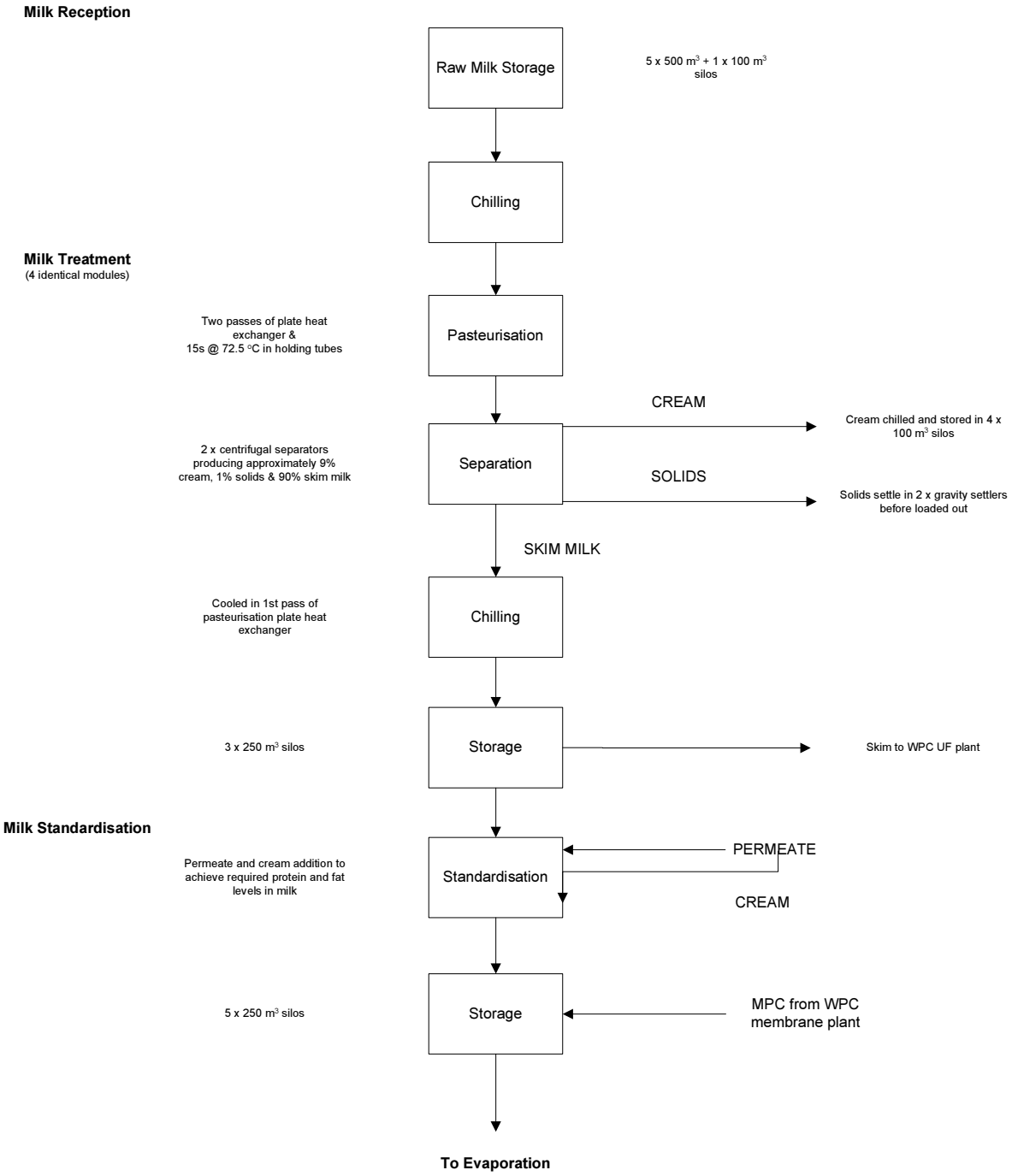
Milk Reception
Raw Milk Storage
5 x 500 m3 + 1 x 100 m3 silos
Chilling
Milk Treatment
(4 identical modules)
Two passes of plate heat exchanger & 15s @ 72.5 °C in holding tubes
Pasteurisation
CREAM
Cream chilled and stored in 4 x 100 m3 silos
2 x centrifugal separators producing approximately 9% cream, 1% solids & 90% skim milk
Separation
SOLIDS
Solids settle in 2 x gravity settlers before loaded out
SKIM MILK
Cooled in 1st pass of pasteurisation plate heat exchanger
Chilling
3 x 250 m3 silos
Storage
Skim to WPC UF plant
Milk Standardisation
Permeate and cream addition to achieve required protein and fat levels in milk
Standardisation
PERMEATE
CREAM
5 x 250 m3 silos
Storage
MPC from WPC membrane plant
To Evaporation

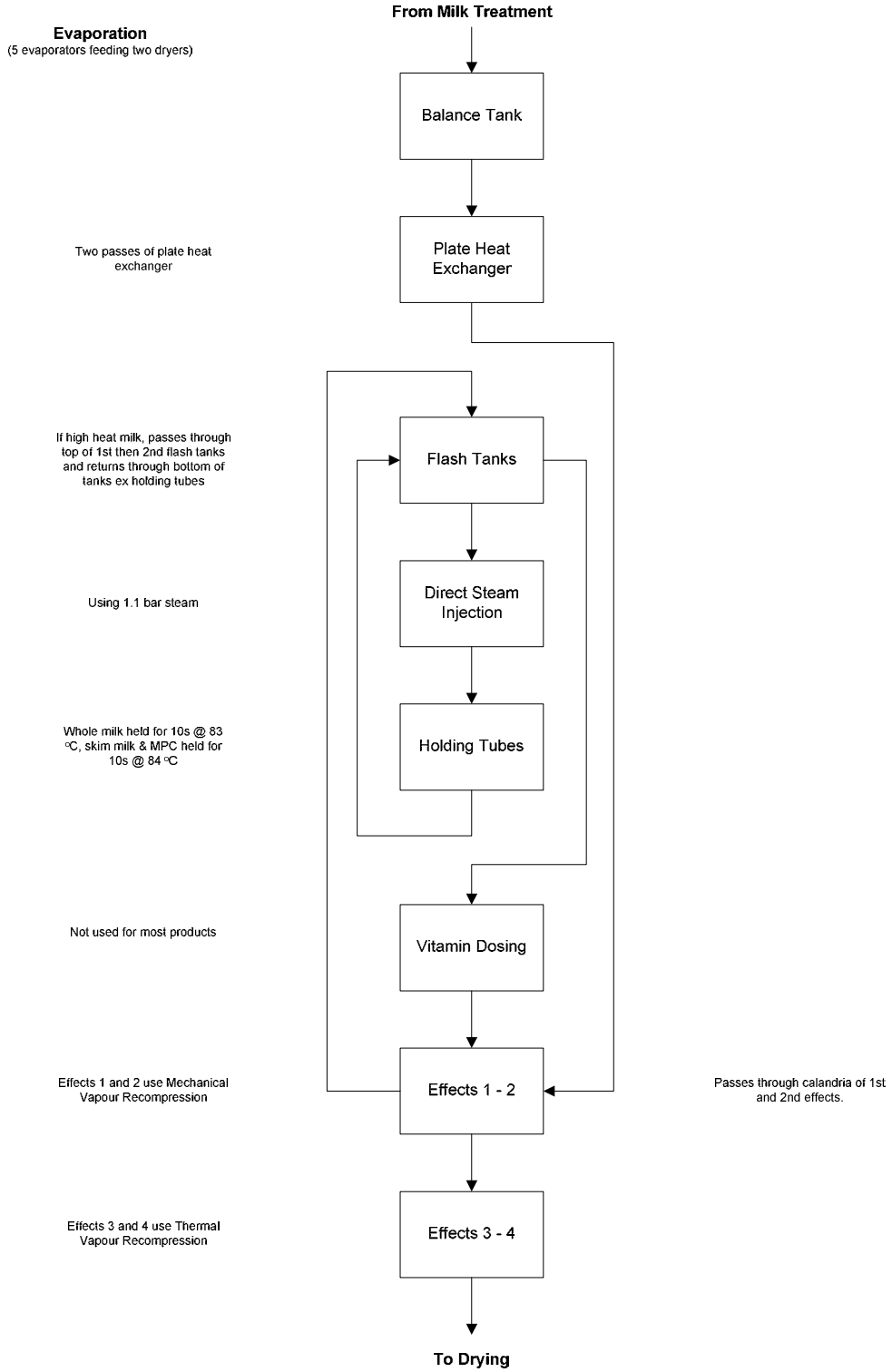
From Milk Treatment
Evaporation
(5 evaporators feeding two dryers)
Balance Tank
Two passes of plate heat exchanger
Plate Heat Exchanger
If high heat milk, passes through top of 1st then 2nd flash tanks and returns through bottom of tanks ex holding tubes
Flash Tanks
Using 1.1 bar steam
Direct Steam Injection
Whole milk held for 10s @ 83 °C, skim milk & MPC held for 10s @ 84 °C
Holding Tubes
Not used for most products
Vitamin Dosing
Effects 1 and 2 use Mechanical Vapour Recompression
Effects 1 - 2
Passes through calandria of 1st and 2nd effects.
Effects 3 and 4 use Thermal Vapour Recompression
Effects 3 - 4
To Drying

Drying (Powder Dry Side)

Saturday, 10 November 2007

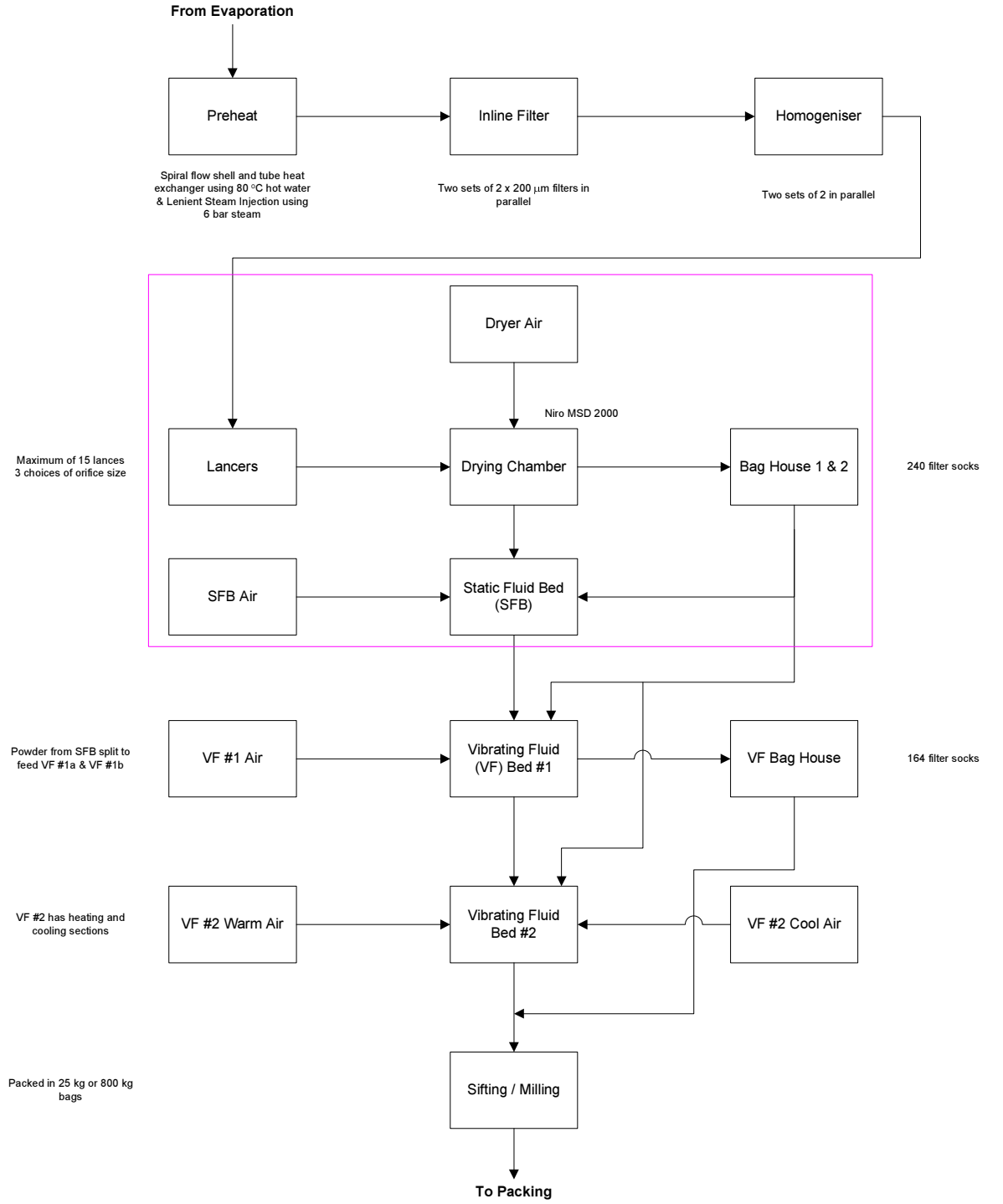

N.B. Dotted box indicates area of study

John Gabites
Department of Chemical and Process Engineering
University of Canterbury
Christchurch, New Zealand

Edendale D2 & D3 Visit

August 2004

Prepared for:

Hong Chen
Tuan Troung
James Winchester
Chris Johnson

Summary

A plant visit to Fonterra Edendale was conducted from 13 to 15 July 2004. The objectives of the visit were to compare the Edendale Dryer 2 (ED2) and Dryer 3 (ED3) milk powder plants with the Clandeboye Dryer 2 (CD2) milk powder plant. A number of photographs of the plants were taken, dimensions were measured in the plants and sourced from building drawings and functional descriptions were used to gather the required information.

It was discovered that Edendale baghouses are vastly different in design to those found at Clandeboye. Specifically, the Edendale baghouses have shorter conical and cylindrical sections and less height in the clean air plenums. The clean air outlet ducts are rectangular at Edendale with smaller cross sectional areas, whereas they are circular at CD2.

Other differences found between the baghouses were that Edendale bags have longer pulse cleaning cycle times and pulse cleaning guide bodies that are pinned rather than welded to the compressed air supply. Also, the Edendale plants have easier access to the pulse cleaning solenoid valves and manholes in the clean air plenums. Finally, fewer bags are housed in the Edendale vibrating fluid bed (VF) baghouses. The vibrating fluid beds themselves are smaller at Edendale than those at Clandeboye but the superficial velocities through the beds are the same in all three plants.

Major differences noted between the dryer buildings are that the Edendale plants have better access between the baghouse sections, better walkways in and around the vibrating fluid beds and along the VF outlet air ducts, and greater floor space allowing for easier access to all fans and baghouse powder rotary valves.

Finally, special features only found in the Edendale plants are an operator screen on top of both dryers, a pole for breaking up powder in the static fluid bed in ED3 and no lenient steam injection in the concentrate feed line in ED3.

Contents

Summary **A29**
Contents **A30**
1. Introduction **A31**
1.1. Aim **A31**
1.2. Methods **A31**
2. Findings **A32**
2.1. Concentrate Feed Lines **A32**
2.2. Drying Chamber **A33**
2.3. Vibrating Fluid Beds **A34**
2.4. Baghouses **A37**
2.5. Building **A44**
2.6. Dryer Operation **A45**
3. Conclusions **A46**
4. Acknowledgements **A47**

1. Introduction

The three plants used in this comparison were designed by GEA Niro A/S. CD2 was built in the 2000/2001 season, ED2 in the 2001/2002 season and ED3 in the 2002/2003 season. The three designs are of the Niro MSD 2000 series, designed for the production of agglomerated milk powders. Each plant was designed with a capacity of 14 tonnes / hour. CD2 produces whole milk, skim milk and milk protein concentrate (MPC) powders, ED2 fat filled and instant whole milk powders and ED3 whole milk and skim milk powders.

1.1. Aim

At the recent Fonterra Baghouse User Group Meeting held at Edendale it was noticed that there were a number of differences between the Niro designed Clandeboye and Edendale milk powder plants. At this meeting it was highlighted that the Edendale baghouse operation had been more successful than that at Clandeboye. It was the aim of this investigation to record the differences between the two sites and to identify whether the difference in plant design was a potential cause of the difference in operational performance.

1.2. Methods

The data to be gathered included baghouse layout and pulse cleaning sequences, dryer and baghouse dimensions and plant operating conditions. Physical dimensions were sourced from measurements in the plant and from building layout drawings. Functional descriptions and instruction manuals were used for pulse cleaning information, and discussions with plant operators and the use of plant logbooks provided operating conditions. In addition, a number of photos were taken inside the plant to be used as a means of comparison.

2. Findings

2.1. Concentrate Feed Lines

2.1.1. Concentrate Filters

Milk concentrate fed to the three dryers passes through identical concentrate filters. A difference between the ED2 and ED3 filters is the direction of the differential pressure gauges. As Figures 1a and 1b show, the ED2 instruments face away from an operator performing a filter swap, making the exercise slightly more difficult

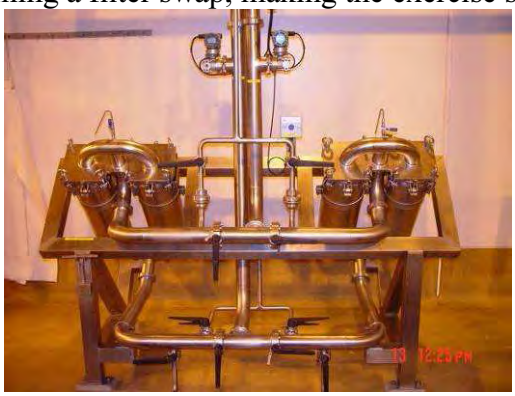

Figure 19a: Edendale D3 Concentrate Filters

Figure 1b: Edendale D2 Concentrate Filters

Figure 2a: Edendale D2 Concentrate Heater

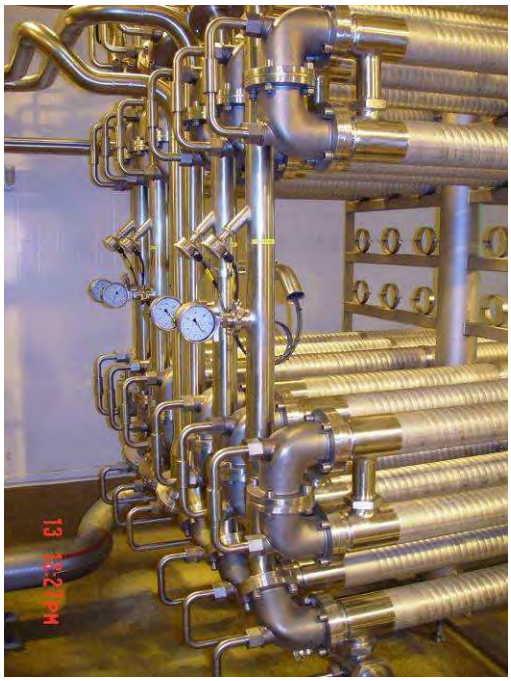

Figure 2b: Edendale D3 Concentrate Heater

2.1.2. Concentrate Heating

There is no lenient steam injection in the concentrate feed line on ED3. Consequently the concentrate heat exchanger is different to those on CD2 and ED2; the milk concentrate flows

through an anulus surrounded by an inner pipe and an outer anulus conveying hot water. Figures 2a and 2b above show the two different concentrate heaters. The advantage of the ED3 set up is that the concentrate total solids are not reduced as a result of the steam injection.

2.2. Drying Chamber

There is no difference in dimensions between the three drying chambers. The dimensions of the three chambers are represented in Figure 3 below.

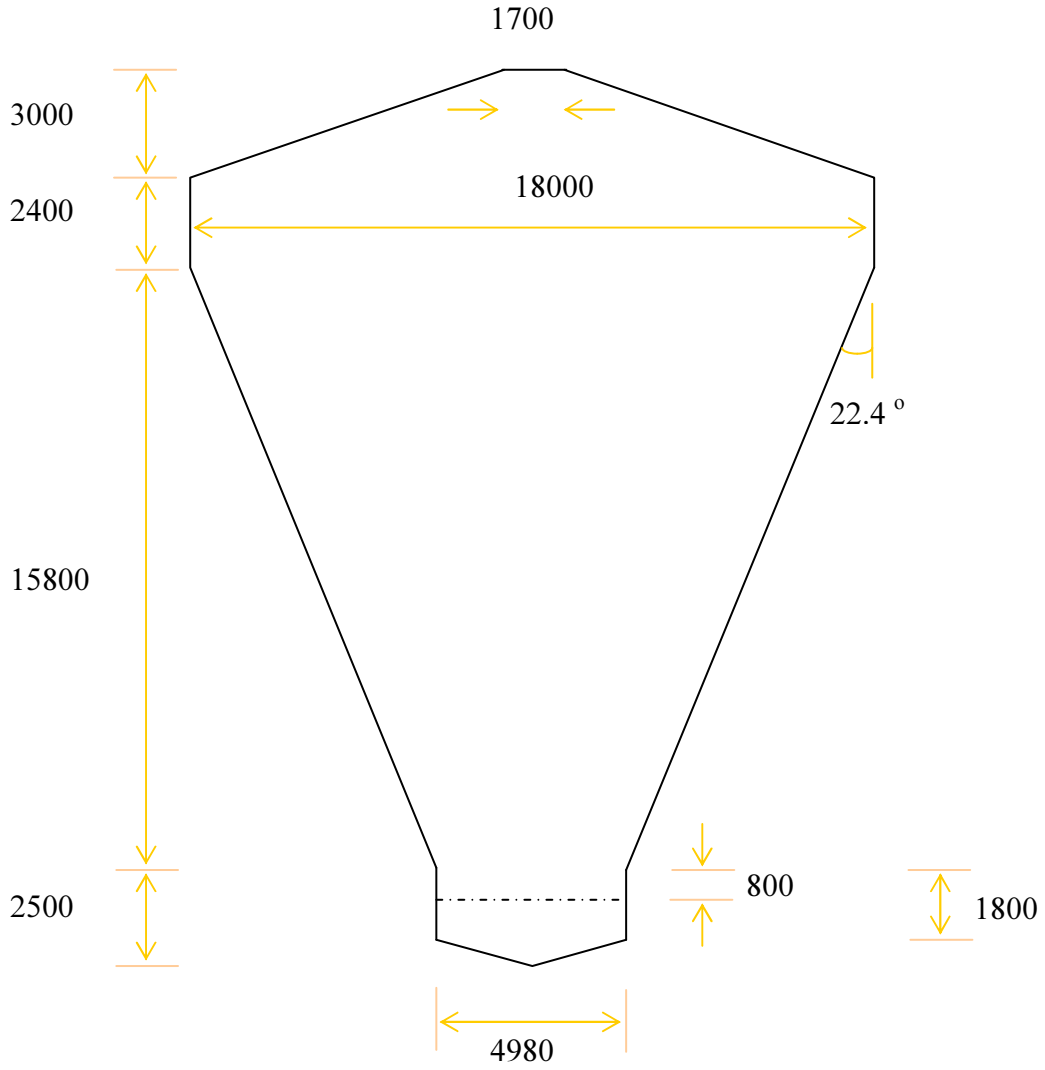

Figure 3: Niro MSD 2000 Drying Chamber Dimensions

The internal lighting of the Edendale chambers is far superior to that at Clandeboye, giving the impression that the Edendale cones are steeper. However, this is not the case. A feature found only on the ED3 dryer is a 'pole hole' at the static fluid bed (SFB). As Figure 4 shows, the hole, located next to the overflow weir, is used to insert a long rod so operators can break up powder lumps in the SFB

Figure 4: Edendale D3 SFB 'Pole Hole'

Both the Edendale plants have an operator screen on top of the dyer as shown in Figure 5. This screen is very useful for operators performing feed line swaps as both feed lines can be viewed a the same time. This screen is not installed at Clandeboye.

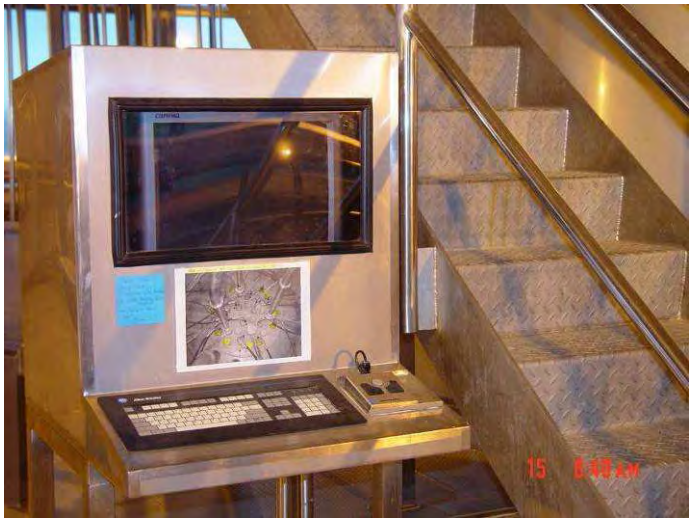

Figure 5: Edendale D2 Operator Screen in Plant

2.3. Vibrating Fluid Beds

The Edendale Vibrating Fluid Beds are smaller than those at Clandeboye; all the ED2 and ED3 beds are 13.3 m long and 1.95 m wide whereas the CD2 beds are 15.1 m long and 2.2 m wide. Due to this difference, the airflows through the Edendale beds are lower than those at Clandeboye as Table 1 below illustrates.

A second major difference in the operation of the VF beds between the plants is the temperature of the air used. The first two beds and the ambient section of the last beds at Edendale use 30 ^{o}C air. Both ED2 and ED3 VF cooling section air temperatures are 15 ^{o}C. At Clandeboye, VFs 1a and 1b use 70 ^{o}C air, the VF 2 ambient section 40 ^{o}C air and the VF 2 ambient section 25 ^{o}C.

Table 1: Vibrating Fluid Bed Mass Flow Rates

	VF 1a [tonne / hr]	VF 1b [tonne / hr]	VF 2 Ambient [tonne / hr]	VF 2 Cooling [tonne / hr]
Edendale D2	22	22	12	12
Edendale D3	22	22	10	10
Clandeboye D2	27	31	22	20

The constant parameter in all three plants is the superficial air velocity through each bed. As Table 2 below shows, the superficial velocities are almost identical except for the CD2 VF #2 value of 0.30 m / s. This is due to the CD2 VF 2 air flows being almost twice those used at Edendale.

Table 2: Vibrating Fluid Bed Superficial Velocities

	VF 1a [m / s]	VF 1b [m / s]	VF 2 [m / s]
Edendale D2	0.20	0.20	0.18
Edendale D3	0.20	0.20	0.21
Clandeboye D2	0.18	0.21	0.30

Another subtle difference between the two sites' VF beds is the outlet air pipe work. This ducting increases in diameter en route to the VF baghouses in all three plants. Figure 6 below shows how the pipe work from the three ED3 VF beds is merged. The changes in pipe diameter occur through expanders which are much more abrupt at the Edendale plants.

Figure 6: VF Bed Outlet Air Pipe Work, Edendale D3

Figure 7 also shows the sharp increase in pipe diameter from one of the first vibrating fluid beds. Note the powder that has fallen from the inspection port, indicating powder is falling from the air stream at this location due to a decrease in air velocity at the expansion. This is not known to occur at Clandeboye because of the gradual increase in pipe diameter.

Figure 7: VF Bed Outlet Air Pipe Work and Walkway, Edendale D2

The Edendale plants allow for better access to the mentioned outlet air stream. Walkways exist, as shown in Figure 7, next to the outlet air ducts from the first stage of VF beds. It is more difficult to check this pipe work at Clandeboye, as operators have to climb down a ladder to a platform that gives access to one inspection hatch only.

The walkways above the second VF bed at the Edendale plants are also better than at Clandeboye. As Figure 8 shows, two stair cases give easy access to the walkway above the bed that lead to inspection hatches in the VF #2 outlet air duct and in the bottom of the first series of VF beds. Access to this area at Clandeboye is achieved by climbing down one of two ladders and onto a large grill plate, which is obviously not as easy or as safe as the Edendale set up.

Figure 8: Walkway Above VF #2, Edendale D2

2.4. Baghouses

As Figure 9 shows, the outlet air from the drying chamber in each plant is fed tangentially into the baghouses via a 1900 x 1300 mm rectangular duct. To compensate for the effect of the high internal velocities, cages around the perimeter of the bag bundle are heavier than those in the centre.

Figure 9: Edendale D3 East Baghouse Entry

2.4.1. Main Dimensions

The major difference between the Edendale and Clandeboye baghouses are the overall dimensions (see Figures 10 and 11). The Edendale baghouses are much shorter than those at Clandeboye but the diameter of the baghouses is the same in all three plants.

Figure 12 reveals the result of the differences in dimensions for the main baghouses. The ceiling in both photos is at the top of the baghouse cones and the distance between the ceiling and the floor is the same in both photos. Therefore the longer Clandeboye cone is clearly shown in the figure. Because of the shorter Edendale cones, these baghouses have a much longer leg feeding the powder rotary valves, which in both plants are located on the fourth floor. Also note that the angle of the Clandeboye baghouse cone is much steeper than that of the Edendale main baghouses.

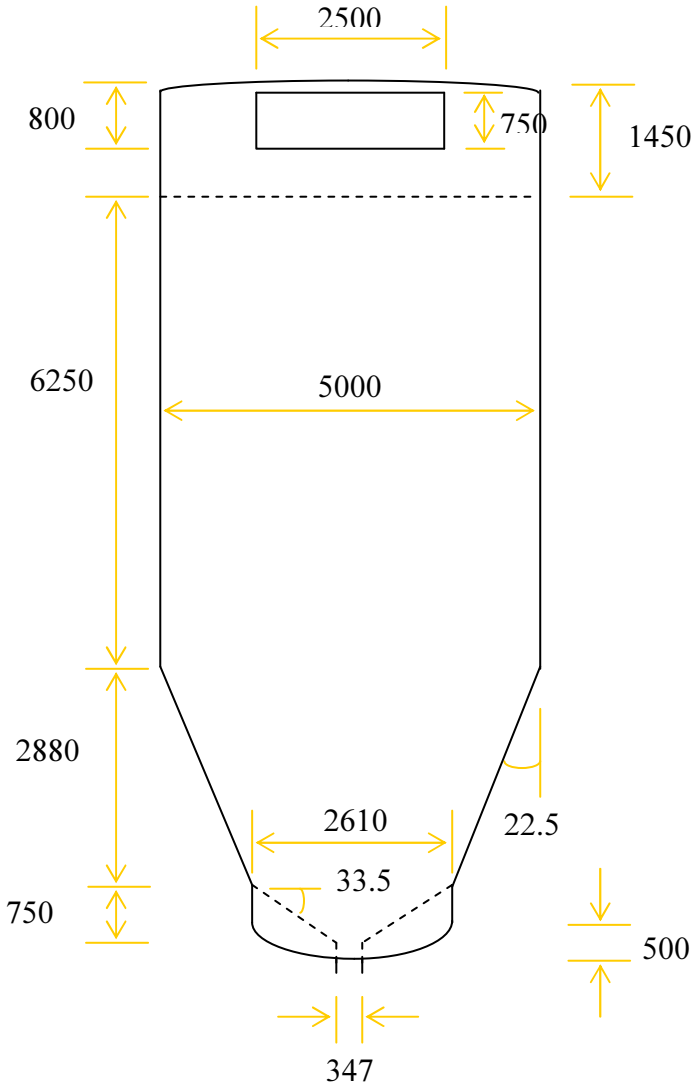

Figure 10a: Edendale Main Baghouses Dimensions

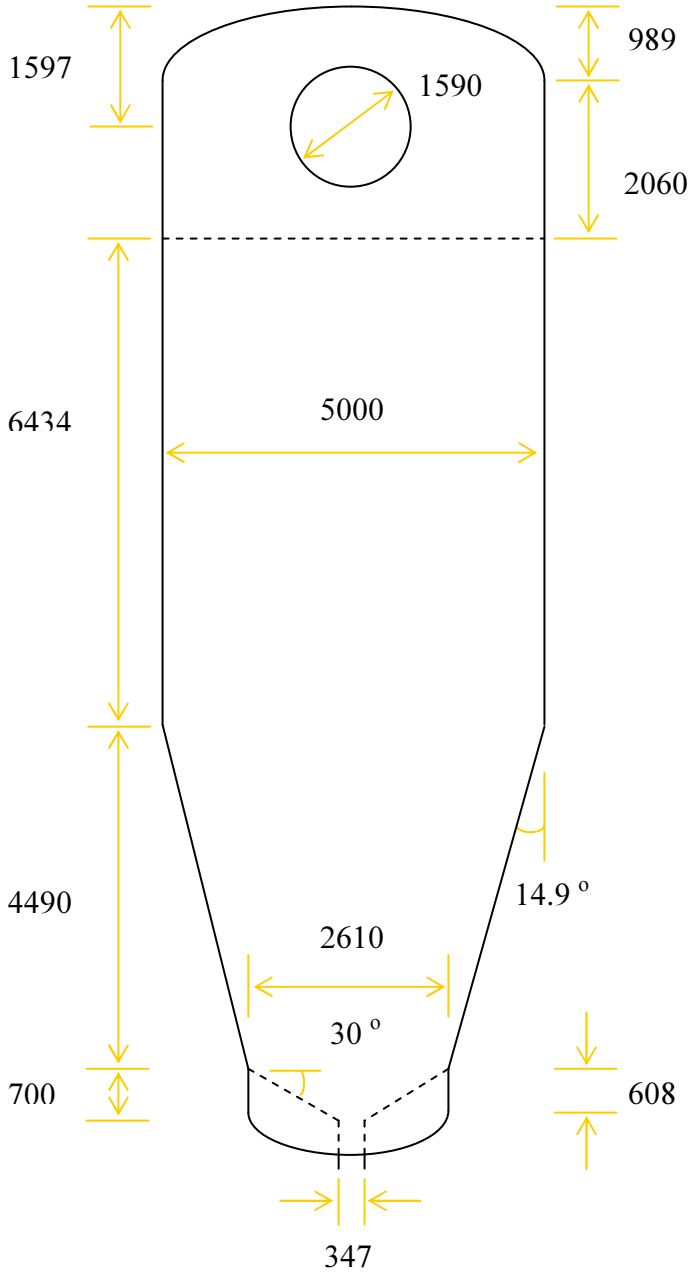

Figure 10b: Clandeboye Main Baghouses Dimensions

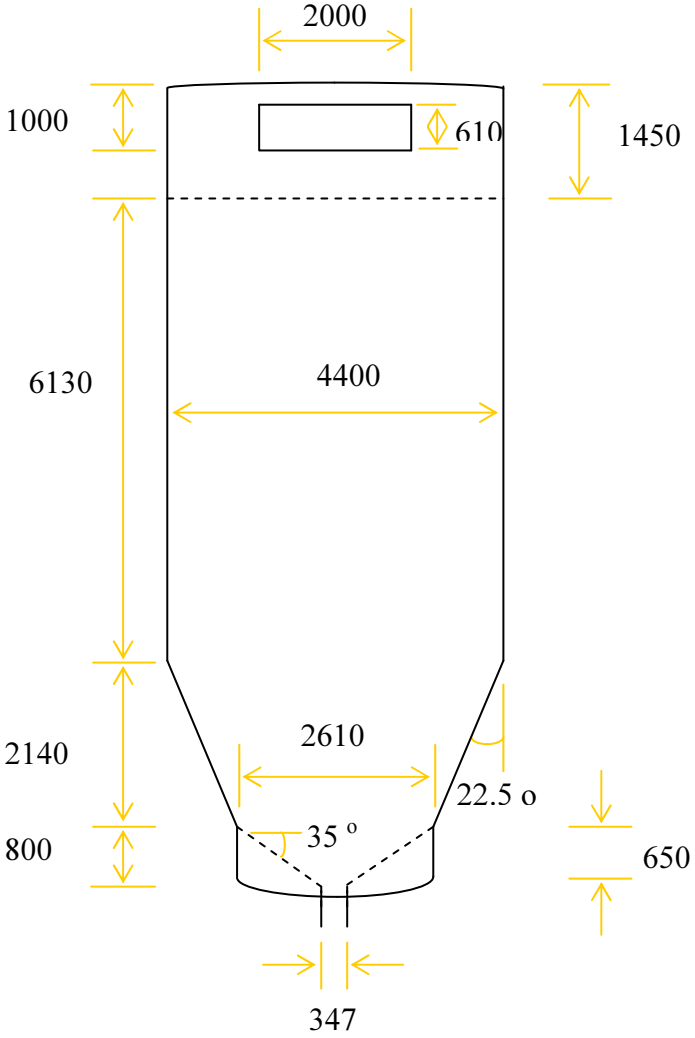

Figure 11a: Edendale VF Baghouse Dimensions

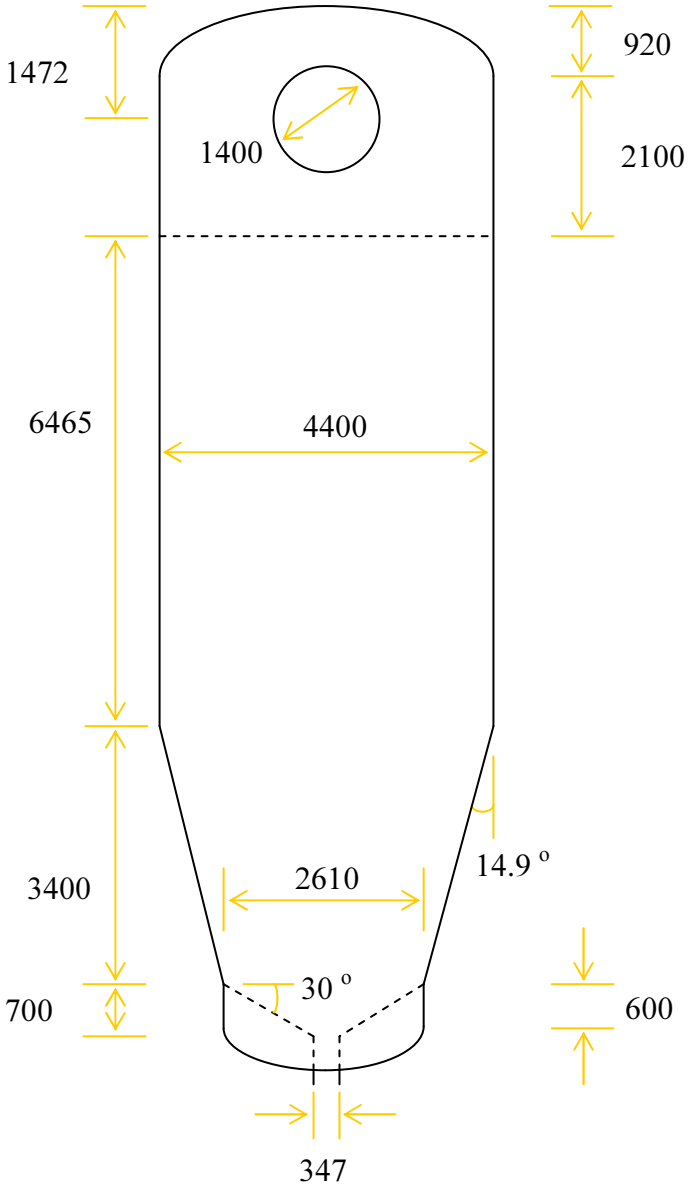

Figure 11b: Clandeboye VF Baghouse Dimensions

Figure 12a: Clandeboye D2 #1 Baghouse

Figure 12b: Edendale D3 East Baghouse

2.4.2. Clean Air Plenums

Figures 10 and 11 above show the difference in design of the baghouse clean air plenums. As Figure 13 shows, the different Edendale design allows for much better access to the solenoid valves placed on top of the baghouse. Note that an inspection hatch for access into the clean air plenum can be seen in Figure 13a. No such hatch is fitted in any of the Clandeboye baghouses.

Figure 13a: Top of Edendale D3 West Baghouse

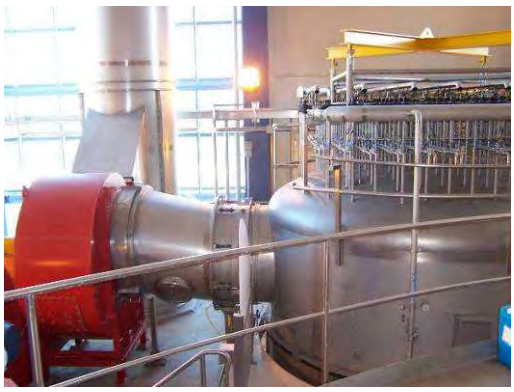

Figure 13b: Top of Clandeboye D2 VF Baghouse

Due to the difference in clean air plenum design, the clean air outlet ducting is also different. Figure 13 shows that the Edendale outlets diverge from a rectangular duct to a round pipe prior to entering the exhaust fans, whereas the Clandeboye outlets have round pipes from the baghouse to the exhaust fans. This different outlet air design means the flow areas are slightly different: 1.88.m^2 for Edendale and 1.99 m^2 for the Clandeboye main baghouses, 1.22

m^2 and 1.54 m^2 for the VF Baghouses. Consequently, it could be expected that the air velocities out of the clean air plenums are higher at Edendale than at Clandeboye.

Again due to the difference in clean air plenum design, the lid lifting mechanisms are different at the Edendale and Clandeboye plants. Hoisting the baghouse lids is achieved manually at Edendale. At Clandeboye, the hoist is automated and the baghouse lid can be rested on a stand when work is being carried out in the baghouses. No stands exist at Edendale so the baghouse lids hang from the hoist once removed, thus clearly not as safe as at Clandeboye.

Figure 14: Edendale D3 East Baghouse Lifting Mechanism

2.4.3. Bottom of Baghouse

The perforated plates at the bottom of the Edendale baghouses are different to those at Clandeboye. The Edendale plates, now that they have been installed the right way up, have holes that are punched from below whereas the Clandeboye holes are punched from above. The Edendale plate is shown in Figure 15.

Figure 15: Edendale D2 North Baghouse Perforated Plate

The access to the manholes at the bottom of the VF baghouses is much more difficult at Edendale. This is due to the floor level being lower than the equivalent floor level at Clandeboye and there being no rail above the man hole to hold onto when climbing into the baghouse.

2.4.4. Filter Area

The main baghouses in the three plants have an identical number and same sized filter bags. Each of the 240 bags is 0.20 m in diameter and 6.0 m in length. In both the main and VF baghouses, bags are spaced 0.26 m apart. There are a different number of bags in the Edendale VF baghouses compared to the Clandeboye VF baghouse. The Edendale VF baghouse contains 136 0.20 m diameter by 6.0 m long bags, but there are 164 of the same dimension bags at Clandeboye.

The air to cloth ratios of the main baghouses based on the dryer operating conditions for each product produced is shown in Table 3 below. These air to cloth ratios or filtration velocities are very similar for all products in all three plants. This is not surprising as the three plants have the same filtration area of 905 m^2 in the main baghouses and operate each plant almost identically.

Table 3: Main Baghouse Air to Cloth Ratios

	SMP [m^3 / m^2 / min]	WMP [m^3 / m^2 / min]	MPC [m^3 / m^2 / min]
Edendale D2	-	2.2	-
Edendale D3	2.4	2.3	-
Clandeboye D2	2.3	-	2.2

Table 4 below displays the filtration area and air to cloth ratios for the VF baghouses. Note there is a smaller filtration area at Edendale as a result of fewer bags in the VF baghouse. The air to cloth ratios of the VF baghouses at Edendale are lower than those of the main baghouses. The air to cloth ratios for the three baghouses at Clandeboye are similar.

Table 4: VF Baghouse Filtration Area and Air to Cloth Ratios

	Filtration Area [m^2]	Air to Cloth Ratio [m^3 / m^2 / min]
Edendale D2	513	1.7
Edendale D3	513	1.9
Clandeboye D2	681	2.3

There is an appreciable difference between the state of CIPed Edendale and Clandeboye bags. The Edendale bags are much softer than the more rigid Clandeboye bags, which suggests the different powders produced in the three plants behave differently when in contact with CIP fluid. Filter bag samples from both plants have now been analysed using a scanning electron microscope in an attempt to identify the cause of the difference (see Chapter 5).

2.4.5. Pulse Cleaning

The pulse cleaning sequences of the main and VF baghouses in the three plants is shown in Table 5 below. The CD2 values were taken from the plant functional descriptions while the ED2 and ED3 values were sourced from Craig Cooke, ED3 Production Supervisor.

Table 5: Main Baghouse Pulse Cleaning Sequence

	Pulse Duration [s]	Hold Period [s]	Reset Delay [s]	Cycle Time [s]
Edendale D2	0.25	2.00	5	275
Edendale D3	0.28	1.80	5	255
Clandeboye D2	0.15	2.40	1	307

Table 6 displays the VF baghouse pulse cleaning sequence for each of the three plants. It is interesting to note that the pulse duration and hold period for the VF and main baghouses in ED2 are the same while the pulse durations for ED3 are slightly different. The Edendale VF baghouse pulse cleaning cycle times are much shorter than these used at Clandeboye.

Table 6: VF Baghouse Pulse Cleaning Sequence

	Pulse Duration [s]	Hold Period [s]	Reset Delay [s]	Cycle Time [s]
Edendale D2	0.25	2.00	5	158
Edendale D3	0.25	2.00	5	158
Clandeboye D2	0.15	3.99	1	340

The guide bodies used for the pulse cleaning at Edendale are fixed to the compressed air line with a removable pin (Figure 16). This is not the case at Clandeboye as the identical guide bodies are welded to the compressed air line, even though the Niro Baghouse instruction manual states they should be fixed with the pin assembly.

Figure 16: Edendale D2 Pulse Air Guide Body Pin

2.5. Building

There are significant differences between the Edendale and Clandeboye buildings. Where there is a void around the dryer chamber on the fourth floor at Clandeboye, in the Edendale plants it has been filled with flooring as Figure 17 below shows. This increase in floor space gives more room for operators to walk around the baghouse powder outlets and for the fans supplying air to the SFB and VF beds.

Figure 17: Edendale D2 Fourth Floor Extra Floor Space

The extra floor space above has also meant that walkways have been built at the Edendale plants all the way around the baghouses (see Figure 19 below). As Figure 18 below shows, the walkway around the Clandeboye baghouses covers only one third of the baghouse cones.

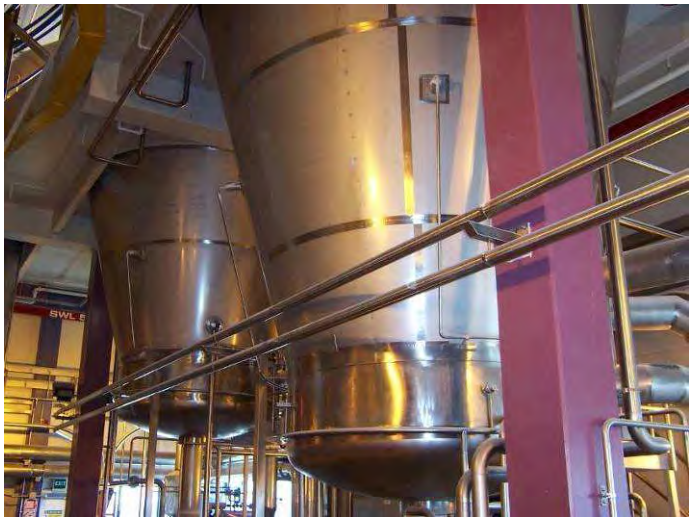

Figure 18: Clandeboye D2 #2 and VF Baghouse

The access between the different baghouse sections is also much better in both Edendale plants. Figure 19 shows the stair well that links the 26 m level to the bottom of the VF baghouse and continues to the bottom of the main baghouse on the same side of the building. The 26 metre level is the top of each of the baghouse's conical section. This better access would allow for a quicker set up for CIP and faster completion of pre start checks. To move

from the top of the conical section to the base of the baghouses at Clandeboye requires use of the main stair well between D1 and D2 or use of the elevator, both requiring one to effectively exit the D2 building.

Figure 19: Stair Access from the 26 m Level and Full Baghouse Walkway, Edendale D3 VF Baghouse

2.6. Dryer Operation

From the information gathered there is very little difference in the operation of the ED3 and CD2 dryers. The slight differences noted are that when producing whole milk powder, ED3 processes a higher concentrate flow and consequently uses a lower outlet temperature (75 ^{o}C c.f. 79 ^{o}C). Also, the SFB air temperature of 85 to 90 ^{o}C is lower than the 95 to 100 ^{o}C used at Clandeboye. Both use similar main inlet air and SFB flows.

There are also subtle differences between ED3 and CD2 for the production of skim milk powder. Again, the Edendale concentrate flow is slightly higher than the Clandeboye flow. The Clandeboye inlet air temperature is greater than that at Edendale (225 ^{o}C c.f. 220 ^{o}C), but the SFB inlet air temperature is lower (100 to 105 ^{o}C c.f. 110 to 115 ^{o}C). The outlet air temperatures for both plants are the same at approximately 80 ^{o}C. Air flows are also approximately the same.

3. Conclusions

From the findings discussed above, it can be concluded that the differences between the Clandeboye and Edendale baghouses are such that the two designs cannot be deemed similar. This proves industry personnel to be incorrect in believing this was not the case.

The list below summarises the differences between the Edendale and Clandeboye plants:
The Edendale baghouses have:

- shorter conical and cylindrical sections
- less height in the clean air plenums
- rectangular versus round clean air outlet ducts with smaller cross sectional areas
- easier access to the pulse cleaning solenoid valves
- longer pulse cleaning cycle times
- pinned rather than welded pulse cleaning guide bodies
- man holes in the clean air plenums
- fewer bags in the VF baghouses (136 versus 164)

The Edendale vibrating fluid beds:

- are shorter in length and width
- operate with lower air flow rates

The Edendale dryer buildings have:

- better access between the baghouse sections
- better walkways in and around the vibrating fluid beds and along the VF outlet air ducts
- greater floor space allowing for easier access to all fans and baghouse powder rotary valves

Special features only found in the Edendale plants are:

- an operator screen on top of both dryers
- a pole for breaking up powder in the SFB in D3
- no LSI in the concentrate feed line in D3

4. Acknowledgements

Many thanks to Craig Cooke for sourcing and supplying additional information after the visit.

Also, thanks to Steve Keelty and the ED2 and ED3 staff for their hospitality and help.

Appendix B – Supporting Information for Torbar 402 Averaging Pitot Tube

---

B1 – Torbar 402 Averaging Pitot Tube Differential Pressure to Volumetric Air Flow Conversion Calculation B2

B2 – Torbar 402 Averaging Pitot Tube Differential Pressure Transmitter CAPEX B3

Torbar 402 Averaging Pitot Tube

Volumetric Flow from Differential Pressure

Equation

$$Q = \sqrt{\Delta P}\left(\frac{KA\sqrt{T+273}}{4.0323\sqrt{S}\sqrt{P}}\right)$$

Variables

Q = volumetric flow [actual m^3 / h]

- Unknown variable to be equated and displayed on operators screens

ΔP = measured differential pressure [mbar]

- Difference between the total and stack static pressures measured by ΔP transmitter.
- Resulting 4 – 20 mA output to be fed to the PLC.

T = actual stack air temperature [^oC]

- The possible temperatures already recorded in the PLC that could be used here are:
  - Dryer outlet air duct probes (5005TT001 and 5006TT002)
  - Fire system probes (7411TT01 and 7411TT02)
  - BH #2 stack probe (2301TT003)

P = actual stack static pressure [bar abs]

- The Torbar measures this, but the electrical signal to the PLC is the ΔP.
- This value is more a constant than a variable and can be assumed to equal the atmospheric pressure (1.01 bar abs).

Constants

K = Torbar 402 coefficient
= 0.7476

A = internal duct cross sectional area
= π (100 cm)^2
= 10,000 π cm^2

S = specific gravity of air
= 1

Equation Simplification

$$Q = \sqrt{\Delta P}\left(\frac{KA\sqrt{T+273}}{4.0323\sqrt{S}\sqrt{P}}\right)$$

Subbing in the constants from above

$$Q = \sqrt{\Delta P}\left(\frac{0.7476\times 10000\pi\sqrt{T+273}}{4.0323\sqrt{1}\sqrt{1.01}}\right)$$

$$= 5795.6966\sqrt{\Delta P}\sqrt{T+273}$$

TO: Chris Johnson

FROM: John Gabites

SUBJECT: CD2 Torbar Differential Pressure Transmitters CAPEX Application

DATE: 9th March 2005

Background

A Torbar Averaging Pitot Tube (Torbar Flowmeters Ltd., UK) was installed in each of the CD2 main baghouse stacks in September 2004. The purpose of these instruments was to measure the air flow through the main baghouses and allow correction of any air flow bias detected. An air flow bias is not desirable for two main reasons. Firstly, when running on air or product a bias means one baghouse has a higher filtration velocity. The higher the filtration velocity, the higher the baghouse emissions and the shorter the bag life through increased bag damage. Secondly on CIP, a bias means it takes longer to dry out one baghouse than the other and hence adds to the CIP turn around time.

Therefore the justification for these instruments was that by balancing the air flow through each baghouse, plant operators could prolong bag life, reduce stack emissions and decrease CIP turnaround time. Prolonged bag life would mean less plant downtime for bag replacement and reduced operating costs by less frequent bag replacement, lower stack emissions would increase plant revenue and shorter CIP times would also reduce plant downtime.

Since their installation, the differential pressure measured by the instrument so that calculation of the air flow can be performed, has been conducted manually with a hand held digital manometer. The error in these readings is high because there is no way of damping out the noise present.

Data obtained has shown that an imbalance exists between the air flows to the two main baghouses. This bias can be corrected by adjusting the ratio of extractor fan speeds. However, because these readings are not continuous, it is unclear whether the bias is affected by different stages of operation such as running on air, product or during a CIP.

Operators often use personal judgement in an attempt to correct the air flow bias. This becomes an issue when different operators use different conditions to balance the air flows. If an extractor fan speed ratio has been suggested from the differential pressure measurements, later shifts are often not aware of this information and hence, attempts to correct the balance could actually make it worse.

Finally, because the differential pressure readings have been taken manually to date, the asset sits idle for 99 % of the time the dryer is running.

Problem / Opportunity Under Consideration

The opportunity that presents itself is to purchase and install instrumentation to automatically take the two differential pressure readings, link these readings into the PLC where the calculation of air flow can be conducted, and present this information on the Dryer 2 operator screens.

How Will This Fix The Problem?

This will fix the problems and reap the potential benefits as follows:

1. Through use of the PLC, the accuracy of the readings will be improved as the noise currently recorded manually will be dampened out.
2. With the air flow result presented on the operators' screens:
    a. Operators will be able to adjust the extractor fan speed ratios as changes in production occur that affect the air flow balance.
    b. All operators will receive the same information, which will prevent different shifts using different extractor fan speed ratios.
3. With a continuous reading, the use of the current assets (i.e. the Torbar averaging Pitot tubes) will increase from 1 % to 100 % of the time the dryer is running.
4. With an automatic online measurement, the air flow data combined with baghouse differential pressure information will allow bag permeability to be calculated. This variable will become a very important management tool for baghouse operation:
    a. Minimum limits could be set for when a baghouse CIP should be conducted and when bag replacement should occur.
    b. The effectiveness of a baghouse CIP can be checked by viewing the filter bag permeability after a wash.
    c. The use of CD2 for trials into Fonterra suppliers of filter bags would use this information for comparison of potential bags.

Alternatives Considered

The alternative to the proposed work is to continue to take the differential pressure readings manually. A procedure could be written for how this task is performed and passed onto a suitable member of staff who would take the readings regularly; currently these readings are being taken by Canterbury University PhD student John Gabites. Operator logs could also record the time and result of the readings, so information would be shared more efficiently between shifts. This alternative will not eliminate the problems or reap the benefits mentioned above.

An alternative to purchasing new differential pressure transmitters was investigated; the Clandeboye site was searched for spare suitable differential pressure transmitters to reduce the cost. However, no suitable instruments were found.

Recommendation For Why We Are Going Down This Route

It is recommended that we go down this route for three mains reasons. Firstly by continually balancing the main baghouse air flows, filter bag life will be prolonged, operating costs will be reduced and less downtime for bag replacement and baghouse dry out post CIP will result.

Secondly, doing this work will greatly improve the usefulness of the September 2004 installation of the Torbar averaging Pitot tubes. Connecting these instruments to the PLC will take their use from virtually zero to 100 % of the time the plant is running.

Finally, continuous measurement and display of the baghouse air flows will give more information to plant management that will allow more informed decisions on baghouse operation, e.g. when to CIP the baghouse, when to replace filter bags and how effective a CIP has been.

Appendix C – Paper submitted to Food and Bioproducts Processing (2007)

Fines loadings in milk powder plants with washable baghouses

J.R. Gabites[1], J. Abrahamson[1 *] and J.A. Winchester[2]

[1]Department of Chemical and Process Engineering, University of Canterbury, Christchurch, New Zealand

[2] Heat Transfer and Drying Team, Clandeboye Site, Fonterra Co-operative Group Ltd, Temuka, New Zealand

* *Corresponding Author*: Associate Professor J Abrahamson, Department of Chemical and Process Engineering, University of Canterbury, Private Bag 4800, Christchurch, New Zealand
E-mail: john.abrahamson@canterbury.ac.nz

Abstract

Washable baghouses are increasingly used to filter the small size fractions of milk powder, known as fines, which become entrained with spray dryer outlet air streams in milk powder plants. Surprisingly, very little is known about the quantity of powder that becomes fines, an important parameter for both the control of agglomeration rates and washable baghouse design. A convenient method is reported here that gives estimates of the fines fraction (the ratio of fines flow to total powder flow), using powder size distributions of samples from around the plant. This method was checked against isokinetic sampling using a thimble filter to independently determine powder flow rates. Results showed that that the fines fractions ranged from 49 ± 8 % to 86 ± 2 % depending on the powder type and plant operating conditions. These values are much greater than what was traditional thought (10 – 20 %). Also, as part of this study results were compared with those from an online optical

scintillation instrument. It was concluded that the newly developed particle size distribution method is a simple and reliable way to estimate fines fractions, yet is sensitive enough to detect changes in operating conditions.

Keywords: Fines Loading, Milk Powder, Optical Scintillation, Spray Dryer, Baghouse

Introduction

A recent change in the design of milk powder plants has seen replacement of the traditional cyclone system used for fines recovery by washable baghouse systems. Fonterra, the world's largest exporter of milk products, has installed or retrofitted seven such designs in milk powder plants throughout New Zealand since the year 2000. One such plant is the world's largest milk powder plant.

Baghouses were traditionally used to remove fines not recovered by cyclones receiving the exit flow from spray dryer systems, but these baghouses were always thought to be a source of microbial contamination because powder may have long residence times in the bags. Therefore approximately 10% of these cyclone fines were downgraded to stock food. Another disadvantage of this traditional system was that cyclones often blocked, thus interrupting dryer operation.

Washable baghouses, with their ability to be cleaned-in-place (CIP), have changed the perception of baghouses as being a source of microbial contamination. Consequently, all fines collected by them retain the microbial product quality of the dryer chamber powder, thereby increasing profits. Because all fines are collected in a single stage, fewer unit operations are required. This leads to reduced building space requirements, lower capital costs and simplified plants (Westergaard, 2003). The final advantage of the new system is that baghouse collection is a gentler form of product collection when compared to cyclones. This is more suited to the high fat and high protein powders of the dairy industry (Machen, 2001).

In the milk powder plant, the inlet powder concentration of the main washable baghouse is the spray dryer outlet air powder concentration. This powder is usually termed fines and thus the inlet powder concentration is known as the fines loading. Currently, the fines loading is not measured in any milk powder plant washable baghouse in New Zealand. Consequently, there is great uncertainty about what the fines loadings are for different milk powders.

Masters (1972) presents results from a pilot scale spray dryer showing that up to 35 % of the powder can become fines depending on the powder particle size and the outlet air duct arrangement. It is uncertain how well these results apply to the modern industrial scale spray dryer which, unlike the pilot scale dryer, have internal fluidised beds at the base of the chamber and, in an increasing number of modern spray dryers, outlet air ducts located near the top rather than the bottom of the chamber (Westergaard, 2003). It is likely that these two features will influence the amount of powder that becomes fines.

When producing agglomerated milk powders, collected fines are returned to the top of the dryer chamber to interact with the atomised droplets in an area known as the collision zone. The agglomeration process is not well understood and consequently operators find it difficult to control and fine tune the powder properties (Williams *et al*., 2006). Choice or knowledge of key parameters such as spray angles, pressure nozzle sizes and fines return flow rates are issues for agglomeration and therefore, the ability to measure fine powder flows in a milk powder plant is important.

The fines loading is more generally a key parameter required for plant design, including baghouse design (Gabites *et al*., 2007). Baghouse air to cloth ratio guidelines require the fines loading as an input to determine suitable values (Croom, 1995; Intensiv-Filter, 1999;

Loffler *et al*., 1988; Turner *et al*., 1998). Providing too little filtration area because of low estimates of the fines loadings could have expensive operational consequences. Sizing pneumatic transport systems also requires knowledge of powder flow rates. Issues can arise if blowers are undersized or underpowered because of designs based on lower powder flows than the actual.

Finally, knowledge of the fines loading may help explain differences in baghouse operation among the different milk powders, as industrial operational data has shown large differences in the baghouse differential pressure among the products. It has been hypothesised that these differences are largely due to differences in fines loadings because the average baghouse differential pressure has been shown to be a strong function of the inlet powder concentration (Caputo and Pelagagge, 2000; Cora and Hung, 2002; Ellenbecker and Leith, 1980; Rothwell, 1987).

This paper examines the fines loadings in milk powder plants with washable baghouses. The aim of the work was to develop a new method for determining the fines loadings of milk powder products produced in milk powder plants with washable baghouses. These results were to be checked by isokinetic sampling and use of an optical scintillation instrument located in an outlet duct of an industrial milk powder spray dryer.

Methods and Materials

Particle Size Distribution Method

The particle size distribution outlined here determines the fines fraction X_{BH} the ratio of baghouse powder flow to total product flow as defined in equation 1:

$$X_{BH} = \frac{m_{BH}}{m_{Sift}} \tag{1}$$

A typical milk powder process using washable baghouses is shown in Figure 1. The dried powder exits the spray drying chamber either through the static fluid bed (SFB) overflow weirs or through the outlet air ducts to the washable baghouses. In the baghouse (BH), the majority of the powder is collected and discharged into the fines return lines and a very small fraction is emitted to the atmosphere with the dyer outlet air stream.

Fines from the main baghouses and the powder from the SFB are passed through the vibrating fluid beds (VFs). Here, some powder is elutriated to the vibrating fluid bed baghouse (VF BH), where again a very small amount of powder is lost to atmosphere while the majority is returned to the end of the second vibrating fluid bed. These fines are reunited with the majority of the powder that has flowed through the VFs and this total is fed to the sifter.

If a mass balance is carried out over the system shown with a dotted boundary in Figure 1, then the flow exiting the spray drying chamber through the SFB and the total flow from the base of the main washable baghouses is equal to the powder flowing through the sifter plus the emissions through the VF baghouse. Baghouses usually have collection efficiencies exceeding 99.9 % (Turner et al., 1998). If it is assumed that both the main and VF baghouses have 100 % collection efficiencies, then the emissions from each baghouse equals zero and

hence, the powder flows to each baghouse equal the powder flows into the fines return system from each baghouse. Therefore the mass balance simplifies to give the powder flow through the sifter being equal to the powder that has exited the chamber through the SFB plus the powder that has exited the chamber through the baghouses as equation 2 shows:.

$$m_{Sift} = m_{SFB} + m_{BH} \tag{2}$$

The main baghouse fines can be recycled to one of three locations in the VFs: the start of VF #1 as drawn in Figure 1, the start of VF #2 or the end of VF #2. The VF baghouse fines can also be recycled to one of these three locations. However, the location of these return lines to the VFs does not impact on the mass balance above, so equation (2) will always hold.

If it is assumed that a) no breakage or agglomeration of powder occurs in the fines return lines or during the VF process, b) that the flow of powder and particle size distribution of the powder is the same in both the main baghouses, and c) that representative samples of powder have been collected, then the particle size distribution at the sifter should be equal to a combination of the SFB powder particle size distribution and the main baghouse particle size distribution. The amount that the SFB and baghouse particle size distribution contribute to the sifter particle size distribution is determined by the powder flows exiting through the SFB and baghouses respectively, expressed as a fraction of the total powder flow. A mass balance corresponding to equation (2) but for one size interval then gives equation (3):

$$\Delta Q_{m,Sift} = \Delta Q_{m,SFB} X_{SFB} + \Delta Q_{m,BH} X_{BH} \tag{3}$$

where ΔQ_m is the mass fraction of a sample of powder in the given particle size band, and the subscripts Sift, SFB and BH represent the sifter, static fluid bed and baghouse samples respectively. The remaining term in equation (3) is X_{SFB} the ratio of SFB powder flow to the total powder flow given by equation (4):

$$X_{SFB} = \frac{m_{SFB}}{m_{Sift}} \tag{4}$$

Dividing equation (2) by m_{Sift} and substituting equations (1) and (4) gives

$$X_{SFB} + X_{BH} = 1 \tag{5}$$

Thus, equation (3) can be written as

$$\Delta Q_{m,Sift} = \Delta Q_{m,SFB}\left(1 - X_{BH}\right) + \Delta Q_{m,BH} X_{BH} \tag{6}$$

The measured particle size distributions yielded volume fractions ΔQ_3. If the densities of all particles are common, that is, the particle densities are constant for all sizes, then the size distribution by mass is equal to the size distribution by volume. For this work, it was assumed that the particle density is constant for each product hence, the mass fractions in equation (6) were replaced with volume fractions (ΔQ_3).

An estimate of the fines loadings can then be made by measuring the sifter, SFB and baghouse samples volume fractions in each particle size range i, and determining the value of X_{BH} across all particle size bands that minimises the sum of the squares of the residuals e_i, where

$$e_i = \Delta Q_{3,Sift,i} - \Delta Q_{3,Sift,\mathrm{Pr}ed,i} \tag{7}$$

and $\Delta Q_{3,Sift,Pred}$ is calculated from the volume fraction equivalent of equation (6). An optimisation package such as Microsoft Excel Solver can be used to carry out this minimisation.

On some occasions (for example during the production of Product A) fines from one of the main baghouses are recycled to the drying chamber. If BH #1 fines were being recycled to

the chamber for example, and again assuming that the fines flows from each baghouse are equal, equation (2) would become

$$m_{Sift} = m_{SFB} + \frac{m_{BH}}{2} \tag{8}$$

In this situation, equation (5) would become equation (9) as only half of the fines flow is contributing to the sifter flow.

$$X_{SFB} + \frac{X_{BH}}{2} = 1 \tag{9}$$

The volume fraction equivalent of equation (6) would also be modified to account for the smaller contribution from the fines as shown in equation (10)

$$\Delta Q_{3,Sift} = \Delta Q_{3,SFB}\left(1 - \frac{X_{BH}}{2}\right) + \Delta Q_{3,BH}\,\frac{X_{BH}}{2} \tag{10}$$

This minimisation of the sum of the squared residuals using either the volume fraction equivalent of equation (6), or equation (10) where appropriate, was used for Products A, B, C, D and E produced in an industrial scale milk powder spray dryer operated by Fonterra. In each case, sets of samples from different batches were obtained from the SFB overflow weir, the inspection hatch above the BH hopper and from the sample point at the start of the sifter. Samples of 200-500 g were collected in a 500 mL sample jar with a 100 mm mouth diameter inserted into the process line through a sample hatch at each location. The jar intercepted approximately 25% in the middle of SFB and sifter solids streams and approximately 2% on the edge of the BH solids stream. Sampling times ranged from 15 to 120 s. The minimisation used Microsoft Excel Solver.

Particle size distributions were measured using a Microtrac X-100 (Leeds & Northrup, North Wales, USA). This unit is a laser diffraction based instrument capable of measuring particles

sizes between 1 μm and 700 μm across 25 size intervals. The powder samples in this case were elutriated in air and the suspension passed through the laser beam. For each sample, the particle size distribution was measured three times and individual interval ΔQ_3 had a pooled variance of 0.32 $(\%)^2$ with 150 degrees of freedom.

An alternative method to evaluate the fines fraction could be to rearrange Equation (6) and calculate X_{BH} for each particle size interval. An overall fines fraction could be determined from the average of these 25 values of X_{BH}. However, because of the uncertainties structure from this approach being greater than that outlined above, the sum of squares approach is preferred.

Isokinetic Sampling

An assembly to allow isokinetic sampling of the gas stream was placed in one of the two spray dryer outlet air ducts during plant downtime. This assembly consisted of a cylindrical stainless steel housing for a fibre glass thimble filter fixed to the end of a 1200 mm long stainless pole. The pole ran through the centre of a 335 mm diameter circular stainless mounting that was bolted to the side of the duct. Rubber air hosing from the back of the thimble was fed through the middle of the pole and came out near the handle of the pole. This was connected to the sampling pump.

The air stream was sampled following a standard isokinetic sampling method such as "Method 5 – Determination of Particulate Matter Emissions from Stationary Sources" (USEPA Emissions Measurement Centre, 1977). The mass flow of air in the duct was determined from a mass balance of the spray dryer. These main inlet and SFB air flows,

along with the temperature in the duct, were taken from the plant operators' screens, allowing the volumetric flow and then the average velocity in the duct to be calculated. Also taken from the operators' screens was the dryer outlet air relative humidity, which enabled the water vapour concentration in the duct air stream to be determined using psychometric charts. It was assumed that, because of the small size of the duct relative to the size of the dryer chamber, and because of the close proximity of the sampling station to the chamber exit (one duct diameter), the velocity in the duct was uniform.

Optical Scintillation Instrument

An optical scintillation based powder flow measurement instrument (CPM 5003, BHA Group, Kansas City, USA) was located in one of the two spray dryer outlet air ducts. This instrument consisted of a transmitter head emitting light at a wavelength of 660 nm from an LED light source. Both the transmitter and receiver surfaces were flushed with plant compressed air to prevent excessive build-up of powder. A key assumption in using this instrument is that the fluctuations in the extinction coefficient of the Beer-Lambert law are solely caused by changes in concentration (Clarke, 1996). Secondly, use of this instrument assumes that the fluctuations in concentration are proportional to the mean concentration.

Results and Analyses

Particle Size Distribution Method

Table 1 shows the results of the milk powder fines fractions (the ratio of the fines flow to the total powder flow) and the total fines flow for the five milk powder products. The error values presented are the average difference between the extreme and mean values. It can be seen that there is a range in fines fractions from 49 ± 8 % for Product B to 86 ± 2 % for Product A at operating condition one (A (1)). As a mass flow of fines powder, the range is from 3.5 ± 0.1 t h^{-1} for Product D to 10.5 ± 0.2 t h^{-1} for Product A (1).

Isokinetic sampling of Products D and E was carried out to check the accuracy of the particle size distribution methods results. The results are also shown in Table 1, where the error values in powder concentration are the calculated contribution of errors associated with each measurement required to calculate the concentration, and the fines fraction error then reflects this. The Product E fines fractions showed excellent repeatability giving an average value of 76 ± 2 %. An average value of 85 ± 5 % was obtained for Product D.

Table 1 also has design values obtained from the plant designer. These estimates were obtained from plant measurements on a smaller industrial scale plant. It has been indicated that the designers would expect 10 t h^{-1} of Product A and 5 t h^{-1} of Product B to be fines, which equate to fines fractions of 82 % for Product A and 42 % for Product B.

Figure 2 shows the average scintillation values for each product measured by the online optical scintillation instrument. The scintillation values plotted are an indication of the level of powder entering the baghouse; the higher the scintillation value, the higher the level of fines. The error bars plotted in Figure 2 show the range (minimum to maximum) in the

observed scintillation values for each product, which are larger than the expected random error. These observations were made over periods ranging from 3 to 30 days.

The fines flow estimates from the particle size distribution method, from the isokinetic sampling and from the plant designers can be compiled with the corresponding optical scintillation readings to form a calibration curve (Figure 3) for the optical scintillation instrument. The scintillation readings for the isokinetic sampling results correspond to those obtained at the same time as the isokinetic sampling. The average scintillation reading for the different products was used with the particle size distribution method and plant designer estimates. This calibration curve is based on the assumption that extinction coefficient has the same value for the different milk powders at a given concentration. The errors shown in this figure correspond to those in Table 1.

Discussion

Particle Size Distribution Results

Assuming that the error variance in the SFB, baghouse and sifter samples is the same and constant among the different milk powders, then the particle size distribution method has an error variance of approximately 0.004 $(\%)^2$ (the method used to calculate this error variance is outlined in the Appendix). This error variance equates to a standard deviation of 0.06%. It can be seen from the fines fraction values in Table 1 that three standard deviations from the mean value is much smaller than the batch-to-batch variation among samples of around 5%, with the exception of Product A at operating condition two (A (2)). Under these operating conditions, fines from one baghouse are returned to the top of the spray drying chamber. It is likely that increased agglomeration occurred under these conditions and because the agglomeration process is difficult to control (Williams *et al*., 2006), the large range in fines fractions observed is a result of varying rates of agglomeration. This increased agglomeration is also the likely reason for the fines fractions at operating condition two being significantly lower than those at operating condition one; increased agglomeration would increase the average particle size of the sifter sample and therefore reduce the amount of fines present. It appears that the inherent scatter in the fines fraction estimate is not a result of contributions of experimental error, but can largely be explained by batch-to-batch variation.

Table 1 shows that the particle size distribution method was used for Product E at two different operating conditions. At the first operating point, an average value of 69 ± 5% was obtained. However, operating point two, where the feed concentrate total solids was approximately 4% lower than that at operating point one, had an average value of 83 ± 1%. A t-Test with a 0.5% probability showed there is more than sufficient evidence to suggest that the two means are different, and thus the change in operating conditions created a change in

the fines fraction. This result is supported by the fact that a reduction in static fluid bed height was observed, indicating that less powder was at the base of the chamber and more powder was exiting the dryer as fines in the outlet air ducts. Therefore, it is clear that the reduction in total solids caused an increase in fines loading. This indicates that the particle size distribution method is sensitive enough to detect changes in fines loadings caused by key changes in plant operating conditions.

The average fines fraction by the particle size distribution method of 96 ± 4 % for product D, which equates to approximately 3.5 ± 0.1 t h^{-1}, indicates that almost all of this powder is exiting the chamber through the baghouses. Therefore, the sifter and baghouse particle size distributions would be expected to be almost identical, which was shown to be the case.

Plant observations support the particle size distribution results. The plant operators struggle to retain powder on the SFB when producing Products C and D, and the time required to obtain a sufficient sample of Products C and D from the SFB overflow weir is much longer than for Products A, B and E. This indicates that most of Products C and D exit the chamber through the baghouses. The time required to obtain a Product B SFB sample was the shortest of all powders. This suggests that compared with the other powders, more Product B is flowing through the SFB and, therefore, less powder flows through the baghouses.

Isokinetic Sampling

Table 1 shows that fines fractions from the isokinetic sampling are slightly lower than those obtained using the particle size distribution method. Two possible sources of experimental error during the isokinetic sampling exist. Firstly, the thimble assembly may not have been

perfectly aligned in the horizontal position during sampling. This would mean that the effective cross sectional area of the nozzle perpendicular to the flow would be reduced and a smaller mass of powder than expected was collected.

Secondly, there may have been errors in determining the velocity for isokinetic sampling. This velocity was calculated by carrying out a mass balance on the air flow in the dryer also accounting for the moisture in the outlet air stream. Slight variation in the values taken from the operators' screens to achieve this was observed and these values may have changed during the time it took to calculate the pump flow rate and carry out the sampling. This same velocity was used to calculate the required sampling flow, and therefore, this may not have been truly isokinetic.

Design Estimates

The Product A at operating condition one and Product B fines loading values obtained from the PSD method show good agreement with the estimates from the plant designers. A fines fraction of 42 % from the plant designers for Product B gives a fines flow of 5.0 t h^{-1}. This fines flow is approximately equal to the Product C fines flow. The scintillation results also show Products B and C to have equal fines flows. This suggests that the Product B fines fractions from the particle size distribution method are slightly higher than the actual, although the two estimates agree within experimental uncertainty. This could be possible if the samples clumped during storage, thus giving a larger particle size distribution than the actual; Product B had a greater tendency for clumping because of its composition.

Online Optical Scintillation Instrument

The optical scintillation instrument results show very good agreement with those from the particle size distribution method. Both methods showed that Product A has the highest fines loading of all products and Product E was shown to be the product with the second highest fines loading. Both methods showed that Product D had the lowest fines loading (3.5 ± 0.1 t h^{-1}) and scintillation (15.8 ± 6 %) of all products.

The particle size distribution and optical scintillation findings are supported by average baghouse differential pressure and fines return line pressure plant operating data. This operating data shows that Product A has the highest baghouse differential pressures and fines return line pressures for all products, and Products C and D the lowest baghouse differential pressures of all products. Although the baghouse differential pressures and fines return line pressures are functions of more than just the fines loadings, the significant difference observed in these parameters among the products are likely to be mostly due to the large difference in fines loadings.

The average scintillation for Product B and Product C was approximately 20 %. This finding that Products B and C have similar amount of fines agrees with a hypothesis from plant operating data; approximately equal fines return line (pneumatic conveying lines taking powder from the bottom of the baghouses to the external fluid beds) pressure drops for these two powders suggest these products have a similar amount of fines. The particle size distribution method and scintillation result above shows this to be true, even though the powders are significantly different in terms of particle size and density.

Online Optical Scintillation Instrument Calibration Curve

Figure 3 shows that a reasonably good straight line fit can be drawn through the data including the origin. This reiterates the fact that the particle size distribution method and the isokinetic sampling results are in good agreement, and also suggests that the extinction coefficient is constant for the different milk powders at a given concentration. This calibration curve means that the optical scintillation values obtained could with some confidence be converted to fines flows and displayed as an additional operating parameter on the operators' screens. This would give operators another tool to help minimise baghouse differential pressures as running conditions that minimised the fines flows to the baghouses could be obtained.

This calibration curve is a very good result considering the instrument is operating at powder concentrations above the supposed maximum; the supposed limit was stated as 10 g m^{-3} but these results indicate the instrument has responded to concentrations as high as 42 g m^{-3}. Also, the data is obtained from the industrial scale, where there is very little control when compared with that at the laboratory scale.

Parameters Influencing Fines Fractions

Table 2 shows some of the key difference in powder properties among the five products produced during this investigation. It would be expected that Product A has the highest fines loading because it has the higher product powder flow (12.2 t h^{-1}) and therefore the greatest quantity of powder that can become fines. At the other extreme, Product D would be expected to have the lowest fines loading because it has the lowest product powder flow of all products (3.7 t h^{-1}). However, Product E (11.1 t h^{-1}) has a slightly lower total powder flow than Product B (11.9 t h^{-1}) but a much higher fines loading, and, Products B and C (4.5 t h^{-1})

have similar fines loadings even though they have very different product powder flows. This indicates that the fines levels are a function of more than just the total powder flow.

Table 2 shows that Product B and Product E have a similar average particle size from the baghouses samples, but a slight difference in powder bulk density. It is likely that, because Product E has the lower powder bulk density, the lighter particles are more easily entrained in the outlet air stream and hence, Product E has a higher fines loading than Product B. Also, because Product E has a mass flow much greater than Products C and D, it places a higher fines loading on the baghouse.

Although Products C and D have the larger particle sizes, the fact that these particles are likely to have lower particle densities than the majority of the other powders, potentially indicates that this powder will have a greater percentage of fines. Therefore, although Product C has a much lower powder flow rate than Product B, because of the differences in powder density, these two powders have a similar level of fines.

Conclusions

This investigation has established a new method for determining the fines loadings in milk powder plants with washable baghouses. The method is based on a comparison of the particle size distributions of powder samples obtained from the SFB, the baghouse and the sifter and determining the percentage of sifter powder from the SFB and the baghouses.

The particle size distribution method results led to the conclusion that the fines fractions are significantly higher than what was traditionally thought to be 10% to 20%. Values of 49 ± 8% for Product B, 96 ± 4% for Products C and D, and either 86 ± 2% or 53 ± 23% for Product A and 64 ± 5% or 83 ± 1% for Product E depending on the operating conditions were obtained. Thus, the particle size distribution method is sensitive enough to detect changes in fines fractions caused by changes in the fines recycle location and the concentrate total solids. Because the results compared well with isokinetic sampling results where available (Products D and E), it was concluded that the particle size distribution method developed is a relatively simple, but accurate method for estimating fines flows.

Readings from an optical scintillation instrument were taken during sampling and a consistency check was made with the particle size distribution method estimates. These readings showed that Product A has the highest fines flow, Product E the second highest and Product D the lowest. These readings were found to be consistent with the particle size distribution method results. It is also concluded that the optical scintillation instrument can be used to measure fines concentrations in milk powder plants. This was despite the powder concentration experienced being high than the upper limits of the instrument stated by the supplier.

Finally, it can be concluded from this work that the fraction of fines in a milk powder plant with washable baghouses is a function of the total dry powder flow rate, the concentrate total solids, and the powder particle size and density.

Nomenclature

ΔQ	percent of powder in the given particle size band, %
c	powder concentration, g m^{-3}
e	residual, %
m	mass flow of powder, t h^{-1}
$M_{1,2}$	average particle size, μm
n	number of samples
ρ_b	powder bulk density, g mL
TS	concentrate total solids, %
X	ratio of source powder flow to the total powder flow, %

Subscripts

A	product A
BH	main baghouse
i	particle size band
In	powder to baghouse
j	product type
m	particle size based on mass
Out	baghouse powder emissions
Pred	calculated value
SFB	static fluid bed
Sift	sifter
VFBH	vibrating fluid bed baghouse
#1	baghouse #1
#2	baghouse #2

3	particle size based on volume

References

Caputo, A.C. and Pelagagge, P.M., 2000, Baghouse system design based on economic optimization, *Environ Prog*, 19(4): 238-245.

Clarke, A.G., 1996, Cross-duct monitoring of particulate emissions by opacity fluctuations, *Environ Technol*, 17: 101-106.

Cora, M.G. and Hung, Y., 2002, Controlling industrial particulate emissions: a practical overview of baghouse technology, *Envir Qual Man*, 11(4): 53-64.

Croom, M.L., 1995, *Filter Dust Collectors: Design and Application*, (McGraw-Hill, New York, USA).

Ellenbecker, M.J. and Leith, D., 1980, The effect of dust retention on pressure drop in a high velocity pulse-jet fabric filter, *Powder Technol*, 25(2): 147-154.

Gabites, J.R., Abrahamson, J., and Winchester, J.A., 2007, Design of baghouses for fines collection in milk powder plants, submitted to *Powder Technol*.

Intensiv-Filter, 1999, *Dedusting Technology Filter Media*, (Intensiv-Filter GmbH & Co, Langenberg, Germany).

Loffler, F., Dietrich, H. and Flatt, W., 1988, *Dust Collection with Bag Filters and Envelope Filters*, (Wiley, Chichester, UK).

Machen, K., 2001, *Characterisation of a washable baghouse in a milk powder manufacturing plant*, Master's thesis, Massey University, Palmerston North, New Zealand.

Masters, K. 1972, *Spray Drying - An Introduction to Principles, Operating Practice and Applications*, (Leonard Hill Books, London, UK).

Rothwell, E., 1987, Who needs better filter media. *Filtr Sep*, 24(2): 104-108.

Turner, J.H., McKenna, J.D., Mycock, J.C., Nunn, A.B. and Vatavuk, W.M., 1998, Baghouses and filters, in *EPA Air Pollution Cost Control Manual: Section 6: Particulate Matter Controls*, Mussatti, D. C. (ed.) (United States Environmental Protection Agency, Research Triangle Park, USA), pp 1-59.

Westergaard, V., 2003, *Milk Powder Technology*, (GEA Niro A/S, Gladsaxevej, Denmark).

Williams, A.M., Jones, J.R., Paterson, A.H.J. and Pearce, D.L., 2006, Agglomeration in the spray zone of a spray drier: determining an agglomeration index, *Proceedings of 5th World Congress on Particle Technology.*, Orlando, USA, April.

USEPA Emissions Measurement Centre, 1977, *Method 5 – Determination of Particulate Matter Emissions from Stationary Sources*, (United States Environmental Protection Agency, Research Triangle Park, USA).

Acknowledgements

The support of Fonterra milk powder plant staff and financial support from the Foundation for Research Science and Technology (FRST) and Fonterra is gratefully acknowledged.

Appendix

Triplicates of the particle size distribution measurements were made for each sample location for each different product sample. Because the Microtrac X-100 measured particle sizes across 25 size intervals, 50 degrees of freedom resulted. The error variances for each size interval for the SFB, baghouse and sifter samples were 0.35 $(\%)^2$, 0.32 $(\%)^2$ and 0.30 $(\%)^2$ respectively. The small difference between each was deemed insignificant and therefore the error variance for each size interval (ΔQ_3) was taken as being 0.32 $(\%)^2$. This variance was related to the variance of the predicted X_{BH} using standard error propagation where partial derivatives of X_{BH} with respect to $\Delta Q_{3,SFB}$, $\Delta Q_{3,BH}$ and $\Delta Q_{3,Sift}$ were calculated. This procedure gave an X_{BH} variance of 0.11 $(\%)^2$ for an individual particle size interval. The analysis contribution to the variance for the mean value of X_{BH} from 25 size intervals was then 0.004 $(\%)^2$ (0.11 $(\%)^2$ / 25).

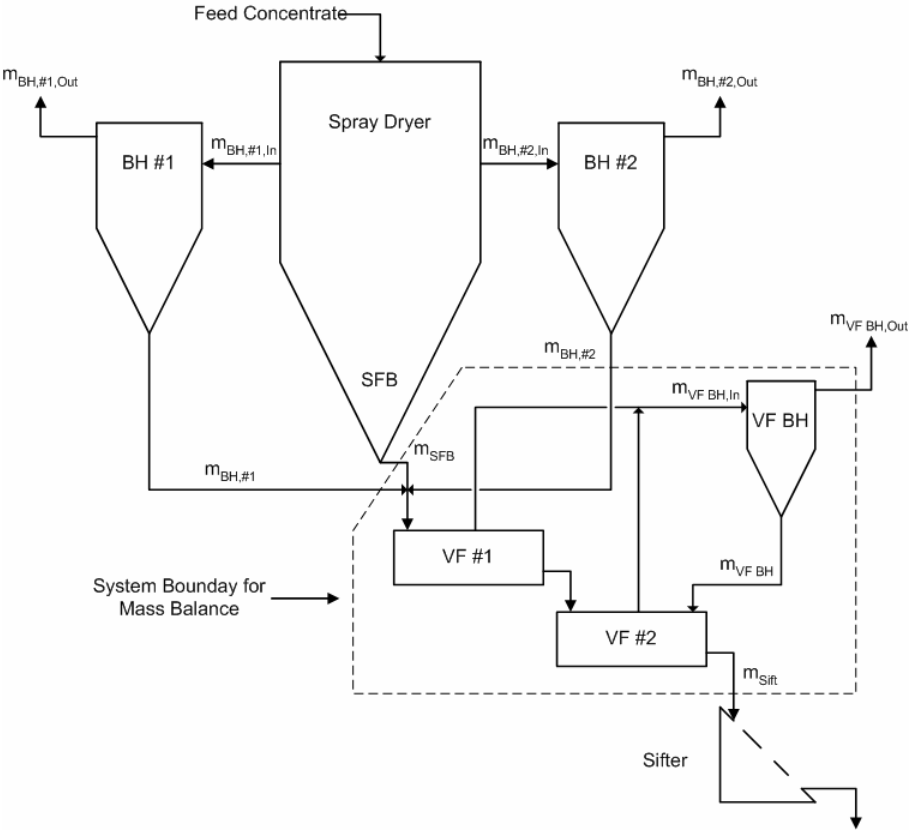

Figure 1. Powder flows in typical milk powder plant with washable baghouses

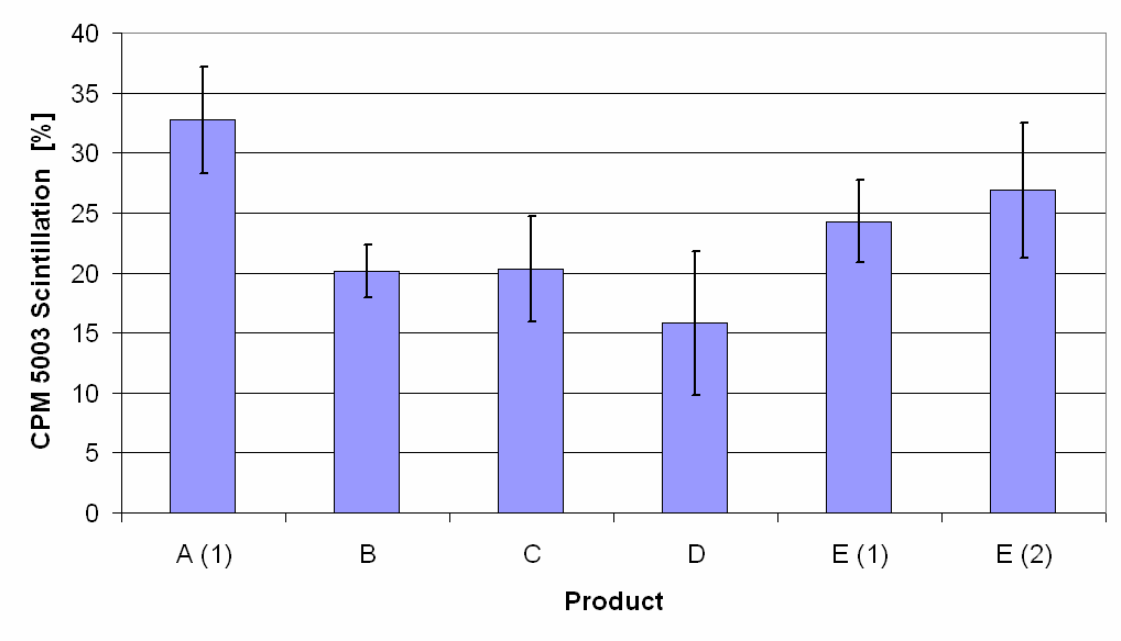

Figure 2. Average optical scintillation instrument values in an industrial Fonterra milk powder spray dryer outlet air duct for various milk powders

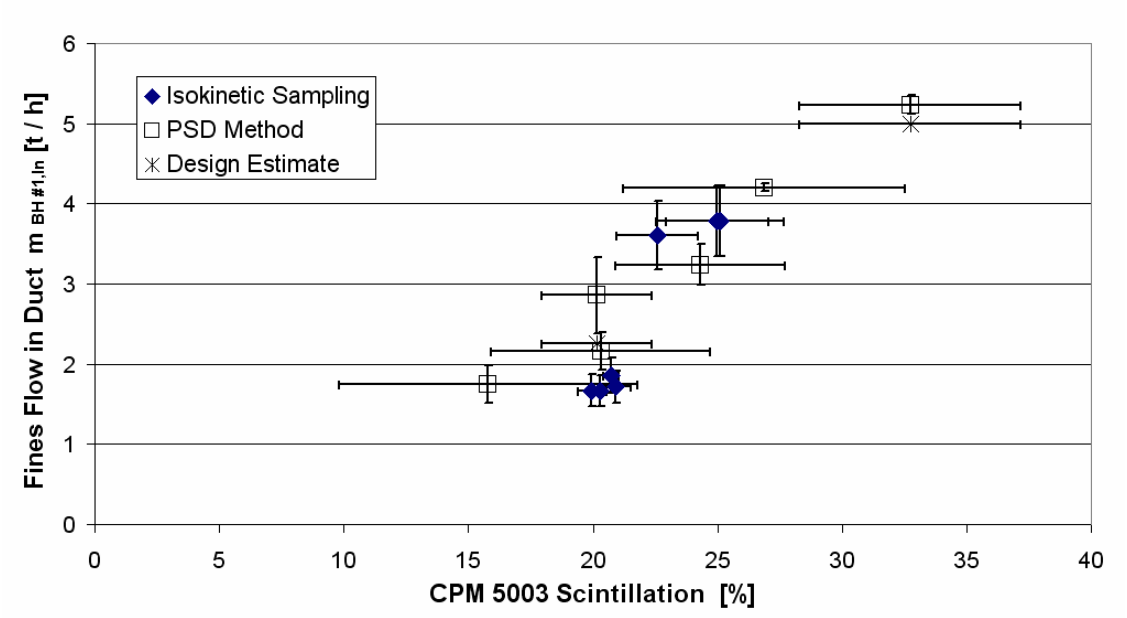

Figure 3. Optical scintillation instrument calibration curve for milk powder flows in an industrial Fonterra milk powder spray dryer outlet air duct

Table 1. Comparison of the particle size distribution method and isokinetic sampling to provide fines fraction estimates, total fines flow rates and powder concentrations for various milk powders produced in an industrial Fonterra milk powder plant

Product	Particle Size Distribution Method			Isokinetic Sampling		
	Number of Samples	Fines Fraction	Total Fines Flow	Number of Samples	Powder Concentration	Fines Fraction
	n	X_{BH} [%]	m_{BH} [t h^{-1}]	n	c_{BH} [g m^{-3}]	X_{BH} [%]
A (1)	2	86 ± 2	10.5 ± 0.2	0	-	-
A (2)	3	53 ± 23	6.5 ± 1.4	0	-	-
B	7	49 ± 8	5.7 ± 1.0	0	-	-
C	3	96 ± 4	4.3 ± 0.2	0	-	-
D	3	96 ± 4	3.5 ± 0.1	3	16.0 ± 0.9	85 ± 5
E (1)	3	64 ± 5	6.7 ± 0.3	0	-	-
E (2)	3	83 ± 1	8.7 ± 0.1	4	36.7 ± 1.5	76 ± 2

(1) = operating condition one
(2) = operating condition two

Table 2. Comparison of parameters influencing fines loadings for milk powders made in an industrial Fonterra milk powder spray dryer

Product	Product Flow Rate	Relative* Concentrate Total Solids	Relative* Average Particle Size	Relative* Bulk Density
	m_{Sift} [t hr^{-1}]	TS_j / TS_A [%]	$M_{1,2,j} / M_{1,2,A}$ [%]	$\rho_{b,j} / \rho_{b,A}$ [%]
A	12.2	100	100	100
B	11.9	102	108	77
C	4.5	54	122	70
D	3.7	50	120	56
E	11.1	83	108	72

* Data given relative to product A

Appendix D – Laboratory Scale Single Cell Baghouse finding proposal submitted to Fonterra

---

John Gabites & Assoc Prof John Abrahamson
Department of Chemical and Process Engineering
University of Canterbury
Christchurch, New Zealand

Laboratory Scale Single Cell Baghouse

Funding Proposal to Fonterra Co-Operative Group Ltd

December 2004

Prepared for:

Hong Chen
Tuan Truong
James Winchester
Chris Johnson

1. Project Overview

A single cell laboratory scale baghouse will be set up within the Department of Chemical and Process Engineering at the University of Canterbury. The rationale behind this proposal is that because of the many potential benefits to Fonterra, funding will be forthcoming.

The rig will initially be used to conduct experiments investigating issues that have arisen from washable baghouse use at Fonterra Clandeboye for a PhD titled Washable Baghouse Operation and Design, as Applied to Milk Powder Production.

These experiments will investigate the amount of bag movement in the baghouse, how pulse jet cleaning parameters can be manipulated to improve cleaning efficiency and prevent powder build up at the top of the filter bags and why an increasing fat content in skim milk powder reduces baghouse differential pressures. It is envisaged that Fonterra will use this rig as a permanent filter bag testing facility to compare filter bags from different suppliers. Finally, it is predicted that the Canterbury PhD will lead to more work on fabric filtration in the dairy industry that will require the use of this rig.

The rig design is novel in that it uses a 3 m long filter bag and the dust used will be milk powder. Most fabric filtration research to date has used bags either 2.5 m long or small circles of bag fabric. Dusts used have generally been limestone, fly ash or coal dust, which are quite different to hygroscopic milk powders.

Benefits of this rig are that experiments conducted will use conditions almost identical to those experienced in the industrial environment and because the work is novel, it will lend itself to publication. Further, this rig will give the flexibility to vary a number of process parameters that would not be possible in the industrial environment because of restrictions on product specifications. Also, by having a bag testing facility, Fonterra will be able to gain data on filter bags of more relevance than that provided by filter bag suppliers, giving them better information for choosing suitable filter bags.

2. Introduction

2.1 Background Information

A recent change in the design of milk powder plants in New Zealand has seen the traditional cyclone system used for fines recovery replaced with washable baghouses. Washable baghouses that have been installed at Fonterra Co-operative Group Limited plants are Powder 2 at Whareroa (2000/2001 season), on the Whey Protein Concentrate Dryer at Lichfield (00/01 season), Dryers 2 and 3 at Edendale (2001/2002 and 2002/2003 seasons) and on Dryers 2 and 3 at Clandeboye (2000/2001 and 2004/0205 season).

GEA Niro A/S installed three Sanicip washable baghouses with the Clandeboye Dryer 2 (D2) in the 2001 off-season. This was the first of the Niro Sanicip designs installed in New Zealand. Since their installation, the baghouses have performed well below expectation. A number of baghouse problems led to a total of 66 hours of plant downtime between August 2002 and January 2003.

In the peak of the dairy season, the milk to be processed at Clandeboye is almost equal to the capacity of the site. Any reduction in site capacity due to production issues is very costly; it was estimated that the downtime due to baghouse issues in the 2002/2003 season cost $100 a minute (Personal communications, 2004).

The downtime was mostly due to bag failure in the main baghouses. Bags wear when they rub against each other and the sharp sections of the internal cages that support them. This movement arises not only because of the nature of pulse cleaning but also because of cage movement due to the dirty airflow in the baghouse. These high internal air flows can bend cages, resulting in more sharp sections for bags to rub on.

A number of different suppliers of filter socks have been used in an attempt to improve bag longevity. Filtercorp International Ltd, Canterbury Filters, supplying Madison bags, and Intensiv Filter have all been trialled with limited success. The technical information supplied by these companies is often irrelevant as the dusts used to generate pressure drop or cleaning efficiency data are often fly ash or coal dust, both of which are vastly different to hygroscopic milk powders. The laboratory conditions for gathering this data are often quite different to those bags' experience in the plant. Small sections of bag fabric, say 15 cm diameter circles, rather than full length bags is an example of how the laboratory and plant comparisons differ. Therefore, the ability to compare filter bags in operating conditions almost identical to their end use would be a real advantage.

Plant experience shows that different powder products allow for better baghouse performance. Baghouses operate at lower differential pressures when manufacturing whole milk powder compared to skim milk powder. Even within the small range of skim milk powder fat contents, baghouse differential pressures vary. The mechanism behind this phenomenon is unknown but one hypothesis is that as the fat content in milk powders increases, the resulting cake on the filter bags is more porous and or less adhesive. Measuring these parameters in an industrial environment would be very difficult, but a purpose built laboratory rig would allow this data to be gathered with relative ease.

Clandeboye powder plant staff have observed that a large amount of powder builds up under the cell plate at the top of the bags (Personal communications, 2004). These findings are consistent with those of Loffler and Sievert (1987), who showed that negative pressures in the

top of the bag developed when the compressed air jet initiated the bag cleaning. This resulted in dust and the filter bag being sucked onto the supporting cage instead of being accelerated away from the cage and releasing the collected cake. It is believed that the location of the jet ejector relative to the top of the bag has a large impact on the amount of powder that builds up under the cell plate. Again however, quantifying these findings and generating a solution in the industrial environment would be very difficult. Therefore, use of a purpose built laboratory rig would be a much better approach to solving this problem.

Finally, how pulse jet cleaning cycle times impact on baghouse differential pressures in the short term and bag life time in the long term is not well known. A plant visit to Edendale revealed different pulse cleaning sequences to those used at Clandeboye, even though the plants are virtually identical. Models are available (Ju et al., 2001; Calle et al., 2002; Neiva and Goldstein, 2003) for predicting pressure drop development over time but the models rely on empirical constants, most of which were developed with dusts dissimilar to milk powders. Therefore, the application of these models to the dairy industry is limited. Quantifying the influence of pulse jet cleaning cycle times and compressed air pressures on baghouse differential pressures would be valuable for improving baghouse performance. Only a laboratory scale apparatus would give the flexibility needed to achieve this.

2.2 Laboratory Baghouse Rigs in Literature

A number of examples in literature can be found of laboratory or pilot scale baghouses (Morris and Allen (1996), Leith, First and Gibson (1978), Loffler and Sievert (1987), Klingle and Loffler (1984), Ellenbecker and Leith (1980)). Most of these rigs were vertical and used bags 2.5 m in length. These authors investigated fabric filtration topics such as cleaning efficiency, dust density profiles on bags, pressure drop modelling and the influence of cake compaction. As mentioned above, however, none of the dusts used were milk powder.

The proposed rig would be novel in that it would use 3 m long bags, half the length as those used in the Fonterra Niro Sanicip baghouses. The advantage of using these 3 m long bags is that almost identical conditions would be replicated in the laboratory rig. This should allow a superior understanding of the mechanisms that create the problems mentioned above and therefore allow for better solutions to be developed.

2.3 Project Location

The location of washable baghouses in the New Zealand Dairy Industry is predominantly in the South Island. Fonterra currently operate four large milk powder plants, with a total of ten main washable baghouses, in the South Island, six of which are found at the Clandeboye site. With the current projections for milk volumes, it is envisaged that another milk powder plant will be built at Clandeboye in the near future, and there is every likelihood that this plant will use washable baghouses as the fines collection equipment.

Because of its close proximity to the Clandeboye site, the University of Canterbury Department of Chemical and Process Engineering (CAPE) is the ideal location to house a laboratory scale single cell baghouse. Associate Professor John Abrahamson, has a large amount of experience in the field of powder technology and the department has facilities, such as Scanning Electron Microscopy and Particle Size Distribution analysis equipment, which may be helpful tools to assist with the proposed work.

3. Project Detail

3.1 Goals and Objectives

John Gabites' University of Canterbury Washable Baghouse Operation and Design PhD thesis will endeavour to achieve the following objectives and goals:

Goal #1 - Investigate the bag movement as a result of internal baghouse air flows and pulse jet cleaning

- Objective 1.1: Video the bag movement in the laboratory rig
- Objective 1.2: Compare the video analysis of the laboratory and industrial baghouses
- Objective 1.3: Measure the bag displacement in the laboratory rig
- Objective 1.4: Evaluate the change in bag movement as a result of welding the cage finger joint

Goal #2 – Limit the amount of powder build up under the cell plate

- Objective 2.1: Observe the effect of changing the position of the compressed air ejector above the cell plate
- Objective 2.2: Observe the effect of modifying the pressure of the compressed air jet
- Objective 2.3: Using the gathered data, generate a model of pulse jet cleaning, relating it to powder properties such as stickiness to the bag

Goal #3 - Determine why baghouse differential pressures drop as the percentage of fat in skim milk powder increases

- Objective 3.1: Measure the filter cake adhesion force to the bag fabric of milk powders at different fat contents
- Objective 3.2: Measure the filter cake permeability of milk powders at different fat contents
- Objective 3.3: Examine filter cake structures of milk powders at different fat contents using scanning electron microscopy (SEM)
- Objective 3.4: Use the Peschl Shear Cell to give an indication of the internal angle of friction for milk powders at different fat contents

Other Use

This rig could also be used as a filter bag testing facility for Fonterra. New filter bags from suppliers, both fabric and pleated, could be compared in this rig at conditions very similar to those that bags would experience in the plant. This would give Fonterra an upper hand over suppliers who provide technical information based on work conducted with dusts other than milk powder.

3.2 Clientele

Those groups with an interest in the results from this project, and those who follow on from it are:

- Fonterra Co-Operative Group Ltd Clandeboye Milk Powder Plant Management
    - Chris Johnson

- Fonterra Co-Operative Group Ltd Clandeboye Heat Transfer and Drying Process Technologists
    - James Winchester
    - Tuan Truong
- Fonterra Co-Operative Group Ltd Washable Baghouse User Group
    - Whareroa
    - Lichfield
    - Edendale
    - Clandeboye
- Filter Bag Suppliers
    - Filtercorp International Ltd
    - Intensiv Filter
    - Madison Filter
- Baghouse Design Companies
    - GEA Niro A/S
    - Intensiv Filter

3.3 Methods

The proposed operation of the single cell rig is as follows:
Air at varying flow rates and humidities will be supplied from the CAPE laboratory scale GEA Niro A/S spray drier running on water. Powder will be injected into this air stream using the current CAPE powder ejector and then fed into the vessel from below the bag. Powder will collect on the filter bag and a pulse jet ejector will use compressed air taken off the laboratory mains for bag cleaning. The falling powder will collect in a hopper at the bottom of the baghouse where transport air flowing through the perforated hopper plate will force this powder through the powder outlet.

A brief description of some of the methods for measuring the variables mentioned in section 3.1 follows.

- Bag Movement – a glass inspection window at the bottom of the bag will allow bag movement to be recorded with a high speed video camera. Displacement guides (wire pushed up against the bag surface and forced out when the bag moves) will be used to measure the maximum amount of bag movement.

- Pulse Jet Cleaning – the effect of various pulse cleaning pressures, ejector positions and cycle times will be discovered by measuring the mass of powder released during cleaning and conducting SEM work on the bag surfaces to deduce the degree of penetration and bag blinding.

- Bag Permeability – two methods will be used. Firstly, a Pitot tube bundle hanging inside the bags will measure the internal bag air flow at five heights. The second method will see a vacuum cleaner blow air through the bag and powder cake while the resulting pressure drop is measured, again at various heights.

- Cake Adhesion Force – the vacuum cleaner set up will be used to suck powder off the bag surface at a fixed flow and the amount of powder removed will be measured using a thimble filter to give an indication of the cake adhesion force. Measuring the

adhesion force this way would replicate as best as possible the exact location where it is important.

3.4 People Involved

John Gabites and Associate Professor John Abrahamson from CAPE will design this rig. Input will also be sought from department safety officer David Brown and Mechanical Workshop Technician Paul Tolson. Paul Tolson will conduct the mechanical construction of the rig, with electrical support from Bob Gordon**,** Electrical and Electronics Workshop Technician.

John Gabites will conduct the initial operation of the rig with supervision from John Abrahamson. At the completion of the Washable Baghouse PhD thesis it is envisaged that opportunities for further use will arise. Therefore, future operators of the rig could be Chemical and Process Engineering Third Professional, Post-Graduate or research students and/or Fonterra summer students.

3.5 Resources

Available Resources

The Department of Chemical and Process Engineering has the following resources available for this project:

- Laboratory space
- Technicians for rig construction
- Easy access to compressed air, humidified air
- Instrumentation
    - Flow meters
    - Pressure gauges
    - Load cell
- Powder ejector
- High speed video camera
- SEM facilities

Needed Resources

The following is a list of resources that would be needed for this project:

- Baghouse vessel and support structure
- Milk powder samples (could use lab scale drier to generate these but for better application of results to the industrial environment, industrial powder should be used)
    - Skim milk powder (fat content varying from 0.5 to 1.1 %)
    - Whole milk powder
    - Milk protein concentrate
- Filter bags
    - New
    - Used
    - CIPed
- Filter bag support cage
- Pulse jet air ejector

- Instrumentation
    - Pitot tube bundle
    - Bag movement ruler
    - Cake permeability/adhesion force test nozzle

A ballpark figure for construction of the rig, support structure and required instrumentation is $10,000 to $15,000. The CAPE PhD project has funding of $5,000 per annum for experimental consumables, which obviously leaves a shortfall. Since this rig would see a collaborative effort between the University of Canterbury and Fonterra Co-Operative Group, it is suggested that an agreement be reached between the two parties to cover the cost of this rig.

3.6 Benefits

The benefits seen to arise from this project are:
For Fonterra

- Gaining a better understanding of baghouse operation and design which will allow for stronger positions when dealing with design companies and filter bag suppliers
- Access to knowledge in the fabric filtration field without great expense
- Resources to conduct research work that otherwise would not be carried out
- Development of relationships that will allow for further collaborative research

For CAPE

- Application of research to an industrial environment
- Exposure for students to industrial environment and therefore networking opportunities
- Development of relationships that may see further collaborative research or funding opportunities
- Exposure of the department and its research activities

3.7 Measures of Success

The measures of success for this project are listed below:

1. The rig construction and operation is such that the industrial conditions are replicated, i.e. the rig can operate at the temperatures, humidities, powder concentrations experienced at Clandeboye and the issues (bag movement, powder build up around the cell plate) are observed in the laboratory scale rig

2. The pulse jet cleaning process is modified (jet ejector position, compressed air pressure, pulse duration and cycle time) such that cleaning efficiency is improved preventing powder build up under the cell plate

3. The pulse jet cleaning model that is developed is successfully used in computational fluid dynamics work for baghouse design

4. The mechanisms behind increasing baghouse differential pressures with decreasing skim milk powder fat contents are found

5. The quality of the work is such that non-commercially sensitive results will be published in relevant journals

6. Fonterra continue to use the rig for comparing filter bags and gain data that is superior to that supplied by filter bag companies

4. Bibliography

1. Personal Communications, Clandeboye Powder Plant Staff, March – June 2004

2. F. Loffler and J. Sievert, *Cleaning mechanisms in pulse jet fabric filters*. Filtr. Sep., Mar/Apr, (1987), 110-113.

3. J. Ju, M. Chiu, C. Tien, *Further work on pulse-jet fabric filtration modeling*. Powder Technol., 118, (2001), 79-89.

4. S. Calle, P. Contal, D. Thomas, D. Bemer, D. Leclerc, *Description of the clogging and cleaning cycles of filter media*. Powder Technol., 123, (2002), 40-52.

5. A.C.B. Neiva, L. Goldstein, *A procedure for calculating pressure drop during the build-up of dust filter cakes*. Chem. Eng. Process., 42, (2003), 495-501.

6. K. Morris and R.W.K. Allen, *The influence of dust and gas properties on cake adhesion in fabric filters*. Filtr. Sep., Apr (1996) 339-343.

7. D. Leith, M.W. First and D.D. Gibson, *Effect of modified cleaning pulses on pulse jet filter performance*. Filtr. Sep. Sep/Oct (1978) 400-406.

8. R. Klingle and F. Loffler, *Investigations on optimal cleaning conditions for bag filters with pulse-jet cleaning*. Chem. Eng. Process., 18 (1984), 189-198.

9. M.J. Ellenbecker and D. Leith, *The effect of dust retention on pressure drop in a high velocity pulse-jet fabric filter*. Powder Technol., 25, (1980), 147-154.

Appendix E – Publications from Baghouse Design work

E1 – Design of washable baghouses for fines collection in milk powder plants, presented in 5th World Congress on Particle Technology (2006) E2

E2 – Design of baghouses for fines collection in milk powder plants, submitted to Powder Technology (2006) E13

Design of Washable Baghouses for Fines Collection in Milk Powder plants

J.R. Gabites[1], J. Abrahamson[1] and J.A. Winchester[2]
[1]Department of Chemical and Process Engineering, University of Canterbury, Christchurch, New Zealand
[2] Heat Transfer and Drying Team, Clandeboye Site, Fonterra Co-operative Group Ltd, Temuka, New Zealand

ABSTRACT

The design of pulse-jet baghouses for fines collection has been investigated. Firstly, the key design parameters and recommended values for these are presented, showing a large variation among sources. A procedure for determining the optimal combination of these parameters has been developed that differs from those found in the literature by including a previously ignored area outside the bag bundle. A comparison was then made between the four air to cloth ratio design guidelines of Croom (1995), Loffler Dietrich and Flatt (1988), Turner et al. (1998) and Intensiv Filter (1999), for the case of milk powder collection. Again large variation is found. Finally, a comparison between industrial experience and these guideline values for the dairy industry shows that in this case, the guideline of Loffler et al. (1988) is the best compromise between high capital costs and operational difficulties.

KEYWORDS: Baghouse, Fines Collection, Milk Powder, Washable

1. INTRODUCTION

Fabric filtration is one of the oldest and most reliable forms of particulate collection [1]. Fabric filters or baghouses have been chosen in an increasing number of industrial processes for controlling atmospheric emissions [2]. Examples include powder generation, chemical, food, metal and mineral industries [3]. As particle emission regulations become more stringent, baghouses will find increasing use because of their high efficiency [4].

A recent change in the design of milk powder plants has seen the traditional cyclone system used for fines recovery replaced with washable baghouse systems. Fonterra Co-operative Group Ltd, the world's largest exporter of milk products, has installed or retrofitted five such designs in milk powder plants throughout New Zealand since the year 2000. One such plant is the world's largest milk powder plant, situated on the Clandeboye site near Temuka in the South Island.

Baghouses were traditionally used to remove fines not recovered by cyclones attached to spray dryer systems, but were always thought to be a source of microbial contamination because powder may have long residence times in the bags. Therefore approximately 10% of these cyclone fines were downgraded to stock food. Another disadvantage of this traditional system was that cyclones often blocked, thus interrupting dryer operation.

Washable baghouses, with their ability to be cleaned-in-place (CIP), have changed the perception of baghouses as being a source of microbial contamination. Consequently, all fines collected by them retain the microbial product quality of the dryer chamber powder, thereby increasing profits. Because all fines are collected in a single stage, fewer unit operations are required. This leads to reduced building space requirements, lower capital costs and simplified plants [5]. The final advantage of the new system is that baghouse collection is a gentler form of product collection when compared to cyclones. This is more suited to the high fat and high protein powders of the dairy industry [6].

Despite the numerous advantages of this new system, high differential pressures, some blinding and bag damage due to bag movement have caused frequent interruptions to the dryer operation.

This paper examines the design of pulse-jet baghouses as applied to milk powder production. The aim of this investigation is to explore the key design parameters, compare the available design guidelines for milk powder baghouses and assess the suitability of each

2. METHOD

Key baghouse design parameters and recommended values for these separate parameters were found from the literature. A procedure for baghouse design was developed building on this information. Microsoft Excel was used to generate a spreadsheet that used the Solver feature to calculate the optimal combination of these parameters.

Specifically for the collection of milk powder, several procedures for calculating recommended air to cloth ratios were found from the literature. Using typical parameter values found in a milk powder plant, these air to cloth ratios were calculated. Based on Fonterra's industrial experience, these air to cloth ratios were assessed for their suitability for milk powder collection.

3. RESULTS AND DISCUSSION

3.1. Baghouse Design Parameters

The key baghouse parameters appear to be as follows; [7-11]

Air to Cloth Ratio (V_f [usual units m^3 / m^2 / min]), also termed the filtration velocity, is the ratio of the inlet gas flow Q_{in} [m^3 / min] to the required filtration area A_f [m^2] as shown in Equation 1.

$$V_f = \frac{Q_{in}}{A_f} \tag{1}$$

where A_f is given by

$$A_f = nA_b \tag{2}$$

n is the total number of bags and A_b the filtration area [m^2] of a single bag given by

$$A_b = \pi D_b L_b \tag{3}$$

where D_b [m] and L_b [m] are the bag diameter and length.

Recommended values have been determined from experience and laboratory or pilot scale experiments. Values were tanked from pulse-cleaned baghouses. Suggested maximum values shown with their sources in Figure 1, vary by approximately 90 %, from a value of 2.4 m^3 / m^2 / min [10] [12] to 4.6 m^3 / m^2 / min [13].

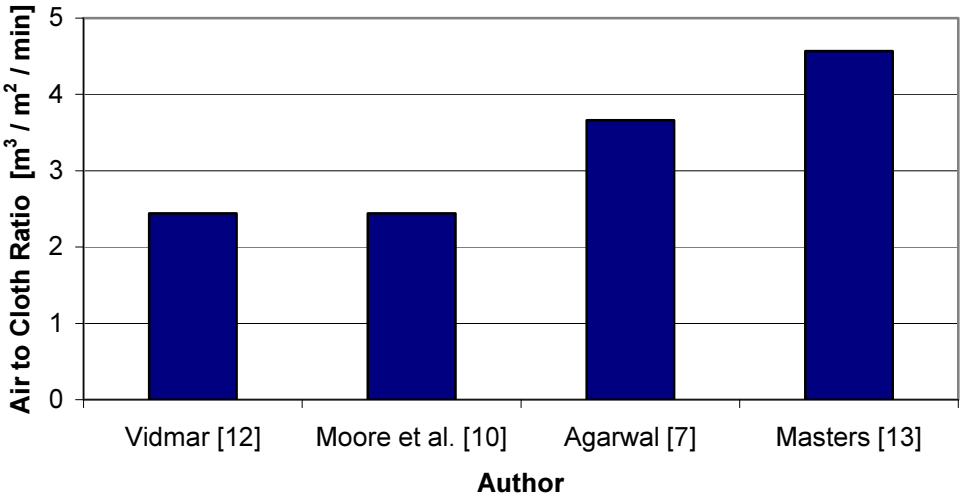

Fig. 1: Maximum pulse-cleaned baghouse air to cloth ratios recommended by various authors

Elutriation Velocity (V_e) is determined by dividing the gas flow by the cross sectional area of the vessel minus that of the bags (Equation 4).

$$V_e = \frac{Q_{in}}{A_{BH} - A_{Bags}} \tag{4}$$

For a circular baghouse the footprint A_{BH} [m^2] is given by Equation 5 where D_{BH} [m] is the baghouse diameter.

$$A_{BH} = \pi\left(\frac{D_{BH}}{2}\right)^2 \tag{5}$$

A_{Bags} [m^2] is the total cross sectional area of the bags given by

$$A_{Bags} = n\pi\left(\frac{D_b}{2}\right)^2 \quad (6)$$

Although the definition of Equation 4 uses the total baghouse area, a more accurate definition would use the bag bundle area as the re-entrainment of dust removed from the bags during cleaning within the bag bundle is of more interest (see Figure 2). The upper limits of the elutriation velocity, again with their sources, are given in Table 1. The basis for the elutriation velocities is a single particle terminal velocity in the baghouse [7]. However, the terminal velocity is strongly dependant on particle size, and it is unclear which size should represent the powder falling off the bags.

Table 1: Recommended maximum elutriation velocities

Author	[m / s]
Croom [8]	1.27
Agarwal [7	1.52
Moore et al. [10]	1.83

Bag Spacing (X_b) is defined as the perimeter-to-perimeter distance between neighbouring bags. Values equal or larger than 25 mm [14] and 80 mm [9] are recommended to ensure that dust removed by pulse cleaning is not pulsed onto neighbouring bags.

Choice of Filter Medium is recommended to be based on testing as well as performance guarantees [8]. Bag properties such as weight, thickness and permeability must be considered. The choice is made between woven and non-woven, natural and synthetic fabrics [3]. A range of mechanical and chemical surface treatments is available to improve bag features such as cake release, resist abrasion and protection against high temperatures [15].

The *Operating Differential Pressure* arises from the resistance of the air passing through the filter bags and cake. There are several models available [3] [16-20] that take account of the filtration velocity, dust concentration, time between cleaning pulses as well as bag and cake resistance. This pressure difference heavily impacts on the operating costs: the higher the differential pressure, the higher the electricity costs to run baghouse fans or blowers. It is agreed that the pulse cleaning should maintain a mean pressure difference across the bags of less than 200 mm H_2O [7] [13].

To maintain the differential pressure below a selected maximum pulse cleaning is used. The pulsing control can either be initiated by an upper differential pressure, where pulsing continues until a lower differential pressure is reached, or by using a timed control, where the pulse will occur periodically independent of the differential pressure. It should be noted, more frequent pulse cleaning creates higher emissions, accelerated bag wear and greater use of compressed air [17]. Further design choices are made between online and offline cleaning and the type of ejector.

Bag Dimensions of diameter (D_b) and length (L_b) are chosen to suit the required filtration area determined from Equation 1. The upper limits given in Table 2 are to ensure that adequate pulse cleaning occurs because cleaning performance decreases as diameter and length increase [7]. Also, as the bag length increases, the abrasion caused by swinging bags also increases and it is suggested that the air to cloth ratio be decreased when the bag length exceeds 3.0 m [9].

Table 2: Recommended maximum bag dimensions

Author	Diameter [mm]		Length [m]	
	Optimal	Maximum	Optimal	Maximum
Agarwal [7]	127 – 152	152	1.8 – 2.4	3.7
Moore et al. [10]	152	–	3.0	3.7
Loffler et al. [9]	120 – 150	200	–	–

Baghouse Footprint (plan area) impacts severely on the cost of an installation. However, larger collectors will increase bag life and reduce maintenance costs [12]. The footprint must be such that elutriation velocity limits for the chosen bag diameter and spacing are satisfied [8]. The baghouse footprint A_{BH} [m^2] consists of the area of the bag bundle A_{BB} [m^2] and the area between the edge of the bag bundle and the baghouse walls. Equation 7 gives the bag bundle area, where N [m^{-2}] is the bag density (number of bags per unit are of A_{BB}).

$$A_{BB} = \frac{n}{N} \tag{7}$$

For bags arranged in a square matrix spaced a perimeter-to-perimeter distance X_b apart, the bag density is given by

$$N = \frac{1}{\left(D_b + X_b\right)^2} \tag{8}$$

Therefore, for a circular baghouse, the diameter of the bag bundle D_{BB} [m] is given by Equation 9

$$D_{BB} = 2\left(D_b + X_b\right)\sqrt{\frac{n}{\pi}} \tag{9}$$

It is often more convenient to state the baghouse diameter instead of the baghouse footprint. The baghouse diameter is the sum of the bag bundle diameter and twice the distance from the edge of the bag bundle to the baghouse wall as shown in Figure 2 and given by Equation 10.

$$D_{BH} = D_{BB} + 2A \tag{10}$$

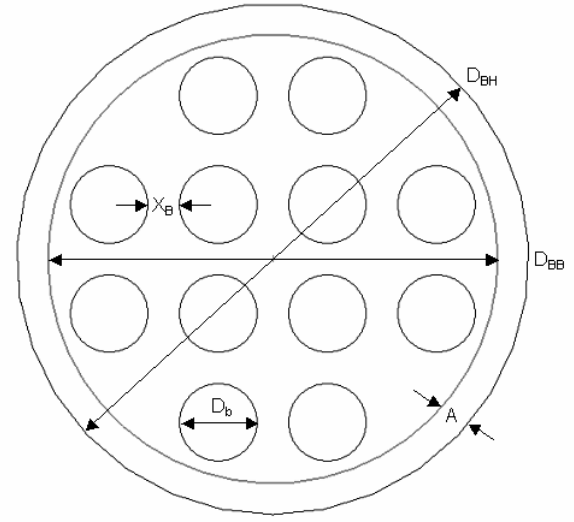

Fig. 2: Definition of parameters required to determine baghouse footprint in a circular baghouse

Three other purportedly less important design parameters are: the inlet air arrangement (bottom or top entry, radial or tangential entry); the baghouse shape (rectangular vs. circular); and the steepness of the hopper walls below the bags (at least 60o from the horizontal [7]).

The findings above indicate that significant variation exists in published recommended values of the key design parameters: the maximum air to cloth ratios vary by approximately 90 %, the maximum elutriation velocities vary by 50 % and optimal bag length varies by over 1 m. Caution is recommended especially for new applications, where field, pilot plant or laboratory measurements may be required [11].

3.2. Design Procedure

There exist nine baghouse design parameters: Q_{in}, V_f, V_e, n, L_b, D_b, X_b, G and D_{BH}. Rearranging Equations 1, 4 and 10 with respect to these parameters gives Equations 11, 12 and 13.

$$V_f = \frac{Q_{in}}{n\pi L_b D_b} \tag{11}$$

$$V_e = \frac{4Q_{in}}{\pi\left(D_{BH}^2 - nD_b^2\right)} \tag{12}$$

$$D_{BH} = 2A + \sqrt{\frac{4n}{\pi}\left(D_b + X_b\right)^2} \tag{13}$$

Because there are nine parameters and three equations, six parameters must be specified. The inlet air flow is specific to the application and determined from the upstream process feeding the baghouse. Upper limits for air to cloth ratio, elutriation velocity, bag length and bag spacing are discussed above and can be used as the specified values or the initial stage of the design. The distance between the edge of the bag bundle and the baghouse walls may be chosen such that it is greater than the between-bag distance. In the interest of distributing the incoming airflow evenly to the bag bundle, a baffle to deflect a radial inflow, or a tangential inflow may be used, both in conjunction with a sufficiently large annular flow area. Initial annular tangential velocities should be no larger than the inlet velocity, meaning that the area (GL_b) should be no less than the inflow area. This is normally set so that the inlet duct velocity is larger than the minimum particle carrying velocity, generally around 15 m/s. Thus all six parameters have been specified.

The system of equations can easily be solved using standard optimisation packages, e.g. Microsoft Excel Solver. A spreadsheet can be created listing the values of the six specified parameters, initial guesses for the three remaining unknowns (n, D_b and D_{BH}) and calculated values of the air to cloth ratio, the elutriation velocity and the baghouse diameter. The solver target cell is calculated as the squared difference between the repeatedly guessed baghouse diameter and that calculated from Equation 13. The solver is run to minimise this target cell by changing the values of the three guessed unknowns with constraints placed on the maximum air to cloth ratio, elutriation velocity and bag diameter.

Although this process generates one optimal design, a cost optimisation may be the next step e.g. [17] who deals with some of the above parameters. The cost of accessories (bags, cages, solenoid valves, air ejectors) will feature in this optimisation.

By including the area between the edge of the bag bundle and the baghouse walls, which is significant in practice, this sequence differs slightly to those found in the literature. Loffler et al. [9] list seven design parameters (Q_{in}, V_f, L_b, D_b, n, X_b, D_{BH}), specify five values (Q_{in}, V_f, L_b, D_b and X_b) and solve two equations (n, D_{BH}) based on a square bag matrix.

Loffler et al. vary the bag diameter and bag spacing to minimise the capital cost within the recommended limits of the parameters above (as long as cleaning performance and bag life are not compromised).

Croom [8] lists eight design parameters (Q_{in}, V_f, V_e, L_b, D_b, n, X_b, D_{BH}) as he also includes the elutriation velocity, specifies six values (Q_{in}, V_f, V_e L_b, D_b and X_b) and solves two equations (n, D_{BH}) based on a square bag matrix. From the resulting numbers, the elutriation velocity is checked. To suit design standards and supplier templates, and to minimise the capital cost related to number of bags and the baghouse footprint (while maintaining velocity limits), the bag diameter or length is varied.

The procedure developed by the authors may be illustrated by using a baghouse application where the inlet air flow is 1000 m^3 / min. The value of the six parameters requiring specification are set at: an air to cloth ratio of 1.6 m^3 / m^2 / min; a maximum elutriation velocity of 68.4 m / min; a bag length 3.0 m; a bag spacing of 0.08 m; and a distance between the bag bundle and the baghouse wall of 0.1 m. Solving using Microsoft Excel Solver from an initial guess of n = 380, D_b = 0.15 m and D_{BH} = 7 m gives the values shown in column two of Table 3.

Table 3: Results of example baghouse design procedure

Parameter	Solver	Option 1*	Option 2*
Q_{in} [m^3 / min]	1000	1000	1000
X_b [m]	0.08	0.08	0.08
L_b [m]	3.0	3.0	3.0
A [m]	0.1	0.1	0.1
n [-]	380	442	332
D_b [m]	0.17	0.15	0.20
D_{BH} [m]	5.9	5.7	6.0
V_f [m^3 / m^2 / min]	1.6	1.6	1.6
V_e [m / min]	56.0	56.0	55.6

* These options correspond to commercially available bag diameters

The range of bag diameters available from bag suppliers affects the chosen bag diameter. In the example above, if 0.17 m bags are not available, a choice is made between 0.15 m and 0.20 m bags. The results of calculations run using these values are shown in columns three and four of Table 3. Using 0.20 m rather than 0.15 m diameter bags requires 110 fewer bags. Although the baghouse diameter increases from 5.7 to 6.0 m and will therefore have a higher material cost than the first option, it is likely that having 110 fewer bags, support cages, solenoid valves and compressed air ejectors will make the second option cheaper.

Another point to note is that the total number of bags required may need to be adjusted. Bags are arranged in a uniform manner, so if 442 or 332 bags do not produce a uniform pattern, extra bags will need to be added until the arrangement is uniform. The number of bags should never be rounded down to create a uniform pattern, as this would cause the desired air to cloth ratios to be exceeded.

3.3. Milk Powder Collection

Clearly, the air to cloth ratio is one of the key baghouse design parameters. Several authors have a separate design procedure to establish suitable values for air to cloth ratios for milk powder collection. Each is based on applying a number of factors that take account of gas and dust properties when estimating an initial air to cloth ratio for milk powder.

Croom [8] applies correction factors as shown in Equation 14, where a nominal filtration velocity V_{fn} [m^3 / m^2 / min] is modified by correction factors for the application type (B), gas temperature (T), particle size (P) and dust load (D) to give a final filtration velocity V_{fe} [m^3 / m^2 / min]. For pulse-jet cleaning V_{fn} is 2.44 m^3 / m^2 / min (8.0 ft / min). The application factor B is based on the collection situation: oily moist or agglomeration dusts, product collection or nuisance collection.

$$V_{fe} = V_{fn} \times B \times T \times P \times D \tag{14}$$

Loffler et al. [9] determine the effective air to cloth ratio V_{fe} [m^3 / m^2 / min] from Equation 15.

$$V_{fe} = V_{fn} \times A_n \times B \times P \times D \times T \times F \times I \times H \tag{15}$$

Like Croom, factors are applied for application type (B), gas temperature (T), particle size (P) and dust load (D). Additional factors are;

- bulk flow behaviour (F), for dusts with bulk densities less than 0.60 g / m^3
- flue gas flow (I), for online cleaning and upwards gas flow past the bags
- tropical climate factor (H), applicable for food production and dusts with hygroscopic tendencies
- filter system factor (A_n), distinguishing between single bag or group pulsing, and on line or offline cleaning.

Loffler et al. vary the base air to cloth ratio V_{fn} between 1.6 – 2.5 m^3 / m^2 / min, depending on the fat contentment of the milk powder.

Turner et al. [20] published a design procedure for the United States Environmental Protection Agency (USEPA) in 1998, with a specific method for pulse-jet baghouses. Again, factors for application type (B), gas temperature (T [^oF]), dust loadings (D_T [gr / ft^3]) and particle size (P [μm]) are applied. The USEPA guideline uses the material factor, A_T, instead of a base air to cloth ratio used by Croom and Loffler et al., to distinguish between different dusts. Once these five factors are determined, the recommended air to cloth ratio, V_{fe} [ft / min], is calculated using Equation 16.

$$V_{fe} = 2.878 A_T B T^{-0.2335} D_T^{-0.06021} \left(0.7471 + 0.0853 \ln P\right) \tag{16}$$

The Intensiv Filter [21] guideline comes in tabulated form. The suggested air to cloth ratio is based on dust size and then a chosen combination of gas temperature, application type and dust loadings. Factors are then applied for dust loadings, if different to those initially chosen, and bag length, both of which inversely affect the air to cloth ratio. Only the Intensiv Filter guideline applies a factor for bag length.

Using conditions for a typical milk powder plant as inputs, the estimated air to cloth ratios for the four design guidelines above were calculated. Figure 3 shows that there was a large variation among the four guidelines with an order of magnitude separating the values of Turner et al. and Croom. The results imply that plants based on the Turner et al., Loffler et al. and Intensiv Filter guidelines would need 250 %, 75 % and 56 % respectively more filtration area than one using the Croom guideline. Although the Turner et al. plant would operate at much lower differential pressures, thus improving collection efficiency and increasing bag life, the capital cost would be significantly greater than for the Croom plant.

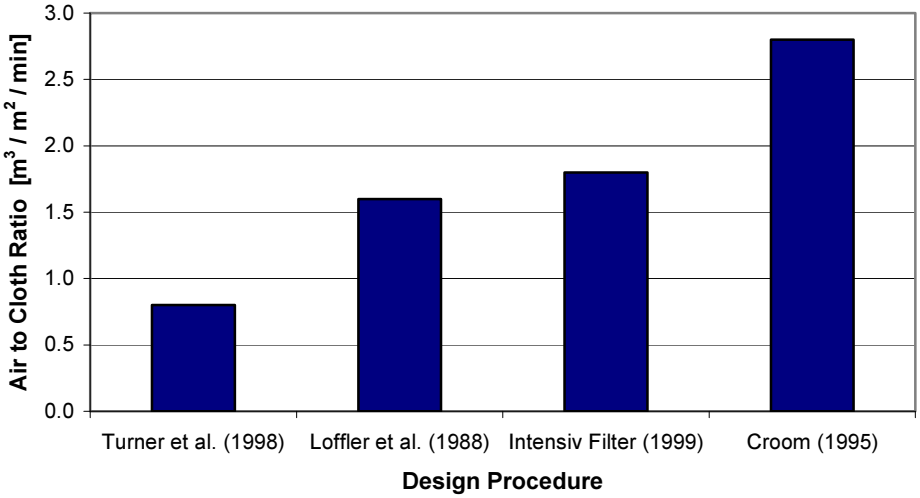

Fig. 3: Recommended baghouse air to cloth ratios for a typical milk powder plant

The air to cloth ratio from Croom is greater than values used by Fonterra. Thus it is likely that using the Croom design would compound the issues experienced to date by Fonterra. The air to cloth ratio from the Turner et al. guideline is much lower than those used by Fonterra, but the high capital cost of such a design would not be acceptable to them. The Loffler et al. and Intensiv Filter guidelines agree well with each other, and may indicate a compromise design between high capital cost and operation interruptions.

Loffler et al. are the only authors to vary the base air to cloth ratio for different types of milk powder. In support of this, Fonterra finds baghouse performance varies with different types of milk powder. Therefore, these results indicate that the guidelines of Loffler et al. would be the most suited for application to milk powder baghouses.

4. CONCLUSIONS

It has been established that there is a large variation in the recommended appropriate values for air to cloth ratio, elutriation velocity, bag spacing and bag dimensions. Other key design parameters are the choice of filter medium, operating differential pressure and baghouse footprint.

A procedure for baghouse design has been developed that differs from previous work in that it includes the area outside the bag bundle as a key design parameter and uses an optimisation routine to solve the system of equations.

Significant variation has been observed among the four design procedures found to determine the air to cloth ratio for baghouses collecting milk powder. It appears the methods of Loffler et al. (1988) and Intensiv Filter (1999) are both reasonable in comparison with industrial experience, and the method of Loffler et al. is more specific for fines collection in milk powder plants.

5. ACKNOWLEDGEMENTS

Financial support from the Foundation for Research Science and Technology (FRST) and Fonterra Co-operative Group Ltd is acknowledged. Main points presented in poster at the Fifth World Congress on Particle Technology, 2006, Orlando, Apr. 23-27.

6. REFERENCES

1. Ruthven, D.M., *Encyclopaedia of separation technology*. Vol. 2. 1997: John Wiley & Sons, New York.
2. Silva, C.R.N., et al., *Influence of gas velocity on cake formation and detachment.* Powder Technology, 1999. **101**(2): p. 165-172.
3. Cora, M.G. and Y. Hung, *Controlling industrial particulate emissions: a practical overview of baghouse technology.* Environmental Quality Management, 2002. **11**(4): p. 53.
4. Ellenbecker, M.J. and D. Leith, *The effect of dust retention on pressure drop in a high velocity pulse-jet fabric filter.* Powder Technology, 1980. **25**(2): p. 147-154.
5. Westergaard, V. *Sanitary bag filter - SANICIP*. [Brochure] 2003 [cited 26/3/04]; Available from: http://www.niro.com/ndk_website/NIRO/CMSResources.nsf/filenames/160303_SANICIP.pdf/$file/160303_SANICIP.pdf.
6. Machen, K., *Characterisation of a washable baghouse in a milk powder manufacturing plant*, in *Food Science and Technology*. 2001, Massey University: Palmerston North. p. 104.
7. Agarwal, A.T., *Design guide for dust collectors.* Chemical Engineering, 2005. **112**(2): p. 42-49.
8. Croom, M.L., *Filter dust collectors: design and application*. 1995, New York: McGraw-Hill. xi, 253.
9. Loffler, F., H. Dietrich, and W. Flatt, *Dust collection with bag filters and envelope filters*. 1988, Chichester, U.K: Wiley.
10. Moore, S., J. Rubak, and M. Jolin, *Selecting baghouse dust collectors.* Plant Engineering, 1996. **50**(11): p. 58-62.
11. Morgan, L. and M. Walters, *Test your dust - getting dust collection right.* Ceramic Industry, 1999. **149**(7): p. 24-29.
12. Vidmar, T.J., *Selecting a dust collection system.* Plant Engineering, 1990. **44**(8): p. 70-73.
13. Masters, K., *Spray drying: an introduction to principles, operational practice and applications*. 1972, London: L. Hill. 668.
14. Bergmann, L., *Beating the bag house blues.* Chemical Engineering, 2001. **108**(1): p.65-67.
15. Zielinski, R., *Keep pulse-jet baghouses running well.* Chemical Engineering, 2003. **110**(6): p. 58 - 61.
16. Rothwell, E., *Who needs better filter media.* Filtration & Separation, 1987. **24**(2): p.104 - 108.
17. Caputo, A.C. and P.M. Pelagagge, *Baghouse system design based on economic optimization.* Environmental Progress, 2000. **19**(4): p. 238 - 245.
18. Neiva, A. and L. Goldstein, *A procedure for calculating pressure drop during the build-up of dust filter cakes.* Chemical Engineering and Processing, 2003. **42**(6): p.495 - 501.

19. Kavouras, A. and G. Krammer, *Distributions of age, thickness and gas velocity in the cake of jet pulsed filters - application and validation of a generations filter model.* Chemical Engineering Science, 2003. **58**(1): p. 223 - 238.

20. Turner, J.H., et al., *Section 6: Particulate Matter Controls - Chapter 1: baghouses and filters*, in *EPA/452/B-02-001*. 1998, United States Environmental Protection Agency.

21. Intensiv-Filter, *Dedusting technology filter media*. 1999, Langenberg: Intensiv-Filter GmbH & Co.

Design of baghouses for fines collection in milk powder plants

J.R. Gabites[1], J. Abrahamson[1] and J.A. Winchester[2]
[1]Department of Chemical and Process Engineering, University of Canterbury, Christchurch, New Zealand
[2] Heat Transfer and Drying Team, Clandeboye Site, Fonterra Co-operative Group Ltd, Temuka, New Zealand

Abstract

The design of pulse-jet baghouses for fines collection has been investigated. Firstly, the key design parameters and recommended values for these baghouse are presented, showing a large variation among sources. A procedure for determining the optimal combination of these parameters has been developed that differs from those found in previous literature by including a hitherto ignored area outside the bag bundle. More specifically, a comparison was made among the recommended air to cloth ratios from four design guidelines (Croom [1], Lőffler Dietrich and Flatt [2], Turner et al. [3] and Intensiv Filter [4]), for the case of milk powder collection. Even here, large variation was found. Finally, a comparison between our industrial experience and these guideline values shows that at least for the dairy industry, the guideline of Lőffler et al. [2] is the best compromise between high capital costs and operational difficulties.

Keywords: Baghouse, Fines Collection, Milk Powder, Washable

Introduction

Fabric filtration is one of the oldest and most reliable forms of particulate collection [5]. Fabric filters or baghouses have been chosen in an increasing number of industrial processes for controlling atmospheric emissions [6]. Examples include power generation, chemical, food, metal and mineral industries [7]. As particle emission regulations become more stringent, baghouses will find increasing use because of their high efficiency [8].

A recent change in the design of milk powder plants has seen replacement of the traditional cyclone system used for fines recovery replaced by washable baghouse systems. Fonterra Co-operative Group Ltd, the world's largest exporter of milk products, has installed or retrofitted five such designs in milk powder plants throughout New Zealand since the year 2000. One such plant is the world's largest milk powder plant, situated on the Clandeboye site near Temuka in the South Island.

Baghouses were traditionally used to remove fines not recovered by cyclones receiving the exit flow from spray dryer systems, but were always thought to be a source of microbial contamination because powder may have long residence times in the bags. Therefore approximately 10 % of these cyclone fines were downgraded to stock food. Another disadvantage of this traditional system was that cyclones often blocked, thus interrupting dryer operation.

Washable baghouses, with their ability to be cleaned-in-place (CIP), have changed the perception of baghouses as being a source of microbial contamination. Consequently, all fines collected by them retain the microbial product quality of the dryer chamber powder, thereby increasing profits. Because all fines are collected in a single stage, fewer unit operations are required. This leads to reduced building space requirements, lower capital costs and simplified plants [9]. The final advantage of the new system is that baghouse collection is a gentler form of product collection when compared to cyclones. This is more suited to the high fat and high protein powders of the dairy industry [10].

Despite the numerous advantages of this new system, high differential pressures, some blinding and bag damage in the main washable baghouses have caused interruptions to the dryer operation. It is likely that these operational issues are a result of the baghouse designs used in these installations.

As the baghouse air to cloth ratio (see below) increases, penetration of powder into the bag fabric during operation also increases [11-13]. These particles imbedded in the pores of the filter medium cannot be removed by reverse flow or pulse cleaning [11, 14-16] and consequently, higher differential pressures result. Baghouse operating costs increase when operating at higher differential pressures, firstly because the energy costs for running the fans

that suck or blow air through the baghouse are higher [7, 17] and secondly, because bag replacement costs increase as bag life is shortened by operating at higher differential pressures.

Baghouse design is likely to affect bag movement which causes the mechanical failure of filter bags [15]. If bags can swing and rub against each other, bag abrasion is likely to occur. Significant bag movement can bend the bag support cages, create sharp sections which the bags could rub on [18] and possibly even puncture the bags.

This paper examines the design of pulse-jet baghouses. The aim of this investigation is to explore the key design parameters and establish a more complete design procedure. Previously reported design guidelines are compared for milk powder baghouses and their suitability assessed in light of practical experience.

Method

Key baghouse design parameters and recommended values for these separate parameters were found from the literature. A new procedure for baghouse design was developed building on this information. Microsoft Excel was used to generate a spreadsheet that used the Solver feature to calculate the optimal combination of these parameters.

Specifically for the collection of milk powder, several procedures for calculating recommended air to cloth ratios were found from the literature. Using typical parameter values found in a milk powder plant, these air to cloth ratios were calculated. Based on Fonterra's industrial experience, these air to cloth ratios were assessed for their suitability for milk powder collection.

Results and Discussion

Baghouse Design Parameters

The key baghouse parameters appear to be as follows [1, 2, 11, 14, 15];

Air to Cloth Ratio (V_f [usual units $m^3 / m^2 / min$]), also termed the filtration velocity, is the ratio of the inlet gas flow Q_{in} [m^3 / min] to the required filtration area A_f [m^2] as shown in Equation 1.

$$V_f = \frac{Q_{in}}{A_f} \tag{1}$$

where A_f is given by

$$A_f = nA_b \tag{2}$$

n is the total number of bags and A_b the filtration area [m^2] of a single bag given by

$$A_b = \pi D_b L_b \tag{3}$$

where D_b [m] and L_b [m] are the bag diameter and length.

Recommended values in the literature have been determined from experience and laboratory or pilot scale experiments. Values were taken from pulse-cleaned baghouses. Suggested maximum values are shown with their sources in Figure 1. These vary by approximately 90%, from a value of 2.4 $m^3 / m^2 / min$ [14, 16] to 4.6 $m^3 / m^2 / min$ [19].

Elutriation Velocity (V_e) is determined by dividing the gas flow Q_{in} by the cross-sectional area of the vessel minus that of the bags (Equation 4).

$$V_e = \frac{Q_{in}}{A_{BH} - A_{Bags}} \tag{4}$$

For a circular baghouse the baghouse footprint A_{BH} [m^2] is given by Equation 5 where D_{BH} [m] is the baghouse diameter.

$$A_{BH} = \pi\left(\frac{D_{BH}}{2}\right)^2 \tag{5}$$

A_{Bags} [m^2] is the total plan cross sectional area of the bags given by

$$A_{Bags} = n\pi\left(\frac{D_b}{2}\right)^2 \tag{6}$$

Although the definition of Equation 4 uses the total plan baghouse area, a more accurate definition would replace this with the smaller bag bundle area. This is because the re-entrainment of dust removed from the bags during cleaning *within* the bag bundle is of more interest (see Figure 2).

Equation 4 implicitly assumes that the gas velocity within the bag bundle is uniform, both between the bags and along the length of each bag. This is believed to be an extreme case as not all gas flows down the annular area outside of the bag bundle from a top entry inlet or is evenly distributed across the bundle for a bottom entry inlet; there will have been some radial flow into the bag bundle and into the clean side of the bags.

The upper limits of the elutriation velocity, again with their sources, are given in Table 1. The basis for the elutriation velocities is a single particle terminal velocity in the baghouse [11]. However, the terminal velocity of individual particles is strongly dependent on particle size. It is unclear which size should represent the powder falling off the bags. This is expected to be in clusters of particles, formed from the breakup of sections of cake.

Bag Spacing (X_b) is defined as the perimeter-to-perimeter distance between neighbouring bags. Values of 25 mm [20] and 80 mm [2] are recommended to ensure that dust removed by pulse cleaning is not pulsed onto neighbouring bags.

It is surprising that no source mentions a relationship between bag spacing and bag length. One would expect that the longer the bag, the greater the bag spacing required to prevent the long bags rubbing and abrading near the base of the bags.

The elutriation velocity is influenced by the bag spacing, however each parameter accounts for a unique mechanism. The elutriation velocity represents the mechanism where powder falling from a bag could potentially become entrained in the gas stream and redeposited onto the filter bags. The bag spacing represents the distance that must be set so powder pulse cleaned off a bag does not land onto a neighbouring bag, but instead falls to the dust hopper below.

Choice of Filter Medium is recommended to be based on testing as well as performance guarantees [1]. Bag properties such as weight, thickness and permeability must be

considered. The choice is made between woven and non-woven, natural and synthetic fabrics [7]. A range of mechanical and chemical surface treatments is available to improve bag features such as cake release, resistance to abrasion and protection against high temperatures [21].

The *Operating Differential Pressure* arises from the resistance of the air passing through the filter bags and cake. There are several models available [3, 7, 17, 22-24] that take account of the filtration velocity, dust concentration, time between cleaning pulses as well as bag and cake resistance. This pressure difference impacts heavily on the operating costs: the higher the differential pressure, the higher the electricity costs to run baghouse fans or blowers. It is agreed that the pulse cleaning should maintain a mean pressure difference across the bags of less than 2000 Pa [11, 19].

To maintain the differential pressure below a selected maximum, pulse cleaning is used. The pulsing control can either be initiated by an upper differential pressure, where pulsing continues until a lower differential pressure is reached, or by using a timed control, where the pulse will occur periodically independent of the differential pressure. It should be noted that more frequent pulse cleaning creates higher emissions, accelerated bag wear and greater use of compressed air [17]. Further design choices are made between online and offline cleaning and the type of ejector.

Bag Dimensions of diameter (D_b) and length (L_b) are chosen to suit the required filtration area determined from Equation 1. The upper limits of these given in Table 2 are to ensure that adequate pulse cleaning occurs because cleaning performance decreases as diameter and length increase [11]. Also, as the bag length increases, the abrasion caused by swinging bags also increases and it has been suggested that the air to cloth ratio be decreased when the bag length exceeds 3.0 m [2].

Baghouse Footprint (plan area) impacts severely on the cost of an installation. However, larger collectors will increase bag life and reduce maintenance costs [16]. The footprint must be such that elutriation velocity limits for the chosen bag diameter and spacing are satisfied [1]. The baghouse footprint A_{BH} [m^2] consists of the area of the bag bundle A_{BB} [m^2] and the area between the edge of the bag bundle and the baghouse walls. Equation 7 gives the bag bundle area, where N [m^{-2}] is the bag density (number of bags per unit area of A_{BB}).

$$A_{BB} = \frac{n}{N} \tag{7}$$

For bags arranged in a square matrix spaced a perimeter-to-perimeter distance X_b apart, the bag density is given by

$$N = \frac{1}{(D_b + X_b)^2} \tag{8}$$

Therefore, for a circular baghouse, the diameter of the bag bundle D_{BB} [m] is given by Equation 9

$$D_{BB} = 2(D_b + X_b)\sqrt{\frac{n}{\pi}} \tag{9}$$

It is often more convenient to express the baghouse diameter instead of the baghouse footprint. The baghouse diameter is the sum of the bag bundle diameter and twice the gap from the edge of the bag bundle to the baghouse wall as shown in Figure 2 and given by Equation 10.

$$D_{BH} = D_{BB} + 2G \tag{10}$$

The baghouse *Collection Efficiency* is a key parameter used to assess the performance of a baghouse. The overall collection efficiency ϕ of a baghouse is defined in Equation 11 [2] where m_{col} [kg / s] is the mass flow of collected powder and m_{in} [kg / s] the mass flow of powder in the feed stream:

$$\phi = \frac{m_{col}}{m_{in}} \tag{11}$$

Equation 11 can be rewritten in terms of the outlet air powder flow m_{out} [kg / s] as shown in Equation 12:

$$\phi = 1 - \frac{m_{out}}{m_{in}} \tag{12}$$

More frequently the inlet air and outlet air stream powder concentrations are known due to online monitoring. If the total feed air flow is equal to the outlet air flow, then Equation 12 can be rewritten as Equation 13, where c_{in} [g / m^3] and c_{out} [g / m^3] are the inlet and outlet air powder concentrations respectively:

$$\phi = 1 - \frac{c_{out}}{c_{in}} \tag{13}$$

It has been shown [25] that between 60 and 90 % of emissions are related to pulse cleaning. Once the filter cake has been removed from the filter bag, particles pass more easily through the bag polluting the clean air. The emissions then decrease because as the filter cake grows, its collection efficiency increases. Therefore, the emissions peak immediately after the cleaning pulse, and decrease with time until the next cleaning pulse [2].

Three other purportedly less important design parameters are: the inlet air arrangement (bottom or top entry, radial or tangential entry); the baghouse shape (rectangular vs. circular); and the steepness of the hopper walls below the bags (at least 60^o from the horizontal [11]).

The findings above indicate that significant variation exists in published recommended values of the key design parameters. The maximum air to cloth ratios vary by approximately 90 %, the maximum elutriation velocities vary by 50 % and optimal bag length varies by over 1 m. Caution is recommended for new applications, where field, pilot plant or laboratory measurements should be made [15].

Design Procedure

There exist nine baghouse design parameters (previously defined): Q_{in}, V_f, V_e, n, L_b, D_b, X_b, G and D_{BH}. Rearranging Equations 1, 4 and 10 with respect to these parameters gives Equations 14, 15 and 16.

$$V_f = \frac{Q_{in}}{n\pi L_b D_b} \tag{14}$$

$$V_e = \frac{4Q_{in}}{\pi\left(D_{BH}^2 - nD_b^2\right)} \tag{15}$$

$$D_{BH} = 2G + \sqrt{\frac{4n}{\pi}\left(D_b + X_b\right)^2} \tag{16}$$

Because there are nine parameters and three equations, six parameters must be specified. The inlet air flow Q_{in} is specific to the application and determined from the upstream process feeding the baghouse. Upper limits for air to cloth ratio V_f, elutriation velocity V_e, bag length L_b and bag spacing X_b are discussed above and can be used as the specified values for the

initial stage of the design. The gap G between the edge of the bag bundle and the baghouse walls may be chosen such that it is greater than the between-bag distance. In the interest of distributing the incoming airflow evenly to the bag bundle, a baffle to deflect a radial inflow, or a tangential inflow may be used, both in conjunction with a sufficiently large annular flow area. Initial annular tangential velocities, defined by Equation 17, should be no larger than the velocity in the inlet duct, meaning that the area (GL_b) should be no less than the inflow area. This is normally set so that the inlet duct velocity is larger than the minimum particle carrying velocity in a horizontal duct, generally around 15 m / s. Thus all six parameters have been specified.

$$V_{Anl} = \frac{Q_{in}}{GL_b} \tag{17}$$

The system of equations can easily be solved using standard optimisation packages, e.g. Microsoft Excel Solver. A spreadsheet can be created listing the values of Q_{in}, V_f, X_b, L_b, G and the maximum value of V_e. Three cells are required for the initial guesses of the three unknowns (n, D_b and D_{BH}). Good initial guesses will ensure that a converged solution is obtained. Previous baghouse experience or literature on other baghouse applications could be used for the initial guess for the number of bags. The recommended optimal bag diameters shown in Table 2 are good initial guesses for the bag diameter. The guesses for the number of bags and the bag diameter can be used in Equation 16 to give an initial guess for the baghouse diameter.

Three other cells are included in the spreadsheet for the values of V_f, V_e and D_{BH} calculated from Equations 14, 15 and 16 respectively. The final cell required is the solver target cell. This cell is calculated as the squared difference between the guessed baghouse diameter and that calculated from Equation 16.

Solver is run to minimise the target cell by changing the values of the three guessed unknowns subject to two constraints. Firstly, the calculated air to cloth ratio must be equal to the specified value and secondly, the calculated elutriation velocity must be less than or equal to the specified maximum. The bag diameter could also be constrained between the range of available bag diameters of 0.05 to 0.20 m [11]. As the solver runs, the values of the three guessed unknowns are changed. Once the target cell is minimised subject to the constraints, the given values of the three unknowns become the final solution and an initial design results.

The procedure developed here may be illustrated by using a baghouse application where the inlet air flow is 1000 m^3 / min. The value of the six parameters requiring specification are set at: an air to cloth ratio of 1.6 m^3 / m^2 / min; a maximum elutriation velocity of 68.4 m / min; a bag length 3.0 m; a bag spacing of 0.08 m; and a distance between the bag bundle and the baghouse wall of 0.37 m. Solving using Microsoft Excel Solver from an initial guess of n = 380, D_b = 0.15 m and D_{BH} = 5.8 m gives the values shown in column two of Table 3.

Although this process generates an initial design, a cost optimisation is required to determine the final design. The set of specific bag diameters available from bag suppliers affects the chosen bag diameter and the number of bags may also need to be adjusted so the bags are arranged in a uniform manner. These parameters impact on the overall cost of the baghouse because they influence the baghouse diameter and the required number of accessories (bags, cages, solenoid valves, air ejectors). Caputo and Pelagagge [17] deals with the cost aspects of some of the above parameters.

It can be tempting, in an attempt to reduce the capital cost of the design, to increase the air to cloth ratio and the elutriation velocity, and decrease the bag spacing and outer gap. However, as highlighted above, such designs are likely to operate at higher differential pressures and result in greater operating costs. Therefore, in the long term, the overall costs of such designs will probably exceed those from a more suitable design and hence, the influence of the design on the operating costs must not be overlooked.

In the example above, if 0.17 m bags are not available, a choice is made between 0.15 m and 0.20 m bags. The results of calculations run using these values are shown in columns three and four of Table 3. In all three cases, the value of the Solver target cells were zero and the elutriation velocities were less than the specified maximum. Using 0.20 m rather than 0.15 m diameter bags requires 110 fewer bags. Although the baghouse diameter increases from 6.2 to 6.5 m and will therefore have a higher material cost than the first option, it is likely that having 110 fewer bags, support cages, solenoid valves and compressed air ejectors will make the second option (fourth column) cheaper.

The number of bags in the example may need to be adjusted to create a uniform pattern. If 442 or 332 bags do not produce a uniform pattern, extra bags will need to be added until the

arrangement is uniform. The number of bags should never be rounded down to create a uniform pattern, as this would cause the desired air to cloth ratios to be exceeded and hence, the operating costs to increase as a result of increased differential pressures.

By including the void area between the edge of the bag bundle and the baghouse walls, which is significant in practice, this design sequence differs somewhat to those found in the literature. Lőffler et al. [2] list seven design parameters (Q_{in}, V_f, L_b, D_b, n, X_b, D_{BH}), specify five values (Q_{in}, V_f, L_b, D_b and X_b) and solve two equations (for n, D_{BH}) based on a square bag matrix. Lőffler et al. [2] vary the bag diameter and bag spacing to minimise the capital cost within the recommended limits of the parameters above such that cleaning performance and bag life are not compromised. Unfortunately Lőffler et al. [2] do not quantify cleaning performance or bag life.

Croom [1] lists eight design parameters (Q_{in}, V_f, V_e, L_b, D_b, n, X_b, D_{BH}) as he also includes the elutriation velocity, specifies six values (Q_{in}, V_f, V_e, L_b, D_b and X_b) and solves two equations (for n, D_{BH}) based on a square bag matrix. From the resulting numbers, the elutriation velocity is checked. To suit design standards and supplier templates, and to minimise the capital cost related to number of bags and the baghouse footprint (while maintaining velocity limits), the bag diameter or length is varied.

Milk Powder Collection Design

Clearly, the air to cloth ratio is one of the key baghouse design parameters. Several authors have a separate design procedure to establish suitable values for air to cloth ratios. Each is based on applying a number of factors that take account of gas and dust properties when estimating an initial air to cloth ratio. Four procedures are discussed below where the air to cloth ratios shown are specifically for milk powder collection.

Croom [1] applied correction factors as shown in Equation 18, where a nominal filtration velocity V_{fn} [m^3 / m^2 / min] is modified by correction factors for the application type (B), gas temperature (T), particle size (P) and dust load (D) to give a final filtration velocity V_{fe} [m^3 / m^2 / min]. For pulse-jet cleaning V_{fn} is 2.44 m^3 / m^2 / min (8.0 ft / min). The application

factor B is based on the collection situation: oily moist or agglomeration dusts, product collection or nuisance collection.

$$V_{fe} = V_{fn} \times B \times T \times P \times D \tag{18}$$

Lőffler et al. [2] determine the effective air to cloth ratio V_{fe} m^3 / m^2 / min] from Equation 19:

$$V_{fe} = V_{fn} \times A_n \times B \times P \times D \times T \times F \times I \times H \tag{19}$$

Like Croom [1], factors are applied for application type (B), gas temperature (T), particle size (P) and dust load (D). Additional factors are;

- bulk flow behaviour (F), for dusts with bulk densities less than 600 kg / m^3
- flue gas flow (I), for online cleaning and upward gas flow past the bags
- tropical climate factor (H), applicable for food production and dusts with hygroscopic tendencies
- filter system factor (A_n), distinguishing between single bag or group pulsing, and on-line or offline cleaning.

Lőffler et al. [2] vary the base air to cloth ratio V_{fn} between 1.6 – 2.5 m^3 / m^2 / min, depending on the fat content of the milk powder.

Turner et al. [3] published a design procedure for the United States Environmental Protection Agency (USEPA) in 1998, with a specific method for pulse-jet baghouses. Again, factors for application type (B), gas temperature (T [^oF]), dust loading (D_T [gr / ft^3]) and particle size (P [μm]) are applied. The USEPA guideline uses the material factor, A_T, instead of a base air to cloth ratio as used by Croom [1] and Lőffler et al. [2], to distinguish between different dusts. Once these five factors are determined, the recommended air to cloth ratio, V_{fe} [ft / min], is calculated using Equation 20.

$$V_{fe} = 2.878 A_T B T^{-0.2335} D_T^{-0.06021} \left(0.7471 + 0.0853 \ln P\right) \tag{20}$$

The Intensiv Filter guideline [4] comes in tabulated form. The suggested air to cloth ratio is based on dust size and then a chosen combination of gas temperature, application type and dust loadings. Factors are then applied for dust loadings, if different to those initially chosen, and bag length, both of which inversely affect the air to cloth ratio. Only the Intensiv Filter guideline [4] applies a factor for bag length.

Using conditions for a typical milk powder plant as inputs, the estimated air to cloth ratios for the four design guidelines above were calculated. Figure 3 shows that there was a large variation among the four guidelines with a three fold difference separating the values of Turner et al. [3] and Croom [1]. The results imply that plants based on the Turner et al. [3], Lőffler et al. [2] and Intensiv Filter [4] guidelines would need 250 %, 75 % and 56 % respectively more filtration area than one using the Croom guideline [1]. Although the Turner et al. [3] plant would operate at much lower differential pressures, thus improving collection efficiency and increasing bag life, the capital cost would be significantly greater than for the Croom [1] plant.

A vibrating fluid bed baghouse filters the powder elutriated from the external vibrating fluid beds that are the final stages of drying in the milk powder process. Within the Fonterra plants, operating experience has found that these baghouses have had no operational difficulties even though the air to cloth ratios of these designs are much greater than that suggested by the Turner et al. guideline [3]. This finding indicates that the air to cloth ratio from the Turner et al. guideline [3] is too conservative, and the resulting capital cost would not be acceptable to an industrial operator such as Fonterra.

The air to cloth ratio from Croom [1] is greater than values used by Fonterra in the main dryer baghouses. Thus it is likely that using the Croom [1] design would compound the operational issues experienced to date by Fonterra in these baghouses. The Lőffler et al. [2] and Intensiv Filter [4] guidelines agree well with each other. These guidelines give air to cloth ratios that are similar to those used by Fonterra in their vibrating fluid bed baghouses. Fonterra experience has shown that air to cloth ratios higher than those from the Lőffler et al. [2] and Intensiv Filter [4] guidelines has been related to operational issues. This suggests that these guidelines give a good compromise design between high capital costs and operational interruptions.

Lőffler et al. [2] are the only authors to vary the base air to cloth ratio for different types of milk powder. From their industrial experience Fonterra finds baghouse performance varies with different types of milk powder. The variations in base air to cloth ratio from Lőffler et al. [2] are also in the same direction as Fonterra's industrial experience. Therefore, these

results indicate that the guidelines of Lőffler et al. [2] are the most suited for application to milk powder baghouses.

Milk Powder Collection Efficiency

In the Canterbury region of the South Island of New Zealand, the regional council (Environment Canterbury) states that particulate emission concentrations must not exceed 20 mg / Nm^3. Washable baghouses operated by Fonterra Co-operative Group Ltd normally meet this regulation as outlet air stream powder concentrations usually range between 6 – 10 mg / Nm^3.

Table 4 shows that over the range of expected inlet powder concentrations, the Fonterra Clandeboye washable baghouses have very high collection efficiencies. For assumed inlet powder concentrations ranging from 2.0 – 40.8 g / m^3 with an outlet powder concentration of 10 mg / m^3, the overall calculated collection efficiency ranges from 99.5 % to 99.98 %. Such high collection efficiencies are to be expected, as one of the main advantages of baghouses over other forms of particulate collection equipment is their high collection efficiencies, which can often be beyond 99 % [5].

Conclusions

It has been established from a review of published baghouse design procedures, that there is a large variation in the recommended appropriate values for air to cloth ratio, elutriation velocity, bag spacing and bag dimensions. Other key design parameters are the choice of filter medium, operating differential pressure and baghouse footprint.

A procedure for baghouse design has been developed that differs from previous work in that it includes the area outside the bag bundle as a key design parameter and uses an optimisation routine to solve the system of equations.

Significant variation has been observed among the four design procedures found to determine the air to cloth ratio when applied to baghouses collecting milk powder. It appears the methods of Lőffler et al. [2] and Intensiv Filter [4] are both reasonable in comparison with industrial experience. The method of Lőffler et al. [2] is more specific for fines collection in milk powder plants, and is recommended.

Acknowledgements

Financial support from the Foundation for Research Science and Technology (FRST) and Fonterra Co-operative Group Ltd is acknowledged.

References

1. M.L. Croom, Filter dust collectors: design and application, McGraw-Hill, 1995.

2. F. Loffler, H. Dietrich, and W. Flatt, Dust collection with bag filters and envelope filters, Wiley, 1988.

3. J.H. Turner, et al., Chapter 1: baghouses and filters, in Section 6: Particulate Matter Controls, United States Environmental Protection Agency, 1998.

4. Intensiv-Filter, Dedusting technology filter media, Intensiv-Filter GmbH & Co, 1999.

5. D.M. Ruthven, Encyclopaedia of separation technology, John Wiley & Sons, 1997.

6. C.R.N. Silva, et al., Influence of gas velocity on cake formation and detachment, Powder Technol. 101 (2) (1999) 165-172.

7. M.G. Cora, Y. Hung, Controlling industrial particulate emissions: a practical overview of baghouse technology, Envir. Qual. Man. 11 (4) (2002). 53-64.

8. M.J. Ellenbecker, D. Leith, The effect of dust retention on pressure drop in a high velocity pulse-jet fabric filter, Powder Technol. 25 (1980) 147-154.

9. V. Westergaard, Sanitary bag filter - SANICIP. [Brochure] 2003 [cited 26/3/04]; Available from: http://www.niro.com/ndk_website/NIRO/CMSResources.nsf/filenames/160303_SANICIP.pdf/$file/160303_SANICIP.pdf.

10. K. Machen, Characterisation of a washable baghouse in a milk powder manufacturing plant, Masters Dissertation, Massey University, New Zealand, 2001.

11. A.T. Agarwal, Design guide for dust collectors, Chem. Eng. 112 (2) (2005) 42-49.

12. D.S. Leith, M.W. First, Performance of a pulse-jet filter at high filtration velocity, 3. Penetration by fault processes. J. Air Pollut. Cont. Assoc. 27 (8) (1977) 754-762.

13. D.S. Leith, M.W. First, and D.D. Gibson, Effect of modified cleaning pulses on pulse jet filter performance, Filtr. Sep. 15 (5) (1978) 400-406.

14. S. Moore, J. Rubak, M. Jolin, Selecting baghouse dust collectors, Plant Eng. 50 (11) (1996) 58-62.

15. L. Morgan, M. Walters, Test your dust - getting dust collection right, Ceramic Ind. 149 (7) (1999) 24-29.

16. T.J. Vidmar, Selecting a dust collection system, Plant Eng. 44 (8) (1990) 70-73.

17. A.C. Caputo, P.M. Pelagagge, Baghouse system design based on economic optimization, Environ. Prog. 19 (4) (2000) 238-245.

18. K.R. Parker, Technological advances in high-efficiency particulate collection, Proc Instn Mech Engrs. 211 (1) (1997) 53-65.

19. K. Masters, Spray drying: an introduction to principles, operational practice and applications, L. Hill, 1972.

20. L. Bergmann, Beating the baghouse blues, Chem. Eng. 108 (1) (2001) 65-67.

21. R. Zielinski, Keep pulse-jet baghouses running well, Chem. Eng. 110 (6) (2003) 58-61.

22. A. Kavouras, G. Krammer, Distributions of age, thickness and gas velocity in the cake of jet pulsed filters - application and validation of a generations filter model, Chem. Eng. Sci. 58 (1) (2003) 223-238.

23. A. Neiva, L. Goldstein, A procedure for calculating pressure drop during the build-up of dust filter cakes, Chem. Eng. Proc. 42 (6) (2003) 495-501.

24. E. Rothwell, Who needs better filter media, Filtr. Sep. 24 (2) (1987) 104-108.

25. E. Schmidt, Experimental investigation into the compression of dust cakes deposited on filter media, Filtr. Sep. 32 (8) (1995) 789-793.

Appendix F – Clandeboye Dryer 2 Baghouse Inspection Hatches CAPEX

TO: Mike Moore

FROM: John Gabites

SUBJECT: CD2 Baghouse Inspection Hatches CAPEX

DATE: 31st March 2005

Problem

Since their installation in the 2001 off season, the Clandeboye Dryer 2 main baghouses have performed below expectation. Major issues have been excessive bag damage and poor CIP performance, both of which have created too much plant downtime; a total of 66 hours of plant downtime between August 2002 and January 2003 was attributed to baghouse issues.

One of the great difficulties in operating these Niro designed washable baghouses (BH) is that there is no effective way of viewing the inside of the bag section of the baghouses. Unlike a fluid bed or sifter, which have a number of inspection hatches at important locations, there are no inspection hatches that give access to baghouse filter bags (currently, the only inspection hatche in the BH is located above the BH hopper).

To identify bag cleanliness during a CIP, a torch is shone onto the bottom of the bags from the BH hopper hatch. The limitation here is that operators often have to wait for liquid to drain off the bags before they can put their head into the baghouse, which may take up to 30 minutes and therefore prolongs the CIP turn around. Also, the distance from the BH hopper hatch to the bottom of the bags is 4.5 metres, which is a long way considering the only light source is from a torch. Adding to this, approximately only 5 % of the total filtration area can be seen from this position so it is extremely difficult to deduce how clean bags become.

University of Canterbury PhD work has shown that a poor baghouse CIP can increase, rather than reduce, baghouse differential pressures. This work has also shown that high protein powders have the potential to cover filter bags with a gel layer created by contact with caustic solutions. Without access to the bags, plant staff have no idea whether a sufficient cleaning film has developed on the surface of the bags and therefore cleaned the bags effectively.

Stack emissions data shows when a filter bag is leaking. However, the only current way to identify the cause bag is to shine a torch down the inside of the bags from the cell plate when the baghouse lid has been removed. This can only be achieved if there is sufficient plant down time that allows for lid lifting.

Plant managers use BH differential pressure and stack emissions data to decide whether a CIP is required or bags need replacing. The use of plant instrumentation to make these decisions is a reactive approach to operation as once the emissions or differentials have increased, both of which are unrecoverable, then action is taken to correct the issue.

Finally, one of the aims of the University of Canterbury Department of Chemical and Process Engineering PhD titled ‘Washable Baghouse Operation and Design, as Applied to Milk Powder Production’ is to analyse the amount of bag movement in the baghouses. This would

be achieved through the use of a high-speed video camera. However, as there is no current inspection port at the bag level, this work is not possible.

Opportunity

The opportunity that presents itself is to install inspection hatches in two locations in the main baghouses. This will bring the CD2 baghouses in line with the other Fonterra washable baghouses.

The first location for the hatches is at the bottom of the bags where a hinged hatch with site glass will be installed, similar to the hatches in the same location on the Clandeboye Dryer 3 baghouses. The site glass is needed to see the bags during operation. A hinged hatch is required so the operators can put their heads inside and look around the baghouse, so the hatch can not be dropped into the baghouse hopper 6 m below and so the inner surface of the site glass can be wiped clean. For photography work a second site glass will be required at the same height to allow a light source. Again this needs to be hinged so the inner surface of the hatch can be wiped clean.

The second hatch will be installed in the clean air plenum above the bags. The Edendale Dryer 2 and 3 baghouses have hatches located in this position but they are not see through. The desired hatches are similar to those found around the CD2 SFB. No hinge is required on these hatches as they could only fall 0.5 meters to the cell plate.

How Will This Resolve The Problem / Benefits

The ability to view the state of the bags during operation and periods of plant down time would be valuable. Firstly, CIP downtime would be reduced as operators could more quickly inspect the cleanliness of the bags. Reduced downtime generates more time to be running on product.

Secondly, by being able to view the CIP of the bags, and by being able to make more accurate decisions about the state of the bags, a better CIP would result. A more effective CIP means that the bag life will be increased, therefore lower operating costs because of less frequent bag replacement and less plant downtime. The baghouses will also run at lower differential pressures, the advantages of which are:

1. Baghouse extractor fan speeds can be reduced while still maintaining the required chamber vacuum; a lower fan speed means reduced electricity costs.
2. Bags experience less wear as fewer pores are created in the bags, bags last longer and hence savings are made through less frequent bag replacement and less plant downtime.
3. Lower emission of fines as there is less of a driving force to allow particles to migrate all the way through the bags and hence more powder is recovered; higher collection efficiency means greater profits.

Thirdly, the bag hatches will allow for more proactive decisions to be made on when bags should be replaced. This will mean that bags can be replaced before excessive stack emissions result, which will increase profits through greater fines collection.

Better access to the clean air plenum of the baghouse will mean operators will be able to remove powder more easily from the cell plate, thus reducing the fire and explosion risk associated with dry powder sitting in a warm environment.

Finally, the bag hatches will mean the Canterbury PhD photography work can be carried out which will lead to a better understanding of baghouse operation and hence improved designs for the future.

Appendix G – Paper presented in 5th International Conference on CFD in the process Industries (2006)

AIR FLOW PATTERNS IN AN INDUSTRIAL MILK POWDER SPRAY DRYER

John R. GABITES[1], John ABRAHAMSON[1] and James A. WINCHESTER[2]

[1] Department of Chemical and Process Engineering, University of Canterbury, Christchurch, NEW ZEALAND
[2]Heat Transfer & Drying Team, Clandeboye Site, Fonterra Co-operative Group Ltd, Temuka, NEW ZEALAND

ABSTRACT

The air flow patterns in an industrial milk powder spray dryer were investigated. Isothermal three-dimensional transient simulations were carried out using the commercial CFD code CFX10.0. The Shear Stress Transport (SST) turbulence model was implemented to model the effects of turbulence.

These simulations differ from previously published studies of spray dryer air flows in that they include features found in industrial scale plant. First, they include a second inlet air stream through the internal fluid bed at the bottom of the drying chamber. Second, the two outlet ducts are located near the top rather than the bottom of the dryer, which has been the case in most previous studies.

It was found that the main air jet oscillated and precessed about the central axis. In turn, the recirculation zones between the main jet and the chamber walls fluctuated in size relative to the movement of the jet.

Validation was achieved by observing the oscillation of the main air jet of a large dryer visualised by tell-tail tufts attached to a central pole.

INTRODUCTION

Spray drying is the transformation of a feed from a fluid state into a dried form by spraying the feed into a hot drying medium (Masters, 1972). This drying technique is used in a number of process industries for the production of foodstuffs, detergents, pharmaceuticals and cosmetics (Masters, 1972).

Fonterra Co-operative Group Ltd, the world's largest exporter of milk products, operates some 40 spray dryers across 25 manufacturing sites within New Zealand. One such plant is the world's largest milk powder plant, situated on the Clandeboye site near Temuka in the South Island.

Computational Fluid Dynamics (CFD) methods have become a powerful tool due to computational advances, and have been used to study spray dryers (Nijdam et al., 2004). These CFD techniques have been used to compare the performance of rotary disc and pressure nozzle atomisation (Huang et al., 2006), assess chamber design alternatives (Huang et al., 2003, Southwell et al., 2001) and predict drying performance (Li and Zbicinski, 2005, Southwell et al., 1999).

Air flow patterns in spray dryers have been the subject of numerous experimental and CFD studies. (Langrish et al., 1992) give a review of flow visualisations. Numerous CFD simulations on spray dryers have been published (Fletcher et al., 2003, Guo et al., 2003, Harvie et al., 2002, Kieviet et al., 1997, Langrish, 1993, Langrish et al., 2004, LeBarbier et al., 2001, Oakley and Bahu, 1990, Stafford et al., 1996, Straatsma et al., 1999).

Stafford et al. (1996) used particle image velocimetry (PIV) to measure the velocity field in a small spray dryer with pressure nozzle atomisation. They observed for the case of no inlet swirl, an off centre jet and no symmetrical recirculation zone. The left hand and right hand wall flows were seen to flow upwards and downwards respectively. This flow pattern was attributed to maldistribution of the inlet air.

Kieviet et al. (1997) compared 2D simulations with experimental measurements of a pilot scale spray dryer (height 0.373 m) without atomisation. The results for the no inlet swirl case indicated a fast flowing core that diverged as it progressed into the chamber. Measurements of sensible mean velocities in the recirculation zones near the walls were not possible due to the unstable flow. These instabilities were attributed to a wiggling core.

Guo et al. (2003) performed transient 3D simulations with CFX 4.4 on a sudden expansion/sudden contraction, as well as a laboratory scale spray dryer (height 2.8 m). They found that with no inlet swirl to the spray dryer, the flow was unstable and a periodic oscillation resulted. The downward flowing jet moved in a quasi flapping pattern with a period of 4.6 s. They concluded the movement of the central jet was due to pressure fluctuations in the large recirculation zones between the jet and the walls, and that future simulations had to be 3D to fully capture these effects.

Langrish et al. (2004) simulated the effects of inlet swirl on the flow patterns in a pilot-scale spray dryer (height 1.61 m). For the case of no inlet swirl, these authors found that the base of the central jet moved or precessed slightly around the axis with time, indicating that steady state simulations of spray dryers are of limited validity. They modelled the effects of turbulence with the shear stress transport (SST) model. The SST model is a statistical turbulence model that solves the k-ω model at the wall and solves the k-ε model in the bulk. A blending function is employed in CFX 10.0 to create a smooth transition between the two (ANSYS, 2005a). This model is one of the most effective models to overcome the problems of the standard k-ε model with non-equilibrium boundary conditions (ANSYS, 2005b).

The majority of spray dryer studies have been conducted on laboratory or pilot scale equipment. This allows for easier measurement of flow properties using experimental techniques such as hot wire anemometry and Laser Doppler Anemometry and hence, validation of CFD simulations.

These studies provide valuable information about the mechanisms within a spray dryer, but they do not truly represent the industrial situation. Modern spray dryers

(Figure 1) are two stage dryers where internal fluidised beds at the base of the chamber provide the second stage of drying. This allows for lower outlet air temperatures because of the evaporation occurring in the fluid bed, thus improving dryer efficiency and making the operation even more suitable for drying heat sensitive materials (Westergaard, 2003).

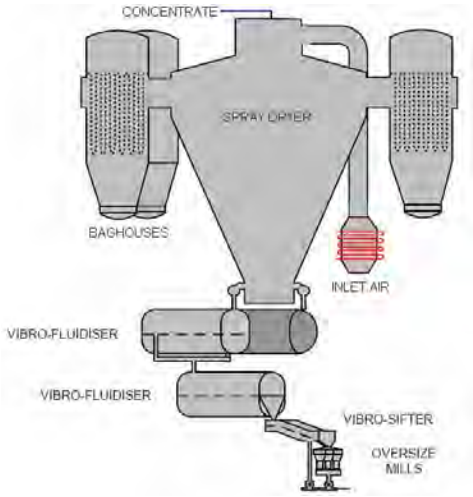

Figure 1: Schematic of modern milk powder plant

The difficulty with experiments and therefore validation on industrial dryers is their large sizes, the massive costs involved and the hostile environment for flow, temperature and humidity measurements (Huang et al., 2006). Also, industrial scale simulations that include transient particle tracking, hindered drying and wall deposition are extremely expensive computationally (Fletcher et al., 2003).

Straatsma et al. (1999) developed a 2D drying simulation model to investigate two industrial spray dryers (heights 14 and 17 m) used for milk powder production. The air outlets in both cases were at the top of the chamber but no internal fluid bed was included. The flow field predicted for the larger of the two chambers that used nozzle atomisers was a fast flowing core with large recirculation zones between the central jet and the walls. These simulations were steady state and included no validation, so no transient behaviour was reported.

Fletcher et al. (2003) conducted a full transient simulation with particle tracking, hindered drying and wall deposition for an industrial spray dryer (height 30 m). A deflected main inflow jet precessed slowly with time around the central axis. The offset outlet pipe at the base of the chamber caused the central jet to be significantly off the dryer axis. However, like the simulations of Straatsma et al. (1999), there was no internal fluid bed flow nor any validation attempted.

Also, in an increasing number of modern spray dryers, the outlet air passes through ducts located near the top of the chamber rather than through a single outlet near the bottom of the chamber. The presence of the outlet air ducts at the top of the chamber means dry fine powder is recirculated to the top of the chamber to interact with the atomiser cloud, thus increasing agglomeration. This mechanism is known as spontaneous secondary agglomeration (Westergaard, 2003).

This paper examines the flow patterns in an industrial spray dryer used for milk powder production. The aim was to determine the transient behaviour of the flow field where a fluid bed air flow was included, and validate the simulations against data collected from the industrial scale.

MODEL DESCRIPTION

Geometry

The industrial chamber geometry used (Figure 2) is a modified conical type. Due to confidentiality the actual dimensions cannot be reported, but it should be noted that they are larger than those of Straatsma et al. (1999).

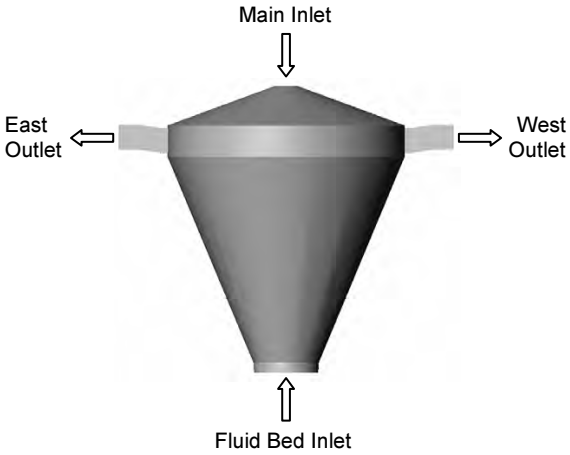

Figure 2: Industrial spray dryer geometry used for simulations and experimental work

The main airflow enters the chamber between the pressure nozzle lances and external recycle fines return holes in the circular flat plate at the top of the chamber. This flow has passed through an air disperser designed to ensure a uniform flow pattern, so it can be assumed there is no swirl in the inlet. The fluid bed air enters a plenum chamber then flows up through the perforated plate, inducing some swirl, which is the base of the chamber in Figure 2. Both air streams are drawn out through the two identical ducts located near the top of the chamber by extractor fans, and hence the chamber and ducts are under vacuum.

Boundary Conditions

The air flow in this simulation was assumed to be incompressible and isothermal at 25 ^{o}C.

The inlet velocity was set at 17.5 m/s with a turbulent intensity of 3.7 % and a turbulent length scale based on the inlet diameter. This inlet turbulence approach is identical to that of a number of studies (Guo et al., 2003, Harvie et al., 2001, Harvie et al., 2002, LeBarbier et al., 2001).

The fluid bed air inlet is modelled as a circular inlet where the velocity is set at 0.77 m/s with no swirl. Again a turbulence intensity of 3.7 % was used with a turbulent length scale based on the fluid bed inlet diameter.

Average static pressures of – 60 Pa were specified in the two outlet air ducts. The chamber walls were treated with the default CFX 10.0 boundary conditions of no slip, with smooth, adiabatic walls.

Simulation Procedure

3D simulations were carried out using the commercial CFD package CFX 10.0. The transient Reynolds Averaged Navier-Stokes equations and the Shear Stress Transport (SST) turbulence equation were used to model

the effects of turbulence. Second order discretization schemes were used in both time and space to convert the partial differential equations into a system of algebraic equations.

Using this scheme, convergence was not possible for steady state simulations, indicating, as expected, that the simulations needed to be run in transient mode. The unconverged steady state results were used as an initial guess for the transient simulations.

A convergence criterion of a maximum residual of 1 x 10^{-4} was used to terminate the coefficient iterations. Usually only two or three iterations at each time step were required when using a time step of 0.01 s. A total simulation time of 40 s was specified.

An unstructured mesh was used with inflation layers at the walls, to ensure boundary layer effects were properly captured. The mesh density was increased in the region around the main inlet air stream at the top of the chamber and in the outlet air ducts, where large gradients exist.

To check that the solutions obtained were independent of the mesh, the simulations were repeated using mesh consisting of approximately 270000, 326000 and 354000 nodes. The results from each compared favourably and the simulation was deduced to be mesh independent. The mesh with 326,000 nodes was used for the results presented here.

Velocity components in the x, y and z directions, along with the pressure at four fixed points, were recorded for each time step.

EXPERIMENTAL

The spray dryer was run on ambient air with a main inlet air flow giving an inlet velocity of 19.1 m/s and a fluid bed flow that gave a measured velocity of 0.77 m/s. The main inlet velocity was slightly higher than that simulated.

Figure 3: Tell tail pole located at centre of dryer fluid bed for observing the movement of the main air jet

The period of oscillation of the main air jet was measured using a tell tail pole (Figure 3). The 3 m pole placed in the centre of the fluid bed, had fabric tufts placed every 200 mm up the pole and enabled the motion of the jet to be recorded with a video camera (Sony Mini DV Digital Handycam).

RESULTS

Simulation

The major flow feature in the drying chamber is the main axial jet entering the top of the chamber. It diverges slightly, slows as it moves further into the dryer and moves about the central axis with time. There is very little flow normal to the dryer axis, with the axial flows dominating.

The low velocity fluid bed air flows up and creates a stagnation point with the main jet approximately 1 m above the fluid bed. At this point, the flow is radial, but the flow switches from being split to both walls or all favouring one wall or the other due to the movement of the main jet. The position of the stagnation point moves up and down.

Between the main jet and the walls of the chamber, slow recirculation zones are evident. The sizes of these zones swell and compress causing the main jet to also change in size and move about the central axis. This movement of the jet also increases the velocities near the walls; they increase when the jet is on the opposite side and decrease when it moves close to the wall.

The movement of the main jet can be observed through a series of 3D snapshots. The three snapshots of the jet behaviour in Figure 4 are taken 30, 33 and 36 seconds from the start of the simulation. It can be seen that the jet flaps through the central axis of the dryer and not along any distinct plane.

At 33 s, the main jet is seen to move close to the chamber walls. Thus, it is likely that wet droplets entrained in the main air jet will impact on the wall. If these droplets adhere, they can brown and therefore have a negative impact on product quality as well as becoming a fire and explosion risk.

Interestingly, the vector plots in Figure 4 show some flow from the main inlet travels straight to the outlets along the roof of the chamber. This implies that some particles will have much shorter residence times compared to those that flow to the bottom of the chamber or become caught in the recirculation zones, and therefore will have higher moisture contents. Smaller particles from the atomiser are more likely to be entrained in this air flow and thus exit the drying chamber through one of the two outlets. Future particle tracking simulations aim to deduce if this is so.

The air velocities in the outlet ducts are high. As expected, they are much higher in magnitude than the majority of velocities in the chamber, as these ducts, are quite small in cross section area when compared to the cross sectional area of the chamber. These velocities are seen to surge slightly with the movement of the main jet in the chamber. This could possibly be the explanation of what is termed by industrial operators as ‘breathing’.

Langrish et al. (2004) found from experimental and simulations on a pilot scale spray dryer that for the case of no inlet swirl, no distinct frequency. From simulations of an industrial scale spray dryer, Fletcher et al. (2003) found the main jet had a frequency of approximately 1 Hz, but stated the presence of higher frequencies were evident.

Therefore, it is to be expected that no apparent frequency exists, which the simulations have shown. The presence of a fluid bed flow could add to the instability of the flow field, as no fluid bed flow was modelled by Langrish et al. (2004) or Fletcher et al. (2003).

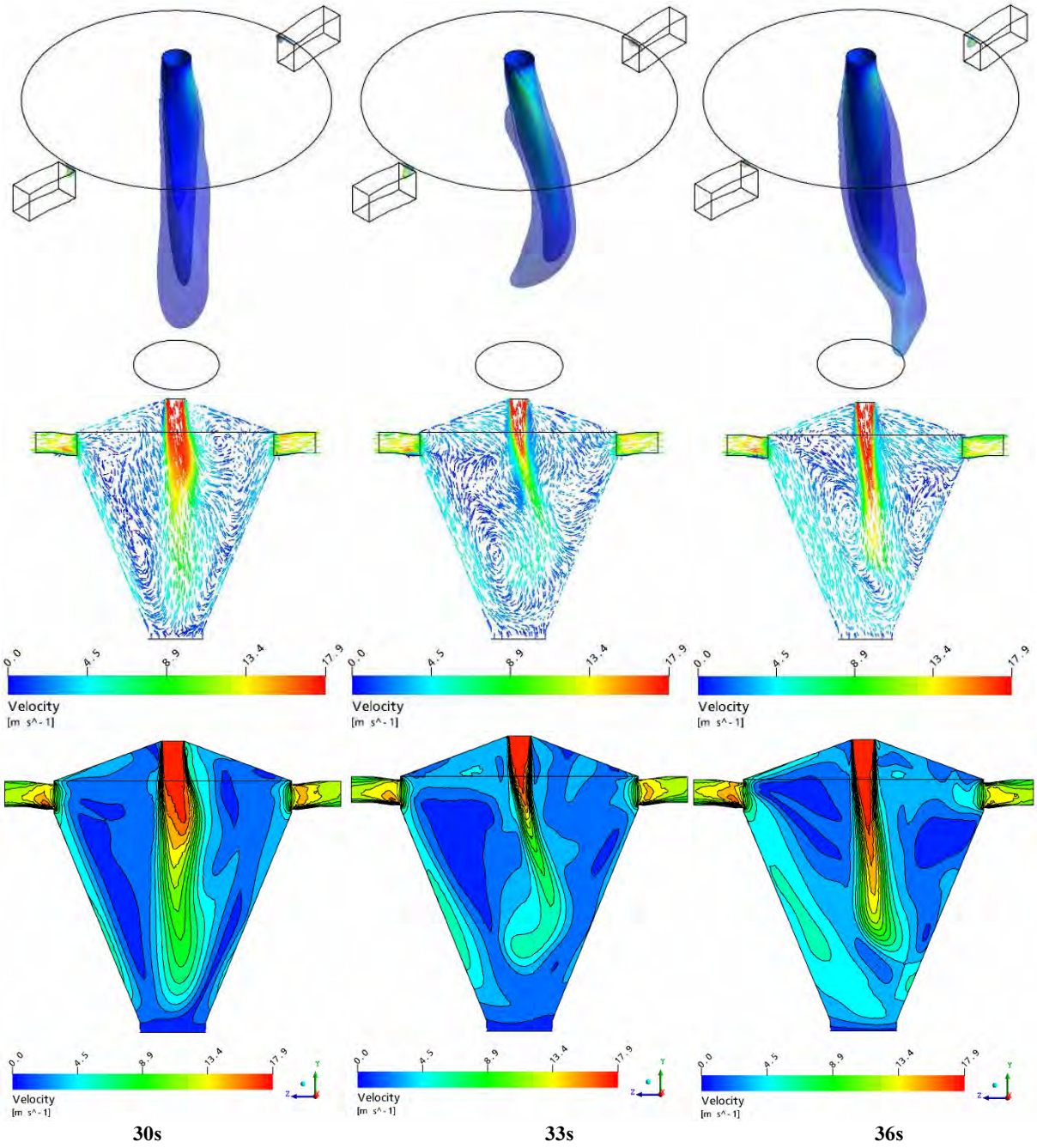

Figure 4: Snapshots of 3D axial velocity contour of the main jet, 2D velocity vector and 2D velocity contour plots through the central plane of the dryer axis 30, 33 and 36 seconds from the start of the simulation

Experimental

The tell-tail tuft observations showed a reasonably consistent behaviour: the tufts would flap in one direction, the flapping would die away as the tails pointed toward the fluid bed at the bottom of the chamber, and then flap again but in the opposite direction. The period of oscillation was estimated by determining the time between directional changes of the tails. The estimated periods ranged from approximately 2 s to around 10 s.

CONCLUSIONS

The air flow patterns in an industrial spray dryer used for milk powder production have been modelled using the transient Reynolds Averaged Navier-Stokes equations with the SST turbulence model. This is possibly the first published work to include the influence of a spray dryer's internal fluid bed airflow on the flow patterns in spray dryers. Also, the geometry in this work has outlet air ducts near the top rather than the bottom of the drying chamber.

The results showed that the main axial jet dominates the flow field and moves about the central axis of the dryer with time. Recirculation zones were observed between this jet and the dryer walls that change in size relative to the motion of the main jet. No apparent distinct frequency is observed which agrees well with the literature and experimental measurements made on the industrial scale dryer.

Although the fluid bed flow had a small impact on the total flow field, it is likely to have destabilised the flow field.

Visualisation of the main jet movement was achieved by running the industrial dryer on ambient air and measuring the main jet period with tell tails in the dryer. These observations confirmed the transient nature of the main jet and that no apparent distinct frequency exists, as the tuft movements had periods ranging from approximately 2 s to 10 s.

These findings reiterate the conclusions of previous authors that transient, 3D simulations are required to fully capture the flow features of spray dryers.

ACKNOWLEDGEMENTS

The authors wish to thank Mr Nathan Bushnell (Department of Chemical and Process Engineering, University of Canterbury) for his academic support and Fonterra Clandeboye Powder plant staff for their industrial support. This work has received funding from the Foundation for Research Science and Technology (FRST) and Fonterra Co-operative Group Ltd.

REFERENCES

ANSYS (2005a) *CFX 10.0 Manual,* Canonsburg.

ANSYS (2005b) Innovative turbulence modelling: SST model in ANSYS CFX. Canonsburg.

FLETCHER, D. F., GUO, B., HARVIE, D. J. E., LANGRISH, T. A. G., NIJDAM, J. J. & WILLIAMS, J. (2003) What is important in the simulation of spray dryer performance and how do current CFD models perform. *Third International Conference on CFD in the Minerals and Process Industries.* Melbourne.

GUO, B., LANGRISH, T. A. G. & FLETCHER, D. F. (2003) Simulation of gas flow instability in a spray dryer. *Trans IChemE, Part A, Chem Eng Res Des,* 81**,** 631-638.

HARVIE, D. J. E., LANGRISH, T. A. G. & FLETCHER, D. F. (2001) Numerical simulations of gas flow patterns within a tall-from spray dryer. *Trans IChemE, Part A, Chem Eng Res Des,* 79**,** 235-248.

HARVIE, D. J. E., LANGRISH, T. A. G. & FLETCHER, D. F. (2002) A computational fluid dynamics study of a tall-from spray dryer. *Trans IChemE, Part C, Food Bioprod Process,* 80**,** 163-175.

HUANG, L., KUMAR, K. & MUJUMDAR, A. S. (2003) Use of computational fluid dynamics to evaluate alternative spray dryer chamber configurations. *Drying Technol,* 21**,** 385-412.

HUANG, L., KUMAR, K. & MUJUMDAR, A. S. (2006) A comparative study of a spray dryer with rotary disc atomizer and pressure nozzle using computational fluid dynamic simulations. *Chem. Eng. Process,* 45**,** 461-470.

KIEVIET, F. G., VAN RAAIJ, J., DE MOOR, P. P. E. A. & KERKHOF, P. J. A. M. (1997) Measurement and modelling of the air low pattern in a pilot-plant spray dryer. *Trans IChemE, Part A, Chem Eng Res Des,* 75**,** 321-328.

LANGRISH, T. A. G. (1993) The flow patterns of gas and particles in spray dryers. *Chem Eng Aust,* 18**,** 16-20.

LANGRISH, T. A. G., KEEY, R. B. & HUTCHINSON, C. A. (1992) Flow visualization in a spray dryer fitted with a vaned-wheel atomizer. *Trans IChemE, Part A, Chem Eng Res Des,* 70**,** 385-394.

LANGRISH, T. A. G., WILLIAMS, J. & FLETCHER, D. F. (2004) Simulation of the effects of inlet swirl on gas flow patterns in a pilot-scale spray dryer. *Trans IChemE, Part A, Chem Eng Res Des,* 82**,** 821-833.

LEBARBIER, C., KOCKEL, T. K., FLETCHER, D. F. & LANGRISH, T. A. G. (2001) Experimental measurement and numerical simulation of the effect of swirl on flow stability in spray dryers. *Trans IChemE, Part A, Chem Eng Res Des,* 79**,** 260-268.

LI, X. & ZBICINSKI, I. (2005) A sensitivity study on CFD modelling of cocurrent spray-drying process. *Drying Technol,* 23**,** 1681-1691.

MASTERS, K. (1972) *Spray drying - an Introduction to principles, operating practises and applications,* London, Leonard Hill Books.

NIJDAM, J. J., GUO, B., FLETCHER, D. F. & LANGRISH, T. A. G. (2004) Challenges of simulating droplet coalescence within a spray. *Drying Technol,* 22**,** 1463-1488.

OAKLEY, D. E. & BAHU, R. E. (1990) Computational modelling of spray dryers. *European Symposium on Computer Aided Process Engineering - 2.* Toulouse.

SOUTHWELL, D. B., LANGRISH, T. A. G. & FLETCHER, D. F. (1999) Process intensification in spray dryers by turbulence enhancement. *Trans IChemE, Part A, Chem Eng Res Des,* 77**,** 189-205.

SOUTHWELL, D. B., LANGRISH, T. A. G. & FLETCHER, D. F. (2001) Use of computational fluid dynamics techniques to assess design alternatives for the plenum chamber of a small spray dryer. *Drying Technol,* 19**,** 257-268.

STAFFORD, R. A., FAUROUX, O. & GLASS, D. H. (1996) Flow visualisation and instantaneous velocity measurements of spray dryer gas and spray flows using particle image velocimetry. *10th International Drying Symposium.* Krakow.

STRAATSMA, J., VAN HOUWELINGEN, G., STEENBERGEN, A. E. & DE JONG, P. (1999) Spray drying of food products: 1. simulation model. *J Food Eng,* 42**,** 67-72.

WESTERGAARD, V. (2003) *Milk powder technology,* Gladsaxevej, GEA Niro A/S.